République Algérienne Démocratique et Populaire

Ministère de l'Enseignement Supérieur et de la Recherche Scientifique

Université Kasdi Merbah-Ouargla

Faculté des Mathématiques et des Sciences de la matière

Département de Chimie

THÈSE PRÉSENTÉE EN VUE DE L'OBTENTION DU DIPLÔME DE DOCTORAT 3ème Cycle (LMD)

Spécialité : Chimie des produits naturels

Intitulé *:*

Étude phytochimique et évaluation des activités biologique de *Atractylis aristata* (Asteraceae)

Présentée par :

Asma Abid

Soutenue publiquement le 09/10/2023

Devant le jury composé de :

Mr. Mohamed Lakhder Belfar	**Professeur**	**Univ. Ouargla**	**Président**
Mme. DEKMOUCHE Messaouda	**Professeur**	**Univ. Ouargla**	**Rapporteur**
Mr. Lazher Bechki	**Professeur**	**Univ. Ouargla**	**Co- Rapporteur**
Mr. Hamada HABA	**Professeur**	**Univ. Batna**	**Examinateur**
Mr. Mohamed Yousfi	**Professeur**	**Univ. Laghouat**	**Examinateur**
Mr. Tarak Mekhelfi	**Professeur**	**Univ. Ouargla**	**Examinateur**
Mr. Mahdi Belguidoum	**MCA**	**Univ. Ghardaia**	**Invité**

Année universitaire: 2022/2023

THESIS SUBMITTED WITH A VIEW TO OBTAINING A 3rd Cycle DOCTORAL DEGREE (LMD)

Ordre number: ....

Serial number:......

Speciality: Chemistry of natural products

Entitled:

Phytochemical study and evaluation of the biological activities of *Atractylis aristata* (Asteraceae)

Presented by:

Asma Abid

Publicly discussed on 09/10/2023

In front of the jury composed of:

Mr. Mohamed Lakhder Belfar	**Professor**	**Univ. Ouargla**	**President**
Mrs. Messaouda Dekmouche	**Professor**	**Univ. Ouargla**	**Supervisor**
Mr. Lazher Bechki	**Professor**	**Univ. Ouargla**	**Co-Supervisor**
Mr. Hamada HABA	**Professor**	**Univ. Batna**	**Examiner**
Mr. Mohamed Yousfi	**Professor**	**Univ. Laghouat**	**Examiner**
Mr. Tarak Mekhelfi	**Professor**	**Univ. Ouargla**	**Examiner**
Mr. Mahdi Belguidoum	**MCA**	**Univ. Ghardaia**	**Invited**

University year: 2022/2023

I dedicate this work to

my dear parents:

My father Mahmoud and my mother Noura who have never stopped supporting me since I was born and constantly encouraging me throughout my school years. Without you, I could not be who I am and could not progress and complete this work. May God Almighty protect you, and grant you a happy life.

my brothers:

Ali, Bachir and Mouhamed

my sisters:

Zineb and Mabrouka

To the memory of:

My grandfather Mouhamed and my uncle Tedjeni You recommended me to study, and here I am today dedicating a PhD thesis to your soul.

my grandmother uncles and aunts:

To my paternal aunts and my uncle Lakhder, to all my cousins and the whole **Abid** family.

To my grandmother Khadra to all my maternal uncles and aunts, to all my cousins. and the whole **Dida** family

Abstract

Atractylis aristata batt. is an endemic plant from Asteraceae family occupying an important place in traditional medicine in the Hoggar region in Algeria. The different extracts of the plant were obtained after maceration then liquid-liquid extraction using solvents of increasing polarity. The obtained extracts were tested for their content in total phenolic, total flavonoids and condensed tannins using colorimetric methods. The biological activities of different extracts were evaluated by *in vitro* antioxidant and antidiabetic activities and by *in vivo* acute toxicity and anti-inflammatory and sedative activities. The antioxidant activity was tested using five methods DPPH, ABTS, reducing power, superoxide anion radical scavenging and Fe^{2+} chelating activity assays and the antidiabetic activity was evaluated using α-amylase inhibitory Power test. The *in vivo* acute toxicity was tested using the limit dose test according to the test guidelines on acute oral toxicity OECD guideline No. 423. Anti-inflammatory activity was evaluated using carrageenan-induced paw edema method. Sedative activity was carried out using the measurement of locomotor method. The quantitative analysis of the extracts of the plant *A. aristata* by spectroscopic methods have shown moderate levels of polyphenols, flavonoids and condensed tannins. Our results reveals that the crude extract had the highest biological activity in relation to the antioxidant activity by DPPH and ABTS free radicals and the Fe^{+2} chelating methods, with values IC_{50} 0.04 mg/mL (DPPH), IC_{50} 0.005 mg/mL (ABTS) and inhibition 95% (Fe^{+2} chelating). The highlighted significant IC_{50} value for the crude extract exhibited noteworthy activity ten times higher than the standard ascorbic acid against ABTS free radical. It is also important to highlight the antidiabetic activity of crude extract, which showed an alpha-amylase inhibition rate (57.62 %) very close to the drug acarbose. In the same case, the crude also showed a robust capacity of anti-inflammatory and sedative activities *in vivo*, with inhibition values (62.98 and 52.12 %, respectively). Depending on our findings in the evaluation of *in vitro* and *in vivo* biological activity, the extracts of the plant *A. aristata* could be safely used therapeutically in pharmaceutical formulations aimed at researching new antioxidant, antidiabetic, anti-inflammatory and sedative agents.

In order to study the phytochemical composition of the plant *A. aristata* maceration, extraction, separation and purification were carried out using different chromatographic techniques, TLC silica gel and column chromatography CC using various supports (normal silica, RP-18 grafted silica, polyamide and Sephadex LH-20). The structural identification of the compounds thus obtained was ensured by 1D and 2D NMR and ESI-MS spectroscopic methods, which made it possible to identify 24 compounds, including four phenolic compounds (two flavonoids and two phenolic acids), 20 triterpene compounds (three lupane, thirteen pentacyclic triterpenes) and four polysaccharides. Among these compounds, twenty compounds were identified for the first time in the genus and three new compounds.

Key words: Asteraceae, triterpenoid, phenolic compounds, flavonoid, polysaccharides, biological activity.

Résumé

Atractylis aristata batt. est une plante endémique de la famille des Astéracées occupant une place importante en médecine traditionnelle dans la région du Hoggar en Algérie. Les différents extraits de la plante ont été obtenus après macération puis extraction liquide-liquide à l'aide de solvants de polarité croissante. Les extraits obtenus ont été testés pour leur teneur en phénols totaux, flavonoïdes totaux et tanins condensés à l'aide de méthodes colorimétriques. Les activités biologiques des différents extraits ont été évaluées par des activités antioxydantes et antidiabétiques *in vitro* et une toxicité aiguë des activités anti-inflammatoires et sédatives *in vivo*. L'activité antioxydante a été testée à l'aide de cinq méthodes DPPH, ABTS, pouvoir réducteur, piégeage des radicaux anions superoxydes et dosages de l'activité chélatrice Fe^{2+}. L'activité antidiabétique a été évaluée à l'aide du test de puissance inhibitrice de l'α-amylase. La toxicité aiguë a été testée à l'aide du test de dose limite conformément aux directives de test sur la toxicité orale aiguë, directive OCDE n° 423. L'activité anti-inflammatoire a été évaluée à l'aide de la méthode de l'œdème de la patte induit par la carragénine. L'activité sédative a été réalisée en utilisant la mesure de la méthode locomotrice. L'analyse quantitative des extraits de la plante *A. aristata* par des méthodes spectroscopiques a montré des niveaux modérés de polyphénols, de flavonoïdes et de tanins condensés. Nos résultats montrent que l'extrait brut avait l'activité biologique la plus élevée par rapport à l'activité antioxydante par les radicaux libres DPPH et ABTS et les méthodes de chélation Fe^{+2}, avec des valeurs IC_{50} 0,04 mg/mL (DPPH), IC_{50} 0,005 mg/mL (ABTS) et 95% (chélatant Fe^{+2}). La valeur IC_{50} significative mise en évidence pour l'extrait brut a montré une activité remarquable dix fois supérieure à celle de l'acide ascorbique standard contre le radical libre ABTS. Il est également important de souligner l'activité antidiabétique de l'extrait brut, qui a montré un taux d'inhibition de l'alpha-amylase (57,62 %) très proche du médicament acarbose. Dans le même cas, le brut a également montré une capacité robuste d'activités anti-inflammatoires et sédatives *in vivo*, avec des valeurs d'inhibition (62,98 et 52,12 %, respectivement). Selon nos découvertes dans l'évaluation de l'activité biologique *in vitro* et *in vivo*, les extraits de la plante *A. aristata* pourraient être utilisés en toute sécurité en thérapeutique dans des formulations pharmaceutiques visant à rechercher de nouveaux agents antioxydants, antidiabétiques, anti-inflammatoires et sédatifs.

Afin d'étudier la composition phytochimique de la plante *A. aristata*, macération, extraction, séparation et purification ont été réalisées à l'aide de différentes techniques chromatographiques ; CCM utilisant le support silice normale et chromatographie sur colonne CC utilisant différents supports (silice normale, silice greffée RP-18, polyamide et Sephadex LH-20). L'identification structurale des composés ainsi obtenus a été assurée par des méthodes spectroscopiques RMN 1D et 2D et ESI-MS, qui ont permis d'identifier 24 composés, dont quatre composés phénoliques (deux flavonoïdes et deux acides phénoliques), 16 composés triterpéniques (trois lupane, treize triterpènes pentacycliques) et quatre polysaccharides. Parmi ces composés, une vingtaine de composés ont été identifiés pour la première fois dans le genre et trois nouveaux composés.

ملخص

Atractylis aristata هو نبات مستوطن من عائلة Asteraceae يحتل مكانة مهمة في الطب التقليدي في منطقة الهقار في الجزائر. بعد النقع ثم الاستخلاص سائل-سائل باستخدام مذيبات ذات قطبية متزايدة تمكنا من الحصول على المستخلصات المختلفة للنبات. المستخلصات المتحصل عليها تم تحديد محتواها من الفينولات الكلية والفلافونويد الكلي والعفص المكثف باستخدام طرق القياس اللوني. قيمت الأنشطة البيولوجية للمستخلصات المختلفة من خلال الأنشطة المضادة للأكسدة ومضادات السكر في المختبر والسمية الحادة الفعالية المضادة للالتهابات والمهدئة في الجسم الحي. اختبر النشاط المضاد للأكسدة باستخدام خمس طرق DPPH، ABTS، القدرة الارجاعية، الكسح الجذري للأكسيد الفائق و نشاط تمخلب Fe^{2+}. قيم النشاط المضاد لمرض السكر باستخدام اختبار الفاعلية المثبطة لأنزيم ألفا أميلاز. السمية الحادة حددت باستخدام اختبار الجرعة المحددة وفقًا لإرشادات اختبار السمية الفموية الحادة، المبدأ التوجيهي رقم 423. كما قيم النشاط المضاد للالتهابات والنشاط المهدئ باستخدام طريقة وذمة القدم التي يسببها الكاراجينان وقياس الطريقة الحركية، على التوالي. أظهر التحليل الكمي لمستخلصات نبات *A. aristata* بالطرق الطيفية مستويات معتدلة من البوليفينول والفلافونويد والعفص المكثف. أظهرت نتائجنا أن المستخلص الخام كان له أعلى نشاط بيولوجي فيما يتعلق بالنشاط المضاد للأكسدة بواسطة الجذور الحرة DPPH و ABTS وطرق مخلب Fe^{2+}، بقيم IC_{50} 0.04 مجم / مل (DPPH)، IC_{50} 0.005 مجم / مل (ABTS)) و95٪ (Fe^{2+} مخلب). أظهرت قيمة IC_{50} المميزة للمستخلص الخام نشاطًا ملحوظًا أعلى بعشر مرات من حمض الأسكوربيك القياسي ضد الجذر الحر ABTS. من المهم أيضًا إبراز النشاط المضاد لمرض السكر في المستخلص الخام، والذي أظهر معدل تثبيط ألفا أميليز (57.62٪) قريبًا جدًا من عقار أكاربوز. في نفس الحالة، أعطى المستخلص الخام أيضًا قدرة قوية للأنشطة المضادة للالتهابات والمسكنات في الجسم الحي، مع قيم تثبيط (62.98 و52.12٪ على التوالي). اعتمادًا على النتائج التي توصلنا إليها في تقييم النشاط البيولوجي في المختبر وفي الجسم الحي، يمكن استخدام مستخلصات نبات *A. aristata* بأمان علاجيًا في المستحضرات الصيدلانية التي تهدف إلى البحث عن عوامل جديدة مضادة للأكسدة ومضادة لمرض السكر ومضادة للالتهابات ومهدئة.

من أجل دراسة التركيب الكيميائي النباتي لنبات *A. aristata*، أجريت عملية النقع والاستخلاص والفصل والتنقية باستخدام تقنيات كروماتوغرافية مختلفة، باستخدام كروماتوغرافيا الطبقة الرقيقة باستخدام الطور الثابت هلام السيليكا وكروماتوغرافيا العمود باستعمال أطوار ثابتة مختلفة (السيليكا العادية، RP-18، مادة متعدد الأميد وsephadex LH-20). حددت هياكل المركبات التي تم الحصول عليها بهذه الطريقة من خلال طرق التحليل الطيفي أحادية البعد وثنائية البعد وكذلك مطيافية الكتلة ESI-MS، مما جعل من الممكن تحديد 24 مركبًا، بما في ذلك أربع مركبات فينولية (اثنان من مركبات الفلافونويد وحمضان فينوليان)، و16 مركبًا من مركبات ترايتيربين (ثلاثة لوبان، ثلاثة عشر ترايتيربين خماسي الحلقي) وأربعة عديدات سكريات. من بين هذه المركبات، تم تحديد عشرون مركبًا لأول مرة في الجنس وثلاثة مركبات جديدة في الطبيعة.

الكلمات المفتاحية: Asteraceae، تربان ثلاثي، مركبات فينولية، فلافونويد، عديدات سكريات، فعالية بيولوجية.

Abbreviation

1D	one-dimensional
2D	two-dimensional
ABTS	2,2`-azinobis-(3-ethylbenzothiazolin-6-sulfonic)
BHT	Butyl Hydroxy Toluene
brs	Broad singulet
brd	Broad doublet
CC	Column Chromatography
COSY	Correlated Spectroscopy
d	Doublet
dd	Doublet of Doublet
ddd	Doublet of Double Doublet
DEPT	Distortionless Enhanced Polarization Transfer
DPPH	1,1-Diphényl-2-PicrylHydrazyl
J	Coupling constant
Hz	Hertz
HMBC	Heteronuclear Multiple Bond Coherence
HSQC	Heteronuclear Single Quantum Coherence
IC 50	Concentration Inhibitory at 50%
ESI-MS	Electrospray Ionization Mass Spectrometry
m	Multiplet
m/z	Mass to charge ratio
NMR	Nuclear magnetic resonance
RP C-18	Reversed-phase C-18 column
S	Singulet
TLC	Thin-Layer Chromatography
TOCSY	Total Correlation Spectroscopy
δ (ppm)	Chemical shift
OECD	Organisation for Economic Co-operation and Development

Chapter IV: Isolation, purification and structural identification of natural compounds

List of content

Chapter I: Asteraceae family, Atractylis genus

Chapter II: Primary and secondary metabolites

Chapter III: Phytochemical screening, in vitro and in vivo biological activities

Chapter IV: Isolation, purification and structural identification of natural compounds

Introduction

──────*Introduction*──────

Recent studies have shown that many manufactured medicines used in the treatment of many diseases have side effects, even some of them are carcinogenic, as some of them have been completely withdrawn from pharmacies. Currently, there is a great worldwide interest in the search for new biologically active molecules from natural sources, in order to prevent various diseases especially those caused by oxidative stress through the process of free radicals scavenging, as well as discovered new drugs to treat many diseases, including diabetes, inflammation, in addition to cancer, which claims the lives of millions each year. The plant kingdom offers a wide range of molecules with very varied biological and pharmacological activity, in particular flavonoids, triterpenoids, saponins and also polysaccharides, which have been studied with the aim of finding compounds capable of protecting against a certain number of diseases.

Throughout history, humans have relied on Nature using the plants for food, shelter, clothes, drugs etc. [1]. About 70–90% of the population living in developing countries continue to use ancient medicines based on plant extracts [2]. The interest in Nature as a source of potential chemotherapeutic agents continues, more than 50% of therapeutic medications have become natural compounds or their derivatives [1].

One of the families of plants often recommended in pharmacies is the Asteraceae family. This family is one of the largest families in the plant world with more than 23,000 species and it is also one of the most evolved. This family is widespread throughout the world, with a predominance in temperate regions. The Asteraceae family was a great diversity of genera and species. Indeed, this family includes plants with different interests. Some of them are used for their medicinal properties, others are used in the ornamental field; and also the Asteraceae plants have a food interest [3]. The Asteraceae is classified as one of the dominant family of plants in Algerian Sahara.

The Sahara, which occupies 10% of the surface of the African continent, is the largest hot desert in the world. Despite its vast expanse, species richness and endemism are low. Despite this, some acclimatized species survive with extraordinary forms of adaptation. This ecoregion includes the northern part of the Sahara, where rainfall occurs during the winter, nurturing a variety of plants that bloom before the hot, dry

summer. The flora of the northern Sahara is very poor considering the vastness of the ecozone. On the other hand, although the Sahara holds 80% of the surface of Algeria, it has been the subject of very little work relating to the development of biological resources [4]. The Algerian Sahara flora contains about 960 species [5], of which 162 species are endemic, endemism represents about 25% [6].

The Algerian Sahara vegetation in the Hoggar region impacted by the moderate Mediterranean climate and tropical Sudan climate. Due to its unusual geographic location, Hoggar is surrounded by a true natural sanctuary with a tremendous floristic diversity. A cosmopolitan, saharosindian, soudano-decanian, Mediterranean, and indigenous flora existed based on biogeography [7].

In this context, the focus of this study is on investigating Asteraceae plants for the discovery of novel natural compounds. The main objective of this work is the evaluation of *in vitro* and *in vivo* biological activities and the extraction, isolation and identification of compounds isolated from organic extracts of a Saharan medicinal plant belonging to the genus Atractylis, namely *Atractylis aristata* of the Asteraceae family. This choice is justified by the fact that this plant is widely used in traditional medicine in Algeria in the Hoggar region to treat stomach diseases, colic, spasms and fever [8]. It should be noted that few phytochemical and biological studies have been devoted to this genus represented in North Africa. The previous pharmacological studies have demonstrated that *Atractylis* extracts have anti-inflammatory, anti-pyretic and acute toxicity [9], antioxidant [10], antidiabetic [11, 12] and anticancer [13] activities.

Our thesis work consists of four chapters:

➢ The first chapter is devoted to the bibliographical and botanical research. This study begins with a bibliographic research and botanical description of the Asteraceae family and the Atractylis genus as well as previous studies carried out on the Atractylis genus.

➢ The second chapter includes some primary and secondary metabolites. A theoretical overview of primary and secondary metabolites in particular, carbohydrates, flavonoids, triterpenes and saponins. By showing the biosynthesis, classifications and biological interests of each family of compounds.

> ➤ The third chapter presents the personal work on the quantification of total phenols, total flavonoids and condensed tannins as well as the evaluation of *in vitro* and *in vivo* biological activities of *A. aristata* extracts. Including *in vitro* antioxidant and antidiabetic activities and *in vivo* acute toxicity, anti-inflammatory and sedative activities.

> ➤ The fourth chapter reports in detail the extraction, separation, purification and structural elucidation of the compounds isolated from the dichloromethane, n-butanol and petroleum ether extracts of *Atractylis aristata*.

Chapter I:

Asteraceae family, Atractylis genus.

I.1. Asteraceae family

The family Asteraceae, also called Compositae, is the largest flowering plant families. It is containing the largest number of species of any plant family; the total number is estimated at about 30,000 species and there are 1600-1700 genera. Assuming that there are 250,000-350,000 species of flowering plants and about 10% of them are present in family Compositae [14, 15], which is mainly distributed in temperate, subtropical, or tropical regions, often in the mountainous region [16].

Plants of the Asteraceae family are distributed entire surface of the earth (**Figure. I. 1**) except Antarctica, it is a cosmopolitan family with greater diversification in dry regions, such as, for example, in the Mediterranean basin, South Africa, Mexico and South America as well as the southwestern United States [3, 14].
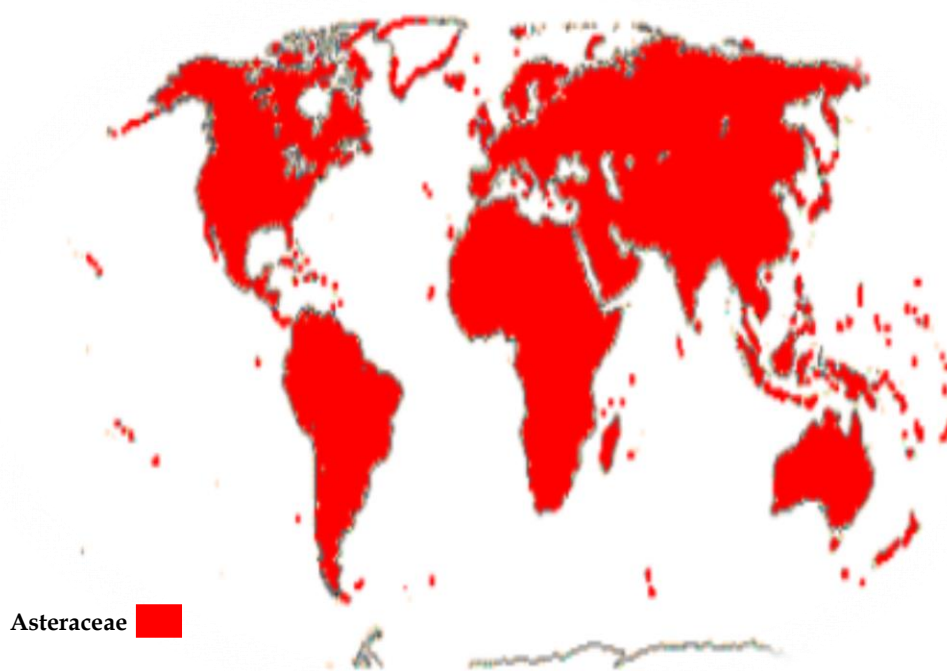
Asteraceae ▉

Figure. I. 1: Distribution of the Asteraceae family in the world [3].

The family Asteraceae is identified by two characters; the grouping of the flowers in heads and welding of the stamens by their anthers, the Asteraceae have the common characteristic of having flowers united in capitula, that is to say, tight together, without peduncles placed on the end of a branch or stem or surrounded by a structure, This cup-shaped or flanged structure is called an involucre [6] (**Figure. I. 2**).

The Characters of Asteraceae (Compositae) are given below:
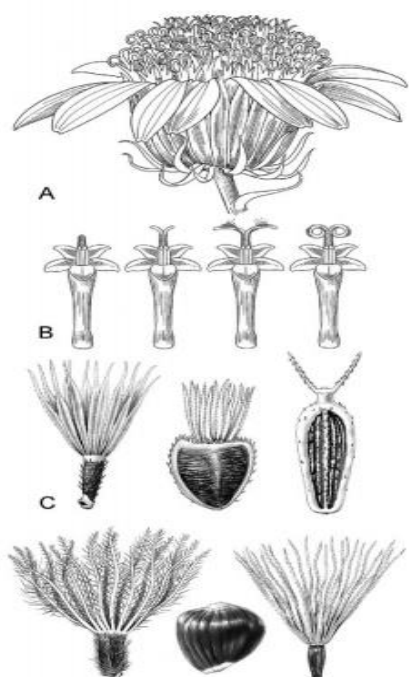
A: The head with ray florets arranged around the perimeter, disc florets in the center, and an involucre with bracts (phyllaries) surrounding the outermost florets.

B: The pollen is released via the style pushing out through the anthers, which are fused at the margins; sometimes the style branches are recurved and come in contact with the style shaft.

C: Some of the achene (cypsela) and pappus types found in Compositae.

Figure. I. 2: Characters of Asteraceae (Compositae) [15].

The morphology of the Asteraceae plants is also diverse. Some species are trees reaching more than 30 m, many others are shrubs, like rabbit brush or rosette-trees, and most are perennial or less annual herbs, ranging from 1–3 m [17].

According to the classification of two groups of researchers (Baldwin *et al*. 2002; Panero and Funk 2002, 2007 and 2008) the Asteraceae family divided into 12 subfamilies and 43 tribes. These subfamilies are: Barnadesioideae, Stifftioideae, Mutisioideae, Wunderlichioideae, Gochnatioideae, Hecastocleidoideae, Carduoideae, Pertyoideae, Gymnarrhenoideae, Cichorioideae, Corymbioideae and Asteroideae [18-21]. Cardueae is one of the largest tribes in Compositae family, with some of 2400 species grouped in 73 genera comprising four subtribes: Echinopsinae, Carlininae, Carduinae, and Centaureinae [22].

It has been reported that the sesquiterpene lactones is the most important groups of compounds in the Asteraceae family [23], other research reported also the presence of phytochemical components in the Asteraceae family, including essential oils, lignans, saponins, flavonoids, polyphenolic compounds, phenolic acids, sterols and polysaccharides [24].

In many cases, the therapeutic effects of the Asteraceae plants have been correlated with the presence of secondary metabolites. One of the best-known cases is certainly that of

artemisinin, a sesquiterpene lactone with antimalarial properties, isolated from *Artemisia annua* [25]. The therapeutic properties attributed to Asteraceae are very numerous, including antitumor [26], cytotoxic [27], immunosuppressive [28], antioxidant [29, 30], anti-acetylcholinesterase [31], antimicrobial [32], antiviral [33], antifungal [34], antiulcer [35], anti-inflammatory [36] and antidiabetic [37].

I.2. Atractylis genus

The *Atractylis* is a sister group of *Atractylodes* and *Carlina*, which belongs to the subtribe Carlininae [38, 39]. This mainly based on characteristics of the flower head, whereas the sexuality of flowers is the main feature that distinguished *Atractylodes* from *Atractylis*. *Atractylodes* are dioecious and *Atractylis* are monoecious [38].

Carlininae Subtribe

The subtribe Carlininae is perennial herbs or shrubs, less often annual plants. Leaves usually spiny, deeply pinnatisect, rarely unarmed and entire. Capitula frequently subtended by pectinate leaf-like bracts, homogamous or heterogamous, sometimes with radiate florets. The only genera presently included in Carlininae are *Atractylis*, *Atractylodes*, *Carlina*, *Thevenotia* and *Tugarinovia* [22].

Cardueae Tribe

The tribe Cardueae is perennial, biennial, or monocarpic herbs or shrubs, less often annual herbs, very rarely small trees, often spiny. Leaves alternate, frequently forming a rosette, rarely in terminal whorls. Resin-ducts always present in roots, less frequent in aerial parts; laticiferous cells often present but only in aerial parts [22].

Botanical description of Atractylis genus

The plants of *Atractylis* genus are characterized as very thorny plants [6], this genus comprises about 30 species including 16 species in North Africa, the *Atractylis* is more centered in North Africa [22].

The characters of the *Atractylis* plants:

➢ Flowers: Ray flowers neutral and in a row, sometimes transformed into radiating ligules [40].
➢ Leaves: the upper leaves (called involucral leaves) [6].

➢ The roots hail, the stem branched from the base, with very spreading branches and few leaves [6].

➢ Achenes: cylindrical oblong achenes, with pappus of 1-2 serial hairs, free or fused in a ring at the base and feathery above [40].

➢ Bracts: the external bracts are themselves spiny (often lined with a regular row of bifurcated spines) [6] (**Figure. I. 3**).
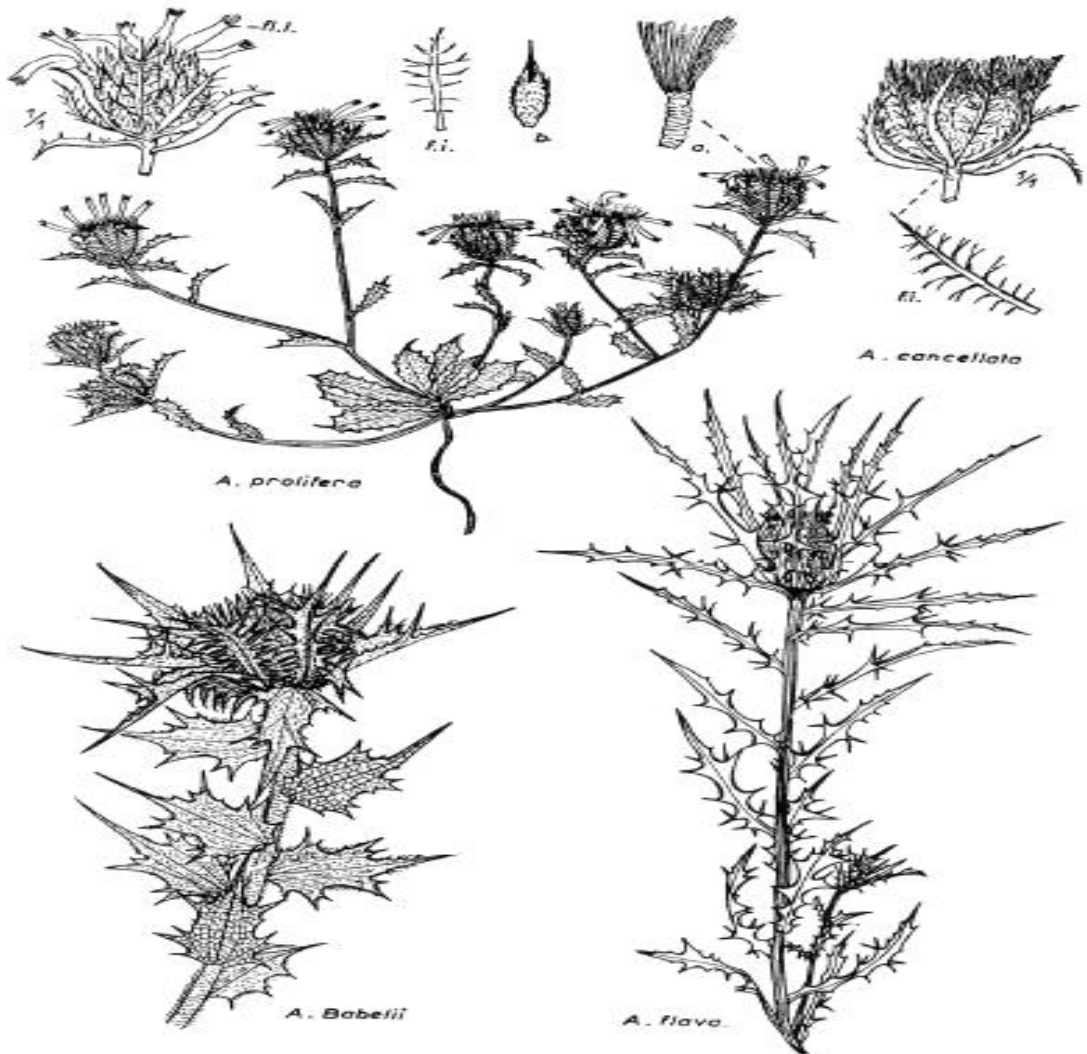
Figure. I. 3: Some plants of *Atractylis* genus [6].

I.3. Traditional uses of Atractylis genus

El Rhaffari and Zaid (2002) reported the folk uses of four species of *Atractylis* genus: *A. serratuloides*, *A. delicatula, A. flava* and *A. babeli,* these plants that are recommended in the decoction form for treatments of diuretic, cholelithiasis, circulatory disorders, as well as hepatitis [41].

It has been reported also that *Atractylis lancea* is used in traditional medicine to treat gastric and intestinal problems, also used for the improvement of gastrointestinal views and disorders [42, 43].

Atractylis gummifera used against intestinal pests, ulcers and snake bites. In addition, it is recommended in the form of decoction or cataplasm for its diuretic, dermatological, antipyretic and purgative effects, as well as for the treatment of syphilis [44].

The decoction of the stems and leaves parts of the plant *Atractylis cancellata* is also used in folk medicine for treatment of dermatological diseases [45].

I.4. Biological activities of *Atractylis* genus

Few biological investigations are focused on the genus *Atractylis*. However, studies are being carried out on the following species:

Atractylis carduus (Atractylis flava): A biological study carried out on the plant *Atractylis carduus* growing in Egypt, revealed that the methanolic and hexane extracts of the aerial parts of this species present a remarkable antibacterial activity [46].

Other study indicated that the Ethyl acetate and n-butanol extracts prepared from whole plant *Atractylis flava* exhibit strong antioxidant activities [10].

The n-BuOH extract of *Atractylis flava* showed a significant cytotoxic effect against cancer cell line THP-1 [13], this extract also showed an *in vitro* antidiabetic activities by the inhibition of the enzymes α-amylase and α-glucosidase [47] and *in vivo* anti-inflammatory, anti-pyretic and acute toxicity effects [9].

A study carried out on the ethyl acetate extract of the aerial parts of the plant *Atractylis serratuloides* growing in Tunisia have shown that this extract is active against the bacterial of *pseudomonas aeruginosa, Escherichia coli* and *salmonella enterica* [48].

Atractylis lancea: A study conducted on this plant showed that the ethanol extract has the power to cause cell death and inhibited cell proliferation, which could be beneficial in cancer. The major components of *Atractylis lancea* induce apoptosis and reduce the proliferation of lung cancer cells [43].

Atractylis babeli: the extracts of this plant obtained by two extraction methods have shown good antioxidant activity [49].

Atractylis cancellata: A study conducted by Badaoui *et al*. (2021) revealed that n-BuOH extract of the whole plant *Atractylis cancellata* showed good acetylcholinesterase and butyrylcholinesterase inhibitory activities (anticholinesterase activities) [50].

I.5. *Atractylis aristata*

Our study is focused on one of the *Atractylis* species *Atractylis aristata*, which is growing in Algerian central Sahara (**Figure. I. 4**).

I.5.1. Description of studied species *Atractylis aristata*

Atractylis aristata is a perennial plant, forming large hemispherical tufts. It is characterized by capitula 8-14 mm in diameter not including the leaves surrounding it; limp **leaves** 3-5 mm wide; yellow **thorns**. Yellow or purplish **flowers** [6].

Leaves lanceolate, spiny-toothed with weak spines, covered on both sides with gray pubescence. **Capitula** solitary and cylindrical. Bracts of involucre proper hairy-spider, narrow. acute and aristae. Very large achenes, pappus shorter than the florets [40].

Figure. I. 4: Picture of the plant *Atractylis aristata*.

I.5.2. Traditional uses of *Atractylis aristata*

Atractylis aristata batt. its tamahaq name is "Ameskeki", endemic plant of central Sahara occupying an important place in traditional medicine in Tamanghasset in Ahaggar region, which is used on internal treatment by infusion of aerial parts for stomach diseases: colic, spasms and fever [8].

I.5.3. Systematic

The systematic classification of plant is presented below:

Kingdom: Plantae

Branch: Spermaphytes

Class: Dicotyledon

Order: Aster

Family: Asteraceae

Subfamily: Carduoideae

Tribe: Cardueae

Subtribe: Carlininae

Genus: Atractylis L.

Species: *Atractylis aristata* batt.

I.6. Phytochemical studies conducted on the genus *Atractylis*

The results of the phytochemical investigations obtained from the studied species of the genus *Atractylis* (*Atractylis gummifera*, *Atractylis flava*, *Atractylis cancellata* and *Atractylis humilis*) confirm well their richness in triterpenoids and flavonoids, which are the major compounds of the plants of the family Asteraceae. Also, *Atractylis* genus contains of different types of phytochemical compounds as: diterpene, alkaloids, acetylenes, phenolic acids and lignans.

I.6.1. Triterpenes

The major compounds isolated from *Atractylis* genus, were triterpenoids of tetracyclic and pentacyclic type derivatives of oleanolic acid, lupeol sterol, α amyrin and β amyrin (**Figure. I. 5**, **Figure. I. 6**, **Figure. I. 7**, **Figure. I. 8** and **Figure. I. 9**). The study of CH_2Cl_2 and n-BuOH extracts *A. flava*, *A. serratuloides*, *A. cancellata* and *A. humilis* allowed to isolate and identify different derivatives of triterpenoids.

Lupeol derivative:

	R$_1$	R$_2$	compound	Species and reference
1	O	CH$_3$	Lupenon	*A. serratuloides* [51]
2	OAc	CH$_3$	Lupeol acetate	*A. serratuloides* [51], *A. flava* [52]
3	OH	CH$_3$	Lupeol	*A. serratuloides* [51], *A. flava* [52] *A. cancellata* [50], *A. humilis* [53]
4	OH	CH$_2$OH	Betulin	*A. flava [54]*
5	OH	COOH	Betulinic acid	*A. flava [52]*
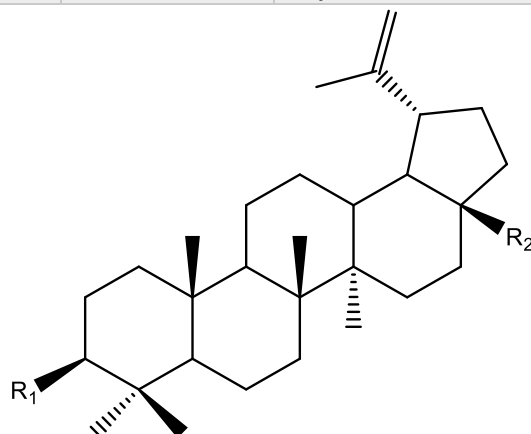
Figure. I. 5: Structures of lupeol derivatives isolated from *Atractylis* genus.

Oleanane derivative

	R$_1$	R$_2$	R$_3$	R$_4$	compound	Species and reference
6	OH	H	H	H	Oleanolic acid	*A. serratuloides* [51] *A. flava* [55] *A. cancellata* [50] *A. humilis* [53]
7	OH	OH	H	H	Hederagenin	*A. flava* [55]
8	OH	OH	OH	H	Caulophyllogenin	*A. serratuloides* [51] *A. flava* [52]
9	OAc	H	H	H	Oleanolic acid acetate	*A. serratuloides* [51]
10	OH	H	H	OH	22β-hydroxy Oleanolic acid	*A. flava* [55]
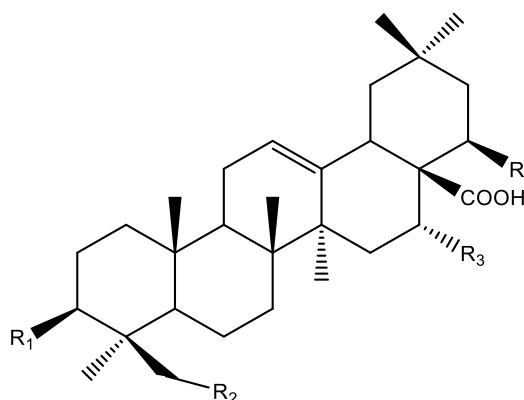
Figure. I. 6: Structures of oleanolic derivatives isolated from *Atractylis* genus.

α amyrin and β amyrin derivative:

Three derivatives of β-amyrin and two derivatives of α-amyrin were isolated and identified from the CH$_2$Cl$_2$ extract of *A. flava*: β-amyrin **11**, oleana-9(11), 12-dien-3-yl acetate **12**, ursa-9(11), 12-dien-3-ylacetate **13**, 11-oxo-β-amyrin acetate **14**, and 11-oxo-α-amyrin acetate **15** [52].
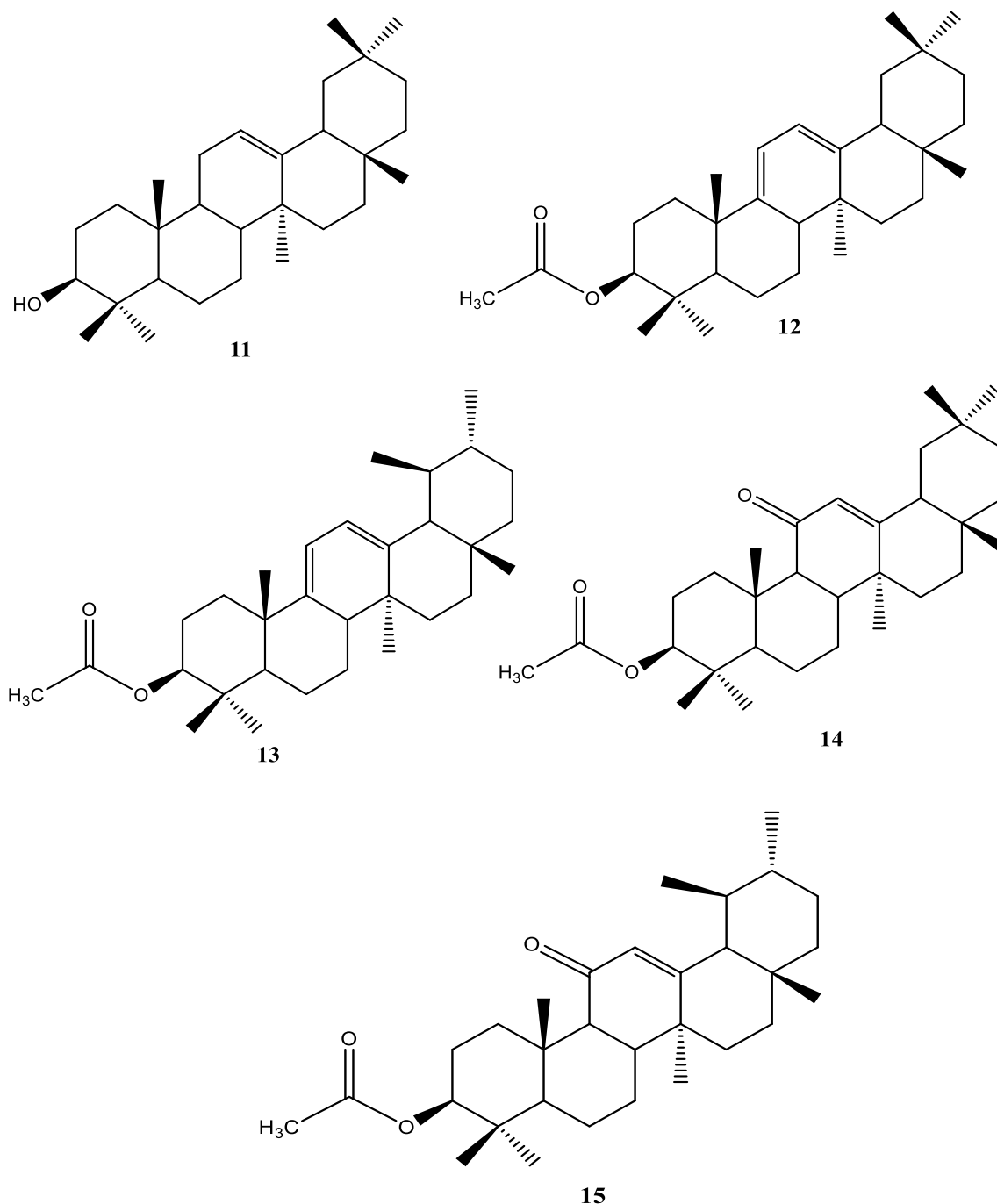
Figure. I. 7: Structures of α amyrin and β amyrin isolated from *Atractylis flava.*

Sterol derivatives:

	R	compound	Species and reference
16	H	β-sitosterol	*A. serratuloides* [51], *A. cancellata* [50], *A. humilis* [53]
17	Glucose	Daucosterol	*A. serratuloides* [9], *A. flava* [13], *A. cancellata* [11]
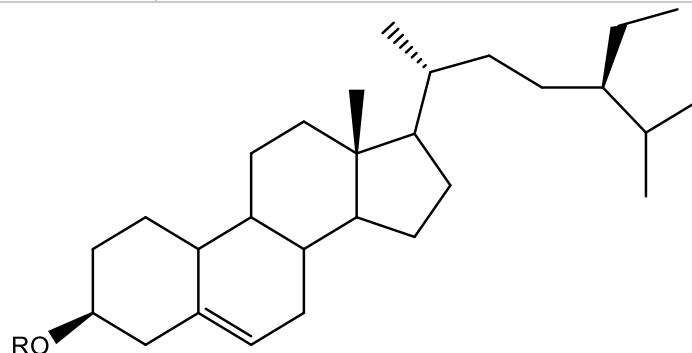
Figure. I. 8: Structures of sterol derivatives isolated from *Atractylis* genus.

	R	compound	Species and reference
18	OH	Stigmasterol	*A. flava* [52] [54]
19	Glucose	Stigmasterol -3-*O*-glucoside	*A. flava* [52] [54]
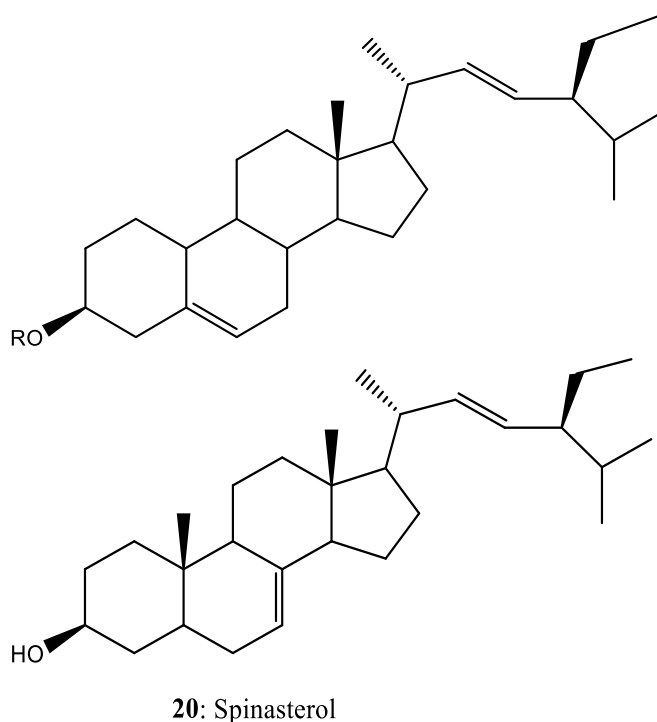
20: Spinasterol

Figure. I. 9: Structure of stigmasterol and spinasterol derivative isolated from *Atractylis* genus.

I.6.2. Flavonoids

The chemical studies of *Atractylis* genus allowed to isolate and identify different flavonoids skeletons with different osidic parts from EtOAc and n-BuOH extracts of the plants *A. flava*, *A. cancellata*, *A. humilis* and *A. gummifera*.

Due to the presence of different type of flavonoids with different osidic parts, the isolated flavonoids can be divided according to the number of sugar derivatives. Starting with the non-glycosylated flavonoids type, we note the isolation and identification of six non-glycosylated flavonoids (Chrysin **21**, Apigenin **22**, Quercetin **23**, Ladanein **24**, Isorhamnetin **25** and Tricine **26**) (**Figure. I. 10**) were isolated from *Artactylis* plants.

N	Flavonoid	Species	Reference
21	Chrysin	*A. flava*	[55]
		A. cancellata	[50]
22	Apigenin	*A. flava*	[55]
		A. cancellata	[50]
23	Quercetin	*A. flava*	[55]
			[54]
		A. cancellata	[50]
24	ladanein	*A. flava*	[52]
25	Isorhamnetin	*A. flava*	[54]
26	Tricin	*A. cancellata*	[50]
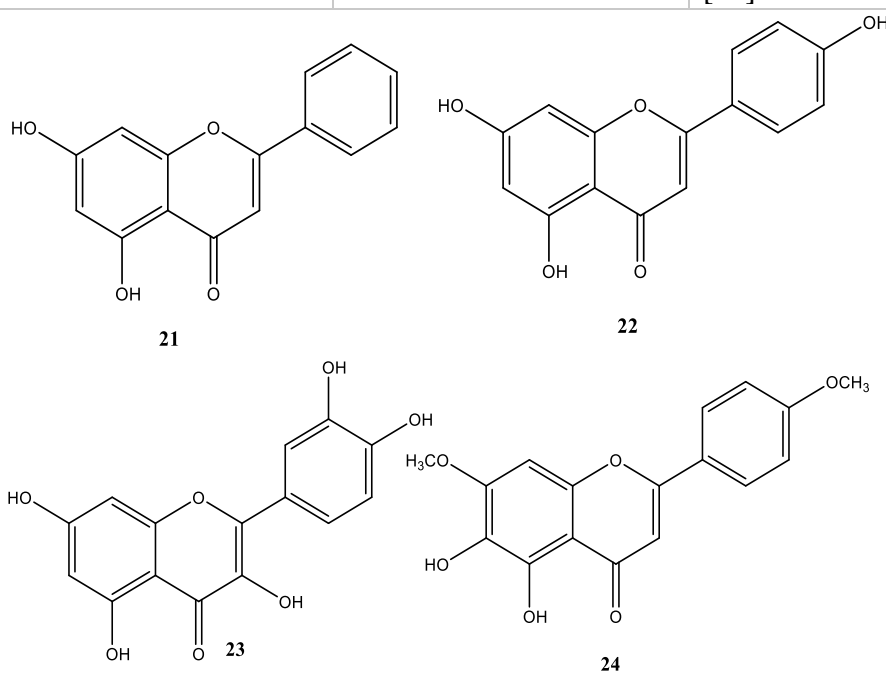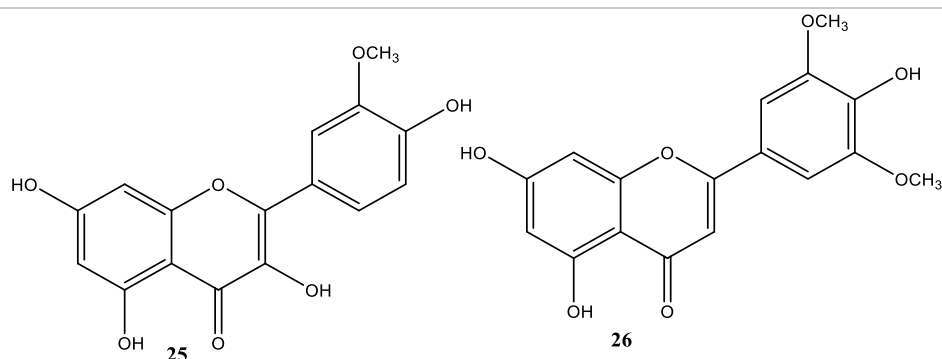
Figure. I. 10: Structure of non-glycosylated flavonoids isolated from *Atractylis* genus.

Eight mono-glycosylated flavonoids (Isorhamnetin-3-O-glucopyranoside **27**, Orientin **28**, Atraflavoside A **29**, Isoorientin **30**, Tiliroside **31**, Quercetin-3-O-*β*-glucopyranoside **32**, 7,3′-Dimethylether isoorientin **33**, Swertisin **34**, were isolated from *Artactylis* plants.

N	Flavonoid	Spiece	Reference
27	Isorhamnetin-3-O-glucopyranoside	*A. flava*	[54]
28	Orientin	*A. gummifera*	[56]
29	Atraflavoside A	*A. flava*	[55]
30	Isoorientin	*A. gummifera* *A. cancellata*	[50]
31	Tiliroside	*A. flava*	[52]
32	Quercetin-3-O-*B*-glucopyranoside	*A. cancellata*	[50]
33	7,3′-dimethylether isoorientin	*A. humilis*	[53]
34	Swertisin	*A. humilis*	[53]
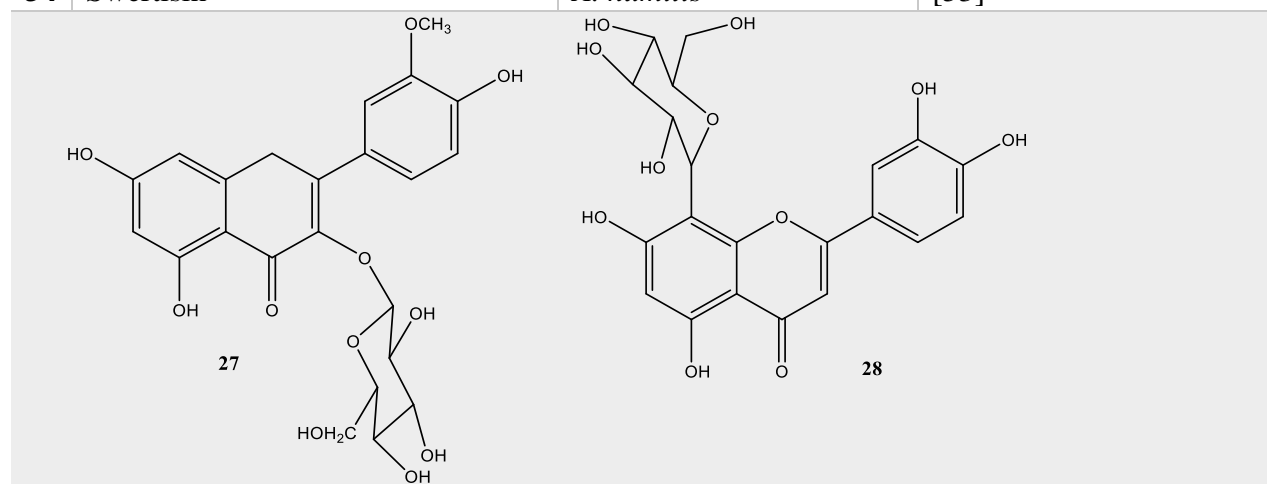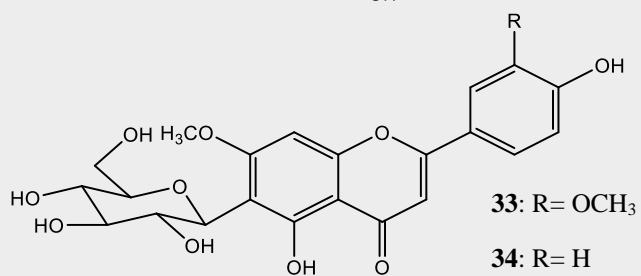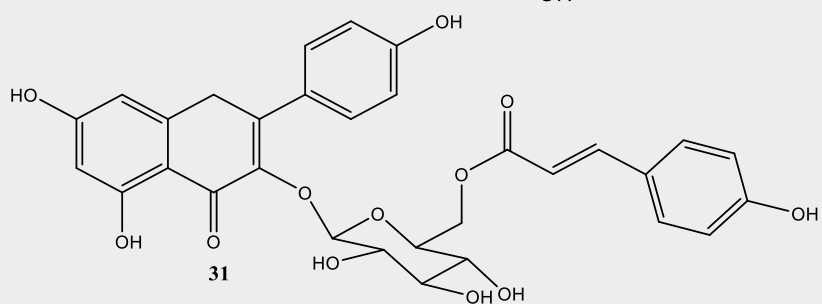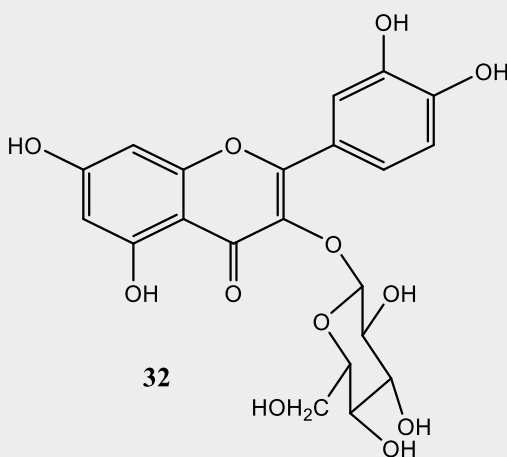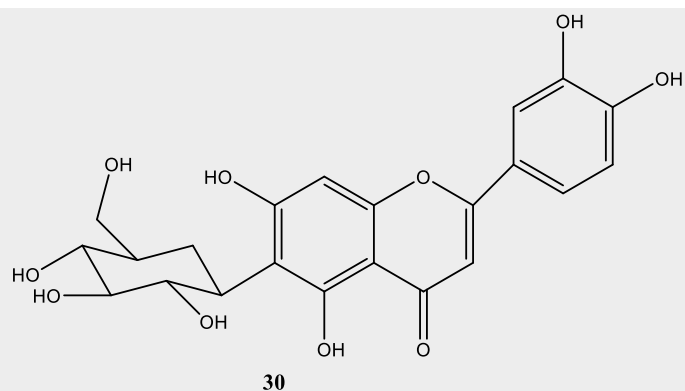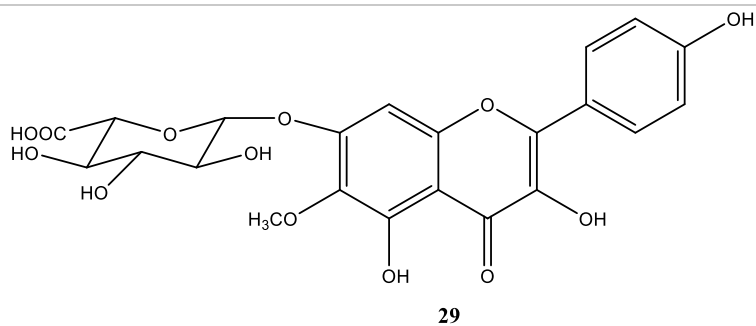
Figure. I. 11: Structure of mono-glycosylated flavonoids isolated from *Atractylis* genus.

Moreover, nine diglycosylated flavonoids were isolated from *Atractylis* genus (Narcissin **35**, Isorhamnetin-3-O-robinobioside **36**, Schaftoside **37**, Isoschaftoside **38**, Neocorymboside **39**, Vicenin 3 **40**, Vicenin 2 **41**, Atraflavoside B **42**, Diosmin **43**) **Figure. I. 12**.

N	Flavonoid	Spiece	Reference
35	Narcissin	*A. flava*	[55] [54]
36	Isorhamnetin-3-O-robinobioside	*A. flava*	[51]
37	Schaftoside	*A. flava*	[55] [54]
38	Isoschaftoside	*A. gummifera*	[56]
39	Neocorymboside	*A. gummifera*	[56]
40	Vicenin 3	*A. flava*	[55]
41	Vicenin 2	*A. flava*	[54]
42	Atraflavoside B	*A. flava*	[55]
43	Diosmin	*A. cancellata*	[50]
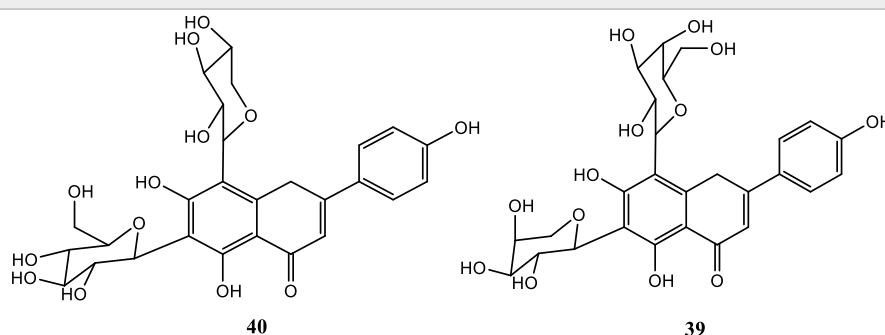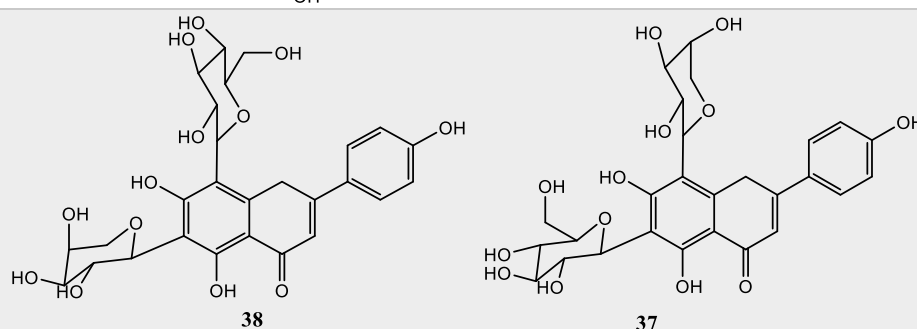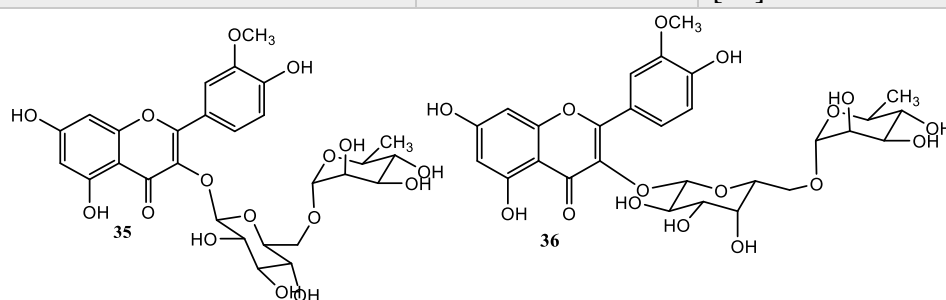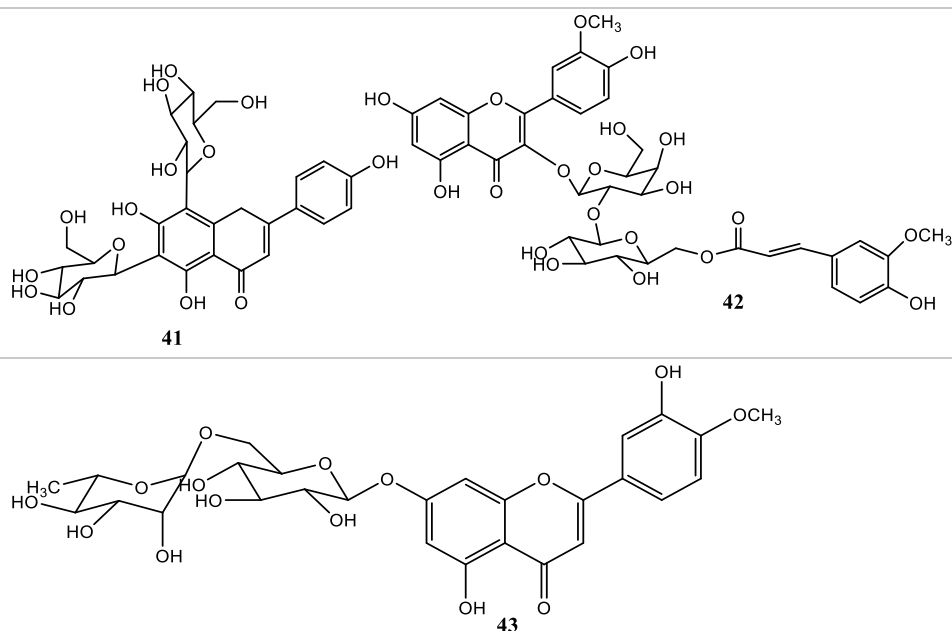
Figure. I. 12: Structures of di-glycosylated flavonoids isolated from *Atractylis* genus.

I.6.3. Diterpenes

The phytochemical investigations were made on the methanolic extract of the plant *Atractylis gummifera* allowed the isolation and identification of two glycosylated diterpenes, Atractyloside and Carboxyatractyloside, which are characterized by their toxicity. Several biological studies have been carried out on these diterpenes showing the high toxicity of these compounds [42, 57, 59] (**Figure. I. 13**).

N	Diterpene	Species	Reference
44	Atractyloside	*Atractylis gummifera*	[57, 58]
45	4-Carboxyatractyloside	*Atractylis gummifera*	[58, 59]

44: R= H
45: R= COOH
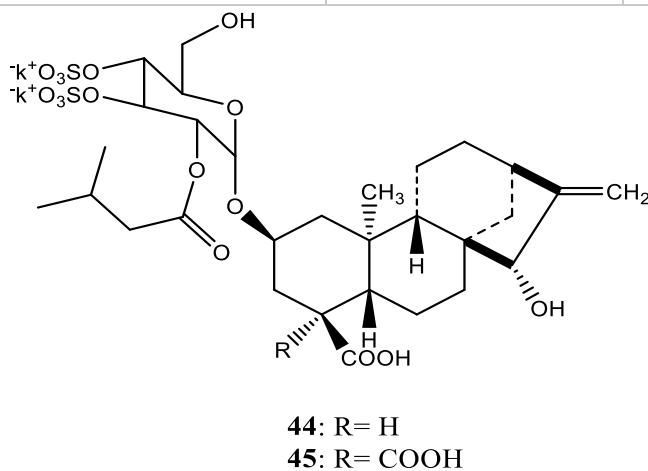
Figure. I. 13: Structures of di-glycosylated flavonoids isolated from *Atractylis* genus.

Moreover, other study made on the petroleum ether extract of the plant *A. koreana*, allowed the isolation and identification of four oxidated diterpenes, the result of this study is the identification of three new oxidated diterpenes namely Atractylone **46**, Atractylenolide I **47** and Atractylenolide III **48** [60] (**Figure. I. 14**).

N	Diterpene
46	Atractylone
47	Atractylenolide I
48	Atractylenolide III
49	5α-H-10β-Selina-4(14),7(11)-dien-8-one
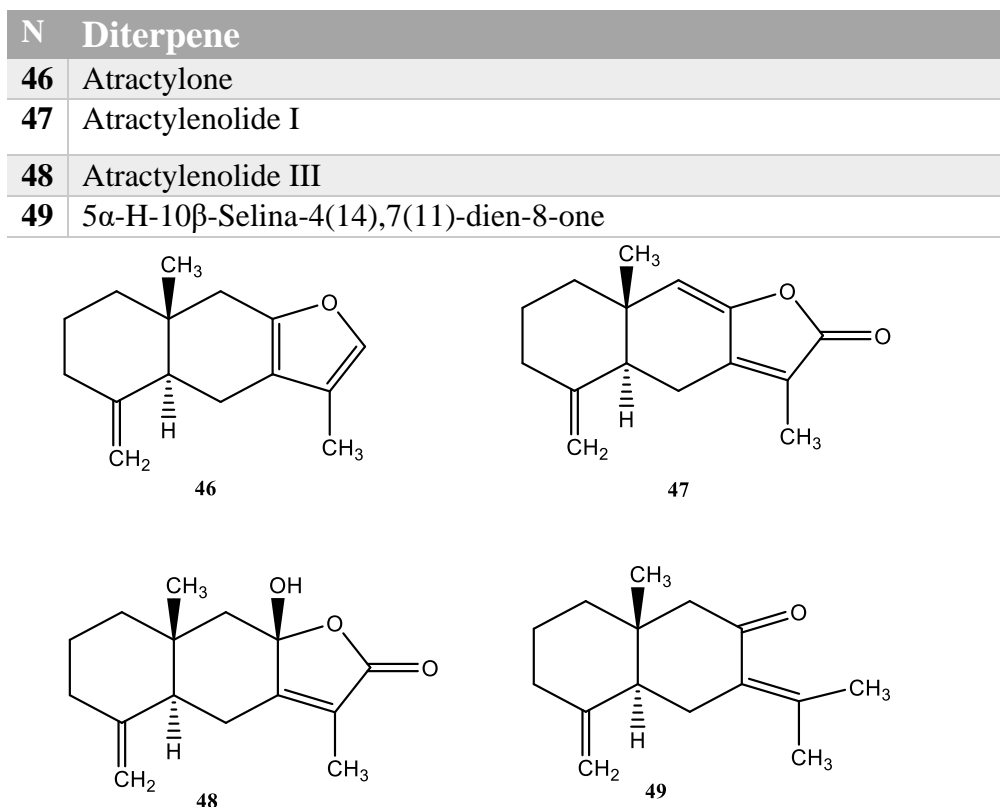
Figure. I. 14: Structures of oxygenated diterpenes isolated from *Atractylis koreana*.

I.6.4. Saponins

A study conducted by Chabani *et al*. (2016), which reports for the first time the occurrence of saponins in the *Atractylis* genus. This study allowed the isolation and identification of three new oleanane-type triterpene saponins from the n-BuOH extract of *Atractylis flava* plant [52].

N	Saponin	Species	Reference
50	3-O-[β-1-glucuronopyranosyl]- 28-O- [β-D-xylopyranosyl-(1→ 4)-α-L-rhamnopyranosyl-(1→2)-β-D-xylopyranosyl] -16α-hydroxy gypsogenic acid	*Atractylis flava*	[52]
51	3-O-[β-1-glucuronopyranosyl] - 28-O-[β-D-xylopyranosyl-(1→4)-α-L-rhamnopyranosyl-(1→2) -α-L-arabinopyranosyl] -16α-hydroxy gypsogenic Acid	*Atractylis flava*	[52]

| 52 | 3-O-[β-D-galactopyranosyl-(1→2) -β-D-glucuronopyranosyl] -28-O-[((3-O-acetyl) -β-D-xylopyranosyl)- (1→4)-((3-O-acetyl)- α-L-rhamnopyranosyl-(1→2)- β-D-xylopyranosyl] -quillaic acid | *Atractylis flava* | [52] |

50: R1= H, R2= OH.

51: R1= OH, R2=H.

52
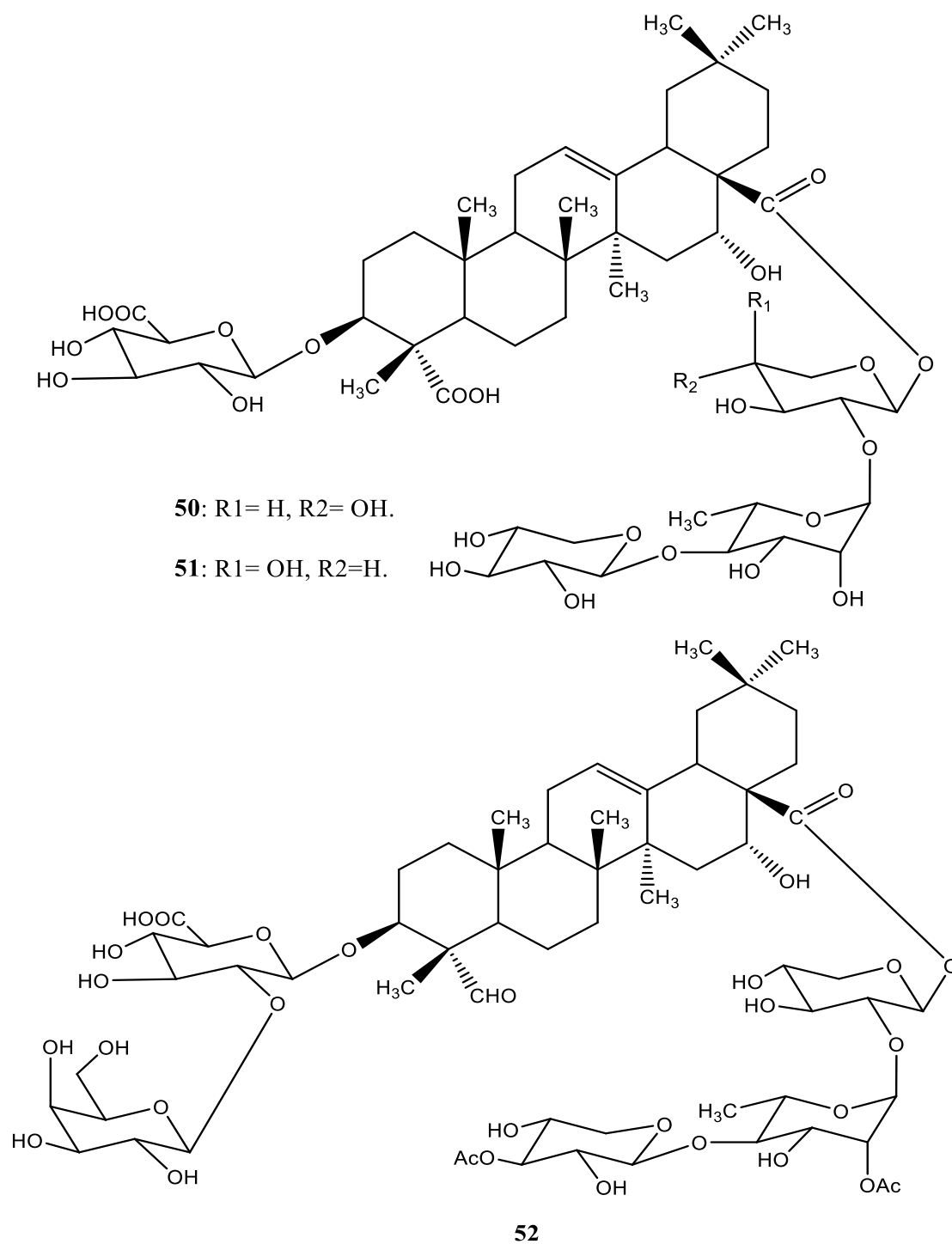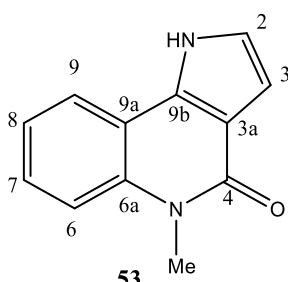
Figure. I. 15: Structures of saponins isolated from *Atractylis flava*.

I.6.5. Alkaloids
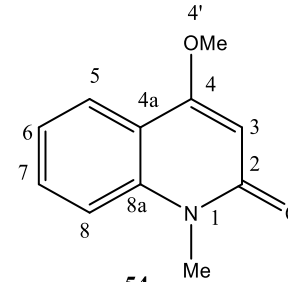
New study conducted by Badaoui *et al*. (2019) reports for the first time the occurrence of alkaloids in the *Atractylis* genus. This study allowed the isolation and identification of two alkaloid compounds from the n-BuOH extract of *A. cancellata* plant. This study allowed the separation of new alkaloid compound **Pyrroloquinolone A** [50] (**Figure. I. 16**).

N	Alkaloid	Species
53	Pyrroloquinolone A	*A. cancellata*
54	4-methoxy-1-methyl-2-quinolone	
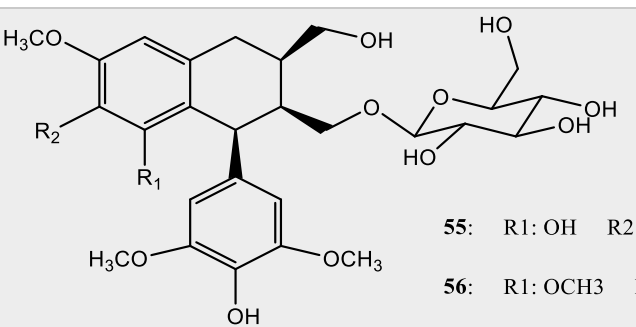
Figure. I. 16: Structures of Alkaloids isolated from *Atractylis cancellata*.

I.6.6. Lignans

New study conducted by Sifouane *et al*. (2020) reports for the first time the occurrence of lignans in the *Atractylis* genus. This study allowed to isolate and identify two cyclo-lignans compounds from the EtOAc and n-BuOH extracts of *A. humilis* plant. This study allowed the separation of new aryltetralin lignan compound namely **(8R,7′S,8′S)-9′-β-D-glucopyranosyl-3,4′,9-trihydroxy-3′,4,5,5′-tetramethoxy-2,7′-cyclolignan** [53].

N	Lignan
55	(8R,7′S,8′S)-9′-β-D-glucopyranosyl-3,4′,9-trihydroxy-3′,4,5,5′-tetramethoxy-2,7′-cyclolignan
56	(7′S,8R,8′S)-7a-[(β-D-glucopyranosyl)-oxy] lyoniresinol

55: R1: OH   R2: OCH3

56: R1: OCH3   R2: OH

Figure. I. 17: Structure of lignans isolated from *Atractylis humilis*.

I.6.7. Phenolic compounds

The study performed on the EtOAc and n-BuOH extracts of *Atractylis humilis* , has allowed the isolation and identification of five phenolic compounds, 2,5-dihydroxyethyl cinnamate, 3,4,5-trimethoxyphenol 1-O-β-D-glucopyranoside, tachioside, vanillic acid, 2,6-dimethoxy 1,4-benzoquinone [53] (**Figure. I. 18**).

N	Phenolic compound
57	2,5-dihydroxyethyl cinnamate
58	3,4,5-trimethoxyphenol1-O-β-D-glucopyranoside
59	tachioside
60	vanillic acid
61	2,6-dimethoxy 1,4-benzoquinone
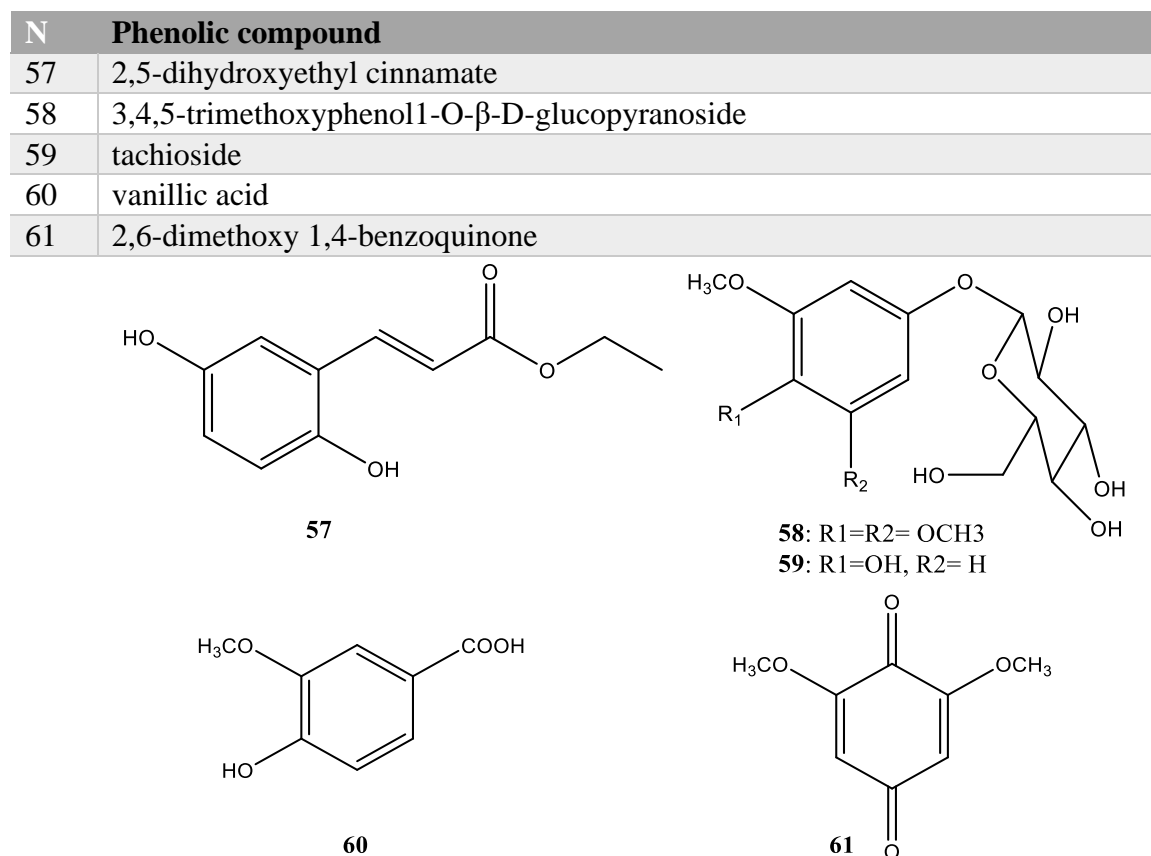
Figure. I. 18: Structures of phenolic compounds isolated from *Atractylis humilis*.

Moreover, others phenolic compounds were isolated from *Atractylis* genus antiarol rutinoside **62** from *Atractylis serratuloides* and 4-O-caffeoyl-2-C-methyl-D-threonic acid **63**, chlorogenic acid methyl ester **64** and 5-O-caffeoylshikimic acid **65** from *Atractylis cancellata*.

N	Phenolic acid	Species	Reference
62	antiarol rutinoside	*A. serratuloides*	[51]
63	4-O-caffeoyl-2-C-methyl-D-threonic acid	*A. cancellata*	[50]
64	chlorogenic acid methyl ester	*A. cancellata*	[50]
65	5-O-caffeoylshikimic acid	*A. cancellata*	[50]
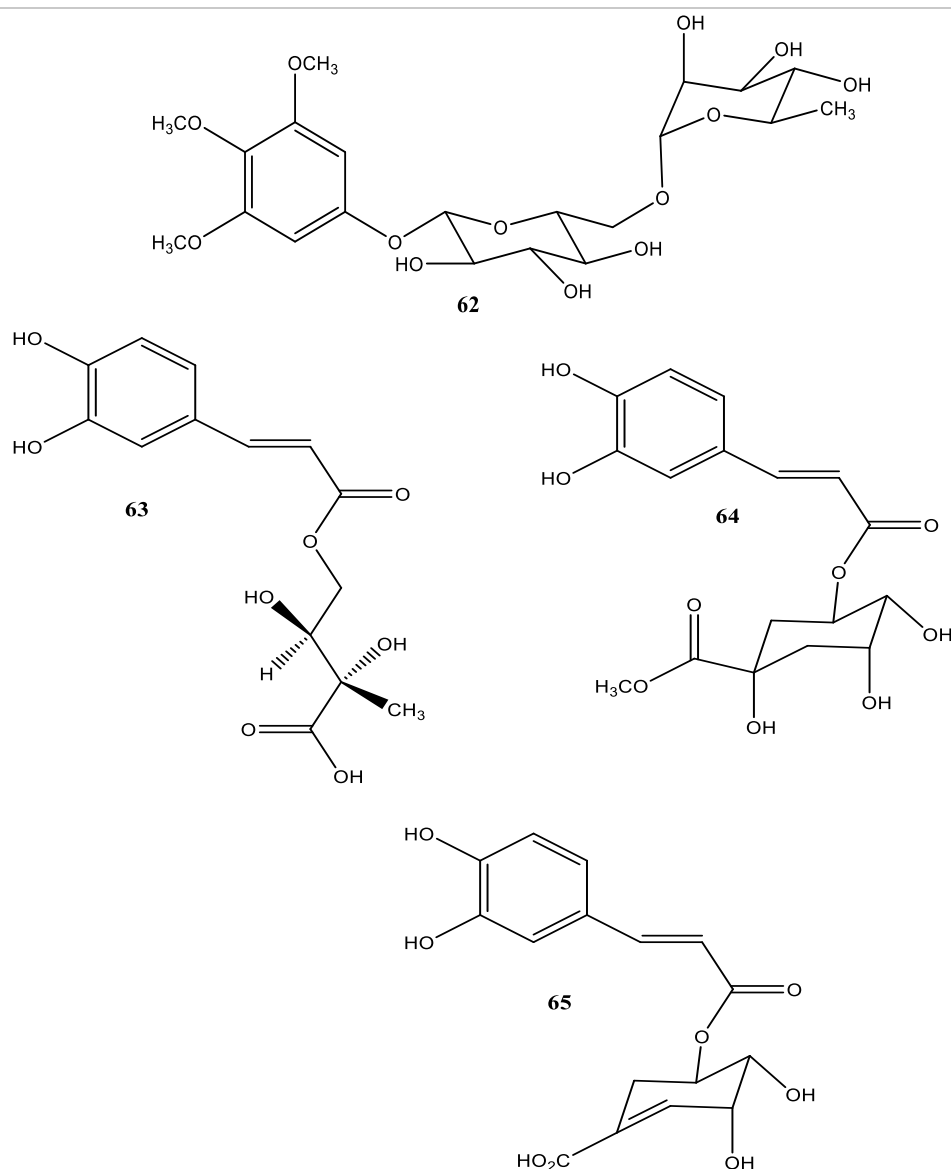
Figure. I. 19: Structures of other phenolic compounds isolated from *Atractylis* genus.

I.6.8. Polyacetylene compounds

A study performed on the petroleum ether extract of *A. koreana* has allowed the isolation and identification of six polyacetylene compounds. (6*E*,12*E*)-tetradeca-6,12-dien-8,10-diyne- 1,3-diyl diacetate **58**, (6*E*, 12*E*)-3-hydroxytetradeca-6,12-dien-8,10-diyn-1-yl acetate **59**, (6*E*, 12*E*)-1-hydroxytetradeca-6,12-dien-8,10-diyn-3-yl acetate **60**, (3*E*,5*E*,11*E*)-trideca-3,5,11-trien-7,9-diyn-1-ol **61**, (3*E*,5*Z*,11*E*)-trideca-3,5,11-trien-7,9-diyn-1-ol **62**, (4*E*, 6*E*, 12*E*)-tetradeca-4,6,12-trién-8,10-diyne-1,3-diyl diacetate **63** [61] (**Figure. I. 20**).

N	Acetylenes
66	(6*E*,12*E*)-tetradeca-6,12-dien-8,10-diyne- 1,3-diyl diacetate
67	(6*E*, 12*E*)-3-hydroxytetradeca-6,12-dien-8,10-diyn-1-yl acetate
68	(6*E*, 12*E*)-1-hydroxytetradeca-6,12-dien-8,10-diyn-3-yl acetate
69	(3*E*,5*E*,11*E*)-trideca-3,5,11-trien-7,9-diyn-1-ol
70	(3*E*,5*Z*,11*E*)-trideca-3,5,11-trien-7,9-diyn-1-ol
71	(4*E*, 6*E*, 12*E*)-tetradeca-4,6,12-trién-8,10-diyne-1,3-diyl diacetate
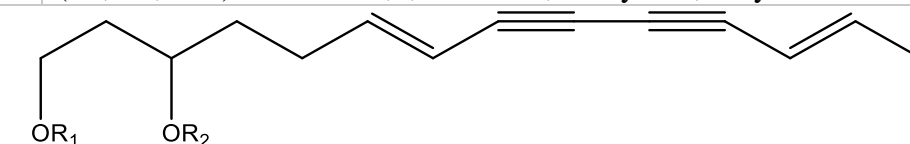
66: R1=R1= Ac

67: R1=Ac, R2=H

68: R1=H, R2=Ac
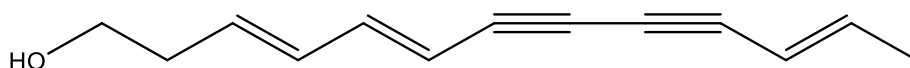
69: 4E, 6E, 12E

70: 4E, 6Z, 12E
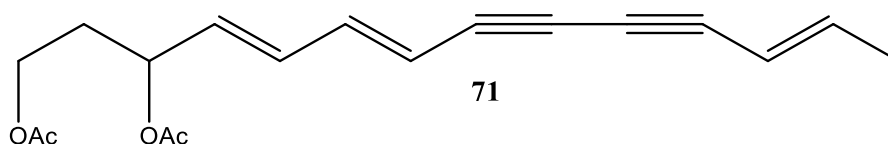
71

Figure. I. 20: Structure of Polyacetylene compounds isolated from *Atractylis koreana*.

I.6.9. Osidic compounds

Two osidic compounds were isolated and identified form the extracts of *Atractylis humilis* 1-O-ethyl-D-xylose **72** and 1-O-ethyl-β-D-glucopyranoside **73** [53] (**Figure. I. 21**).

72

73
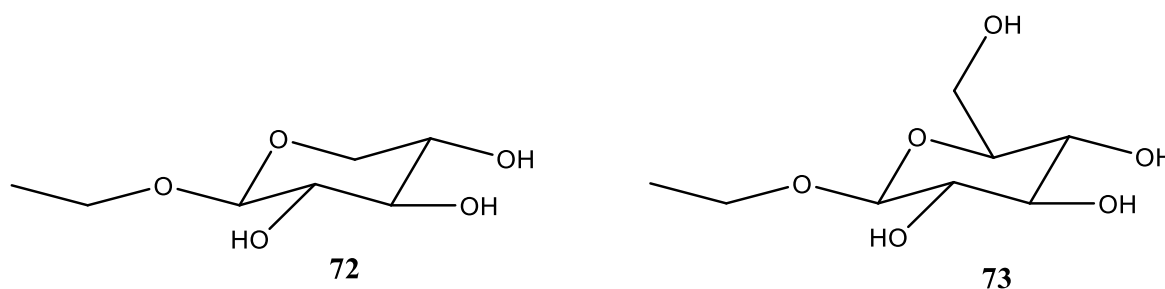
Figure. I. 21: Structure of osidic compounds isolated from *Atractylis humilis*.

Chapter II:

Primary and secondary metabolites.

II. Primary and secondary metabolites

Plants form metabolites with various functions within the plant. These metabolites are produced by chemical reactions called metabolism. In plants, there are two main types of metabolites (**Figure. II. 1**):

❖ Primary metabolites correspond to the organic molecules present in all plant cells. The main primary metabolites are lipids, proteins and carbohydrates.

❖ Secondary metabolites are more complex molecules which differ according to the species and are present in smaller quantities. They have a role in particular of protection against insects, predators and pathogens. The main classes of secondary metabolites are terpenes, phenolic compounds, saponins, cardiac and cyanogenic glycosides and alkaloids.
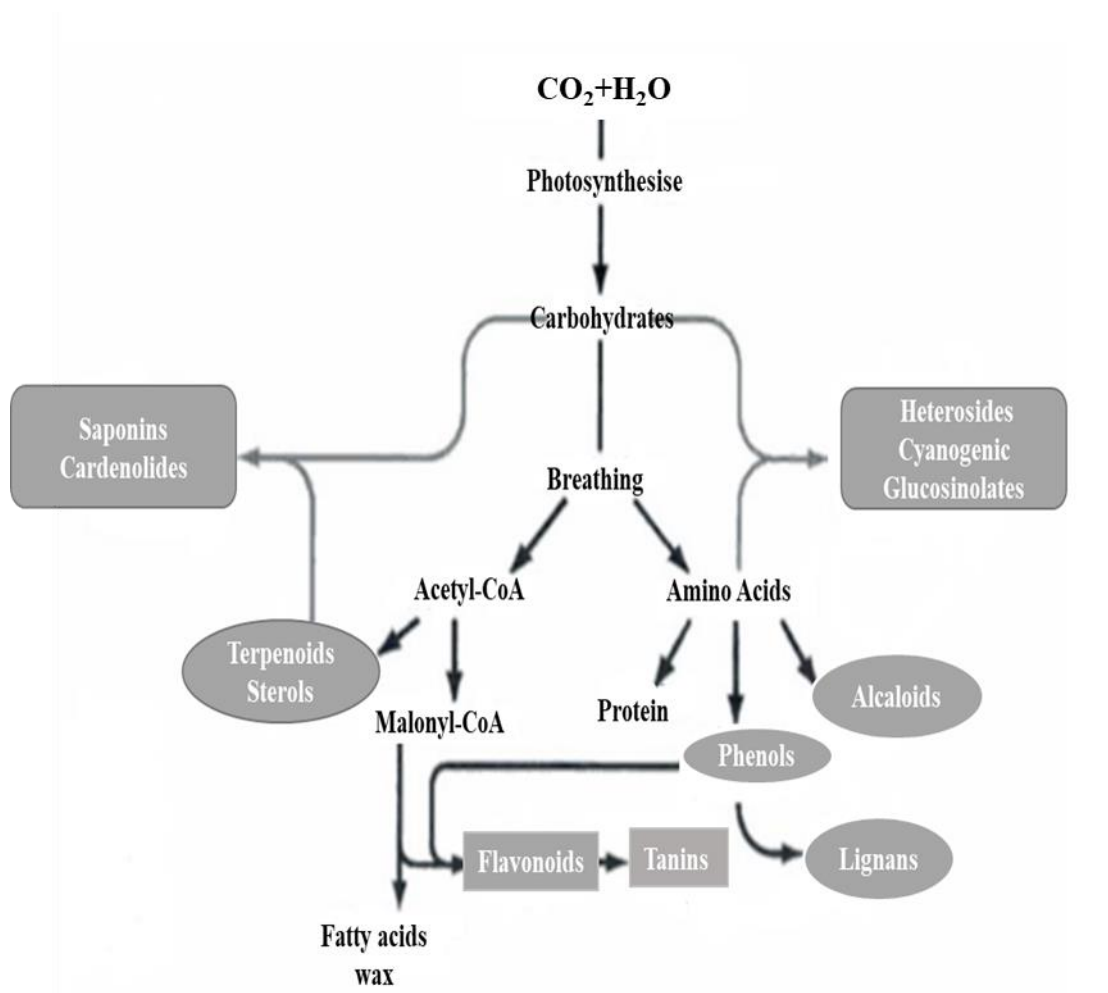
Figure. II. 1: Schematic representation illustrating the relationships between primary and secondary metabolites [62].

II.1. Primary metabolites (Carbohydrates)

The term "carbohydrate" refers to a hydrate of carbon that is widely distributed in nature, particularly in plants. The majority of these compounds take the form of $C_nH_{2n}O_n$ or $C_n(H_2O)_n$. As a result, carbohydrates are a collection of linear and cyclic polyols, as well as polyhydroxy aldehydes, ketones, acids, or their derivatives. Sometimes, sugars and their compounds are used to refer to carbohydrate. Our muscles and brains mostly use carbohydrates as fuel. Eating a high carbohydrate diet will ensure maintenance of muscle and liver glycogen (storage forms of carbohydrate), improve performance and delay fatigue [63].

II.1.1. Classification

Generally, carbohydrates are classified into four different main classes, monosaccharides, di-, tri- and tetrasaccharides, oligosaccharides and polysaccharides.

II.1.1. I. Monosaccharide

These sugars, which are often referred to as carbohydrates, range in carbon atom count from three to nine. The majority of naturally occurring monosaccharides have five (pentose, $C_5H_{10}O_5$) or six (hexose, $C_6H_{12}O_6$) carbon atoms. The most prevalent monosaccharide is glucose, a sugar with six carbons that is used to provide energy by human bodies. Fructose is another hexose that found in many fruits [63].

Glucose

Fructose

Monosaccharides are classified according to functional groups and carbon numbers. Aldehyde and ketone are the two functional groups that are most frequently found in monosaccharides (in open chain form). A monosaccharide is referred to as an aldose when it contains an aldehyde, such as glucose, and as a ketose or keto sugar when it contains a ketone, such as fructose [63].
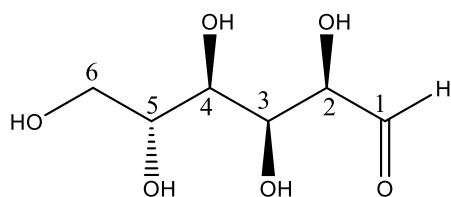
D-Glucose, an aldose
Contains an aldehyde group
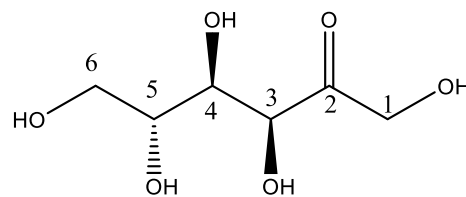
D-Fructose, a ketose
Contains a ketone group

Monosaccharides are classified as triose, tetrose, pentose, or hexose depending on how many carbon atoms they contain—three, four, five, or six, respectively. For instance, since it has six carbon atoms and an aldehyde group, glucose can be classified as an aldohexose. The crucial structural difference between hemiacetals and hemiketals is the presence of -OH and -OR connected to the same carbon. Sugars can take on the pyranose and/or furanose forms through cyclization [63].
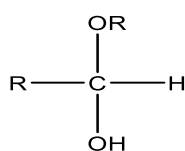
Hemiacetal
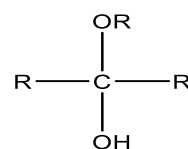
Hemiketal

In addition to being open chain molecules (acyclic), monosaccharides can also be cyclic compounds. The intramolecular nucleophilic addition reaction between a -OH and a CO group causes cyclization, which results in the creation of cyclic hemiacetals or hemiketals. Numerous monosaccharides exist in equilibrium between an open chain and cyclic forms [63] (**Figure. II. 2**).

D-Glucose

ß-D-Glucopyranose
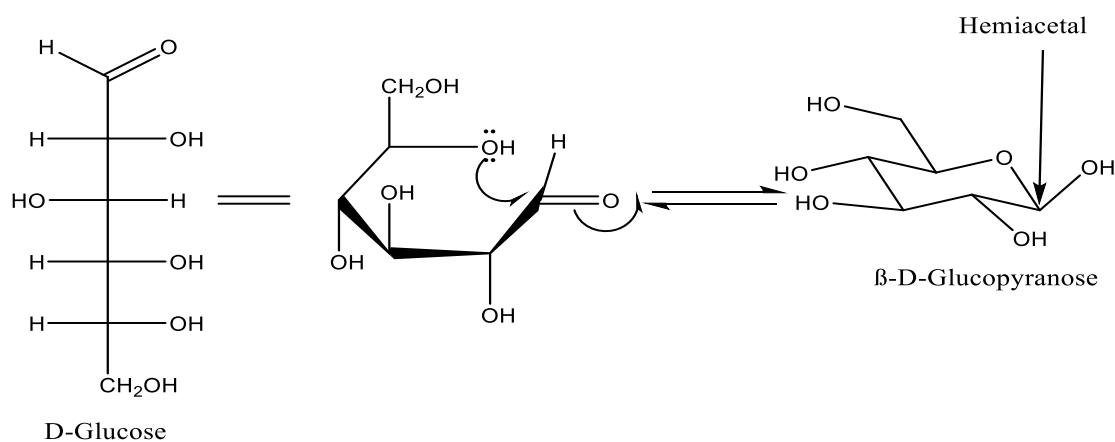
Figure. II. 2: Cyclisation of D-Glucose.
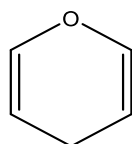
Pyran
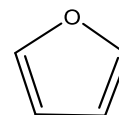
Furan

A new chiral center is created during cyclization at position C-1. The anomeric carbon is this substance. At the anomeric carbon, the –OH group can project upwards (β configuration) or downwards (α configuration) [63] (**Figure. II. 3** and **Figure. II. 4**).

a Anomer (a configuration)

D-Glucose

C-1 (anomeric carbon)

ß Anomer (ß configuration)
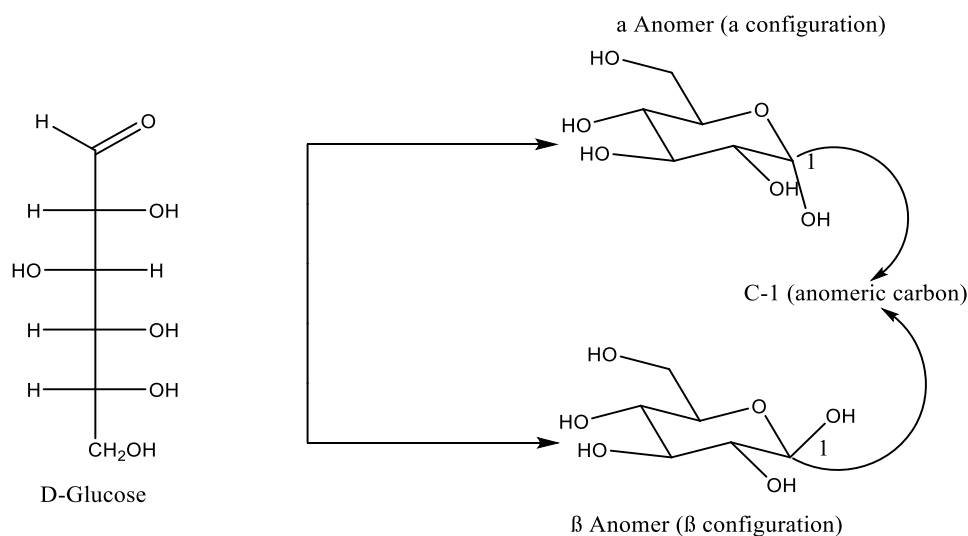
Figure. II. 3: D-Glucose configurations.

D-Fructose

Hemiketal

Pyranose form of fructose

Hemiketal

Furanose form of fructose
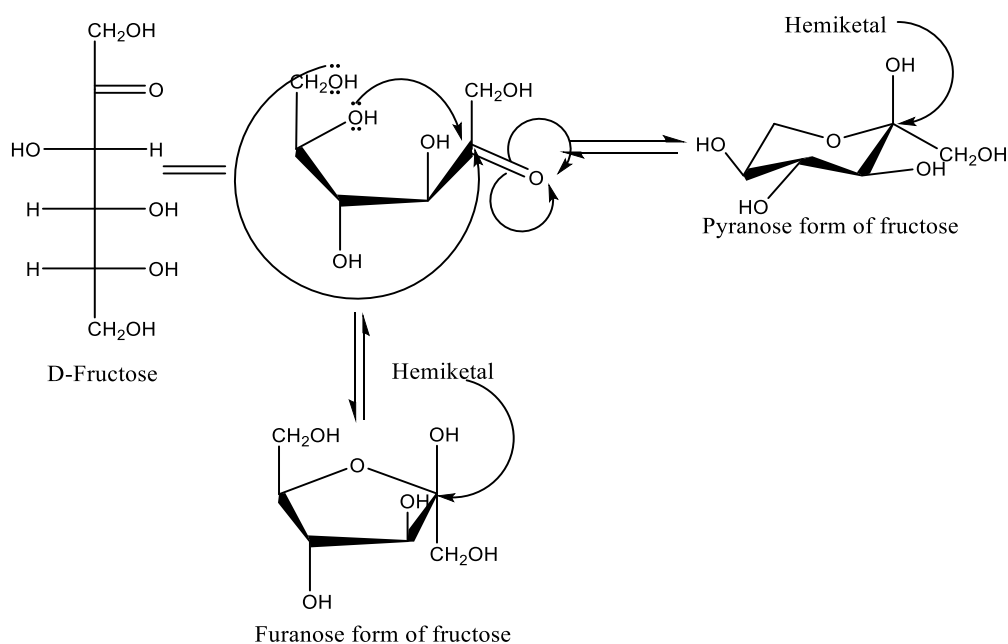
Figure. II. 4: Cyclisation of D- fructose.

II.1.1. II. Di-, tri- and tetrasaccharides

These saccharides are generated from two, three, or four monosaccharide molecules with the removal of one, two, or three water molecules to form dimers, trimers, and tetramers of carbohydrates. For instance, sucrose, a disaccharide made up of the monosaccharide fructose and glucose (**Figure. II. 5**) [63].
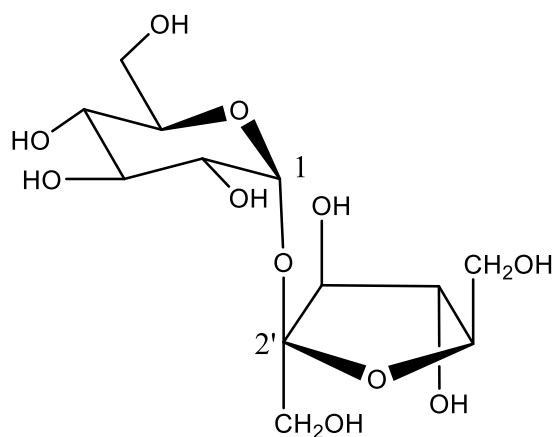
Sucrose

Figure. II. 5: Structure of the disaccharide; Sucrose [64].

II.1.1. III. Oligosaccharides

The name 'oligosaccharide' refers to saccharides containing two to ten, monosaccharides. For example, raffinose, found in beans and pulses, is an oligosaccharide composed of three monosaccharide units, i.e., galactose, glucose and fructose (**Figure. II. 6**).
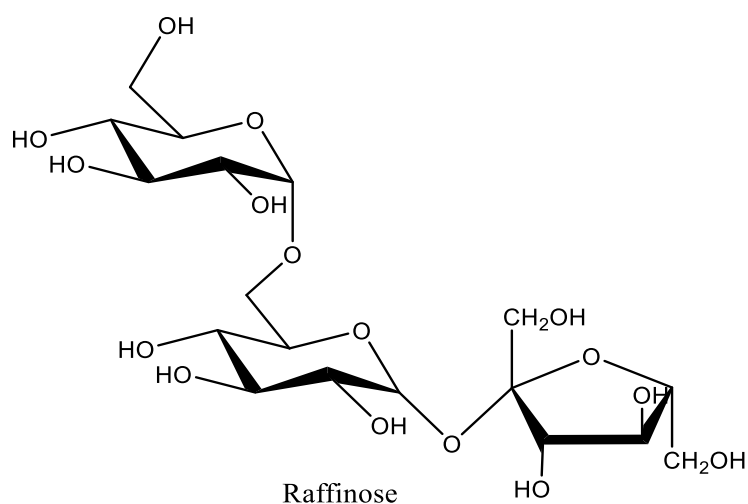
Raffinose

Figure. II. 6: Structure of the trisaccharide; Raffinose.

II.1.1. IV. Polysaccharides

Polysaccharides are composed of a numerous of monosaccharide units, and the number forming the molecule is often approximately known. For example, the polysaccharides cellulose and starch, which contain hundreds of glucose units [63].

II.1.2. Biological activity of the polysaccharides

II.1.2. I. Antioxidant activity

A very promising source of antioxidants is natural extracts, particularly polysaccharides, which have the capacity to scavenge free radicals. Antioxidant activity of polysaccharides have received a lot of attention lately and are crucial for the development and manufacture of natural medicine. Some polysaccharides, according to studies, can reduce lipid peroxidation and improve the body's capacity to scavenge free radicals [65, 66]. As example, three polysaccharides (GLP-H, GLP-V and GLP-F) isolated from *Ganoderma lucidum* showed the stronger radical scavenging activities and was proved that exhibited antioxidant activities in vitro against superoxide radical, hydroxyl radical, reducing power, DPPH free radical and Ferric-reducing antioxidant power (FRAP) assay [67]. Other study conducted by Houfang et al, 2010 that investigated the antioxidant activities of polysaccharides extracted from Bryopsis plumosa, employing various established in vitro systems, these in vitro results clearly establish the possibility that this polysaccharides could be effectively employed as ingredient in health or functional food, to all deviate oxidative stress [68].

II.1.2. *II*. Anti-inflammatory activity

One of the most significant bioactivities of polysaccharides is their anti-inflammatory properties. It has been reported the strong anti-inflammatory activity of polysaccharides employing in vivo models, using the formalin-induced (chronic) and carrageenan-induced (acute) inflammatory tests [69]. Furthermore, polysaccharides' anti-inflammatory effects are primarily brought about by their ability to block the expression of chemokines and adhesion factors as well as the activity of crucial inflammatory enzymes [70].

II.1.2. III. Antidiabetic activity

It is obvious that polysaccharides derived from natural resources, such as higher plants, mushrooms, and algae, all have significant potential for use in the treatment of diabetes mellitus and serve as a valuable resource for the discovery and future

development of new compounds with therapeutic potential. Polysaccharides have garnered the interest of numerous researchers as the primary active components of various natural anti-diabetic medicines [71]. According to reports, *Astragalus* polysaccharide can improve the lipid and glucose metabolisms of T2DM rats by boosting insulin production and having a protective effect on islet beta cells in the pancreas [72]. *Rehmannia glutinosa* polysaccharide can successfully reduce hyperglycemia, hyperlipemia, vascular inflammation, and oxidative stress in STZ-induced diabetic mice, making it a possible treatment for type 1 diabetes [73].

II.1.2. IV. Anticancer activity

The biological activity of polysaccharides has recently become a hot topic for domestic and international experts and scholars in the medical field due to a study that revealed polysaccharides from natural sources have significant anti-tumor activity and the toxic side effects of the human body are relatively small. More anticancer polysaccharides have currently been discovered, such as lentinan, polysaccharides, and schizophyllan, which can enhance T cells' immunological activity, increase the production and activation of macrophages, and lower the expression of macromolecules [74]. As a result, it strongly inhibitory effect on cancer cells. Clinical trials have used lentinan, *Polyporus umbellatus* polysaccharide, *Ganoderma lucidum* polysaccharide, and *Astragalus* polysaccharides. Even certain polysaccharides have been used in the treatment of cancer as immunostimulatory agents in combination with chemotherapy medicines [75-78].

II.1.2. V. Antiviral activity

One of the biggest risks to human health is virus infection, thus finding specialized, safe, and effective antiviral medications has always been a top priority. An underused novel source of natural chemicals for drug discovery, polysaccharides serve a huge diversity of activities in organisms. Numerous polysaccharides have been discovered to have antiviral activity, minimal toxicity, and low resistance in studies [79]. In vitro studies on pig pseudorabies virus revealed that polysaccharides had a strong blocking impact, directly suppressing and killing the virus [70]. The flavivirus, togavirus, arenavirus, rhabdovirus, orthopoxvirus, and herpesvirus families of enveloped viruses have all been found to be inhibited by complex structural sulfated polysaccharides, which are particularly abundant in many species of marine algae [80].

II.2. Secondary metabolites

II.2.1. Triterpenoids

The triterpenes compounds belong to the terpene group, that is one of the most popular groups of natural products with approximately 30,000 identified structures [81]. All terpenes are derived from C5 isoprene units, and based on the isoprene units' number, terpenes subdivided into hemiterpenes (C5) monoterpenes (C10), sesquiterpenes (C15), diterpenes (C20), sesterpenes (C25), triterpenes (C30) and tetraterpene (C40) [82]. Triterpenes consist of a large number of different types of compounds which, according to the various features of their skeletons, can be divided into monocyclic-, bi-, tri- tetra- or pentacyclic structures [83]. In nature, triterpenoids are most often found as tetracyclic or pentacyclic structures, the pentacyclic triterpenes can be divided into three main classes: lupane, oleanane, and ursane (figure), also the tetracyclic triterpenes most abundant in nature are : protostanes, cycloartanes, dammaranes [83, 84].

The pentacyclic triterpenes are found naturally in many medicinal plants, which widely distributed all over the world, in large variety vegetables, in aromatic herbs and consumed fruit especially in fruit peel, they have also found in trees, such as eucalyptus, for this the pentacyclic triterpenes is a part of human diet [84]. It is estimated that the average human consumption of a triterpene is estimated to be around 250 mg per day in the Western world and in Mediterranean countries the average consumption can be as high as 400 mg per day [85]. Pentacyclic triterpenes have received much attention, and several of them, including pentacyclic triterpene derivatives, are being marketed as therapeutic agents or dietary supplements around the world [83]. It has been reported that the beneficial health effects of fruits, vegetables and medicinal plants have associated with their triterpene content [84, 86].

II.2.2. Biosynthesis of triterpene

The precursor of all terpenoids is 3R-(+)-mevalonic acid, the initial step of formation of this precursor involves the condensation of thioethers of acetic acid: formation of aceto-acetate and condensation of this with an acetylcoenzyme A molecule [87].

The precursor 3R-(+)-mevalonic acid is enzymatically catalyzed to give 3R-(+)-metrononic acid 5-diphosphate, which is transformed into isopentenyl diphosphate, also

called isopentenyl pyrophosphate (IPP), the latter is isomerized by isopentenyl isomerase to dimethylallylpyrophosphate (DMAPP) (**Figure. II. 7**).

3R (+)-Mevalonic acid 5-diphosphate   3R (+)-Mevalonic acid 5-phosphate   mevalonic acid

Isopentenyl diphosphate   Dimethylallylpyrophosphate
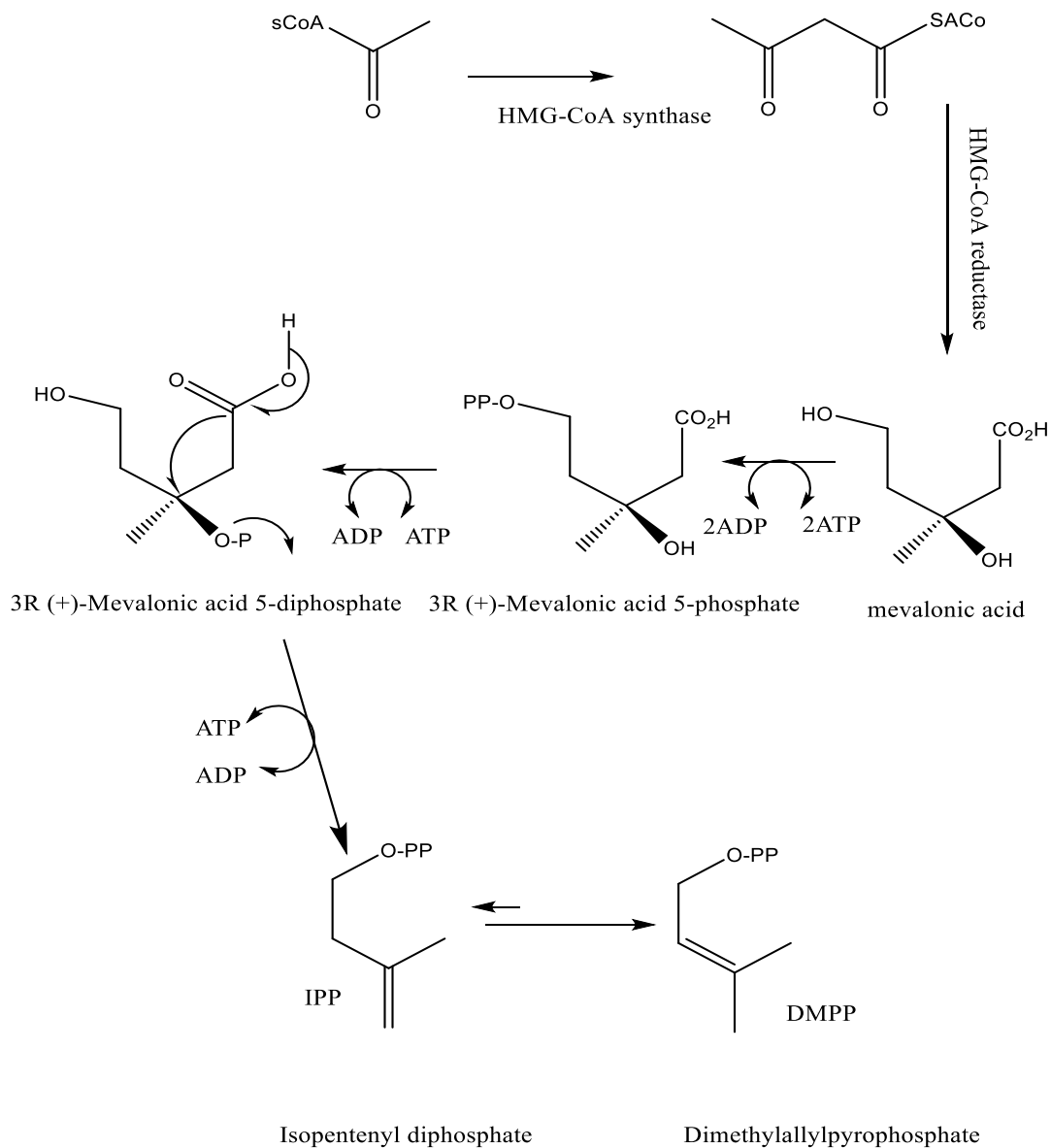
Figure. II. 7: formation of IPP and DMPP [62, 85].

The combination of isopentenyl pyrophosphate (IPP) unit with dimethylallylpyrophosphate (DMAPP) head to tail by dimethylallyl transferase form the geranyl pyrophosphate (GPP). The addition of isopentenyl pyrophosphate (IPP) to geranyl pyrophosphate (GPP) produces farnesyl pyrophosphate (FPP) [63] (**Figure. II. 8**).
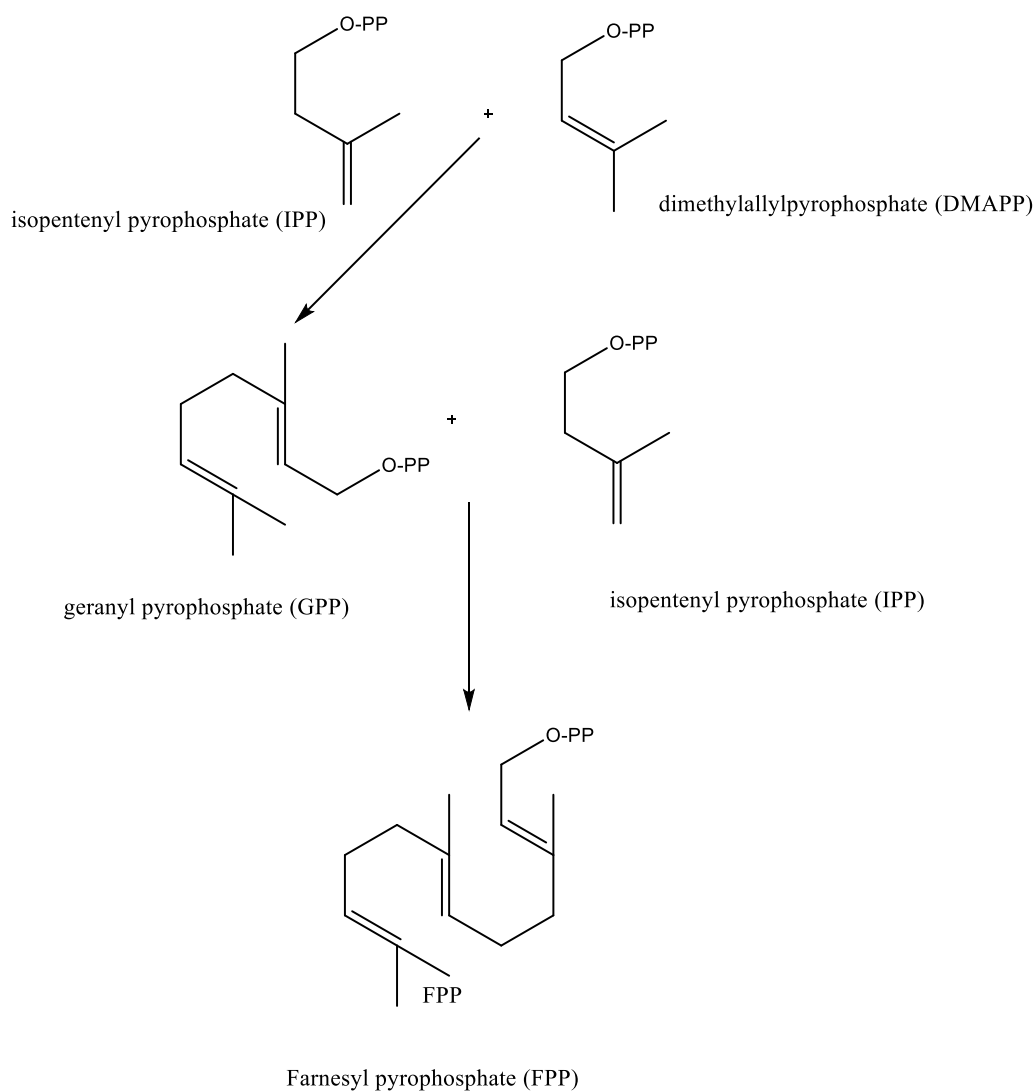
Figure. II. 8: The formation of farnesyl pyrophosphate (FPP).

Two molecules of farnesyl pyrophosphate are joined tail-to-tail to yield squalene, this last transformed to 2,3-oxidosqualene by squalene synthase, which is the common starting point for cyclization reactions in triterpenoid biosynthesis. The opening of the epoxy of 2,3-oxidosqualene initiates the cyclization, which oriented the biosynthesis to the sterols on the hand and triterpene on the other hand [63, 88] (**Figure. II. 9**).

➢ If the 2,3-oxidosqualene is held in a chair-chair-boat (CBC) conformation, cyclization leads to the sterols (**Figure. II. 10**).

➢ If 2,3-oxidosqualene is held into a chair-chair-chair conformation (CCC) a different conformation, cyclization leads to the triterpene (**Figure. II. 11**).
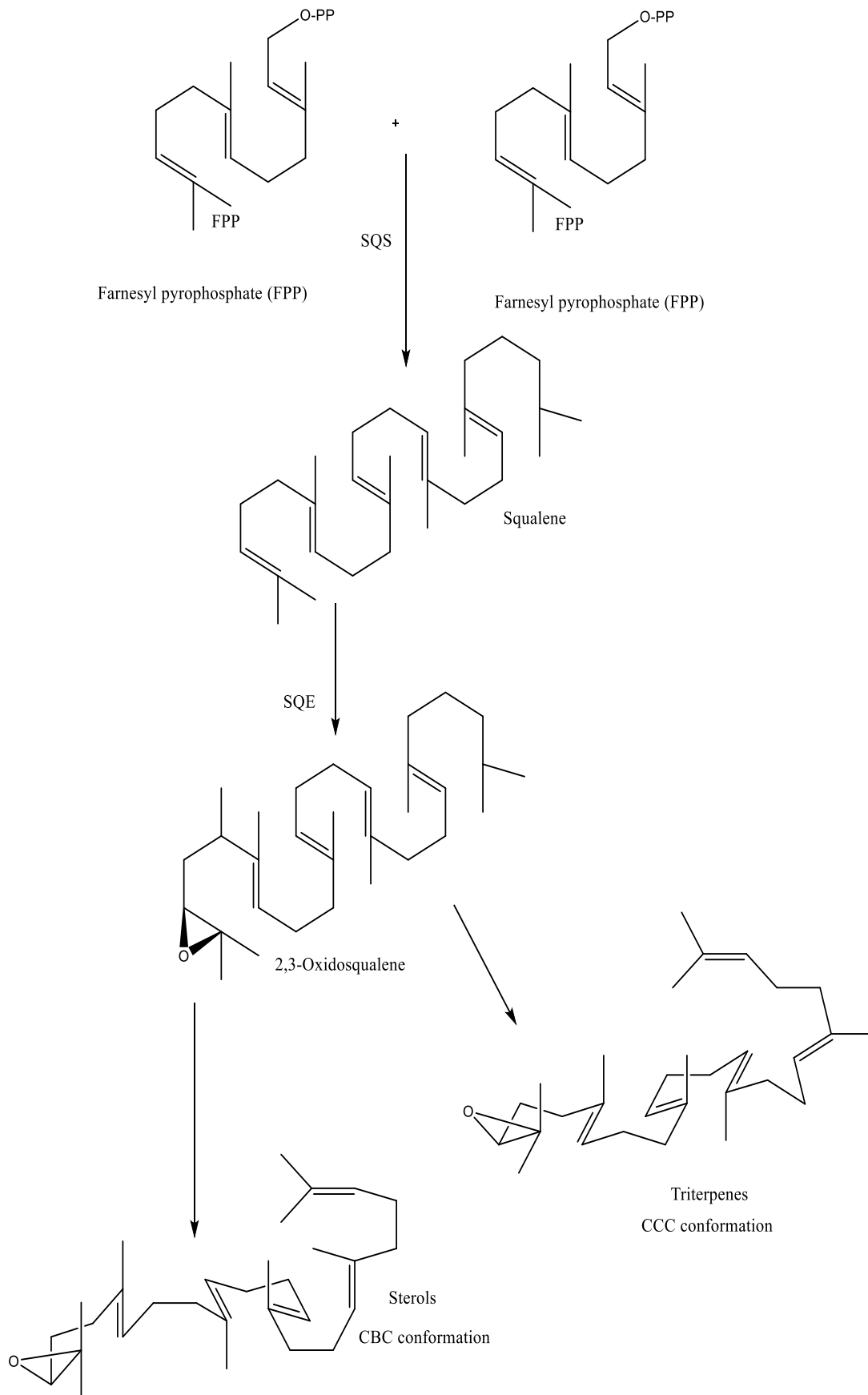
Figure. II. 9: Biosynthesis of triterpene [62, 86].

Protostane

cycloartane

Dammarane
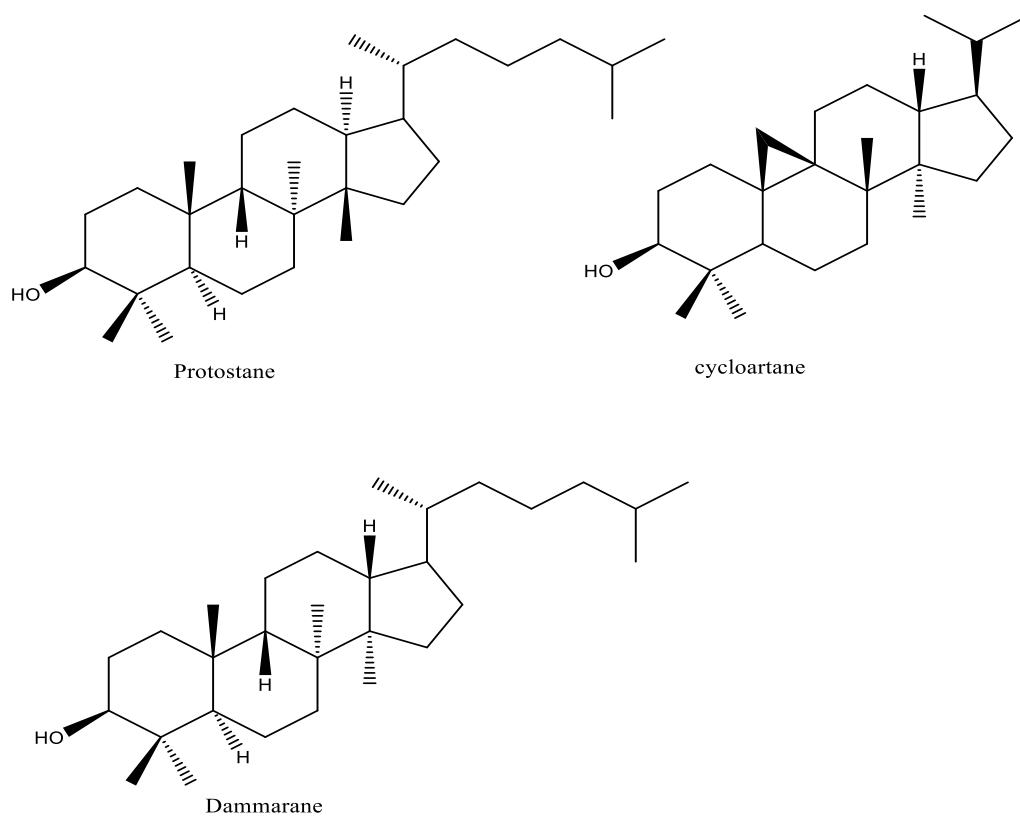
Figure. II. 10: Structures of triterpenes tetracyclic.

Oleanolic acid

Ursolic acid

Lupeol
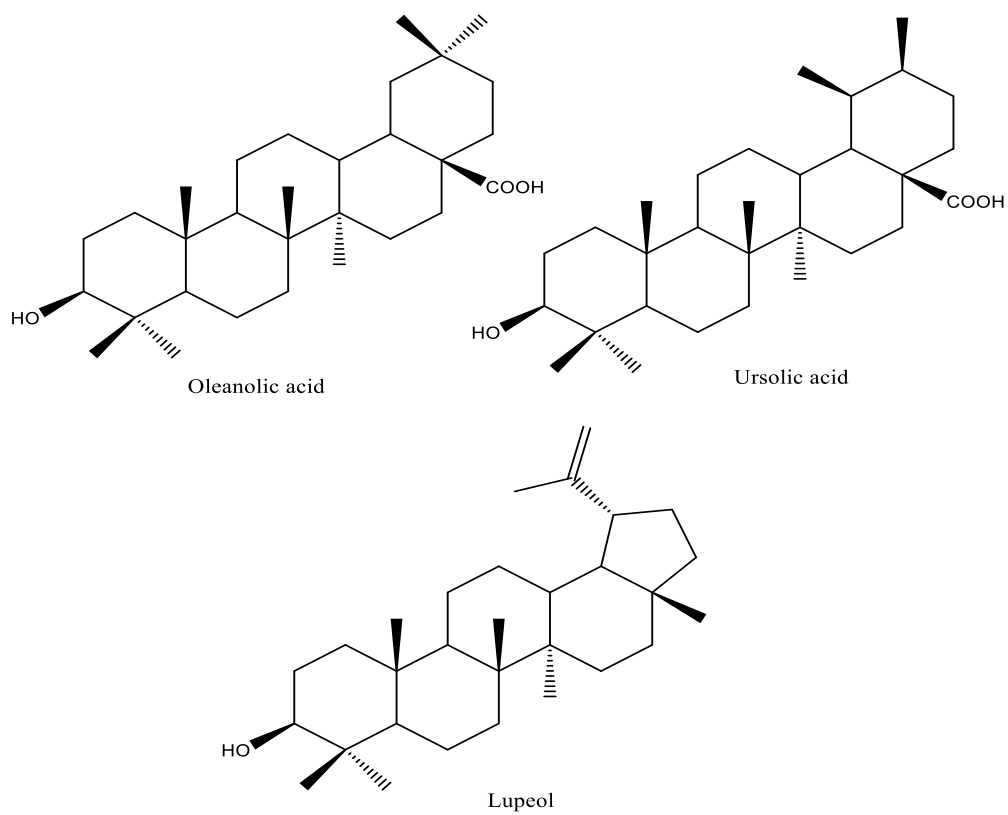
Figure. II. 11: Structures of triterpenes pentacyclic.

II.2.3. Biological activities of triterpene

A study of electronic databases revealed an increase in the number of publications and patents relating to the biological activities and medicinal potential of triterpenes. The estimated number of references in 2017 was 6910 in SciFinder Scholar, 2908 in PubMed, 2223 in Web of Science, and 2103 in Thomson Reuters Integrity[84]. In reality, this group of substances exhibits a wide range of biological properties, including:

II.2.3. I. Antioxidant activity

The triterpenes have the potential to be used as antioxidants due to their capacity to scavenge free radicals and strengthen the body's antioxidant defense mechanisms. that shows highly effective in lowering *in vitro* lipid peroxidation and successfully scavenged DPPH$^{\bullet+}$, ABTS$^{\bullet+}$, and superoxide radicals, they also shown considerable ferric reducing activity. The triterpenes also show *in vivo* antioxidant activity, that confirmed by injection of triterpenes to Swiss albino mice where boosted the activities of the antioxidant enzymes in the blood and tissue [89].

II.2.3. II. Anti-inflammatory activity

Triterpenes, which are widely dispersed in plants, are frequently the bioactive compounds that give them their anti-inflammatory properties. Numerous of these substances are effective in a variety of in vivo experimental models, including adjuvant arthritis and allergy simulations, ear edema caused by phorbol and daphnane esters, ethylphenylpropiolate, arachidonic acid, and capsaicin, and hind paw edema caused by carrageenan, serotonin, and phospholipase A2. Some triterpenes are active against inflammatory enzymes such 5-1ipoxygenase, elastase, and phospholipase A2, according to in vitro research on additional effects. Some of these blocks the release of histamine, collagenase, interleukin, lipid peroxidation, and free radical-mediated processes, as well as complement and protein kinase activities [90].

II.2.3. III. Antidiabetic activity

Numerous studies have demonstrated that the triterpenes substances have various antidiabetic actions. They can normalize plasma glucose and insulin levels, stop the onset of insulin resistance, and inhibit enzymes involved in glucose metabolism. In contrast to synthetic medications, these natural substances have been reported to exhibit

hypolipidemic and anti-obesity activity in addition to a hypoglycemic impact. Triterpenes are also promising agents in the prevention of diabetes complications. Preventing the formation of advanced glycemic end products, which are involved in the pathogenesis of diabetic nephropathy, embryopathy, neuropathy or impaired wound healing [91].

II.2.3. IV. Anticancer activity

On using natural remedies to both prevent and treat cancer, several studies have been conducted. Among bioactive substances, triterpenes are a significant class that has cytotoxic capabilities against tumor cells while having little effect on normal cells [92]. The lupane, oleanane, and ursane groups of triterpenes have the potential to treat cancer in various ways, according to study conducted by Pisha et al in 1995, betulinic acid is a highly promising anticancer medication after causing apoptosis in melanoma cell lines in vitro and in vivo. Experiments focused on the processes by which betulinic acid and other triterpenes induce apoptosis [93]. Later, the antitumor effects were verified in a number of cancer cell lines from different origins, including breast, colon, lung, and neuroblastoma. The expectation that triterpenes are helpful to treat cancer by a variety of mechanisms of action is further supported by the numerous additional benefits that have been demonstrated in recent studies [94].

II.2.3. V. Antiviral activity

According to reports, the triterpenes have a variety of therapeutic uses, including antiviral capabilities. As a whole, 342 triterpenoids were discovered to have antiviral activities against 14 distinct viruses, including: Coronavirus, Coxsackie B3, Cytomegalovirus, Dengue virus, Epstein-Barr virus, Enteroviruses, Hepatitis virus, Herpes simplex virus, Human immunodeficiency viruses, Influenza virus, Porcine epidemic diarrhoea virus, Respiratory syncytial virus, Semliki Forest virus and Zika virus [95].

II.2.3. VI. Hepato-protective

Triterpenes' potential hepatoprotective effects have been studied, where the studies demonstrated that lupeol provides protection against aflatoxin B1, a strong hepatotoxic chemical, when tested in vivo. Aspartate, alanine, aminotransferase, lactate dehydrogenase and alkaline phosphatase are examples of liver function enzymes, which their levels are elevated in serum as a result of eating foods high in aflatoxin. The altered

levels of biomarker enzymes, however, were reversed to normal levels in mice treated with aflatoxin when lupeol (100 mg/kg) was given orally for 7 days. Surprisingly, lupeol has a greater hepatoprotective impact than the well-known natural hepatoprotective substance silymarin [96].

II.2.4. Saponins

Generally speaking, saponins are non-volatile and surface-active substances present throughout nature, particularly in the plant kingdom, which are widely distributed in plant species, being reported in nearly 100 families [97, 98]. The word "saponin" is derived from the Latin word "sapo," which means "soap," because when saponin molecules are agitated with water, they produce foams soap-like [97].

Chemically the saponins are triterpene and steroid glycosides, which are both derived from the 30 carbon atoms containing the precursor oxidosqualene, they are consist of aglycones coupled with one or more monosaccharide moieties [88, 97].

II.2.5. Classification of saponins

Traditionally, saponins can be classified into two groups based on the nature of their aglycone skeleton, triterpenoid saponins and steroidal saponins, which are both derived from precursor oxidosqualene, the group that consists of triterpenoid saponins are the most abundant and mostly occur in dicotyledonous angiosperms. the group that consists of steroidal saponins are essentially only found in monocotyledonous angiosperms [99]. The difference between the two classes lies in the fact that:

II.2.5. I. Triterpenoids saponins

The triterpenoid saponins or triterpenoid glycosides is the most widely distributed saponins type in the plant kingdom, triterpenoid glycosides are pentacyclic compounds having 30 carbon atoms normally having one hydroxyl group (OH) at C-3 and carboxyl group (-COOH) at C-28 [100].

Based on the attached sugar chains number the triterpenoid saponins can be classified as monodesmosidic, bidesmosidic or tridesmosidic [101]. The majority of known saponins are monodesmosidic saponins, which means that only one position of the aglycone is glycosylated, the saponins that glycosylated in two positions with two saccharide chains are bidesmosidic saponins. In monodesmosidic saponins the saccharide chain is often joined to the C3 hydroxy group present in the most of

sapogenins by an ether linkage [97]. These saccharide side groups can be branched and, in most cases, consist of 2–5 monosaccharide units, which may increase up to 11 units. The second saccharide chains are most often attached by an ester linkage to the C28 carboxy group in the bidesmosidic saponins. Finally, three saccharide chains are linked to the aglycone at various positions in the somewhat uncommon tridesmosidic saponins [101].

II.2.5. II. Steroids saponins

Steroid saponins, Steroid glycosides or steroidal saponins are modified triterpenoids, generally the steroidal saponins aglycon comprising of six-rings, where two is a hetero ring, one of both is furan ring and the other is a pyran ring with structure 27 carbon atoms, spirostane skeleton (**Figure. II. 12**), which have one sugar chain at C-3 through an ether linkage. In some cases, the hydroxyl group in the 26-position is engaged in a glycosidic linkage, and so the aglycone structure remains pentacyclic, this is referred to as a furostane skeleton (**Figure. II. 12**). The steroidal saponins is less distributed in nature comparing to triterpenoid saponins [100, 102].

Steroidal spirostane

Steroidal furostane
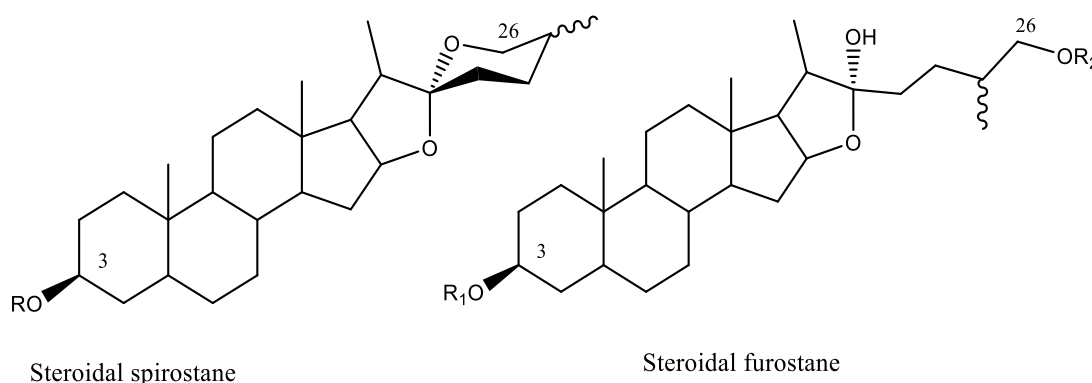
Figure. II. 12: Steroidal saponins skeletons, R= sugar moiety [100].

The sugar chains:

The sugar chains that usually attached to the aglycone are composed of glucose, galactose, glucuronic acid, rhamnose, xylose and arabinose and are added onto hydroxyl groups forming sugar acetals or carboxyl groups forming sugar esters (**Figure. II. 13**). These sugar chains normally attached at the C-3 and/or C-28 positions (although glycosylation at the C-4, C-16, C-20, C-21, C-22, and/or C-23 positions can also occur) [88, 97].
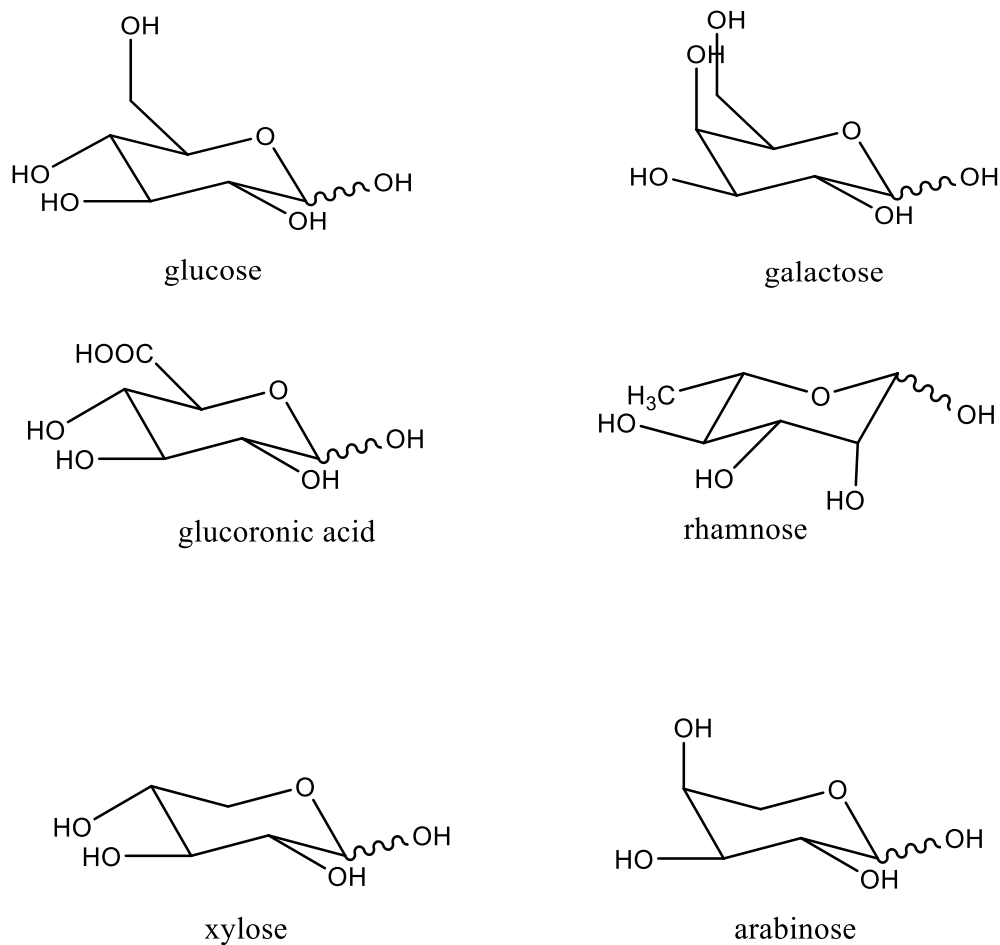
Figure. II. 13: Different structure of sugar.

Vincken *et al.* (2007) proposed a detailed classification of saponins based on the aglycone skeleton that results from the biosynthesis via isoprenoid pathway, the saponins are classified into 11 main classes, which covering the major skeletons of saponins, including dammaranes, tirucallanes, lupanes, hopanes, oleananes, taraxasteranes, ursanes, cucurbitanes, cycloartanes, lanostanes, and steroids. These aglycones are represent the end products of cyclization, rearrangement and degradation reactions that occur on the oxidosqualene can proceed in two ways, either via the chair–chair–chair or chair–boat–chair conformations as shown in **Figure. II. 14** [97].

Via the cyclization of the chair–chair–chair conformation of oxidosqualene

Dammarane type saponins: are all saponins that are formed from the tetracyclic dammarenyl C20 carbocation, which is produced by the proton-initiated cyclization of the "chair-chair-chair" conformation.
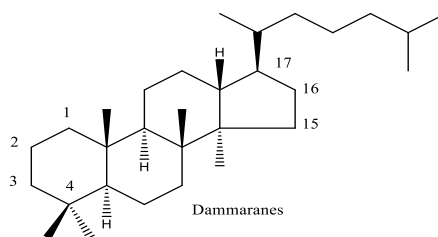
Tirucallane type saponins: the tirucallenyl C8 carbocation is produced by a series of hydride and methyl shifts in the dammarenyl carbocation, and all saponins derived from this carbocation are classified as tirucallane type saponins.
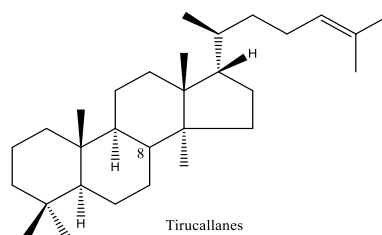
Lupane type saponins: the C16-C17 bond or the C13-C17 bond can be shifted in order to enlarge the five-membered ring close to the C20 dammarenyl carbocation. A reaction involving the C24-C25 double bond might result in the pentacyclic C25 lupenyl carbocation after a shift of the C16-C17 bond yields the tetracyclic C17 baccharenyl carbocation. All saponins produced by this carbocation are classified as lupane type saponins.
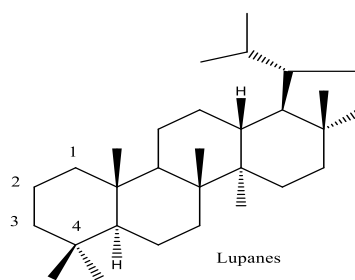
Oleanane type saponins: Further rearrangements of the lupenyl carbocation are possible, first to the C18 germanicenyl carbocation and then, via a series of hydride shifts, to the C13 oleanyl carbocation. All saponins derived from this oleanyl carbocation are classified as oleanane type saponins.
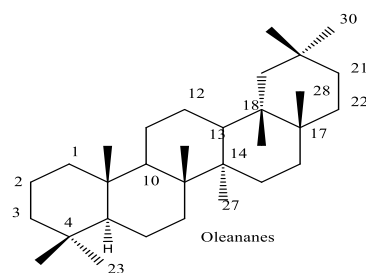
Taraxasterane type saponins: The C20 taraxasterenyl carbocation is produced by shifting the α methyl group in the germanicenyl carbocation, which can be deprotonated to yield taraxasterane type saponins.
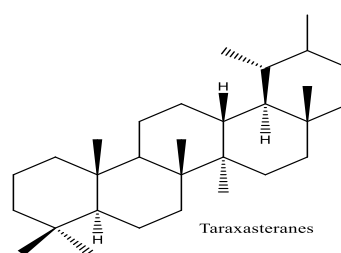
Ursane type saponins: The germanicenyl carbocation undergoes a methyl shift, which is followed by numerous hydrides shifts to form the C13 carbocation, which may then be deprotonated to form saponins of the ursane type.
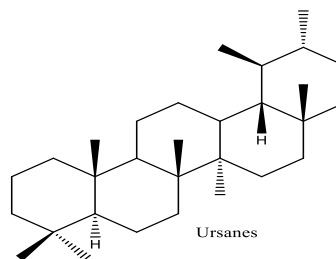
Hopane type saponins: A C17 carbocation is created by shifting the C13-C17 bond in the C20 dammarenyl carbocation. This C17 carbocation can then be cyclized by reacting with the side chain's double bond to create the C25 pentacyclic hopenyl carbocation. All saponins produced by this carbocation are categorized as being of the hopane type.
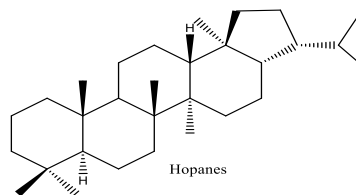
Via the cyclization of the chair–boat–chair conformation of oxidosqualene:

Cucurbitanes type saponins: The intermediate C9 lanosteryl carbocation is produced by starting with a tetracyclic protosteryl C20 carbocation, which then proceeds through a sequence of hydride and methyl shifts. This carbocation is capable of undergoing further methyl and hydride changes to become the C5 cucurbitanyl carbocation. All saponins derived from this carbocation are classified as cucurbitanes type saponins.
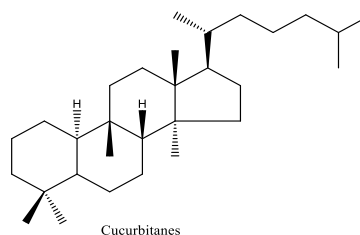
Cycloartane type saponins: A cyclopropane ring, like the one in cycloartenol, may be formed by deprotonating the C19 methyl group on the lanosteryl carbocation. All saponins derived from cycloartenol are classified as cycloartane type saponins.
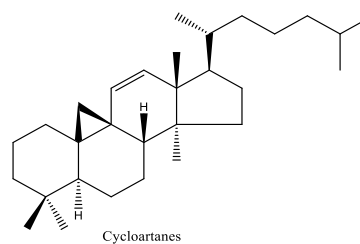
Lanostane type saponins: Lanosterol is produced by deprotonating the lanosteryl carbocation, and all saponins derived from lanosterol are classified as lanostane type saponins.

Lanostanes
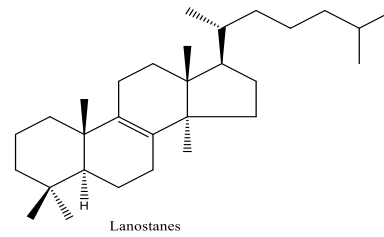
Steroid type saponins: Additionally, the double bond in lanosterol can be isomerized and demethylated to produce cholesterol. The saponins derived from this skeleton are classified as steroid type saponins.

Steroids
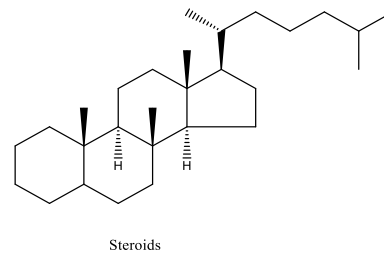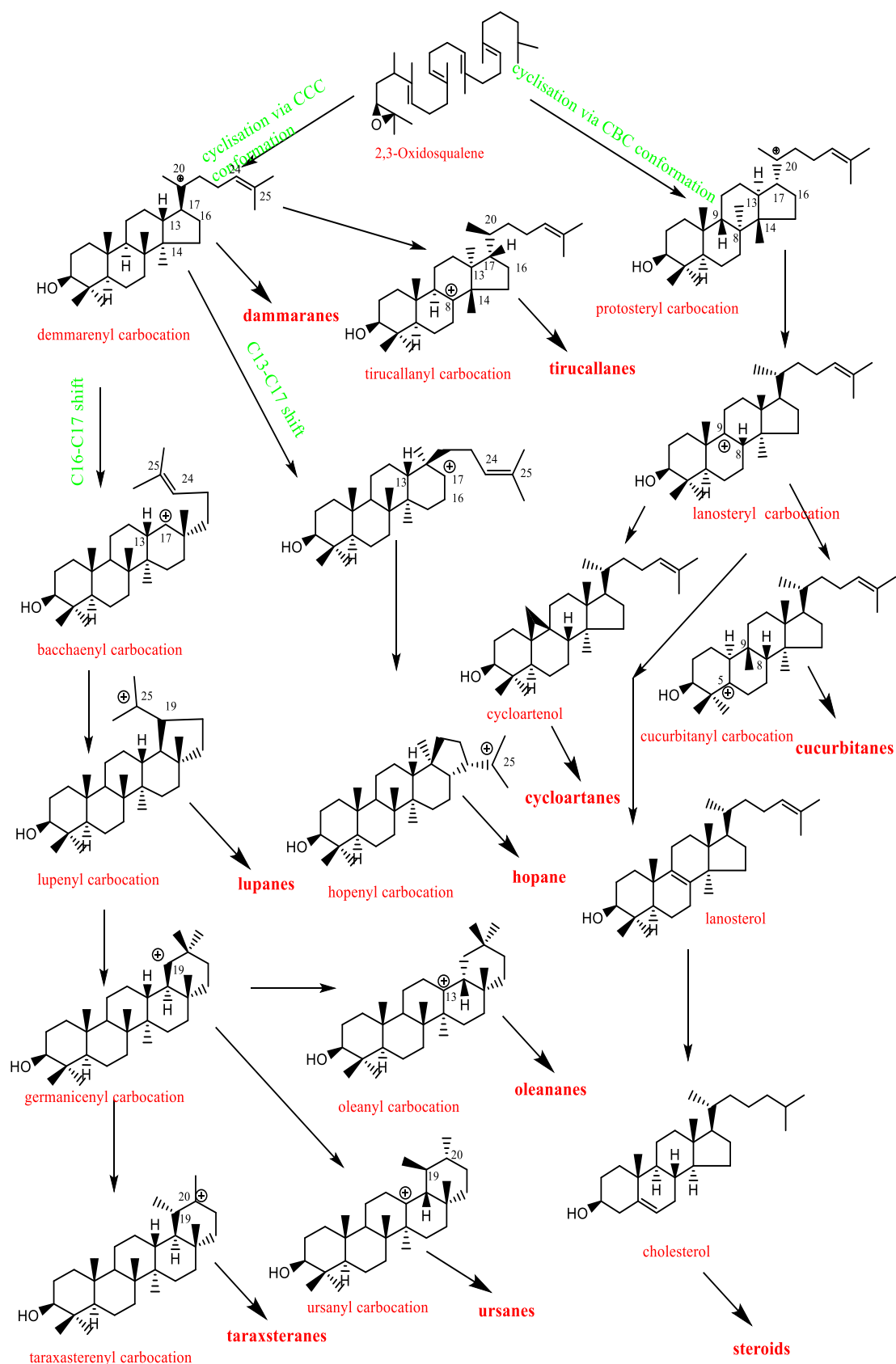
Figure. II. 14: The cyclization of oxidosqualene to various aglycone skeleton of saponins [95].

II.2.6. Biological activities of saponins

II.2.6. I. Antioxidant activity

The saponins extracted from plant sources are reported to have antioxidant activity in many reports. As example, the antioxidant activity of saponins extract from the root of *Curcuma angustifolia* was evaluated against -2,2-diphenyl-1-picrylhydrazyl (DPPH), hydrogen peroxide (H_2O_2), and nitric oxide (NO) assays, this extract saponins demonstrated excellent antioxidant activity [103]. Other study conducted by Hong *et al.* 2017 show that the saponin fractions prepared from the stems and leaves of *Helicteres hirsuta* Lour exhibited strong antioxidant capacity against DPPH radical scavenging, Ferric reducing antioxidant power (FRAP) and Cupric ion reducing antioxidant capacity (CUPRAC) [104].

II.2.6. II. Anti-inflammatory activity

Numerous reports mention that the saponins isolated from plant sources having anti-inflammatory properties. In the mouse carrageenan-induced oedema experiment, many saponins reduce the inflammation. A study conducted by Sirtori 2001, which show that the Aescin, a mixture of triterpenoid saponins have anti-inflammatory, anti-oedematous and venotonic properties [105]. The steroidal saponin was evaluated also for anti-inflammatory activity, utilizing the test for capillary permeability. The steroidal saponin inhibited the increase in vascular permeability caused by acetic acid, which is a typical model for the first stage inflammatory reaction [106].

II.2.6. III. Antidiabetic activity

Recent research has shown that triterpenoid saponins effectively lower plasma glucose and plasma triglyceride levels. Triterpenoid saponins and investigated for their α-glucosidase and α-amylase inhibition properties. Where these compounds displayed obvious inhibitory activities against α-glucosidase, and significant inhibitory activities against α-amylase [107]. Additionally, the steroidal saponins showing strong antidiabetic properties, which could be employed as nutritional supplements to help control systemic glucose levels [108].

II.2.6. IV. Anticancer activity

With low toxicity and excellent efficacy, steroidal saponins are particularly popular for the prevention and treatment of cancers [109]. According to in vitro and in

vivo investigations, the steroidal saponin compounds offer a variety of anticancer effects, including the inhibition of proliferation, induction of apoptosis and autophagy, and suppression of tumor invasion and metastasis [110]. Other study conducted by Jacqueline Eskander et al 2013., showed antitumor activity of steroidal saponins, where this study showed potent activity against HCT116, MCF7, and HepG2 cell lines in comparison with the positive control doxorubicin [111]. The triterpene saponins also show in vitro antitumor activity against five human cancer cell lines (SHG44, HCT116, CEM, MDA-MB-435 and HepG2) by the 3-(4,5- dimethylthiazol-2-yl)-2,5-diphenyltetrazolium bromide (MTT) assay [112].

II.2.6. V. Antiviral activity

There have also been reported that saponins have antiviral properties. a study by Simes *et al*. (1999) examined the antiviral activity of two types of triterpenoids saponins, oleanane-type and ursane-type, obtained from Chinese plants. The oleanane-type inhibited herpes simplex virus type 1 DNA synthesis, whereas the ursane-type saponin inhibited viral capsid protein synthesis of herpes simplex virus type 1 [113].

II.2.7. Flavonoids

Flavonoids are polyphenolic compounds consist of 15 carbons, with two aromatic rings connected by a three-carbon bridge, which have the structure C6-C3-C6. These compounds are the most numerous of the phenolics and are found throughout the plant kingdom [114] (**Figure. II. 15**).
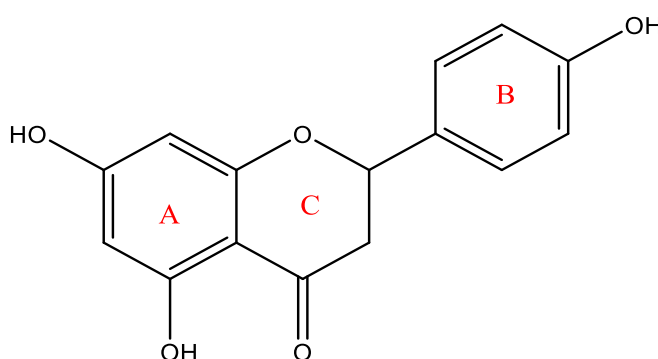
Figure. II. 15: Structure of flavonoid; naringenin.

Flavonoids are almost universal plant pigments. They are responsible for the coloring of the flowers conditioning entomophilous pollination. Such is the case of yellow flavonoids (chalcones, aurones, yellow flavonols) or that of red or purple anthocyanosides [87]. The flavonoids play significant and diversified roles as

secondary metabolites and are found in high concentrations in the epidermis of leaves and the skin of fruits. Flavonoids play a variety of roles in plant biology, including UV defense, pigmentation, promotion of nitrogen-fixing nodules, and disease resistance [114].

II.2.8. Classification of flavonoids

The main subclasses of flavonoids are the flavones, flavonols, flavan-3-ols, isoflavones, flavanones and anthocyanidins [114] (**Figure. II. 16**):
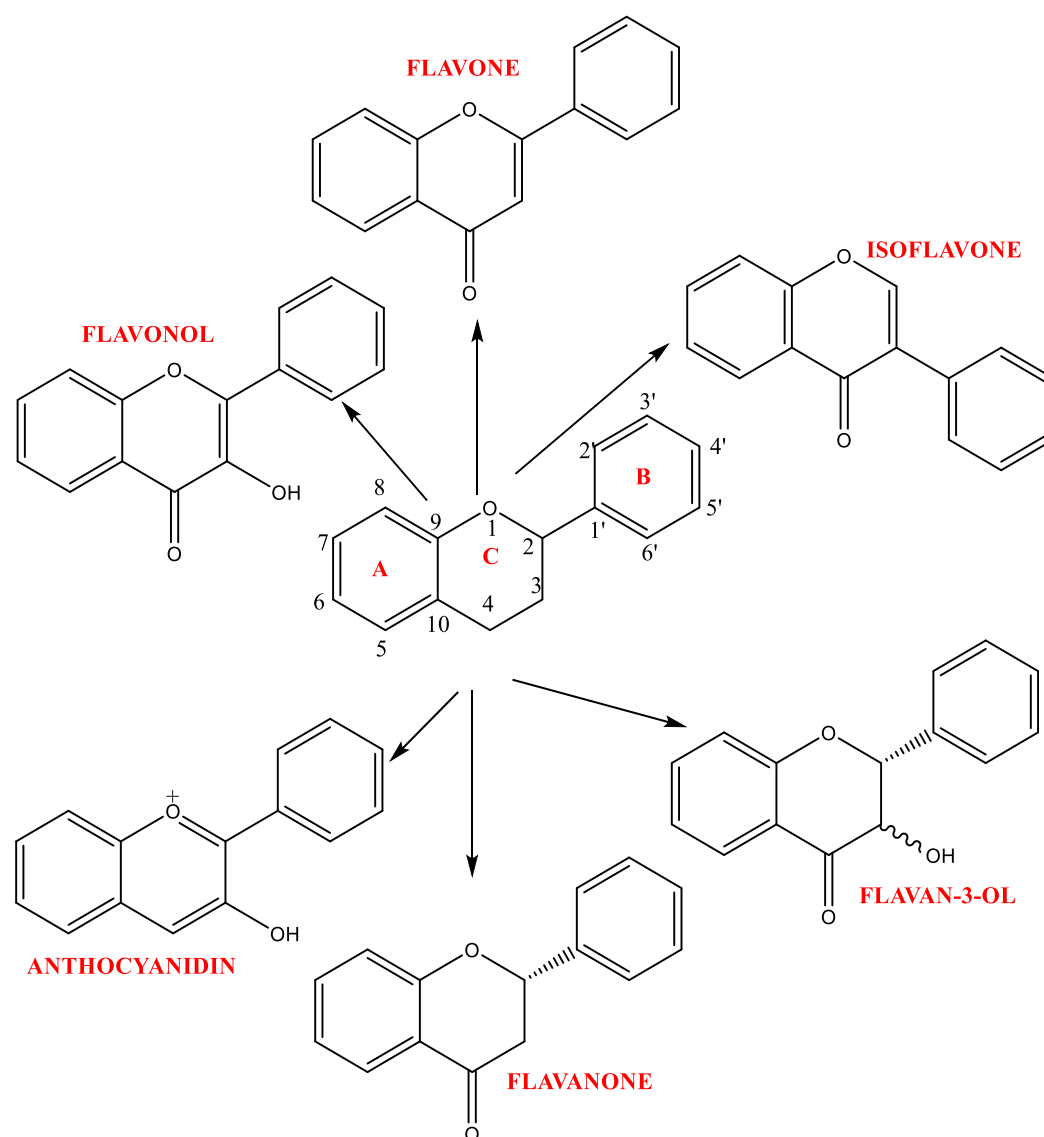
Figure. II. 16: The main subclasses of flavonoids.

II.2.9. Biosynthesis of flavonoids

The structure of the C6-C3-C6 flavonoid is the product of two separate biosynthetic pathways. The bridge and the aromatic B ring constitute a

phenylpropanoid unit synthesized from p-coumaroyl CoA. The six carbons of the A-nucleus come from the condensation of three acetate units by way of malonic acid [114]. The biosynthesis of flavonoids takes place from a common precursor: 4, 2', 4', 6'-tetrahydroxychalcone. Cyclization of this stereospecific chalcone by chalcone isomerase forms (S)-4',5,7-trihydroxyflavanone leading to the basic flavonoid skeleton [115] (**Figure. II. 17**).
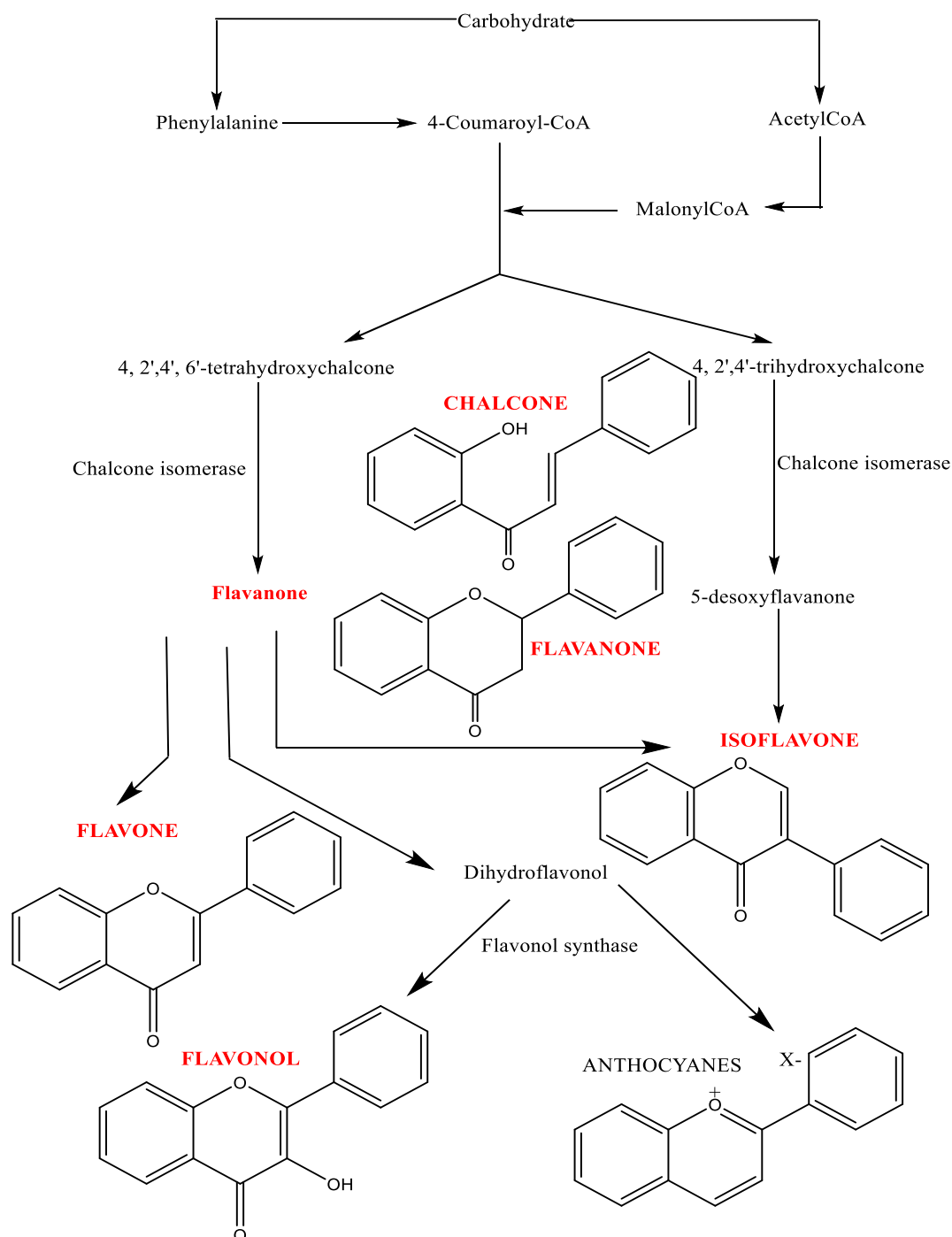
Figure. II. 17: Flavonoid biosynthetic pathway [113].

II.2.10. Biological activity of flavonoids

II.2.10. I. Antioxidant activity

Although flavonoids have a wide range of biochemical characteristics, their ability to function as antioxidants is the one that practically every group of flavonoids is most known for. Numerous aspects of antioxidant activity, including the ability to scavenge free radicals and chelate metal ions [116]. For instance, isorhamnetin is a flavonoid compound, The scavenging of the diphenylpicrylhydrazyl radical (DPPH), iron (III) to iron (II)—reducing, and iron-chelating tests were used to assess the antioxidant capabilities of isorhamnetin. When compared to ascorbic acid and BHT, the findings of the antioxidant assays revealed that isorhamnetin show strong antioxidant activity [117].

II.2.10. II. Anti-inflammatory activity

Many flavonoids have been found to have anti-inflammatory property. Particularly tyrosine and serine-threonine protein kinases, which are crucially implicated in the formation of inflammatory processes, flavonoids may directly alter the operation of these enzyme systems [116]. For example, the myricetin a flavonol compound, was tested for its in vivo anti-inflammatory effects in both acute and chronic models of inflammation, which showed a significant inhibition of xylene-induced ear swelling, carrageenan-induced hind paw swelling, and acetic acid-induced capillary permeability [118].

II.2.10. III. Antidiabetic activity

Various strategies have been developed in recent years to use flavonoids in vitro and in vivo models by adding a few novel techniques to enhance their antidiabetic efficacy [119]. Isorhamnetin was given orally for 10 days and reduced hyperglycemia and oxidative stress in a STZ-induced diabetes model [120]. In another study, Apigenin is a flavone found in many fruits, vegetables, nuts, onion, orange and tea, in diabetic rats caused by STZ, apigenin maintains the cellular architecture of essential tissues toward normal [119]. In studies with rats, Diosmin significantly reduced plasma glucose levels in rats when administered orally for 45 days. It also increased the activity of several key hepatic enzymes, including hexokinase and glucose-6-phosphate dehydrogenase (G6PD), while decreasing the activity of glucose-6-phosphatase

(G6Pase) and fructose-1,6-bisphosphatase (FDPase) in the streptozotocin (STZ)-nicotinamide treated rats exhibiting its antihypeglycemic activities [121].

II.2.10. IV. Anticancer activity

Cancer prevention is significantly influenced by dietary variables. Flavonoids found in fruits and vegetables have been reported to be chemopreventive of cancer. Consumption of apples and/or onions, two important food sources of the flavonol quercetin, which is inversely associated with the incidence of cancer of the prostate, lung, stomach, and breast [116]. A study conducted by Philips *et al*. 2011, suggested that myricetin might possess anticancer properties in pancreatic cancer via obstructing phosphatidylinositol 3-kinase. Tumor regression and reduced *in vivo* metastatic spread served as confirmation of this [122].

II.2.10. V. Antiviral activity

Since the 1940s, naturally occurring flavonoids have been known to have antiviral properties, and several reports on the antiviral properties of different flavonoids are available. The majority of research on antiviral substances focuses on blocking several enzymes involved in the life cycle of viruses. There is a correlation between the structure-function of flavonoids and their ability to suppress enzyme activity [116]. Numerous flavonoids, including dihydroquercetin, dihydrofisetin, leucocyanidin, pelargonidin chloride, and catechin, exhibit antiviral activity against a variety of viruses, including the Sindbis virus, respiratory syncytial virus, poliovirus, and HSV [116].

Chapter III:

Phytochemical screening, in vitro and in vivo biological activities:

III.1. Plant material

The selected species *Atractylis aristata* was collected from its natural habitat. The harvest was carried out in the Algerian Sahara in the Tamanrasset region (22°47′ 13″ N, 5° 31′ 38″ E) Terhanant region, during February of 2019. The harvest location is presented in **Figure. III. 1**. The scientific identification of the plant has been performed by professor Reggani Abdelmalek, professor in university of Tamanrasset. A specimen of the plant has been deposited in the herbarium of the laboratory of Valorization and Promotion of Saharan Resources (VPRS), under the code 201902Tam/AtysAr.

Figure. III. 1: Map represents the place of harvest (google maps).

III.2. Phytochemical screening

10.00 g of plant were macerated in a 8/2 system (MeOH / H_2O) for 24 hours, after filtration, the crude extract retained for carrying out the following phytochemical tests [123-126]:

III.2.1. Flavonoids test: 1 mL of lead acetate (10%) was added to 1 mL of crude extract, the formation of yellow precipitation indicates the presence of flavonoids.

II.2.2. Steroids test: two tests were carried out:

1. **Salkowski test:** 2 mL of crude extract were mixed with 2 mL of $CHCl_3$ and 2 mL of concentrated H_2SO_4, the appearance of a red color indicates presence of steroids.

2. **Librman Burchard test:** 2 mL of crude extract were dissolved in $CHCl_3$, and then 2 mL of concentrated H_2SO_4 and 2 mL of acetic acid were added, the appearance of a greenish coloring indicates the presence of steroids.

III.2.3. Tannins test: To 1 mL of crude extract, 0.5 mL of 1 % $FeCl_3$ were added; the appearance of a greenish or blue-blackish coloration indicates the presence of tannins.

III.2.4. Saponins test: In a test tube, 5 mL of crude extract were stirred for a few seconds and then left standing for 15 min. Persistent foam height indicates the presence of saponins.

III.2.5. Terpenoids test: 5 mL of crude extract were added to 2 mL of chloroform and 3 mL of concentrated H_2SO_4. The formation of two phases and a brown color at the interphase indicates the presence of terpenoids.

III.2.6. Reducing compounds test: 2 mL of Fehling reagents (1 mL Fehling A and 1 mL Fehling B) were added to 1 mL of crude extract. The mixture incubated for 8 minutes in a boiling water bath. The formation of a red brick precipitate indicates the presence of reducing compounds.

III.2.7. Triterpenoids test: two tests were carried out:

1. **Salkowski test:** 5 drops of concentrated H_2SO_4 were added to 2 mL of the crude extract. The appearance of a greenish color indicates the presence of triterpenoids.

2. **Liberman Burchard test:** 10 drops of acetic anhydride were added to 2 mL of crude extract, and then added 5 mL of concentrated H_2SO_4, the appearance of a greenish coloration indicates the presence of triterpenoids.

III.2.8. Free Quinone test: A few drops of NaOH (1%) were added to 5 mL of crude extract. The yellow, red or purple indicates the presence of free quinones.

III.2.9. Cardenolides tests: 2 mL of glacial acetic acid and a drop of $FeCl_3$ solution were added to 5 mL of crude extract and mixed with 1 mL of concentrated H_2SO_4. The

formation of brown ring on the interface indicates the presence of cardenolide glycosides.

III.3. Preparation of extracts

- ✓ The plant has been dried in a dry and ventilated place, protected from direct sunlight, afterwards the plant is completely crushed and then weighed (100 g).

- ✓ The plant has been macerated for 24 h with petroleum ether to remove fats, waxes and chlorophylls.

- ✓ After the filtration, the plant has been dried and macerated with a mixture (methanol / water; 80/20; V / V), this operation was repeated 3 times with renewal of the solvent every 24 hours and one time for 48 hours.

- ✓ After filtration and concentration, the concentrated hydroalcoholic extract is diluted with 60 mL distilled water, then the solution is left to stand overnight and then filtered.

- ✓ The solution was subjected to successive liquid-liquid type extractions using solvents of increasing polarity, starting with dichloromethane (repeated three times) then ethyl acetate (once) and finally with n-butanol (repeated five times).

- ✓ The three organic phases thus obtained (weakly polar: dichloromethane, moderately polar: ethyl acetate and polar: n-butanol) are evaporated to dryness under reduced pressure and weighed, the extracts yields are given in the **Table. III. 2**.

The extraction protocol is summarized in **Figure. III. 2**:
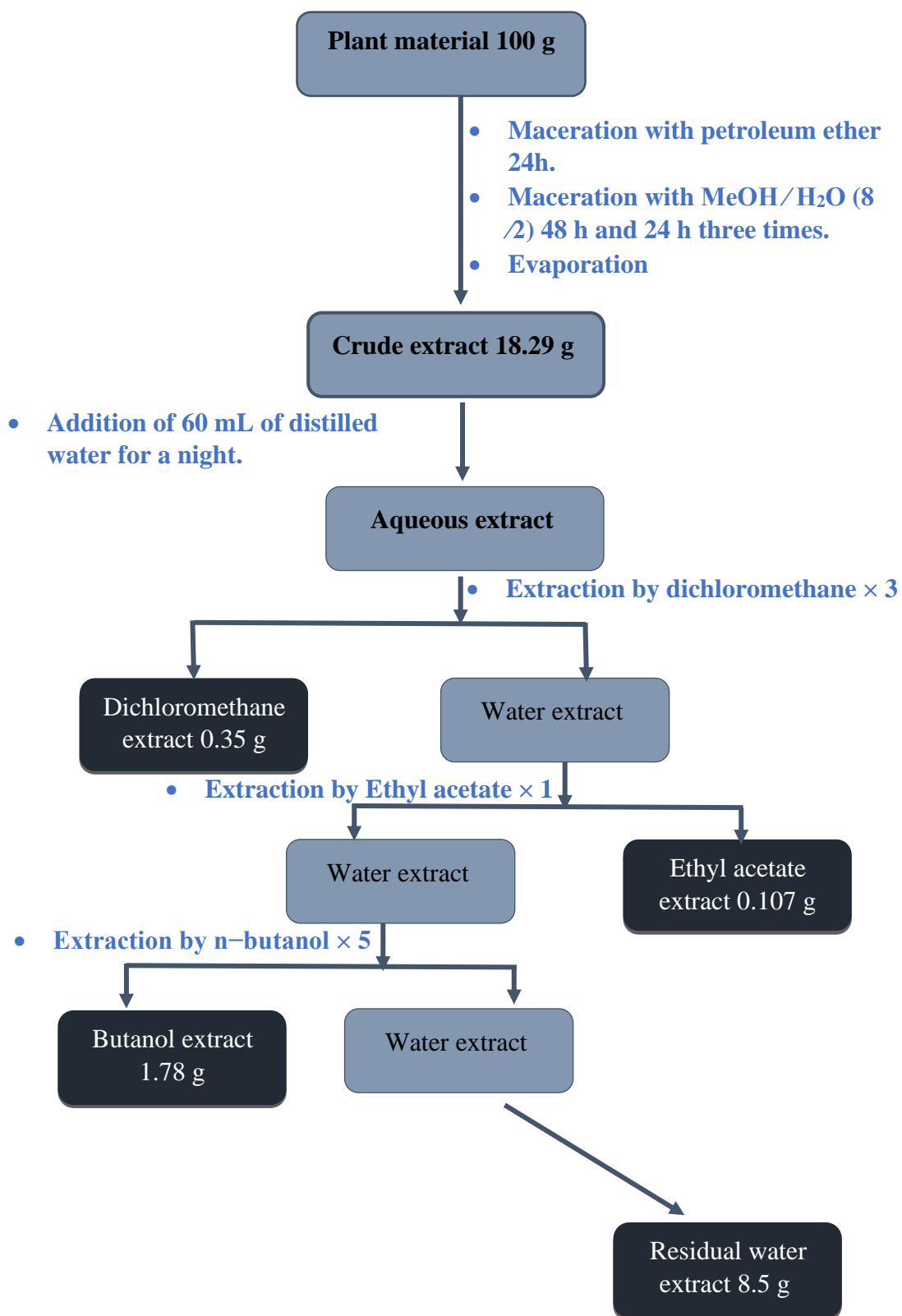
Figure. III. 2: Extraction protocol of different extracts.

III.4. Quantitative analysis

Phenolic compounds are identified using colorimetric methods that allow absorption at a specific wavelength at which the concentration of phenolic compounds is calculated as follow:

$$c\left(\frac{mg}{g}\right) = \frac{nf * v * Abs}{k * m}$$

Where, **nf:** is number of dilutions, **v:** is volume of solvent, **Abs:** is absorbance of sample, **K:** is the slope of the standard curve and **m:** is weight of dried plant material.

III.4.1. Quantification of total phenol

The quantification of total phenolic is carried out according to the method of Singleton and Rossi, the method using Folin–Ciocalteu (F–C) as a reagent [127]. The Folin–Ciocalteu reagent is a mixture of acids phosphotungstic ($H_3PW_{12}O_{40}$) and phosphomolybdic ($H_3PMo_{12}O_{40}$), it is reduced by phenolic compounds giving a mixture of complexes of tungsten oxide W_8O_{23} and molybdenum Mo_8O_3 of blue color [128]. The intensity of the blue coloration proportional to the concentration of polyphenols. Phenols are estimated by UV spectroscopy where gallic acid is used as a standard at a wavelength $\lambda = 760$ nm.

Procedure

0.1 mL of the extract is taken and mixed with the Folin-Ciocalteu reagent (diluted 10 times) left for 5 minutes and then neutralized with 2 mL of 20% sodium carbonate Na_2CO_3 solution, then the solutions were shaken immediately and are incubated in the dark for 30 minutes at room temperature. At 760 nm, the absorbance was measured by spectrophotometry against a blank (same mixture, the extract replaced by methanol) [129]. The phenolic concentration was determined using the linear regression equation obtained from the calibration curve of the gallic acid standard (0.03-0.27 mg/mL). The results were expressed in mg of gallic acid equivalent (GAE) per gram of dry weight (mg GAE / g of dry weight).

III.4.2. Quantification of total flavonoid

The quantification of total flavonoids determined using the aluminum chloride ($AlCl_3$) Colorimetric Method. The principle of this method is that the hydroxyl group of flavones and flavonols forms a stable complexes with the aluminum trichloride,

while the orthodihydroxyl groups in the A- or B-ring of flavonoids form acid labile complexes with aluminum chloride [130]. The complexes produced are yellow in the visible and absorbs visible light at a wavelength 430 nm. The total flavonoids are estimated by UV spectroscopy where the quercetin is used as a standard at a wavelength $\lambda = 430$ nm.

Procedure

1.5 mL of ethanol solution of $AlCl_3$ (2%) is added to 1.5 mL of the extract. The mixture is incubated in the dark for 30 minutes at room temperature. At 430 nm, the absorbance was measured by spectrophotometry against a blank (same mixture, the extract replaced by methanol) [129]. The flavonoids concentration was determined using the linear regression equation obtained from the calibration curve of the quercetin standard (0.003 -0.03 mg/mL). The results were expressed in mg of quercetin equivalent (QE) per gram of dry weight (mg QE / g of dry weight).

III.4.3. Quantification of condensed tannin

The quantification of condensed tannins was carried out depending on the method of vanillin in an acid medium, this method is based on the production of a colored complex measurable at 500 nm. In the presence of an acid, the condensed tannin units react with vanillin where only the first unit of the polymer is involved. The condensed tannins are estimated by UV spectroscopy where the catechin is used as a standard at a wavelength $\lambda = 500$ nm [131].

Procedure

3 mL of vanillin ethanolic (4%) solution are added to 1.5 mL of concentrated HCl and 0.4 mL of the extract. The mixture is incubated in the dark for 15 minutes at room temperature. At 500 nm, the absorbance was measured by spectrophotometry against a blank (same mixture, the extract replaced by methanol) [129]. The condensed tannins concentration was determined using the linear regression equation obtained from the calibration curve of the catechin standard (0.01 -0.08 mg/mL). The results were expressed in mg of catechin equivalent (CE) per gram of dry weight (mg CE/g of dry weight).

III.5. Qualitative analysis using (HPLC-UV) analysis

The analysis of the extracts and 16 standard compounds was carried out using liquid chromatography model (Shimadzu NEXERA XR) in reverse phase, consisting of a solvent delivery system (LC-20ADXR), and a detection system UV equipped with a variable wavelength (190–800 nm). The chromatographic separation was carried out on ultra C18 column (5 µm, 250 x 4.6 mm), the column temperature was set at 30°C. The mobile phase composed of 0.1% Acetic acid/Ultra-pure water (solvent A) and Acetonitrile (Solvent B) at a flow rate of 1 mL/min. The gradient mode elution was 0.01 min (10% B), 55 min (100% B).

Procedure

The stock solution of the samples was prepared at concentration of 1 mg/mL and filtered with 45 µm filter, 10 µL of each extract was injected, the UV absorption spectra were recorded at 250 nm. The identification of the compounds was made by comparing their retention time with the standards.

III.6. Antioxidant activity

In recent years, there has been a significant increase in interest in natural antioxidants for their medicinal effects. The extraction, identification, and quantification of these compounds from a variety of natural sources, such as medicinal plants and agri-food items, has been the subject of research in a number of scientific disciplines. The antioxidant properties it is the capacity of a molecule to inhibit the oxidation of biological substances by free radicals or any pro-oxidant molecules.

III.6. 1. Free radical

A free radical is a chemical species, molecule, or simple atom that has one or more unpaired electrons due to the loss of one or more electrons from the outer orbital. In the human body, free radicals are constantly being formed, under the action of external triggering factors (UV, ionizing radiation, transition metals, combustion fumes, asbestos and silica dust, antiseptics, drugs, pesticides, solvents, etc.). Among the free radicals exposed by the human body, we find reactive oxygen species (ROS) such as superoxide ($O_2^{.-}$), hydroxyl ($OH^.$) and peroxyl ($RO^.$) radicals, hydrogen peroxide (H_2O_2) and singlet oxygen ($1O$). Free-radical mechanisms have been implicated in the pathology of several human diseases, including cancer, atherosclerosis, malaria, and rheumatoid arthritis and neurodegenerative diseases [132].

III.6. 2. Oxidative stress

free radicals are permanently produced in small quantities as tissue mediators or residues of energy or defense reactions, and this physiological production is perfectly controlled by defense systems. In a physiological situation, the balance antioxidant/prooxidant is balanced. Oxidative stress is defined as an imbalance between the level of production of free radicals and the body's antioxidant defenses [132].

III.6. 3. Evaluation of antioxidant activity

Many methods have been developed to determine the antioxidant activity of individual foods, extracts or compounds. These tests including: tests measuring the transfer of electrons or hydrogen also the metals chelating. The study of the antioxidant activity of different extracts of *Atractylis aristata* evaluated using different spectrophotometric methods:

III.6.4. Reducing power assay
Principal

The reducing power of *A. aristata* extracts is evaluated by the phosphomolybdenum method described by Prieto *et al*. (1999) [133]. This technique is based on the reduction of molybdenum Mo (VI) present in the form of molybdate ion MoO_4^{2-} to molybdenum Mo (V) present in the form MoO_2^+ in the presence of the extract to form a green phosphate complex (Mo (V)) at acid pH.

Procedure

3 mL of extract are added to 0.3 mL of a reagent composed of H_2SO_4 (0.6 M), NaH_2PO_4 (28 mM) and ammonium molybdate (4 mM). The mixture was incubated at 95 °C for 90 minutes. After cooling, the absorbance was measured using a UV-Visible Spectrophotometer, at a wavelength of 695 nm against a blank prepared in the same way (except that the extract is replaced by 0.3 mL of water). Ascorbic acid used as a standard antioxidant; the antioxidant capacity is expressed by AEAC (Ascorbic Acid Equivalent Antioxidant Capacity). Which is defined as the molar concentration of the ascorbic acid solution. The Ascorbic Acid Equivalent Antioxidant Capacity (AEAC) of the extract was measured in mM equivalent of Ascorbic acid [134].

III.6.5. 1,1 diphenyl-2-picrylhydrazyl (DPPH free radical) assay

Principal

The antiradical activity of *A. aristata* extracts is evaluated by 1,1-diphenyl-2-picrylhydrazyl (DPPH free radical) method of Brand-Williams *et al*. (1995) [135]. When a purple-colored DPPH˙ reacts with an antioxidant compound, which can give hydrogen, it is reduced to yellow-colored 1,1-diphenyl-2-picrylhydrazine, as showing in the **Figure. III. 3**. The disappearance of the violet color can be measured spectrophotometrically at 517 nm. The color intensity is inversely proportional to the capacity of the antioxidants present in the medium.
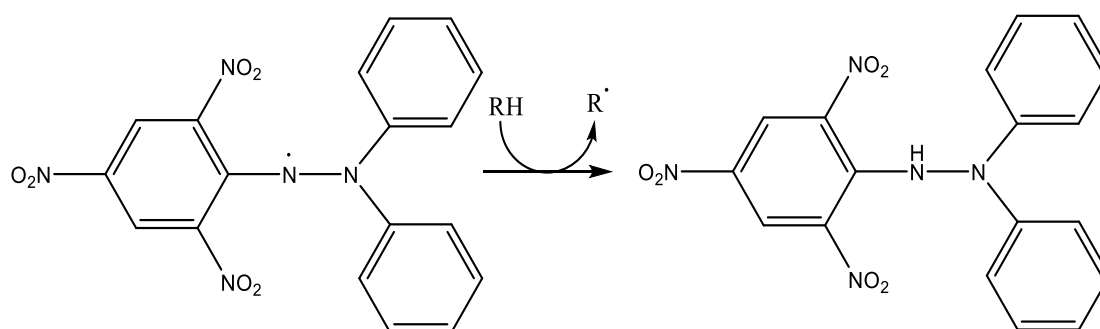
Figure. III. 3: The reduction of the stable radial DPPH˙.

Procedure

1.5 mL of DPPH free radical solution (250 μM) prepared in the ethanol was added to 1.5 mL of each concentration (10-100 mg/mL) of *A. aristata* extracts. The mixture was incubated in the dark at room temperature for 30 minutes. The absorbance was measured at 517 nm. The negative control containing 1.5 mL of DPPH˙ solution and 1.5 mL of water [136]. The antiradical capacity is estimated according to the equation below:

$$DPPH \ scavenging \ effect \ (\%) = \left[\frac{A_0 - A_1}{A_0}\right] * 100$$

Where **A₁** and **A₀** are the sample and the control absorbance at 30 minutes, respectively, BHT and ascorbic acid are used as a positive control.

The IC$_{50}$ (mg/mL) value was used to evaluate the antiradical activity, which is defined as the extract dose required to reduce the absorbance at 517 nm by 50%. Increased antioxidant activity is indicated by a lower IC$_{50}$ value.

III.6.6. 2,2'-azino-bis-3-ethyl benzthiazoline-6-sulfonic acid (ABTS) assay

Principal

Spectrophotometric analysis of 2,2'-azino-bis-3-ethyl benzthiazoline-6-sulfonic acid (ABTS$^{\bullet+}$) cation radical scavenging activity was determined according to the method of Re *et al.* (1999) [137]. The ABTS is a synthetic organic blue-green radical, which can be reduced in the presence of antioxidants, the radical cation ABTS$^{+\bullet}$ was produced by oxidation in the presence of potassium persulfate (**Figure. III. 4**). 7 mM of 2,2'-azino-bis (3-ethylbenzothiozolin-6 sulfonic acid (ABTS) was mixed with 2.45 mM of potassium persulfate ($K_2S_2O_8$) and incubated at room temperature in the dark for 16 hours to give a colored solution in green-blue. The absorbance of ABTS$^{\bullet+}$ solution was adjusted with methanol to 0.7 ± 0.02 at 734 nm.
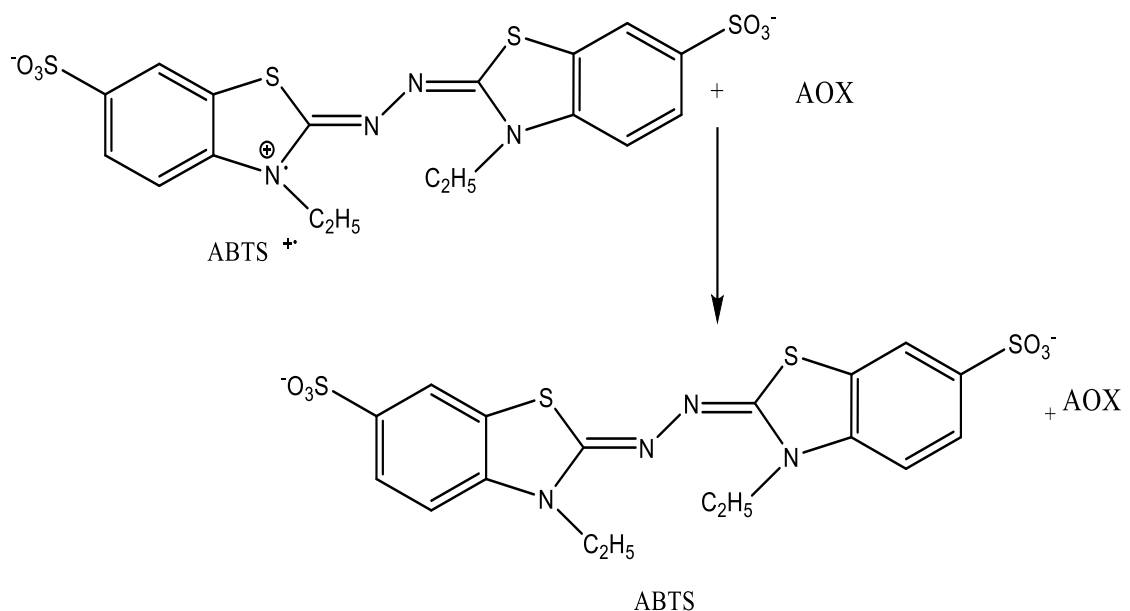
Figure. III. 4: Chemical reaction involved in the ABTS spectrophotometric test.

Procedure

The antioxidant activity of *A. aristata* extracts was evaluated by improving 2,2'-azino-bis-(3-ethylbenzothiazoline-6-sulfonic acid) (ABTS$^{\bullet+}$) radical cation scavenging capacity. 50 µl of different concentrations of extracts mixed with 950 µl solution of ABTS$^{\bullet+}$. The reaction was incubated at room temperature for 6 min in the dark and the absorbance was immediately measured at 734 nm. The negative control (ABTS solution with methanol) also the ascorbic acid was used as positive control. The inhibition percentage was calculated according to the formula of DPPH.

III.6.7. Superoxide anion radical scavenging activity

Principal

Pyrogallol (1,2,3-benzenetriol) has long been known to autoxidize rapidly, especially in alkaline solution. This method has been widely used to evaluate the antioxidant capacities of scavenging the superoxide anion radicals originating from the autoxidation of pyrogallol *in vitro* for some extracts and compounds. The auto-oxidation of pyrogallol will be used as a source of anions; this way depends on the inhibition of the autooxidation of catechol compounds such as adrenaline, 6-hydroxydopamine or pyrogallol (**Figure. III. 5**). Their anionic form like phenolate in an alkaline medium is oxidized and gives quinone accompanied by oxygen consumption [138].
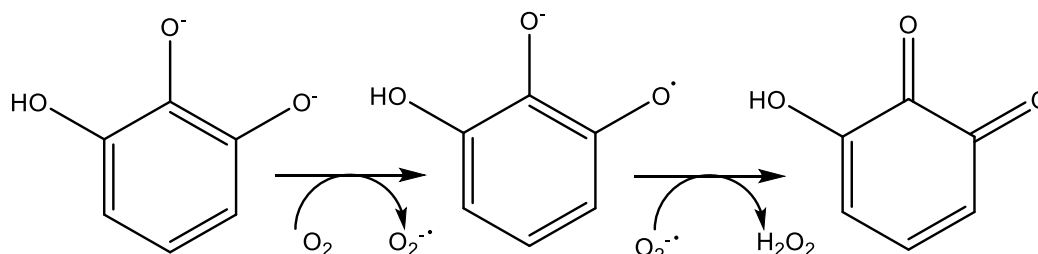
Figure. III. 5: Auto-oxidation of pyrogallol [138].

Procedure

Superoxide anion radical inhibition of *A. aristata* extracts was performed using a simple and rapid spectrophotometric method, described by Marklund S. and Marklund G. (1974) [139]. 0.5 mL of extracts (0.05 mg/mL) was added to the reaction solution containing 0.01 mL of 45 mM pyrogallol (prepared in the buffer solution pH= 8.2) and 4.5 mL of buffer at pH= 8.2. For a total of 5 minutes, the mixture was recoded every 30 seconds, the absorbance was measured at 320 nm [140]. The inhibition rate of pyrogallol auto-oxidation effect was calculated by the following equation:

$$I\% = \frac{(\Delta A_0 - \Delta A)}{\Delta A_0} \times 100\%$$

Where I% is the inhibition rate, **ΔA** and **ΔA₀** are the rates of autoxidation of pyrogallol in the presence and absence of extract respectively.

III.6.8. The Fe^{2+} chelating activity assay

Principal

The chelating effect of the extracts was determined according to the method cited by Zhao *et al*. (2006) [141]. Which is based on the inhibition of the formation of Fe^{2+}-ferrozine complex after treatment of samples with Fe^{2+} ions (**Figure. III. 6**).
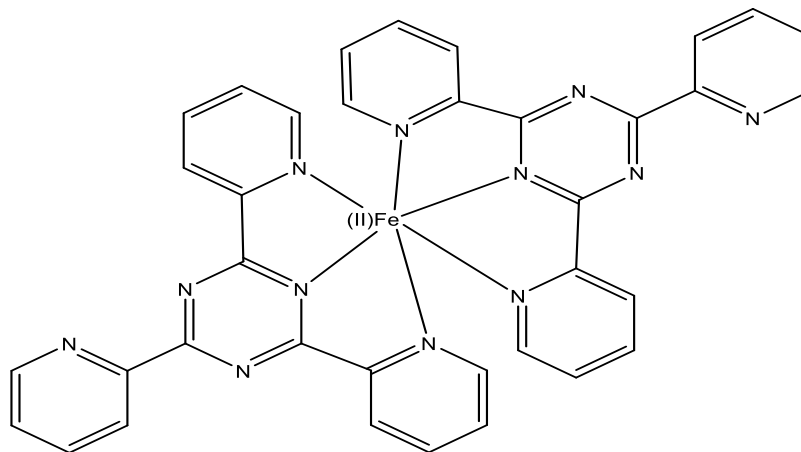
Figure. III. 6: Fe^{2+}-ferrozine complex [142].

Procedure

0.1 mL (5.8 mg/mL) of *A. aristata* extracts was mixed with 0.05 mL of $FeSO_4$ (2 mM). The mixture was incubated at room temperature for 5 min, the reaction was initiated by the addition of 0.1 mL ferrozine (5 mM), the total volume was adjusted to 2.5 mL with methanol. Then, the mixture was incubated at room temperature for 10 min. Absorbance of the solution was measured at 562 nm, the metal chelating activity was compared with the chelating activity of the synthetic metal chelator EDTA. The percentage of inhibition of ferrozine Fe^{2+} complex formation was calculated using the formula given below:

$$\textbf{Fe Chelating rate } (\%) = \left[\frac{A_0 - A_1}{A_0}\right] * 100$$

where A_0 was the absorbance of the control (blank, without extract) and A_1 was the absorbance in the presence of the extract.

III.7. Antidiabetic activity

Recently, it has been reported that numerous medicinal plants are beneficial in the treatment of diabetes and that they have been used empirically as antidiabetic treatment. These plants reduce hyperglycemia via increasing insulin secretion, inhibiting intestinal glucose absorption, or facilitating metabolites in insulin-dependent activities [143].

III.7.1. Diabetes mellitus

Diabetes mellitus is a multifaceted metabolic condition in which the fasting plasma glucose concentration is greater than 126 mg/dL or the blood glucose concentration is greater than 200 mg/dL at any time of the day [144].

Diabetes mellitus refers to a group of metabolic diseases with one common manifestation hyperglycemia. Chronic hyperglycemia is caused by inherited and/or acquired deficiency in production of insulin by the pancreas, or by the ineffectiveness of the insulin produced. It is caused by insufficient insulin hormone secretion, insufficient insulin target cell response, or a combination of these causes [143]. The more common types of diabetes are showing below:

III.7.1. 1. Type I diabetes

Type I diabetes mellitus (T1DM) is a chronic autoimmune illness characterized by elevated blood glucose levels (hyperglycemia) caused by insulin insufficiency due to the loss of pancreatic islet β-cells [145]. In type 1 diabetes, the destruction of pancreatic cells typically results in an absolute insulin deficit [146]. It is estimated at about 5–10% of total patients of T1DM [144].

III.7.1. 2. Type II diabetes

Type II diabetes mellitus (T2DM) is characterized by dysregulation of glucose, lipid, and protein metabolism and is caused by decreased insulin production, insulin resistance, or a combination of the two [147]. Approximately 346 million persons (90–95% of all patients) are estimated to have T2DM due to pancreatic β-cell dysfunction and/or enhanced insulin resistance with reduced glucose tolerance [144].

III.7.1. *In vitro* evaluation of α-amylase inhibitory power

Principal

The α-amylase inhibition test is carried out according to the method of Bernfeld (1955) with slight modifications using dinitrosalicylic (DNS) as a reagent [148]. The enzymatic activity of the *A. aristata* extracts is measured using starch as a substrate. The enzyme catalyzes the hydrolysis of this substrate, resulting in the release of maltose and other products (**Figure. III. 7**). This method is based on the quantification of reducing sugars (maltose equivalent) produced by α-amylase hydrolysis of starch.
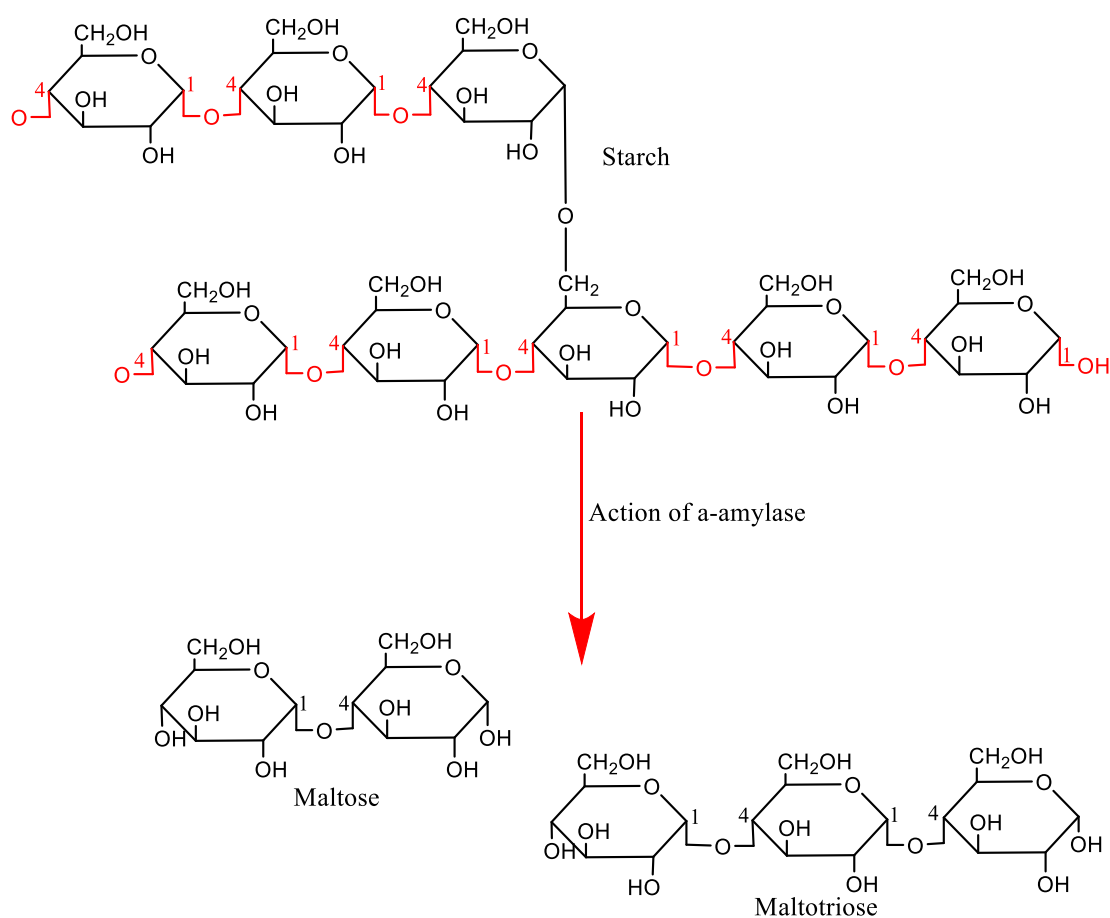
Figure. III. 7: Starch degradation product by α-amylase [149].

Procedure:

200 µL of sodium phosphate buffer saline (pH = 6.9) was mixed with 100 µL of soluble starch (1%) as substrate and 100 µL of each extract diluted at the same concentration (1 mg/mL) for comparison, while 100 µL of buffer was used instead of the extract for the blank sample. After thoroughly mixing, both sample and blank test tubes

were pre-incubated at 37 °C for 5 min. Then, the reaction was launched by the addition of 100 μL of α–amylase (E.C. 3.2.1.1 from *Aspergillus oryzae* 30U/mg; product code 101016460, purchased from Sigma Adrich) (13 units; one unit of enzyme activity is the enzyme amount required to release one micromole of maltose from starch per minute under assay conditions). After incubation at 37 °C for 5 min, the reaction was stopped by adding 1 mL of DNS solution. The reaction mixture was incubated at 100 °C for 5 min; after that, the tubes were cooled with tap water and after cooling, 4 mL of distilled water was added to the mixture. Enzyme activity was determined by measuring optical density proportionally to the quantity of the maltose equivalents released from starch at 530 nm. Different concentrations of acarbose (Acarbose is a drug used to treat type II diabetes) are used to plot the standard curve; the data were expressed relative to the value obtained with acarbose from the calibration curve.

The α-amylase inhibitory activity of the sample calculated using the following formula:

$$\textbf{I\% } (\boldsymbol{\alpha - \textbf{amylase inhibitory activity}}) = \frac{(A_0 - A_1)}{A_0} \times 100$$

Where:

A$_0$: Absorbance of the control and **A$_1$:** Absorbance of sample.

The Acarbose Equivalent Inhibitory Capacity calculated using the following formula:

$$\textbf{AEIC} = \frac{I\% * nf * v}{K * m}$$

I %: α-amylase inhibitory activity. **K:** The slope of the Acarbose curve.

V: volume of solvent. **nf:** dilution number. **m:** weight of extract.

III.8. Results and discussion

III.8.1. Phytochemical screening results

The extracts of medicinal plants are a complex mixture of different types of chemical substances, which are primarily responsible for their pharmacological effects. The phytochemical screening of these substances in plants is essential to determine their medical value. In order to determine the presence of numerous phytoconstituents with potential medical uses, the crude extract of *A. aristata* was subjected to preliminary phytochemical screening using traditional techniques.

The results of phytochemical screening of *A. aristata* showed the presence of different types of compounds such as flavonoids, steroids, tannins, saponins, terpenoids, reducing compounds, triterpenoids, free quinones and cardenolides (**Table. III. 1**).

Table. III. 1: The results of phytochemical screening.

Test	Results
Flavonoids	+
Steroids	+
Tannins	+
Saponins	+
Terpenoids	+
Reducing compounds	+
Triterpenoids	+
Free Quinone	+
Cardenolides	+

Research in this subject has revealed the presence of many different phytochemical substances, which vary by species, genus, and family, making phytochemical screening the first significant test for taking clear information on the composition of plant extracts.

Our investigation focused on the plant *A. aristata* as a result of the existence of these chemicals, which provide strong evidence for the plant's pharmacological significance. For this reason, we chose a working method to extract these compounds. The existence of a modest or big amount might be determined by the degree of coloring or precipitation that resulted. By comparing our results with those of the plants of *Atractylis* genus, a few numbers of *Atractylis* species have been studied for their phytochemical composition. Therefore, the phytochemical investigations of *Atractylis* plants are very scanty, amongst these plants *A. flava* [52, 55], *A. carduus* [54], *A. cancellata* [50], *A. serratuloides* [51], *A. gummifera* [59]

and *A. humilis* [53], from which flavonoids, diterpenes, triterpenes, alkaloids, and osidic compounds.

III.8.2. Extracts yields and concentrations

Solvent extractions with increasingly more polar allow for polarity-based separation of components. As well as the residual water phase and the crude extract, three organic phases (dichloromethane, ethyl acetate, and n-butanol) were obtained. These phases are dried out and weighed before being restored in methanol or water. The yields of extracts are shown in **Table. III. 2**. It should be highlighted that the yields of plant extracts change from one solvent to another based on the degree of solubility of the chemicals in the solvent.

Table. III. 2: Yields and concentration of extracts.

Extract	Yield %
Crude	58.28
Dichloromethane	0.36
Ethyl acetate	0.11
n-Butanol	1.85
Residual water	8.86

The crude extract showed the highest value of yield 58.28% followed by the residual water extract with value of 8.86%. While the Ethyl acetate extract showed the less value of yield which equal to 0.11%. The use of water and the organic solvent methanol in combination may enhance the extraction of compounds that are soluble in water and/or organic solvent. This may be the reason why the crude extract yield is higher than the yields of other extracts [150].

The high yield of n-butanol can be attributed to the abundance of polar molecules in this plant. Due to the highly polar chemicals that are soluble in water, the residual water phase had the highest yield, this extract contains all substances that are insoluble in other solvents. The ethyl acetate extract shows the less yield value followed by dichloromethane. The results show that the extracts yields increase with increasing polarity of the solvent used in extraction, except for the ethyl acetate extract because the extraction process was done only one time compared to other solvents. The solubility of phenolic compounds in different polarity solvents is also determined by their structural differences. Therefore, the type of extraction solvent and the isolation processes can have a significant effect on the yield of polyphenols extracted from plant material [151].

III.8.3. Quantification of total phenol

Following the identical steps taken to establish the calibration curve (**Figure. III. 8**), replacing gallic acid with the extracts, we were able to determine the total phenol content of the various extracts. The amount of total phenols in the extracts is expressed as gallic acid equivalent in milligrams per 1g of dry plant material (mg/g). The results obtained are presented in the **Table. III. 3**.
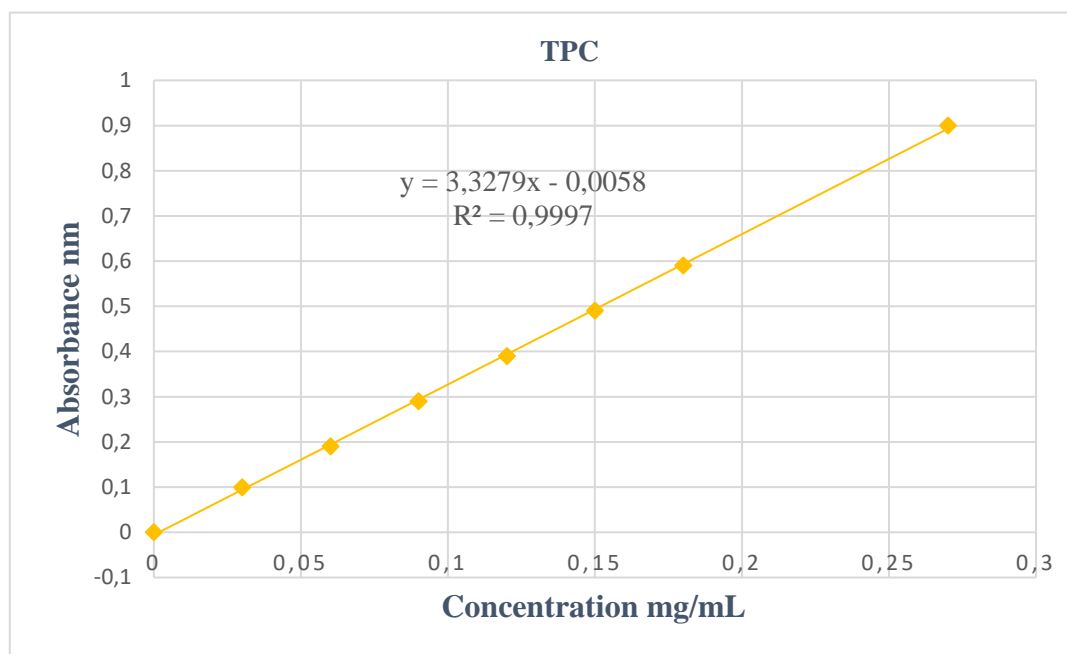
Figure. III. 8: Calibration curve of gallic acid for quantification of total phenol.

The results showed a wide values range of TPC varied from 0.023 ± 0.01 to 3.544 ± 0.738 mg GAE/g of dry weight material. The results for the different extracts are classified in the following descending order: residual water extract > n-butanol extract > dichloromethane extract > ethyl acetate extract > crude extract.

Table. III. 3: The results of total phenolic quantification of extracts on mg GAE/g DW.

Extract	TPC mg GAE/g DW
Crude	0.023 ±0.01
Dichloromethane	1.126 ±0.135
Ethyl acetate	0.900 ±0.262
n-Butanol	2.443 ±1.007
Residual water	3.544 ±0.738
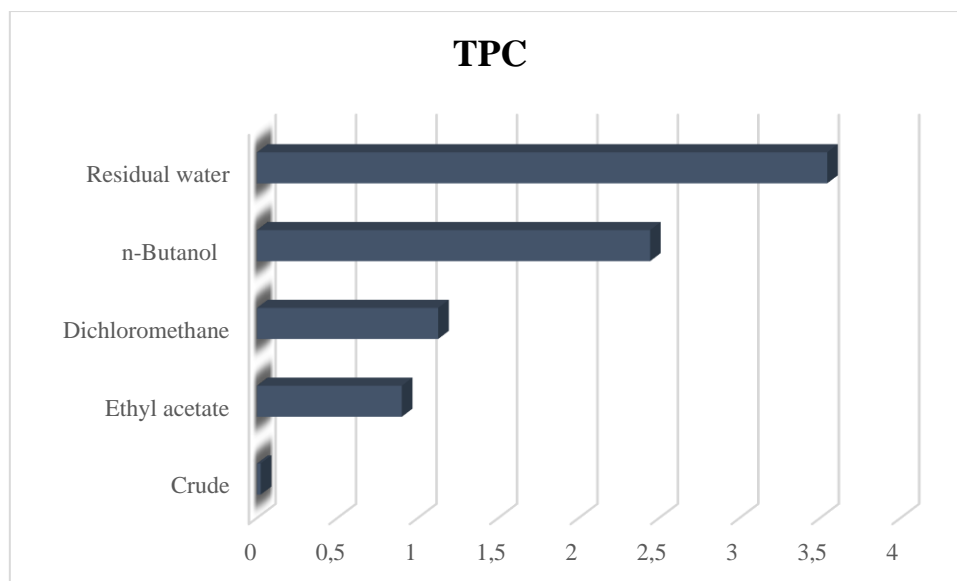
Figure. III. 9 : Comparison of total phenolic content between extracts.

As shown in **Figure. III. 9** and **Table. III. 3**, remarkable differences in TPC amounts in extracts of *A. aristata* were observed, these results show that the residual water and butanol extracts are richness in polyphenols. Where, the highest content is observed in the residual water fraction, it is of the order of 3.544 ±0.738 mg GAE / g, followed by the n-butanol fraction with a content of 2.443 ±1.007 mg GAE / g. The total phenol content of the crude extract of *A. aristata* was 0.023 ± 0.01 mg GAE / g. According to our results, total phenol contents were small compared to the results of species of the genus *Atractylis* varied from 8.36 ± 0.06 GAE / g DW to 17 mg GAE / g DW [49, 152].

By comparing these results, it can be concluded that the crude extract of *A. aristata* has a low content of total phenols. In a study conducted by Fukushima *et al*. (2009), showing that the determination of total polyphenols by the Folin-Ciocalteu test is a non-selective assay with respect to polyphenols, because it is implied that all the reducing molecules, such as reducing saccharides or vitamin C [153]. Methodological difference may partially cause differences in the analytical values, as well as the difference between species, source and seasonality [154].

III.8.4. Quantification of total flavonoid

The quantification of total flavonoids content of extracts was made by adapting the same procedure used for the establishment of the calibration curve (**Figure. III. 10**), replacing quercetin by the extracts.
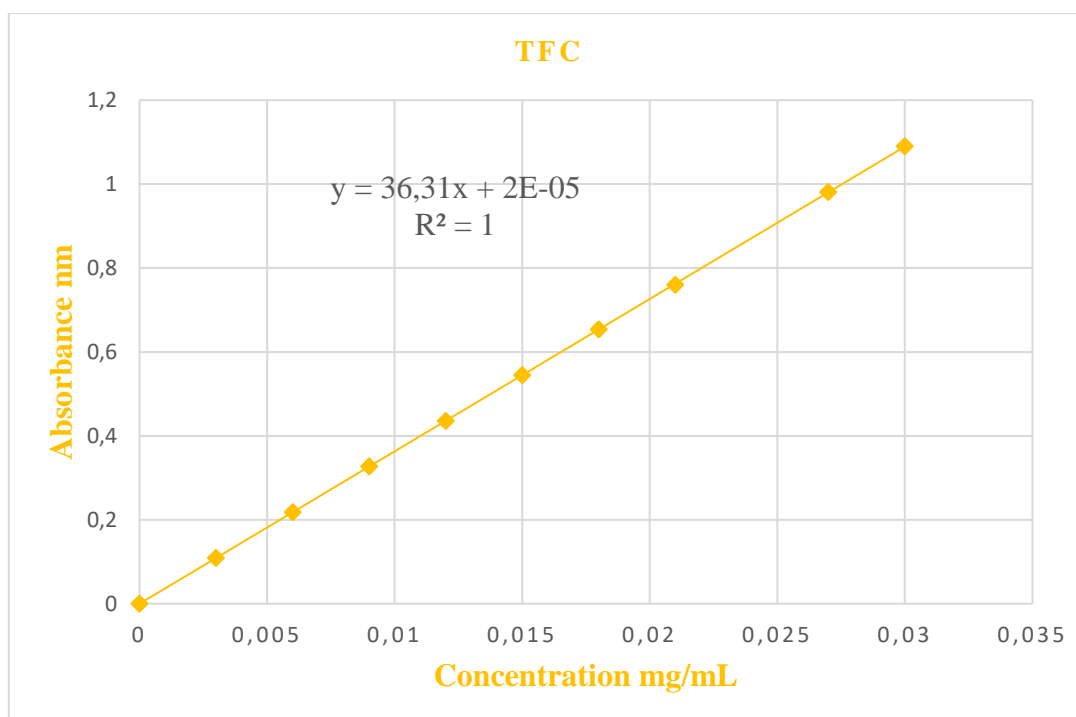
Figure. III. 10: Calibration curve of quercetin for quantification of total flavonoid.

The amount of total flavonoids in the extracts is expressed as equivalent quercetin in milligrams per 1g of dry plant material (mg/g). The results obtained are presented in the **Table. III. 4**.

Table. III. 4: The results of total flavonoid quantification of extracts on mg QE ∕ g DW.

Extract	TFC mg QE ∕ g DW
Crude	0.410 ±0.0004
Dichloromethane	0.380 ±0.060
Ethyl acetate	0.012 ±0.0050
n-Butanol	2.554 ±0.090
Residual water	3.104 ±0.6760

The flavonoids concentration of *A. aristata* extracts was determined by using method based on complex formation between phenolic compounds and aluminum trichloride ($AlCl_3$). The results showed that the concentrations values of the crude, dichloromethane, ethyl acetate, n-butanol and residual water extracts of *A. aristata* aerial parts, are 0.410 ±0.0004; 0.380 ±0.060; 0.012 ±0.0050; 2.554 ±0.090 and 3.104 ± 0.6760 mg QE/g of dry weight material respectively.
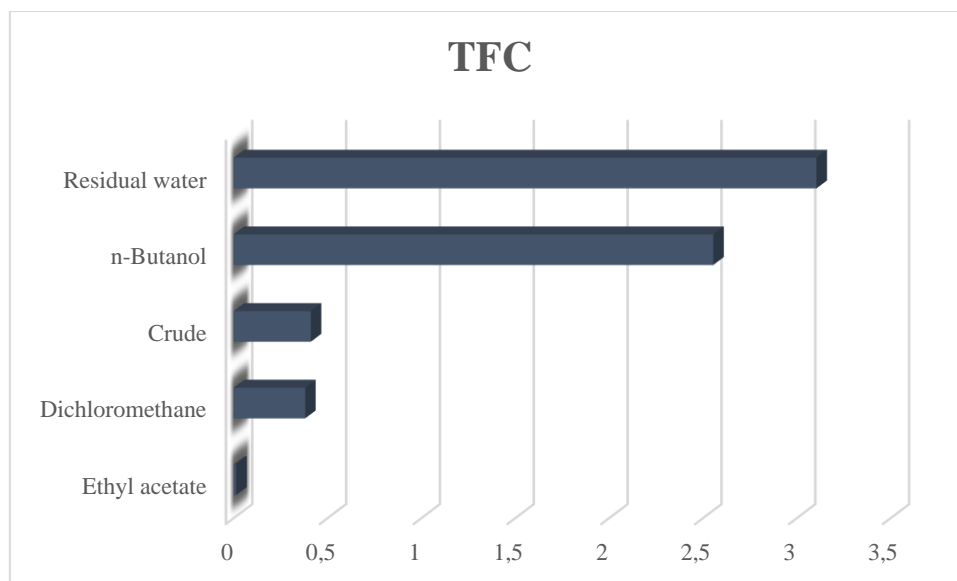
Figure. III. 11: Comparison of total flavonoids content between extracts.

As shown in the **Table. III. 4** and in the **Figure. III. 11**, high differences in TFC amounts in extracts of *A. aristata* were observed. These results show that the residual water and n-butanol extracts have the highest flavonoid content, where the highest content is observed in the residual water fraction, it is of the order of 3.104 ± 0.676 mg QE / g, followed by the n-butanol fraction with a content of 2.554 ± 0.090 mg QE /g. The ethyl acetate fraction exhibited the less value of TFC; it is of the order 0.012 ± 0.0050 mg QE/ g.

These results could be justified by the investigation into flavonoids compounds from *Atractylis* genus [51, 55], that confirm well the presence of flavonoid glycosides, which explains the richness of residual water and n-butanol extracts on flavonoids content. According to our results, flavonoid contents from *A. aristata* extracts are comparable to those of the similar genus *Atractylis gummifera* [152] and *Atractylis babeli* [49]. The results explained by the presence of similar types of flavonoid compositions with the plants of *Atractylis* genus.

III.8.5. Quantification of condensed tannins

The quantification of condensed tannins content of extracts was made by adapting the same procedure used for the establishment of the calibration curve (**Figure. III. 12**), replacing catechin by the extracts.

The chart shows a CTC calibration curve with the equation $y = 4{,}3767x - 0{,}0004$ and $R^2 = 1$, plotting Absorbance nm against Concentration mg/mL.
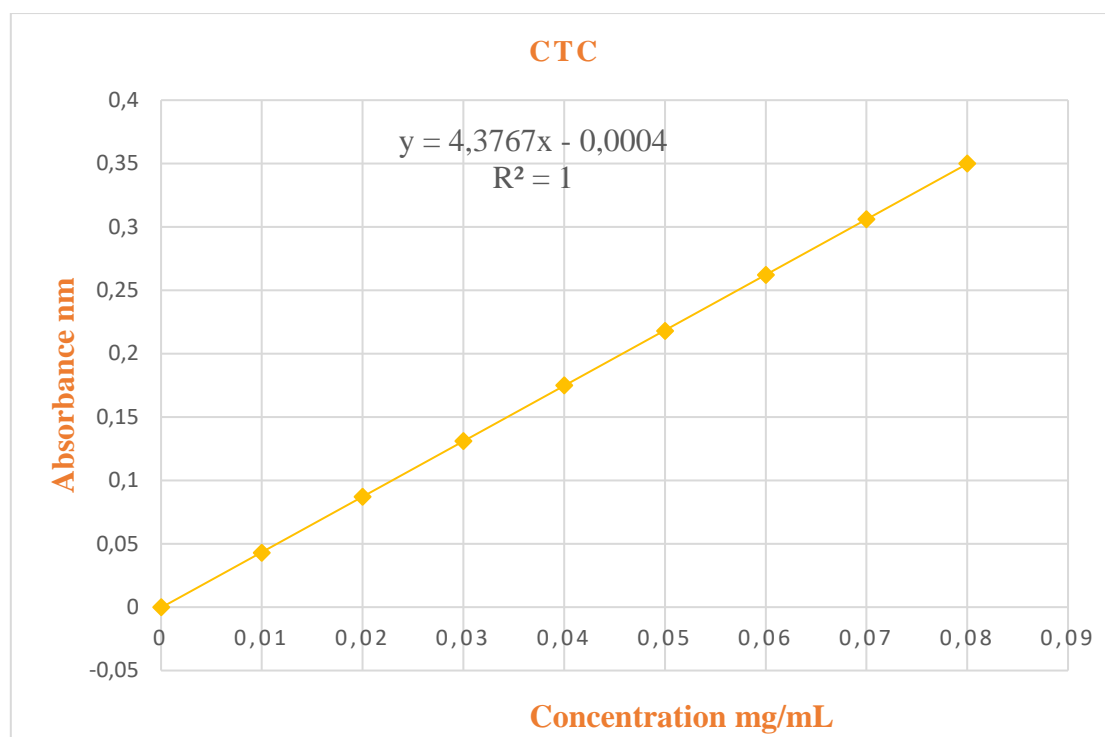
Figure. III. 12: Catechin calibration curve for condensed tannins quantification.

The amount of condensed tannins in the extracts is expressed as equivalent catechin in milligrams per 1g of dry plant material (mg / g). The results obtained are presented in the **Table. III. 5**.

Table. III. 5: The results of condensed tannins quantification of extracts on mg CE⁄g DW.

Extract	CTC mg CE⁄g DW
Crude	0.645 ±0.016
Dichloromethane	0.396±0.047
Ethyl acetate	0.683±0.199
n-Butanol	1.856±0.765
Residual water	2.692±0.561

The results of concentration values of condensed tannins content of *A. aristata* extracts were varied from 0.396 ± 0.047 to 2.692 ± 0.561 mg CE/g of dry material. By comparing CTC for the different extracts is classified in the following descending order: residual water extract > n-butanol extract > ethyl acetate extract >dichloromethane extract > crude extract.
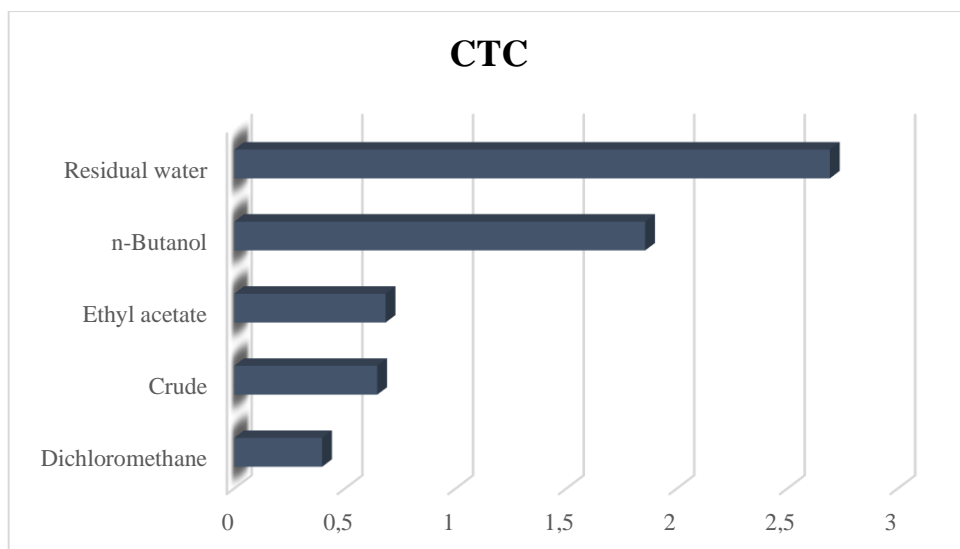
Figure. III. 13: Comparison of condensed tannins content between extracts.

As shown in the **Table. III. 5** and in the **Figure. III. 13**, small differences in CTC amounts in extracts of *A. aristata* were observed. These results show that the residual water and n-butanol extracts are the richest in condensed tannins, where the highest content is observed in the residual water fraction, it is of the order of 2.692 ± 0.561 mg CE / g DW, followed by the n-butanol fraction with a content of 1.856 ± 0.765 mg CE /g DW. The dichloromethane fraction exhibited the less value of CTC; it is of the order 0.396 ± 0.047 mg CE/ g DW, while the crude and the ethyl acetate extracts showed very similar values for the content of condensed tannins, which is equal to 0.6 mg CE/ g DW.

Tannins are polar phenolic compounds soluble in water, which explains the richness of the n-butanol and residual water phases in condensed tannins, our results showed slightly higher amounts of condensed tannin contents on the crude extract (0.645 ± 0.016 mg CE/ g DW), in comparison of the same extract with the other obtained from *Atractylis* genus (0.41 mg CE/g DW) from *A. babeli* [49], and also showed slightly lower amounts (1.7 mg CE/g DW) from *A. gummifera* [152].

Through the quantification of total phenolic, total flavonoids and condensed tannins content, we could be deemed that the crude extract of *Atractylis aristata* gave a moderate amount of phenolic compounds. When compared to others south Sahara plants collected in Tamanrasset from Asteraceae family, that have been collected during the flowering stage, such as *Varthemia sericea* (TPC: 0.283 ± 0.58 GAE mg / g DW; TCF: 0.022 ± 1.7 QE mg / g DW) [155], and *Asteriscus graveolens* (TPC: 0.107 ± 3.01 GAE mg / g DW; TFC: $0.114 \pm$

1.9; QE mg / g DW; TCT: 0.021 ±8.09 CE mg / g DW) [156]. The differences of the results of plants in the similar genus explained by the hard environmental conditions such as hot temperatures, dryness, and short growing season may be lead to varied accumulation of secondary metabolites in Saharan plants that help them cope with such conditions [157]. The amount of phenolic depends on several factors such as temperature, UV-light, nutrition available to the plant, and genetic factors [158].

III.8.6. Liquid chromatography-Ultra violet (HPLC-UV) analysis

The results of HPLC-UV analysis of *Atractylis aristata* extracts are presented in the **Table. III. 6**.

Table. III. 6: The results of HPLC-UV analysis of *Atractylis aristata* extracts.

Bioactive compounds	Extracts				
	Crude	Dichlorom ethane	Ethyl acetate	n-Butanol	Residual water
	RT	RT	RT	RT	RT
Acetylsalicylic acid	17.686	17.662	17.654	17.673	17.682
Ascorbic acid	2.501	2.476	2.472	2.465	ND
Caffeic acid	ND	10.976	10.859	ND	ND
Chlorogenic acid	ND	ND	8.795	ND	ND
Gallic acid	3.960	3.557	3.765	3.949	ND
Para coumaric acid	14.433	ND	14.259	ND	ND
Caffeine	ND	10.111	9.547	ND	ND
Catechin	ND	ND	9.189	ND	ND
Epicatechin	ND	ND	ND	ND	ND
Pyrogallol	4.727	ND	ND	ND	5.240
Quercetin	21.312	21.295	21.283	21.298	21.308
Rutin	ND	13.289	13.304	ND	ND
Vitamin B1	ND	1.767	1.774	ND	ND
Vitamin B6	ND	ND	ND	ND	ND
Vitamin D3	ND	ND	ND	ND	ND
Vanillin	14.433	14.566	14.454	14.423	14.435

RT: Retention Time.   **ND**: Not Detected.

The chromatographic profiles of the standards used for the comparison are shown in the **Figure. III. 14**.
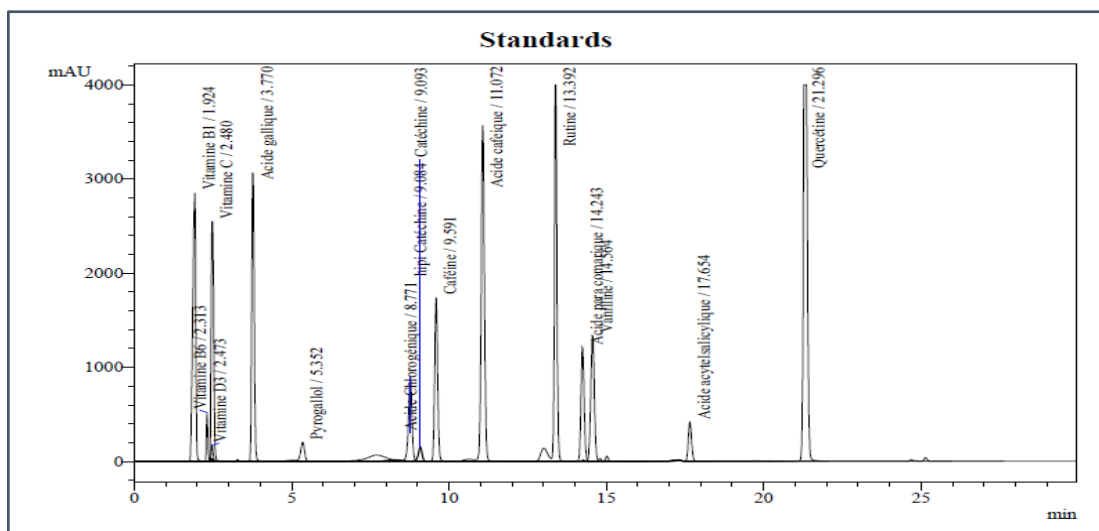
Figure. III. 14: HPLC profile of standards.

In HPLC, some characteristics of the isolated polyphenols can be identified using the detection system, depending on the chemical structure of the molecule. UV-Vis absorption spectra in parallel with retention time can aid in the identification of polyphenols, with the use of authenticated standards [159]. The analysis of the chromatograms obtained by *A. aristata* extracts (**Figure. III. 15**) reveals the richness of our extracts in different types of bioactive compounds. Among the peaks recorded on the chromatographic profile of the extracts, twelve compounds are identified in the different extracts by comparison of their retention time with those of the different standards. The analysis of UV chromatograms revealed the presence of three bioactive compounds in all the extracts, which were: acetylsalicylic acid, quercetin and vanillin. Also, the UV chromatograms led to detection of gallic acid in dichloromethane, ethyl acetate and butanol extracts and the detection of caffeic acid and rutin in dichloromethane and ethyl acetate extracts (**Table. III. 6**).

According to other studies, these compounds have been identified as the major phenolic chemicals in several Asteraceae plants, with different biological activities [160]. In general, other not identified peaks at retention time 17.188 min and 17.431 min, are present in ethyl acetate extract (figure 2B **Figure. III. 15**), and three not identified peaks at retention times 16.971 min, 17.192 min and 17.436 min are detected

in dichloromethane extract (figure 2A **Figure. III. 15**), the chemicals in the extracts were not all detected due to inadequate standards, these not identified peaks demonstrated the richness of the extracts by different bioactive compounds.
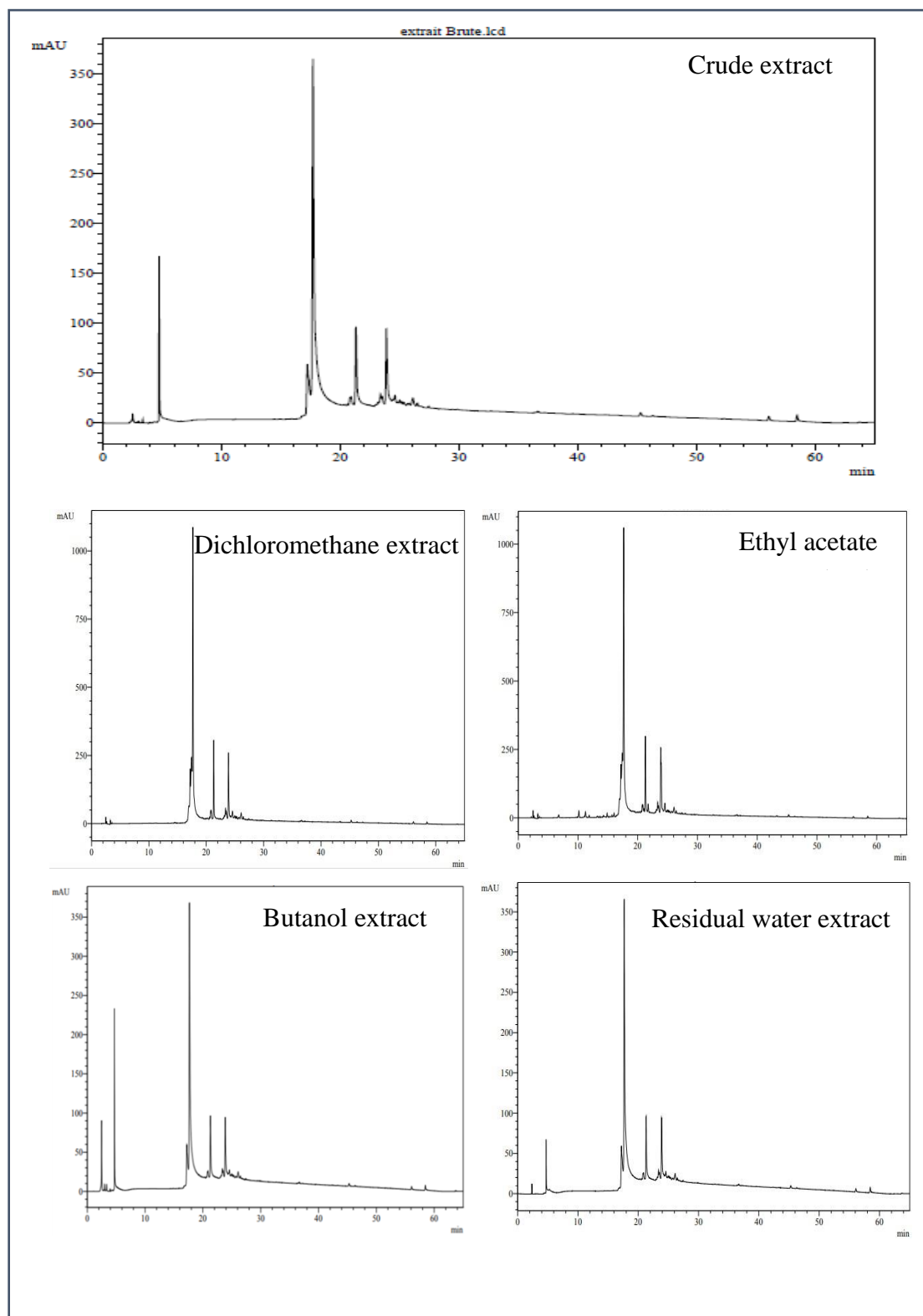
Figure. III. 15: HPLC chromatograms of different extracts.

The chemical structures of the main compounds detected in our extracts by the HPLC analysis are represented in the **Figure. III. 16**.

Gallic acid

Caffeic acid

Vanillin

Rutin

Quercetin

Acetylsalicylic acid
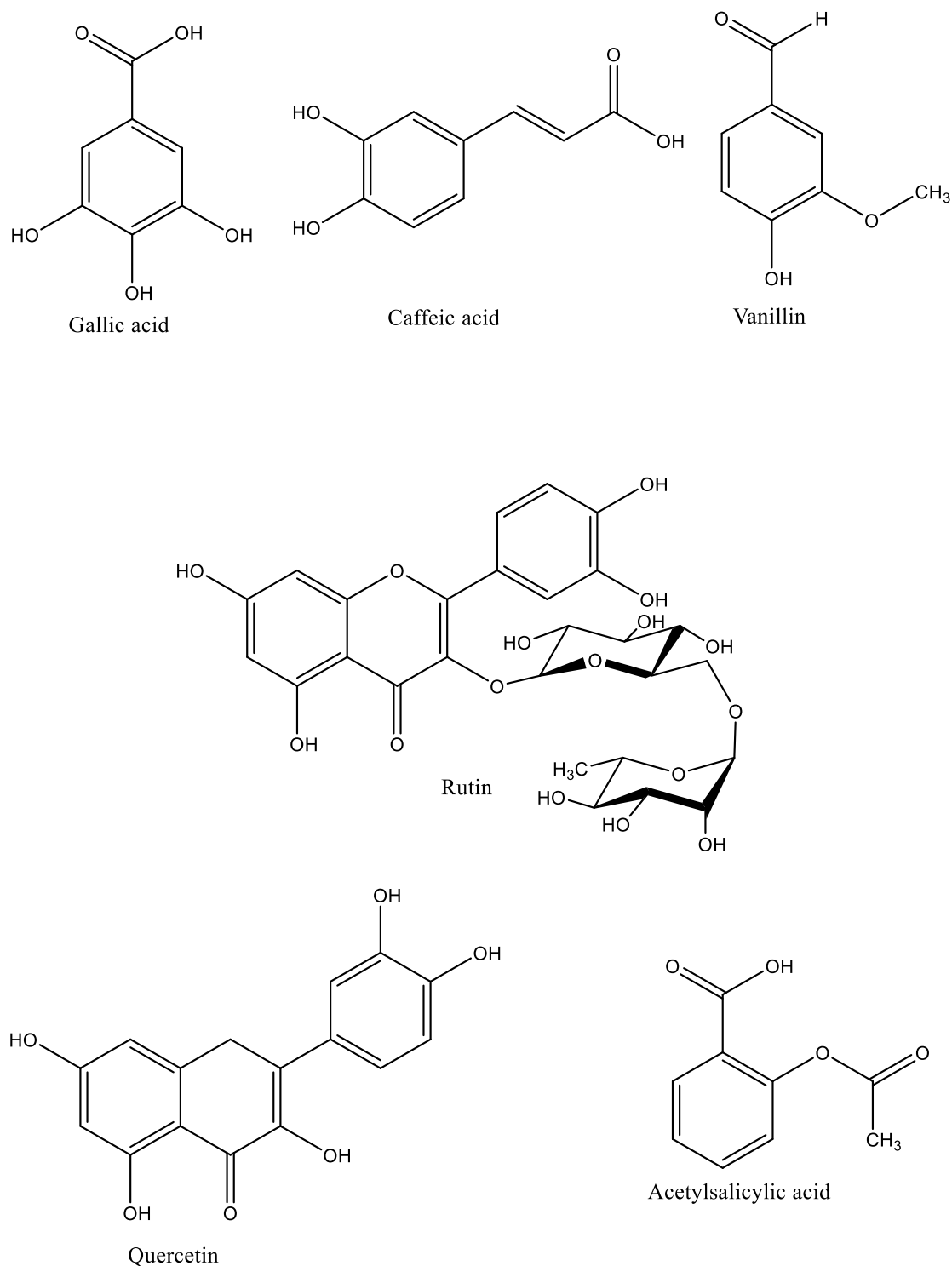
Figure. III. 16: Structures of the main compounds detected in the extracts by HPLC analysis.

III.8.7. Antioxidant activity

III.8.7. 1. Reducing power assay

Antioxidant activity is measured using the term AEAC (Ascorbic Acid Equivalent Antioxidant Capacity). The different extracts are treated in the same way as those of standard ascorbic acid solutions (**Figure. III. 17**). We have plotted the curves representing the variation in reducing capacity expressed in absorbance as a function of the inverse of the number of dilutions of standard BHT (**Figure. III. 18**) and extracts (**Figure. III. 19**). The results are expressed by the AEAC values, this value is proportional to antioxidant activity, i.e., the higher AEAC value, has the higher antioxidant activity. The test results of reducing capacity are summarized in the **Table. III. 7**.

Ascorbic acid

$$y = 0{,}4205x - 0{,}0416$$
$$R^2 = 0{,}9913$$

Absorbance nm

Concentration mg/mL
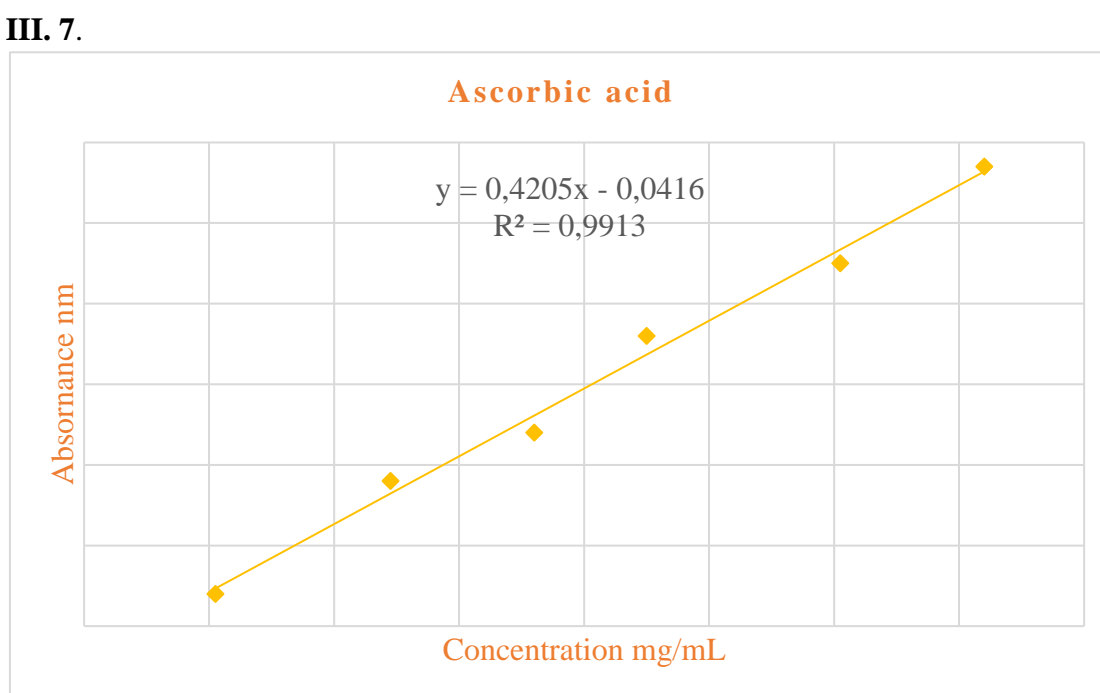
Figure. III. 17: Ascorbic acid calibration curve for reducing power assay.

The reducing Mo(VI) to Mo(V) of different extracts of *A. aristata* varied from 49.30 ± 1.405 to 219.34 ± 6.496 mM. The highest activity is found in the Residual water fraction whereas the lowest activity is recorded in the ethyl acetate fraction. The reducing power of extracts was expressed as AEAC, the more valuable it was, the higher the antioxidant capacity. The synthetic antioxidant BHT (3,5-di-tertbutyl-4hydroxytoluene) is widely used in antioxidant capacity as standards. These synthetic antioxidants are used as a positive control in order to compare the activities of our extracts with those of the reference antioxidants.

Table. III. 7: Reduction Mo(VI) to Mo(V) of different extracts.

Extract	Total antioxidant capacity mM
Crude	91.15 ± 3.921
Dichloromethane	128.48 ± 5.421
Ethyl acetate	49.30 ± 1.405
Butanol	106.62 ± 3.786
Residual water	219.34 ± 6.496
BHT	11.10 ± 7.55

All the extracts showed power antioxidant capacity, higher than the standard used BHT. The residual water extract exhibited the highest value of antioxidant activity, which is 19 times higher than BHT, followed by the dichloromethane fraction which is 11.5 times higher than BHT. The lowest value of antioxidant activity corresponds to the ethyl acetate fraction, which is 4 times higher than BHT.
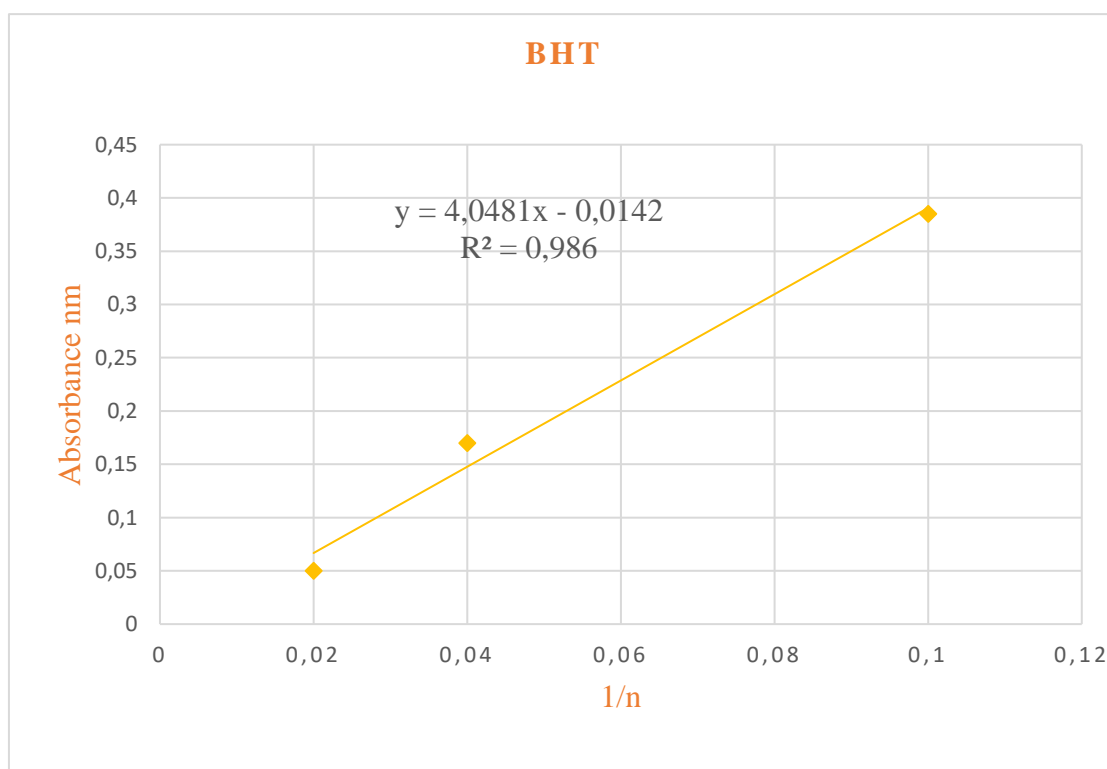
Figure. III. 18: Curves representing the total antioxidant activity of the standard BHT.
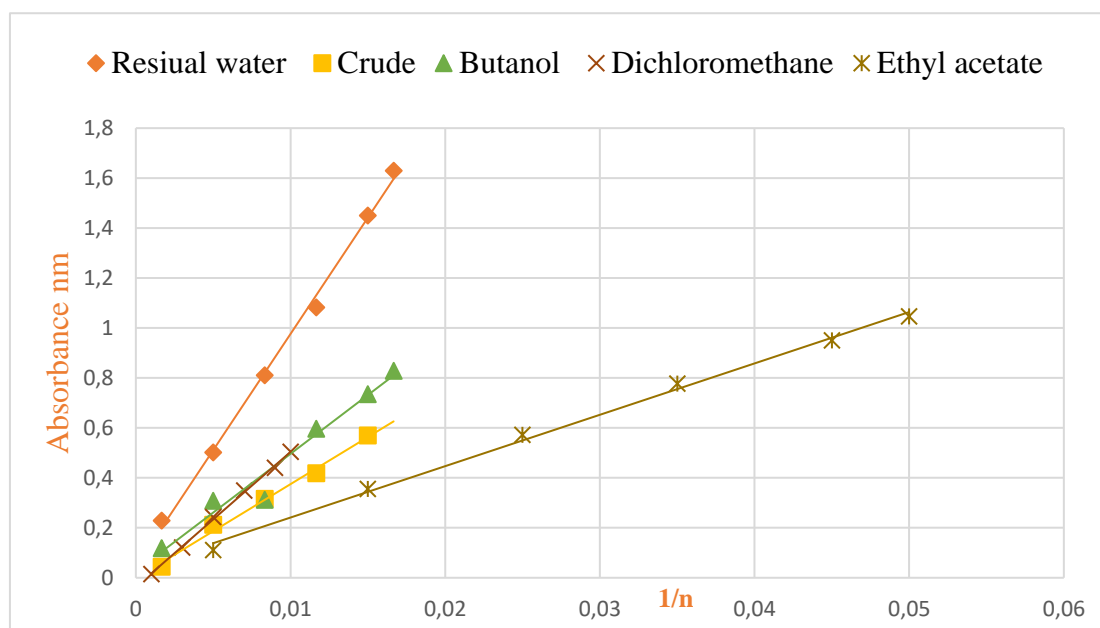
Figure. III. 19: Curves representing the reduction Mo(VI) to Mo(V) of the various extracts.

The AEAC values of the different extracts of *A. aristata* are classified in the following descending order: residual water fraction> dichloromethane fraction> butanol fraction> ethyl acetate fraction. Also, the correlation between AEAC and the phenolic content was $R^2 = 0.604$, with flavonoids was $R^2 = 0.560$ and with condensed tannins was $R^2 = 0.526$ (**Table. III. 11**). This allows us to conclude that the capacity of AEAC is mainly due to the 60.4% of total phenol content, 56.0% of flavonoids, and 52.6% of condensed tannins. This may confirmed with previous research, which showing that the phenolic compounds play an important role as a reducing agent [161].

III.8.7. 2. Free radicals DPPH and ABTS scavenging activity

The free radical scavenging activity of the different extracts was estimated using two free radicals DPPH and ABTS tests. We have plotted the curves representing the variation in radical scavenging expressed in inhibition as a function of the concentration. The results are expressed by the IC_{50} value, this value is inversely proportional to the antioxidant activity, i.e., the smaller IC_{50} value, has the higher antioxidant activity.

All the extracts exhibited high antiradical activity against DPPH and ABTS free radicals, the activity differed between the extracts, and we note that the extracts were

in the same order in both methods. This can be explained by the fact that the efficiency, whether related to quantity or quality, if the reaction mechanics are the same, the extracts are in the same order despite the different values between the two methods. There are remarkable correlations between the two methods of antioxidant activity (DPPH and ABTS) R^2=0.96 **Table. III. 11**, these correlations attribute to the similar mechanism of action of antioxidant compounds in the assay followed.

III.8.7. 3. 1,1 diphenyl-2-picrylhydrazyl (DPPH) assay

The different extracts are treated in the same way as those of standards ascorbic acid and BHT solutions (**Figure. III. 20**). We have used tow known antioxidant compounds, natural standard as ascorbic acid and synthetic as BHT, the curves representing the variation in radical scavenging of extracts (**Figure. III. 21**) were plotted. The IC_{50} values of the extracts of *A. aristata* as well as the standards are summarized in the **Table. III. 8**.
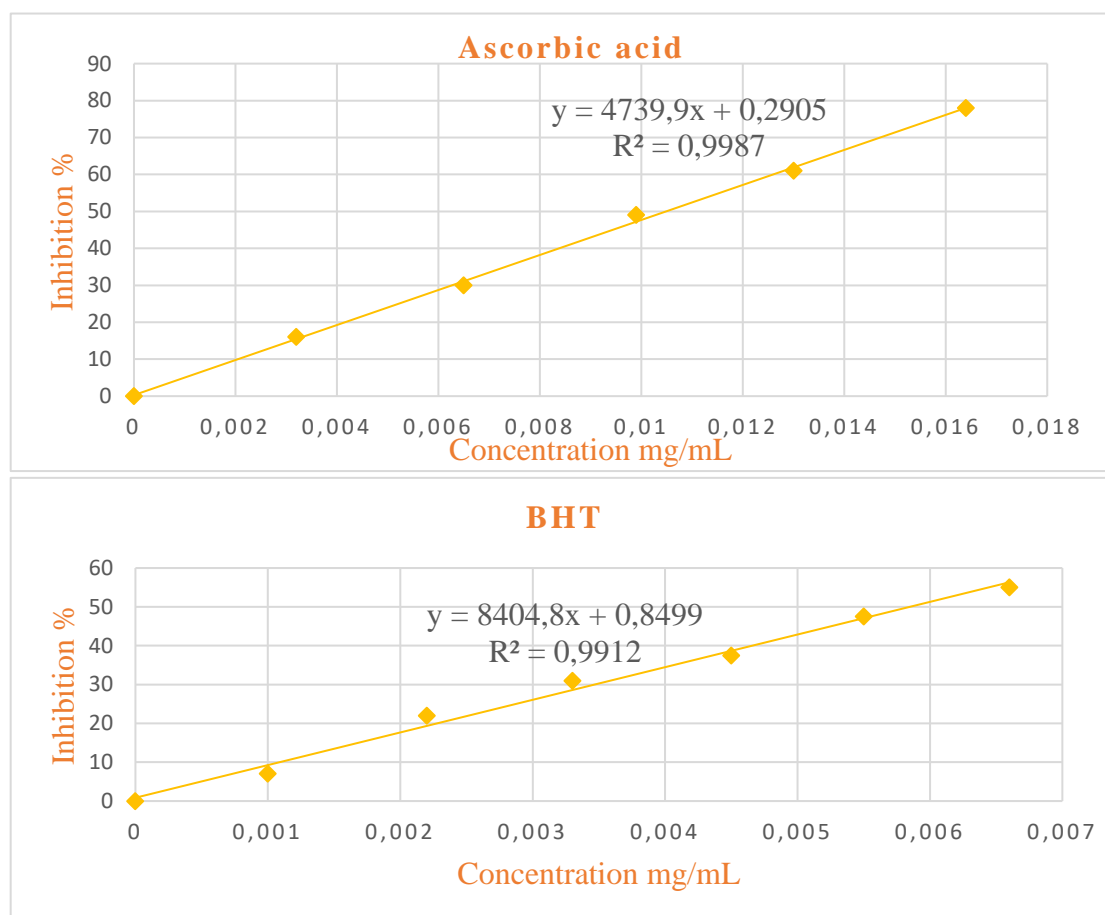
Figure. III. 20: Curves representing the inhibition percentage of DPPH free radical of the standards.
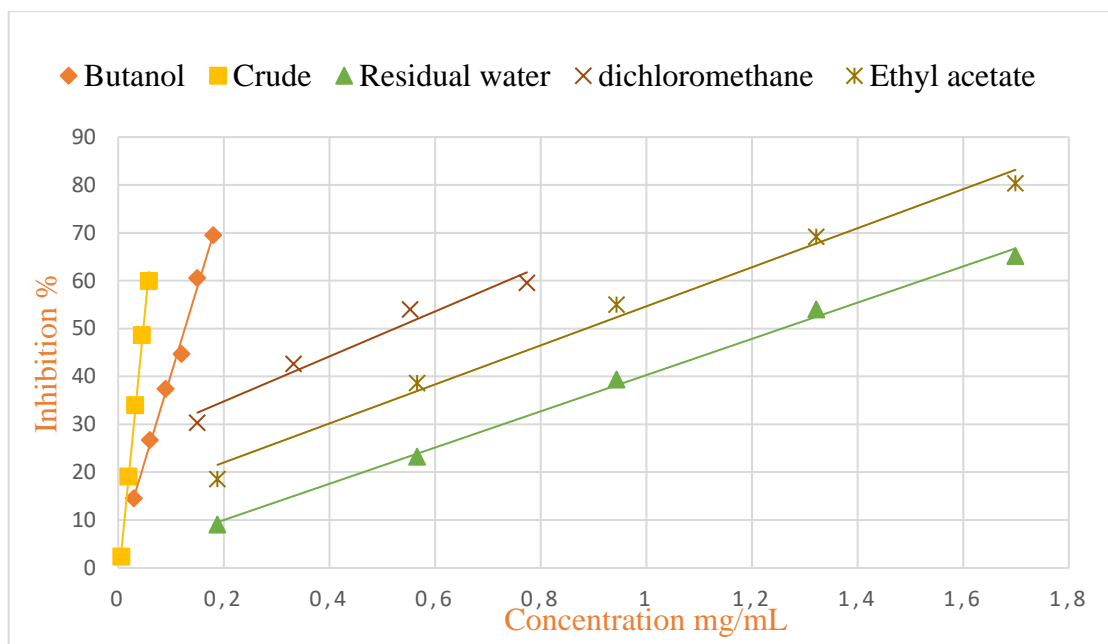
Figure. III. 21: Curves representing the inhibition percentage of DPPH free radical of the various extracts.

III.8.7. 4. 2,2'-azino-bis-3-ethyl benzthiazoline-6-sulfonic acid (ABTS) assay

The different extracts are treated in the same way as standard BHT solutions (**Figure. III. 22**). The curves representing the variation in radical scavenging of extracts (**Figure. III. 23**) were plotted. The IC_{50} values of the extracts of *A. aristata* as well as the standards are summarized in the **Table. III. 8**.
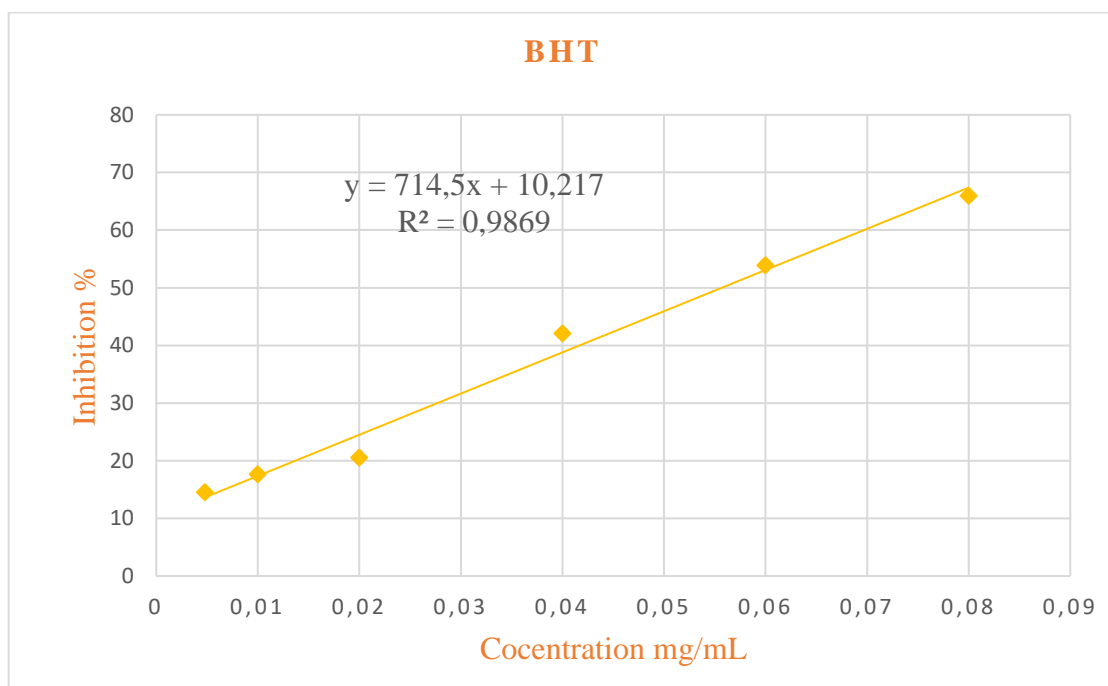
Figure. III. 22: Curves representing the inhibition percentage of ABTS free radical of the standard.
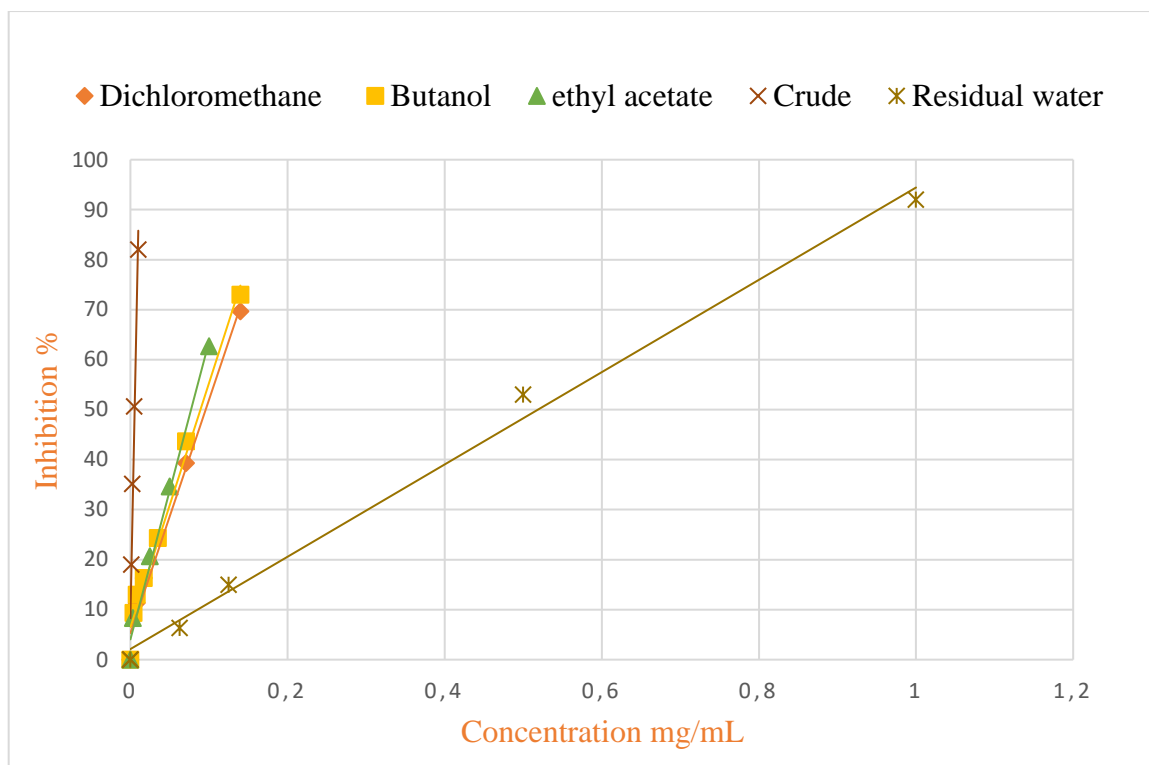
Figure. III. 23: Curves representing the reducing capacity of ABTS free radical of the various extracts.

Table. III. 8: The IC_{50} values of *A. aristata* extracts of DPPH and ABTS free radical.

Extract	ABTS IC_{50} mg∕mL	DPPH IC_{50} mg∕mL
Crude	$0.005 \pm 5.77 \times 10^{-5}$	0.040 ± 0.003
Dichloromethane	0.094 ± 0.002	0.364 ± 0.117
Ethyl acetate	0.077 ± 0.003	0.097 ± 0.003
Butanol	0.088 ± 0.002	0.124 ± 0.005
Residual water	0.515 ± 0.017	1.256 ± 0.013
Ascorbic acid	0.057 ± 0.012	0.009 ± 0.0005
BHT	/	0.004 ± 0.0004

All the extracts demonstrated high antiradical activity towards the stable radicals DPPH and ABTS. The IC_{50} values of the different extracts of *A. aristata* vary between 0.040 ± 0.003 and 1.256 ± 0.013 mg∕mL against the free radical DPPH and vary between $0.005 \pm 5.77 \times 10^{-5}$ and 0.515 ± 0.017 mg∕mL against the free radical ABTS. As we mentioned before the lowest IC_{50} value corresponding the higher antiradical activity.

The results achieved are higher than those found by Melakhessou *et al.* (2018), in different extracts of *A. flava* [10]. However, our results appeared to be more closely related to Bouabid *et al.* (2020) findings in aqueous extract of *A. gummifera* [162].

Nevertheless, the results of the antioxidant activity obtained by the ABTS free radical of the chloroformic extract of the plant *A. gummifera* shows high IC_{50} values compared with results obtained in our study. While, our results shows that crude extract has IC_{50} values more higher than the methanolic extract of *A. gummifera* [162]. The differences in IC_{50} values between plants of the same genus are due to several factors, among them the flowering time, picking time, temperature, UV-light and nutrition available to the plant.

In our study, the highest antioxidant activity against the both DPPH and ABTS free radicals was achieved by the crude extract and the lowest was recorded on the residual water extract. The IC_{50} values are classified in the same ascending order: crude extract <ethyl acetate extract < butanol extract < dichloromethane extract < residual water extract. The crude extract was the highest active extract against the both free radicals despite the low content of phenolic compounds, this could be explained either by the number of hydroxyl groups in the chemical structures of phenolic compound's present in this extract, which is correlated with its antioxidant activity. This means that the relative amounts of these groups in the sample will determine the manner in which they reduced free radicals. Also, phenolic compounds can counteract reactive species in a variety of ways, including synergistically, additively, and antagonistically [163]. The high antioxidant activity of this extract could be confirmed also by the presence of other types of compounds such as reducing compounds, triterpenoids, free quinones and cardenolides, these compounds are known by their antioxidant capacity.

In general, the correlation between DPPH IC_{50} and the phenolic content was $R^2 = 0.626$, with flavonoids was $R^2=0.466$ and with condensed tannins was $R^2 = 0.569$ (**Table. III. 11**). This allows us to conclude that the capacity of DPPH radical is mainly due to 62.6% of the total phenolic content. ABTS IC_{50} total phenols content and condensed tannins have a high correlation value ($R^2 = 0.723$ and $R^2 = 0.703$ respectively), and a medium correlation with flavonoids ($R^2 = 0.561$) (**Table. III. 11**). This allows us to conclude that the capacity of free radical ABTS is mainly due to the 72.3% of total phenol content, 56.1% of flavonoids, and 70.3% of condensed tannins. Almost majority of polyphenols display significant antioxidant action. The flavonoids are phenolic compounds isolated from a vast array of plant species [164]. Also, the tannins are phenolic compounds.

Numerous research has revealed that flavonoids have antioxidant activity, the ability of flavonoids to function as antioxidants has been the topic of a number of research in recent years, and significant structure-activity correlations of the antioxidant activity have been identified [165]. The connection between the chemical structure of flavonoids and their radical-scavenging properties was investigated. In general, the presence of a 3-hydroxy group in conjunction with a 2,3 double bond in the flavonoid structure improves the resonance stabilization for electron delocalization; hence, it has a greater antioxidant effect [166]. On the other hand, tannins are thought to be strong antioxidants because of their richness in phenolic hydroxyl groups [167].

III.8.7. 5. Superoxide anion radical scavenging activity

The measurement of the superoxide anion scavenging activity by different extracts of *A. aristata* is estimated using the auto-oxidation reaction of pyrogallol occurring under alkaline conditions. The different extracts were treated in the same way as negative control distilled water. We have plotted the curves representing the variation in auto-oxidation of pyrogallol expressed in inhibition rate as a function of the time (second) (**Figure. III. 24**). The results of measuring the auto-oxidation rate of pyrogallol in the presence of the same concentration are expressed by the I% values, this value is proportional to antioxidant activity, i.e., the higher I% value, has the higher antioxidant activity.
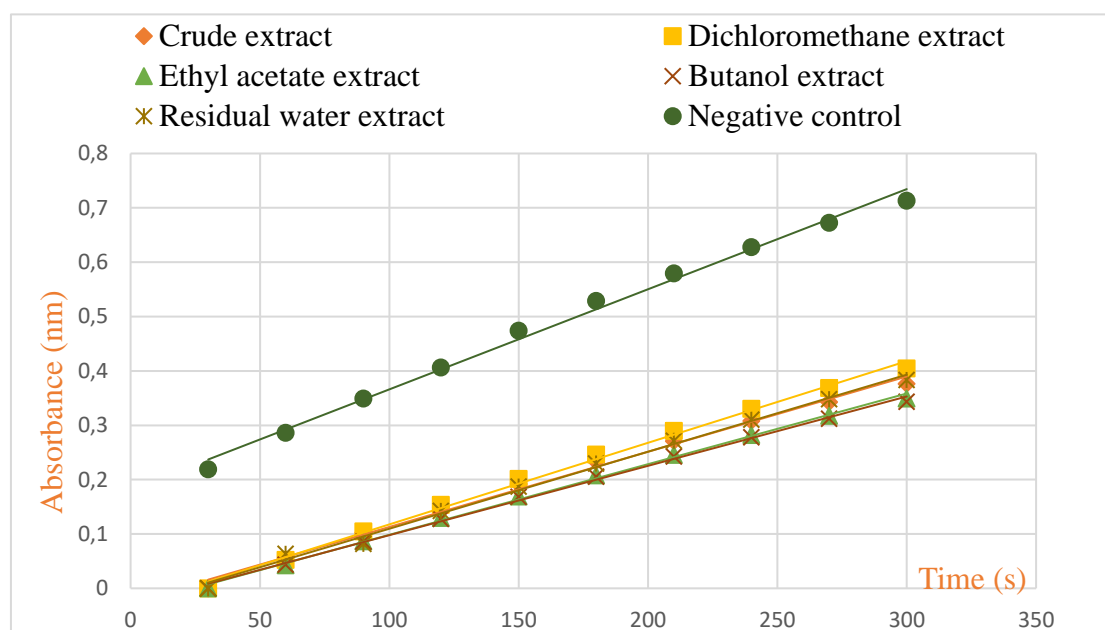
Figure. III. 24: Curves representing the autoxidation of pyrogallol of the various extracts.

The curves of the absorbance as a function of times were plotted, from these curves we deduce the slope, which expresses the rate of the auto-oxidation of pyrogallol. The radical scavenging percentages of all extracts ranged from (30.49 ± 7.653 % and 18.08 ± 2.328) (**Table. III. 9**). The greatest percentages of inhibition were recorded by the butanol and ethyl acetate extracts (30.49 ± 7.653 % and 29.28 ± 2.363 % respectively), while the lowest percentages of inhibition were recorded to the residual water and dichloromethane extracts (22.40 ± 2.935 % and 18.08 ± 2.328 % respectively).

Table. III. 9: The inhibition values of superoxide anion radical scavenging of different extracts.

Extract	I %
Crude	23.81 ± 4.276
Dichloromethane	18.08 ± 2.328
Ethyl acetate	29.28 ± 2.363
Butanol	30.49 ± 7.653
Residual water	22.40 ± 2.935

The superoxide anion radical $O_2^{\bullet-}$, contributes significantly in many human illnesses. As a result, there is a critical need for a validated, quick assay that can accurately quantify an antioxidant's ability to scavenge $O2^{\bullet-}$ [168]. For many years, the auto-oxidation of pyrogallol method have frequently been used to produce superoxide anion radical as can be seen in **Figure. III. 5** of autoxidation of pyrogallol [139].

The structure of compounds affects the $O2^{\bullet-}$ scavenging activity. For instance, the flavonoid compounds have an $O2^{\bullet-}$ scavenging activity, due to its hydroxyl groups, the $O2^{\bullet-}$ scavenging activity would increase with more hydroxyl groups in ring B of flavonoids [168]. In our study at the same concentration 0.05 mg ∕ mL of extracts, the efficiency of *A. aristata* extracts can be classified in the following descending order: butanol extract > ethyl acetate extract> crude extract > residual water extract > dichloromethane extract. The divergent efficacies in *A. aristata* extracts may be explained by the hydroxyl groups, which are known to contribute to increasing polarity, a study mentioned by Chen *et al.* (2013), might support our results. When compared to other flavonoids with only one or no hydroxyl on ring B, luteolin and quercetin both have the catechol moiety on ring B. These compounds have stronger $O2^{\bullet-}$ scavenging capabilities [168].

III.8.7. 6. The Fe^{2+} chelating activity assay

The measurement of the chelating effect of the extracts was estimated using chelation of the Fe^{2+} in the presence of extracts. The different extracts are treated in the same way as standard EDTA solutions. EDTA compound is a potent metal chelator; thus, it was utilized as standard metal chelator factor in this work. We have plotted the curve of standard representing the inhibition of Fe^{2+} chelation as a function of concentration (**Figure. III. 25**).
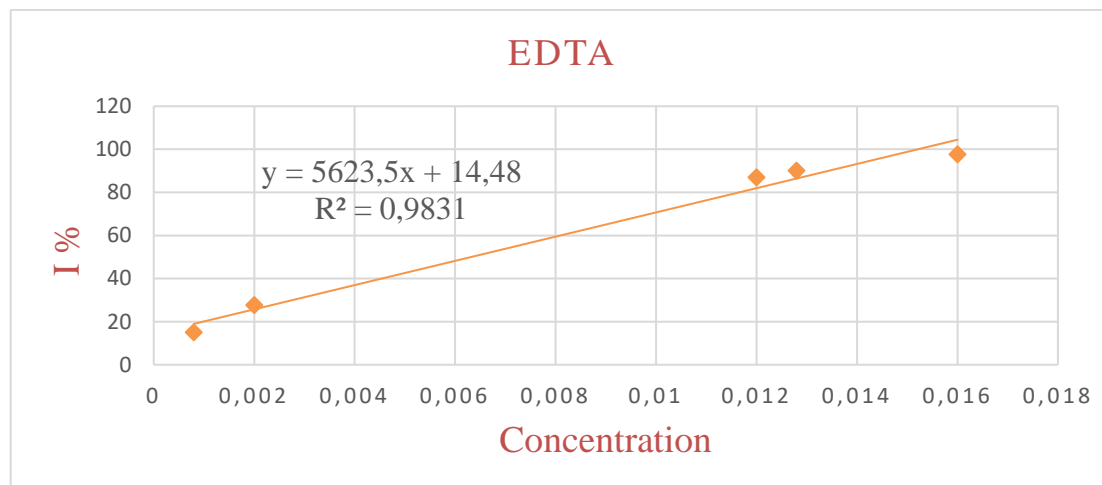
Figure. III. 25: Curve representing the inhibition percentage of the standard EDTA.

The results are expressed by the I % values, this value is proportional to antioxidant activity, i.e., the higher I % value, has the higher antioxidant activity. The results of inhibition chelation are summarized in the **Table. III. 10**. At concentration of 5.8 mg∕mL, the values of inhibition chelation ranged from 24.46 ± 1.947 % to 95.19 ± 1.355. The highest inhibition chelation percentages are recorded by the crude and residual water extracts (95.19 ± 1.355 % and 63.56 ± 0.621% respectively), while the lowest percentages of inhibition chelation were recorded to the butanol and ethyl acetate extracts (22.40 ± 2.935 % and 18.08 ± 2.328 % respectively).

Table. III. 10: The inhibition percentage of Fe^{2+} chelating of different extract.

Extract	I%
Crude	95.19 ± 1.355
Dichloromethane	53.40 ± 5.128
Ethyl acetate	24.46 ± 1.947
Butanol	35.95 ± 4.896
Residual water	63.56 ± 0.621
EDTA	$IC_{50} = 6.31$ µg/mL

At the same concentration 5.8 mg/mL of extracts, we can classify the efficiency the inhibition chelation Fe^{2+} of *A. aristata* extracts in descending order: crude extract > residual water extract > dichloromethane extract > butanol extract > ethyl acetate extract.
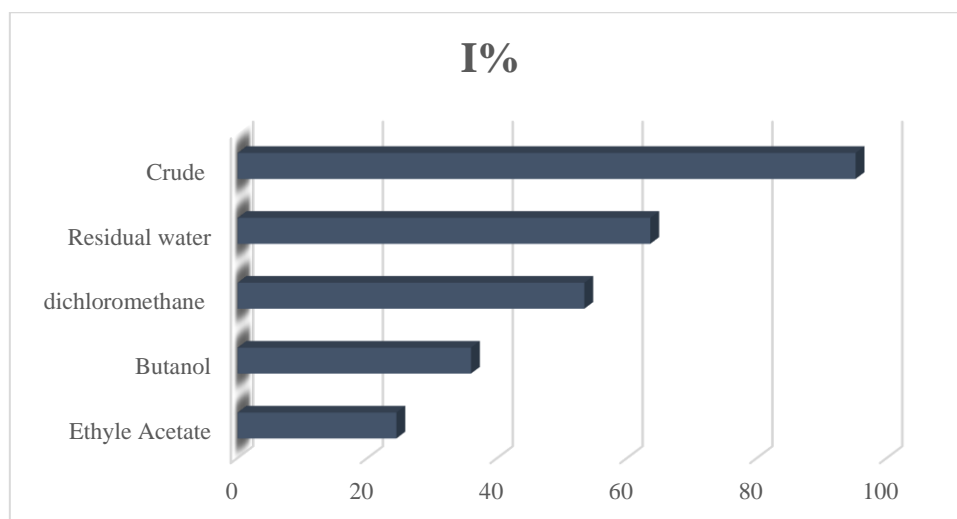
Figure. III. 26: Comparing the metal chelating effect between the extracts.

Metal ions are necessary for the continuation of the vital functions of living organisms, an increase in heavy metals in the human body stimulates the formation of free radicals [169]. For this, the removal of heavy metals from the body via the use of chelating agents is known as metal chelation therapy. When the enhanced creation of reactive oxygen species overwhelms the maintenance of antioxidants in the human body, oxidative stress results. This condition causes lipid peroxidation, protein modification, DNA damage, and other effects that are all symptoms of numerous diseases, including cardiovascular disease, atherosclerosis, cancer, diabetes, neurological disorders like Parkinson's disease AD, chronic inflammation, and others [170]. Metal chelating ability is very important as it reduces the metal concentration, which has a catalytic effect in lipid peroxidation. In addition, metal chelating agents are considered as secondary antioxidants because they decrease the redox potential and thus stabilize the oxidized [169].

The iron chelation assay was carried out to assess the chelation capacity of the extracts of *A. aristata*, Ferrozine can quantitatively form complexes with ferrous iron, in our study, the presence of extracts/EDTA, the complex (ferrozine-Fe^{2+}) formation was disrupted and this was shown by a change in the color of the complex [171].

As can be seen in the **Figure. III. 26**, all extracts displayed chelation of iron. Among extracts, crude extract exhibited stronger chelating ability with an inhibition value of 95.19 % $\pm$ 1.355, when compared to other extracts. In this way, the interaction between the extract and Fe^{2+} is supplied, that is, Fe^{2+} ions are chelated by the extract. EDTA exhibited high stronger chelating effect with an EC_{50} value of 6.31 µg/mL (effective concentration that chelates 50%) when compared to extracts. EDTA is a common metal chelator in antioxidant procedures even though it is not an antioxidant molecule due to its strong chelating ability. In fact, the metal chelation properties of antioxidants or extracts are often represented as EDTA equivalents [169].

Metal chelating is usually considered as a the most putative and common antioxidant method. It has been noted that antioxidants' functional groups, which carry out metal binding, provide them an effective Fe-binding capacity [169]. The main antioxidant compounds present in plants are flavonoids, which operate as reducing agents, hydrogen donors, singlet oxygen quenchers, and metal chelating agents due to their redox characteristics [171]. It has been reported that the major compounds present in the *Atractylis* plants are flavonoids [50-53, 55].

Our results of phytochemical screening of the crude extract shows the presence of flavonoids, also the analysis of the HPLC-UV chromatograms of *A. aristata* extracts reveal the detection of quercetin in all the extracts. Thus, the Fe chelating activity of our extracts can be attributed to the presence of flavonoids, especially the quercetin which is known as an antioxidant and it has been reported the Fe chelating effect of this compound. The mechanism of quercetin's binding to ferrous ions (Fe^{2+}) the chelating sites for Fe to Quercetin were between 3-OH and 4-oxo groups of the heterocyclic ring, also between the A ring and the heterocyclic ring 5-OH and 4-oxo groups, and the catechol moiety of the B ring, the quercetin be able to chelate multiple Fe^{2+} ions across functional hydroxyl (-OH) and carbonyl (-C=O) groups as can be seen in the

Figure. III. 27. Ferrozine had a high affinity for Fe^{2+}, but quercetin may chelate Fe^{2+} before it. Thus, quercetin either changes ferrous ions into metal complexes or sterically inhibits interactions between lipid intermediates and metals [169].
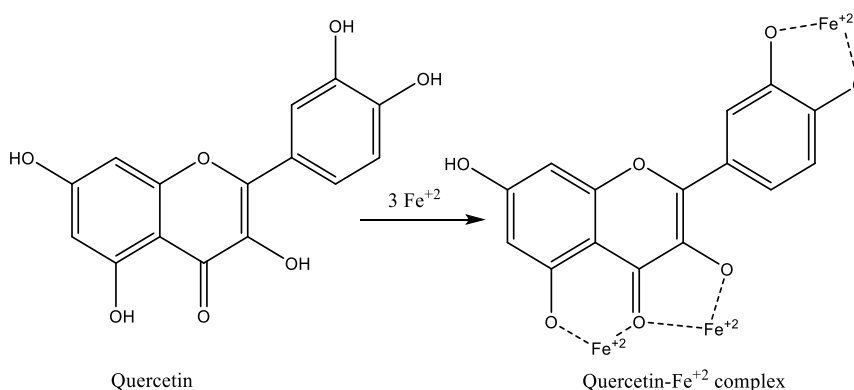
Figure. III. 27: The proposed mechanism of quercetin's binding to ferrous ions (Fe^{2+}) [169].

Table. III. 11: The correlations between antioxidant activity and TPC, TFC and CTC.

	TPC	TFC	CTC	TAC	DPPH	ABTS
TAC	0.604	0.560	0.526	1	0.879	0.797
DPPH	0.626	0.466	0.569		1	0.966
ABTS	0.723	0.561	0.703		0.96	1

III.8.7. *In vitro* evaluation of α-amylase inhibitory power

The absorbance measurements of these inhibition tests carried out at the same concentration of extracts allowed us to calculate the inhibition rates then the parameter AEIC (Acarbose Equivalent Inhibitory Capacity) for each extract using a graph representing the percentage of inhibition (%) acarbose as a standard depending on the concentration (**Figure. III. 28**). The results are expressed by the parameter AEIC which is defined as being the concentration of the standard solution of acarbose having the inhibiting capacity equivalent to a solution of 1 mg/ mL of the studied extract.
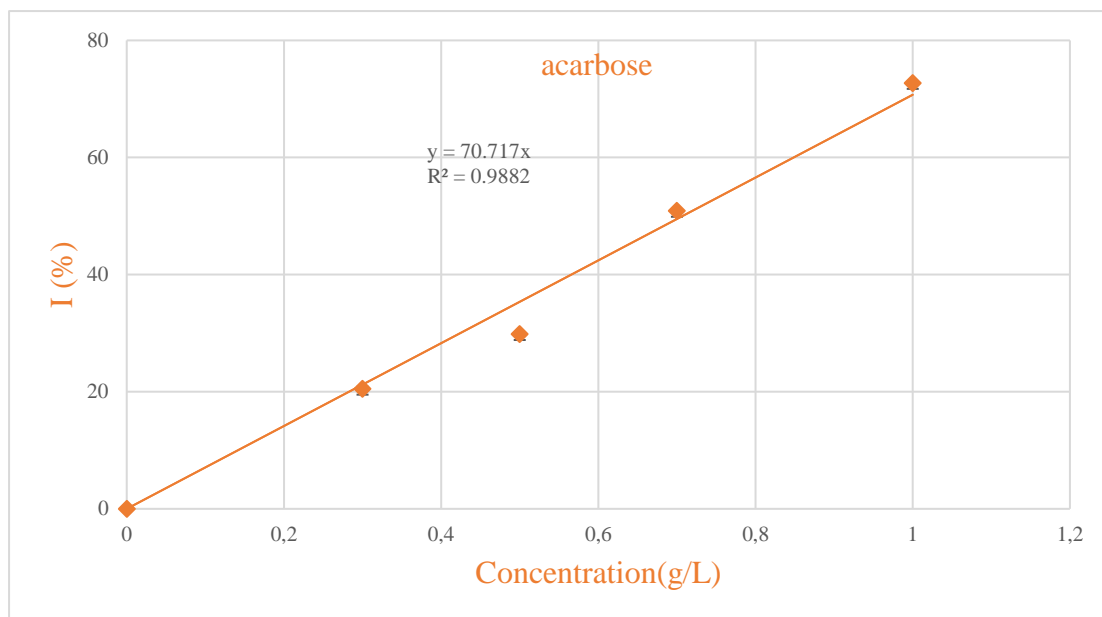
Figure. III. 28: Curves representing the inhibition percentage of acarbose.

The results obtained from this test show that all the studied extracts have inhibitory properties with inhibition values varied between 25.50% and 57.62% and AEIC values between 0.3607 and 0.8148 as can be seen in the **Table. III. 12** and the **Figure. III. 29**. The highest values of AEIC were recorded in the crude, butanol dichloromethane and ethyl acetate extracts, 0.8148, 0.7695, 0.8148 and 0.6934, respectively. While the lowest values of AEIC were recorded in the residual water extract which is equal to 0.3607.

Table. III. 12: I% and AEIC values of α-amylase inhibitory power of different extract.

Extract	I%	AEIC
Crude	57.6241 ± 2.81772	0.8148
Dichloromethane	51.9340 ± 2.79509	0.7343
Ethyl acetate	49.0358 ± 2.67486	0.6934
Butanol	54.4238 ± 3.177	0.7695
Residual water	25.5098 ± 4.22001	0.3607

A. aristata extracts show high inhibition percentage of the enzyme α-amylase at the same concentration of 1 mg/ mL, our results are compared with the anti-diabetic activity of the reference drug acarbose at the concentration of 1 mg/ mL, where exhibited an inhibition percentage equal to 70.71%. As can be seen in the **Figure. III. 29**, the crude and n-butanol extracts show a significant inhibition close to acarbose 57.62% and 54.42 %. Despite the alpha-amylase inhibitory activity of *A. aristata* extracts is relatively less than that of reference drug the acarbose, but this last is a pure

molecule with numerous side effects [172]. However, our extracts still mixtures that likely comprise a number of compounds that must be separated and purified in order to identify the active ingredient.
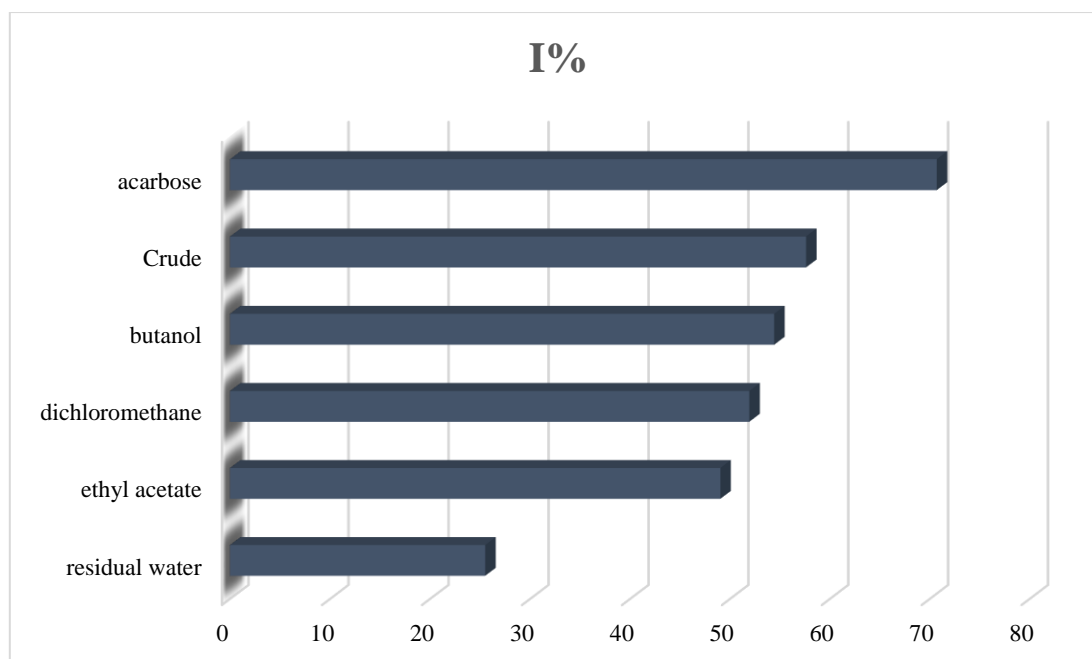
Figure. III. 29: Inhibition percentage of *A. aristata* extracts and acarbose.

For the treatment of various types of diabetes mellitus, several therapeutic options are available. One of the therapeutic techniques is to reduce postprandial glucose levels by inhibiting oligo and disaccharide degradation. This could be accomplished by inhibiting the carbohydrate-hydrolyzing enzymes, α-amylase and α-glucosidase, which are essential enzymes in the digestion of starch and glycogen. These enzymes are found in the small intestine brush border and are responsible for breakdown oligosaccharides and disaccharides into monosaccharides that can be absorbed. Inhibitors of the α -amylase and α-glucosidase enzymes slow sugar digestion, reducing the rate of glucose absorption and, as a result, blunting the postprandial plasma glucose rise [144].

Several synthetic inhibitors, including acarbose, miglitol, voglibose, and orlistat, are currently available and appear to be a successful method of controlling T2D. The increased level of undigested starch in the colon, however, can result in side/adverse consequences (abdominal pain, flatulence, diarrhea, hepatotoxicity) [172]. As a result, the scientific community has focused its attention on looking for new, effective agents that have been identified from edible or medicinal plants [172].

The naturally occurring of active phytochemicals (polyphenols, terpenoids, saponins, polysaccharides, and steroids) found in some plants can offer an alternate strategy at a relatively lower cost [173, 174]. Additionally, the use of plant extracts in combination therapy can help decrease the consumption of pharmaceutical drugs and, consequently, reduce side effects [175]. The anti-diabetic activity of plant extracts attributed to the existence of these phytochemicals, which is confirmed in many reports and books. The differences in the ability of *A. aristata* extracts to inhibit the enzyme α-amylase is due to the differences in the presence of these compounds among the extracts for instance, the residual water extract is the last extract we get from the successive extraction process, the absence of some compounds that made this extract the least effective. Also, it is known that the difference in the polarity of the solvents lead to the extraction of compounds of different nature, this results the difference in effectiveness between the extracts.

It has been reported the antidiabetic activity of some species of the genus *Atractylis*. A study conducted by Bouabid *et al*. (2018) on the extracts of the plant *A. gummifera* has been showed that the macerated methanol extract has a potent antidiabetic activity compared to other extracts with IC_{50} value equal to 0.557 mg/mL using the α-amylase inhibitory method, i.e. at a concentration of 0.557 mg/ml, the inhibition rate is 50% [12]. Thus, our results of the crude extracts are small lower than the results of *A. gummifera*. However, our results of the dichloromethane and the ethyl acetate extracts exhibited similar results compared with their same extracts (chloroform and the ethyl acetate) of *A. gummifera*, where at concentration of 1.25 mg/ mL and 1.39 mg/ml the inhibitory value is 50%. This can be explained by the existence of the same types of molecules in both plants.

III.9. *In vivo* evaluation of biological activities

III.9.1. Animal and management

The *in vivo* study was carried out on mice of the Wistar species (females) obtained from the Pasteur Institute of Algiers, weighing between 18 g and 20 g. These mice are housed in metabolic cages at a temperature of 20 to 24 °C. The animals were fed standard food (O.N.A.B), and water was available at all time, they have free access to water and food. In the all experiments the animals were fasted for 16 hours before treatment. This part of study was carried out in research and development center of the Saidal group, Algiers laboratories.

Experiments that used animals were done in line with the U.S. guidelines and the internationally accepted principles for the use and care of laboratory animals (NIH publication no. 85-23, revised in 1985).

III.9.2. Preparation of the extracts

Crude extract: The crude extract was prepared by maceration of 50 g of the plant *A. aristata* in MeOH/H$_2$O (70/30) for 24 h this operation repeated three times, after the filtration, the mixture evaporated and then it was preserved in the form of a powder.

Aqueous extract: The aqueous extract was prepared by the decoction of 50 g of the plant *A. aristata* in distilled water for 1 h, after the filtration, the mixture evaporated and then it was preserved in the form of a powder.

III.9.3. Acute toxicity study

III.9.3.1. Toxicity and its manifestation in the body

III.9.3.1. I. A toxicant

The word toxicant doesn't have a single, agreed-upon definition. Usually, we call something toxic if it can hurt the health of living organisms. Scientifically, a substance is toxic if it gets into the body in any way, whether it's in a high dose, several close doses, or small doses given over a long period of time, it causes short-term or long-term problems with one or more of the body's functions, which can go as far as stopping them completely and lead to death [176].

III.9.3.1. II. Acute toxicity

Acute toxicity can be defined as that which causes death or very serious physiological disorders within a short period of time after absorption of a relatively large dose of a toxic compound, once or multiple times [176].

III.9.3.1. III. Manifestation of toxicity

The effect of a toxin on the organism essentially depends on the quantity of the toxin or of the reaction substances that it generates (active metabolites, free radicals) which bind to the site of action (enzyme, cytoplasmic receptor, DNA …). This effect is a function not only of the quantity of the active toxicant which reaches the site of action, but also of its affinity for this site [176].

III.9.3.1. Evaluation of *in vivo* Acute toxicity study

The Acute oral toxicity study of the crude and aqueous extracts was carried out using the limit dose test according to the Test Guidelines on Acute Oral Toxicity OECD guideline No. 423 (2002), with a limit dose of 2000 mg/kg body weight/oral route [177].

Procedure

Six females Albino mice were used for each extract, the mice were selected one at a time, weighed, and given an equivalent dose of 2000 mg/kg body weight of the crude and aqueous extracts. All solutions of the crude and aqueous extracts were prepared with 5 mL of distilled water (0.08 mg/mL). A volume of 0.5 mL of extract was administrated to each mouse through stomach tube after 16 h of fasting (**Figure. III. 30**). The mice are fed after two hours of the oral administration of the extracts.

Figure. III. 30: Administration of extracts (acute toxicity test).

Each animal was observed each time for the first 5 min after loading for signs of regurgitation and then kept in a metabolic cage. Each was watched after 2 h after dosing for the short-term outcome, then daily for the successive 24 h for 14 days for the long-term possible outcome.

III.9.4. Anti-inflammatory activity

III.9.4. 1. Inflammation

Inflammation is a local defense response to maintain homeostasis in living organisms by eliminating foreign bodies such as microbial pathogens and abnormal cells. Inflammation is a protective response of the body, can be triggered by physical or chemical trauma or invading microorganisms. It is an important immune response that leads to the elimination of the pathogen and the healing of injured tissue [178].

III.9.4. 2. Type of inflammation

Inflammation is classified into two categories according to the duration and kinetics of the inflammatory process:

Acute inflammation

Acute inflammation occurs right away once an irritant enters the body. Acute inflammation can last anywhere from a few days to a few weeks (is of relatively short duration) depending on the degree of injury. The key features of this process are the leakage of plasma fluids and proteins (edema) and the movement of leukocytes (mostly neutrophils) from blood arteries to the inflammatory site (injured tissue). While innate immunity helps get rid of the infection right away, it also sets off the adaptive response that ultimately does away with the danger [179, 180]. There are three phases to the acute inflammatory response [181]:

➢ The vascular phase.
➢ The cellular phase.
➢ The resolution and repair phase.

Chronic inflammation

Chronic inflammation corresponds to a failure of acute inflammation and induces many pathologies. It is characterized by a prolonged evolution that can last for months or even years, chronic inflammation is defined by a duration of more than six weeks [180].

III.9.4. 3. The causes of the inflammatory reaction

The causes of the inflammatory reaction are multiple [181]:

➢ Infectious agent: contamination by micro-organisms (bacteria, viruses, parasites, fungi);
➢ Physical agents: trauma, heat, cold, radiation;
➢ Chemical agents: caustics, toxins, venoms;
➢ Foreign bodies: exogenous or endogenous;
➢ Defect of vascularization: inflammatory reaction secondary to necrosis by ischemia;
➢ Immune dysregulation (abnormal immune response, allergies, autoimmune) [181].

III.9.4. 4. Evaluation of *in vivo* anti-inflammatory activity

Principle

The injection of carrageenan under the plantar aponeurosis of the mouse paw provokes an inflammatory reaction. this study makes it possible to compare the reduction in plantar edema after administration of equal doses of the anti-inflammatory product to be tested and the corresponding reference product.

Procedure

The anti-inflammatory power of the crude and aqueous extracts was evaluated according to the method described by saidal group using adult mice. The mice were randomly divided into 4 homogeneous groups of 6 mice and fasted for 16 hours before treatment. Then, the mice received the test products intragastrical.

Control batch: The mice in this batch receive orally a 0.5 ml of physiological water.

Test batches: The mice in this batch were treated orally with 0.5 mL of each extract at a rate of 2 g/Kg (0.08 mg/mL).

Reference batch: The mice in this batch were treated orally with 0.5 mL of a reference anti-inflammatory (Ibuprofen).

30 min after the various treatments, 0.025 mL of a solution of carrageenan (1%) was injected into each mouse under the foot pad of the left hind paw. However, the right hind paw did not undergo any treatment (a control) **Figure. III. 31**.

Figure. III. 31: The oral administration and the injection of carrageenan under the plantar pad of the left hind paw.

Expression of results

The percentage increase in paw weights (%edema) is calculated by the following formula:

$$\% \, Edema = \frac{left \, paw \, weight \, average - right \, paw \, weight \, average}{right \, paw \, weight \, average} * 100$$

The percentage of reduction in edema in the treated mice compared to the controls calculated by the following formula:

$$Edema \, Reduction \, Percentage = \frac{\% \, control \, edema - \% \, edema \, test}{\% \, control \, edema} * 100$$

III.9.5. Sedative activity

III.9.5. 1. The sedation

Sedation is a condition characterized by cerebral cortex-mediated central nervous system depression accompanied by drowsiness and some degree of centrally induced muscle relaxation. The patient is usually unaware of their surroundings but can respond to stimuli depending on their intensity. This is therefore different from tranquilization which corresponds to an animal which is aware of its environment but also different from narcosis which is defined by a patient in a state of deep sleep [182].

III.9.5. 2. Evaluation of sedative activity (the measurement of locomotor activity)

Principle

The principle of this study consists of studying spontaneous motility using the Boissier & Simon actophotometer (**Figure. III. 32**) in mice previously treated with a psychotropic drug.

Procedure

The locomotor activity of the crude and aqueous extracts was measured using an actophotometer in accordance with SAIDAL Group method, using adult mice. The animals were divided into 4 homogeneous groups, each consisting of six animals.

Control batch: The mice in this batch receive orally a 0.5 mL of distilled water.

Test batches: The mice in this batch were treated orally with 0.5 mL of each extract at a rate of 2 g/Kg (0.08 mg/mL).

Reference batch: The mice in this batch were treated orally with 0.5 mL of a reference product (haloperidol).

30 minutes after the various treatments, each mouse was placed individually in the actophotometer for a period of 30 minutes. The animal's movement interrupts a beam of light falling on a photocell, where a digital count is recorded and displayed in the corresponding totalizer.

Figure. III. 32: The mouse was placed individually in the actophotometer.

Expression of results

$$movement\ reduction\ percentage\ I\%$$
$$= \frac{moy\ of\ control\ movment - moy\ of\ testmovment}{moy\ of\ control\ movment} * 100$$

III.10. Results and discussion of the *in vivo* biological activities

III.10.1. Acute toxicity test

The *in vivo* toxicological properties of *A. aristata* extracts were investigated according to OECD Guideline 423, consisting of a single-dose 14-day acute oral toxicity study. This method is a stepwise procedure with the use of 3 animals of a same sex (females) per step. The range of acute toxicity of the test substance depends on the mortality and/or moribund status of the animals. Two to four steps may be necessary to determine the toxicity category (**Figure. III. 33**).
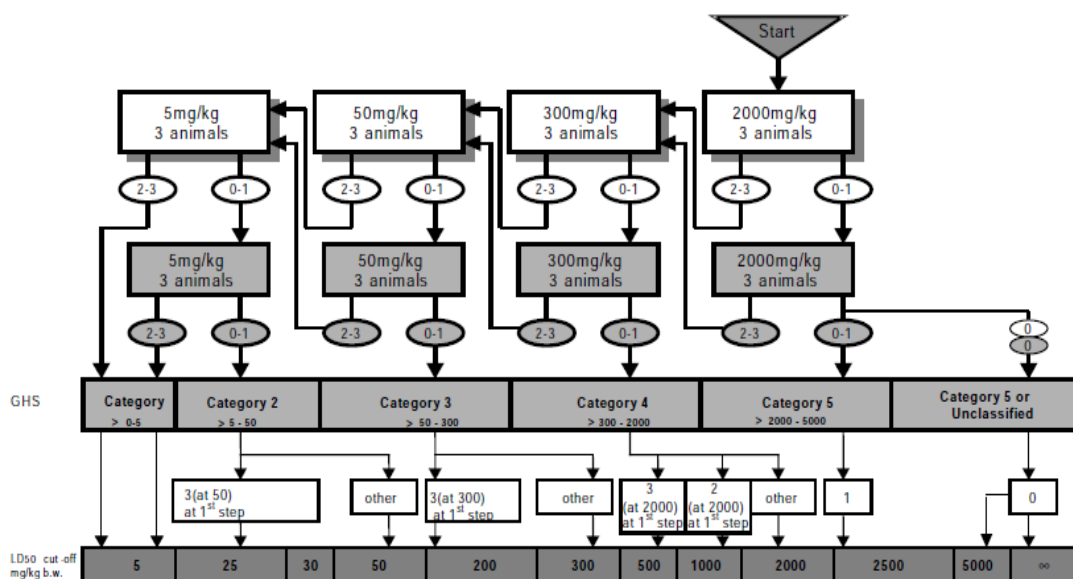
Figure. III. 33: 423 test procedure with a starting dose of 2000 mg/kg body weight.

The acute toxicity study showed no fatalities or noticeable neurobehavioral consequences at the limit test in the *Atractylis aristata* extracts. Hence, this led to their classification in GHS category 5, as recommended by OECD guideline number 423. We were unable to establish the LD_{50} because there was no evidence of toxicity at the 2000 mg/kg dose.

By comparing our results with those of the same genus, the butanol extract of *Atractylis flava* shows that this extract did not bring any signs of toxicity or mortality in treated animals during the 14 days observation period [9].

III.10.2. Anti-inflammatory activity

The *in vivo* anti-inflammatory activity of the crude and aqueous extracts is assessed using the method of carrageenan-induced paw edema. The carrageenan injection under the paws of mice treated with distilled water induces a progressive increase in edema volume after 4h of the treatment. Whilst, the mice treated with the extracts and the ibuprofen show significant decrease in edema volume after 4h of the treatment. The results of the anti-inflammatory activity in mice treated with the distilled water, the ibuprofen and the extracts of *A. aristata* are depicted in **Table. III. 13** and **Figure. III. 34**. The crude and aqueous extracts have a high anti-inflammatory effect after 4 h of the treatment with a percentage of inhibition 62.98% and 56.51% respectively, at a same dose of 2 g/kg. Our results are compared with the anti-

inflammatory activity of the reference drug (ibuprofen) which exhibited an inhibition percentage equal to 83.58% after 4h of the experiment.

Table. III. 13: The results of Edema Reduction Percentage %.

Batch	Left paw weight average (g)	Right paw weight average (g)	%Edema	Edema Reduction Percentage %
Control	0.104	0.07	43.79	/
Reference	0.169	0.139	7.19	83.58
Aqueous extract	0.075	0.063	16.21	56.51
Crude extract	0.086	0.074	19.04	62.98
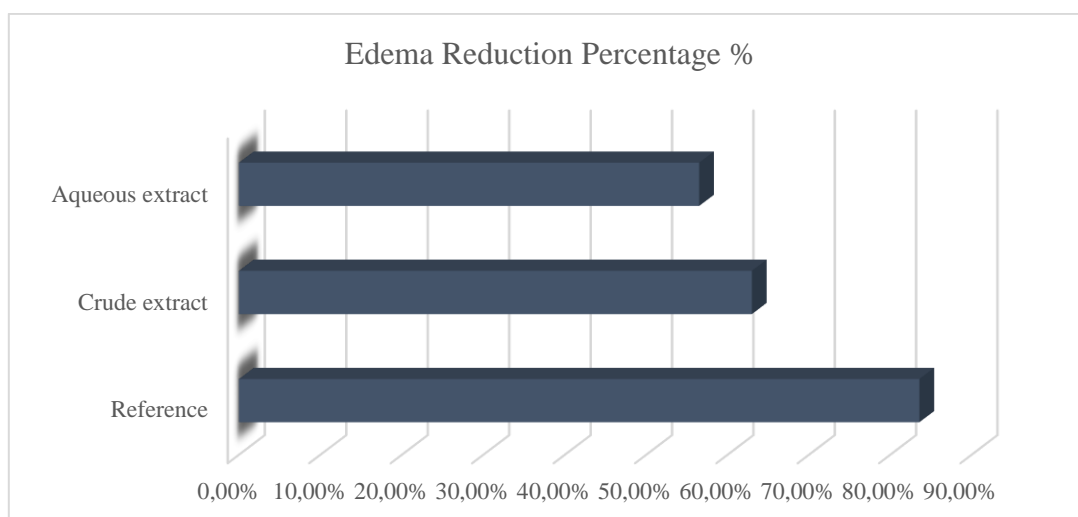
Figure. III. 34: Edema Reduction Percentage of reference and *A. aristata* extracts after 4h.

Synthetic anti-inflammatories often cause several harmful effects on human health such as gastrointestinal ulcers, cardiovascular risk, liver damage and carcinogenesis [183]. Herbal medicines may offer a safer and more effective treatment for inflammatory diseases due to its phytochemical compositions. In which, numerous studies have demonstrated that different flavonoid compounds have anti-inflammatory properties on diverse animal models of inflammation [184]. It has been Also reported the anti-inflammatory activity of the polysaccharides [69], triterpenoids [90] and saponins [105, 106]. Thus, the anti-inflammatory activity of our extracts could be

attributed to the existence of these compounds in the *A. aristata* extracts which mentioned within the phytochemical profile of our plant.

Our results of *in vivo* anti-inflammatory activity show an inhibition of paw edema values after 4h slightly higher than those found by Melakhessou *et al*. (2018) which was evaluated in male rats by the egg albumin induced paw edema method [9].

III.10.3. Sedative activity

The sedative effect of *Atractylis aristata* extracts is assessed using a test of locomotor activity. A decrease in locomotor activity is suggestive of sedative activity, whereas the increase is as an index of alertness [185]. The aqueous and crude extract in doses of 2g/kg produced significant (P < 0.05) reduction in locomotor activity as compared to the control animals. The locomotor activity in mice at test doses of crude and aqueous extracts of *A. aristata* is depicted in **Table. III. 14** and **Figure. III. 35**.

Table. III. 14: The results of sedative activity.

Treatment	Locomotor activity in 30 min	Sedative activity I%
Control	482.16 ± 368.92	/
Aqueous extract	246 ± 239.13	48.98
Crude extract	230.83 ± 104.52	52.12
Reference	44.5 ± 29.81	90.77

Our results showed that crude and aqueous extracts exhibited significant sedative effect at 2 g/kg, as compared to the distilled water treated group. However, this decrease was less than that observed in haloperidol-treated mice. The reduction in amplitude of motion may have been attributable to the sedative effect of *A. aristata*, which was found to exert a mild sedation compared to haloperidol. The measurement of locomotor activity of the extracts, control and the standard (haloperidol) within 30 minutes, are summarized in the **Table. III. 15**, **Table. III. 16** ,**Table. III. 17** and **Table. III. 18**.

Locomotor activity in 30 min
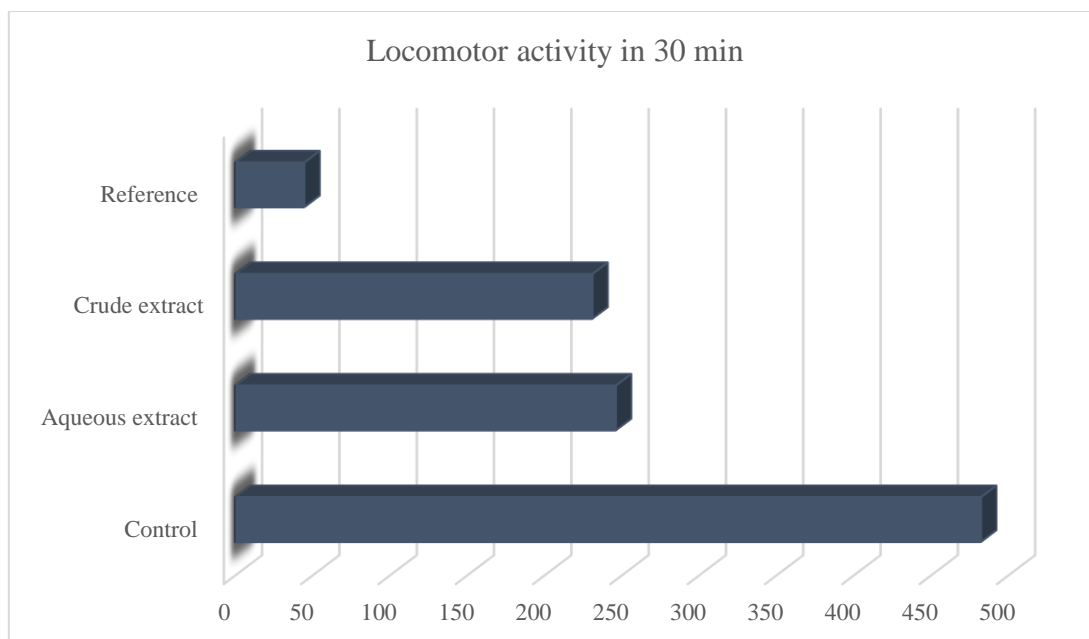
Figure. III. 35: Locomotor activity of *A. aristata* extracts, reference and control in 30 min.

The majority of sedative medications have various side effects, including impairments in memory, cognitive function, and general daytime performance; as a result, their usage beyond four weeks is generally discouraged [186]. Thus, it has been widely reported that several plants can be used as sedatives in traditional medicine. The effectiveness of these plants is due to the presence of several natural compounds. For instance, *Valeriana officinalis*: the sesquiterpenes one of the main categories of molecules that support the activity of valerian [187], also, the existence flavonoid glycosides in Valeriana enhances the sedatives properties of this plant [188]. The plant *Passiflora incarnata* contains alkaloids (harmane and derivatives), sometimes considered a responsible for its sedative activity [187]. Our study was the first test of the sedative activity on the plants of *Atractylis* genus.

Several natural compounds isolated from the plants were used to investigate their sedative effect such as phenolic compounds [189], flavonoids [190, 191], alkaloids [192], saponins [193] and polysaccharides [193]. As a consequence, the existence of these compounds in the *A. aristata* extracts which mentioned within the phytochemical screening and the qualitative analysis of the plant, may significantly contribute the plant's sedative effects.

Table. III. 15: The measurement of locomotor activity of the control group.

Batch	Mouse	5 min	10 min	15 min	30 min
Control	1	58	84	84	97
	2	176	274	420	824
	3	77	102	155	384
	4	11	11	11	25
	5	184	352	454	688
	6	137	294	508	875

Table. III. 16: The measurement of locomotor activity of the aqueous extract group.

Batch	Mouse	5 min	10 min	15 min	30 min
Aqueous extract	1	9	15	17	24
	2	115	176	258	575
	3	1	3	16	29
	4	60	129	192	470
	5	14	15	23	78
	6	68	95	143	300

Table. III. 17: The measurement of locomotor activity of the crude extract group.

Batch	Mouse	5 min	10 min	15 min	30 min
Crude extract	1	117	185	245	404
	2	20	33	56	118
	3	51	92	111	292
	4	57	76	87	210
	5	42	89	132	217
	6	22	67	99	144

Table. III. 18: The measurement of locomotor activity of the reference group.

Batch	Mouse	5 min	10 min	15 min	30 min
Reference	1	1	11	19	26
	2	21	37	44	59
	3	2	2	7	9
	4	33	45	55	58
	5	10	14	20	25
	6	24	72	87	90

In the anti-inflammatory and the sedative activities, in both cases, the crude extract shows higher inhibition percentage compared to the aqueous extract. As we mentioned previously the use of water and the organic solvent methanol in combination may facilitate the extraction of phytochemicals that are soluble in water and/or organic solvent [150]. This could be the reason for this difference in the effectiveness between the two extracts.

Chapter IV:

Isolation, purification and structural identification of natural compounds.

IV.1. Plant material

The selected plant *A. aristata* batt. was collected in its natural habitat. The harvest was carried out in the Algerian Sahara in the Tamanrasset region in January 2019.

IV.2. Preparation of extracts

The plant has been dried in a dry and ventilated place, protected from direct sunlight, and afterwards the plant is completely crushed, and then weighed (917 g).

- ➢ The plant has been macerated for 24 h with petroleum ether to remove fats, waxes and chlorophylls.
- ➢ After the filtration, the plant has been dried and macerated with a mixture (methanol/water; 80/20; V/V), this operation was repeated 3 times with renewal of the solvent every 24 hours and one time for 48 hours.
- ➢ After filtration and concentration, the concentrated hydroalcoholic extract is diluted with 582 mL distilled water, then the solution is left to stand overnight and then filtered.
- ➢ The solution was subjected to successive liquid-liquid type extractions using solvents of increasing polarity, starting with dichloromethane (repeated three times) then ethyl acetate (once) and finally with n-butanol (repeated five times).
- ➢ The four obtained organic phases (weakly polar: petroleum ether and dichloromethane, moderately polar: ethyl acetate and polar: n-butanol) are concentrated to dryness under reduced pressure, weighed and the masses are given in the **Table. IV. 1**.
- ➢ The extraction protocol is summarized in the **Figure. IV. 1**.

Table. IV. 1: Extracts masses on g.

Extract	Weight g
Petroleum ether	7
Dichloromethane	1.918
Ethyl acetate	0.706
n-Butanol	14.48

.

Plant material **917 g**

Petroleum ether extract 7 g

- **Maceration by petroleum ether 24h.**
- **Maceration by MeOH∕H₂O 8∕2 48 h and 24 h three times.**
- **Evaporation**

Crude extract

- **Addition of 582 mL of distillated water for a night.**

Aqueous extract

Water extract

- **Extraction by dichloromethane × 3**

Water extract

- **Extraction by Ethyl acetate × 1**

- **Extraction by n-butanol × 5**

Dichloromethane extract 1.918 g

Ethyl acetate extract 0,706 g

Butanol extract 14.48 g

Figure. IV. 1: Extraction protocol of different extracts of *A. aristata*.

IV.3. Isolation and purification

The dichloromethane, n-butanol and petroleum ether extracts were fractionated and purified using different chromatographic technics. The selection of the extracts was made based on their TLC profile (thin layer chromatography), which confirm the richness of those extracts on secondary metabolites and showed the differences between them. The separation of the products based on the R_f values on the UV lamps UV (254 and 366 nm) and the color of the spots under the revelation.

IV.3.1. Dichloromethane extract

An open column of diameter 2.5 cm filled with an amount of 100 g of normal phase silica gel was used for fractionation of 1.918 g of the dichloromethane extract by liquid chromatography (column chromatography). The elution is carried out with a mixture of solvents: dichloromethane – methanol (100: 0 to 0:100) (**Figure. IV. 5**). The collection of the sub-fractions was carried out in 25 mL tubes, the grouping of the tubes according to their TLC profile under the UV lamp (254 and 366 nm) and revelation with a vanillin sulfuric acid solution and heating provided 4 sub-fractions (FB to FE+J) (**Figure. IV. 2**). These fractions are subsequently subjected to purification operations.
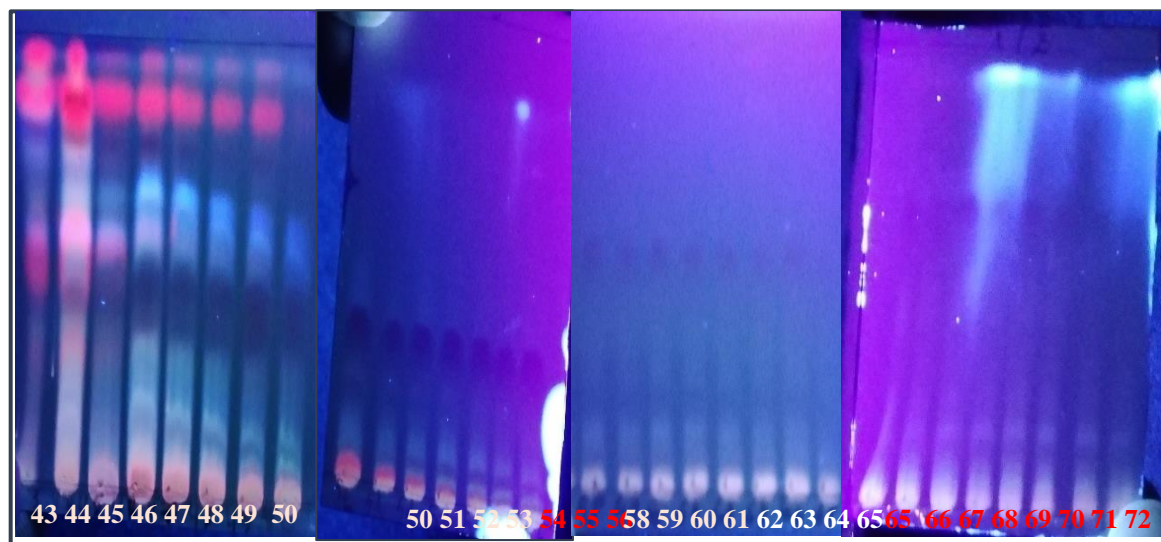
Figure. IV. 2: Follow column by TLC under UV lamp 366 nm.

FB [30−40] fraction: this fraction forms whitened crystals are isolated by normal phase column. The elution is carried out with a mixture of solvents hexane – ethyl acetate – methanol (15:1:0 to 0:1:0 to 0:0:1). The first sub fractions are purified with TLC using the system dichloromethane – methanol (40: 1). Separation gave 48 mg of the pure compound **P1** (**Figure. IV. 3**). This spot invisible under the tow UV light.
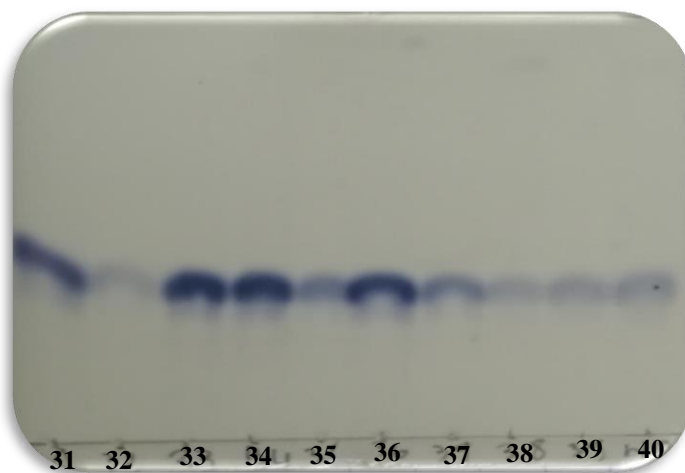
Figure. IV. 3: TLC test of fraction **FB** (the compound **P1**).

FC [43−49] fraction: this fraction is divided into two parts: **crystals** and **supernatant FC`** (**Figure. IV. 4**) they were separated and purified as follows:

Crystals; whitened crystals are purified with RP−18 column. The elution is carried out with a mixture of solvents water–methanol (4:1 to 0:1). The sub fraction **14−18** were combined and then subjected to purification by TLC using the system dichloromethane – methanol (40: 1). The purification gave 20 mg of the pure compound **P2**.
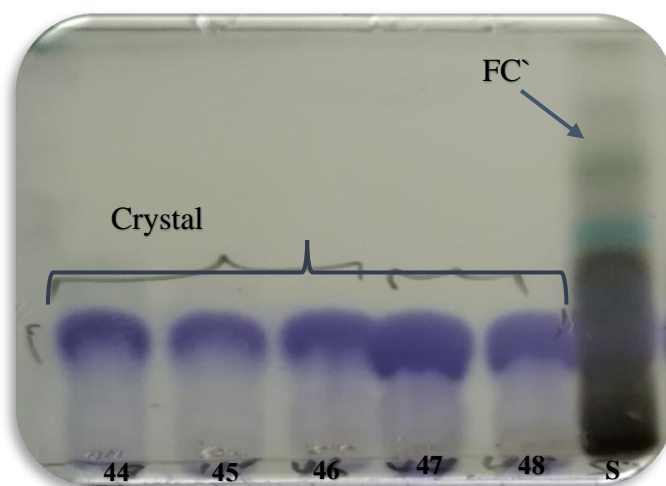
Figure. IV. 4: TLC test of fraction **FC** (the compound **P2**).
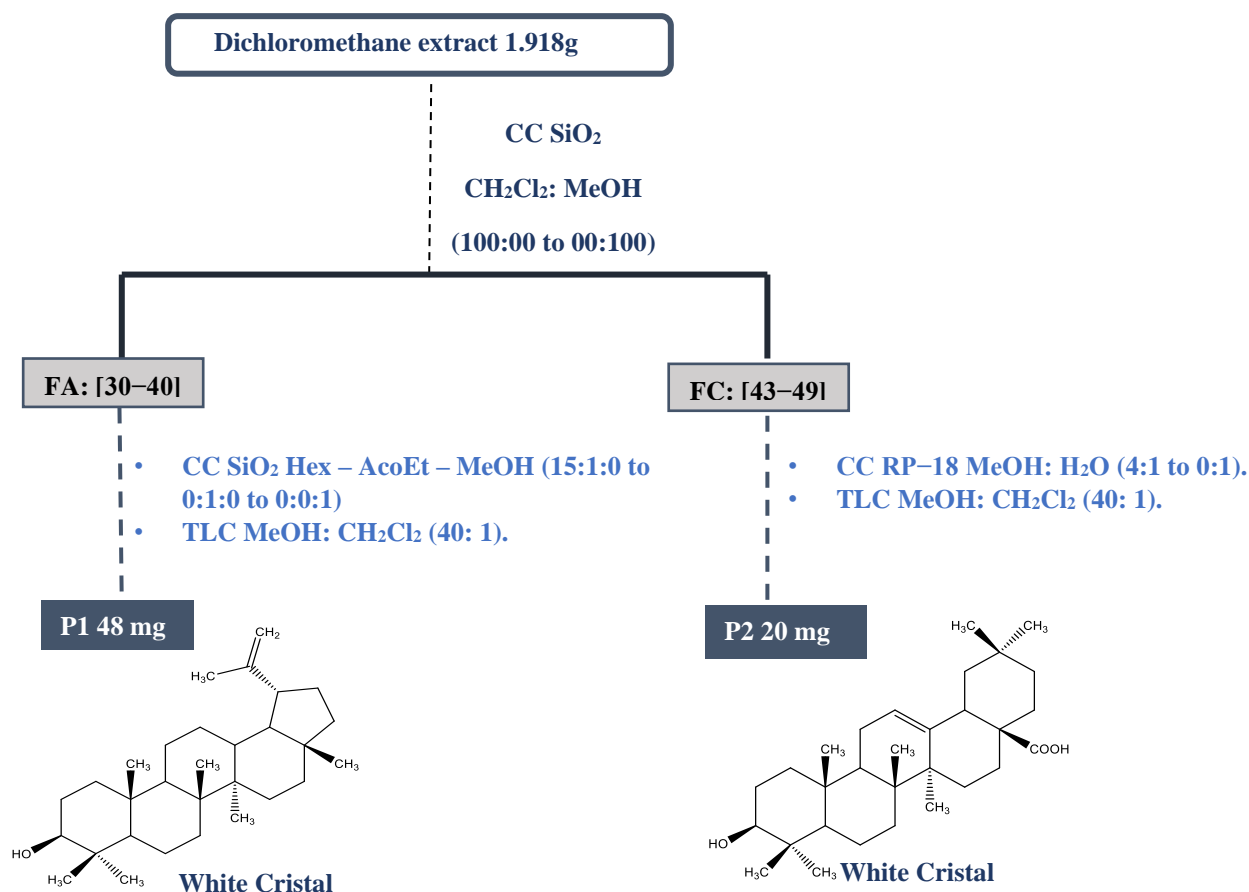
Figure. IV. 5: Diagram of fractionation and purification of the dichloromethane extract.

IV.3.2. n-Butanol extract

After choosing the suitable column (a column with a diameter of 5 cm). The column is filled with 500 g of silica gel 60 (100-210 mesh) mixed with 450 mL of dichloromethane.

10 g of the butanol extract of *Atractylis aristata* are dissolved with methanol then 9 g of thin silica gel is added as an adsorbent. Mix well then, the solvent was removed to obtain a dry powder, after that a mortar was used to obtain a fine and homogeneous powder. The mixture is loaded into the column in such a way as to form a homogeneous layer.

The elution was done using a solvent gradient composed of CH_2Cl_2 and MeOH. The proportions used are: 100:0 to 50:50 and finally only methanol (**Figure. IV. 13**).

56 fractions of 225 mL were collected. By following the progress of the column and basing on the TLC profile of the collected fractions (**Figure. IV. 6**), the latter are grouped according to their similarities (**Figure. IV. 2** and **Table. IV. 2**).

Table. IV. 2: Masses of n-butanol extract fractions.

Eluent	Fractions collected	Mass (mg)
CH$_2$Cl$_2$-MeOH		
100-00 To 90-10	EMPTY TUBE	/
	FA: 17-18	
87-13	FB: 19-21	
	FC: 25-27	177
80-20	FD: 31-39	990.9
75-25 To 50-50	FE: 40-52	2527.0
00-100	FJ: 54-56	2000.0

Following of butanol extract column by TLC under chemical revelation:
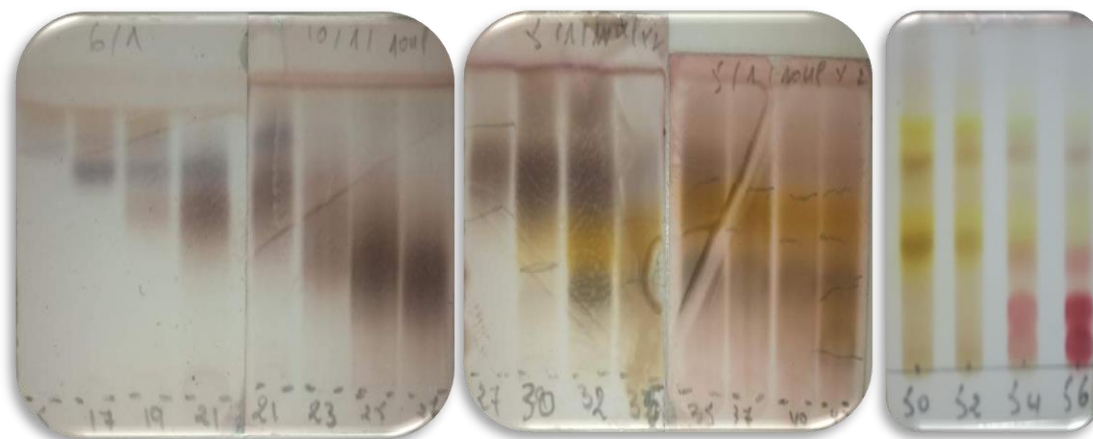
Figure. IV. 6: Following of butanol extract column by TLC under revelation.

The FA fraction is purified by TLC using the eluent: CH$_2$Cl$_2$–MeOH: 6:1. This purification made it possible to obtain compound **V5** (4 mg) in the pure state (**Figure. IV. 7**).

The FB fraction is chromatographed on a column of silica gel in reverse phase RP-18. The elution is carried out by a MeOH–H$_2$O mixture at different gradients (4:1). 5 mL fractions were collected, examined by TLC in normal phase. The FB-1 sub-fraction (17.3 mg), eluted with the MeOH–H$_2$O mixture (4:1), is purified by TLC in the normal

phase, eluted with the eluent: CH_2Cl_2–MeOH– Acetic Acid: 7:1:0.02. This purification made it possible to obtain compound **V4** (5 mg) in the pure state (**Figure. IV. 7**).
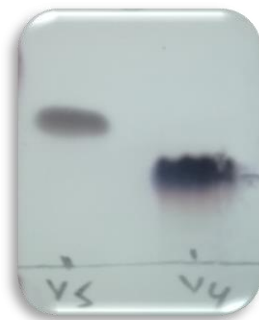
Figure. IV. 7: TLC test of the compounds **V4** and **V5** after revelation.

The FC fraction (177 mg) is chromatographed on a column of RP-18. The elution is carried out by a MeOH–H_2O mixture at different gradients (4:1, 7:1 and 1:0). 5 mL fractions were collected, examined by TLC in normal phase, and finally pooled into 10 sub-fractions. The FC-1 sub-fraction (17.3 mg), eluted with the MeOH–H_2O mixture (4:1), is purified by TLC in the normal phase, eluted with the eluent: CH_2Cl_2–MeOH– Acetic Acid: 7:1:0.02. This purification made it possible to obtain compound **N2** (13 mg) in the pure state (**Figure. IV. 10**).

The FD fraction (990.9 mg) is chromatographed on a column of polyamide, the elution is carried out by an isocratic system of Toluene–MeOH (8:1). 20 ml fractions were collected, examined by TLC in normal phase, and finally pooled into 2 sub-fractions:

The FD-1 sub-fraction (115.6 mg) is chromatographed on a column of silica gel in reverse phase RP-18 repeated 5 times. The elution is carried out by 100% H_2O and washed with MeOH, only the first tube was collected and the rest of the column was subjected of repetitive fractionation under the same conditions (5 times) (**Figure. IV. 8** and **Figure. IV. 10**). The enriched fraction obtained by RP-18 was purified by TLC using the eluent: CH_2Cl_2–MeOH– Acetic Acid: 5:1:0.02. This purification made it possible to obtain compound **N5** (8 mg) in the pure state (**Figure. IV. 10**).
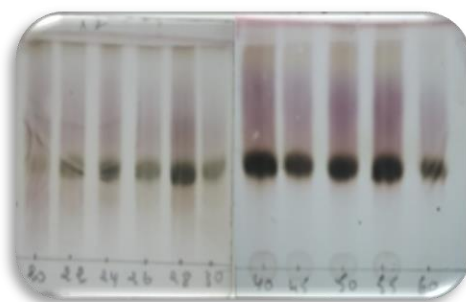
Figure. IV. 8: Follow of RP-18 column **FD-1**.

The FD-2 sub-fraction (168.9 mg) is chromatographed on a column of silica gel in normal phase. The elution is carried out by a CH_2Cl_2–MeOH mixture (10:1). 5 ml fractions were collected (**Figure. IV. 9**). The sub-fractions [8-18] of FD-2 (23 mg) purified by TLC using the eluent: CH_2Cl_2–MeOH– Acetic Acid: 5:1:0.02. This purification made it possible to obtain compound **J2** (18 mg) in the pure state.
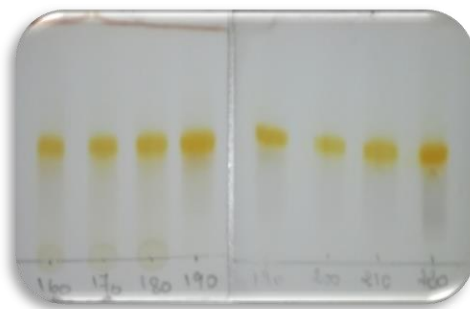
Figure. IV. 9: Follow of silica gel column **FD-2**.

The FE fraction (2527 mg) is chromatographed on a column of polyamide, the elution is carried out by an isocratic system of Toluene–MeOH (8:1). 20 ml fractions were collected, examined by TLC in normal phase, and finally pooled into 2 sub-fractions:

The FE-1 sub-fraction is chromatographed on a column of reverse phase RP-18 repeated, the elution is carried out by 100% H_2O and washed with MeOH, only the first tube was collected and the rest of the column was subjected of repetitive fractionation under the same conditions (6 times). The enriched fraction obtained by RP-18 was purified by TLC using the eluent: CH_2Cl_2–MeOH– Acetic Acid: 5:1:0.02. This purification made it possible to obtain compound **N6** (18 mg) in the pure state (**Figure. IV. 10**).
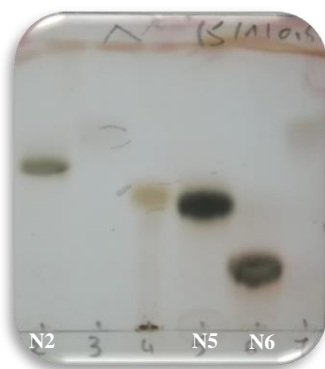
Figure. IV. 10: TLC test of **N2**, **N5** and **N6** after revelation.

The FE-2 sub-fraction is chromatographed on a column of LH-20. The elution is carried out by a CH_2Cl_2–MeOH mixture (5:1). 5 ml fractions were collected. This purification made it possible to obtain compound **J4** (5 mg) in the pure state.

The FJ fraction (2000 mg) is chromatographed on a column of silica gel in normal phase, the elution is carried out by a CH_2Cl_2–MeOH isocratic mode (3:1). 20 ml fractions were collected, examined by TLC in normal phase (**Figure. IV. 11**). The FJ-A [7-15] sub-fraction (163 mg) is chromatographed on a column of silica gel in reverse phase RP-18. The elution is carried out by 100% H_2O and finally pooled into 2 sub-fractions:

The FJ-A1 sub-fraction is purified by TLC using the eluent: CH_2Cl_2–MeOH–Acetic Acid: 2:1:0.4. This purification made it possible to obtain compound **N1** (5 mg) in the pure state (**Figure. IV. 12**).

The FJ-A2 sub-fraction fraction is purified by TLC using the eluent: CH_2Cl_2–MeOH– Acetic Acid: 2:1:0.4. This purification made it possible to obtain the compound **R1** (7 mg), **R2** (11 mg) and **R3** (6 mg) in the pure state (**Figure. IV. 12**).
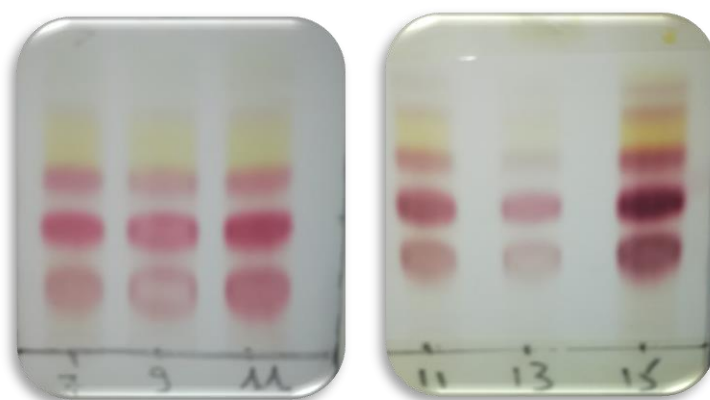
Figure. IV. 11: Follow of silica gel column of the Fraction FJ.
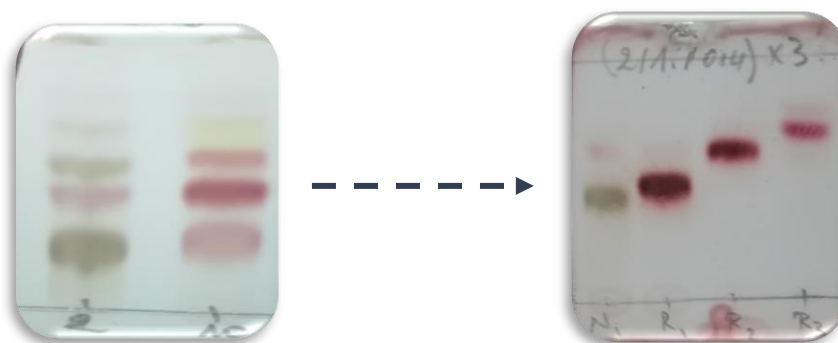
Figure. IV. 12: TLC test of **N1**, **R1**, **R2** and **R3** after revelation.
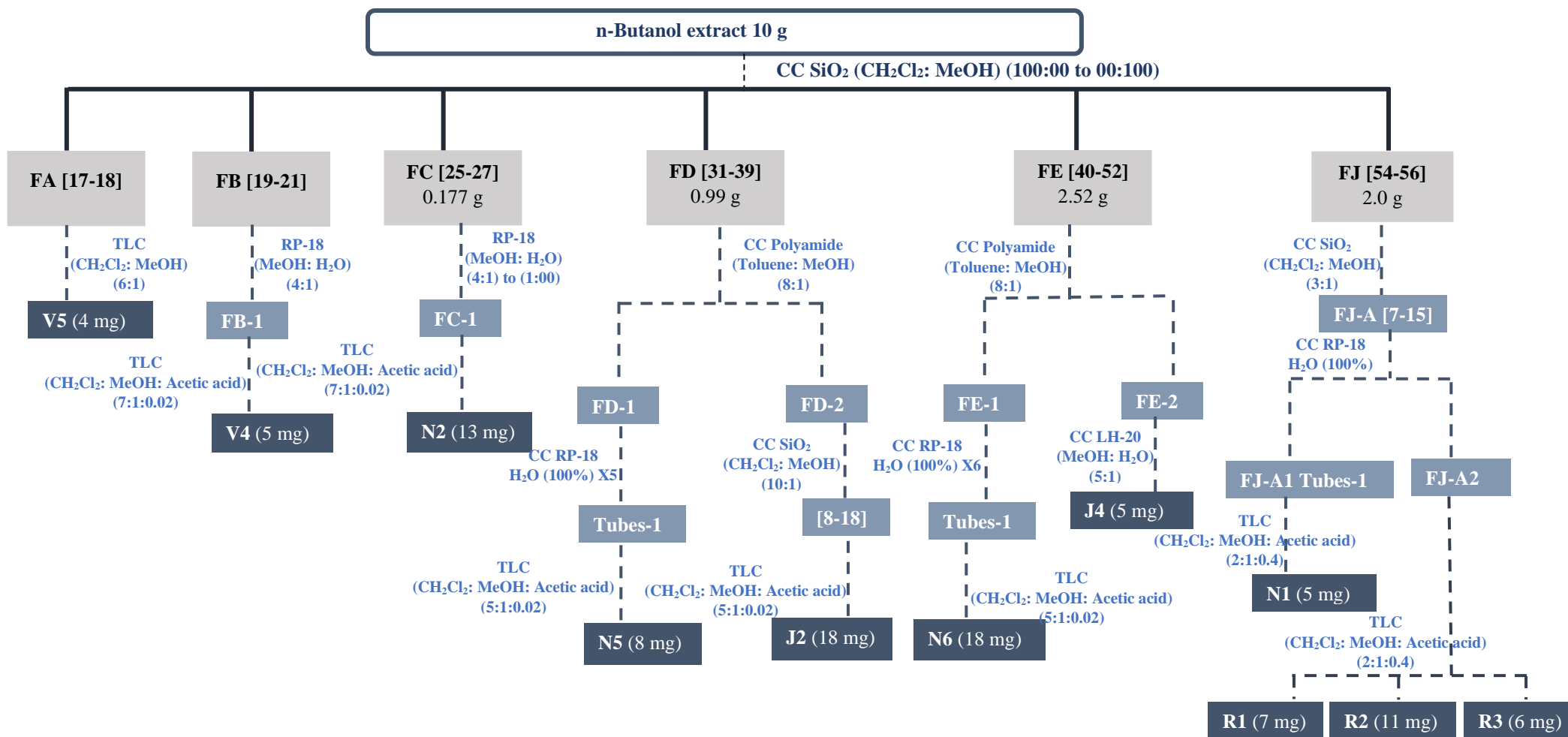
Figure. IV. 13: Diagram of fractionation and purification of the n-butanol extract.

IV.3.3. Petroleum ether extract

An open column filled with an amount of 210 g of normal phase silica gel was used for fractionation of 7 g of the Petroleum Ether extract by liquid chromatography (column chromatography). The elution is carried out with an isocratic mode of solvents: hexane–ethyl acetate (50: 1) (**Figure. IV. 14** and **Figure. IV. 16**). The collection of the sub-fractions was carried out in 25 ml tubes, the **tube 5** was chromatographed by column chromatography, the elution is carried out using an isocratic mode of solvents: cyclohexane–dichloromethane (20: 1), the grouping of the tubes according to their TLC profile under the UV lamp (254 and 366 nm) and revelation with a vanillin sulfuric acid solution and heating provided 2 sub-fractions (**FA** and **FB**). These fractions are subsequently subjected to purification operations (**Figure. IV. 16**).

I. **FA [6-18]** 98 mg: chromatographed by CC SiO₂ cyclohexane–dichloromethane (20: 1) and purified by TLC using system Cyclohexane/dichloromethane/ethyl acetate (50:0.5:0.5) X 2 to give **EP3** and **EP4 (Figure. IV. 15)**.

II. **FB [42-56]** 78 mg: the purification by TLC using system Cyclohexane/dichloromethane/ethyl acetate (50:0.5:0.5) X 4 to give **EP1** and **EP2 (Figure. IV. 15)**.
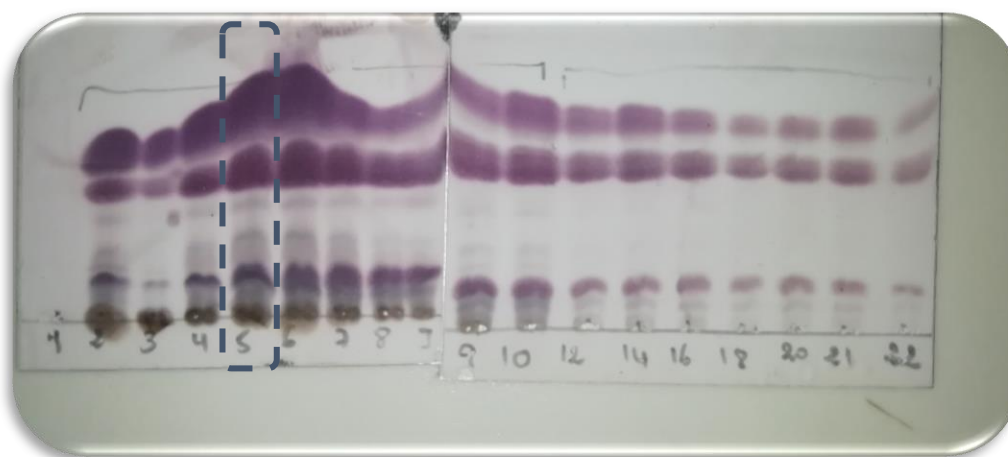
Figure. IV. 14: Follow of first column of the Petroleum Ether extract by TLC under revelation.
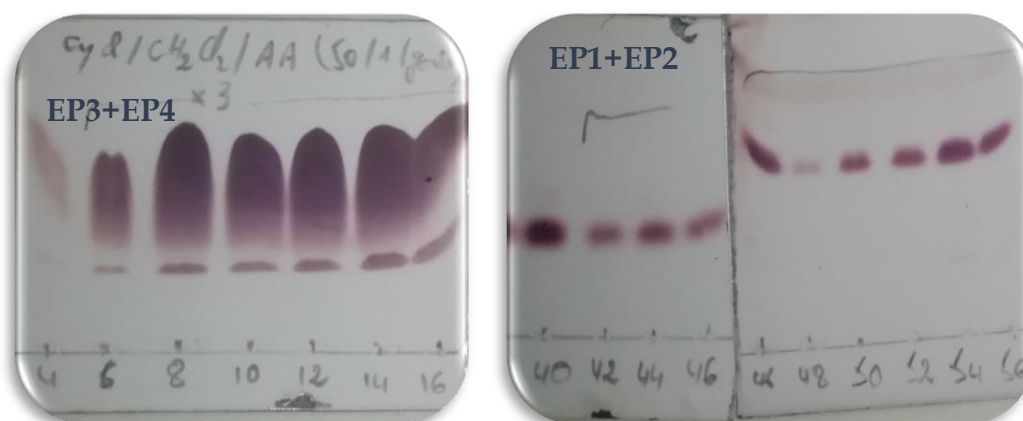
Figure. IV. 15: Follow of second column of the Petroleum Ether extract by TLC under revelation.
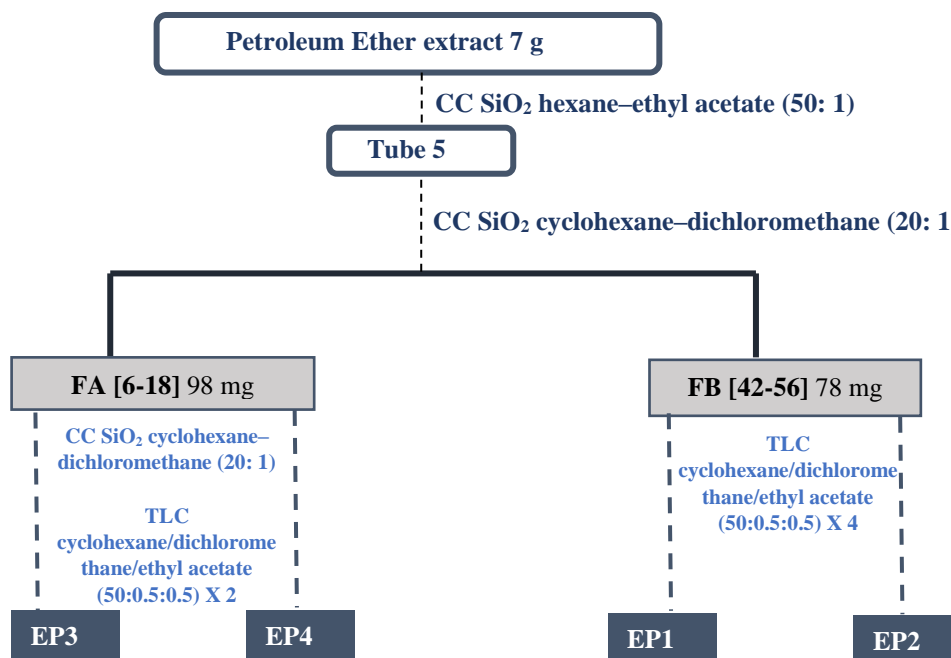
Figure. IV. 16: Diagram of fractionation of the Petroleum Ether extract.

IV.4. Structural elucidation of isolated compounds

The structural elucidation of the isolated compounds was made using different spectroscopic methods including: 1D and 2D NMR, UV-Vis and ESI-MS spectra.

IV.4. 1. Compound P1

The compound **P1** was isolated in the form of white crystals, soluble in dichloromethane. This compound is characterized on TLC test by invisible spot under UV light, which turns purple by revelation using vanillic acid solution and heating.

The ^{1}H NMR spectrum of the compound **P1** (**Figure. IV. 17**) recorded in CDCl$_3$, show the presence of seven methyl groups resonating at δ_H 0.75, 0.77, 0.83, 0.93, 0.97, 1.02 and 1.68 integrating of three protons for each as singlets (S, 3H) except the signal resonating at δ_H 1.68 (bs, 3H). These results lead us to a triterpene skeleton.

This spectrum also shows a signal in the form of double doublet resonating at δ_H 3.19 (dd, J = 11.3, 4.9 Hz, 1H) corresponding to CHO group corresponding to the position 3 of triterpene. The coupling constant value J = 11.3, 4.9 Hz, indicates an α-axial orientation of H-3 and a β-equatorial orientation of the OH group. In addition to the presence of two olefinic protons resonating at δ_H 4.57 (dd, J = 2.3, 1.3 Hz, 1H) and at δ_H 4.69 (d, J = 2.3 Hz, 1H).
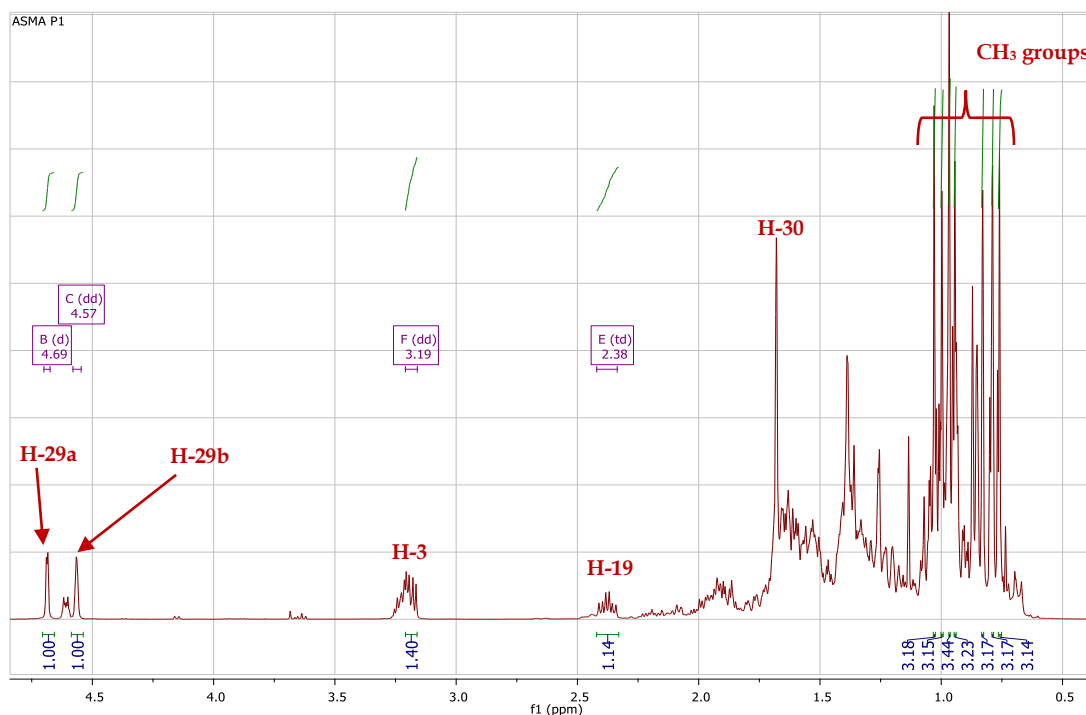
Figure. IV. 17: ^{1}H NMR spectrum (400 MHz, CD$_3$Cl) of the compound **P1**.

The ^{13}C NMR (**Figure. IV. 18**) reveals the presence of 30 thirty signals, confirm the triterpene skeleton of this compound. This spectrum also shows:

- ❖ The presence of seven methyl groups at δ_C 15.44, 17.96, 16.13, 14.57, 28.00, 16.02 and 19.41.

- ❖ The signals resonating between 18 and 55 ppm, attributable to CH_2, CH and quaternary carbons C.

- ❖ A signal at δ_C 79.01 attributable to a carbon with hydroxyl group substitution.

- ❖ Two olefinic carbons at δ_C 150.97 and 109.34.
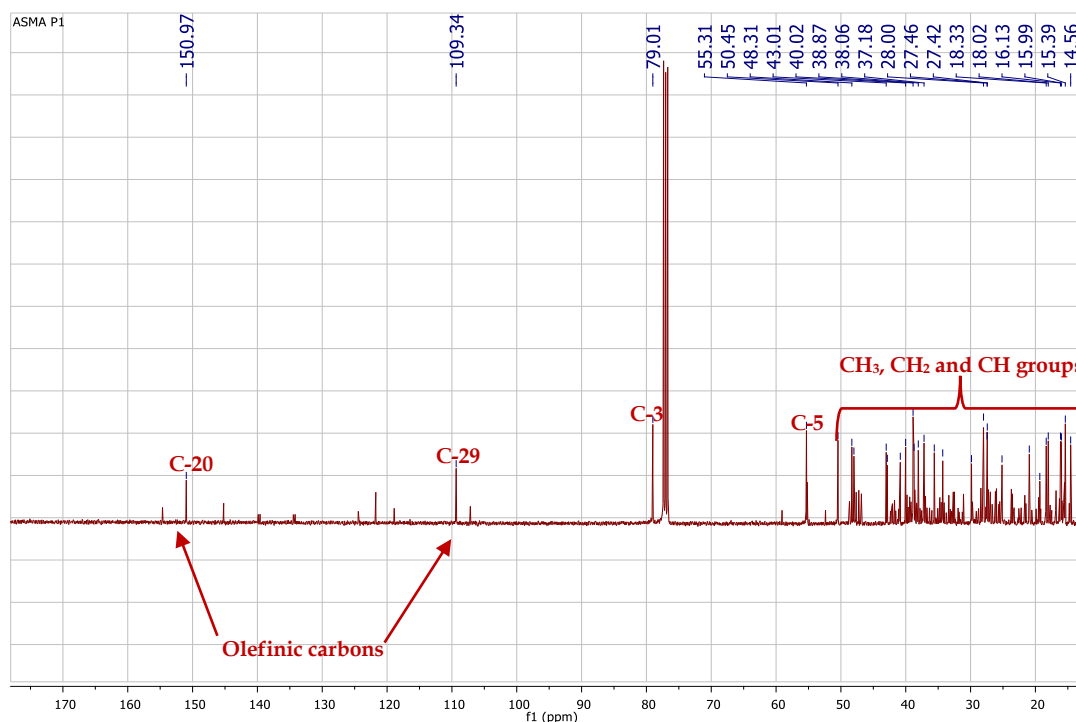
Figure. IV. 18: ^{13}C NMR (100 MHz, CD$_3$Cl) spectrum of the compound **P1.**

The DEPT135 spectrum (**Figure. IV. 19**) displays seven tertiary carbons (CH_3), eleven secondary carbons (CH_2) and six primary carbons (CH). We deduce six quaternary carbons (C). The DEPT135 spectrum confirms that one the olefinic carbons appeared at δ_C 150.97 is a quaternary carbon and the second that appeared at δ_C 109.34 is a methylene carbon.
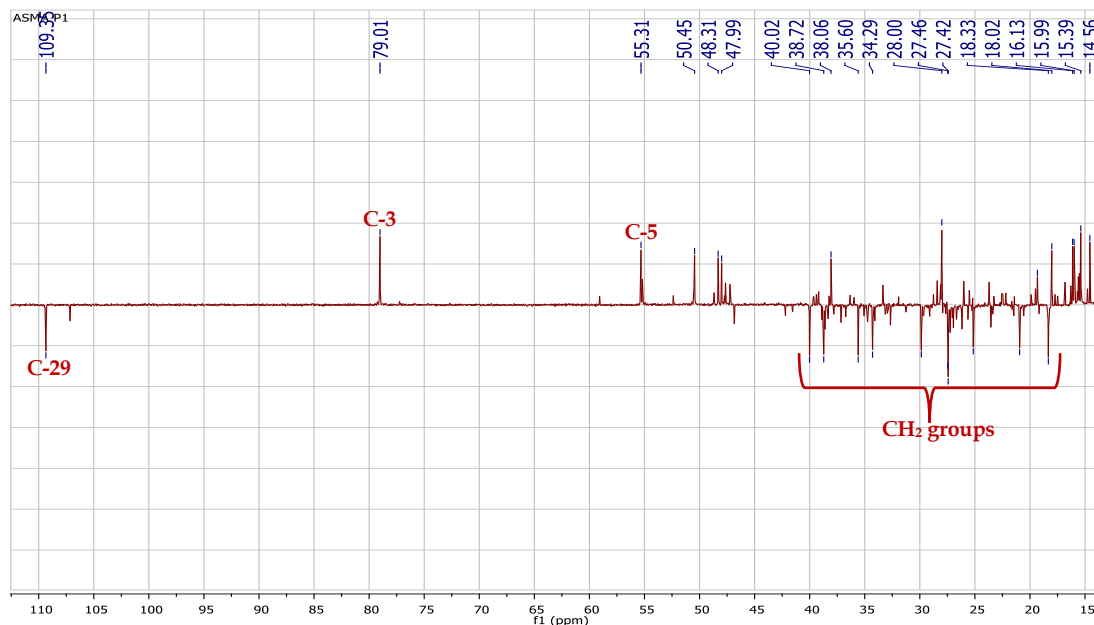
Figure. IV. 19: DEPT135 (100 MHz, CD_3Cl) spectrum of the compound **P1**.

The structural elucidation of **P1** is mainly based on the HSQC, HMBC and COSY spectra. This analysis makes it possible to identify and characterize a large number of carbons and protons of **P1**.

According to COSY spectrum (**Figure. IV. 26**), the proton H-3 shows a correlation with the proton resonating at 1.58 (m) corresponding to H-2, which show also a correlation with two protons resonating at δ_H 1.66 and 0.9 assigned to H-1a and H-1b, respectively.

The corresponding carbons was attributed using the HSQC experiment (**Figure. IV. 30**) as follows:

- ❖ H-1/ C-1 δ_C 38.72.
- ❖ H-2/ C-2 δ_C 27.42.
- ❖ H-3/ C-3 δ_C 79.01.

The HMBC spectrum (**Figure. IV. 32**) shows clear correlation spots between C-3 and two methyl groups resonating at δ_H 0.98 and 0.75 corresponding to H_3-23 and H_3-

24, respectively. These two methyl groups show correlation with a quaternary carbon resonating at δ_C 38.78 attributable to C-4 and with a methine carbon resonating at δ_C 55.31 corresponding to C-5 (**Figure. IV. 20**). The chemical shift of H-5 attributed by HSQC experiment at δ_H 0.67 (**Figure. IV. 30**).
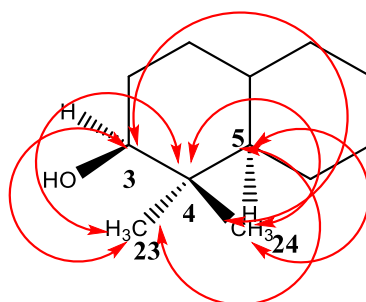
Figure. IV. 20: HMBC correlations of two methyl groups **Me-23** and **Me-24** of the compound **P1**.

The carbon C-5 shows a correlation spot in HMBC spectrum (**Figure. IV. 32**) with the protons of methyl group resonating at δ_H 0.83 attributable to H$_3$-25, which correlate with C-1 that previously identified. The protons of this methyl group H$_3$-25 show correlations with a methine carbon (CH) resonating at δ_C 50.45 and with a quaternary carbon at δ_C 37.18, corresponding to C-9 and C-10, respectively (**Figure. IV. 21**). The chemical shift of H-9 attributed by HSQC experiment at δ_H 1.27 (**Figure. IV. 30**). The carbon C-9 shows a correlation with another methyl group resonating at δ_H 1.03 attributable to the protons of the position 26 (Me-26), that correlate with two other carbons resonating at δ_C 34.30 (CH$_2$) and at δ_C 40.84 (quaternary carbon), corresponding to C-7 and C-8, respectively (**Figure. IV. 21**). The chemical shift of H-7 attributed by HSQC experiment (**Figure. IV. 30**) at δ_H 1.38.
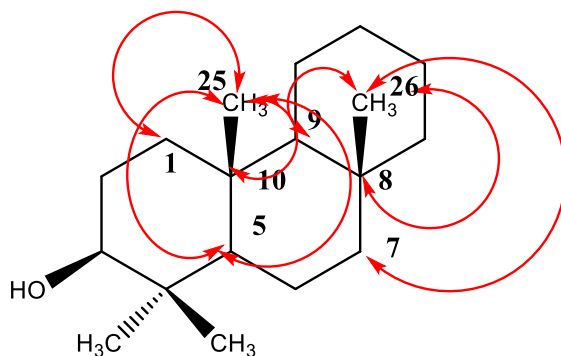
Figure. IV. 21: HMBC correlations of two methyl groups **Me-25** and **Me-26** of the compound **P1**.

According to the analysis of COSY spectrum (**Figure. IV. 26**) the proton H-5 shows correlation spots with two protons resonating at δ_H 1.53 and 1.38 corresponding to H-6a and H-6b, respectively. This spectrum also shows a spin system of six protons starting from H-9, which is make it possible to identify the coupling protons, H-11a at δ_H 1.40 and H-11b at δ_H 1.24, H-12a at δ_H 1.67 and H-12b at δ_H 1.04 and H-13 at δ_H 1.67 (**Figure. IV. 22**).
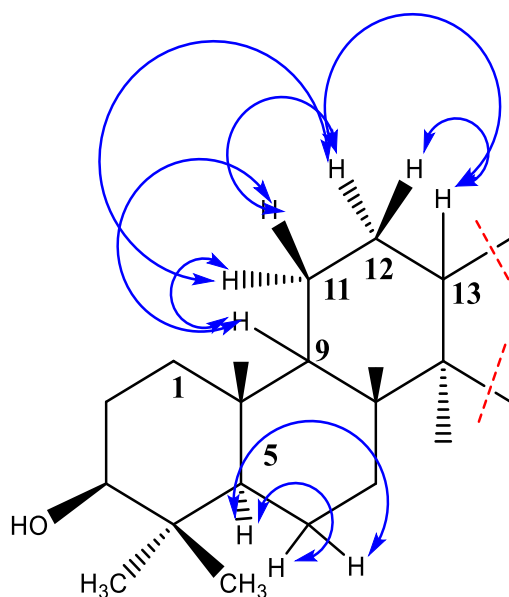
Figure. IV. 22: COSY correlations of H-6 and H-11 of the compound **P1**.

The corresponding carbons of the identified protons were attributed using the HSQC experiment (**Figure. IV. 30**) as follows:

- ❖ H-6/ C-6 δ_C 18.33.
- ❖ H-11/ C-11 δ_C 20.94.
- ❖ H-12/ C-12 δ_C 25.15.
- ❖ H-13/ C-13 δ_C 38.06.

The carbon C-13 shows correlation with the protons of methyl group resonating at δ_H 0.93 ppm corresponding to H_3-27, which shows a correlation with carbons resonating at δ_C 43.01 (quaternary carbon) and 27.46 (CH_2), corresponding to C-14 and C-15 respectively (**Figure. IV. 23**). The chemical shift of the protons H-15a and H-15b attributed by HSQC experiment at δ_H 1.66 and 0.99, respectively (**Figure. IV. 30**).
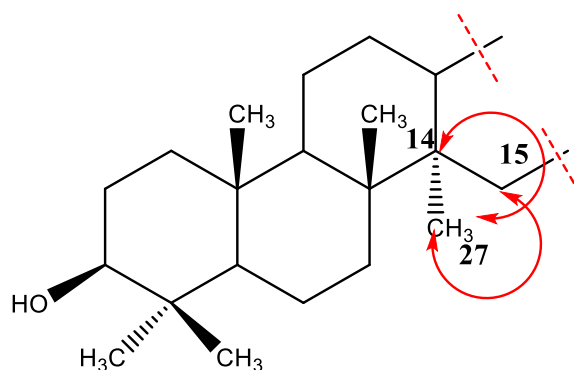
Figure. IV. 23: HMBC correlations of methyl group **Me-27** of **P1**.

According to COSY spectrum (**Figure. IV. 26**) the protons H_2-15 shows a correlation with the proton resonating at δ_H 1.37 assigned to H-16, which correlates in HSQC spectrum (**Figure. IV. 30**) with the C-16 that resonating at δ_C 40.02. The C-16 shows in HMBC spectrum a correlation with a methyl group resonating at δ_H 0.77 corresponding to H_3-28, this last shows also a correlation with three carbons resonating at δ_C 42.84, 48.31 and 35.60 corresponding to C-17, C-18 and C-22, respectively (**Figure. IV. 25**). The HSQC spectrum make it possible to identify their corresponding protons H-18 at δ_H 1.35, H-22a at δ_H 1.47 and H-22b at δ_H 1.37.

The HSQC spectrum (**Figure. IV. 24**) allowed us to link the methyl groups of each proton with its carbon as follows:

- ❖ H-23 (0.98) C-23 (28.00).
- ❖ H-24 (0.75) C-24 (15.39).
- ❖ H-25 (0.83) C-25 (16.21).
- ❖ H-26 (1.03) C-26 (16.02).
- ❖ H-27 (0.93) C-27 (14.56).
- ❖ H-28 (0.77) C-28 (18.02).
- ❖ H-30 (1.68) C-30 (19.32).
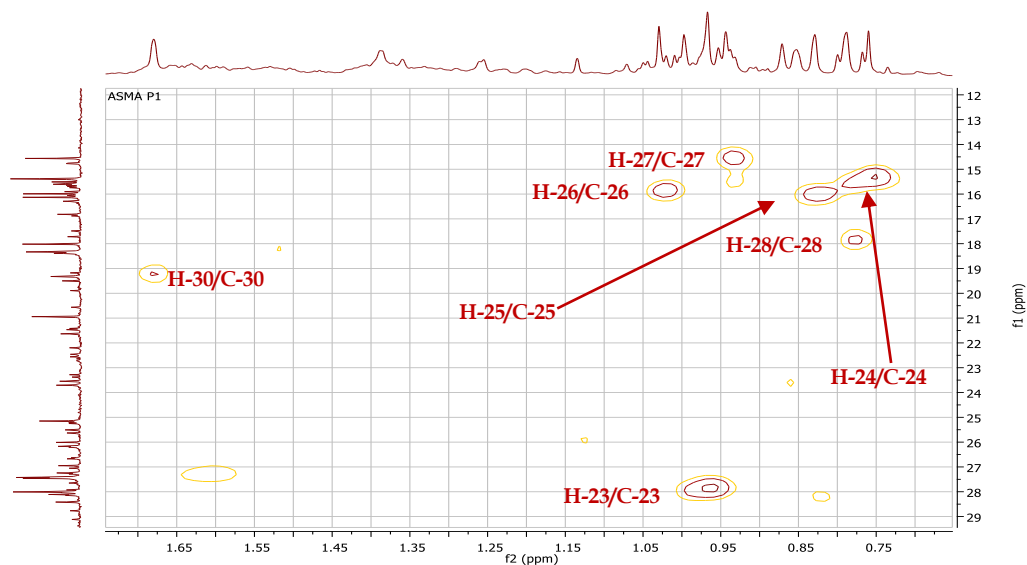
Figure. IV. 24: HSQC spectrum (400 MHz, CD$_3$Cl) of the methyl groups of the compound **P1**.
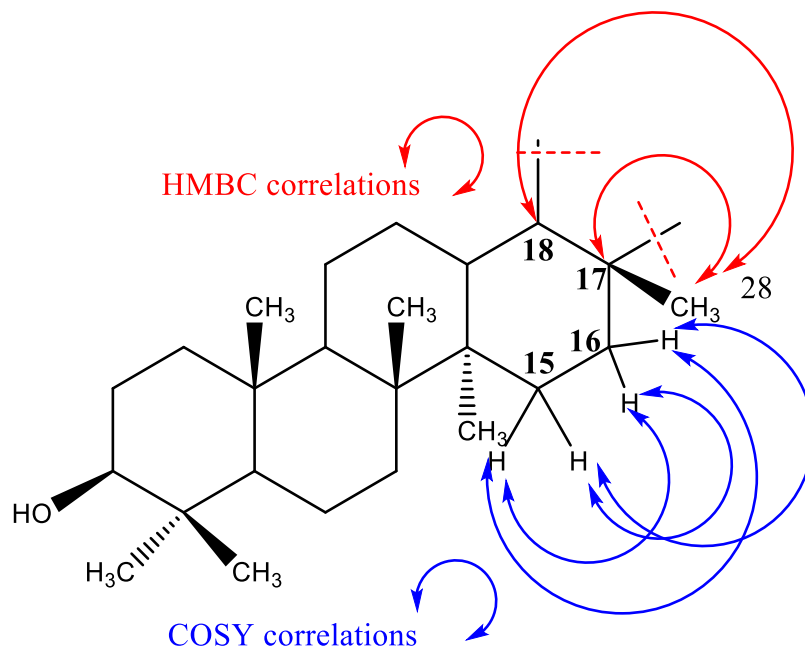
Figure. IV. 25: COSY and HMBC correlations of Me-28 of the compound **P1.**
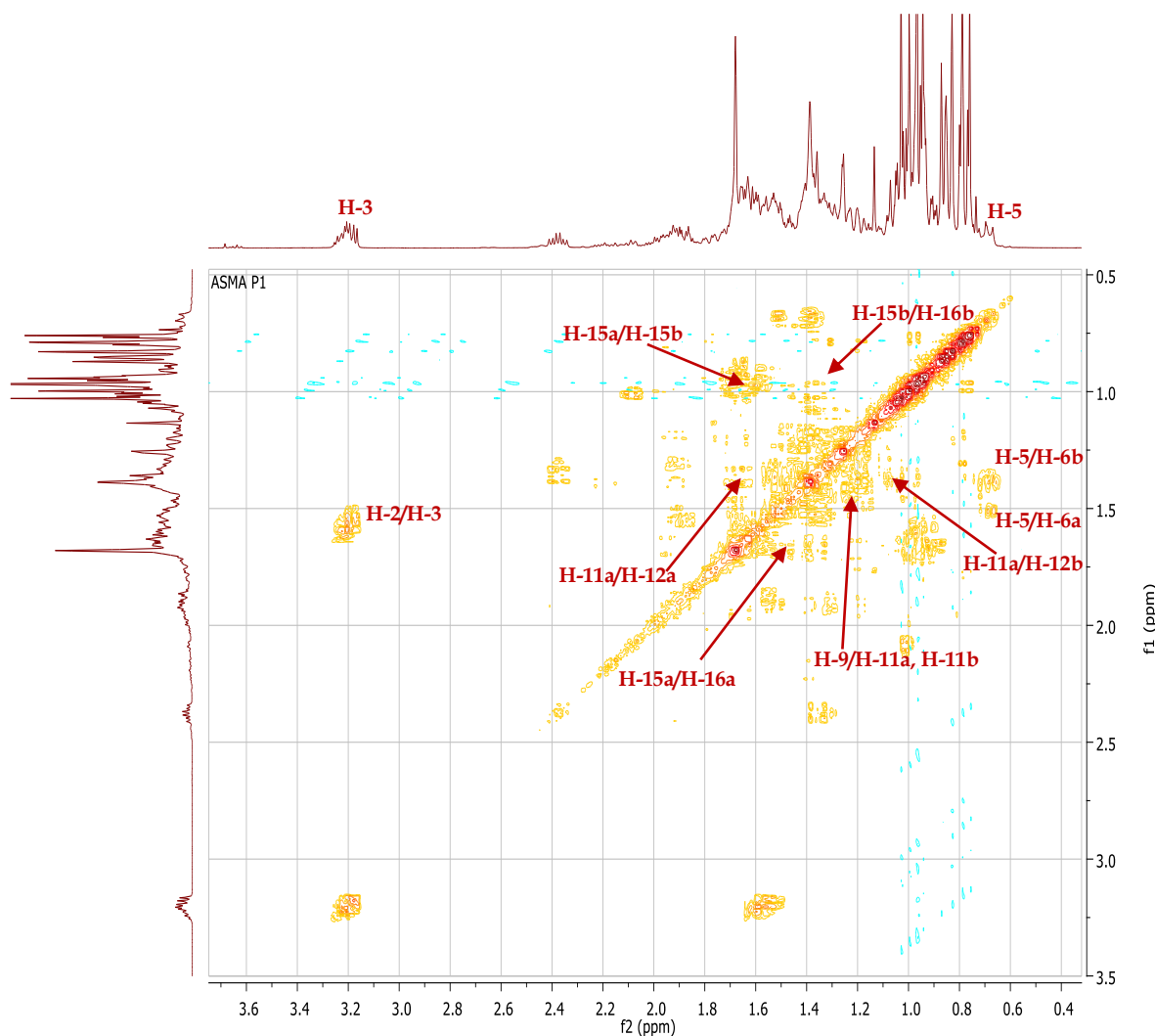
Figure. IV. 26: COSY spectrum from H-3 to H-16 of the compound **P1**.

The two olefinic protons resonating at δ_H 4.57 (dd, J = 2.3, 1.3 Hz, 1H) and δ_H 4.69 (d, J = 2.3 Hz, 1H) correlates in HSQC spectrum (**Figure. IV. 31**) with the methylene carbon (CH$_2$) δ_C 109.35, the coupling constant (1.3 Hz) confirms the presence of isopropenyl group, a characteristic of triterpene lupane type. These two protons assigned to H-29a and H-29b displays a correlation in COSY spectrum (**Figure. IV. 27**) with the methyl group resonating at δ_H 1.68 corresponding to H-30. This last exhibits a correlation in HMBC spectrum with two carbons resonating at δ_C 47.99 and 150.97 corresponding to C-19 and C-20. The chemical shift of the proton H-19 and the carbon C-30 were attributed by HSQC experiment at δ_H 2.37 and at δ_C 19.32, respectively.
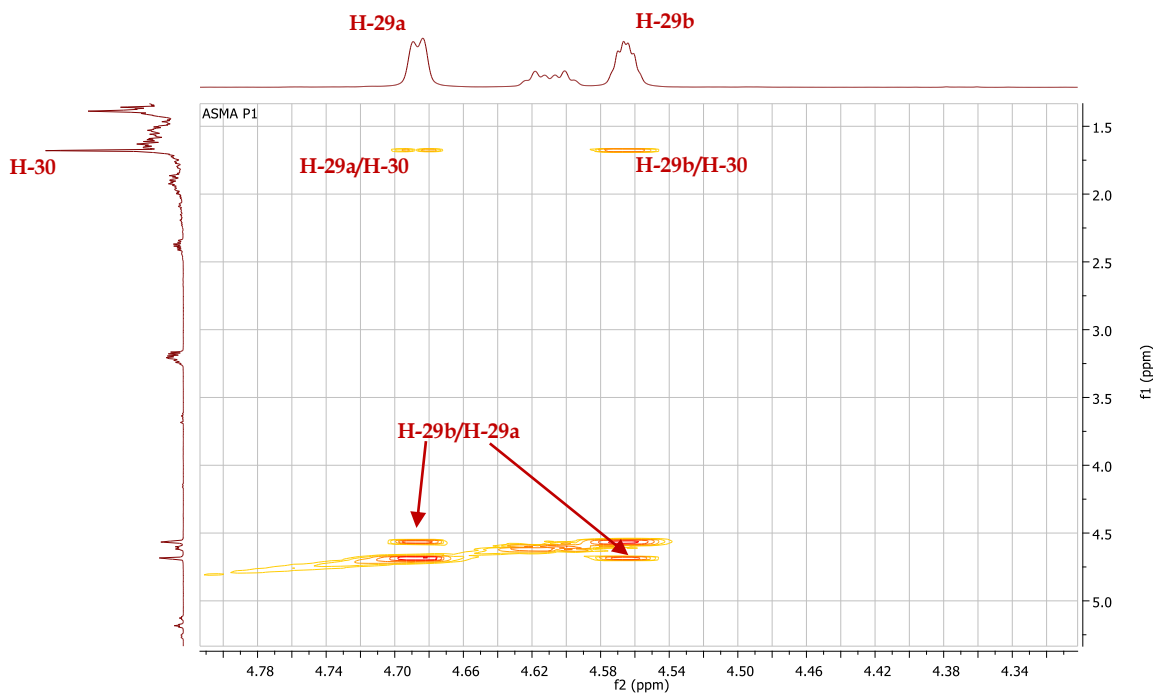
Figure. IV. 27: COSY spectrum (400 MHz, CD$_3$Cl) of H$_2$-29 and H$_3$-30 of the compound **P1**.

According to COSY spectrum spins system of six protons was identified starting from H-18 to H-22 (**Figure. IV. 29**).
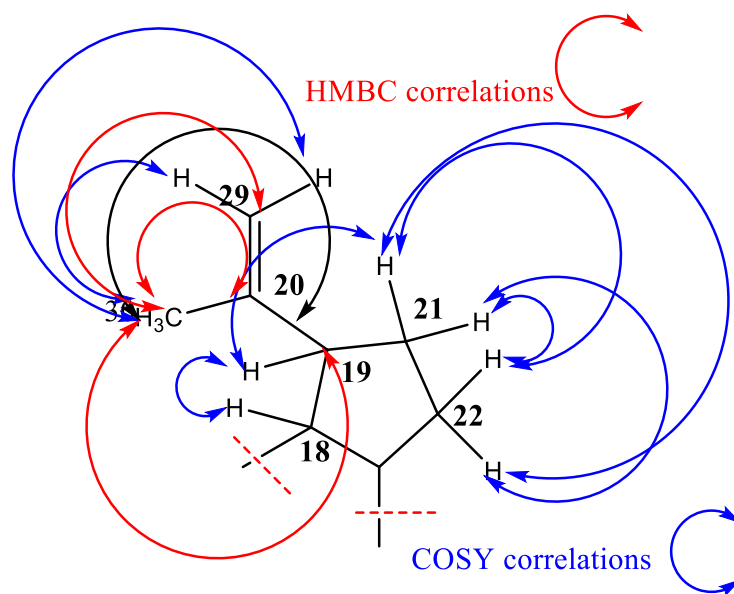
Figure. IV. 28: HMBC and COSY correlations of Me-30 and their vicinal protons of the compound **P1**.
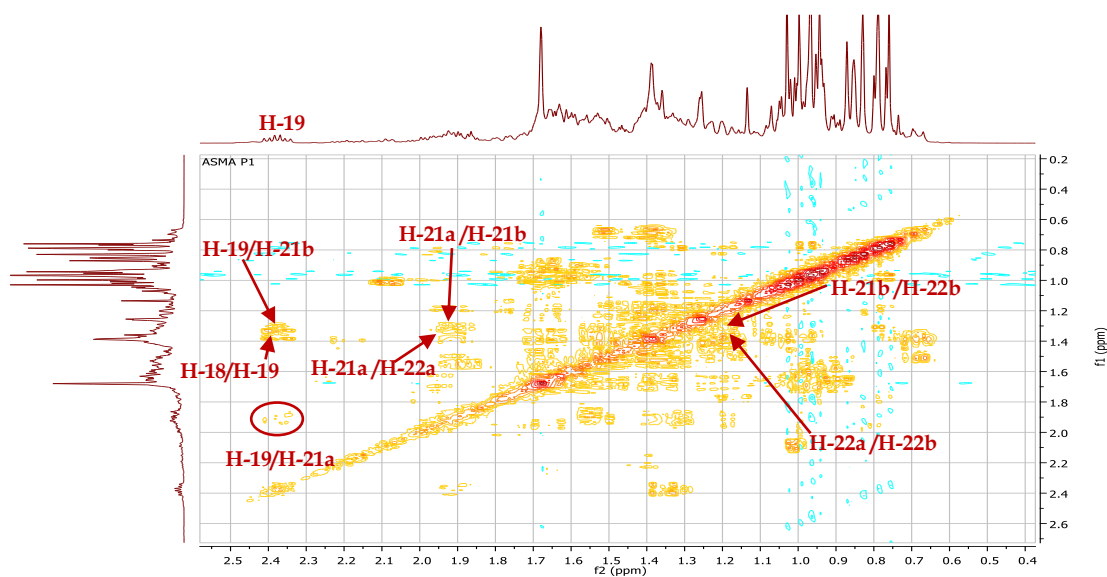
Figure. IV. 29: COSY spectrum (400 MHz, CD$_3$Cl) from H-18 to H-22 of **P1**.
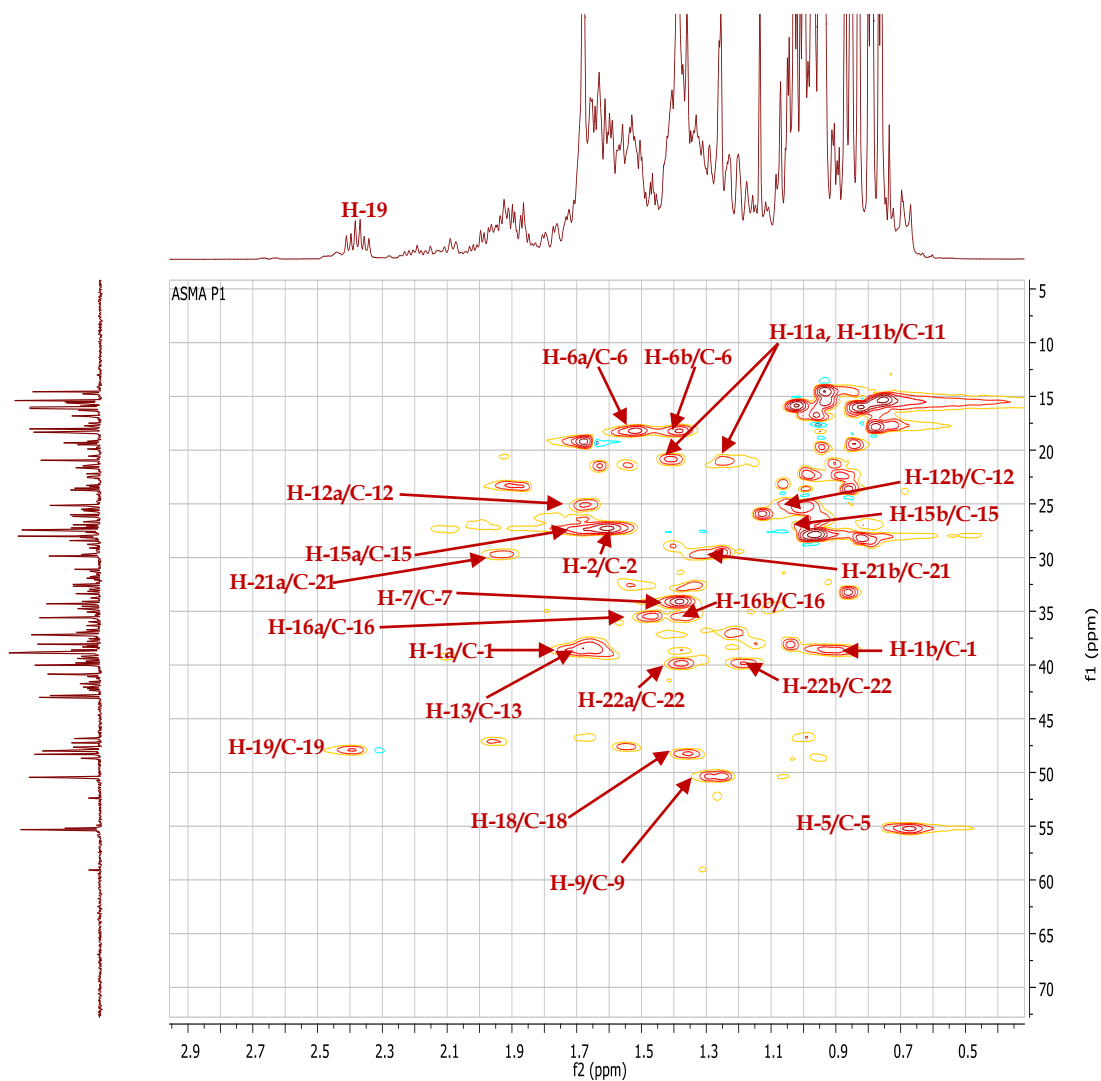
Figure. IV. 30: HSQC spectrum (400 MHz, CD$_3$Cl) of **P1**.
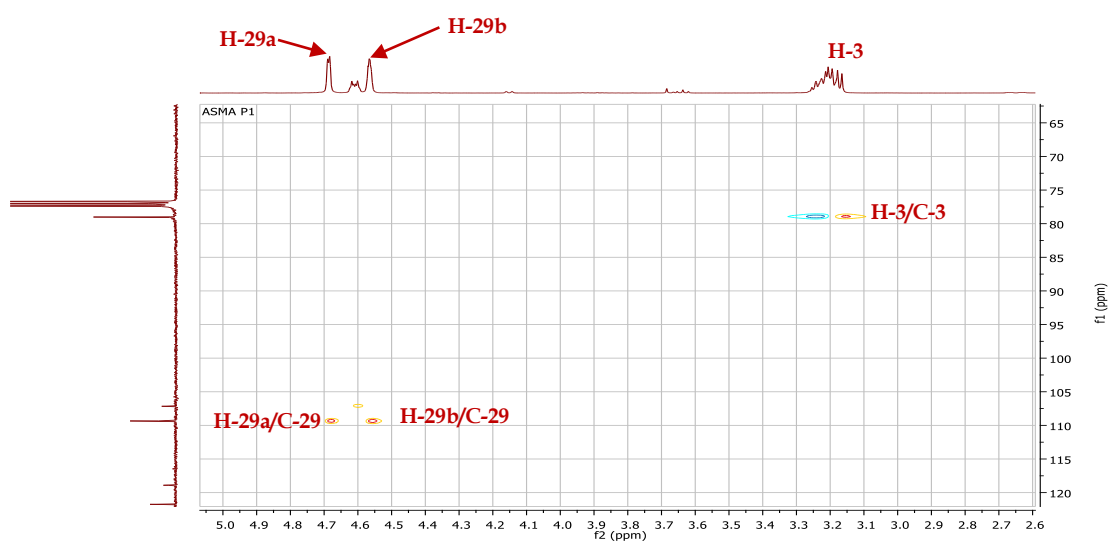
Figure. IV. 31: HSQC spectrum (400 MHz, CD$_3$Cl) of H-29 and H-3 compound **P1**.
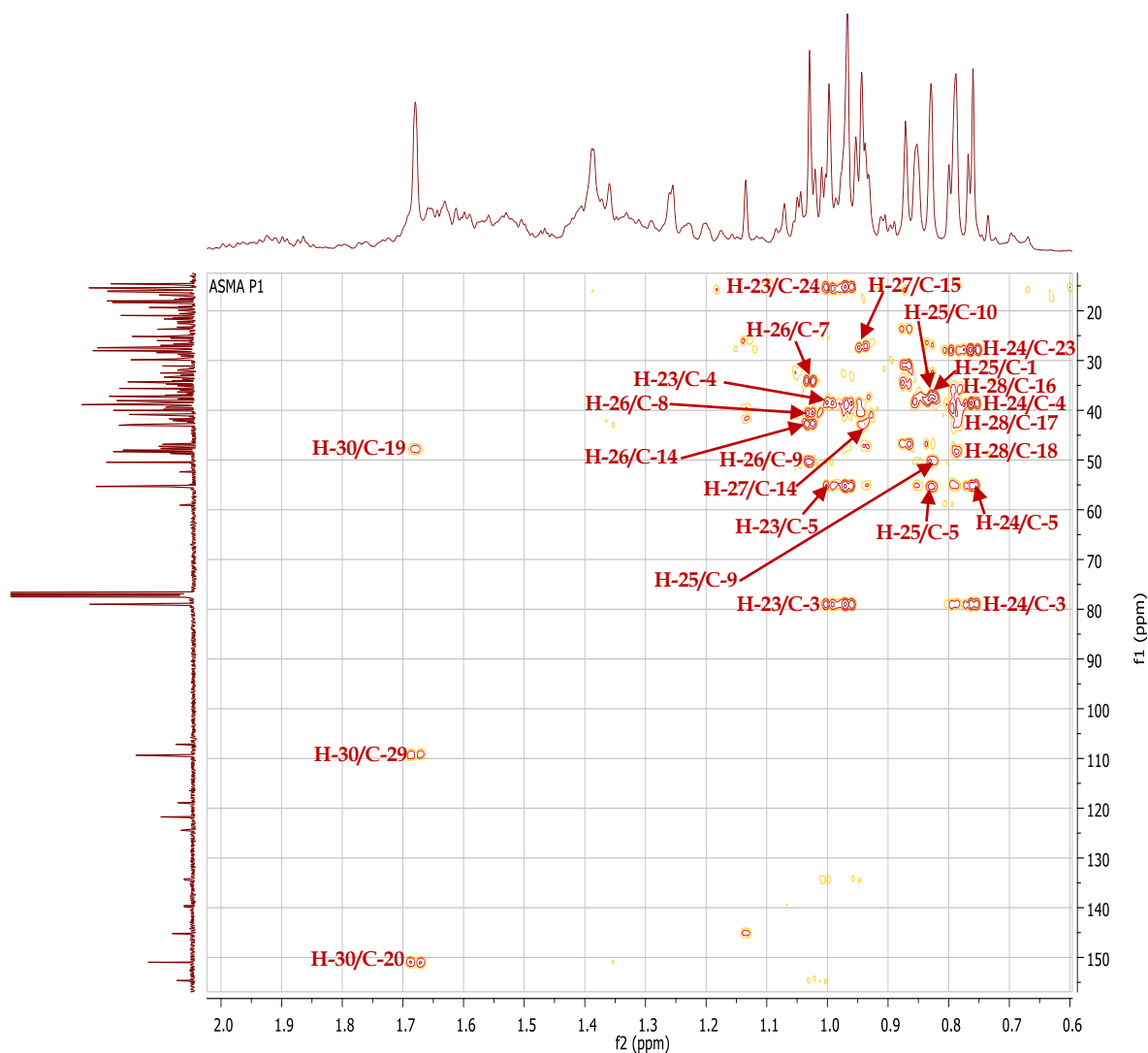
Figure. IV. 32: HMBC spectrum (400 MHz, CD$_3$Cl) of methyl groups of **P1**.

The findings of ^{1}H NMR and ^{13}C NMR and the analysis of HSQC, HMBC and COSY spectra and by comparing the chemical shifts with the literature data, the compound **P1** can be identified as lupeol (**Figure. IV. 33**). This compound has been previously isolated from species *A. flava* [52], *A. serratuloides* [51], *A. cancellata* [50] and *A. humilis* [53], and isolated for the first time form the species *A. aristata*. The ^{1}H and ^{13}C NMR data, are summarized in the **Table. IV. 3**, which are in total agreement with the literature [194, 195].
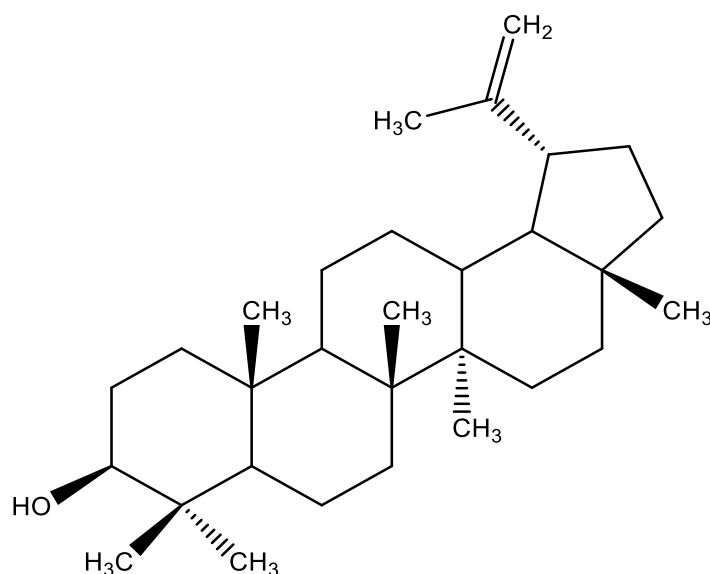
Figure. IV. 33: Structure of compound **P1;** lupeol.

Table. IV. 3: The chemical shifts of ^{1}H (400 MHz) and ^{13}C NMR (100 MHz) on CDCl$_3$ of compound **P1** (δ_C in ppm and δ_H in ppm and J in Hz).

Position	carbon	Proton
1	38.72	1.66 (m) H-1a 0.90 (m) H-1b
2	27.42	1.58 (m)
3	79.01	3.19 (dd, J = 11.3, 4.9 Hz, 1H)
4	38.87	--
5	55.31	0.67 (m)
6	18.33	1.53 (m) H-6a 1.38 (m) H-6b
7	34.30	1.38 (m)
8	40.84	--

9	50.45	1.27 (d, J = 2.2 Hz, 1H) H-9 α
10	37.18	--
11	20.94	1.40 (m) H-11a
		1.24 (m) H-11b
12	25.15	1.67 (m) H-12a
		1.04 (m) H-12b
13	38.06	1.67 (m)
14	43.01	--
15	27.46	1.66 (m) H-15a
		0.99 (m) H-15b
16	35.60	1.47 (m) H-16a
		1.37 (m) H-16b
17	42.84	--
18	48.31	1.35 (m)
19	47.99	2.38 (td, J = 11.0, 5.8 Hz, 1H)
20	150.97	--
21	29.86	1.92 (m) H-21a
		1.33 (m) H-21b
22	40.02	1.37 (m) H-22a
		1.18 (m) H-22b
23	28.00	0.98 (S, 3H)
24	15.39	0.75 (S, 3H)
25	16.21	0.83 (S, 3H)
26	16.02	1.03 (S, 3H)
27	14.56	0.93 (S, 3H)
28	18.02	0.77 (S, 3H)
29	109.34	4.69 (d, J = 2.3 Hz, 1H) H-29a
		4.57 (dd, J = 2.3, 1.3 Hz, 1H) H-29b
30	19.32	1.68 (brs, 3H)

IV.4. 2. Compound P2

The compound **P2** was isolated in the form of white crystals, soluble in methanol. This compound is characterized on TLC test by invisible spot under UV light which turns purple by revelation using vanillic acid solution and heating.

The ^{1}H NMR spectrum (**Figure. IV. 34**) recorded in CD$_3$OD, displays seven methyl singlet signals integrating three protons for each. This leads us to a triterpene skeleton.
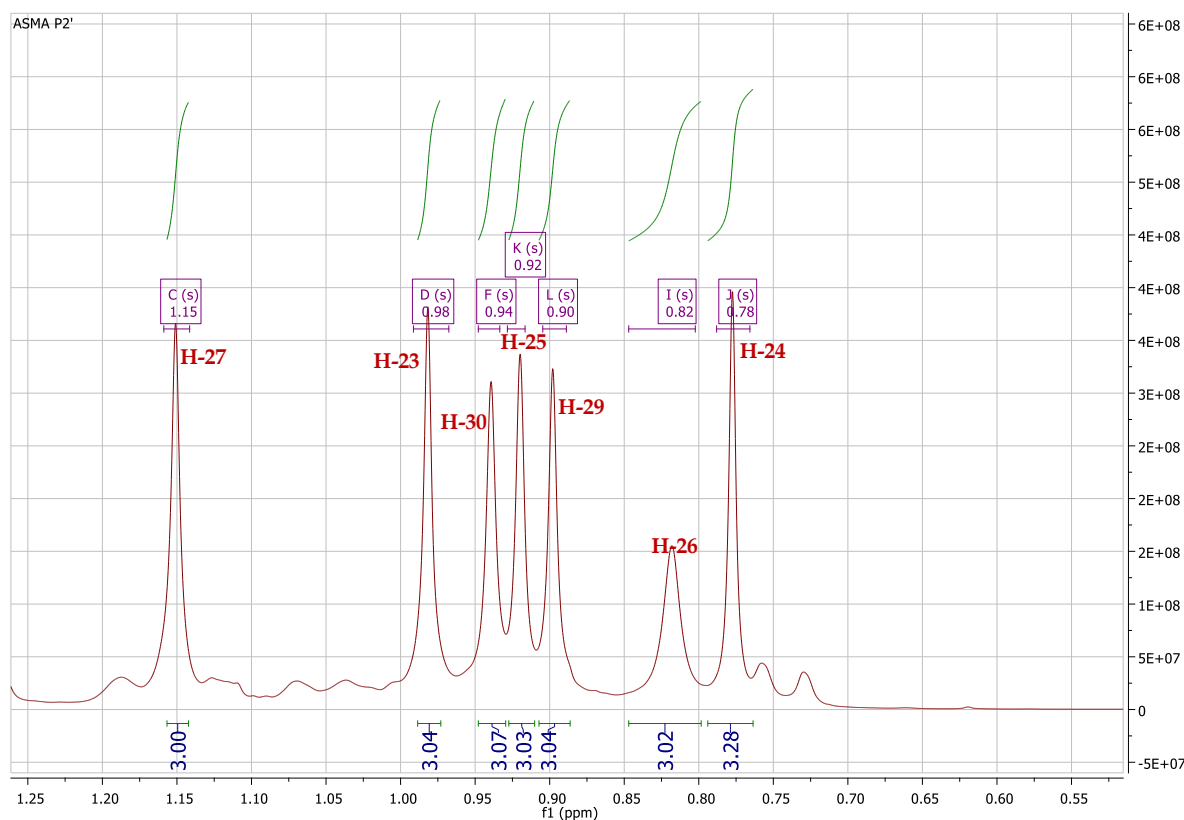
Figure. IV. 34: ^{1}H NMR spectrum (400 MHz, CD$_3$OD) of methyl groups of the compound **P2**.

The ^{1}H NMR spectrum (**Figure. IV. 35**) also shows:

- ❖ a signal in the form of a broad doublet at δ_H 3.19 (brd, J=15.8 Hz, 1H) attributable to the proton H-3. The coupling constant value 15.8 Hz indicates an α-axial orientation of H-3 and by therefore a β- equatorial orientation of the OH group of the same position.
- ❖ A signal in the form of a broad singlet at δ 5.25 ppm characteristic of an olefinic proton.

❖ A mass of protons resonating between 0.9 to 1.9 ppm, corresponding to the CH and CH_2 of the triterpene skeleton.

❖ A signal in the form of a double doublet at δ_H 2.85 (dd, J=13.6 and 3.5 Hz, 1H) attributable to H-18 this indicates that **P2** is an oleanane derivative [196]. Additionally, the multiplicity of the proton H-18 indicates the presence of two adjacent protons which will be H-19a and H-19b, and the coupling constant value that a typical shift in the oleanane series [197]. The coupling constant value of H-18 is very important to distinguish between the α amyrin and β amyrin skeleton.

From the data collected from the ^{1}H NMR spectrum, it is deduced that compound **P2** is a pentacyclic triterpene skeleton of a β-amyrin form precisely of a **3-hydroxy-olean-12-ene**.
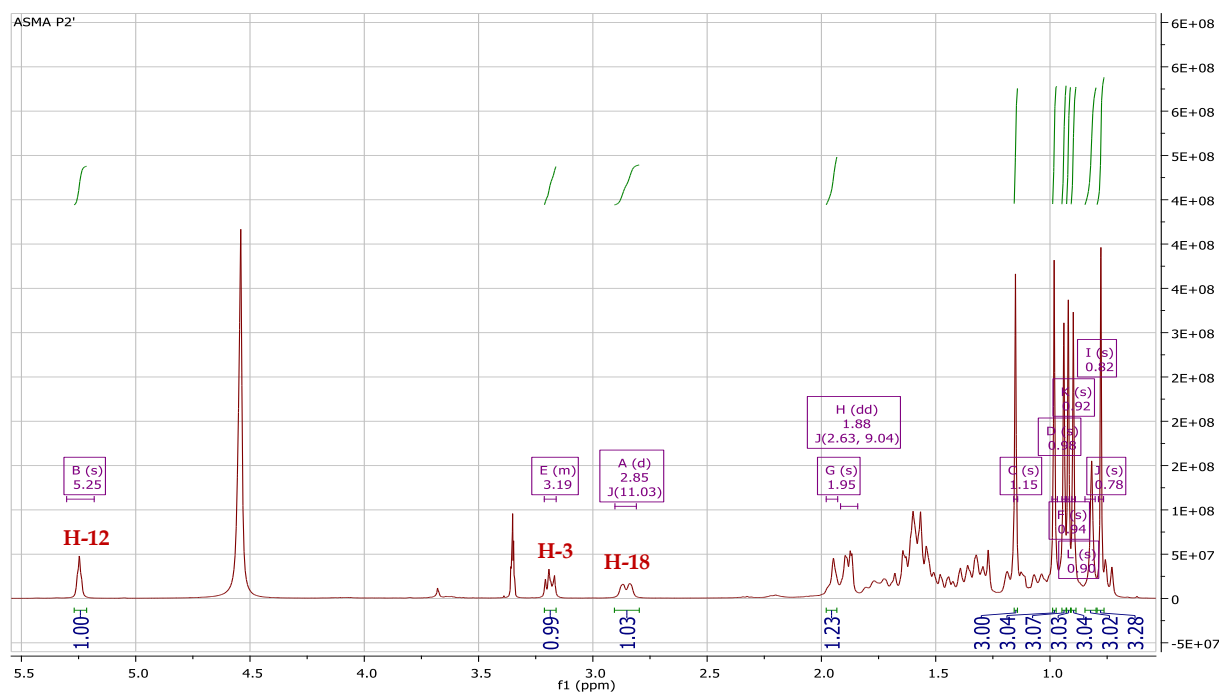
Figure. IV. 35: ^{1}H NMR spectrum (400 MHz, in CD$_3$OD) of **P2**.

The ^{13}C NMR (**Figure. IV. 36**) reveals the presence of thirty carbon signals, confirming the pentacyclic triterpene skeleton. This spectrum also exhibits:

❖ The presence seven methyl groups at 15.04, 15.38, 16.84, 23.32, 25.67, 27.80 and 32.92 ppm.

❖ The chemical shifts of olefinic carbons at δ_C 121.59 and 144.70 are attributable to C-12 and C-13 respectively, are characteristic of the β-amyrin structure [195].

The difference between the chemical shift of the two olefinic carbons is of the order of $\Delta\delta=23.11$ ppm that a typical of **Olean-12-ene**, these values are in total agreement with the literature [195, 198].

❖ A set of carbons resonating between 18 and 55 ppm, attributable to CH_2, CH and quaternary carbons.
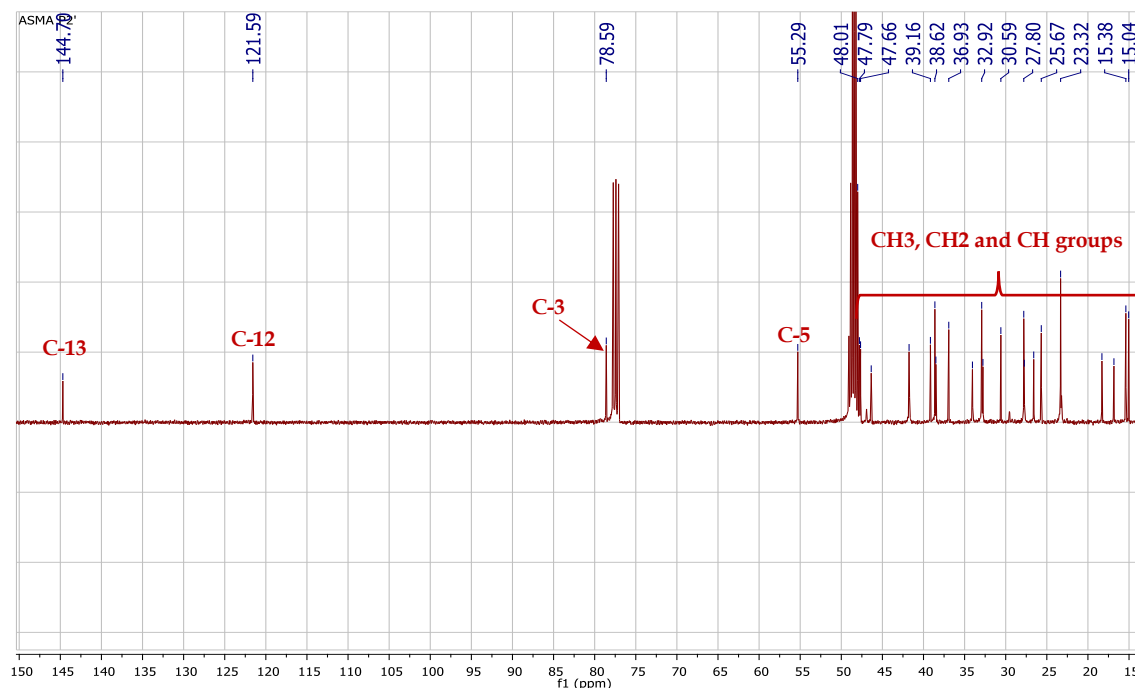
Figure. IV. 36: ^{13}C NMR spectrum (100 MHz, CD$_3$OD) of **P2**.

According to the DEPT 135 spectrum (**Figure. IV. 37**), there are seven tertiary carbons (CH$_3$), ten secondary carbons (CH$_2$) and five primary carbons (CH). We thus deduce seven quaternary carbons (C).
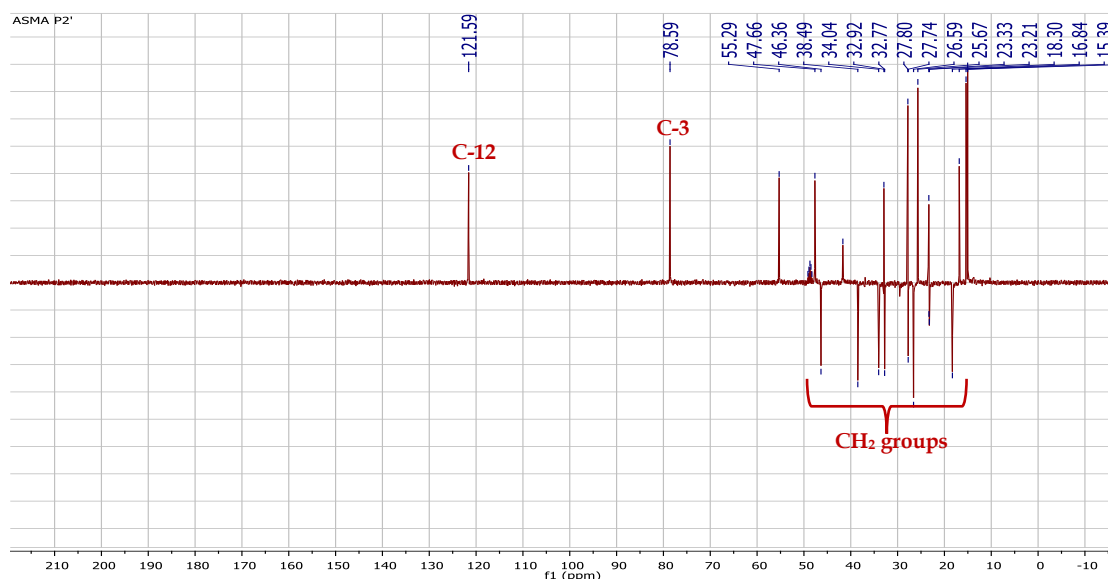
Figure. IV. 37: DEPT135 spectrum (100MHz, CD$_3$OD) of the **P2**.

Starting from the identified proton H-3 and according to COSY (**Figure. IV. 43**), HMBC (**Figure. IV. 41**) and HSQC (**Figure. IV. 42**) spectra, the protons and carbons from (C-1 and H-1) to (C-11 and H-11) are identified, in addition to the methyl groups (Me-23, Me-24, Me-25 and Me-26) as we explained in the previous compound **P1**, as follow:

- ❖ C-1/ H_2-1 (38.49 ppm /H-1b 0.96 and H-1a 1.61 ppm).
- ❖ C-2/ H_2-2 (26.59 ppm / 1.58 ppm).
- ❖ C-3/ H-3 (78.59 ppm / 3.19 ppm).
- ❖ C-4 (38.60 ppm).
- ❖ C-5/ H-5 (55.29 ppm /0.72 ppm).
- ❖ C-6/ H_2-6 (18.30 ppm /H-6b 1.38 and H-6a 1.53 ppm).
- ❖ C-7/ H_2-7 (32.77 ppm /H-7b 1.51 and H-7a 1.71 ppm.
- ❖ C-8 (39.19 ppm).
- ❖ C-9/ H-9 (47.66/1.55 ppm).
- ❖ C-10 (36.93 ppm).
- ❖ C-11/H_2-11 (23.21/1.88 ppm).

The identified protons H_2-11 (1.88 ppm) shows a correlation spot in COSY spectrum with an olefinic proton resonating at 5.25 ppm assigned to H-12. This last reveals a correlation in HMBC spectrum with an olefinic carbon resonating at 144.7 corresponding to C-13. This last identified carbon (C-13) displays a correlation in HMBC spectrum with the protons of methyl group resonating at δ_H 1.14 ppm corresponding to H_3-27, which exhibits correlation spots with carbons resonating at δ_C 41.76 (quaternary carbon) and at δ_C 27.74 (CH_2), corresponding to C-14 and C-15, respectively (**Figure. IV. *38***). The chemical shift of the protons H-15a and H-15b were attributed by HSQC experiment at δ_H 1.75 and 1.03, respectively.
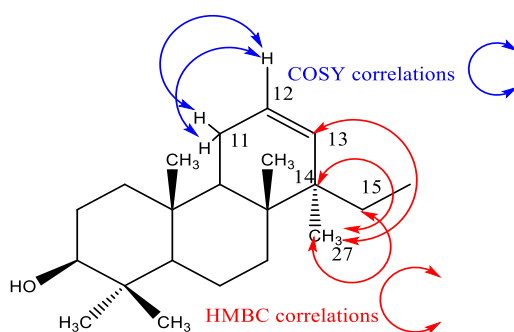
Figure. IV. 38: HMBC and COSY correlations of H-12 and Me-27 of **P2**.

According to COSY spectrum (**Figure. IV. 42**) the protons H$_2$-15 reveals correlations with the protons resonating at δ$_H$ 1.58 and 1.89 assigned to H-16b and H-16a, which correlate in HSQC spectrum with the C-16 δ$_C$ 23.31. The protons H$_2$-16 displays in HMBC spectrum a correlation spot with a quaternary carbon resonating at δ$_C$ 47.79 corresponding to C-17.

The HSQC experiment (**Figure. IV. 42**) established the connectivity between C-18 (41.69) and H-18 (δ$_H$ 2.85, dd, J=13.6 and 3.5 Hz)). This last shows in COSY spectrum correlations with two protons at δ$_H$ 1.12 and 1.64 ppm corresponding to H-19b and H-19a, respectively. Which are reveals a correlation in HMBC spectrum with quaternary carbon at δ$_C$ 30.59, assigned to C-20.

The HMBC experiment (**Figure. IV. 41**) established the connectivity between C-20 and two methyl groups resonating at δ$_H$ 0.89 and 0.94 ppm attributable to H$_3$-29 and H$_3$-30, respectively. This is also very important to confirm the β-amyrin skeleton. These two last identified protons show also correlations with carbon resonating at δ$_C$ 34.04 corresponding to C-21. The analysis of HSQC spectrum makes it possible to identify their corresponding protons H-21b and H-21a at δ$_H$ 1.16 and 1.34, respectively. In the last, these protons reveal in COSY spectrum (**Figure. IV. 43**) correlation spots with two protons resonating at δ$_H$ 1.30 and 1.44 ppm corresponding to H-22b and H-22a, respectively (**Figure. IV. 39**). HSQC spectrum makes it possible to identify its corresponding carbon at δ$_C$ 32.77.
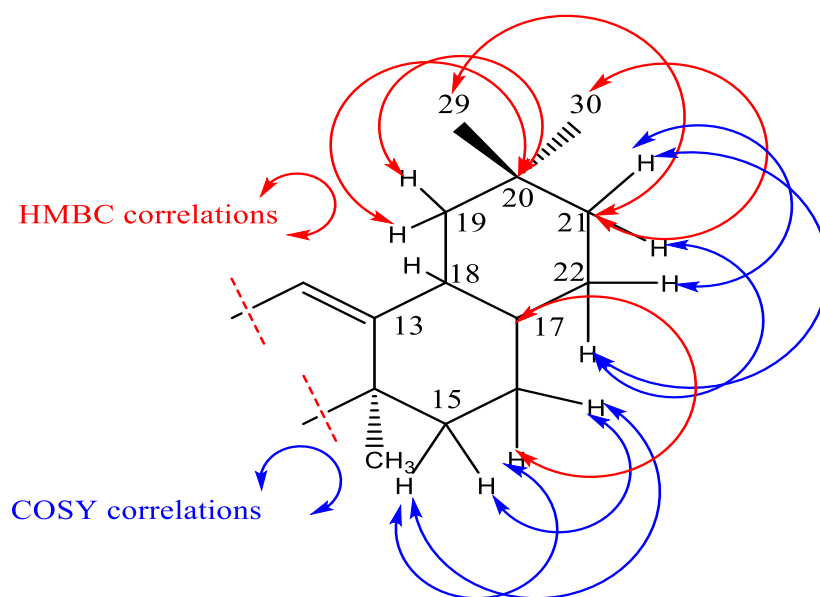
Figure. IV. 39: HMBC and COSY correlations from 15 to 30 positions of **P2**.

The HSQC spectrum (**Figure. IV. 40**) allowed us to link the methyl groups of each proton with its carbon as follows:

- ❖ H_3-23 (0.98) C-23 (27.80).
- ❖ H_3-24 (0.78) C-24 (15.38).
- ❖ H_3-25 (0.92) C-25 (15.04).
- ❖ H_3-26 (0.82) C-26 (16.84).
- ❖ H_3-27 (1.15) C-27 (25.67).
- ❖ H_3-29 (0.90) C-29 (32.92).
- ❖ H_3-30 (0.94) C-30 (23.32).
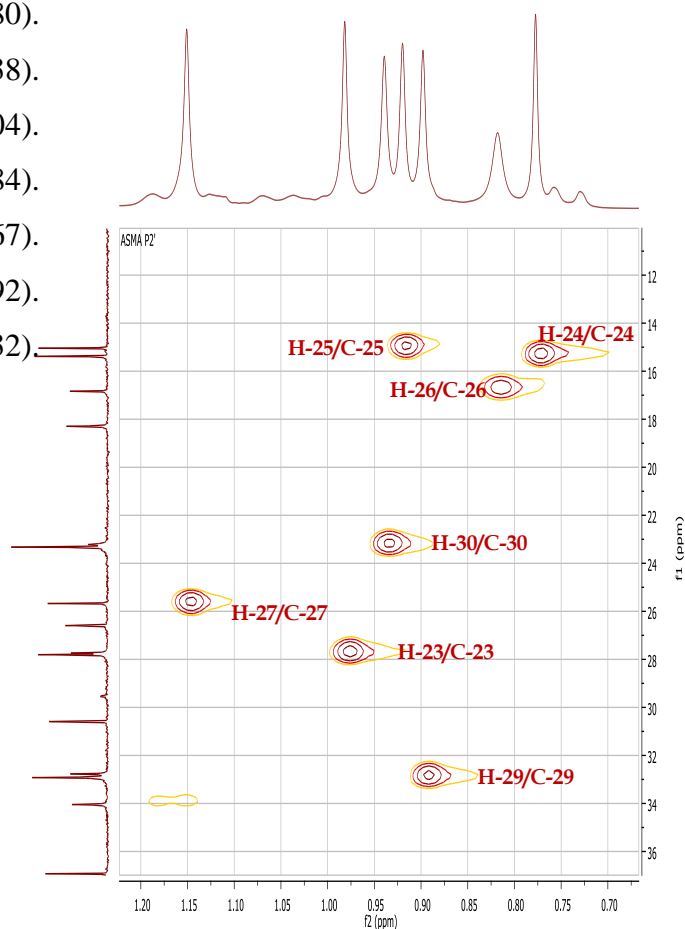
Figure. IV. 40: HSQC Spread Spectrum (400 MHz, CD_3OD) of **P2.**
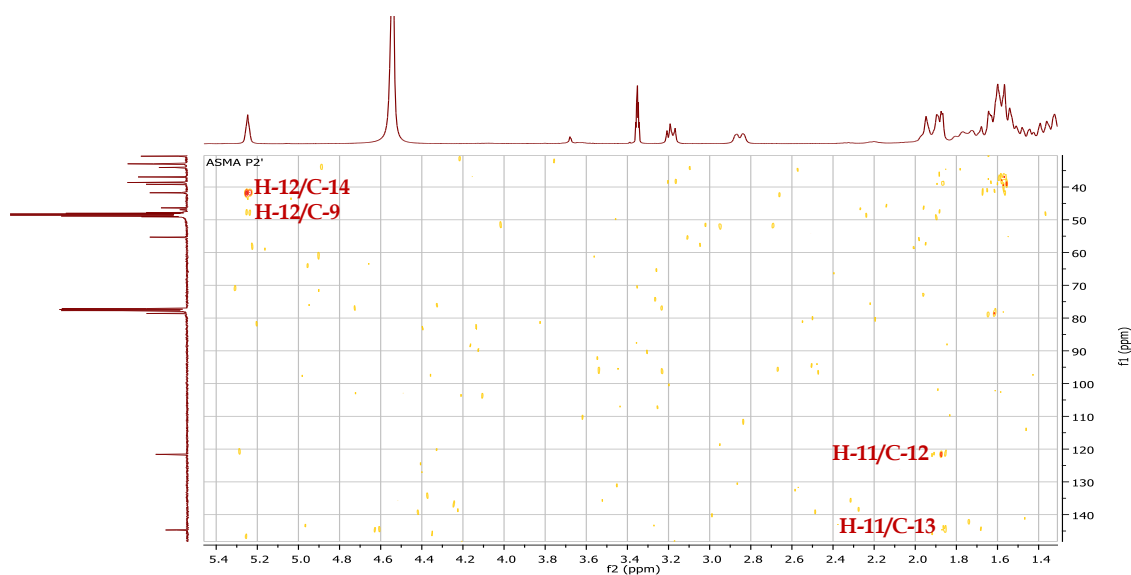
Figure. IV. 41: HMBC Spectrum (400 MHz, CD_3OD) of **P2**.
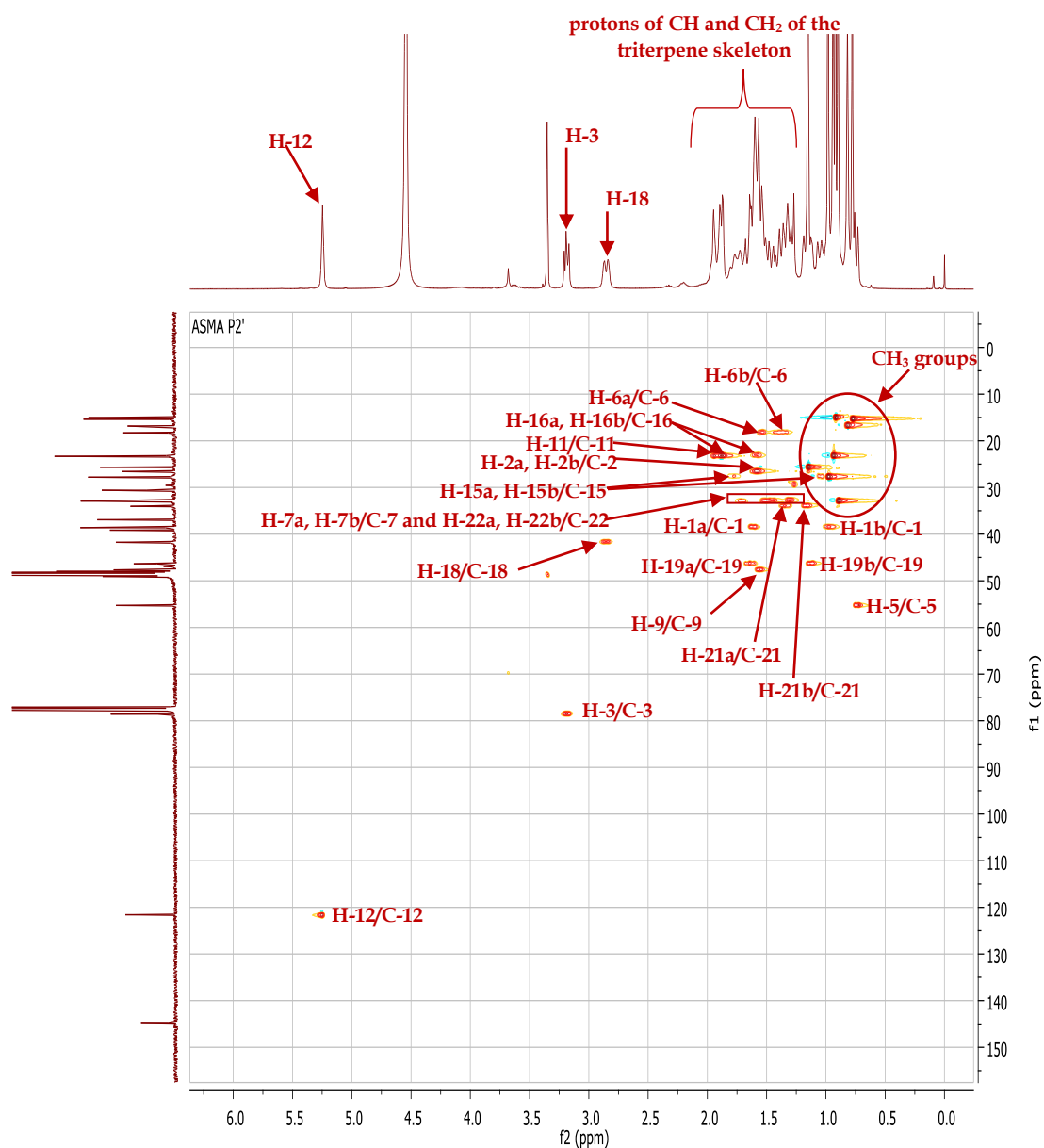
Figure. IV. 42: HSQC Spectrum (400 MHz, CD₃OD) of **P2**.
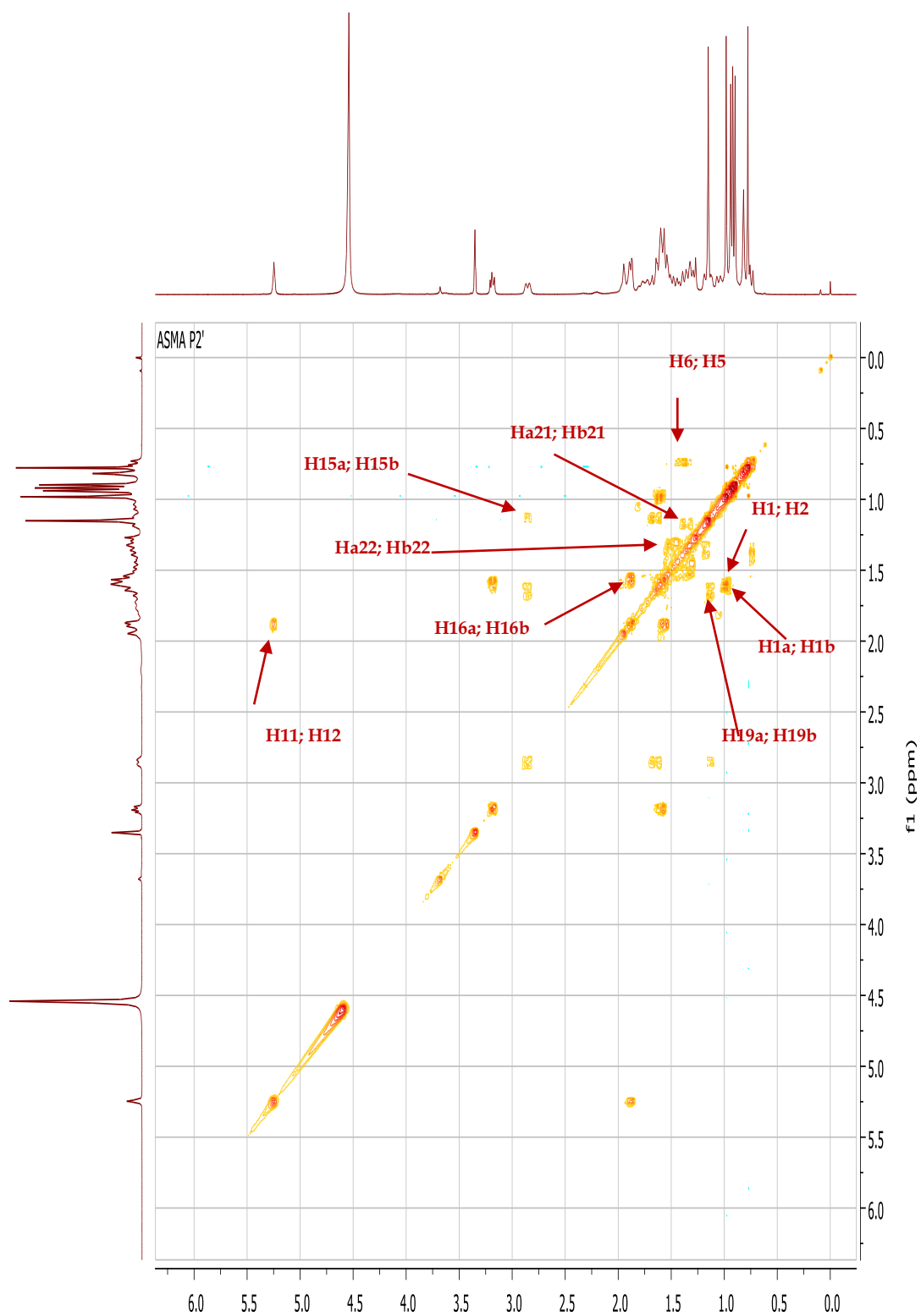
Figure. IV. 43: COSY Spectrum (400 MHz, CD$_3$OD) of **P2**.

The HMBC experiment (**Figure. IV. 44**) shows:

- ➢ Three correlations observed between H-3 (δ_H 3.18 and δ_C 78.59) and:
    - ❖ C-4 (δ_C 38.60).
    - ❖ C-23 (δ_C 27.80).
    - ❖ C-24 (δ_C 15.38).
- ➢ Four correlations observed between H$_3$-23 (δ_H 0.98 and δ_C 27.80) and:
    - ❖ C-3 (δ_C 78.59).
    - ❖ C-4 (δ_C 38.60).
    - ❖ C-5 (δ_C 55.29).
    - ❖ C-24 (δ_C 15.38).
- ➢ Four correlations observed between H$_3$-24 (δ_H 0.77 and δ_C 15.38) and:
    - ❖ C-3 (δ_C 78.59).
    - ❖ C-4 (δ_C 38.60).
    - ❖ C-5 (δ_C 55.29).
    - ❖ C-23 (δ_C 27.80).
- ➢ Four correlations observed between H$_3$-25 (δ_H 0.92 and δ_C 15.04) and:
    - ❖ C-1 (δ_C 38.49).
    - ❖ C-5 (δ_C 55.29).
    - ❖ C-9 (δ_C 47.66).
    - ❖ C-10 (δ_C 36.93).
- ➢ Three correlations observed between H$_3$-26 (δ_H 0.80 and δ_C 16.84) and:
    - ❖ C-7 (δ_C 32.77).
    - ❖ C-8 (δ_C 39.19).
    - ❖ C-9 (δ_C 47.66).
- ➢ Three correlations observed between H$_3$-27 (δ_H 1.14 and δ_C 25.67) and:
    - ❖ C-13 (δ_C 144.7).
    - ❖ C-14 (δ_C 41.76).
    - ❖ C-15 (δ_C 27.74).
- ➢ Three correlations observed between H$_3$-29 (δ_H 0.89 and δ_C 32.92) and:
    - ❖ C-19 (δ_C 46.36).
    - ❖ C-20 (δ_C 30.59).
    - ❖ C-21 (δ_C 34.04).
    - ❖ C-30 (δ_C 23.32).

- ➢ Three correlations observed between H$_3$-30 (δ_H 0.94 and δ_C 23.32) and:
  - ❖ C-19 (δ_C 46.36).
  - ❖ C-20 (δ_C 30.59).
  - ❖ C-21 (δ_C 34.04).
  - ❖ C-29 (δ_C 32.92).
- ➢ a correlation spot between H-12 (5.25) with C-14(41.76) and C-9(47.66).
- ➢ a correlation spot between H-16 (1.58 and 1.89) and C-17(47.79).

all other HMBC correlations are demonstrated in the Figure.
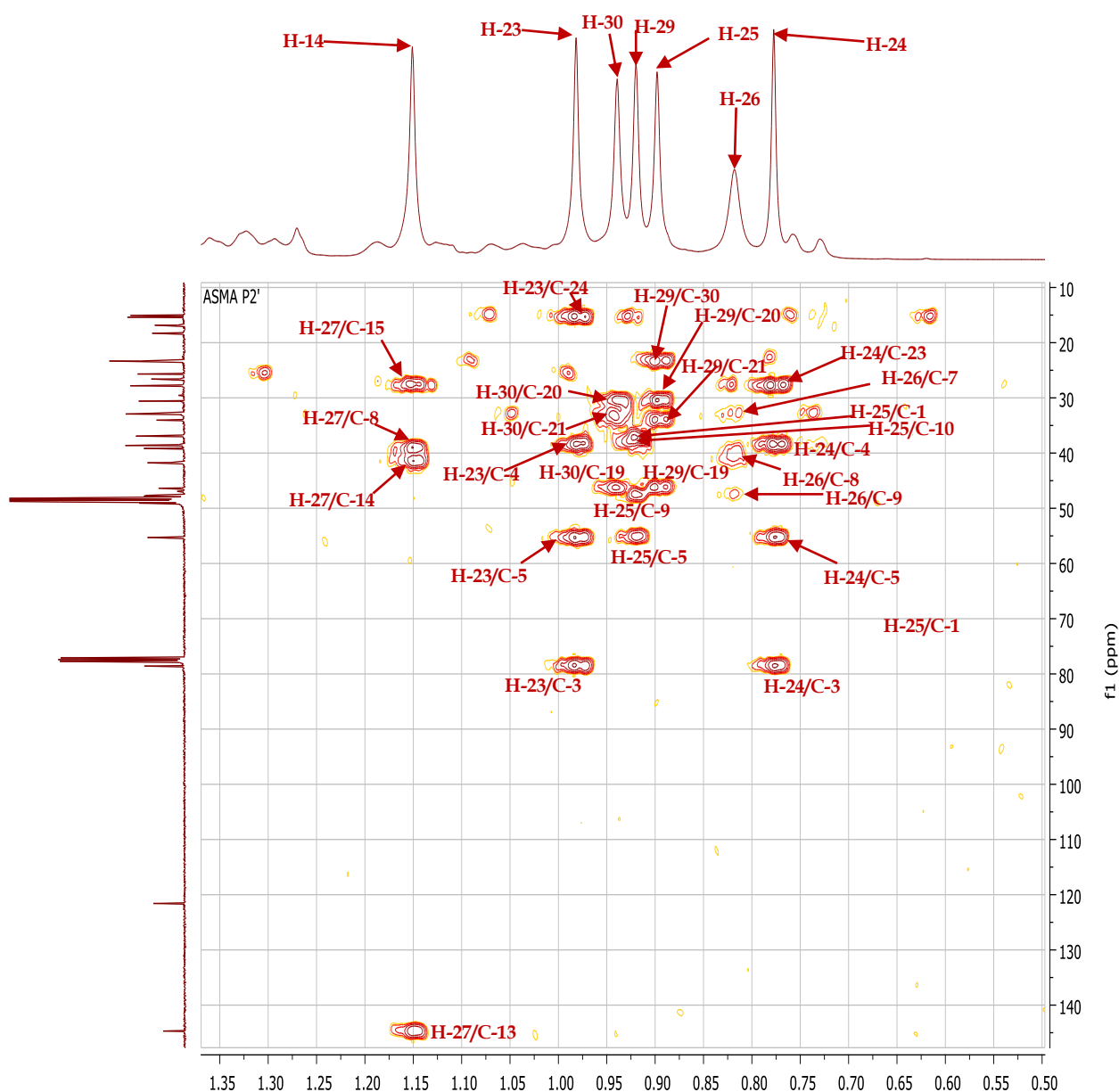
Figure. IV. 44: HMBC of methyl groups (400 MHz, in CD$_3$OD) of compound **P2**.

The Δδ between the olefinic carbons C-12 and C-13, which is of the order of 23.11 ppm that a typical of **Olean-12-enes**. The presence of seven methyl groups supposes the oxidation of one of the eight methyl usually constituting the oleanane skeleton. Also, the absence of characteristic peak of COOH in ^{13}C NMR, makes us guess about the comparison of the chemical shift of C-16, C-17 and C-18 with literature data of Oleanolic acid and beta amyrin [195]. The deshielding of C-17 and C-18 (Δδ=14 ppm and Δδ=6 ppm, respectively) and the shielding of C-16 (Δδ= 3.6 ppm) of the Oleanolic acid compared to the β-amyrin skeleton indicating that C-28 is COOH.

We deduce the structure tends to be an Oleanolic acid. Therefore, the structure of compound **P2** was determined to be a **3-hydroxy-olean-12-ene-28-carboxyl** (Oleanolic acid) (**Figure. IV. 45**), The ^{1}H and ^{13}C NMR data, are summarized in the **Table. IV. 4**, which are in full agreement with the literature [195, 198].

This compound was isolated from *A. cancellata* [50], *A. flava* [55], *A. serratuloides* [51] and *A. humilis* [53], and for the first time form the species *A. aristata*.
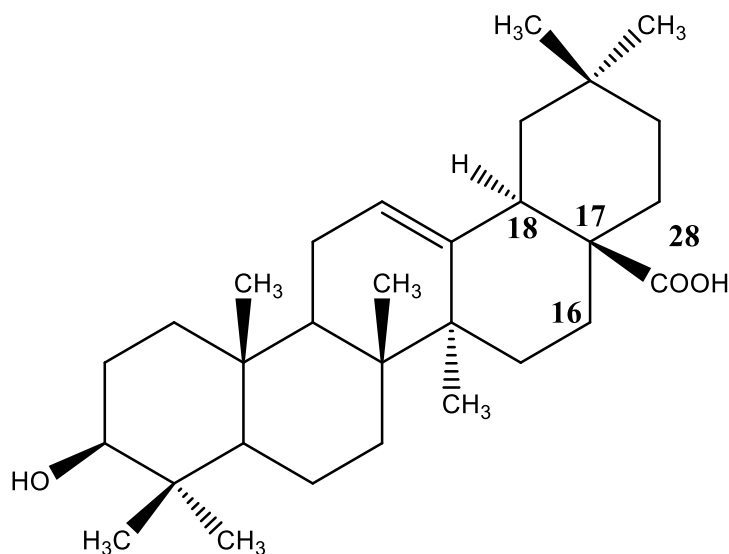
Figure. IV. 45: Chemical structure of the compound **P2;** a 3-hydroxy-olean-12-ene-28-carboxyl (Oleanolic acid).

Table. IV. 4: ^{1}H (400 MHz) and ^{13}C NMR (100 MHz) Chemical shifts in CD$_3$OD of compound **P2** (δ_C in ppm and δ_H in ppm and J in Hz).

Position	carbon	Proton
1	38.49	0.96 (m) 1.61 (m)
2	26.59	1.58 (m)
3	78.59	3.18 (brd, J=15.8 Hz, 1H)
4	38.60	--
5	55.29	0.72 (m)
6	18.30	1.38 (m) 1.53 (m)
7	32.77	1.51 (m) 1.71 (m)
8	39.19	--
9	47.66	1.55 (m)
10	36.93	--
11	23.21	1.88 (m)
12	121.59	5.25 (m)
13	144.7	--
14	41.76	--
15	27.74	1.03 (m) 1.77 (m)
16	23.31	1.58 (m) 1.89 (m)
17	47.79	--
18	41.69	2.85 (dd, J=13.6,3.5 Hz, 1H)
19	46.36	1.12 (m) 1.64 (m)
20	30.59	--
21	34.04	1.16 (m) 1.34 (m)

22	32.77	1.30 (m)
		1.44 (m)
23	27.80	0.98 (S, 3H)
24	15.38	0.78 (S, 3H)
25	15.04	0.92 (S, 3H)
26	16.84	0.82 (S, 3H)
27	25.67	1.15 (S, 3H)
28	--	--
29	32.92	0.90 (S, 3H)
30	23.32	0.94 (S, 3H)

IV.4. 3. Compound N1

Compound **N1** is isolated in the form of a brown amorph soluble in methanol. This compound is characterized on TLC test by invisible spot under UV light which turns black by revelation using acid solution and heating.

The ^{1}H NMR spectrum of the compound **N1** (**Figure. IV. 46**) recorded in CD$_3$OD displays the appearance of peaks in the field from 3.22 to 5.31 ppm characterizing the osidic protons, this may indicate that the compound **N1** was saccharide compound. This spectrum also shows only one signal in the form of doublet at 5.31 ppm (d, 3.9 Hz, 1H) in the anomeric spectral region.

The number of osidic protons that appeared in the field from 3.22 to 4.09 ppm reveals that the compound **N1** consist of more than one saccharide residue with different types. The presence of only one anomeric proton signal suggests the presence of fructose units, since the fructose has no anomeric proton [199].

Figure. IV. 46: ^{1}H NMR spectrum (400 MHz, CD$_3$OD) of compound **N1**.

The analysis of ^{13}C NMR spectrum of **N1** showed 18 osidic carbon signals (**Figure. IV. 47**), the appearance of these peaks in the field from 60 to 103.82 ppm may confirm that the compound **N1** was saccharide compound. Also, because there were 18 signals in the osidic region in addition to the presence of three anomeric carbon signals resonating at δ$_C$ 92.73, 103.56 and 103.82 in anomeric spectral region, it was obviously that the compound **N1** was trisaccharide composed of three saccharide residues. According to the analysis of the ^{13}C NMR spectrum, we deduce that these saccharide residues are hexose type.
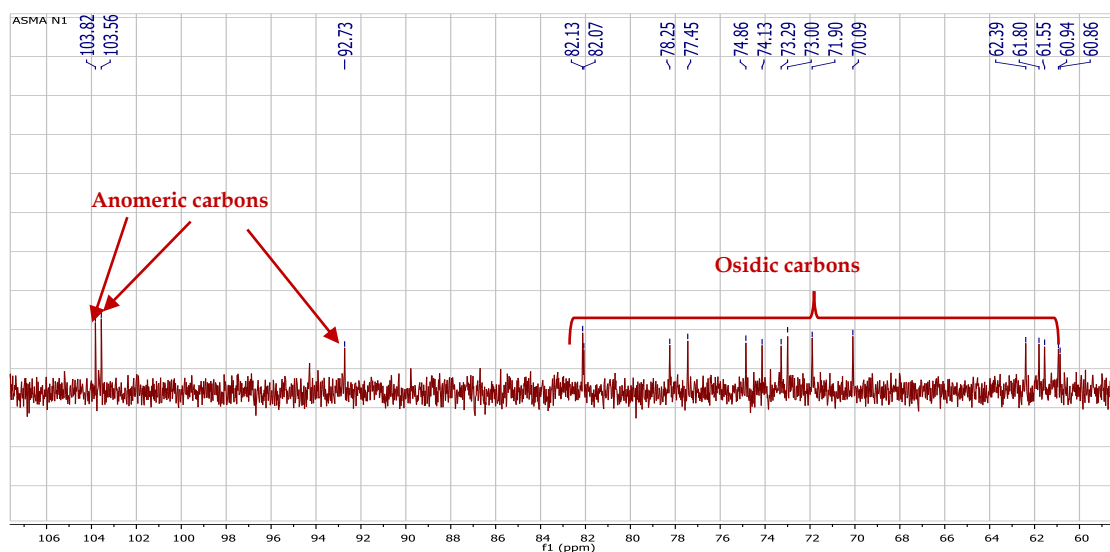
Figure. IV. 47: ^{13}C NMR spectrum (100 MHz, CD$_3$OD) of the compound **N1**.

The DEPT135 spectrum (**Figure. IV. 48**) shows the disappearance of two anomeric carbons that resonating at δ_C 103.56 and 103.82 (quaternary carbon), this spectrum also reveals the presence of five signals characteristic of methylene (CH_2) groups resonating at δ_C 60.93, 61.80, 60.68, 62.39 and 61.55 and elven signals characteristic of CH groups.
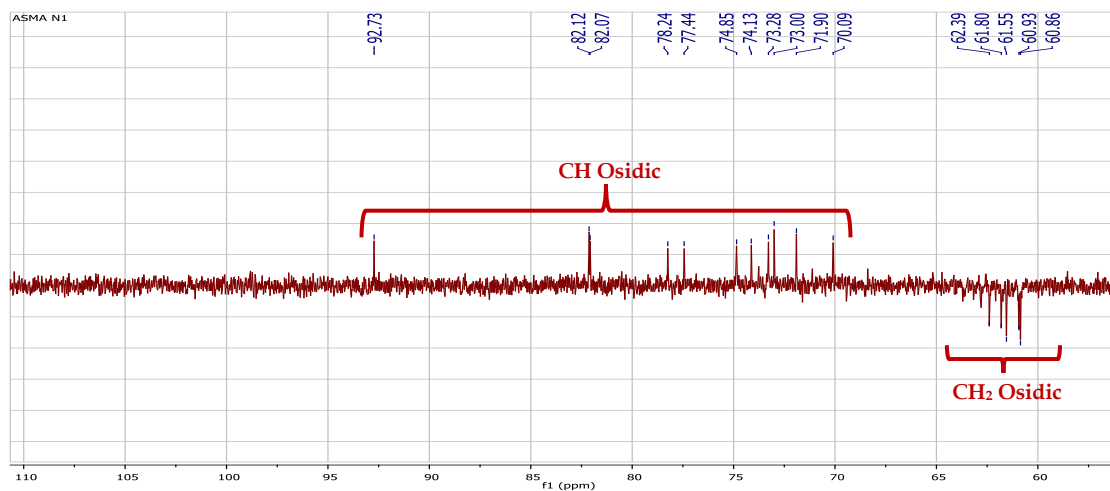
Figure. IV. 48: DEPT135 NMR spectrum (100 MHz, CD_3OD) of the compound **N1**.

According to COSY spectrum (**Figure. IV. 49**) spin system of seven protons of the first hexose was identified starting from the anomeric proton H-1 resonating at δ_H 5.31 (d, J=3.9 Hz, 1H) to H-6. The proton H-1 correlate with a proton resonating at δ_H 3.30 (dd, J = 9.8, 3.9 Hz, 1H) corresponding to H-2, this last also reveals a correlation with a proton resonating at δ_H 3.56 (dd, J = 9.5, 3.6 Hz, 1H) attributable to H-3. The proton H-4 at δ_H 3.24 (dd, J = 7.1, 3.1 Hz, 1H) correlate with a proton resonating at δ_H 3.73 ppm (dd, J = 7.1, 4.5 Hz, 1H) assigned to H-5, this last displays correlation spots with two protons resonating at δ_H 3.58 (d, J = 12.4 Hz, 1H) and at δ_H 3.70 (dd, J = 12.4, 4.5 Hz, 1H) corresponding to H-6b and H-6a, respectively. The coupling constant of the anomeric proton (J=3.9 Hz) indicates the α orientation of this proton. Also, the coupling constant between the protons H-4 and H-5 indicates the trans di-axial position of these protons, based on these results the first hexose was identified as α-d-glucose.

Spin system of five protons of the second hexose was identified starting from H-6' to H-3'. The protons H-6'a and H-6'b resonating at 3.64 and 3.74 ppm, correlate with a proton resonating at δ_H 3.63 ppm (m) assigned to H-5'. The H-4' at δ_H 3.91 (d, J = 8.3 Hz, 1H) correlate with H-3' δ_H 4.09 (d, J = 8.3 Hz, 1H) (**Figure. IV. 49**).

The third hexose reveals also a spin system of five protons starting from H-6''
to H-3''. The protons H_2-6'' resonating at δ_H 3.51 and 3.58 shows a correlation with a
proton at δ_H 3.64 (m) assigned to H-5''. The H-4'' 3.93 (d, J = 8.3 Hz, 1H) correlate with
H-3' δ_H 4.03 (d, J = 8.3 Hz, 1H) (**Figure. IV. 49**).
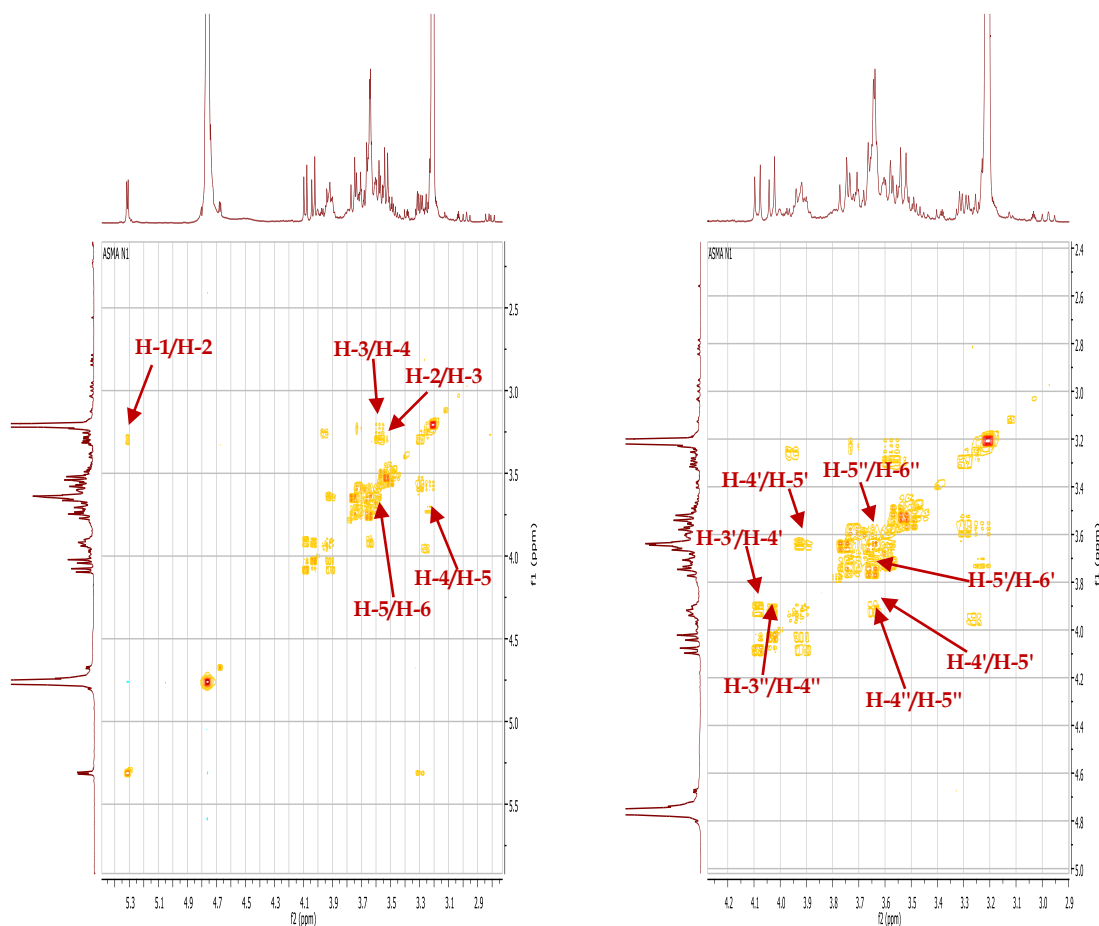
Figure. IV. 49: The COSY spectrum of three hexoses of the compound **N1**.

Depending on the HSQC experiment, each proton is assigned to its
corresponding carbon as shown in the **Figure. IV. 50**.

- ❖ H-1/C-1 δ_C 92.73.
- ❖ H-2/C-2 δ_C 71.90.
- ❖ H-3/C-3 δ_C 73.2.
- ❖ H-4/C-4 δ_C 70.09.
- ❖ H-5/C-5 δ_C 73.00.
- ❖ H-6/C-6 δ_C 60.94.
- ❖ H-1'/C-1' δ_C 61.80.
- ❖ H-2'/C-2' δ_C 103.56.
- ❖ H-3'/C-3' δ_C 78.25.
- ❖ H-4'/C-4' δ_C 74.86.
- ❖ H-5'/C-5' δ_C 82.13.
- ❖ H-6'/C-6' δ_C 61.55.
- ❖ H-1"/C-1" δ_C 62.39.
- ❖ H-2"/C-2" δ_C 103.82.
- ❖ H-3"/C-3" δ_C 77.45.
- ❖ H-4"/C-4" δ_C 74.13.
- ❖ H-5"/C-5" δ_C 82.07.
- ❖ H-6"/C-6" δ_C 60.68.
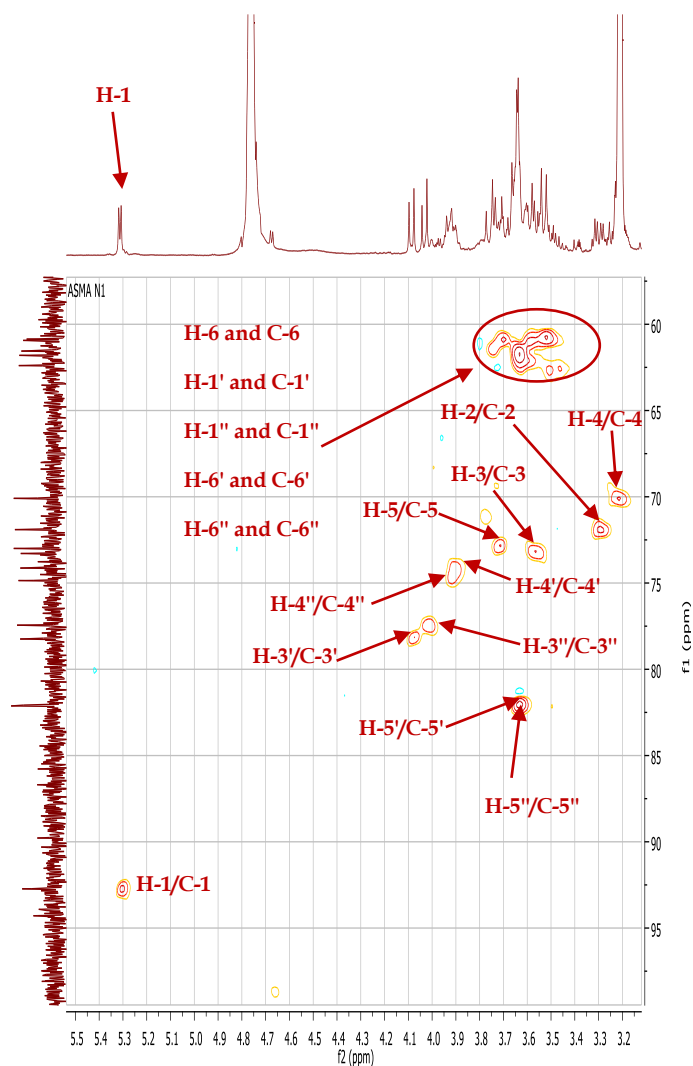
Figure. IV. 50: HSQC spectrum (400 MHz, CD$_3$OD) of the compound **N1**.

Due to the tiny differences of the chemical shifts of the carbons of two saccharide residues, it could be deduced that these signals were attributed to the same type of sugar residue. By comparing the values of the ^{13}C NMR chemical shifts with literature data it could be confirm our suggestion that the two saccharide were ketose (fructose) [200]. These two fructose residues were determined as β-furanoside type. It is known that α-fructoside produces larger chemical shifts compared with β-fructoside. According to previously reported data, the resonances from 102 to 107 ppm in the ^{13}C NMR were attributed to the anomeric carbon of β-D-fructofuranose [201-206].

The HMBC experiment (**Figure. IV. 51**) of **N1** showed strong cross-peaks between ^{1}H and ^{13}C peaks in different residues, which indicated the linkage sites and sequence of different residue:

❖ A correlation spot between H-1 δ_H 5.31 and C-2 δ_C 71.90 and C-3 δ_C 73.29 of the first hexose (α-d-glucose). Also, between H-3 at δ_H 3.56 and C-2 at δ_C 71.90 and C-4 at δ_C 70.09.

❖ A correlation spot between H-1' δ_H 3.63 (S,2H) and C-2' δ_C 103.56, between H-3' δ_H 4.09 and C-4' δ_C 74.13 of β-D-fructose 1.

❖ A correlation between H-1" δ_H 3.52 and C-2" 103.82 ppm, between H-3" δ_H 4.03 and C-4" δ_C 74.13 of β-D-fructose 2.

Also, a cross-peaks among different residues C-2' of fructose 1 and H-1 of glucose (H-1 5.31 and C-2' 103.56), confirms that the O-1 of glucose was linked to fructose (1→2) with ether linkage. The correlation spot between H-6a", H-6b" (3.64; 3.74) and C-2" (103.82), confirming the O-6 of fructose 1 was linked to fructose 2 through (6→2) linkage (**Figure. IV. 52**).
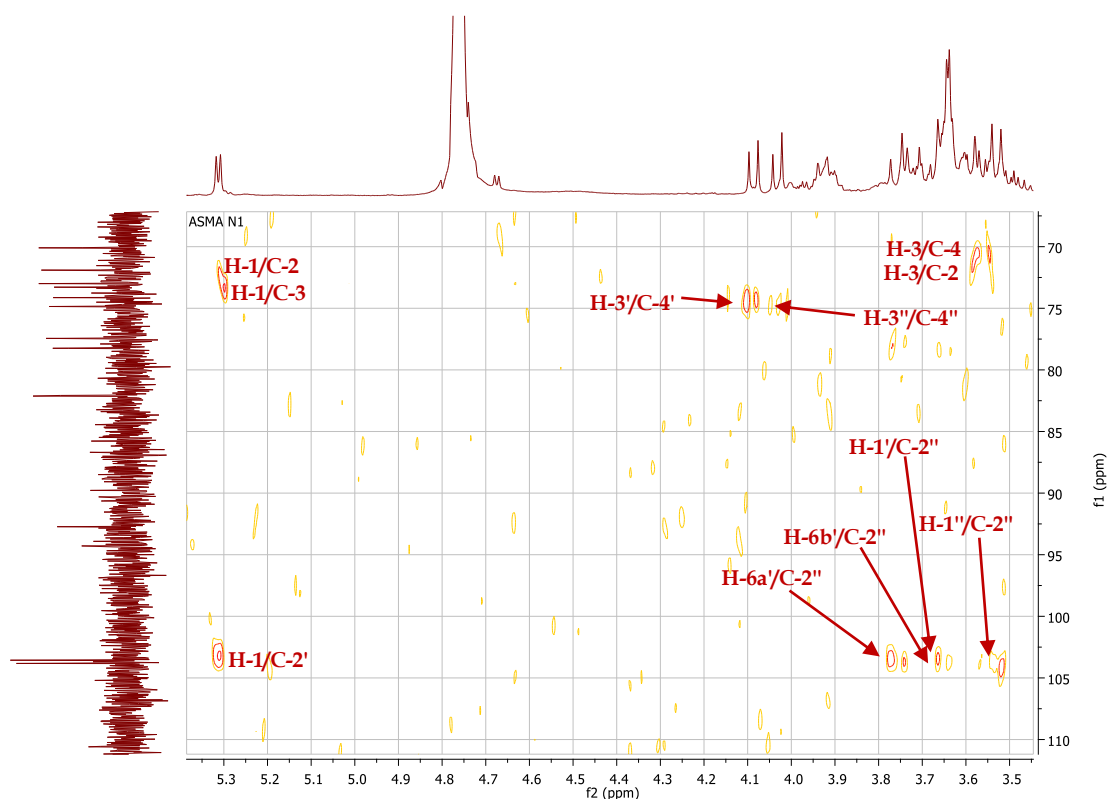
Figure. IV. 51: HMBC spectrum (400 MHz, CD$_3$OD) of the compound **N1**.
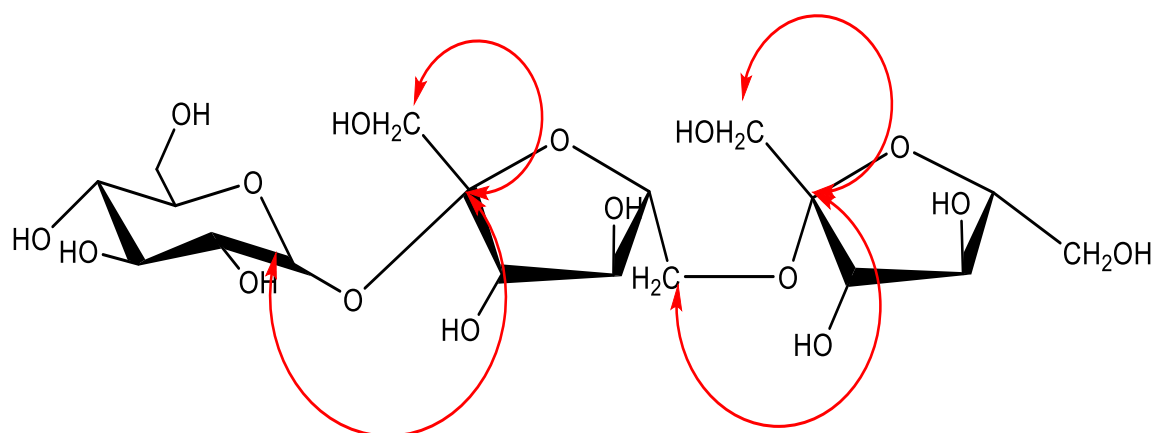
Figure. IV. 52: HMBC correlations of the compound **N1**.

The structural confirmation of the compound **N1** was done based on the ^{1}H and ^{13}C NMR analyses using 1D-NMR and 2D-NMR spectra. These spectra showed that **N1** is trisaccharide containing α-glucose and two β-frucofuranose. From the previous detailed results, it was found that the oligosaccharide **N1** was [O-β-d-fructofuranosyl-(2→6)-β-fructofuranosyl-(2→1)-α-d-glucopyranoside] (**Figure. IV. 53**), this trisaccharide known as **6-Kestose** [207]. The kestoses are trisaccharide which have a fructofuranose attached to sucrose, and they differ only by the linkage of the second fructose residue to the sucrose, including: [O-β-d-fructofuranosyl-(2→1)-β-d-fructofuranosyl-(2→1)-α-d-glucopyranoside] **1-Kestose** [O-β-d-fructofuranosyl-(2→6)-β-d-fructofuranosyl-(2→1)-α-d-glucopyranoside] **6-Kestose** and [O-β-d-fructofuranosyl-(2→6) -α-d-glucopyranosyl-(2→1)-β-d-fructofuranoside] **Neokestose** [207, 208].

The ^{1}H and ^{13}C NMR data, are summarized in (**Table. IV. 5**), which are in total agreement with the literature [200, 207]. **6-Kestose** occurs naturally in numerous plants [207]. This compound was isolated for the first time from the genus *Atractylis*.
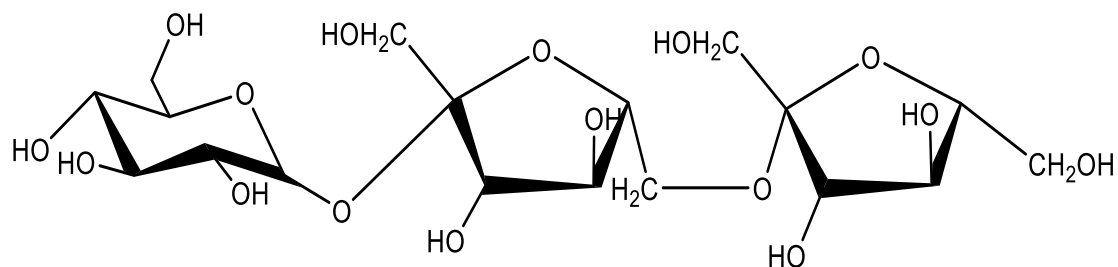
Figure. IV. 53: Structure of the compound **N1**; [O-β-d-fructofuranosyl-(2→6)-β-fructofuranosyl-(2→1)-α-d-glucopyranoside]; **(6- kestose)**.

Table. IV. 5: The chemical shifts of ^{1}H NMR (400 MHz) and ^{13}C NMR (100 MHz) on CD_3OD of compound **N1** (δ_C in ppm and δ_H in ppm and J in Hz).

Position	Carbon	Proton
α-Glucose		
1	92.73	5.31 (d, J=3.9 Hz, 1H)
2	71.90	3.29 (dd, J = 9.8, 3.9 Hz, 1H)
3	73.28	3.57 (dd, J = 9.5, 3.6 Hz, 1H)
4	70.09	3.24 (dd, J = 7.1, 3.1 Hz, 1H)
5	73.17	3.71 (dd, J = 7.1, 4.5 Hz, 1H)
6	60.93	3.58 (d, J = 12.4 Hz, 1H)
		3.70 (dd, J = 12.4, 4.5 Hz, 1H)
β-Fructose1		
1'	61.80	3.63 (m)
2'	103.56	--
3'	78.24	4.09 (d, J = 8.3 Hz, 1H)
4'	74.86	3.91 (brd, J = 8.3 Hz, 1H)
5'	82.12	3.64 (m)
6 '	61.55	3.64 (m)
		3.74
B-Fructose2		
1''	62.39	3.52 (m)
2''	103.82	--
3''	77.44	4.03 (d, J = 8.3 Hz, 1H)
4''	74.13	3.93 (brd, J = 8.3 Hz, 1H)
5''	82.07	3.64 (m)
6''	60.68	3.51(m)
		3.61(m)

IV.4. 4. Compound N2

Compound **N2** is isolated in the form of a brown amorph soluble in methanol. This compound is characterized on TLC test by invisible spot under UV light which turns black by revelation using acid solution and heating.

The ^{1}H NMR spectrum (**Figure. IV. 54**) recorded in CD$_3$OD, showed the appearance of peaks only in the field from 3.47 to 4.01 ppm characterizing osidic protons, this may indicate that the compound **N2** was saccharide compound as mentioned in the compound **N1**. This spectrum also showed no anomeric proton.
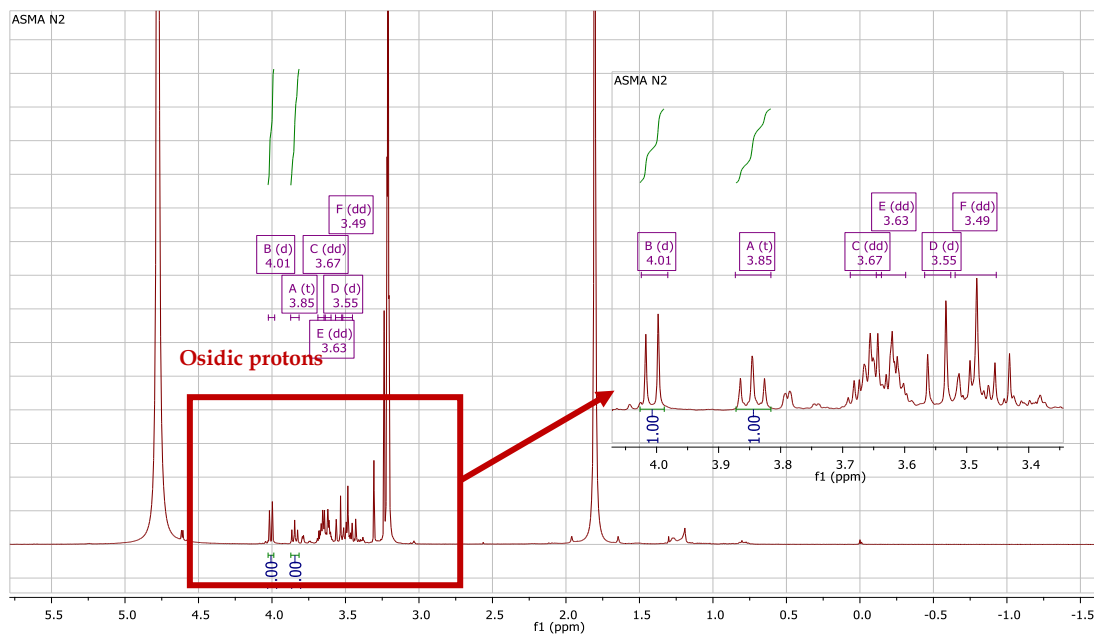
Figure. IV. 54: ^{1}H NMR spectrum (400 MHz, CD$_3$OD) of the compound **N2**.

The ^{13}C NMR spectrum of **N2** showed only six signals (**Figure. IV. 55**), the appearance of these peaks in the field from 60 to 104 ppm may confirms that the compound **N2** was saccharide compound. We deduce that this saccharide is present in the form of hexose type, the ^{13}C NMR spectrum also show one signal at δ$_C$ 103.71 in anomeric spectral region. Depending on the findings it can be concluded that this compound is monosaccharide.
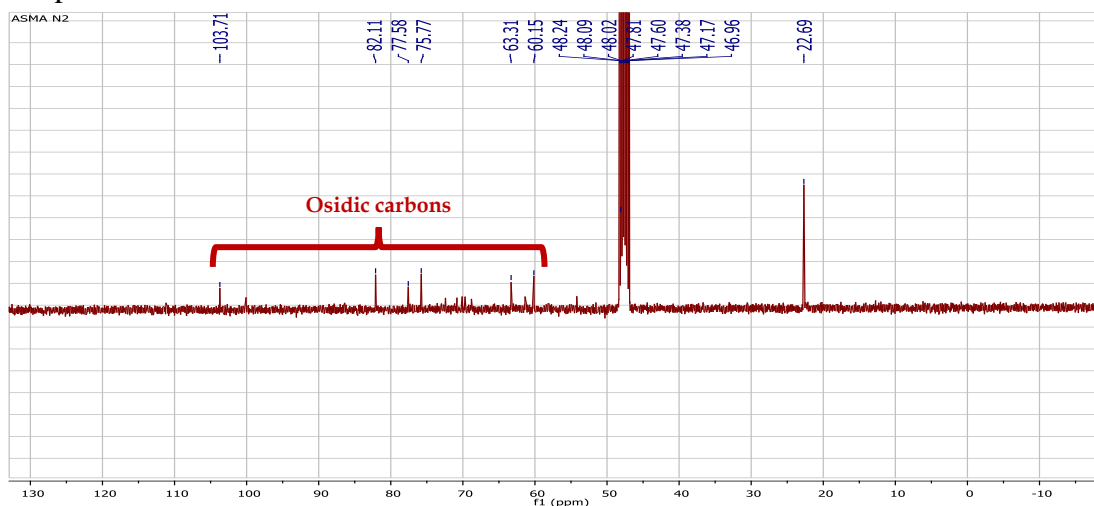
Figure. IV. 55: ^{13}C NMR spectrum (100 MHz, CD$_3$OD) of the compound **N2**.

DEPT 135 spectrum (**Figure. IV. 56**) reveals the disappearance of the carbon signal at δ_C 103.71, quaternary carbons, as previously mentioned that this the characteristic of anomeric carbon of the (C-2) of β-D-fructose, the DEPT 135 spectrum also shows:

❖ Two signals at δ_C 60.15 and 62.31 and characteristic of methylene (CH$_2$) groups that characterizing the β-D-fructose.

❖ Three signals of CH groups, which characterizing the CH of the β-D-fructose.
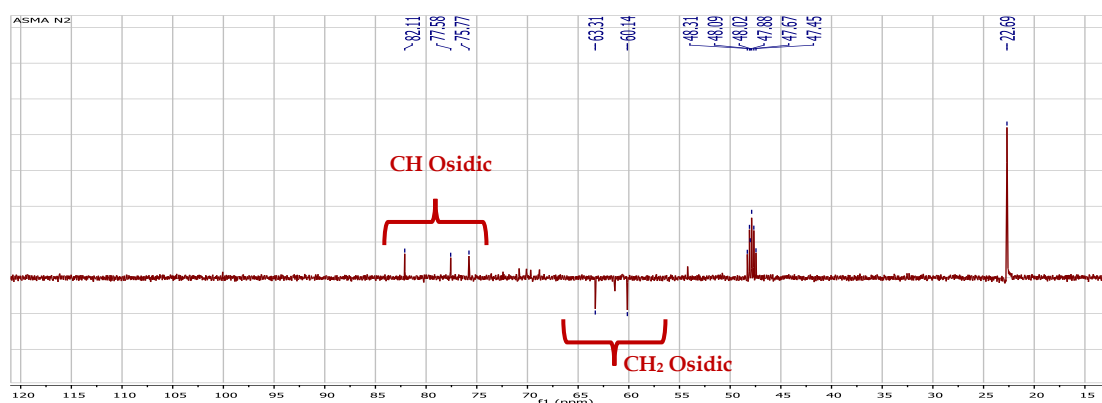
Figure. IV. 56: DEPT 135 spectrum (100 MHz, CD$_3$OD) of compound **N2**.

The structural confirmation of **N2** is mainly based on the COSY (**Figure. IV. 57**) and HSQC (**Figure. IV. 58**) spectra. The COSY spectrum reveals the correlation spots between the adjacent protons, starting from H-3 to H-6. The proton resonating at δ_H 4.01 (d, 7.7 Hz, 1H) assigned to H-3 correlate with H-4 δ_H 3.83 (t, 7.7 Hz, 1H). The proton resonating at δ_H 3.65 (m) correlate with H-6a at δ_H 3.63 (dd, 11.4, 4.5, 1H) and H-6b at δ_H 3.49 (dd, 11.4, 7.1, 1H).
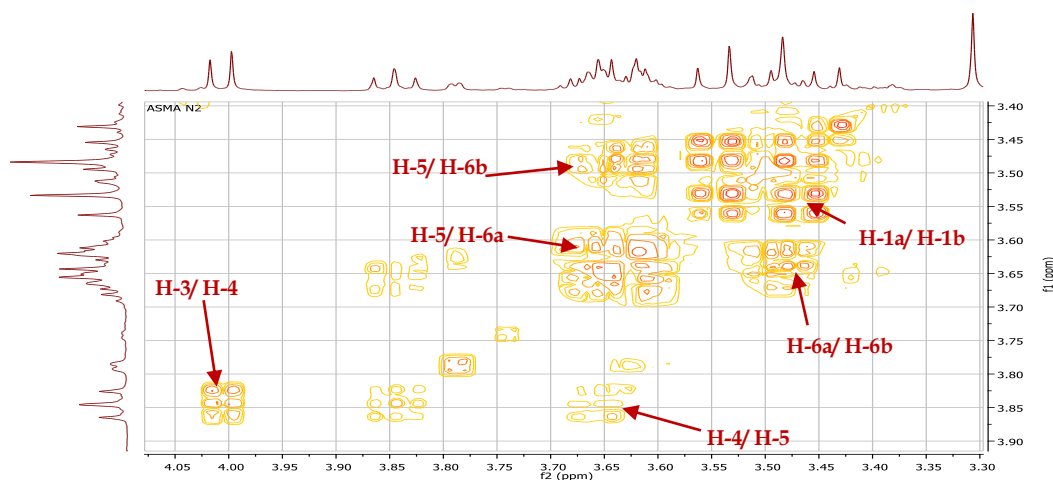
Figure. IV. 57: COSY spectrum (400 MHz, CD$_3$OD) of the compound **N2**.

The corresponding carbons of the mentioned protons were assigned using HSQC spectrum (**Figure. IV. 58**) as follow:

- ❖ H-1/ C-1 δ_C 60.14.
- ❖ H-3/ C-3 δ_C 77.58.
- ❖ H-4/ C-4 δ_C 75.77.
- ❖ H-5/ C-5 δ_C 82.11.
- ❖ H-6a and H-6b/ C-6 δ_C 63.31.
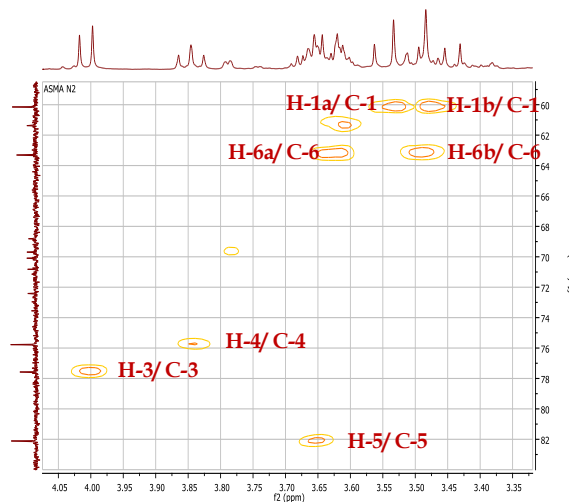
Figure. IV. 58: HSQC spectrum (400 MHz, CD$_3$OD) of the compound **N2**.

The HMBC spectrum (**Figure. IV. 59**) displays the presence of correlation spots between C-2 resonating at δ_C 103.71 and (δ_H 3.48 and 3.54) corresponding to H-1a and H-1b. The absence of correlations between H-6 and C-2 and the unshielded effect observed in C-5 δ_C 82.11 confirms that this fructose present as D-fructofuranose.
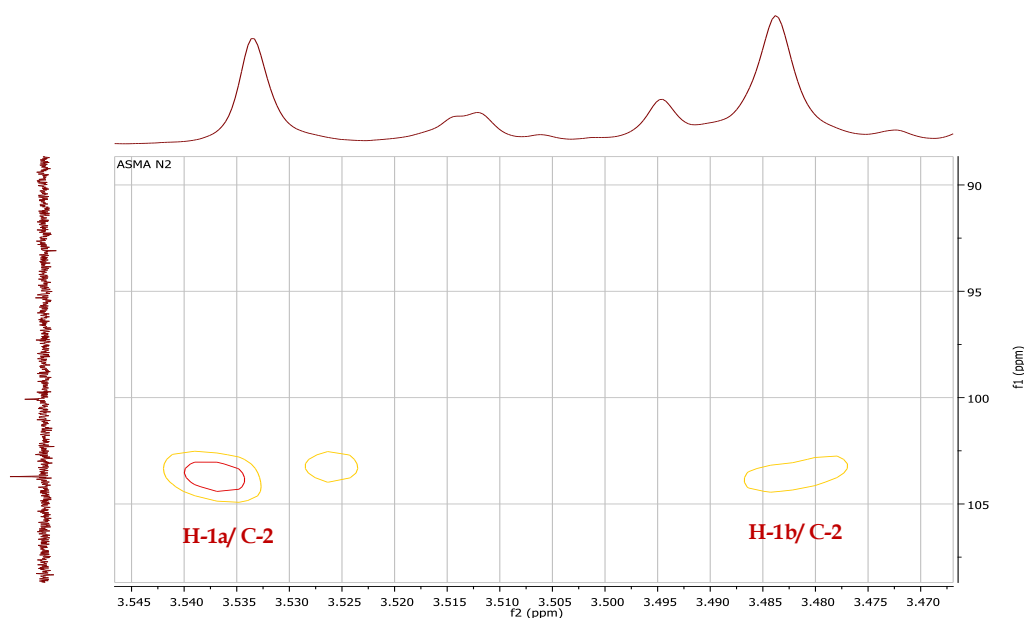
Figure. IV. 59: HMBC spectrum (400 MHz, CD$_3$OD) of the compound **N2**.

The structural elucidation of **N2** was performed according to ^{1}H and ^{13}C NMR analyses using 1D-NMR and 2D-NMR. The findings showed that **N2** it is monosaccharide compound. From the previous detailed results, it was found that this compound was β-D-fructofuranoide (**Figure. IV. 60**).
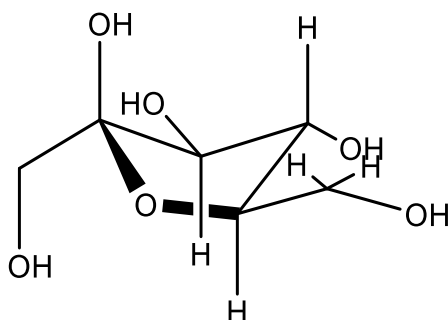
Figure. IV. 60: Structure of compound **N2**; β-D-fructofuranoide.

The ^{1}H and ^{13}C NMR data, are summarized in the **Table. IV. 6**, which are in total agreement with the literature [200]. This compound was isolated from for the first time in the genus *Atractylis.*

Table. IV. 6: The chemical shifts ^{1}H NMR (400 MHz) and ^{13}C NMR (100 MHz) in CD₃OD compound **N2** (δ_C in ppm and δ_H in ppm and J in Hz).

Position	Carbon	Proton
β-Fructofuranose		
1	60.14	3.48 (d, J = 11.7 Hz, 1H)
		3.55 (d, J = 11.8 Hz, 1H)
2	103.74	--
3	77.58	4.01 (d, J = 8.0 Hz, 1H)
4	75.77	3.85 (t, J = 7.7 Hz, 1H)
5	82.11	3.65 m
6	63.31	3.49 (dd, J = 11.7, 7.1 Hz, 1H)
		3.63 (dd, J = 11.4, 5.2 Hz, 1H)

IV.4. 5. Compound N5

Compound **N5** is isolated in the form of a brown amorph soluble in methanol. This compound is characterized on TLC test by invisible spot under UV light which turns black by revelation using acid solution and heating.

The ^{1}H NMR spectrum (**Figure. IV. 61**) of the compound **N5** showed no anomeric proton in the anomeric spectral region, this spectrum reveals other signals resonating between 3.49 and 4.06 ppm. The absence of the anomeric protons it could be deduced that the compound **N5** consist of D-fructose residues.
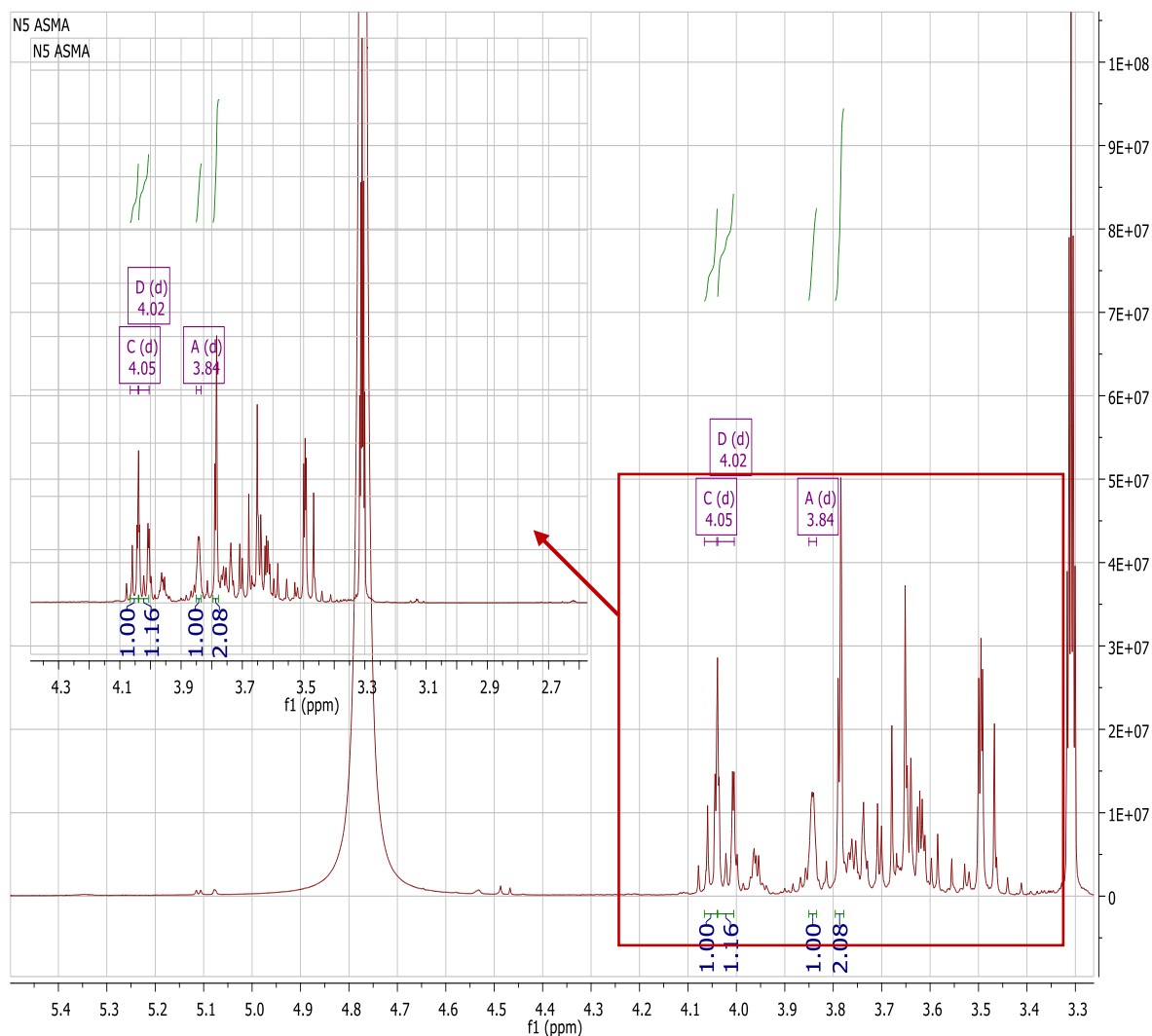
Figure. IV. 61: ^{1}H NMR spectrum (400 MHz, CD$_3$OD) of the compound **N5**.

The ^{13}C NMR spectrum of **N5** showed 12 signals (**Figure. IV. 62**), the appearance of these peaks in the field from 60 to 101.77 ppm may confirm that the compound **N5** was saccharide compound as we mentioned previously. The spectrum also shows two signals (δ_C 97.79 and 101.77) in anomeric spectral region. Because there were 12 signals and two anomeric carbons in the ^{13}C NMR spectrum, it could be deduced that the **N5** is disaccharide composed of two D-fructose residues. The fructose was determined as β-furanoside type, and the comparison of chemical shifts of the fructose with literature data, which revealed that this disaccharide consist of one fructofuranose and one frucropyranose.
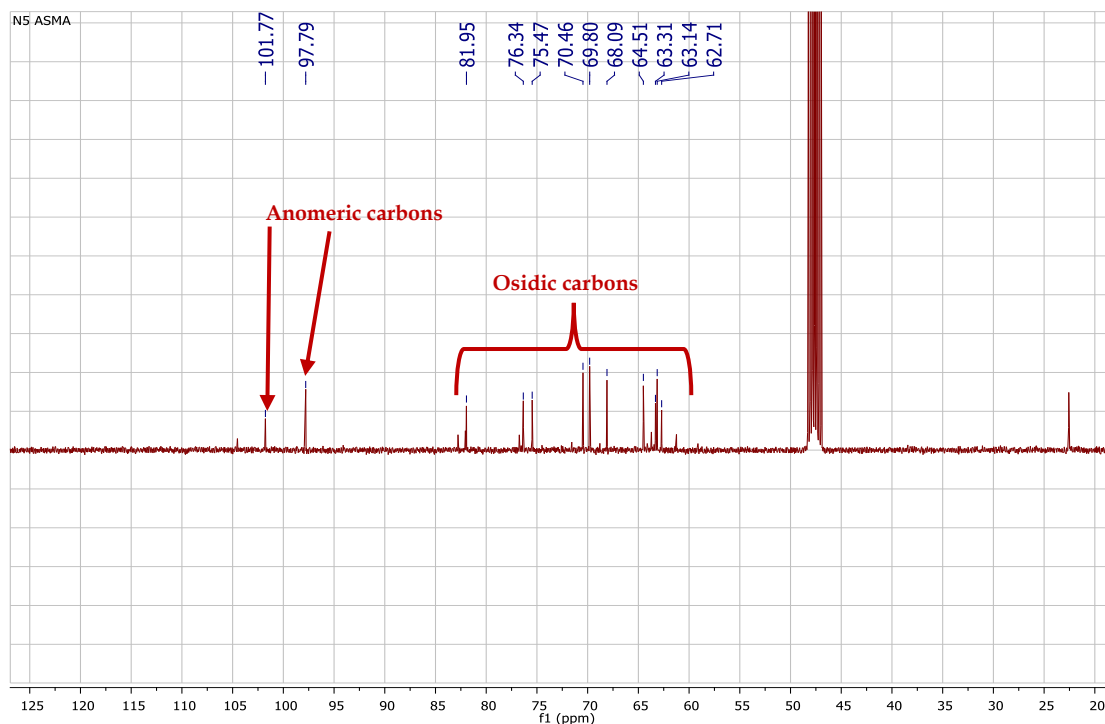
Figure. IV. 62: ^{13}C NMR spectrum (100 MHz, CD_3OD) of compound **N5**.

DEPT 135 (**Figure. IV. 63**) and DEPT 90 (**Figure. IV. 65**) spectra exhibits the disappearance of the anomeric carbon signals at δ_C 101.77 and 97.79 (quaternary carbons), anomeric carbon of the fructose. The DEPT 135 spectrum also shows:

❖ Four signals at δ_C 62.71, 63.61, 63.14 and 64.50 and characteristic of methylene (CH_2) groups that characterizing the D-fructose.

❖ Six signals of CH groups, which characterizing the CH of the D-fructose.
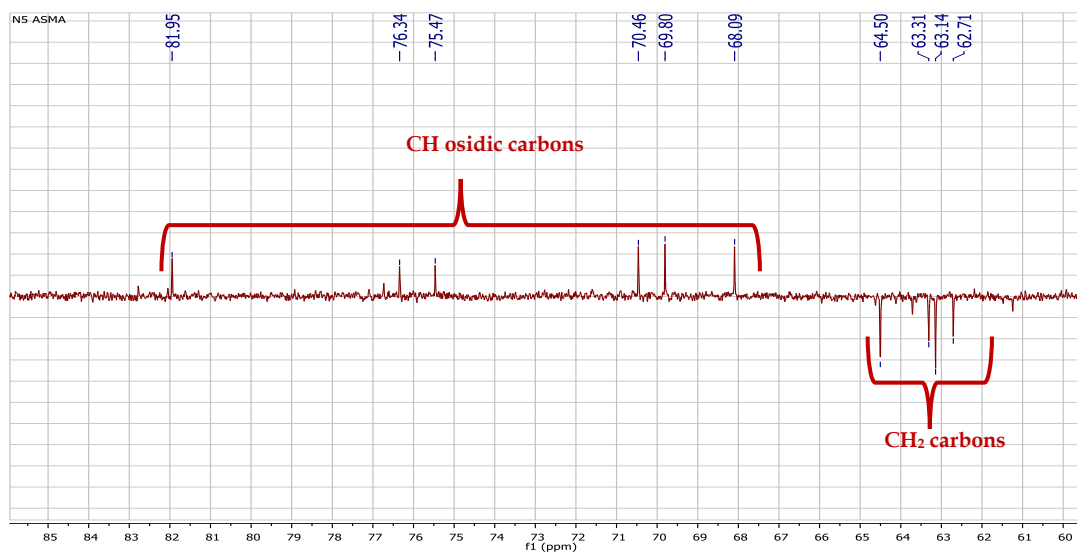
Figure. IV. 63: DEPT 135 spectrum (100 MHz, CD_3OD) of the compound **N5**.

The DEPT 90 (**Figure. IV. 64**) reveals the presence of only six signals of CH group of two fructose.
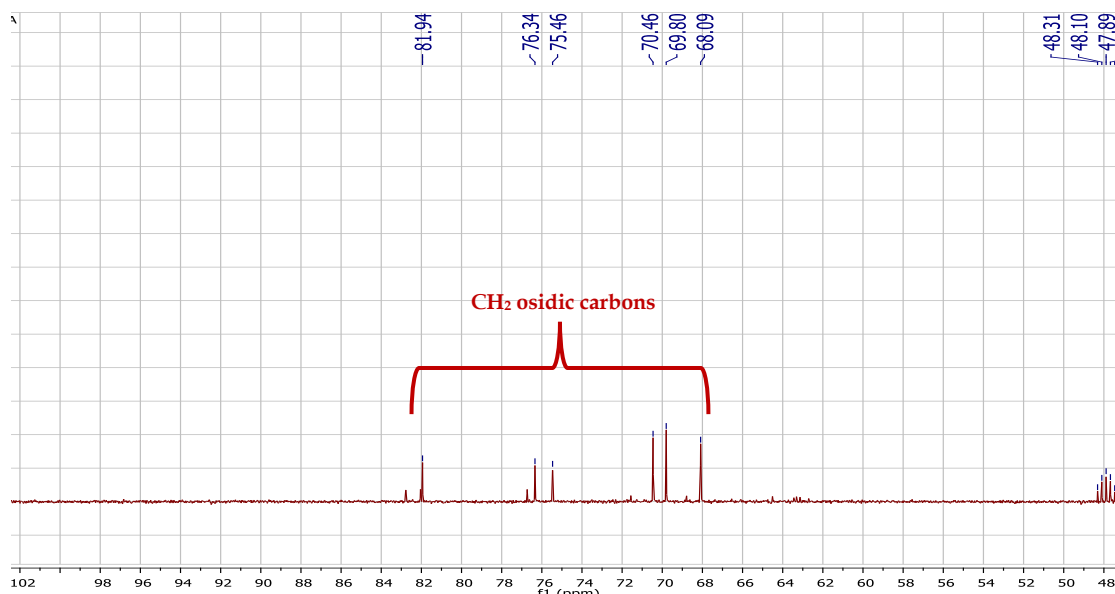
Figure. IV. 65: DEPT 90 spectrum (100 MHz, CD$_3$OD) of the compound **N5**.

The COSY spectrum (**Figure. IV. 67**) assigned the spin system from H-3 to H-6, H-3 resonating at δ_H 3.77 shows a correlation with H-4 δ_H 3.84. The peak that resonating at δ_H 3.78 assigned to H-5, which show a correlation with H-6a δ_H and H-6b δ_H of fructopyranose (**Figure. IV. 66**).

This spectrum (**Figure. IV. 67**) also reveals a spin system of five protons starting from H-3' resonating at 4.03 correlate with H-4' δ_H 4.04 and H-5' exhibits a correlation with H-6a and H-6b of fructofuranose (**Figure. IV. 66**).

Fructopyranose   Fructofuranose
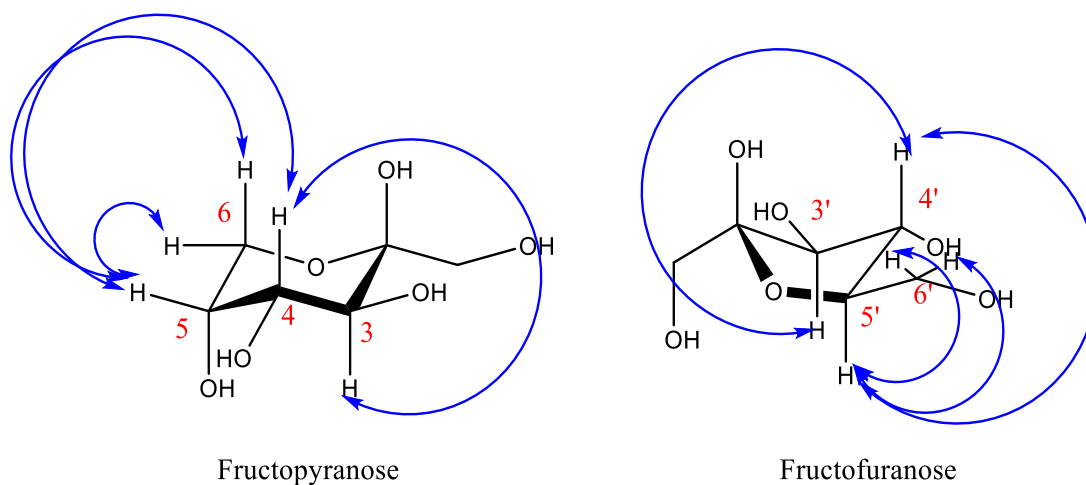
Figure. IV. 66: COSY correlations of fructopyranose and fructofuranose of the compound **N5**.
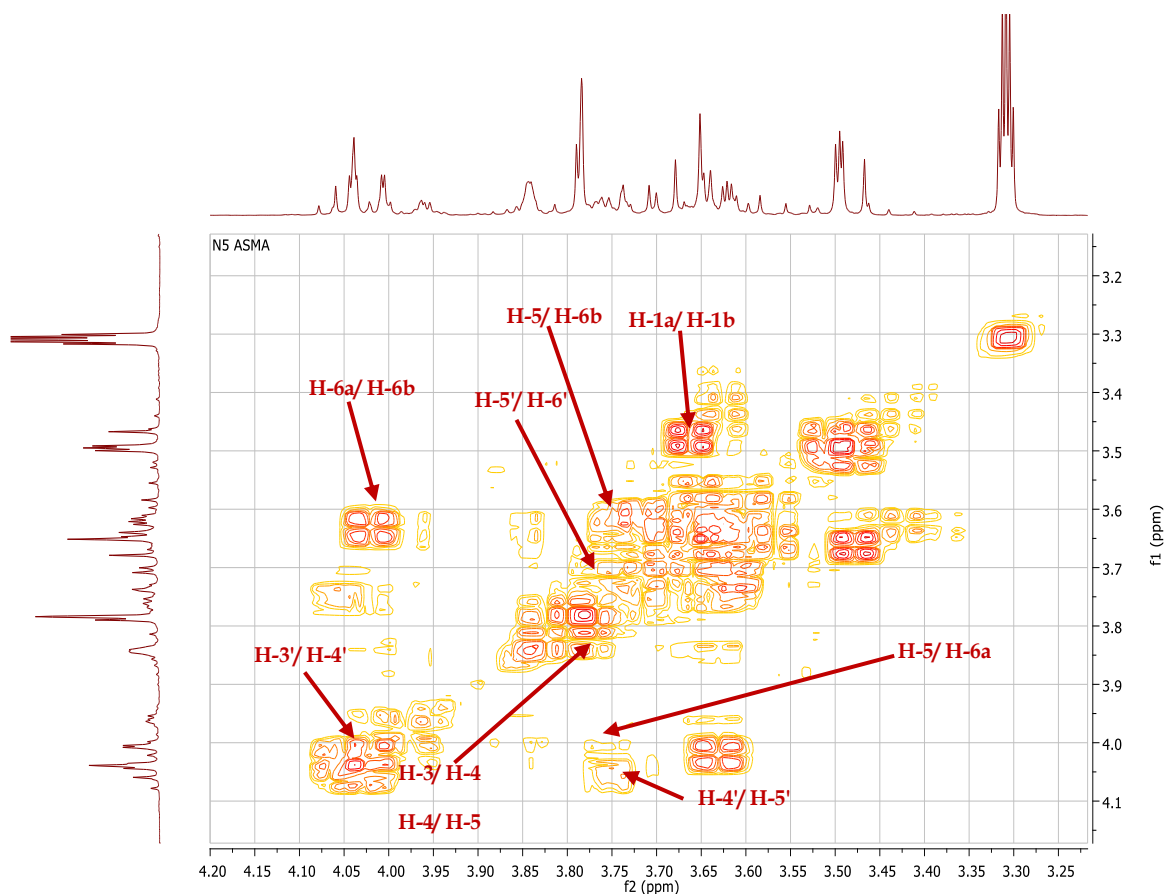
Figure. IV. 67: COSY spectrum (400 MHz, CD₃OD) of compound **N5**.

The corresponding carbons assigned based on HSQC spectrum (**Figure. IV. 68**) as follows:

- ❖ H-1/ C-1(δ_C 64.50).
- ❖ H-3/ C-3 (δ_C 68.12).
- ❖ H-4/ C-4 (δ_C 70.58).
- ❖ H-5/C-5 (δ_C 69.79).
- ❖ H-6/C-6 (δ_C 63.14).
- ❖ H-1'/ C-1' (δ_C 63.61).
- ❖ H-3'/C-3' (δ_C 76.47).
- ❖ H-4'/C-4' (δ_C 75.50).
- ❖ H--5'/ C-5' (δ_C 81.95).
- ❖ H-6'/ C-6' (δ_C 62.71).
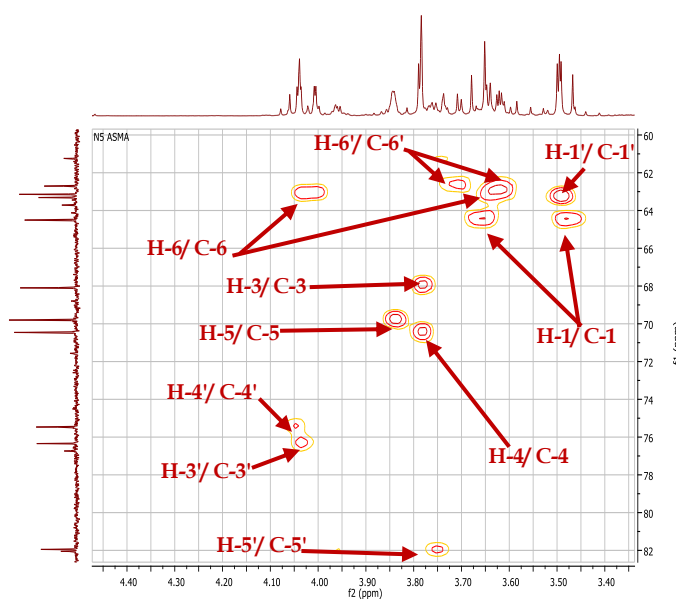
Figure. IV. 68: HSQC spectrum (400 MHz, CD₃OD) of compound **N5**.

The HMBC spectrum (**Figure. IV. 69**) of **N5** showed strong cross-peaks between ^{1}H and ^{13}C peaks in different residues, which indicated the linkage sites and sequence of different residue. All the remaining interactions on the HMBC spectrum confirm the structural elucidated of this compound; including:

- ❖ A correlation spots between H-1a, H-1b with C-2 and C-3, between C-4 with H-3 and H-5 and between C-5 and H-6a, H-6b for D-fructopyranose.
- ❖ A correlation spots between H-1' and C-2' and C-3', and between H-5' and C-6' for D-fructofuranose.
- ❖ A cross-peaks among different residues at H-1 (δ_H 3.49) and C-2' (δ_C 101.77), which indicated the linkage site O-1 of D-fructopyranose was linked to the C-2' of D-fructofuranose (2 →1) linkage (**Figure. IV. 70**).
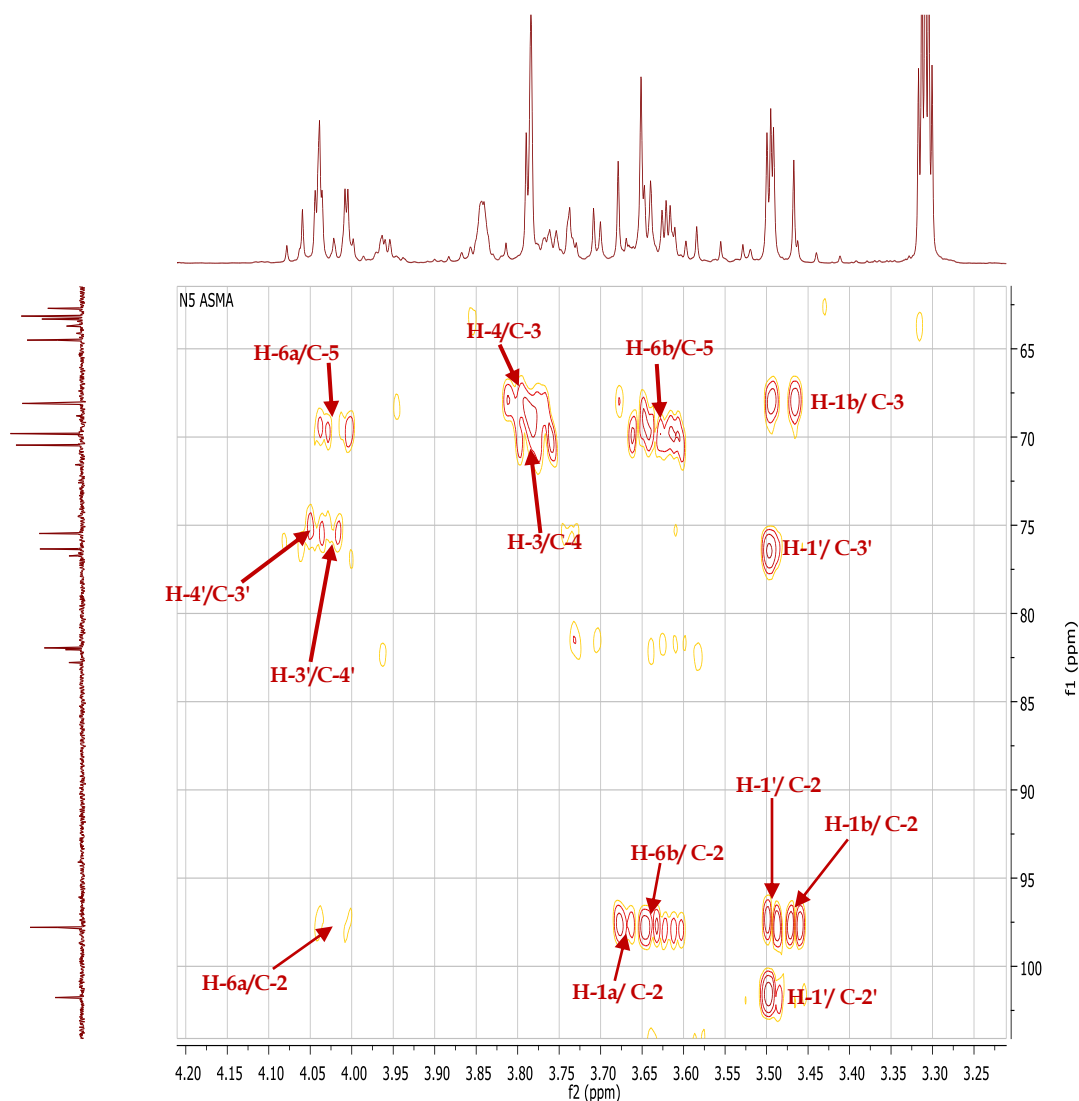
Figure. IV. 69: HMBC spectrum (400 MHz, CD₃OD) of the compound **N5**.
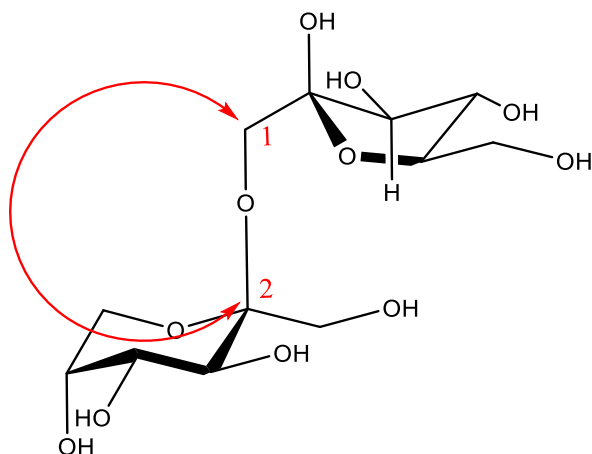
Figure. IV. 70: the linkage site O-1 of fructopyranose with C-2' of fructofuranose (2 →1) linkage.

Structures of compound **N5** was β-D-fructopyranosyl-(2→1)-D-fructofuranose (**Figure. IV. 71**), this compound is isolated for the first time from *Atractylis* genus. The ^{1}H and ^{13}C NMR data, are summarized in the **Table. IV. 7**, which are in total agreement with the literature [200].
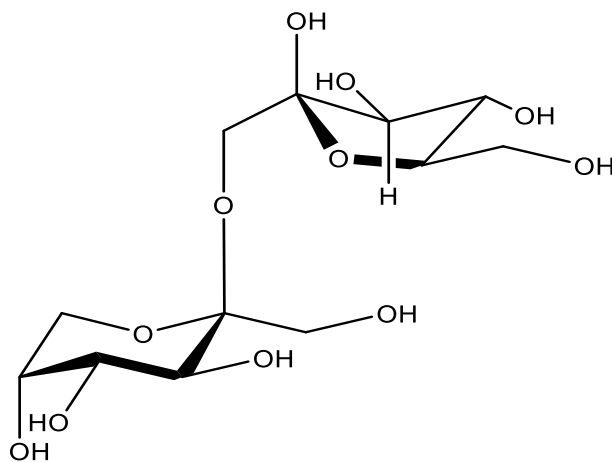
Figure. IV. 71: Structures of compound N5; β-D-fructopyranosyl-(2→1)-D-fructofuranose.

Table. IV. 7: The chemical shifts ^1H NMR (400 MHz) and ^{13}C NMR (400 MHz) on of compound **N5** (δ_C in ppm and δ_H in ppm and J in Hz).

| Position	Carbon	Proton
β-Fructopyranose		
1	64.50	3.49
		3.65
2	97.79	--
3	68.12	3.77
4	70.58	3.78
5	69.79	3.84
6	63.14	3.62
		4.02
β-Fructofuranose		
1'	63.61	3.50
2'	101.77	--
3'	76.47	4.03
4'	75.60	4.04
5'	81.95	3.75
6'	62.71	3.71
		3.62

IV.4. 6. Compound N6

Compound **N6** is isolated in the form of a brown amorph soluble in methanol. This compound is characterized on TLC test by invisible spot under UV light which turns black by revelation using acid solution and heating.

The ^1H NMR spectrum (**Figure. IV. 72**) recorded in CD$_3$OD, showed the appearance of peaks in the field from 3.22 to 5.30 ppm characterizing the osidic protons, as we mentioned previously in the compounds **N1**, **N2** and **N5**, the compound **N6** was saccharide compound. The ^1H NMR spectrum reveals the presence of one anomeric proton resonating at δ_H 5.30 (d, J = 3.8 Hz, 1H).
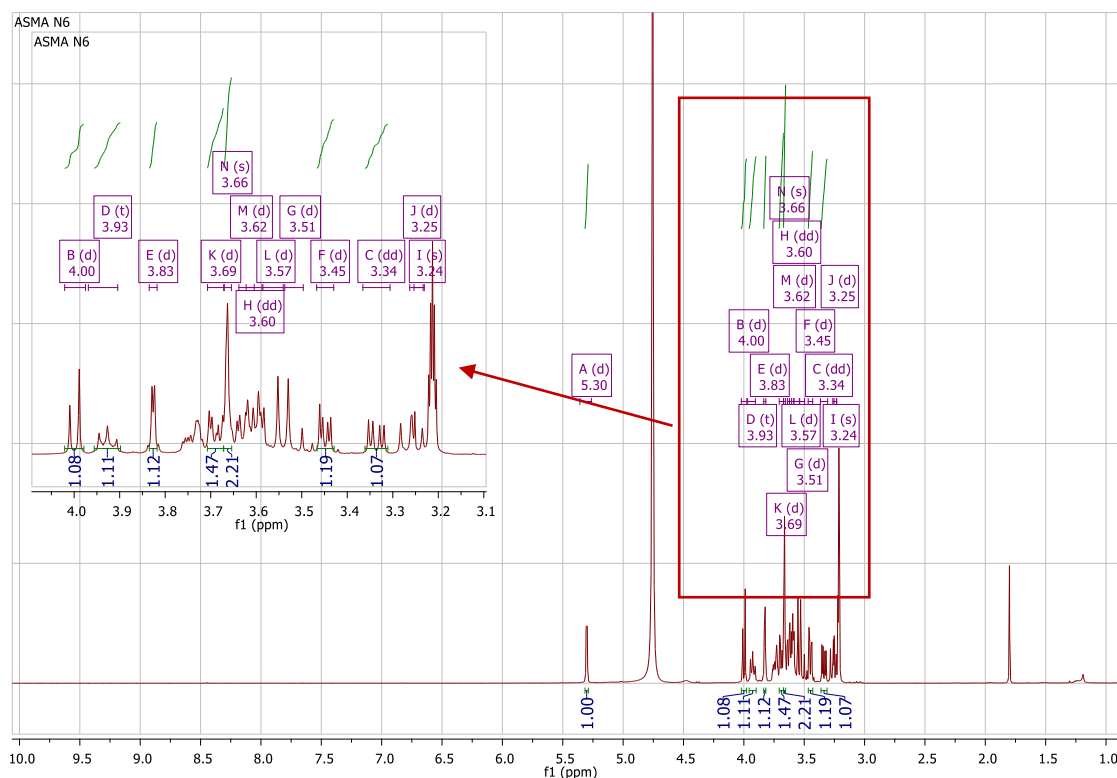
Figure. IV. 72: ^{1}H NMR spectrum (400 MHz, CD$_3$OD) of the compound **N6**.

So, depending on the ^{1}H NMR spectrum and compared with the data of **N1**, **N2** and **N5**, it could be deduced that the compound **N6** containing a fructose residue.

According to COSY spectrum (**Figure. IV. 73**) seven spin system of a hexose identified starting from the anomeric proton H-1 resonating at δ$_H$ 5.30 (d, J= 3.8 Hz, 1H) to H-6. The coupling constant indicate the α position of H-1, this last displays a correlation with the proton resonating at δ$_H$ 3.34 (dd, J= 9.8, 3.8, Hz, 1H) assigned to H-2. The proton H-3 δ$_H$ 3.44 (bd, J= 9.8 Hz, 1H) correlate with H-4 resonating at δ$_H$ 3.23 (bd, J= 9.8 Hz, 1H). Also, the proton H-5 resonating at δ$_H$ 3.60 (dd, J = 9.8, 4.9 Hz, 1H) correlate with two protons δ$_H$ 3.62 (d, J = 12.3 Hz, 1H) and δ$_H$ 3.70 (d, J = 12.3 Hz, 1H) corresponding H-6a and H-6b. The coupling constant between H-4 and H-5 (9.8 Hz) indicate the trans di-axial position of these protons, depending on these findings this hexose identified as α-D-glucose.

Also, a correlation of five spin system of another hexose was identified starting from H-6' to H-3'. The two protons resonating at δ$_H$ 3.65 (m) corresponding H-6a and H-6b correlate with proton resonating δ$_H$ 3.66 (m) assigned to H-5'. The proton H-4' δ$_H$

3.92 (t, J = 8.2 Hz, 1H) shows a correlation with H-3' resonating at δ_H 4.00 (d, J = 8.2 Hz, 1H).
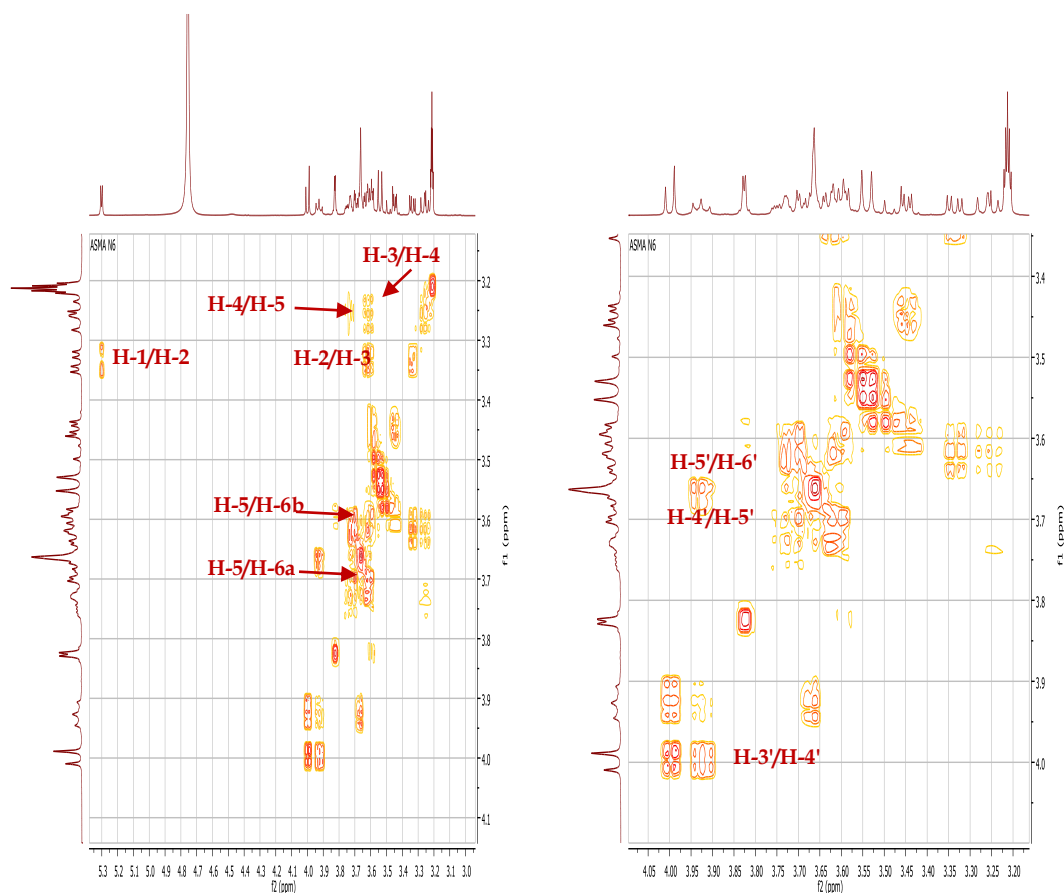
Figure. IV. 73: COSY spectrum (400 MHz, CD$_3$OD) of two hexoses of the compound **N6**.

The analyses of ^{13}C NMR spectrum (**Figure. IV. 74**) shows the presence of 12 peaks in the osidic field from 60 to 103.93 ppm, this confirm that the compound **N6** was disaccharide compound consist of two hexoses. The presence of two signals of anomeric carbons resonating at 92.28 and 103.93 ppm.
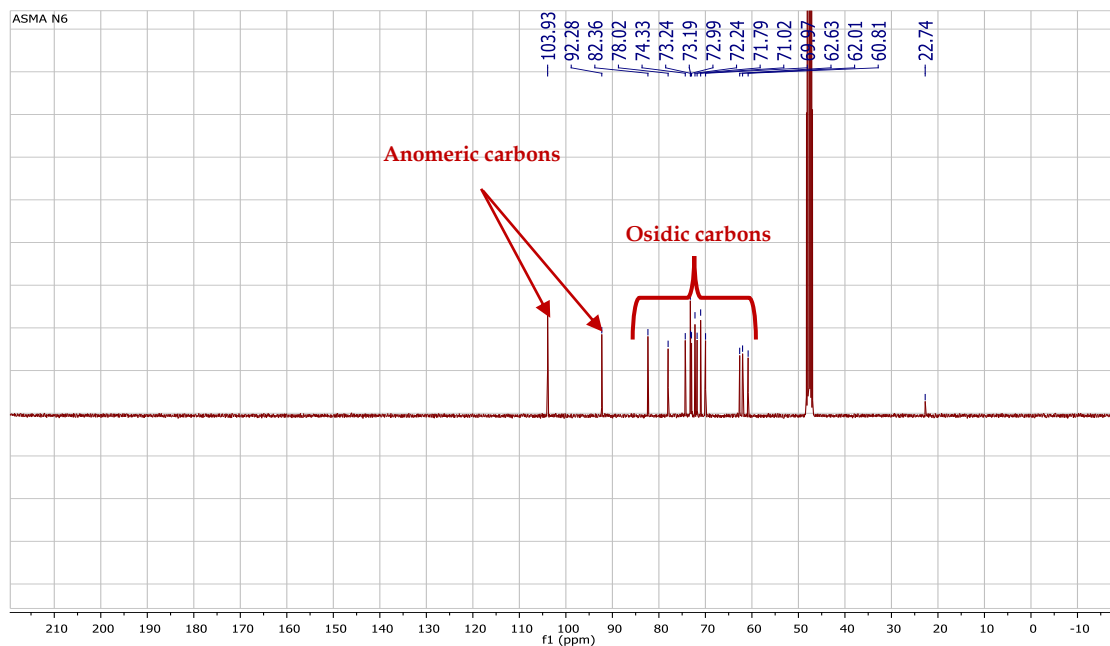
Figure. IV. 74: ^{13}C NMR spectrum (100 MHz, CD$_3$OD) of the compound **N6**.

The DEPT135 spectrum (**Figure. IV. 75**) reveals the disappearance of one anomeric carbon, this indicate that one of two hexose was D-fructose residue.
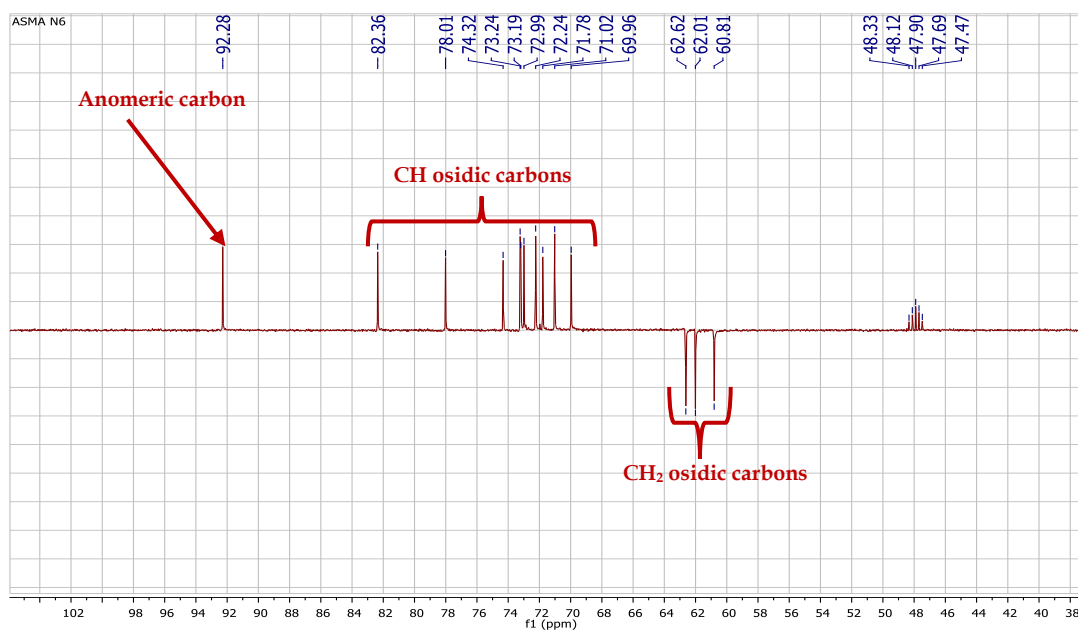
Figure. IV. 75: DEPT135 spectrum (100 MHz, CD$_3$OD) of the compound **N6**.

According to the HSQC experiment (**Figure. IV. 76**), each proton is assigned its corresponding carbon:

- ❖ H-1/ C-1 δ_C 92.28.
- ❖ H-2/ C-2 δ_C 71.79.
- ❖ H-3/ C-3 δ_C 73.19.
- ❖ H-4/ C-4 δ_C 69.97.
- ❖ H-5/ C-5 δ_C 72.99.
- ❖ H-6/ C-6 δ_C 60.81.
- ❖ H-1'/ C-1' δ_C 62.62.
- ❖ H-3'/ C-3' δ_C 78.02.
- ❖ H-4'/ C-4' δ_C 74.33.
- ❖ H-5'/ C-5' δ_C 82.36.
- ❖ H-6'/ C-6' δ_C 62.01.
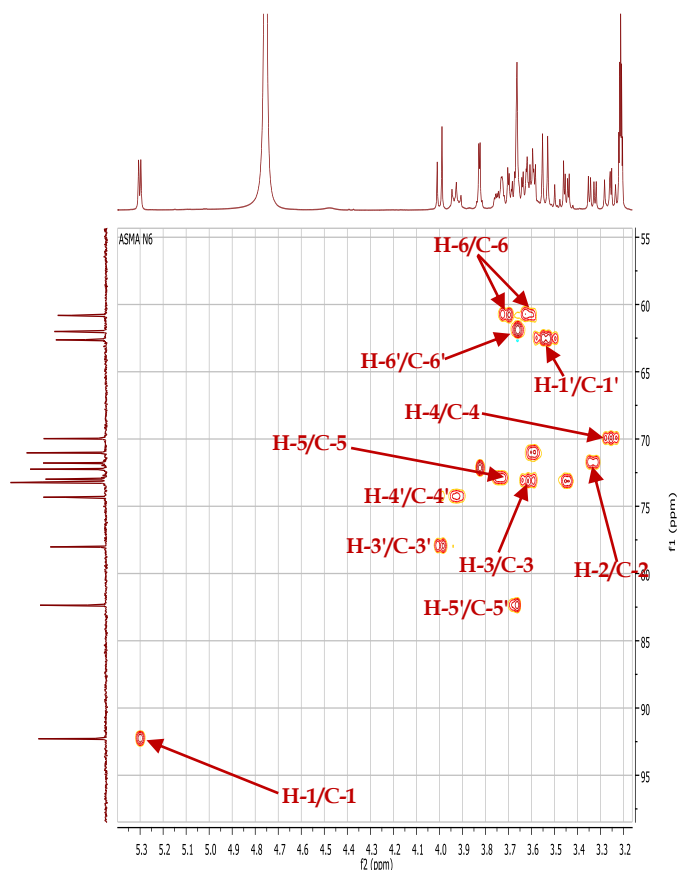
**Figure. IV. 76:** HSQC spectrum (400 MHz, CD$_3$OD) of the compound **N6**.

According to these results it could be deduced that the disaccharide **N6** consist of fructose and glucose. Based on the ^{13}C NMR data and the comparison of the chemical shift values with the values of compound **N1**, **N2** and **N5** and with literature data, the fructose was determined as β-D-furanoside type. The furanose type could be also confirmed by the chemical shift value of C-1' 62.01 ppm a free CH$_2$OH and the clearly correlation observed in HMBC spectrum (**Figure. IV. 78**) between H-5' and the anomeric carbon C-2' 103.93 ppm.

The HMBC experiment (**Figure. IV. 78**) show strong cross-peaks between ^{1}H and ^{13}C peaks in different residues, including:

- ❖ A correlation spot between H-1 δ_H 5.30 ppm with C-2 δ_C 71.79 and C-3 δ_C 73.24, the proton H-4 δ_H 3.23 correlate with C-3 δ_C 73.19, C-5 δ_C 72.99 and C-6 δ_C 60.81.
- ❖ A correlation spot between H$_2$-1' δ_H 3.52 (d, J = 12.3 Hz, 1H) and 3.55 (d, J = 12.3 Hz, 1H)) and C-2' δ_C 103.93, between H-4' δ_H 3.92 with C-3' δ_C 78.02 and C-5' δ_C 82.36 and between C-5' and H-6'.

Also, A cross-peaks among different residues at H-1 (δ_H 5.30) and C-2' (δ_C 103.93), which indicated the linkage site O-1 of α-D-glucopyranose was linked to the C-2' of β-D-fructofuranose (1 →2) linkage (**Figure. IV. 77**).
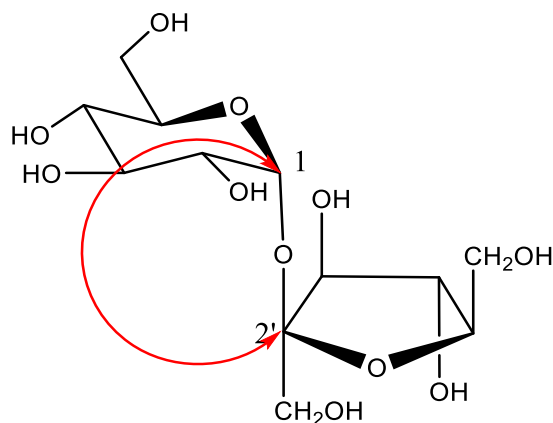
Figure. IV. 77: HMBC correlation of the compound **N6**.
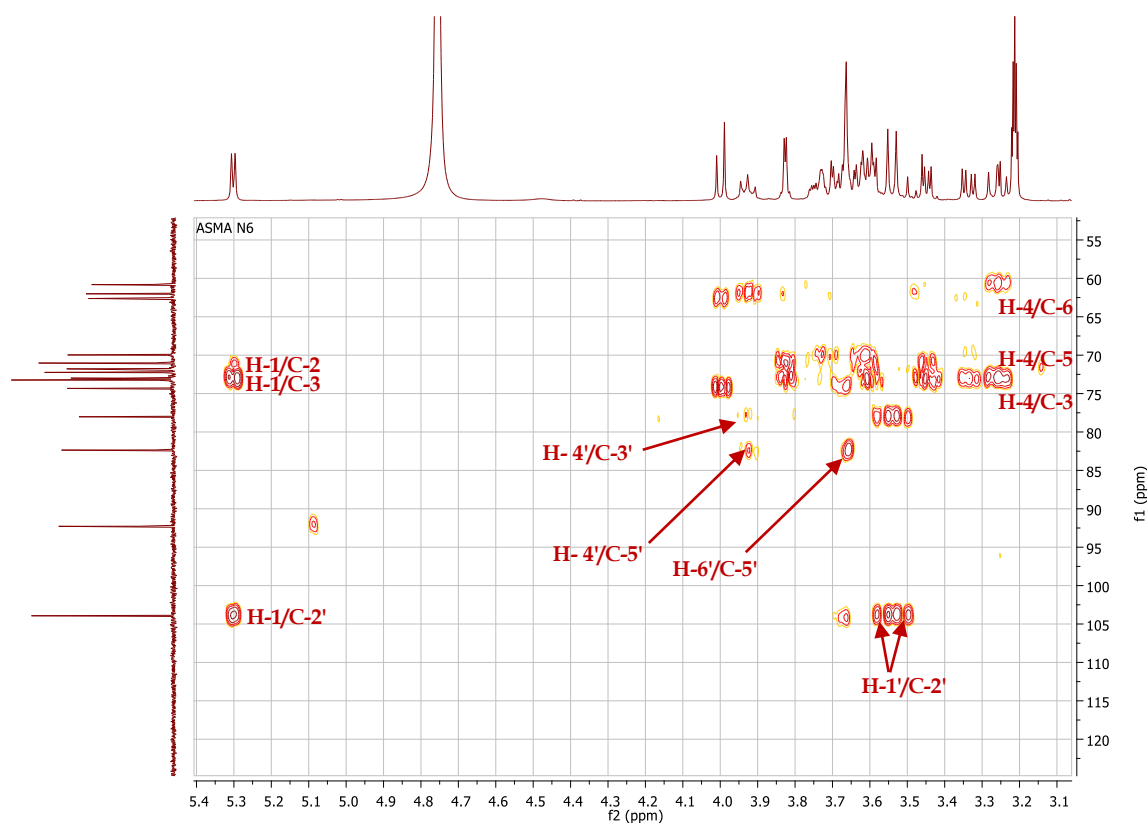
Figure. IV. 78: HMBC spectrum (400 MHz, CD$_3$OD) of the compound **N6**.

The structural confirmation of **N6** according to ^{1}H and ^{13}C NMR analyses using 1D-NMR and 2D-NMR showed that **N6** is disaccharide containing α-D-glucose and β-D-frucofuranose. From the previous detailed results, it was found that the compound

N6 was [O-β-D-fructofuranosyl-(2→1)-α-D-glucopyranoside], this disaccharide known as **Sucrose** (**Figure. IV. 79**) [209].

The ^{1}H and ^{13}C NMR data, are summarized in the **Table. IV. 8**, which are in full agreement with the literature [209]. **Sucrose** is the most naturally occurring polysaccharide [209]. This compound was isolated from for the first time from the genus *Atractylis*.
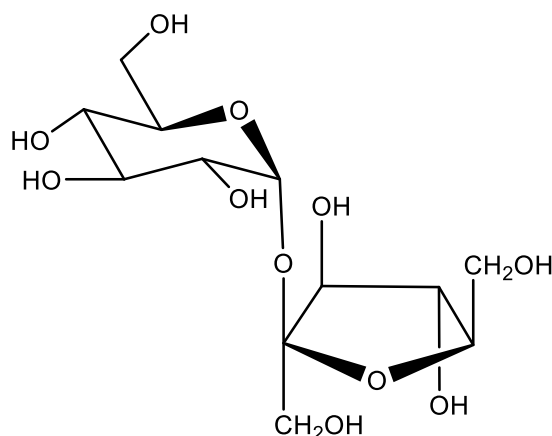
Figure. IV. 79: The structure of compound **N6**; [O-β-D-fructofuranosyl-(2→1)-α-D-glucopyranoside], Sucrose.

Table. IV. 8: ^{1}H NMR (400 MHz) and ^{13}C NMR (100 MHz) spectral data of compound **N6** (δ_C in ppm and δ_H in ppm and J in Hz).

Position	Carbon	Proton
α-D-glucose		
1	92.28	5.30 (d, J = 3.8 Hz, 1H)
2	71.79	3.33 (dd J= 9.8, 3.8 Hz, 1H)
3	73.19	3.60(dd, J = 9.8, 4.9 Hz, 1H)
4	69.97	3.23 m
5	72.99	3.73 m
6	60.81	3.62(d, J = 11.9 Hz, 1H)
		3.70(d, J = 11.9 Hz, 1H)
β Fructofuranose		
1'	62.62	3.52(d, J = 12.3 Hz, 1H)
2'		3.55(d, J = 12.3 Hz, 1H)
3'	103.90	--
4'	78.02	4.00 (d, J = 8.2 Hz, 1H)
5'	74.33	3.92 (t, J = 8.2 Hz, 1H)
6'	82.36	3.66 m
	62.01	3.65(S, 2H)

IV.4. 7. Compound J2

Compound **J2** is isolated in the form of a yellow amorph soluble in methanol. This compound is characterized on TLC test by dark purple fluorescence spot under UV lamp, which turns yellow by revelation using acid solution and heating.

The UV spectrum of compound **J2** recorded in the methanol shows two absorption maxima. Band I around 356 nm corresponding to cycle B and band II around 255 nm corresponding to cycle A (**Figure. IV. 80**), characteristics of flavonoid, flavonols 3-OH substituted type [210]. The bathochromic effects observed in the band I in the presence of NaOH, and the stability of the spectrum are in favor of the presence of a free OH at C4'. Also, the appearance of new band at 331 nm (**Figure. IV. 81**) after the addition of NaOH confirms the presence of 7-OH [210].
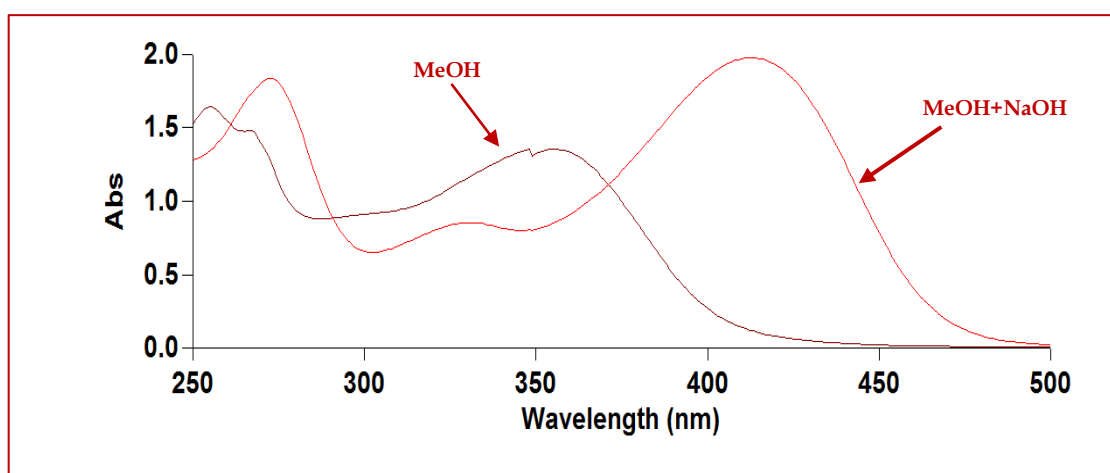
Figure. IV. 80: UV spectrum of compound **J2** recorded in MeOH and MeOH+ NaOH.
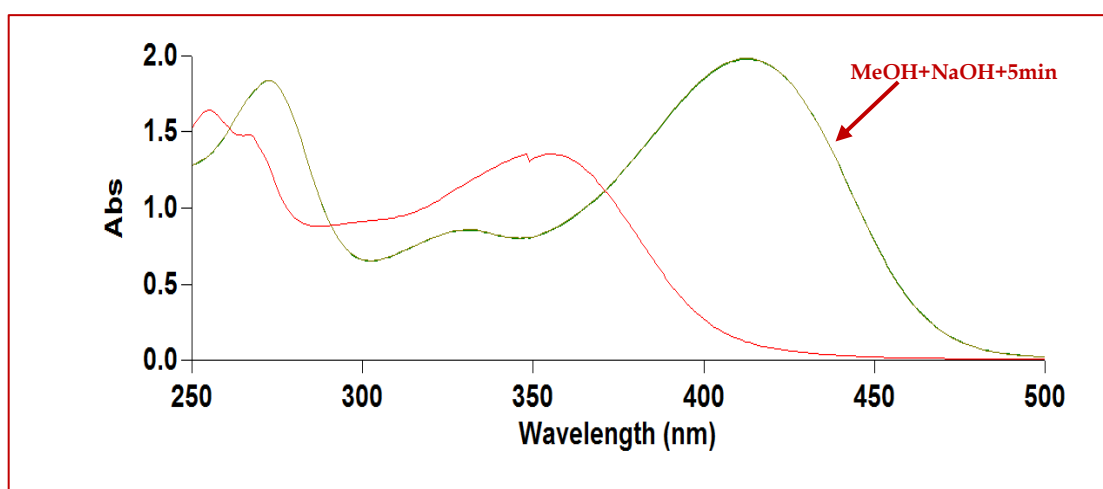
Figure. IV. 81: UV spectrum of compound **J2** recorded in MeOH, MeOH+ NaOH and MeOH+ NaOH after 5min.

The UV spectrum of compound **J2** recorded in the methanol+AlCl$_3$ (**Figure. IV. 82**) and methanol+AlCl$_3$+HCl (**Figure. IV. 83**) shows no changes compared with the UV spectrum of compound **J2** recorded in the methanol, this proposed the possibility of the presence of 5-OH and the absence of ortho dihydroxy [210].

Figure. IV. 82: UV spectrum of compound **J2** recorded in MeOH+AlCl$_3$.

Figure. IV. 83: UV spectrum of compound **J2** recorded in MeOH, AlC$_{l3}$ and AlCl$_3$+HCl.

According to the ^{1}H NMR spectrum (**Figure. IV. 85**) recorded in CD$_3$OD, we distinguish the characteristic signals of the aromatic protons, precisely of a flavonoid. The dark purple fluorescence spot under UV lamp suggests that **J2** is flavone or flavonol substituted in C-3 (3-OR). The ^{1}H NMR spectrum reveals:

❖ Two broad singlets at δ_H 6.11 and 6.31 attributable to H-6 and H-8 respectively, indicated the di-substitution of the aromatic ring A.

❖ Three peaks at δ 7.93 ppm (bs, 1H), 7.50 ppm (d, J = 8.6 Hz, 1H) and 6.81 ppm (bd, J = 7.7 Hz, 1H) are assignable to the aromatic protons of aromatic ring B 3,4 disubstituted.

❖ A peak singlet at δ 3.87 ppm (s, 3H), indicated the presence of methoxy group.

❖ The absence of H-3 peaks of ring C in the aromatic spectral region, confirms that **J2** is flavonol.

The ^{1}H NMR spectrum (**Figure. IV. 84**) displays that **J2** is diglycosylated flavonoid, indeed the spectrum presents two anomeric protons:

❖ Anomeric protons at δ 5.10 ppm (d, J = 7.6 Hz, 1H) was ascribed to H-1 of D-galactose, and signals at δ 1.07 (d, J = 6.2 Hz, 3H) and 4.43 ppm (broad singlet) assigned to H-6 and H-1 of L-rhamnose, respectively [211]. The characteristic coupling constants of anomeric protons of these two sugar residues, confirming the configuration β of the sugar D-galactose and the configuration α of the sugar L-rhamnose.
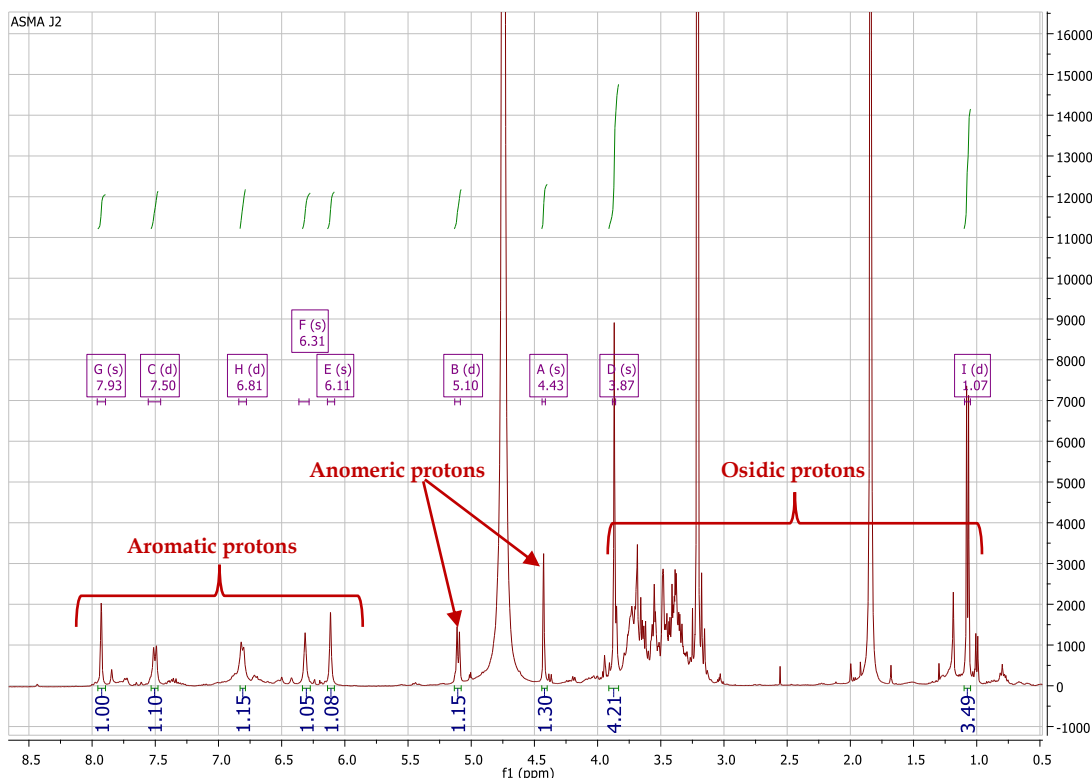
Figure. IV. 84: ^{1}H NMR spectrum (400 MHz, CD$_3$OD) of the compound **J2**.
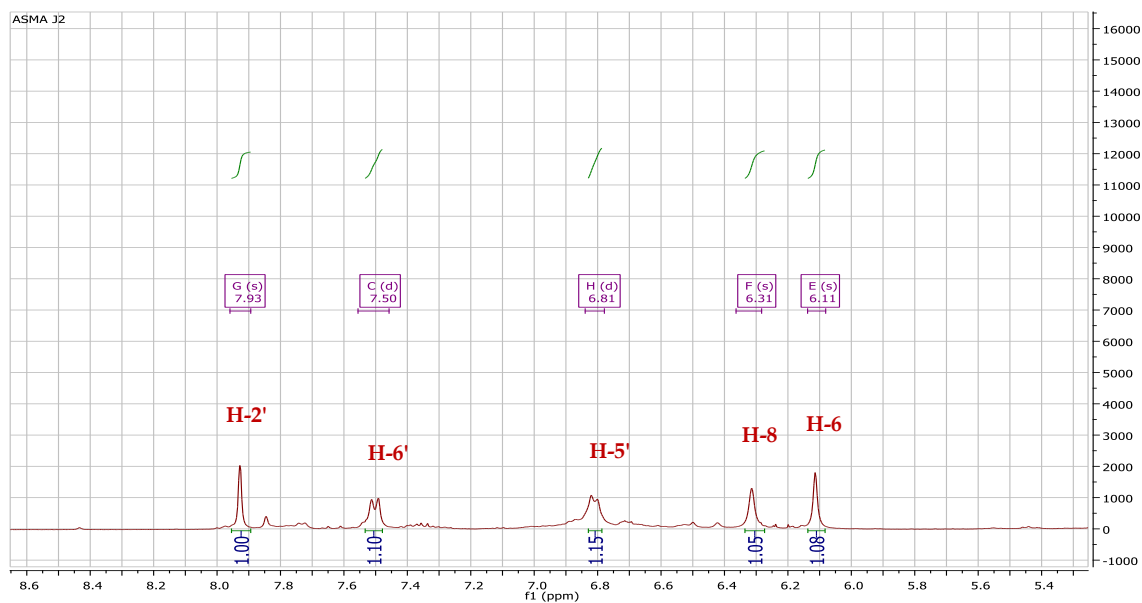
Figure. IV. 85: ^{1}H NMR spectrum (400 MHz, CD$_3$OD) of aromatic region of **J2**.

According to COSY spectrum (**Figure. IV. 88**):

❖ The two aromatic protons at 6.11 ppm (brs, 1H) and 6.31 ppm (brs, 1H) corresponding to H-6 and H-8, respectively of ring A of flavonol, belong to the same spin system. The multiplicity indicates the meta type of these protons.
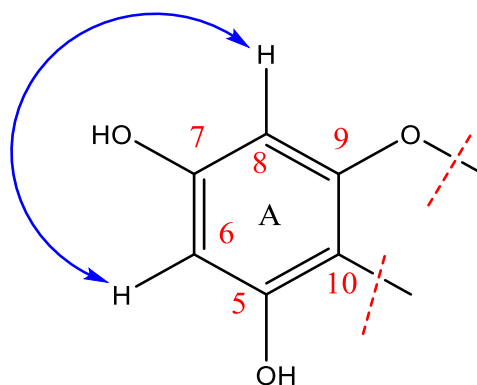
Figure. IV. 86: COSY correlations of aromatic ring A of the compound **J2**.

❖ The three aromatic protons at δ 7.93 ppm (bs, 1H), 7.50 ppm (d, J = 8.6 Hz, 1H) and 6.81 ppm (bd, J = 7.7 Hz, 1H) corresponding to H-2', H-5' and H-6', respectively. The coupling constant of these protons attributable to an ABX coupling system of the aromatic ring B 1',3',4' trisubstituted (**Figure. IV. 87**).
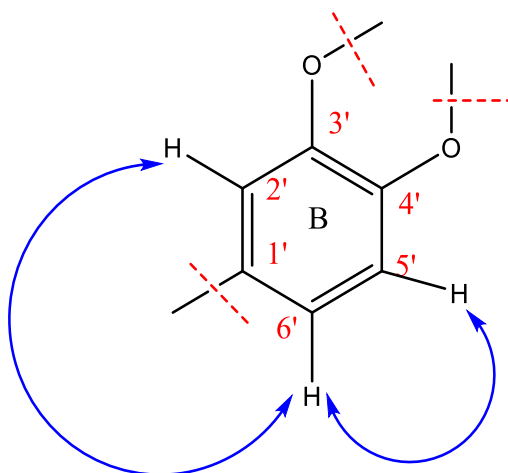
Figure. IV. 87: COSY correlations of aromatic ring B of the compound **J2**.
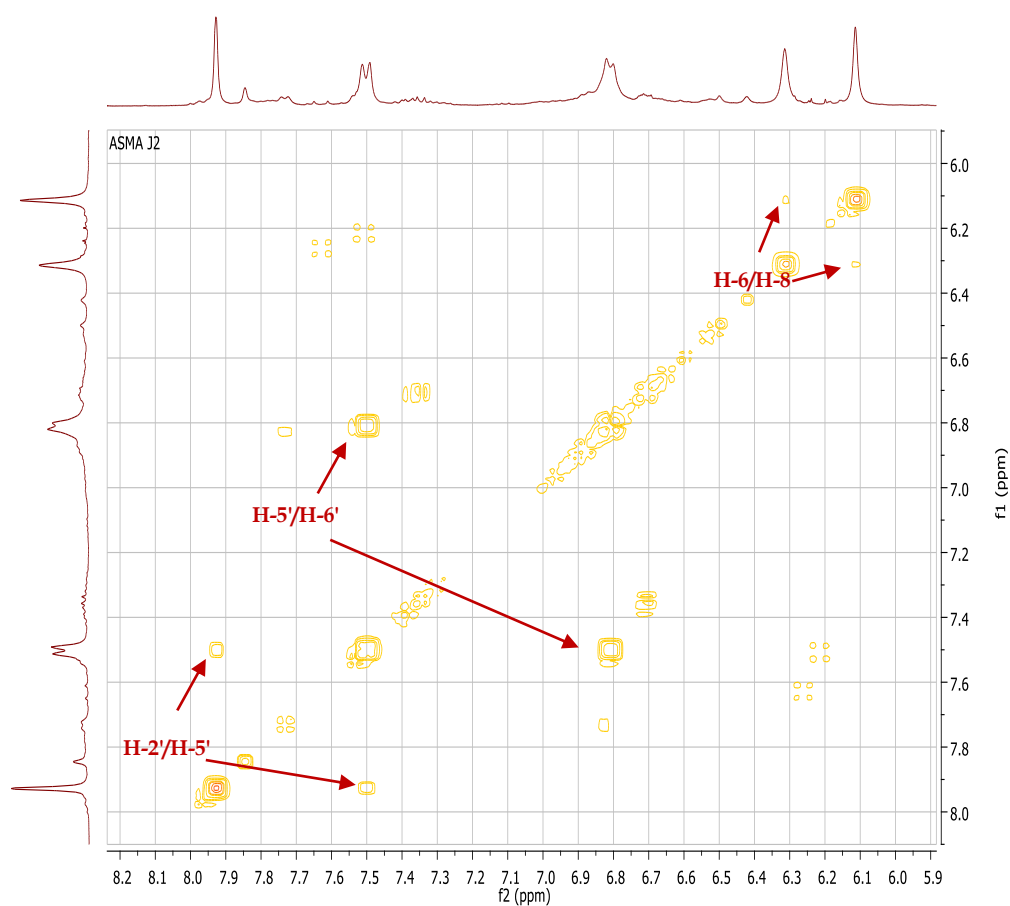
Figure. IV. 88: COSY spectrum (400 MHz, CD₃OD) of the compound **J2**.

The ^{13}C NMR spectrum (**Figure. IV. 96**) gave 28 carbon signals, based on DEPT 135 and (**Figure. IV. 97**) and DEPT 90 (**Figure. IV. 98**) spectra these 28 carbons are distributed as follows:

Aglycon part

- ❖ 10 quaternary carbons distributed in the ring A, B and C.

- ❖ A carbonyl group at δ 178.08 ppm, attributable to C-4 of flavonol.

- ❖ 5 aromatic CH between 93 and 123 ppm corresponding to H-6, H-8, H-2', H-5' and H-6' of aromatic ring A and B. The corresponding carbons assigned based on HSQC spectrum (**Figure. IV. 90**) as follows:

    - ➢ Cycle A: (C-6, H-6; δ 98.66, 6.11) and (H-8, C-8; 93.53; 6.31).

    - ➢ Cycle B: (C-2', H-2'; δ 113.27, 7.93) and (H-5', C-5'; 114.60, 6.81), (H-6', C-6'; 122.40, 7.50).

- ❖ A methoxy group at 55.57 ppm, the methoxy group (δ_H 3.87/ δ_C 55.57) correlates in HMBC (**Figure. IV. 99**) with aromatic carbon at δ_C 147.02, which assigned to the aromatic ring B. In addition, the protons of the methoxy group at δ_H 3.87 correlates in COSY with the proton already identified H-2' (δ_H 7.93). The presence of a correlation between H-2' and the carbon substituted by the methoxy group implies that it is carbon C-3' this indicates that the OH at position C-4' is free. The proton H-2' correlates in HMBC with 3 quaternary carbons at δ_C 121.57, 147.02 and 149.51 attributable to C-1', C-3' and C-4', respectively (**Figure. IV. 89**). The analysis of all these spectra indicates that the aglycon part of flavonol identified as isorhamnetin (**Figure. IV. 91**).
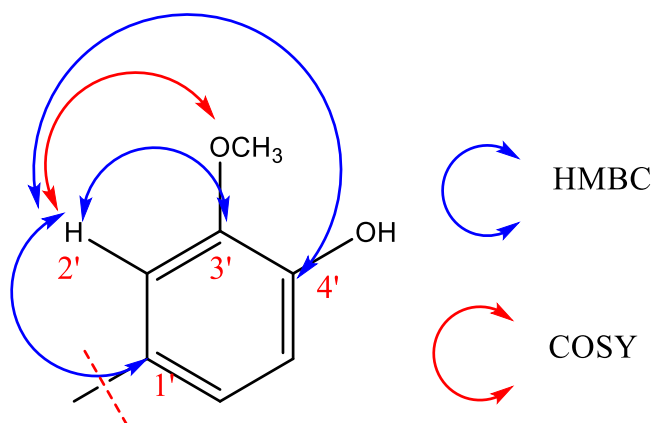
Figure. IV. 89: structure of isorhamnetin and HMBC, COSY correlations of ring B of the compound J2.
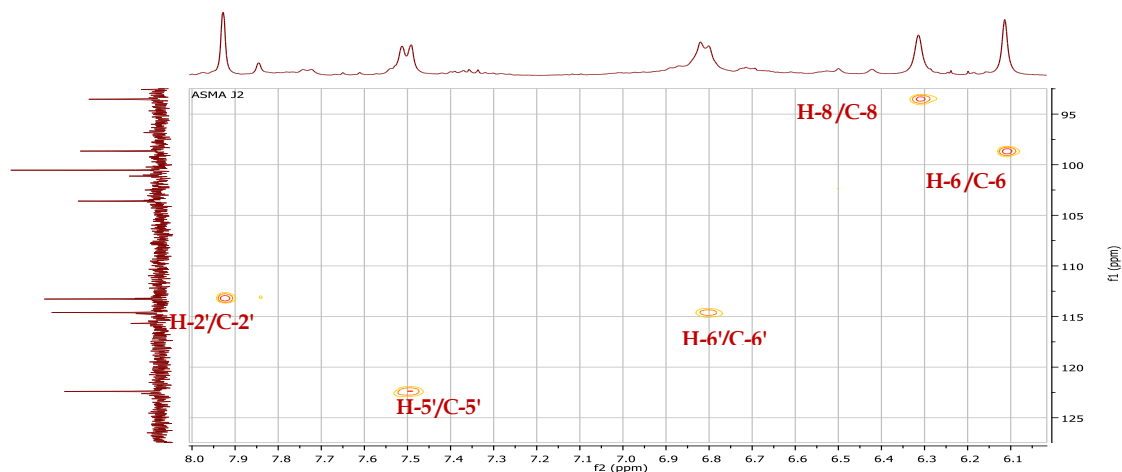
Figure. IV. 90: HSQC spectrum (400 MHz, CD$_3$OD) of aromatic region of **J2**.
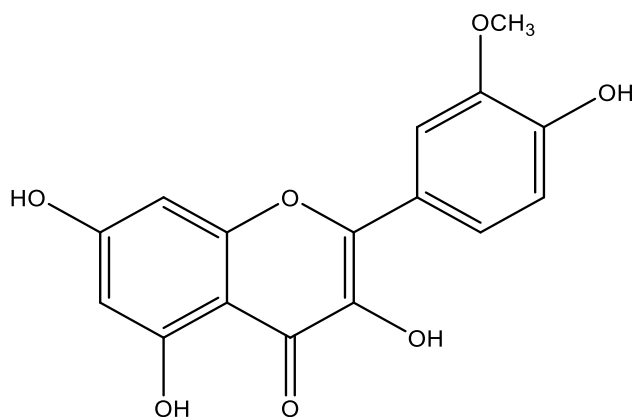
Figure. IV. 91: Structure of isorhamnetin.

Osidic part

- ❖ Two anomeric carbons at δ 100.54 and 103.59 ppm, and 8 CH resonating from 68 to 74 ppm corresponding to carbons of two sugar units.

    The analysis of COSY spectrum (**Figure. IV. 94**), makes it possible to identify a spin system with seven protons from the anomeric proton H-1" (δ$_H$ 5.10) to H-6" (δ$_H$ 3.34 and 3.62) of β-D-galactose (**Figure. IV. 92**):

- ❖ H-1" with H-2" (δ$_{H2"}$ 3.73).
- ❖ H-2" with H-3" (δ$_{H3"}$ 3.45).
- ❖ H-3" with H-4" (δ$_{H4"}$ 3.68).
- ❖ H-4" with H-5" (δ$_{H5"}$ 3.54).
- ❖ H-5" with H-6"a and H-6"b (δ$_{H6"}$ 3.34 and 3.62).
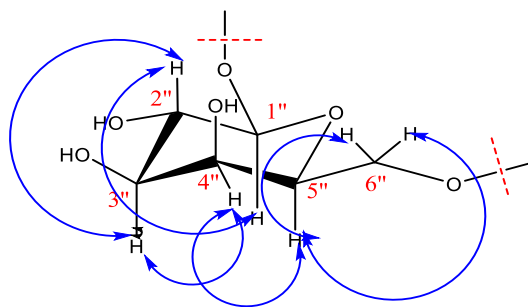
Figure. IV. 92: COSY correlations of β-D-galactose protons of the compound **J2**.

Also, the analysis of COSY spectrum (**Figure. IV. 94**), makes it possible to identify a spin system with eight protons from the anomeric proton H-1''' (δ_H 4.43) to H-6''' CH$_3$ (δ_H 1.07) of α-L-rhamnose (**Figure. IV. 93**).

- ❖ H-1''' with H-2''' ($\delta_{H2'''}$ 3.47).
- ❖ H-2''' with H-3''' ($\delta_{H3'''}$ 3.38).
- ❖ H-3''' with H-4''' ($\delta_{H4'''}$ 3.17).
- ❖ H-4''' with H-5''' ($\delta_{H5'''}$ 3.42).
- ❖ H-5''' with H-6''' ($\delta_{H6'''}$ 1.07).
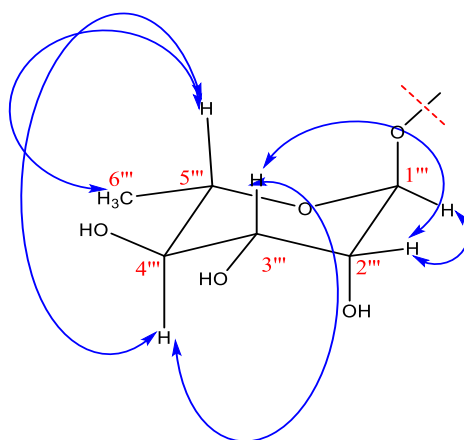
Figure. IV. 93: COSY correlations of α-L-rhamnose protons of the compound **J2**.
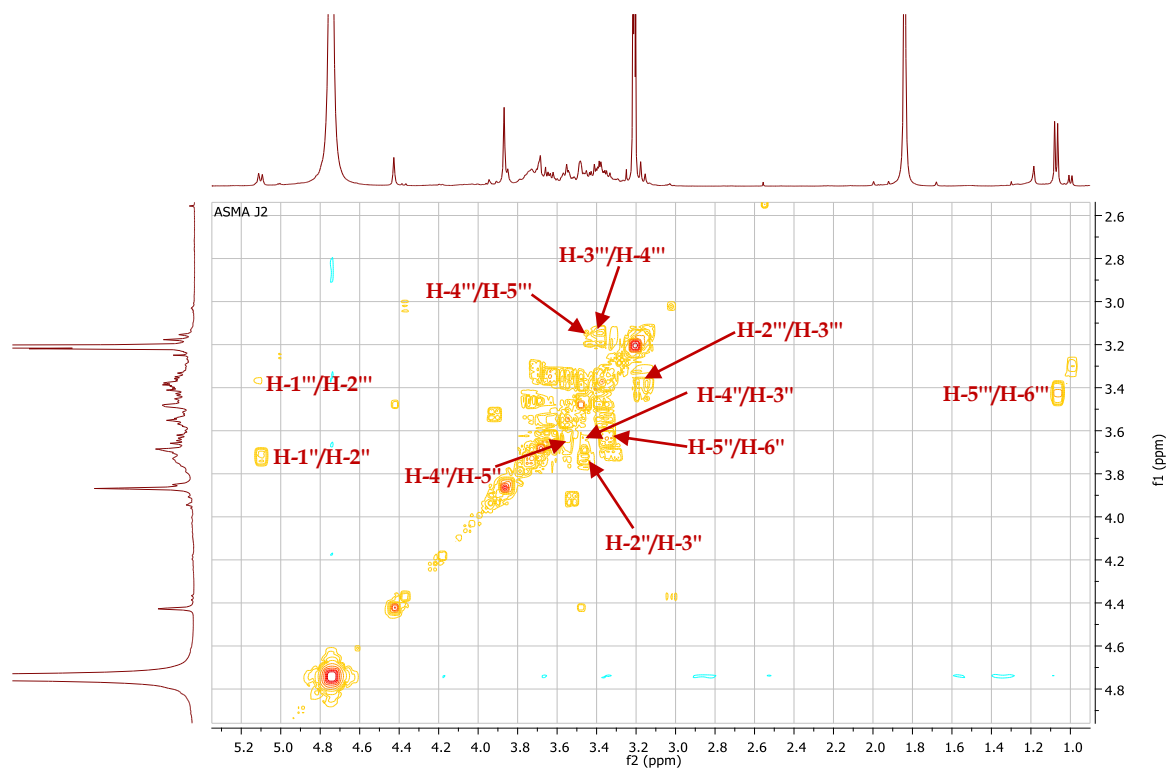
Figure. IV. 94: COSY spectrum (400 MHz, CD$_3$OD) of osidic part of compound **J2**.

The analysis of HSQC spectrum (**Figure. IV. 95**), make it possible to assigns all the corresponding carbons of the protons of the two osidic units as follows:

- ❖ β-D-galactose: the carbons resonating at δ$_C$ 103.59, 71.68, 73.62, 68.63, 74.14 and 66.09 ppm attributable to C-1″, C-2″, C-3″, C-4″, C-5″ and C-6″, respectively.

- ❖ α-L-rhamnose: the carbons resonating at δ$_C$ 100.54, 70.68, 70.90, 72.45, 68.33 and 16.53 ppm attributable to C-1‴, C-2‴, C-3‴, C-4‴, C-5‴ and C-6‴, respectively.
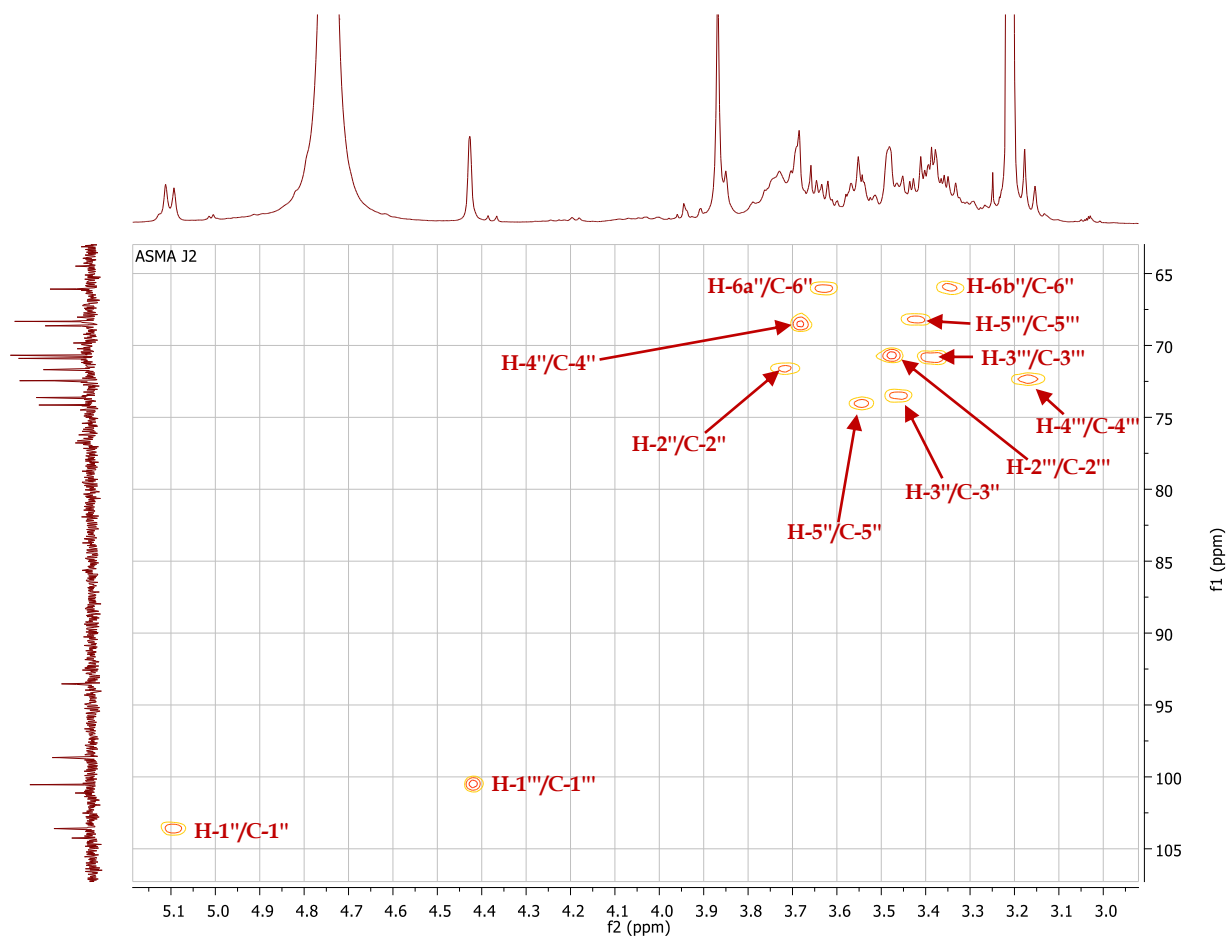
Figure. IV. 95: HSQC spectrum (400 MHz, CD$_3$OD) of osidic protons and carbons of compound **J2**.
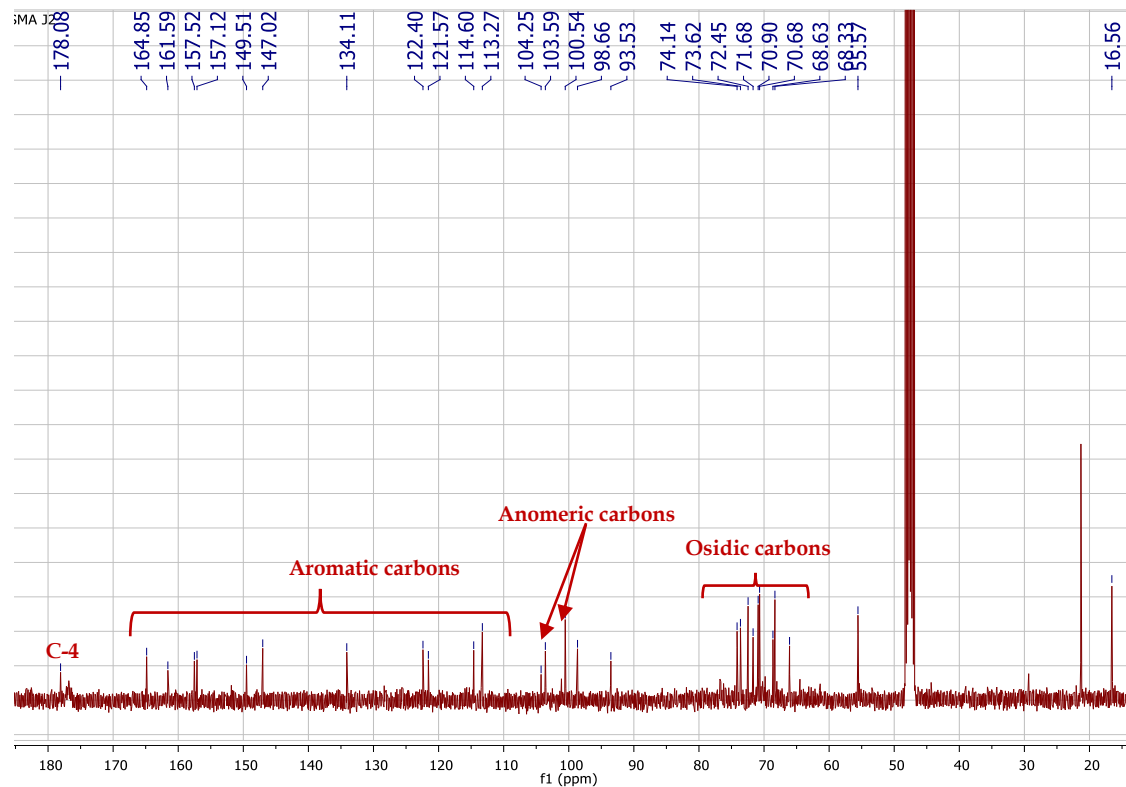
Figure. IV. 96: ^{13}C NMR spectrum (100 MHz, CD$_3$OD) of the compound **J2**.
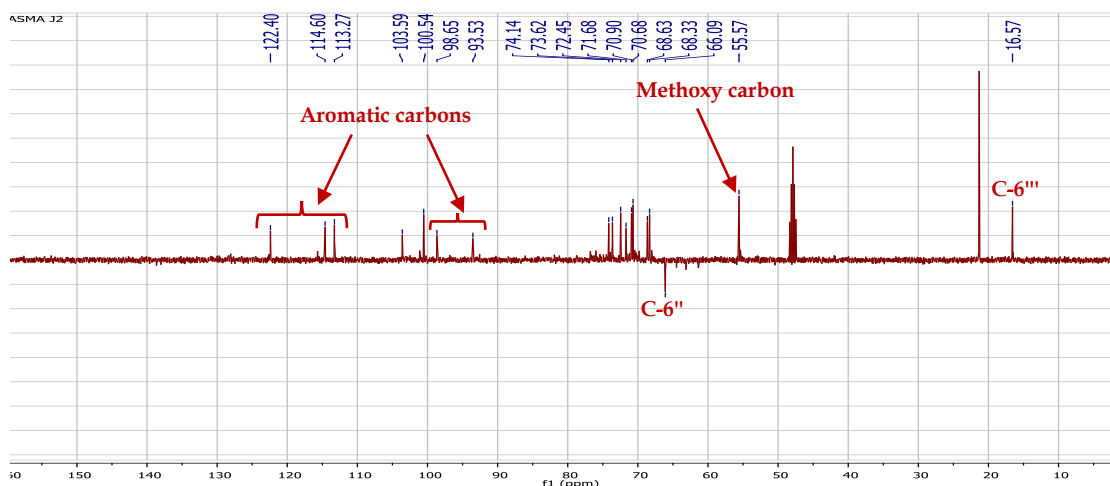
Figure. IV. 97: DEPT 135 spectrum (100 MHz, CD₃OD) of the compound **J2**.
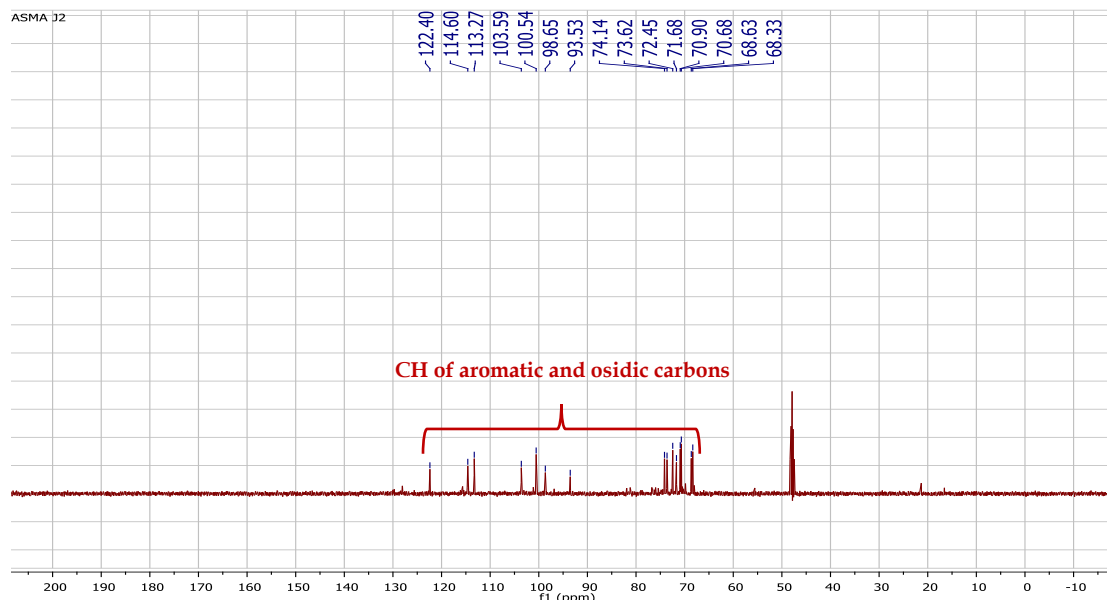
Figure. IV. 98: DEPT 90 spectrum (400 MHz, CD₃OD) of the compound **J2**.

Taking into the consideration the presence of H-6 and H-8 at δ_H 6.11 and 6.31, respectively. Furthermore, a downfield shift of 10.9 ppm of C-2 signal and an up-field shift 1.4 of ppm of C-3 signal in ^{13}C NMR spectrum (**Table. IV. 9**), in comparison with the non-glycosylated isorhamnetin (δ_{C2} 146.6 ppm and δ_{C3} 135.6 ppm) indicated that **J2** is **isorhamnetin-3-O-glycoside** [212, 213].

The HMBC spectrum (**Figure. IV. 99**) also show correlation spot between C-1''' and C-6'', that revealed the attachment rhamnose C-1'''→C-6'' galactose. Which deduced by a remarkable downfield shift of 5.09 ppm of C-6 compared with

isorhamnetin-3-O-β-D-galactoside [212]. This effect is characteristic of rhamnosylation on C-6 of galactose, the attachment rhamnose C-1'''→C-6'' galactose called robinobioside (**Figure. IV. 100**).
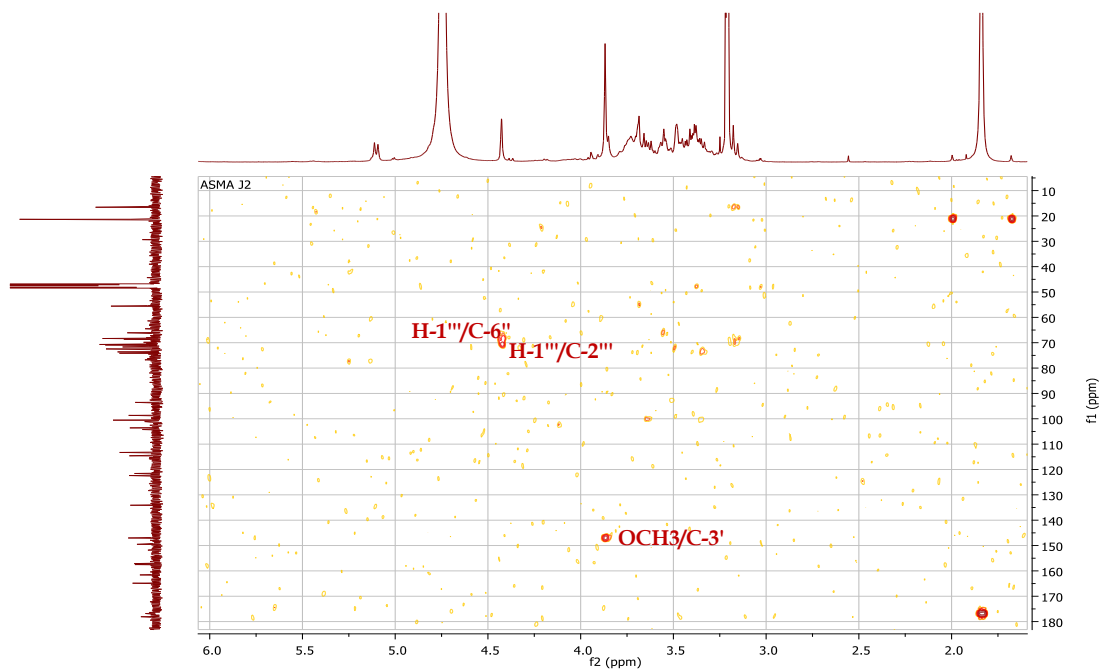
Figure. IV. 99: HMBC spectrum (400 MHz, CD₃OD) of the compound **J2**.
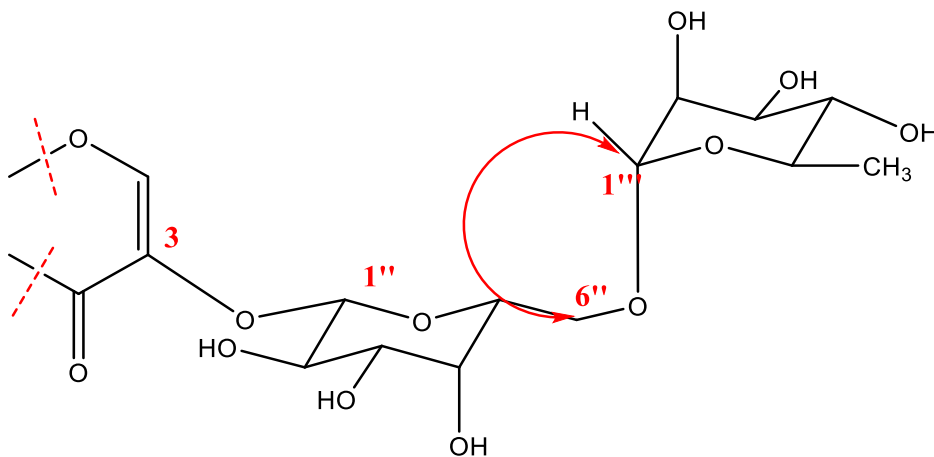
Figure. IV. 100: HMBC correlations between two sugars units and between osidic and aglycon parts of the compound **J2**.

All the data of the compound **J2** are in total agreement with isorhamnetin 3-O-robinobioside (**Figure. IV. 101**), which previously isolated from species *Gomphrenu martiam* (Amaranthaceae) [211], *Atractylis flava* (Asteraceae) [55], *Nitraria retusa* (Nitrariaceae) [214], and for second time from *Artactylis* genus.
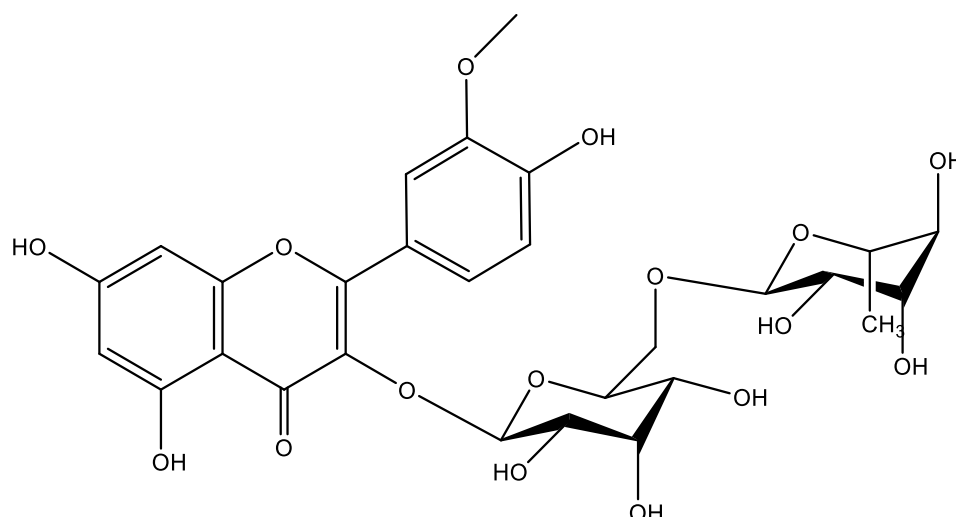
Figure. IV. 101: Structure of compound **J2**; isorhamnetin 3-O-robinobioside.

The ^{1}H and ^{13}C NMR data, are summarized in the **Table. IV. 9**, which are in total agreement with the literature [55].

Table. IV. 9: Chemical shifts ^{1}H NMR (400 MHz) and ^{13}C NMR (100 MHz) in CD$_3$OD of compound **J2** (δ_C in ppm and δ_H in ppm and J in Hz).

Position	Carbon	Proton
1	-O-	--
2	157.52	--
3	134.11	--
4	178.08	--
5	161.59	--
6	98.66	6.11 (brs, 1H)
7	164.85	--
8	93.53	6.31 (brs, 1H)
9	157.12	--
10	104.25	--
1'	121.57	--
2'	113.27	7.93 (brd, 1H)
3'	147.02	--
3'-OCH$_3$	55.57	3.87 (s, 3H)
4'	149.51	--
5'	114.60	6.81 (d, J= 7.7 Hz, 1H)

|		
6'	122.40	7.50 (brd, J = 8.6 Hz, 1H)
3-O-1''- galactose	103.59	5.10 (d, J = 7.6 Hz, 1H)
2''	71.68	3.73 (m)
3''	73.62	3.46 (m)
4''	68.63	3.69 (brd, J = 2.0 Hz, 1H)
5''	74.14	3.54 (m)
6''	66.09	3.62 (dd, J = 12.3, 6.8 Hz, 1H) H-6a 3.34 (dd, J = 12.3, 6.0 Hz, 1H) H-6b
6''-O-1'''-rhamnose	100.54	4.43 (brs, 1H)
2'''	70.68	3.47 (m)
3'''	70.9	3.38 (m)
4'''	72.45	3.17 (brd, J = 9.4 Hz, 1H)
5'''	68.33	3.43 (dd, J = 9.7, 6.5 Hz, 1H)
6'''	16.53	1.07 (d, J = 6.2 Hz, 3H)

IV.4. 8. Compound J4

Compound **J4** is isolated in the form of yellow amorph soluble in methanol. This compound is characterized on TLC test by dark purple fluorescence spot under UV lamp suggests that **J4** is flavone or flavonol substituted in C-3 (3-OR), and by revelation using acid solution and heating the **J4** spot turns yellow.

The UV spectrum of compound **J4** recorded in the methanol shows two absorption maxima. Band I around 356 nm corresponding to cycle B and band II around 255 nm corresponding to cycle A (**Figure. IV. 102**), characteristics of flavonoid flavonols 3-OH substituted type [210] (**Figure. IV. 102**). The bathochromic effects observed in the band I in the presence of NaOH and the stability of the spectrum are in favor of the presence of a free OH at C4'. Also, the appearance of new band at 327 nm after the addition of NaOH confirms the presence of 7-OH [210] (**Figure. IV. 103**). The UV spectrum of compound **J4** recorded in the methanol+AlCl$_3$ (**Figure. IV. 104**) and methanol+AlCl$_3$+HCl (**Figure. IV. 105**) shows no changes compared with the UV spectrum of compound **J4** recorded in the methanol, this proposed the possibility of the presence of 5-OH and the absence of ortho dihydroxy [210].
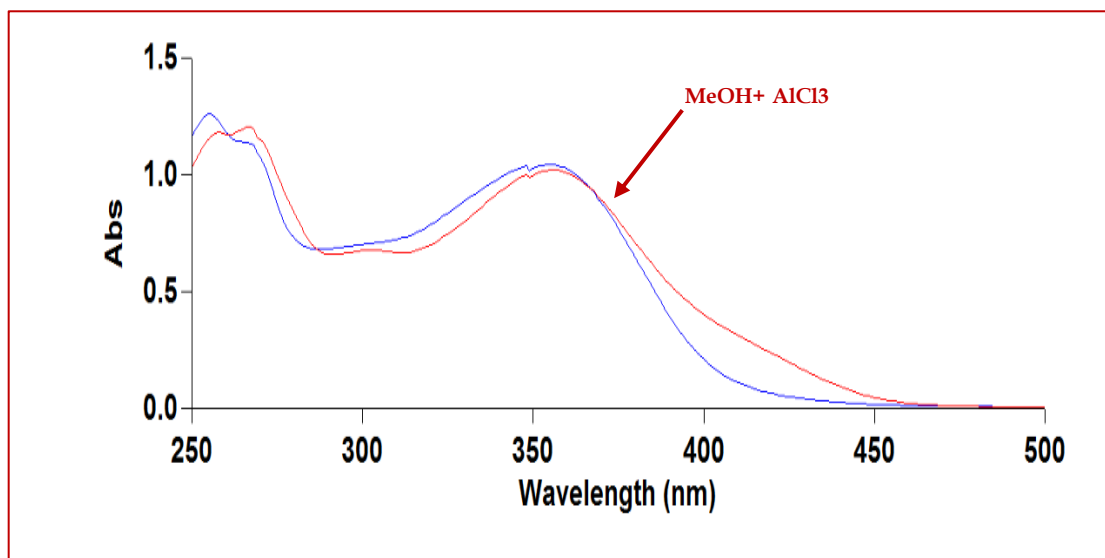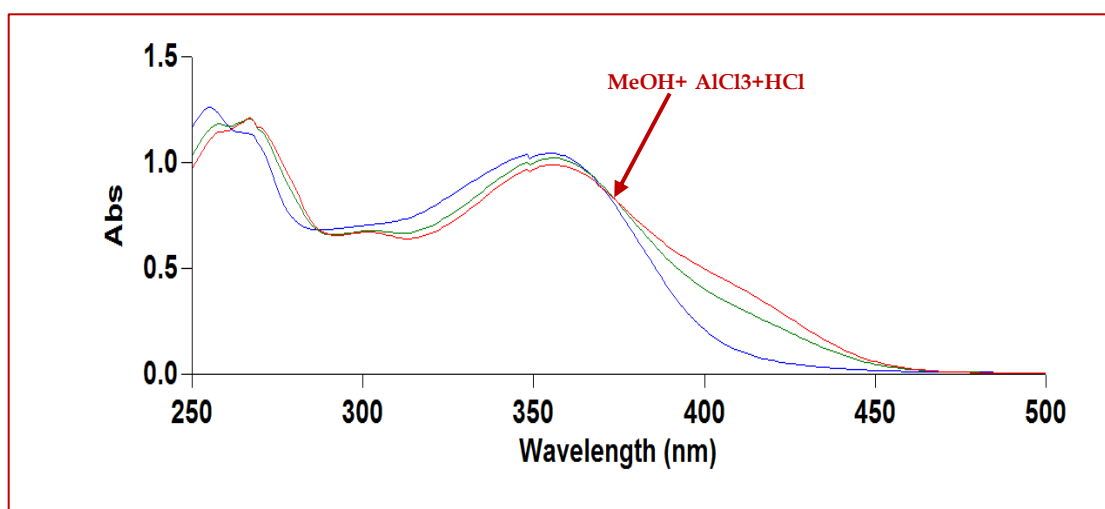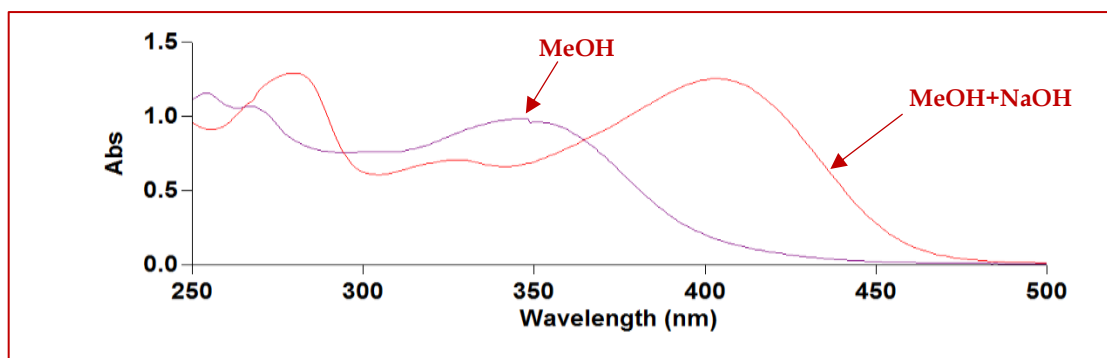
Figure. IV. 102: UV spectrum of compound **J4** recorded in MeOH and MeOH+ NaOH.
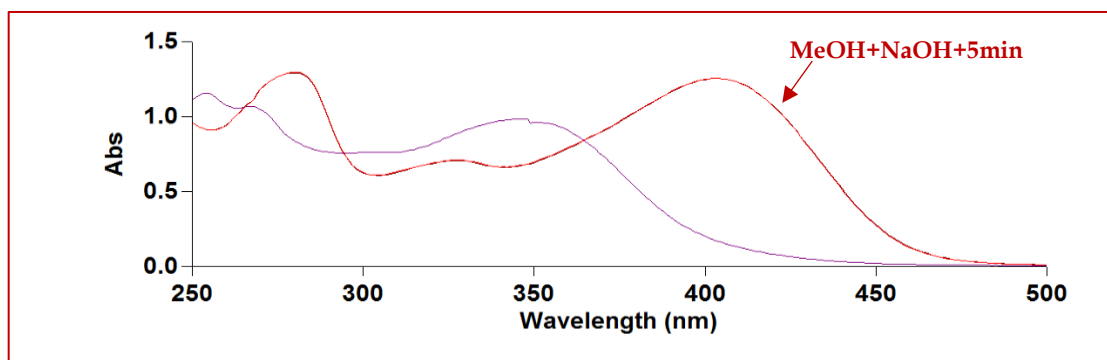
Figure. IV. 103: UV spectrum of compound **J4** recorded in MeOH+ NaOH after 5min.
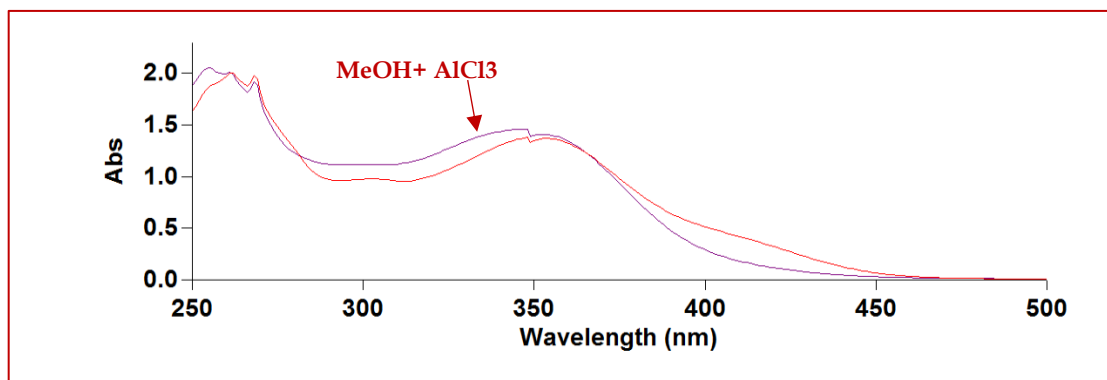
Figure. IV. 104: UV spectrum of compound **J4** recorded in MeOH +$AlCl_3$.
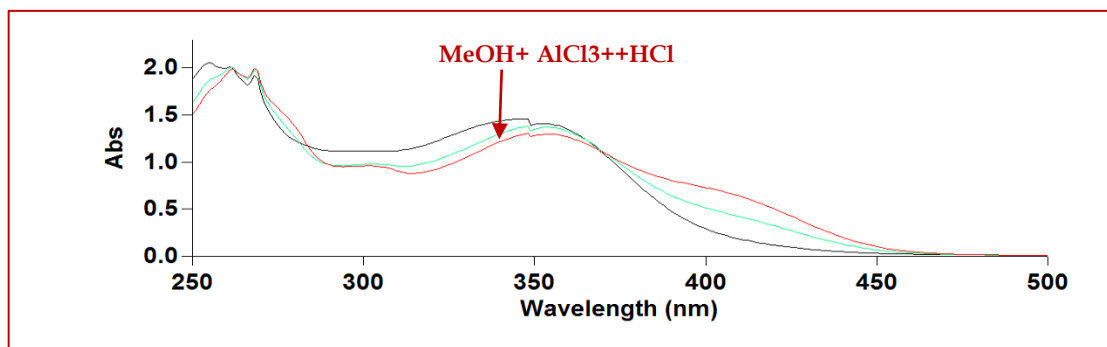
**Figure. IV. 105:** UV spectrum of compound **J4** recorded in $AlCl_3$+HCl.

The ^{1}H NMR spectrum recorded in CD$_3$OD (**Figure. IV. 107**), reveals the characteristic signals of the aromatic protons, precisely of a flavonoid. The ^{1}H and ^{13}C NMR spectral data (**Table. IV. 10** and **Table. IV. 9**) make it possible to deduce that compound **J4** has the same aglycone (isorhamnetin) as compound **J2** previously described.

The ^{1}H NMR spectrum (**Figure. IV. 106**) includes two signals in the form of doublets at δ_H 6.09 and 6.29 ppm with the same coupling constant (J = 2.0 Hz), which are characteristic of aromatic protons H-6 and H-8 of aromatic ring A.

The spectrum also includes three signals corresponding to H-2', H-5' and H-6' respectively of an aromatic ring B, the signal of proton H-6' observed at δ_H 7.43 in the form of a double doublets (J = 8.5; 2.0 Hz).

- ❖ The first doublet corresponds to an ortho coupling with the proton H-5' that resonates at δ_H 6.81 (J = 8.5 Hz).
- ❖ The second doublet, indicating meta coupling with the proton detected at δ_H 7.96 H-2' (J = 2.0 Hz).

The ^{1}H NMR spectrum also show a peak in singlet form at δ_H 3.90 ppm, corresponding to methoxy group of isorhamnetin.
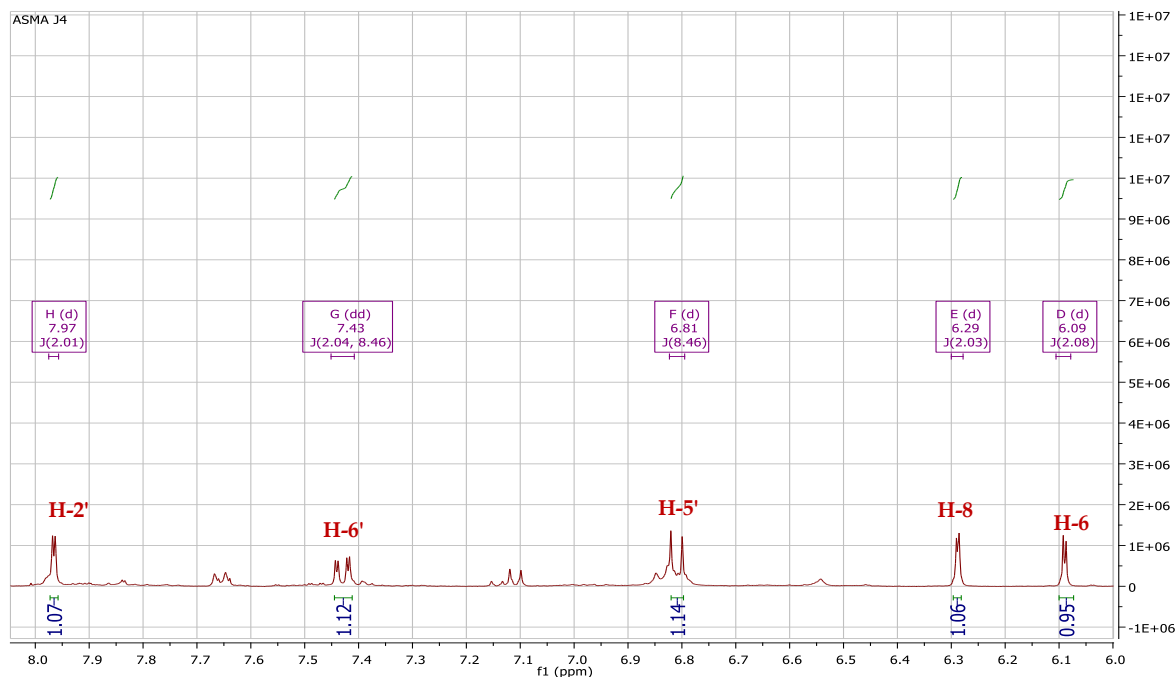
Figure. IV. 106: ^{1}H NMR spectrum (400 MHz, CD$_3$OD) of aromatic part of compound **J4**.

The Osidic protons detected in ^{1}H NMR spectrum (**Figure. IV. 107**) at δ_H 5.69 ppm (d, J = 7.6 Hz, 1H) was ascribed to H-1" of D-galactose with configuration β. The signals at δ_H 1.07 (d, J = 6.2 Hz, 3H), 4.46 (d, J = 1.4 Hz, 1H), 0.78 (d, J = 6.2 Hz, 3H) and 5.06 ppm (d, J = 1.3 Hz, 1H) assigned to H-6''', H-1''', H-6'''' and H-1'''' of two L-rhamnose sugar units, respectively [211]. The characteristic coupling constants of anomeric protons of rhamnose, confirmed the configuration α of L-rhamnose.

The protons present in the osidic spectral regions, indicate the presence of three sugar units.
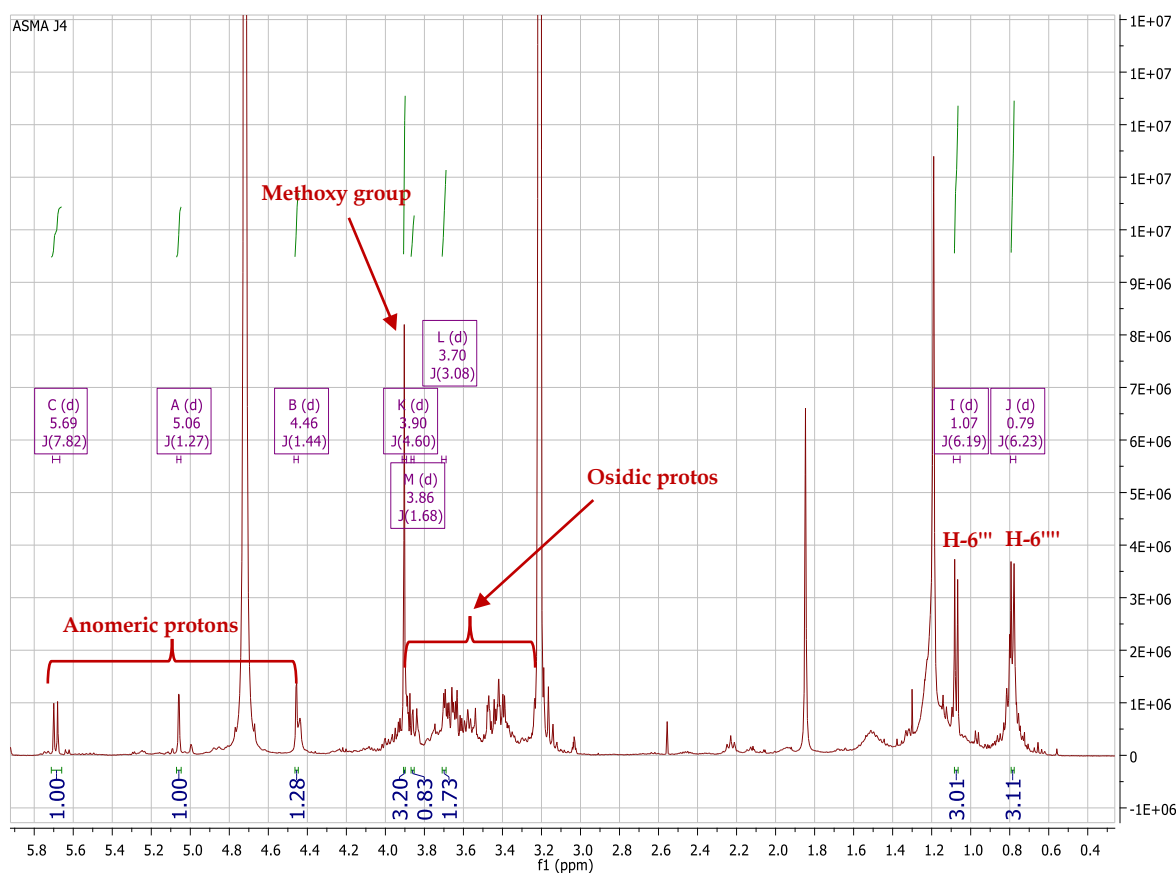
Figure. IV. 107: ^{1}H NMR spectrum (400 MHz, CD$_3$OD) of osidic protons of the compound **J4**.

The ^{13}C NMR spectrum (**Figure. IV. 108**), indicate the presence of 34 carbons; 16 carbons of isorhamnetin and 18 carbons of three sugar units, which are distributed based on DEPT 135 (**Figure. IV. 109**) and DEPT 90 (**Figure. IV. 110**) as follows:

❖ A carbonyl group detected at δ_C 178.76 ppm, corresponding to C-4 of flavonol.
❖ A methoxy group at δ_C 55.80, corresponding to OCH$_3$ - C-3'- of isorhamnetin.

- ❖ 5 CH aromatic of ring A and B resonating between 93 and 122 ppm, C-6, C-8, C-2', C-5' and C-6'.

- ❖ 7 oxygenated quaternary carbons of isorhamnetin resonating between 133 and 164 ppm, corresponding to C-2, C-3, C-5, C-7, C-9, C-3' and C-4'.

- ❖ 15 CH carbons resonating between 68 and 101 corresponding to osidic carbons of three sugar units.

- ❖ Two CH$_3$ groups resonating at δ_C 15.95 and 16.54 ppm, corresponding to C-6''' and C-6'''' of two rhamnose units.

- ❖ The peaks resonating from δ_C 65.82 to 76.42 assigned to osidic carbons.
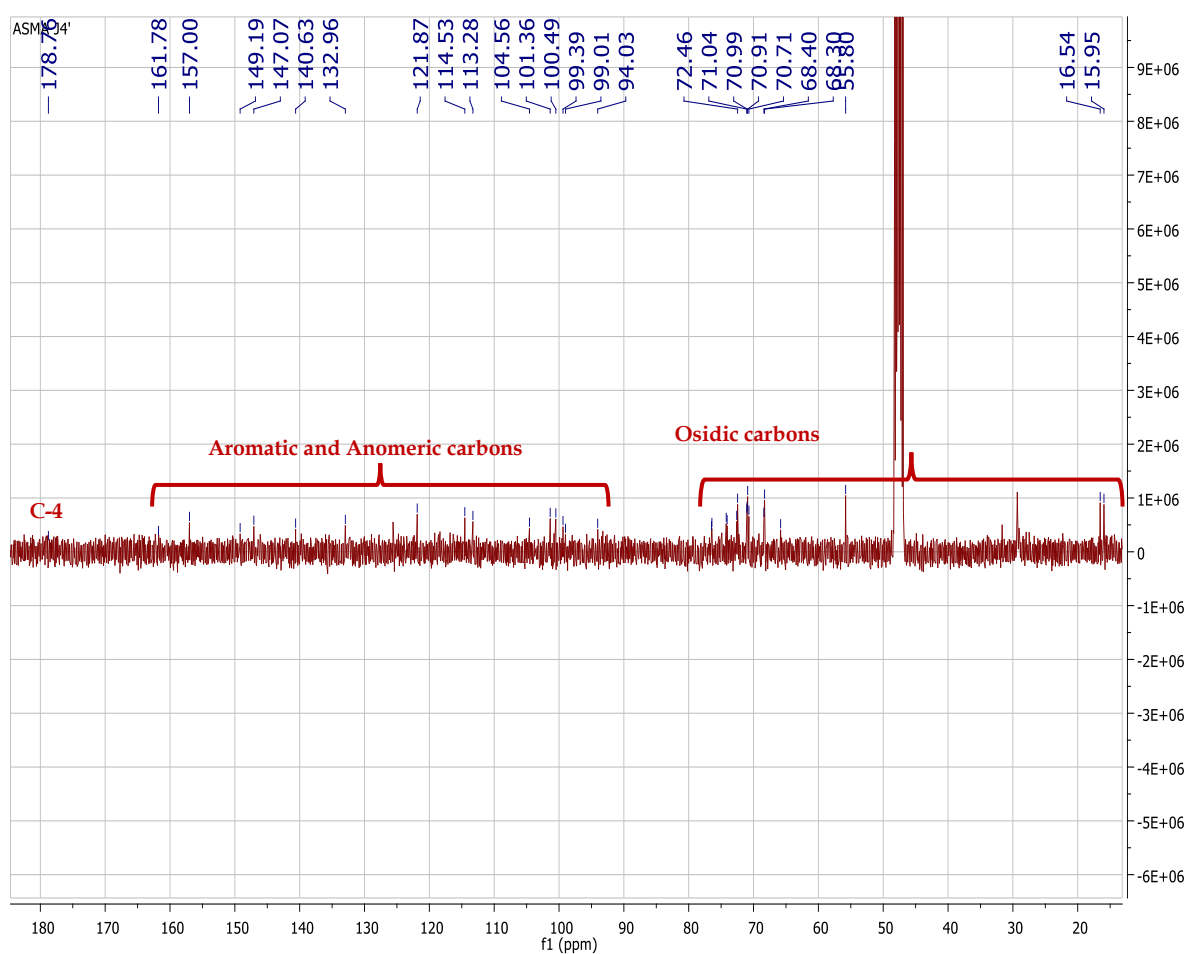
Figure. IV. 108: ^{13}C NMR (100 MHz, CD$_3$OD) spectrum of compound **J4**.
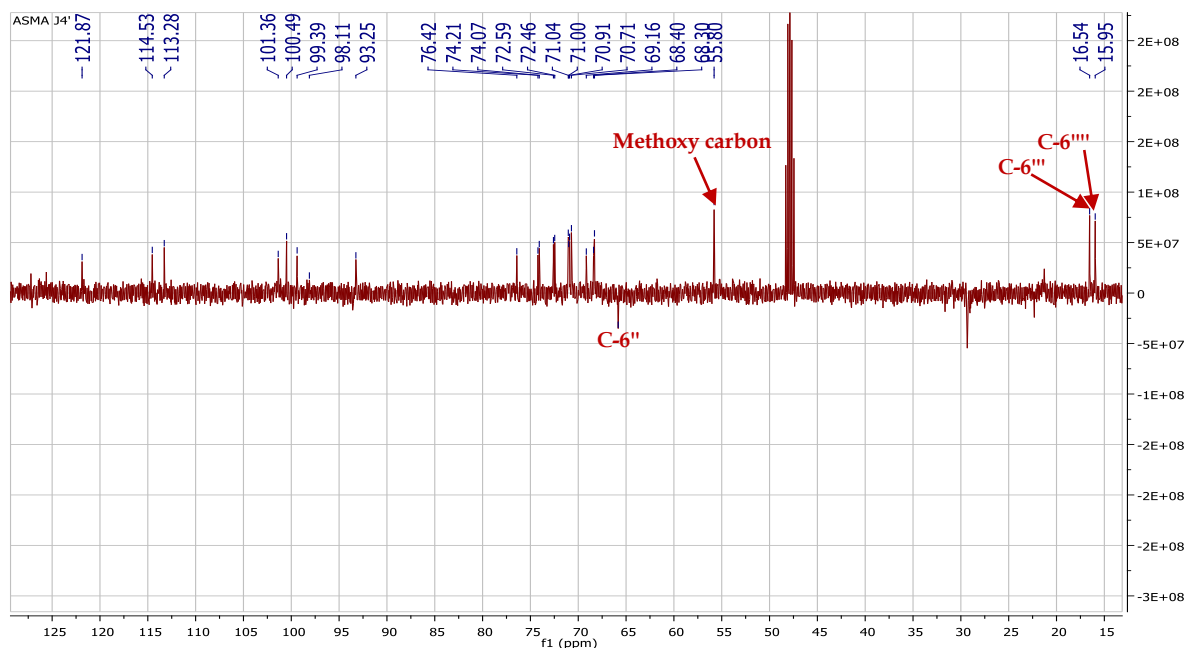
Figure. IV. 109: DEPT 135 spectrum (400 MHz, CD₃OD) of compound **J4**.
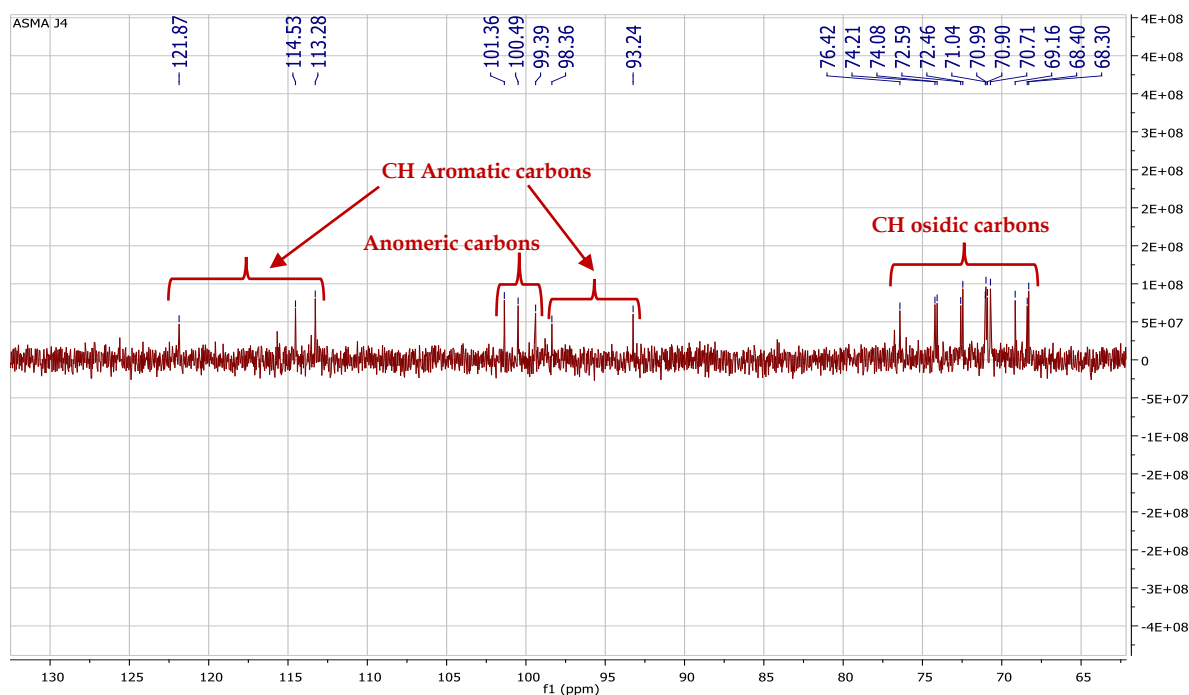
Figure. IV. 110: DEPT 90 spectrum (400 MHz, CD₃OD) of the compound **J4**.

The ^{13}C NMR shifts of the aglycone parts of **J4** corresponded well to the shifts for isorhamnetin-3-O-glycoside as the compound **J2**.

The ^{1}H and ^{13}C NMR spectrum showed that **J4** had two L-rhamnose and D-galactose in its structure, the significant difference being up-field shift of 4.0 ppm for C-2' and 5.3 ppm for C-6' of D-galactose [212].

COSY spectrum shows a correlation spot between the two aromatic protons at 6.09 ppm (d, J= 2.0 Hz, 1H) and 6.29 ppm (d, J= 2.0 Hz, 1H) corresponding to H-6 and H-8 respectively of aromatic ring A. This spectrum also shows a correlation spot between the three aromatic protons of aromatic ring B (**Figure. IV. 111**).
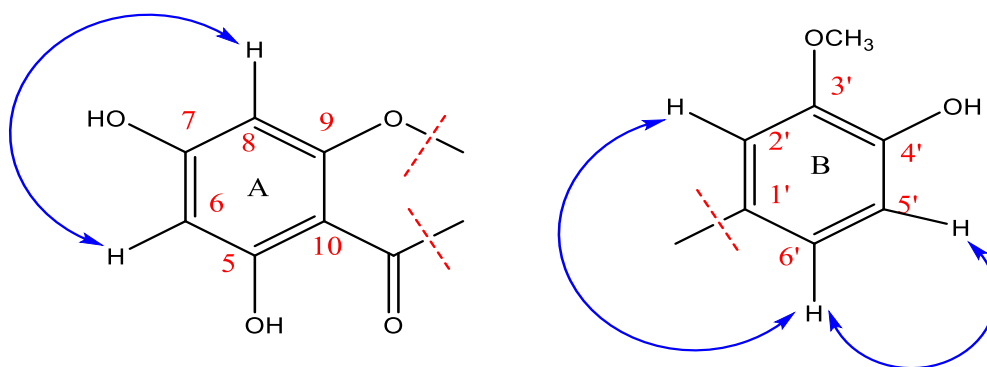
Figure. IV. 111: COSY correlations of aromatic ring A and B of the compound **J4**.

According to the protons already identified using ^{1}H NMR spectrum, the chemical shifts of their corresponding carbons were assigned using HSQC experiment (**Figure. IV. 112**) as follows: C-6 (δ_C 98.36), C-8 (δ_C 93.24), C-2' (δ_C 113.28), C-5' (δ_C 114.53) and C-6' (δ_C 121.87).
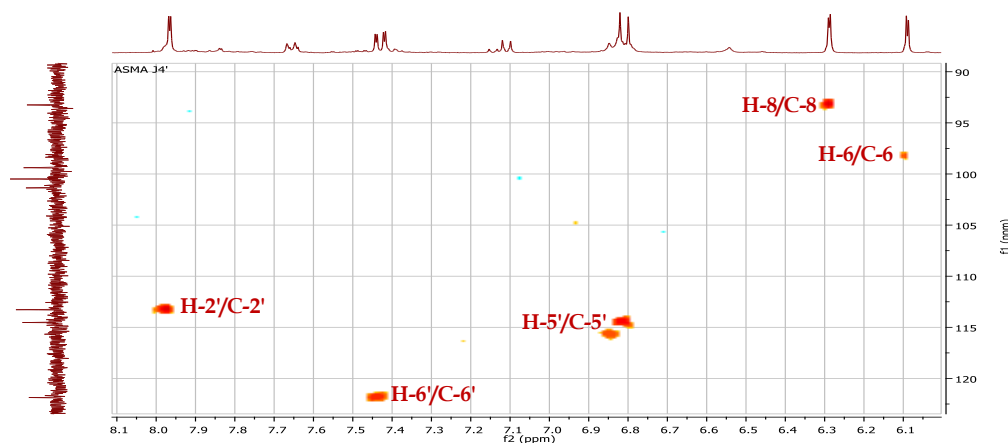
Figure. IV. 112: HSQC spectrum (400 MHz, CD$_3$OD) of aromatic region of compound **J4**.

The analysis of COSY spectrum (**Figure. IV. 115**), makes it possible to identify a spin system with seven protons from the anomeric proton H-1" (δ_H 5.69) to H-6" (3.41 and 3.64) of the galactose: H-1" with H-2" ($\delta_{H2"}$ 3.86)/ H-2" with H-3" ($\delta_{H3"}$

3.57)/ H-3″ with H-4″ ($\delta_{H4″}$ 3.69)/ H-4″ with H-5″ ($\delta_{H5″}$ 3.62) and H-5″ with H-6″a and H-6″b ($\delta_{H6″}$ 3.41 and 3.64) (**Figure. IV. 113**).
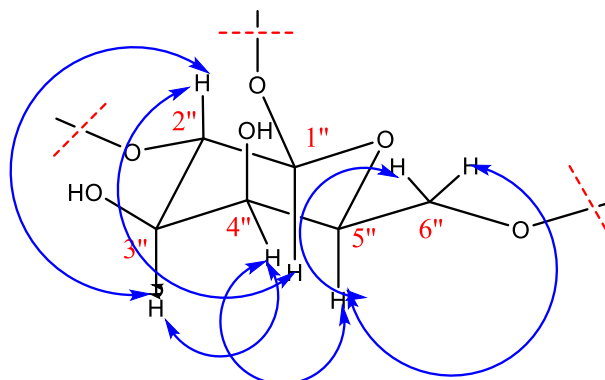
Figure. IV. 113: COSY correlations of galactose protons of the compound **J4**.

COSY spectrum also, makes it possible to identify a spin system with eight protons from the anomeric proton H-1‴ (δ_H 5.06) to H-6‴ (δ_H 0.78) of rhamnose 1 and from the anomeric proton H-1⁗ (δ_H 4.46) to H-6⁗ (δ_H 1.07) of rhamnose 2 (**Figure. IV. 114**) as follows:

- ❖ H-1‴ with H-2‴ ($\delta_{H2‴}$ 3.89).
- ❖ H-2‴ with H-3‴ ($\delta_{H3‴}$ 3.65).
- ❖ H-3‴ with H-4‴ ($\delta_{H4‴}$ 3.21).
- ❖ H-4‴ with H-5‴ ($\delta_{H5‴}$ 3.93).
- ❖ H-5‴ with H-6‴ ($\delta_{H6‴}$ 0.78).
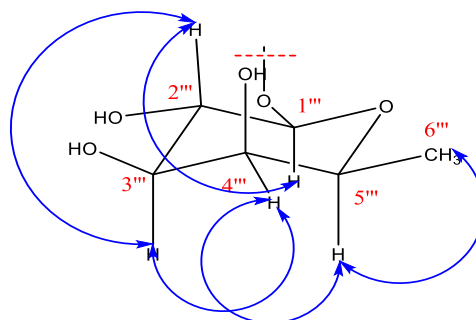
- ❖ H-1⁗ with H-2⁗ ($\delta_{H2⁗}$ 3.47).
- ❖ H-2⁗ with H-3⁗ ($\delta_{H3⁗}$ 3.42).
- ❖ H-3⁗ with H-4⁗ ($\delta_{H4⁗}$ 3.17).
- ❖ H-4⁗ with H-5⁗ ($\delta_{H5⁗}$ 3.43).
- ❖ H-5⁗ with H-6⁗ ($\delta_{H6⁗}$ 1.07).
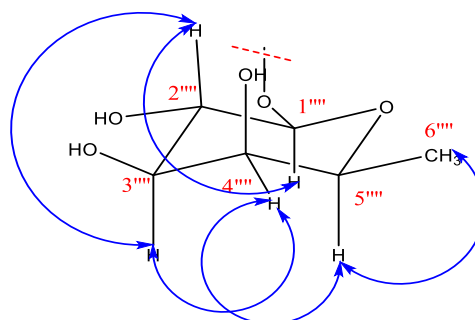
**Figure. IV. 114:** COSY correlations of two rhamnose protons of the compound **J4**.
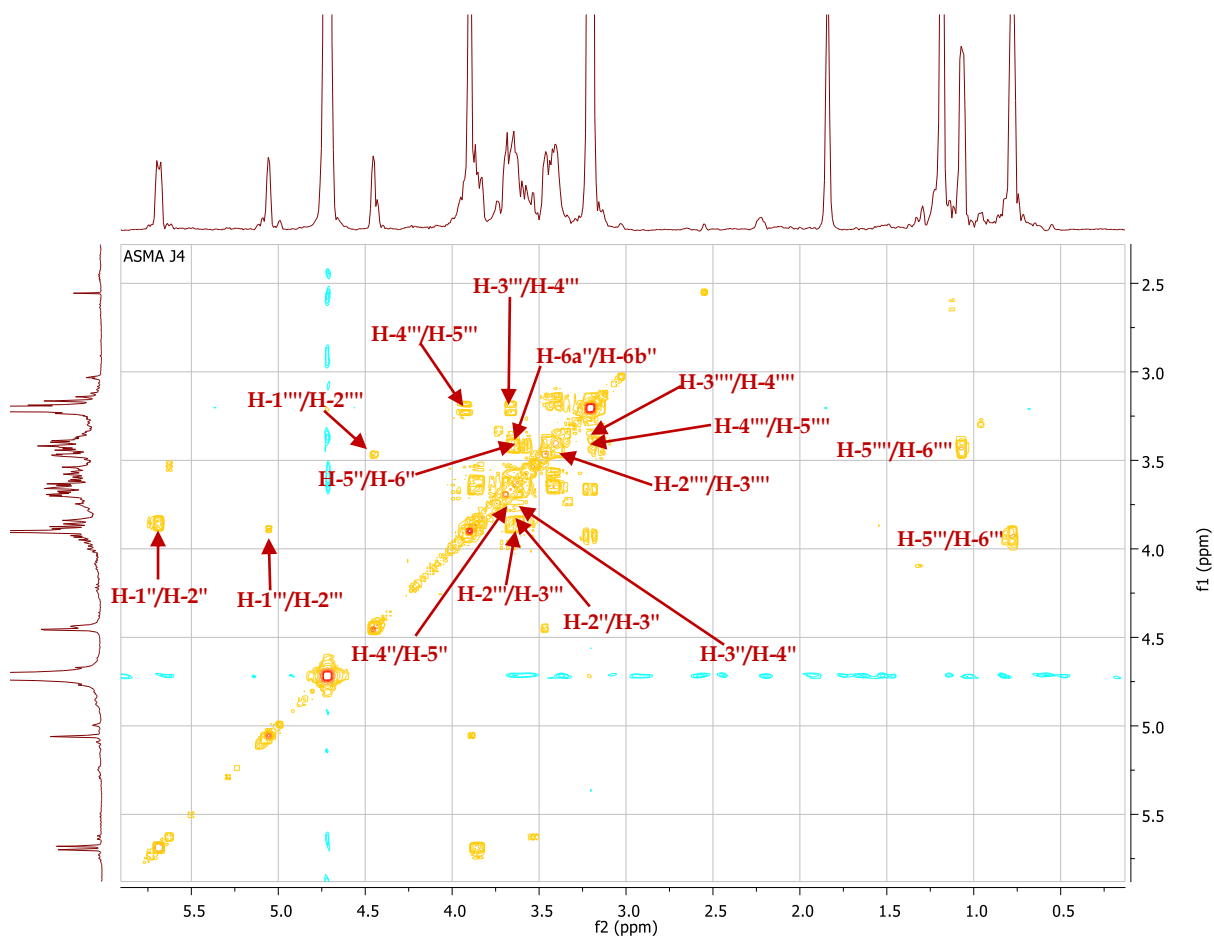
Figure. IV. 115: COSY spectrum (400 MHz, CD$_3$OD) of osidic protons of the compound **J4**.

The analysis of HSQC spectrum (**Figure. IV. 116** and **Figure. IV. 117**), make it possible to correlates the identified protons, which confirmed their correlations by COSY spectrum, of β-D-galactose and the two α-L-rhamnose units with their corresponding carbons that distributed as follows:

➢ β-D-galactose: C-1" ($\delta_{C1"}$ 99.39)/ C-2" ($\delta_{C2"}$ 76.42)/ C-3" ($\delta_{C3"}$ 74.08)/ C-4" ($\delta_{C4"}$ 69.16)/ C-5" ($\delta_{C5"}$ 74.21) and C-6" ($\delta_{C6"}$ 65.82).

➢ α-L-rhamnose 1: C-1"' ($\delta_{C1"'}$ 101.36)/ C-2"' ($\delta_{C2"'}$ 71.04)/ C-3"' ($\delta_{C3"'}$ 71.00)/ C-4"' ($\delta_{C4"'}$ 72.46)/ C-5"' ($\delta_{C5"'}$ 68.40) and C-6"' ($\delta_{C6"'}$ 15.95).

> ➤ α-L-rhamnose 2: C-1'''' ($\delta_{C1''''}$ 100.49)/ C-2'''' ($\delta_{C2''''}$ 70.71)/ C-3'''' ($\delta_{C3''''}$ 70.91)/ C-4'''' ($\delta_{C4''''}$ 72.59)/ C-5'''' ($\delta_{C5''''}$ 68.30) and C-6'''' ($\delta_{C6''''}$ 16.54).
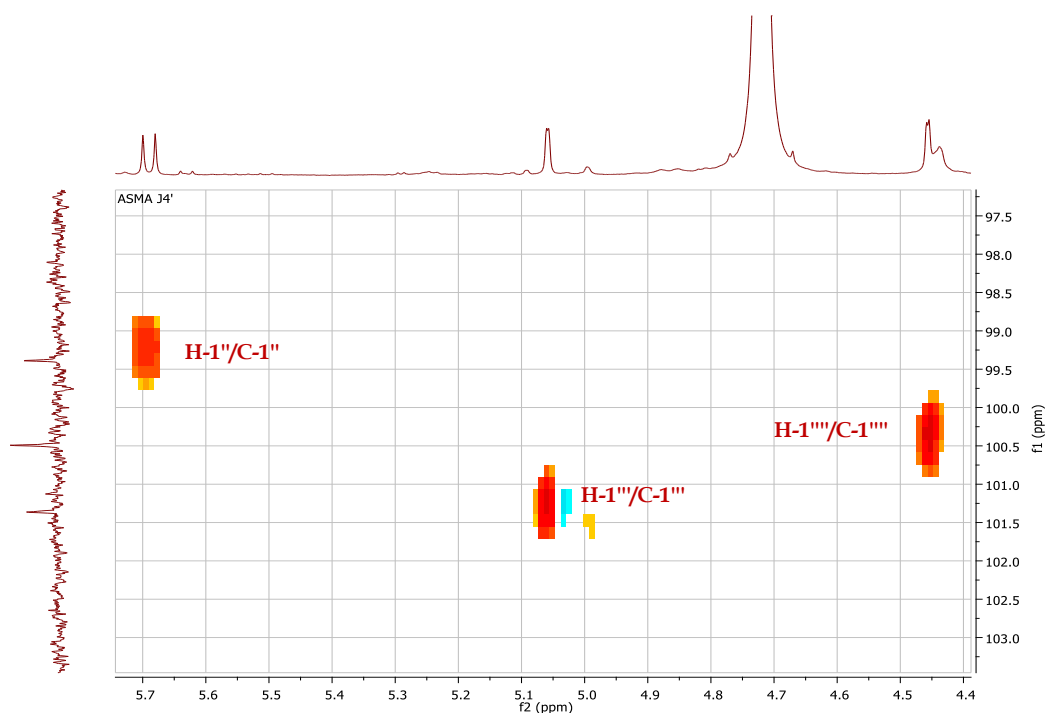
Figure. IV. 116: HSQC spectrum (400 MHz, CD$_3$OD) of anomeric parts of the compound **J4**.
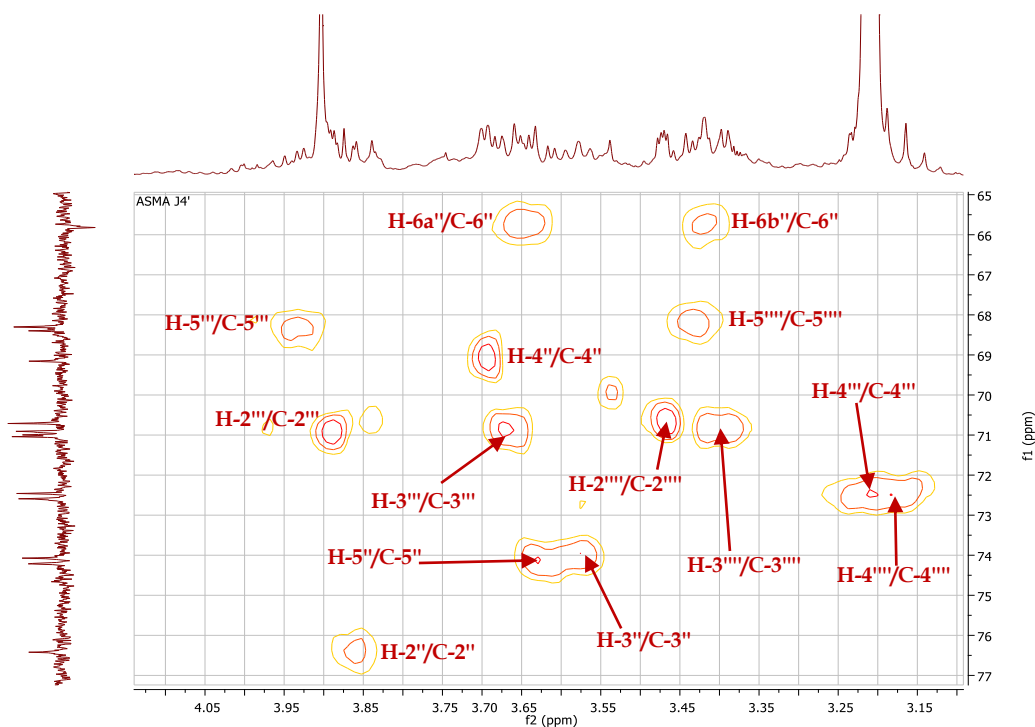
Figure. IV. 117: HSQC spectrum (400 MHz, CD$_3$OD) of osidic parts of the compound **J4**.

The downfield shift of 10.4 ppm of C-2 signal and an up-field shift 2.64 of ppm of C-3 signal in ^{13}C NMR spectrum (**Table. IV. 10**), in comparison to isorhamnetin (δ_{C2} 146.6 and δ_{C3} 135.6) indicated that **J4** is **isorhamnetin-3-O-glycosilated** [212, 213]. By comparing ^{13}C chemical shifts of **J4** with those of the compound **J2** and with those of galactose at C-3, the downfield shift of 6.20 ppm of C-2" and of 6.00 ppm of C-6" of the galactose, indicate that the C-2" and C-6" is the glycosylation sites [212, 215]. Depending on these findings the attachment of the three sugar units are α-L-rhamnose C-1'"→C-2" β-D-galactose and α-L-rhamnose C-1""→C-6" β-D-galactose (**Figure. IV. 118**) [212, 215].
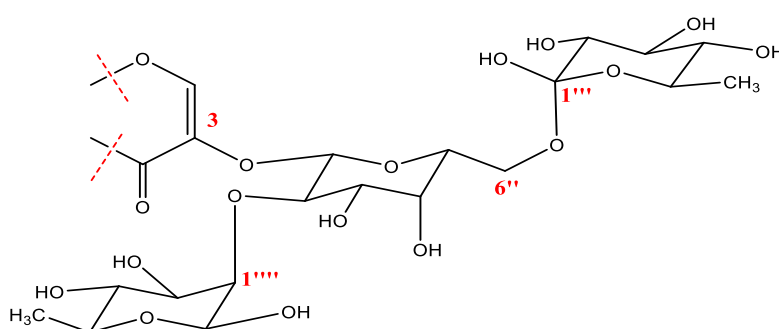
Figure. IV. 118: The attachment of osidic part at C-3 of compound **J4**.

All the data are in total agreement with Isorhamnetin 3-O-(2,6-di- O-α - rhamnopyranosyl -β- galactopyranoside) (**Figure. IV. 119**), which previously isolated from species *Lysimachia fortune* (Primulaceae) [215]. This flavonoid is isolated for the first time from *Atractylis* genus.
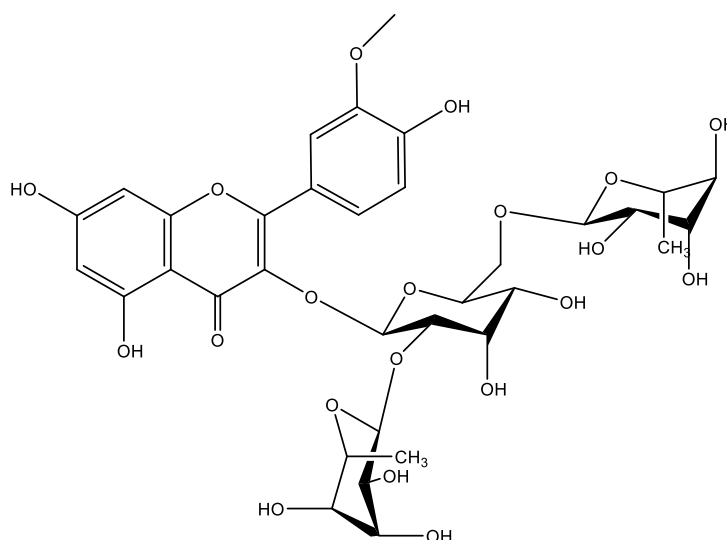
Figure. IV. 119: Structure of compound **J4**; Isorhamnetin 3-O-(2",6"-di-O-α - rhamnopyranosyl-β-galactopyranoside).

The ^{1}H and ^{13}C NMR data, are summarized in the **Table. IV. 10**, which are in total agreement with the literature [215].

Table. IV. 10: Chemical shifts ^{1}H NMR (400 MHz) and ^{13}C NMR (100 MHz) of compound **J4** (δ_C in ppm and δ_H in ppm and J in Hz).

Position	Carbon	Proton
1	-O-	--
2	157.00	--
3	132.96	--
4	178.76	--
5	161.78	--
6	98.36	6.09 (d, J = 2.0 Hz, 1H)
7	164	--
8	93.24	6.29 (d, J = 2.0 Hz, 1H)
9	157.00	--
10	104.50	--
1'	121.57	--
2'	113.28	7.97 (d, J = 2.0 Hz, 1H)
3'	147.07	--
3'-OCH₃	55.80	3.90 (s, 3H)
4'	149.19	--
5'	114.53	6.81 (d, J = 8.5 Hz, 1H)
6'	121.87	7.43 (dd, J = 8.5, 2.0 Hz, 1H)
3-O-1''- galactose	99.39	5.69 (d, J = 7.6 Hz, 1H)
2''	76.42	3.86 (m)
3''	74.08	3.57 (m)
4''	69.16	3.69 (dd, J = 7.0, 3.3 Hz, 1H)
5''	74.21	3.62 (brd, J = 3.4 Hz, 1H)
6''	65.82	3.41 (m)
		3.64 (m)
2''-O-1'''-rhamnose	101.36	5.06 (d, J = 1.3 Hz, 1H)
2'''	71.04	3.89 (m)
3'''	71.00	3.65 (m)

4'''	72.46	3.18 (m)
5'''	68.40	3.93 (m)
6'''	15.95	0.78 (d, J = 6.2 Hz, 3H)
6''-O-1'''-rhamnose	100.49	4.46 (d, J = 1.4 Hz, 1H)
2''''	70.71	3.47 (m)
3''''	70.91	3.42 (m)
4''''	72.59	3.17 (m)
5''''	68.30	3.43 (m)
6''''	16.54	1.07 (d, J = 6.2 Hz, 3H)

IV.4. 9. Compound R1

Compound **R1** is isolated in the form of a white powder soluble in methanol. It is characterized on TLC test by invisible spot under UV (254 and 366 nm) lamp which turns pink by revelation using acid solution and heating.

The mass spectrum of compound **R1** (**Figure. IV. 120**) obtained in negative mode by ESI-MS soft ionization, shows a pseudo-molecular ion peak at m/z 1381.6 [M-H]⁻, i.e., a molecular mass of 1382.6 corresponding to a molecular formula $C_{64}H_{102}O_{32}$.
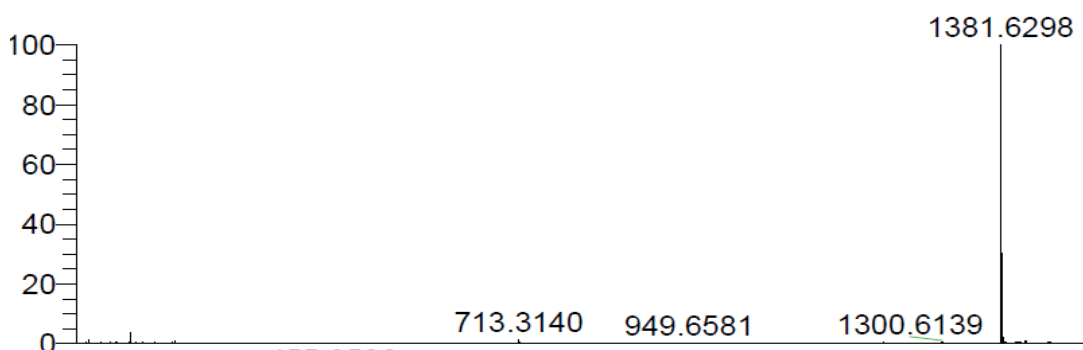
Figure. IV. 120: ESI-MS mass spectrum of the compound **R1**, recorded in negative mode.

The ^{1}H NMR spectrum (**Figure. IV. 121**) recorded in CD_3OD, displays seven methyl groups resonating between 0.6 and 1.3 ppm as singlet form with integrating of three protons (S, 3H) for each, we distinguish the characteristic signals of a triterpene skeleton.
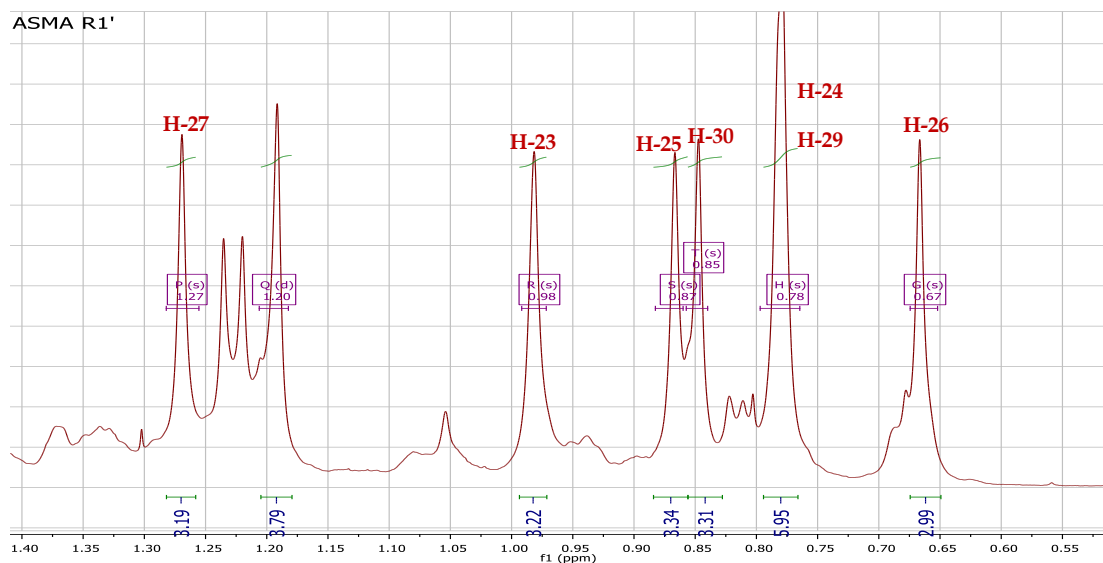
Figure. IV. 121: ^{1}H NMR spectrum (400 MHz, CD$_3$OD) of methyl groups of the compound **R1**.

The ^{1}H NMR spectrum (**Figure. IV. 122**) reveals other signals resonating between 1.00 and 2.30 ppm, corresponding to protons CH and CH$_2$ groups of a triterpene skeleton, other characteristic signals are present in this spectrum:

❖ One olefinic proton at δ_H 5.23 (t, J = 3.5 Hz, 1H), assigned to H-12 of the triterpene pentacyclic.

❖ Two oxygenated methine protons the first at δ_H 3.10 (dd, J=12.4, 3.8 Hz, 1H) assigned to H-3 and second at δ_H 4.36 (t, J = 3.4 Hz).

❖ A signal in the form of a double doublet at δ_H 2.87 (dd, J = 14.3, 4.1 Hz, 1H) corresponding to H-18, its multiplicity indicates the presence of two adjacent protons and the coupling constant assigned the β orientation of H-18.

❖ Six anomeric protons at δ_H 4.36 (d, J = 7.5 Hz, 1H), δ_H 4.43 (d, J = 7.8 Hz, 1H), δ_H 4.46 (d, J = 7.7 Hz, 2H), δ_H 5.20 (d, J = 1.6 Hz, 1H) and δ_H 5.33 (d, J = 6.3 Hz, 1H) and the osidic protons resonating between 3.10 and 3.9 ppm.

❖ The signals at δ_H 1.23 (d, J = 6.1 Hz, 3H) and δ_H 5.20 (d, J = 1.6 Hz, 1H) assigned to H-6 and H-1 of rhamnose, respectively [19].
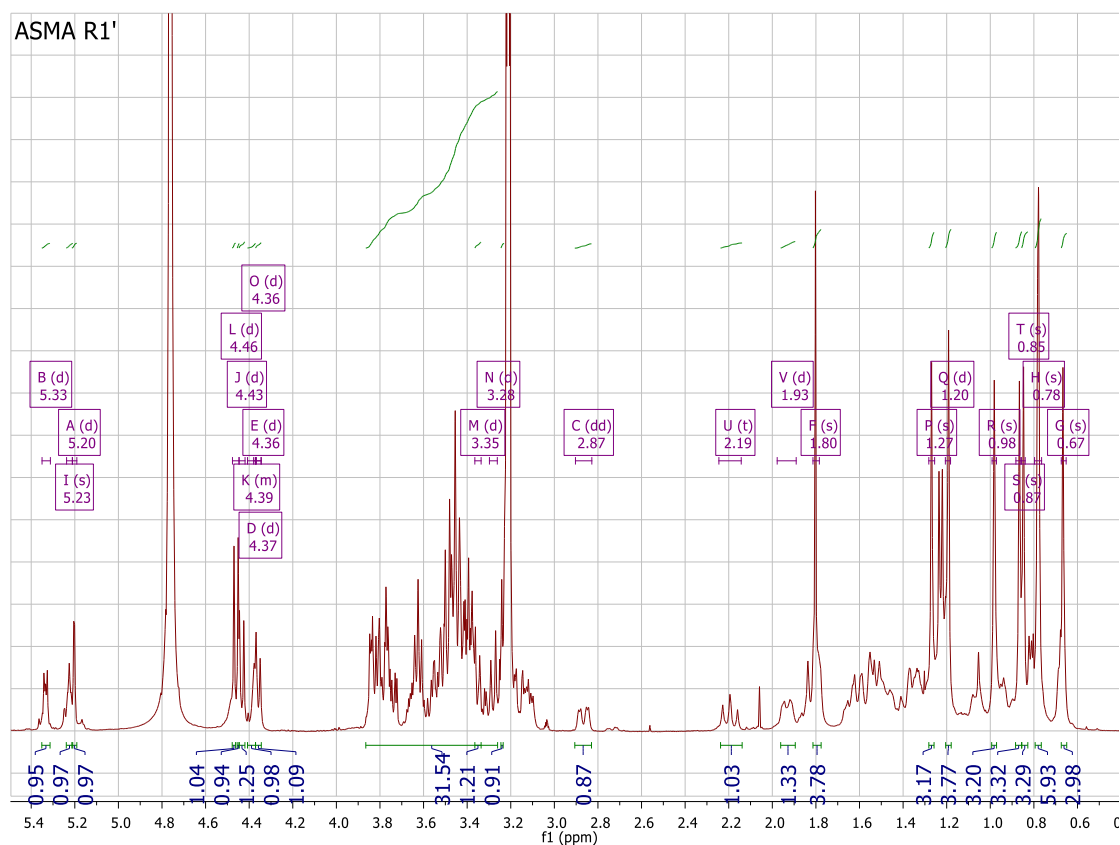
Figure. IV. 122: ^{1}H NMR spectrum (400 MHz, CD$_3$OD) of the compound **R1**.

The COSY spectrum (**Figure. IV. 123**) shows a correlation spot between H-3 (δ_H 3.10) already identified and two protons at δ_H 1.92 and 1.58, corresponding to H-2a and H-2b, respectively. Which also correlates with two protons at δ_H 0.91 and 1.51 attributable to H-1b and H-1a, respectively.

The olefinic proton H-12 at δ_H 5.23 (t, J = 3.5 Hz, 1H) showed a correlation spot in the COSY spectrum (**Figure. IV. 123**) with a proton resonating at δ_H 1.79 (brs, 2H), corresponding to H$_2$-11. This last was also correlated with a proton at δ_H 1.52, which determined that it is H-9.

Two correlation spots observed between H-18 at δ_H 2.87 (dd, J = 14.3, 4.1 Hz, 1H) and two protons that resonating at δ_H 0.94 and 2.19, corresponding to the two adjacent protons H-19b and H-19a, respectively (**Figure. IV. 124**).
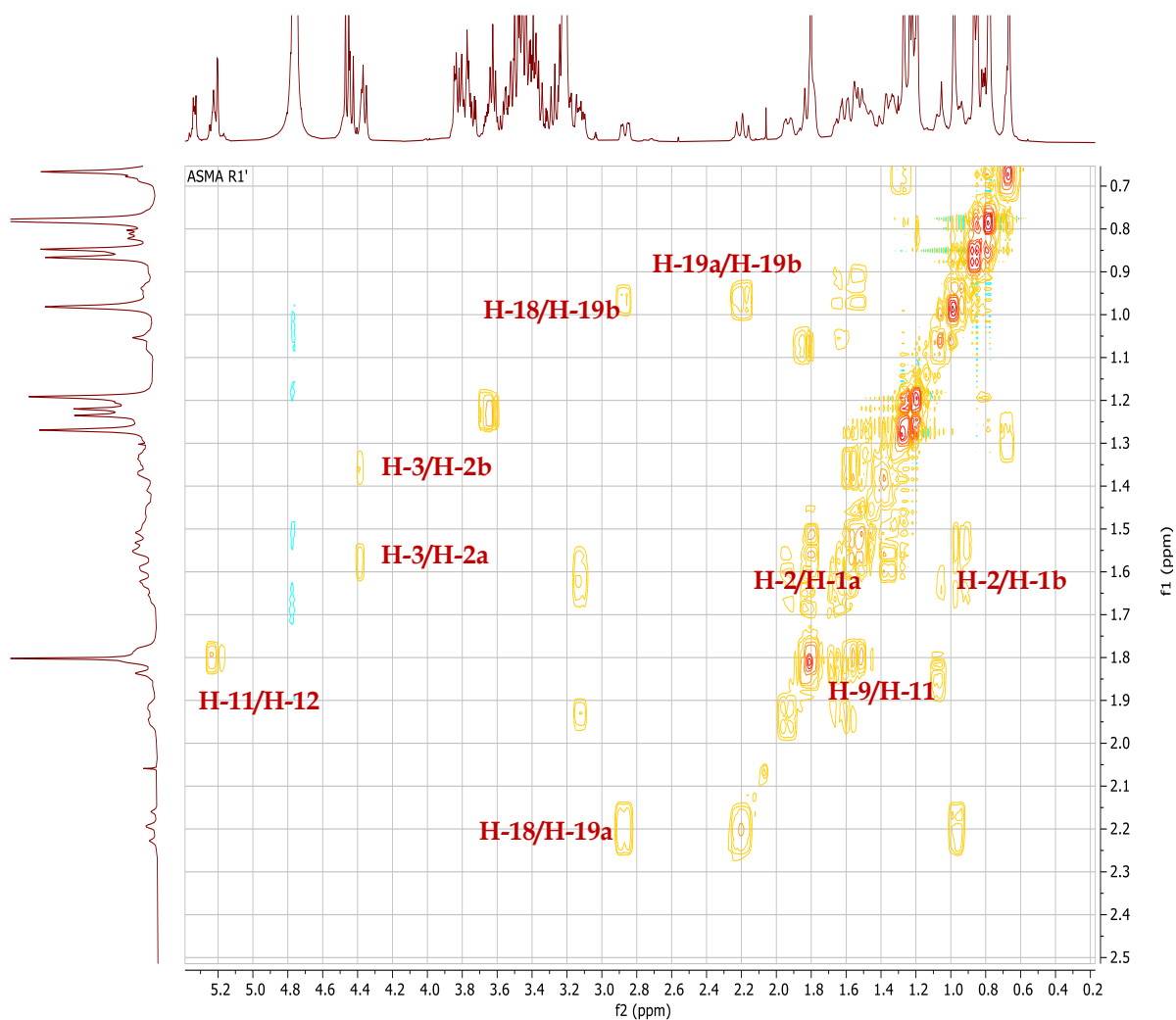
Figure. IV. 123: COSY spectrum (400 MHz, CD₃OD) of the aglycon protons of the compound **R1**.
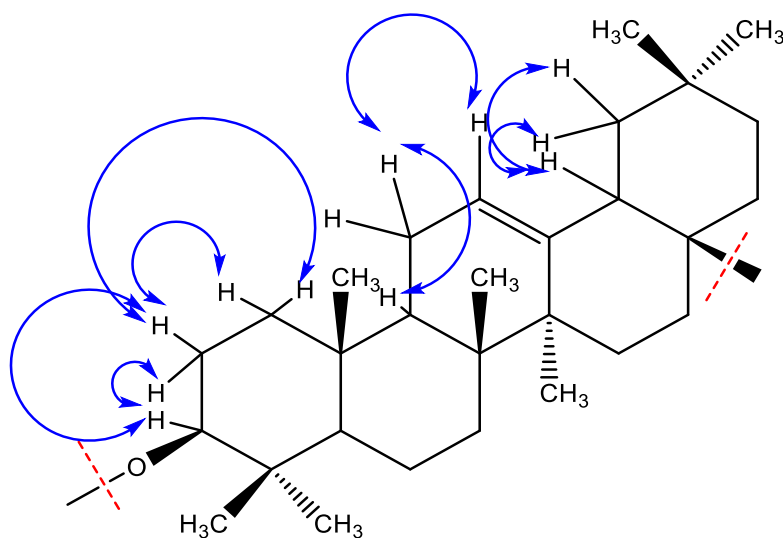
Figure. IV. 124: COSY correlations of the compound **R1**.

The ^{13}C NMR (**Figure. IV. 125**) and DEPT135 (**Figure. IV. 126**) spectra revealed 64 signals, of which 30 were assigned to the aglycone moiety (triterpene pentacyclic) and 34 to a sugar units made up of six sugar units comprising two pentoses and four hexoses. These signals were distributed as follows:

❖ Carbon signals resonating between δ_C 18 and 55.80, attributable to CH, CH_2, CH_3 and quaternary carbons (C).

❖ Seven carbon signals of methyl groups resonating between 14 and 32 ppm.

❖ Two olefinic carbons at δ_C 122.7 and 143.23, were characteristic to an olean-12-ene skeleton.

❖ Two oxygenated carbons at δ_C 74.02, attributable to a free hydroxy group and at δ_C 89.59 corresponding to C-3. The deshielding effect observed in this position compared to the same carbon with hydroxyl group indicated that C-3 is linked to sugar moiety.

❖ Carbonyl group observed at δ_C 175.65.

❖ The spectrum also shows six anomeric carbons at δ_C 94.04, 99.83, 103.73, 103.93, 104.64 and 105.33.

❖ Signals of osidic carbons resonating between 60 and 86.73 ppm, corresponding to CH and CH_2 of sugar units.
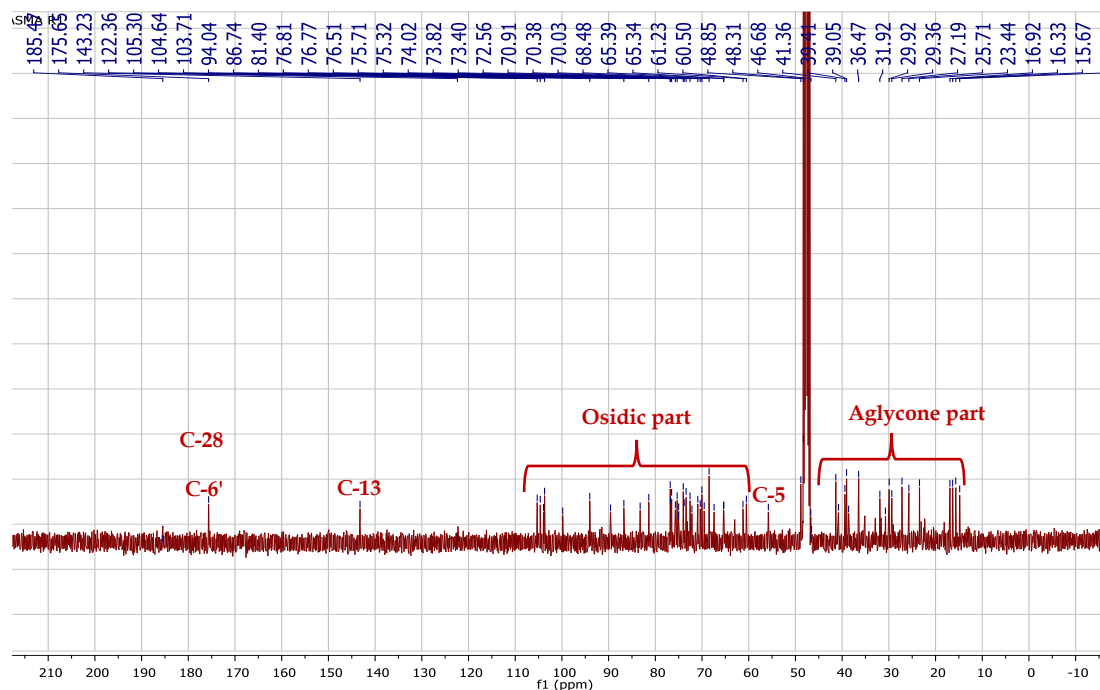
Figure. IV. 125: ^{13}C NMR spectrum (100 MHz, CD_3OD) of the compound **R1**.
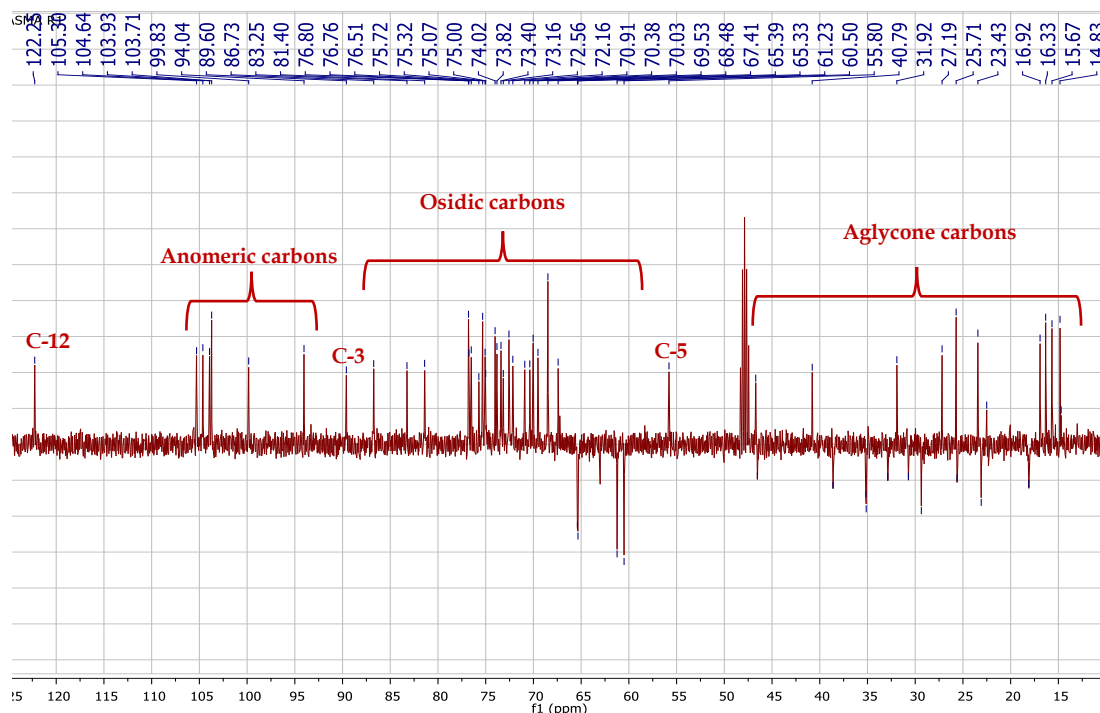
Figure. IV. 126: DEPT 135 spectrum (100 MHz, CD$_3$OD) of the compound **R1**.

According to ^{13}C and ^{1}H NMR spectral data, that indicated the presence of triterpenoid saponin with oleanane skeleton. Contains aglycon moiety of **3-hydroxyolean-12-en** (**Figure. IV. 130**) and six osidic units. The structural elucidation of compound **R1**, was made using the analysis of 2D NMR spectra COSY, HMBC, HSQC and TOCSY.

The corresponding carbons of the protons mentioned previously were attributed with the help of HSQC experiment (**Figure. IV. 127**), C-1 (δ_C 38.61), C-2 (δ_C 25.62), C-11 (δ_C 23.08), C-9 (δ_C 46.71), C-18 (δ_C 40.49), C-19 (46.53). The ^{13}C NMR resonances of C-18 and C-28 (δ_C 40.79 and 175.65, respectively) were in agreement with a β orientation of H-18.

HSQC spectrum (**Figure. IV. 127**) also, makes it possible to assign the seven carbons of CH$_3$ groups resonating at δ_C 14.83, 15.67, 16.33, 23.43, 25.71, 27.19 and 31.92, corresponding to C-25, C-24, C-26, C-30, C-27, C-23, and C-29, respectively.
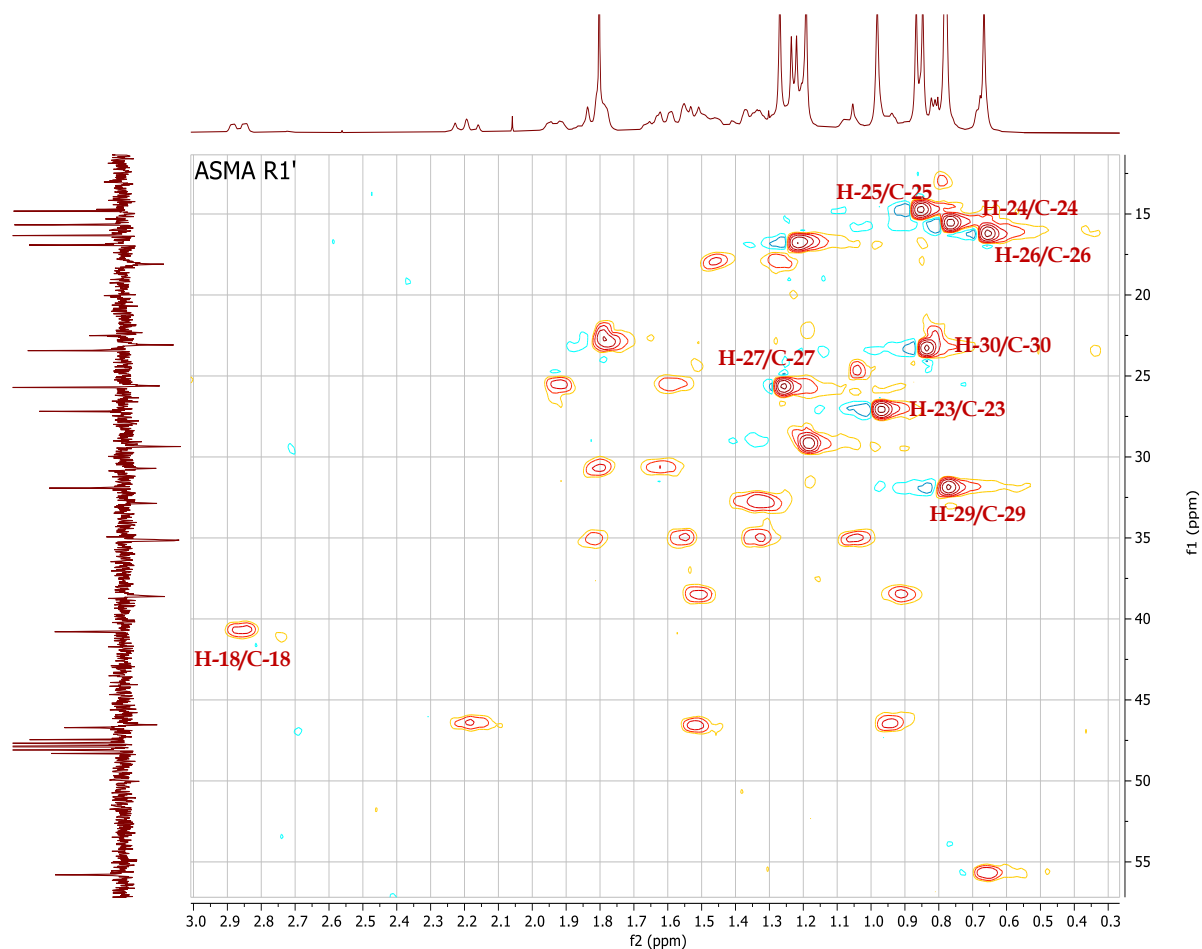
Figure. IV. 127: HSQC spectrum (400 MHz, CD$_3$OD) of the compound **R1**.

The assignment of most aglycone carbons, were done using the long-range correlations observed in the HMBC spectrum (**Figure. IV. 128**) from the methyl protons signals (CH$_3$-23, CH$_3$-24, CH$_3$-25, CH$_3$-26, CH$_3$-27, CH$_3$-29 and CH$_3$-30), the oxygenated carbon at δ_H 3.10 and the olefinic proton at δ_H 5.23 (**Figure. IV. 129**), the HMBC correlations were distributed as follows:

- ❖ Correlation spots observed between the protons at δ_H 0.98 CH$_3$-23 and four carbons resonating at δ_C 89.59, 15.67, corresponding to the carbons already identified C-3 and C-24 respectively, and at δ_C 39.05 and 55.80 ppm attributable to C-4 and C-5 of **R1**.

- ❖ The protons of CH$_3$-24 resonating at δ_H 0.78 shows correlation spots with four carbons that previously identified: C-3 (δ_C 89.59), C-4 (δ_C 39.05), C-5 (δ_C 55.80) and C-23 (δ_C 27.19).

- ❖ Four correlations observed between H$_3$-25 at δ_H 0.87 and C-1 (δ_C 38.49) C-5 (δ_C 55.80), C-9 (δ_C 47.71), already identified and δ_C 36.47 attributable to C-10.

- ❖ Three correlations observed between H_3-26 δ_H 0.67 and δ_C 46.71, which assigned to C-9 and two carbons at δ_C 32.87 and 39.41, attributable to C-7 and C-8, respectively.

- ❖ Three correlations observed between H_3-27 δ_H 1.27 and C-13 δ_C 143.23, and two correlation spots at δ_C 41.36 and 35.14, attributable to C-14 and C-15, respectively.

- ❖ The protons H_3-29 and H_3-30 resonating at δ_H 0.78 and 0.85, respectively. Also, three carbons resonating at δ_C 46.53, 29.92 and 35.15 corresponding to C-19, C-20 and C-21, respectively.
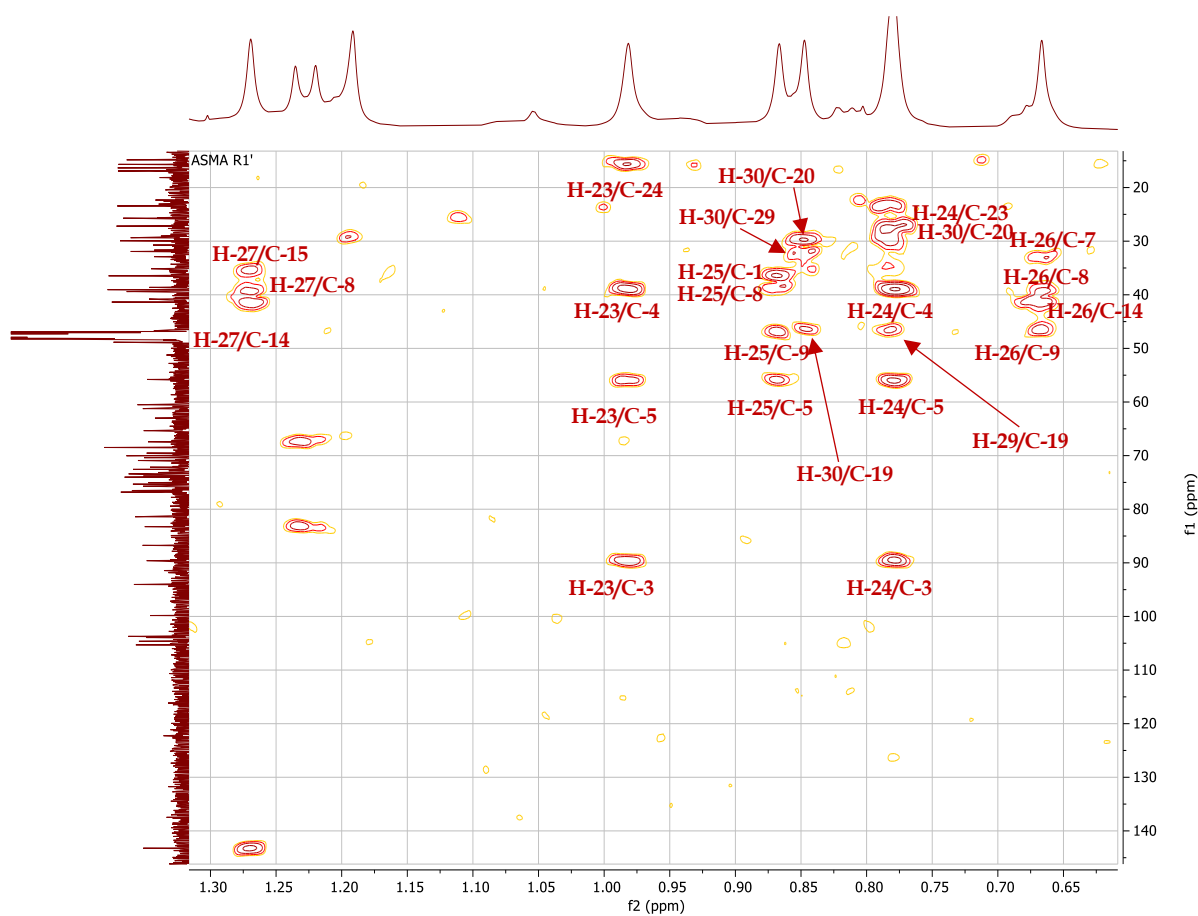
Figure. IV. 128: HMBC spectrum (400 MHz, CD$_3$OD) reveals the correlations of the methyl groups of the compound **R1**.
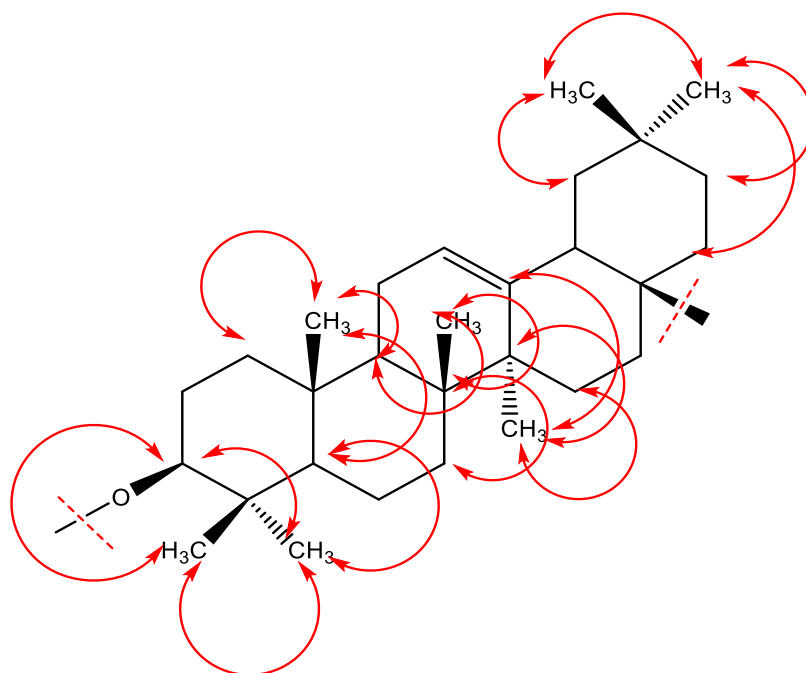
Figure. IV. 129: HMBC correlation of methyl groups of aglycon moiety of compound **R1**.

Based on all the mentioned data of analysis of all spectra of the compound **R1**,

the aglycone moiety of this compound is identified as oleanolic acid (**Figure. IV. 130**)
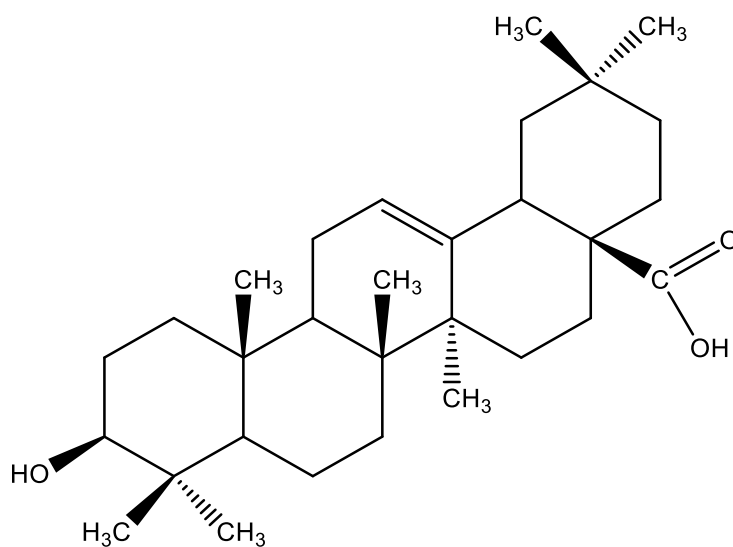
Figure. IV. 130: Structure of oleanolic acid.

The corresponding protons of the identified carbons was assigned using HSQC experiment (**Figure. IV. 131** and **Figure. IV. 132**):

C-5/ δ_H 0.67; C-7/ δ_H 1.34; C-9/ δ_H 1.52; C-15/ δ_H 1.34 and 1.57; C-21/ δ_H 1.14 and 1.92 and C-22/ δ_H 1.62 and 1.81.
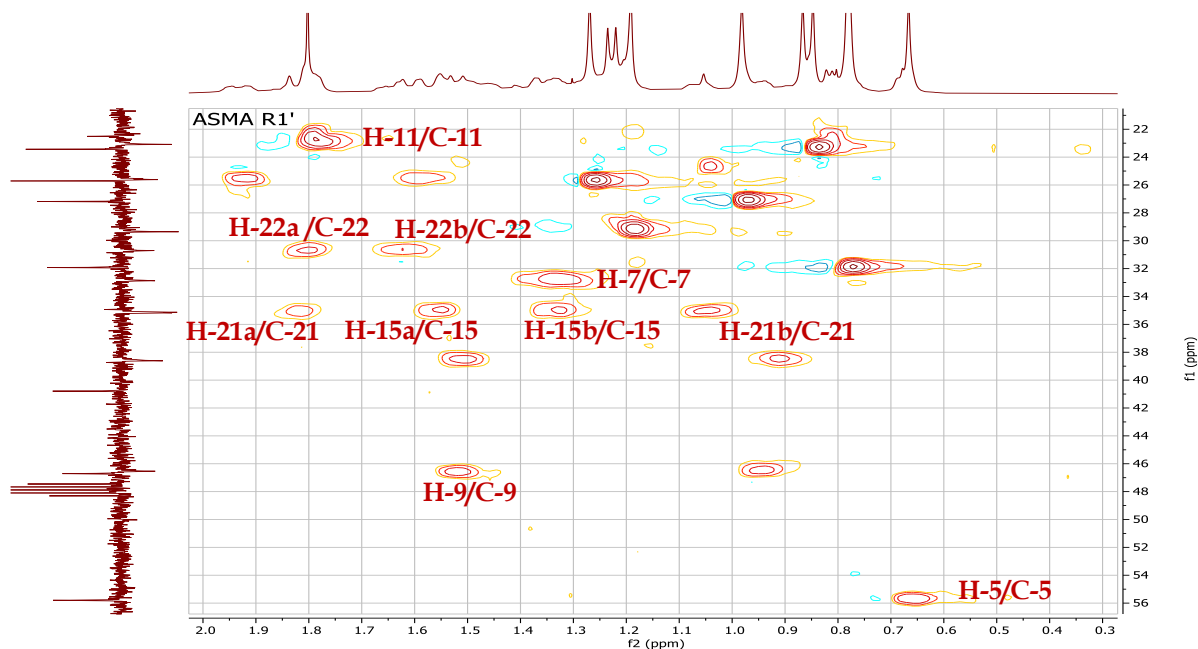
Figure. IV. 131: HSQC spectrum (400 MHz, CD$_3$OD) of the aglycon part of **R1**.
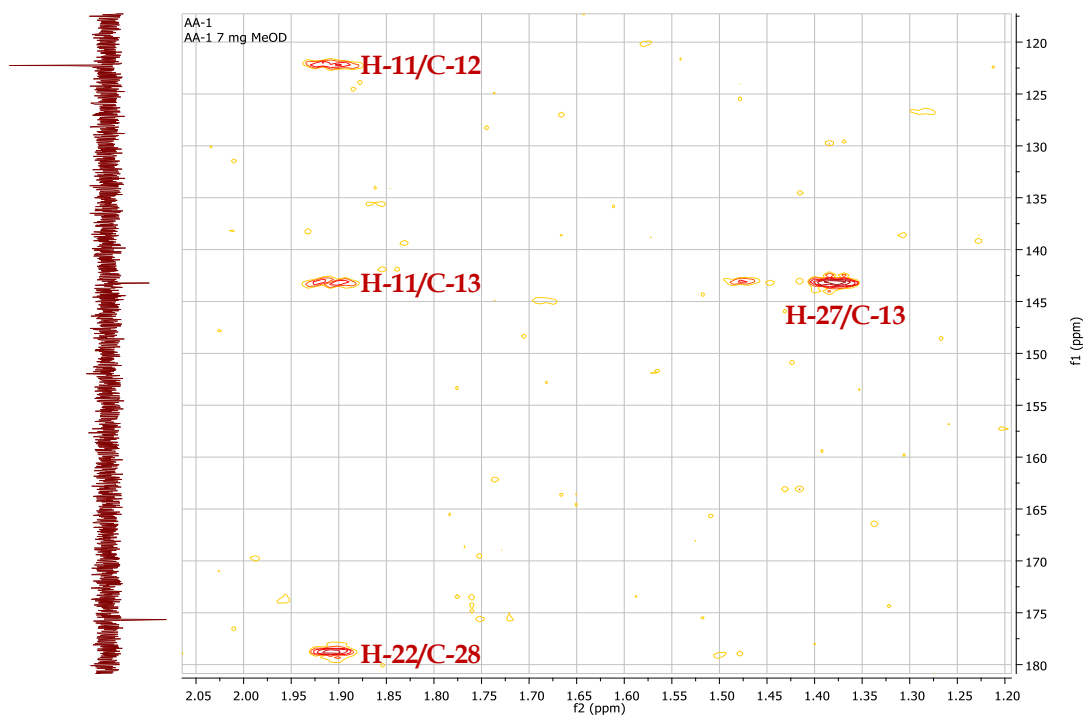
Figure. IV. 132: HMBC spectrum (600 MHz, CD$_3$OD) displays the correlations between H-11, H-22 and H-27 and their adjacent carbons of **R1**.

The rest protons of the aglycon moiety were determined according to their COSY correlations (**Figure. IV. 133** and **Figure. IV. 134**) with the identified protons H-7 and H-15a and H-15b:

- ❖ H-5 and H-7 revealed correlation with two protons resonating at δ_H 1.26 and 1.46, corresponding to H_2-6 and the chemical shit of their carbon was assigned by HSQC experiment δ_C 18.10.
- ❖ H-15a and H-15b show correlation with the oxygenated proton at δ_H 4.36, since all the carbons adjacent of C-15 was quaternary carbons so the correlations with this proton was assigned to H-16, its corresponding carbon in the HSQC spectrum with δ_C 74.02. Indicated that it was correlated with the secondary hydroxyl group of the compound **R1**.
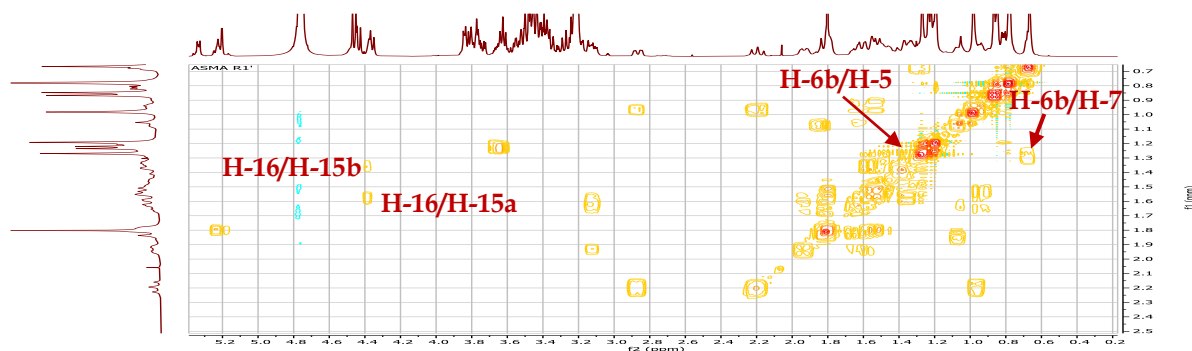
Figure. IV. 133: COSY spectrum of revealed H_2-6 and H-16 correlations of **R1**.
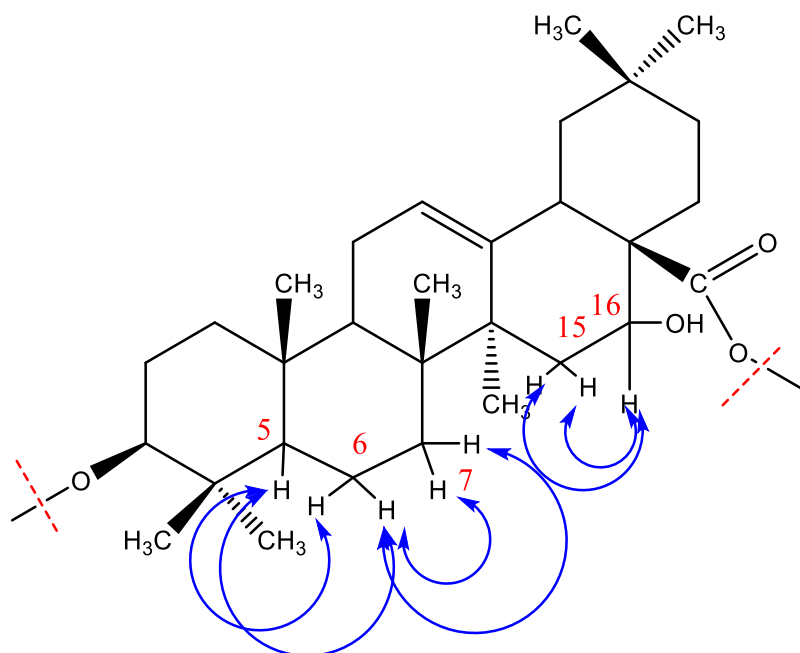
Figure. IV. 134: COSY correlations of H_2-6 and H-16 of compound **R1**.

The aglycone of compound **R1** was a **3-hydroxyolean-12-en-28-oic acid** with a secondary alcoholic function. The correlation observed in COSY spectrum between H-16 δ_H 4.36 (t, J = 3.4 Hz, 1H) and the protons in position 15, were characteristic for 16-α-hydroxy oleanolic acid, which called also echinocystic acid [216]. The α orientation of OH-16 in compound R1 was justified by the relatively small value of the coupling constant of H-16 (J = 3.4 Hz) like in echinocystic acid [216]. By the comparison of the ^{13}C NMR data with aglycone part with that of echinocystic acid showed that the signals of C-3 (δ_C 89.59) and C-28 (δ_C 175.65) were significantly shifted indicating a bidesmosidic structure of the compound **R1** (**Figure. IV. 135**) [217, 218].
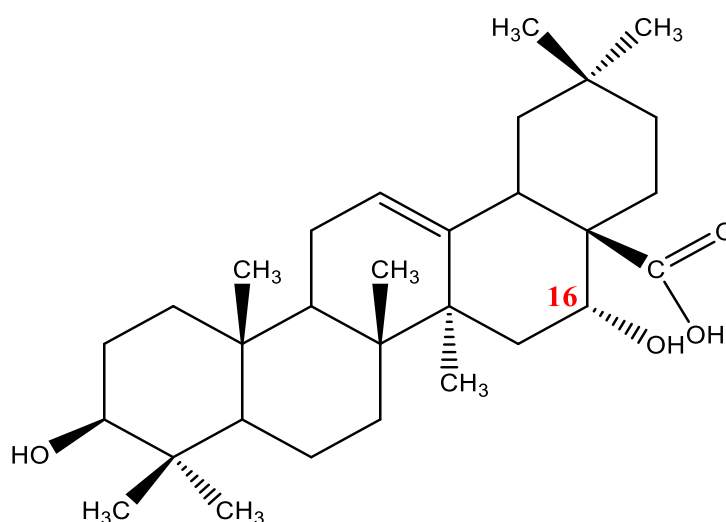
Figure. IV. 135: Structure of **16-α-hydroxy oleanolic acid = echinocystic acid.**

The osidic part

As shown in the ^{1}H NMR spectrum (**Figure. IV. 122**), six anomeric proton signals at δ_H 4.36 (d, J = 7.5 Hz, 1H), δ_H 4.43 (d, J = 7.8 Hz, 1H), δ_H 4.46 (d, J = 7.7 Hz, 2H), δ_H 5.20 (d, J = 1.6 Hz, 1H) and δ_H 5.33 (d, J = 6.3 Hz, 1H) gives correlations in the HSQC spectrum (**Figure. IV. 136**) with their corresponding anomeric carbons at δ_C 103.93, 103.73, 105.33, 104.64, 99.83 and 94.04, respectively, suggesting the occurrence of six sugar units. All the anomeric protons confirm the β configuration, except for anomeric proton at δ_H 5.20 (d, J = 1.6 Hz, 1H) show the α configuration.
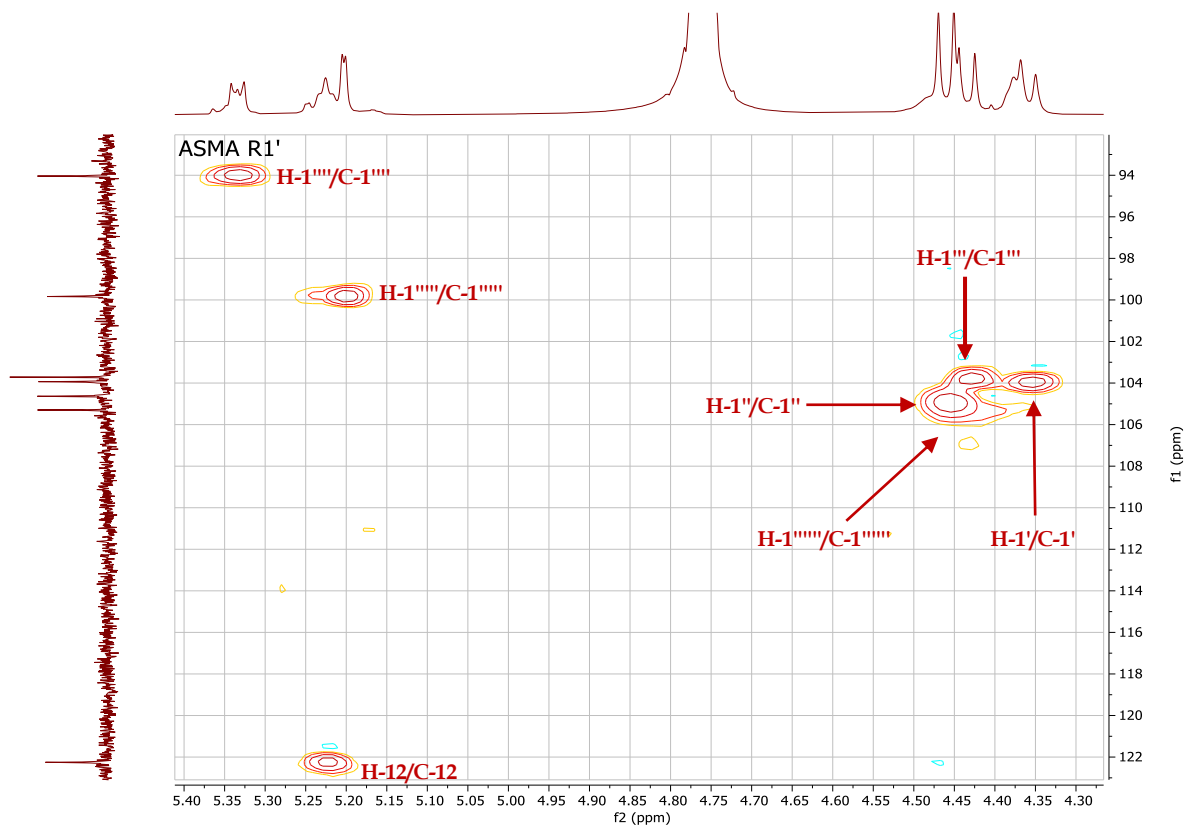
Figure. IV. 136: HSQC spectrum (400 MHz, CD$_3$OD) of anomeric region **R1**.

The protons of the monosaccharide residues were assigned starting from the anomeric protons by means of the COSY, TOCSY, HMBC and HSQC NMR plots.

The analysis of COSY (**Figure. IV. 138**) and TOCSY (**Figure. IV. 139**) spectra, makes it possible to identify spins system of five protons starting from the anomeric proton δ$_H$ 4.36 (d, J = 7.5 Hz, 1H), which show a correlation with an osidic proton resonating at δ$_H$ 3.46 assigned to H-2'. H-3', H-4' and H-5' were determined by assignment of H-H COSY and TOCSY correlations at δ$_H$ 3.40 (m), 3.23 (m) and 3.43 (d, J = 9.7 Hz, 1H), respectively (**Figure. IV. 137**).
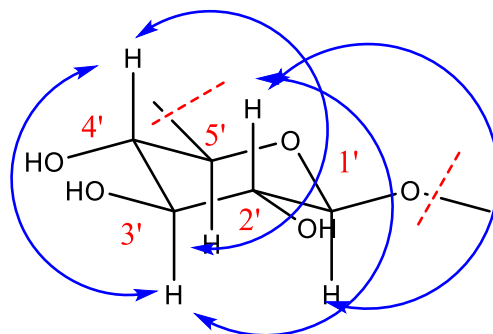
Figure. IV. 137: COSY correlations of first sugar unit of compound **R1**.
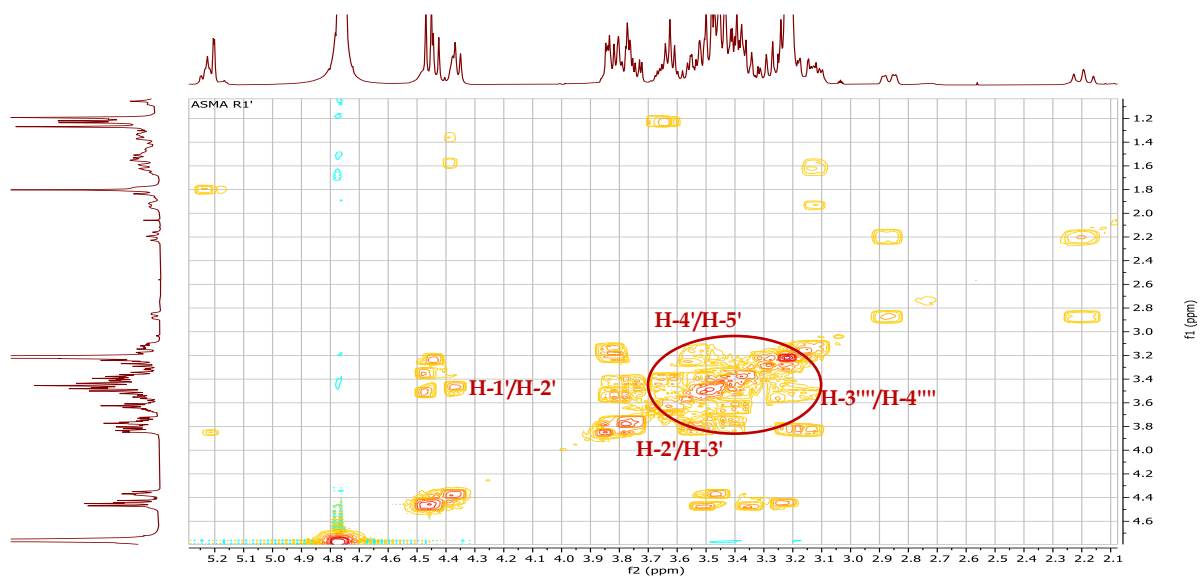
Figure. IV. 138: COSY spectrum (400 MHz, CD$_3$OD) of first sugar unit of compound **R1**.
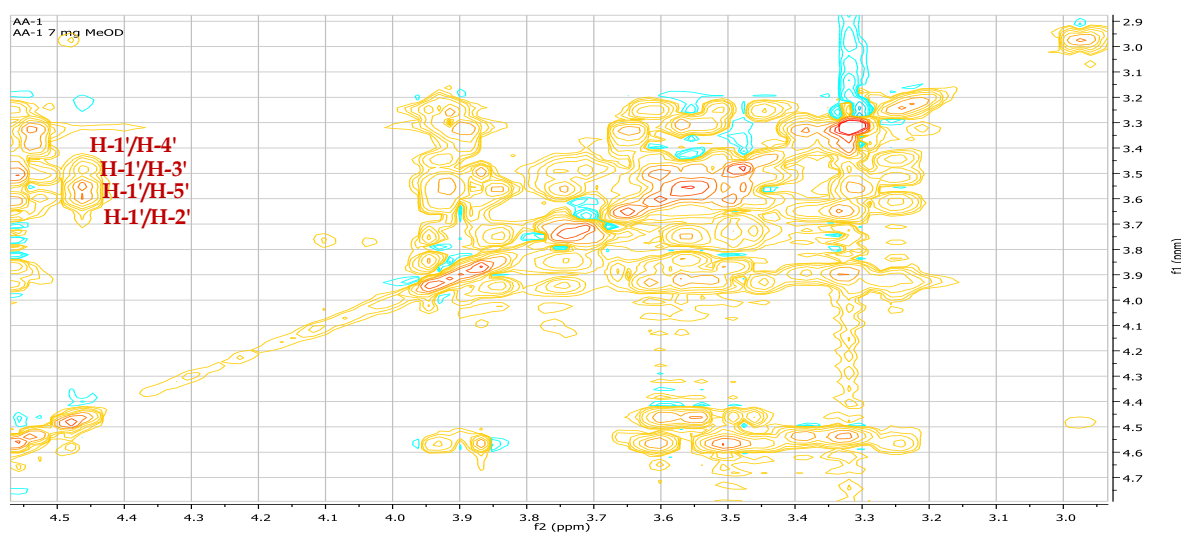
Figure. IV. 139: TOCSY spectrum (600 MHz, CD$_3$OD) of first sugar unit of compound **R1**.

The corresponding carbons assigned based on the HSQC spectrum (**Figure. IV. 140**) as follow:

- ❖ H-2' /C-2' δ$_C$ 81.40.
- ❖ H-3' /C-3' δ$_C$ 86.73.
- ❖ H-4' /C-4' δ$_C$ 73.82.
- ❖ H-5' /C-5' δ$_C$ 75.32.
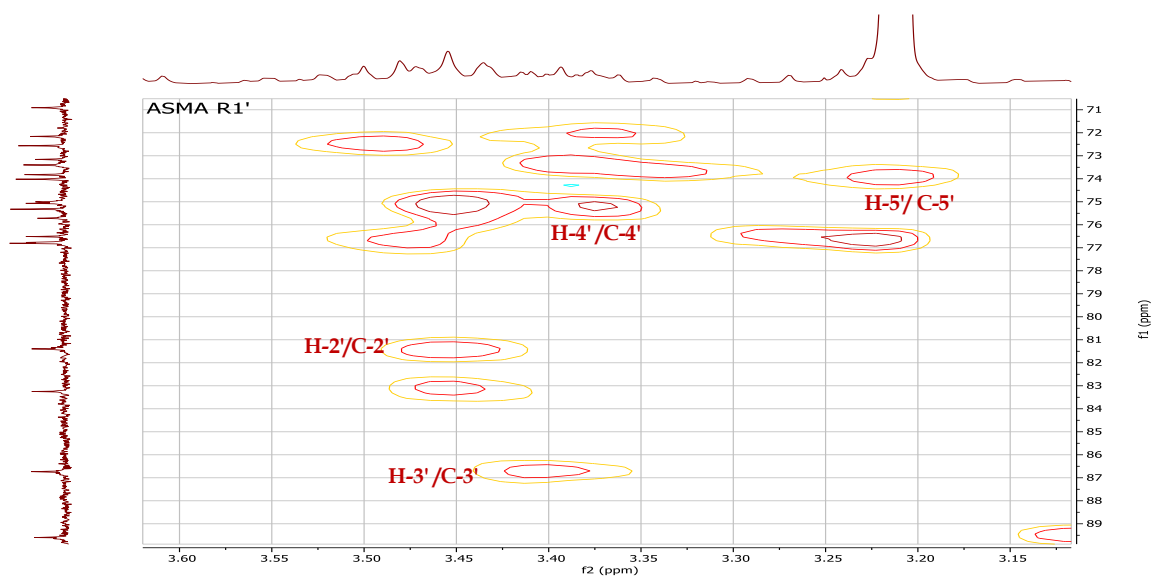
Figure. IV. 140: HSQC spectrum (400 MHz, CD$_3$OD) of first sugar unit of compound **R1**.

The H-5' reveals in HMBC spectrum correlations with the carbonyl group resonating at δ_C 175.65, this last corresponding to C-6' (**Figure. IV. 141** and **Figure. IV. 142**).
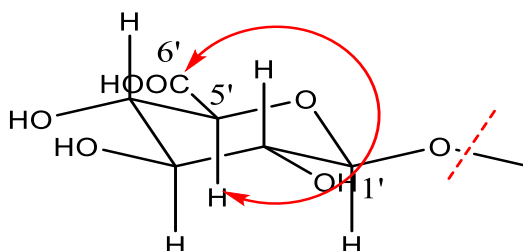
Figure. IV. 141: HMBC correlations of H-5' and C-6' of the compound **R1**.
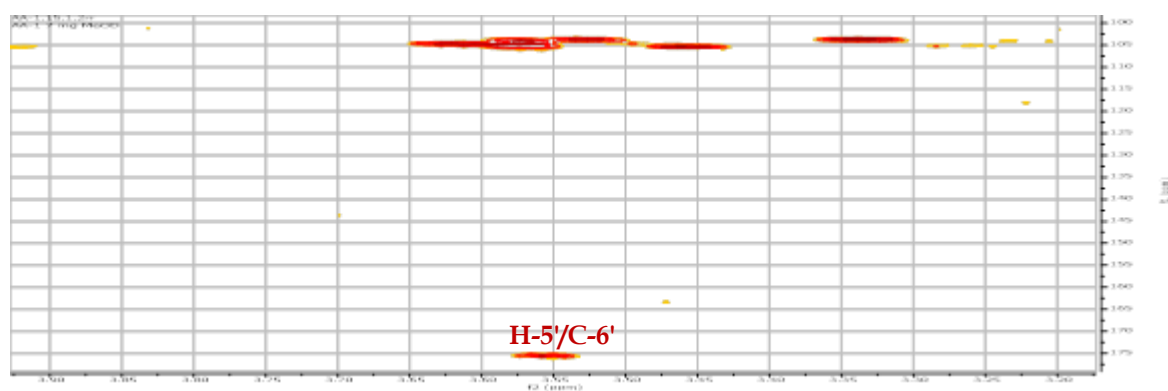
Figure. IV. 142: HMBC spectrum (600 MHz, CD$_3$OD) shows the correlations between H-5' and C-6' of **R1**.

According to the analysis of COSY, TOCSY, HSQC and HMBC spectra, it could be deduced that first sugar was glucuronic acid (**Figure. IV. 143**).
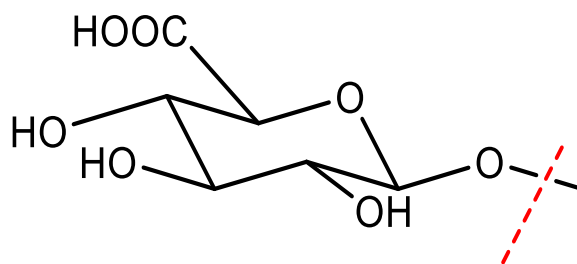
Figure. IV. 143: Structure of Glucoronic acid.

The deshielding effect observed on C-2' and C-3' to 81.40 and 86.74 ppm, respectively, comparing with ^{13}C chemical shifts with those of glucoronic acid, showed glycosylation shift of C-2' by 7.8 ppm and C-3' by 10.64 ppm indicating that the C-2' and C-3' is sites of glycosylation. This confirms by the correlations observed in HMBC spectrum (**Figure. IV. 144**) between H-1" (δ_H 4.46) and C-2' and between H-1''' (δ_H 4.43) and C-3'.
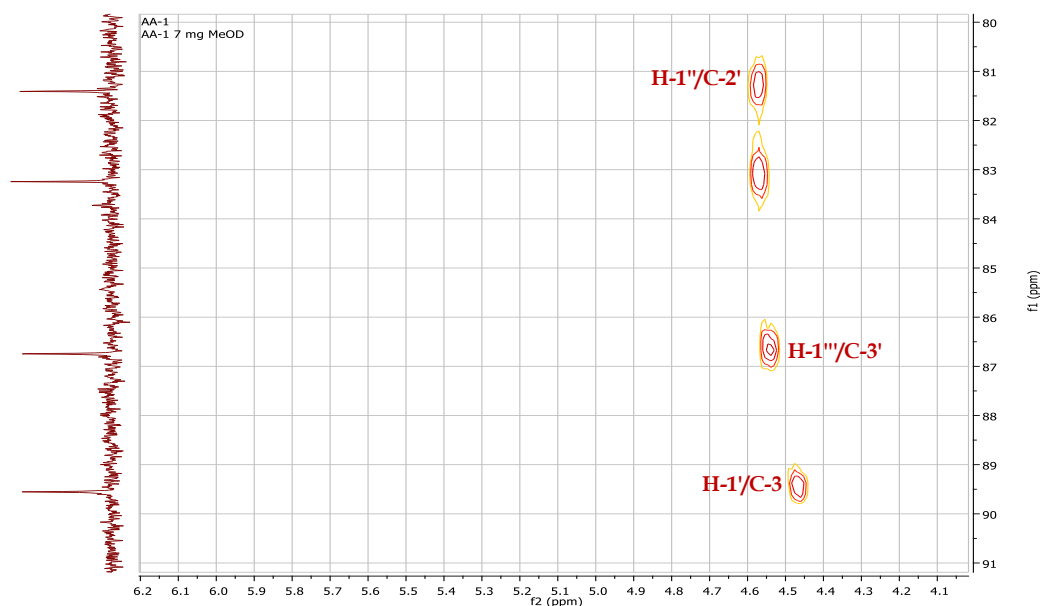
Figure. IV. 144: HMBC spectrum (600 MHz, CD$_3$OD) of anomeric protons of the compound **R1**.

The protons of the monosaccharide residues of these two sugar units were assigned starting from the anomeric protons by means of the COSY, TOCSY, HMBC and HSQC NMR plots.

The analysis of COSY spectrum (**Figure. IV. 146**), makes it possible to identify six spins system of hexose starting from the anomeric proton resonating at δ_H 4.46 (d, J = 7.7 Hz, 1H), which show a correlation with an osidic proton resonating at δ_H 3.52 assigned to H-2". The H-H COSY spectrum show correlations (**Figure. IV. 145**) between:

- ❖ H-2" with H-3" δ_H 3.41.
- ❖ H-3" with H-4" δ_H 3.77.
- ❖ H-4" with H-5" δ_H 3.46.
- ❖ H-5" with H$_2$-6" δ_H 3.61.
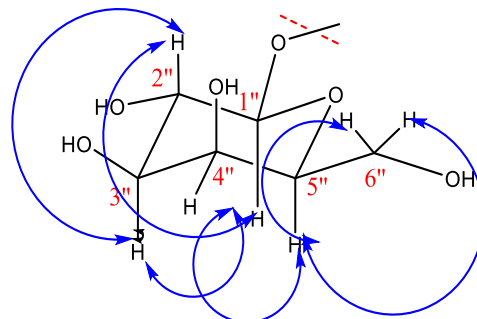
Figure. IV. 145: COSY correlations of the second hexose of compound **R1**.

The protons H-4" detected at δ_H 3.77 (bd, J = 3.5 Hz, 1H), the small coupling constant value of this proton indicated that it is in equatorial position. According to this data the hexose identified as β-D-galactose.
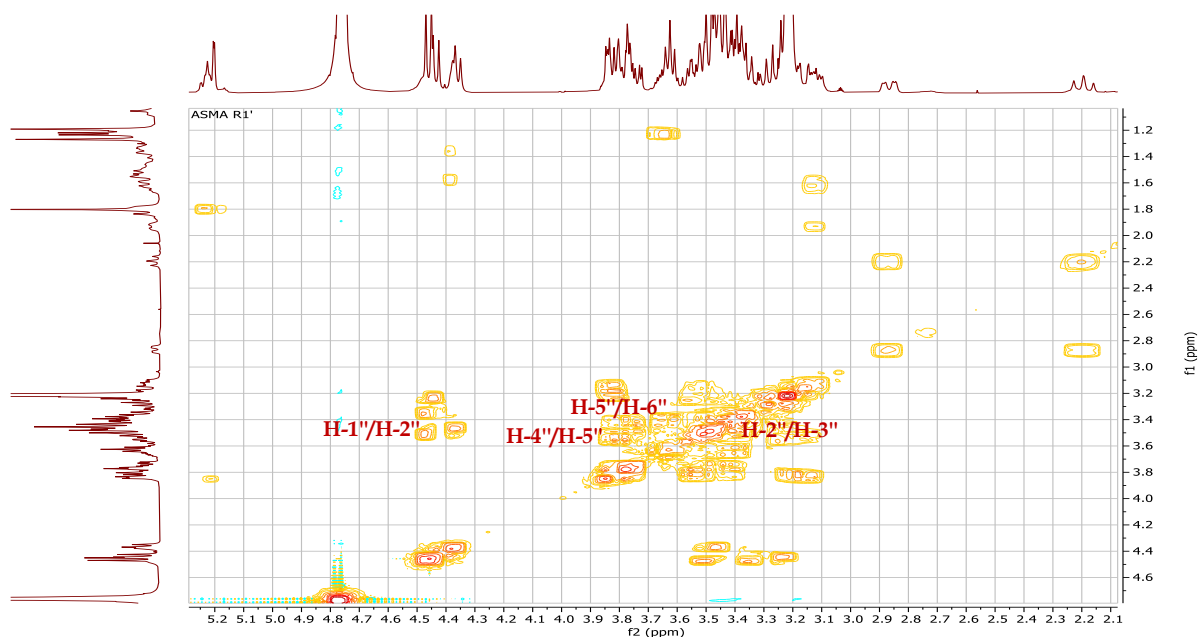
Figure. IV. 146: COSY spectrum (400 MHz, CD$_3$OD) of β-D-galactose of compound **R1**.

The corresponding carbons of the β-D-galactose assigned based on the HSQC spectrum (**Figure. IV. 147**) (H-2" /C-2" δ_C 72.56); (H-3" /C-3" δ_C 73.40); (H-4" /C-4" δ_C 68.40); (H-5" /C-5" δ_C 75.00) and (H$_2$-6"/ C-6" δ_C 60.50).
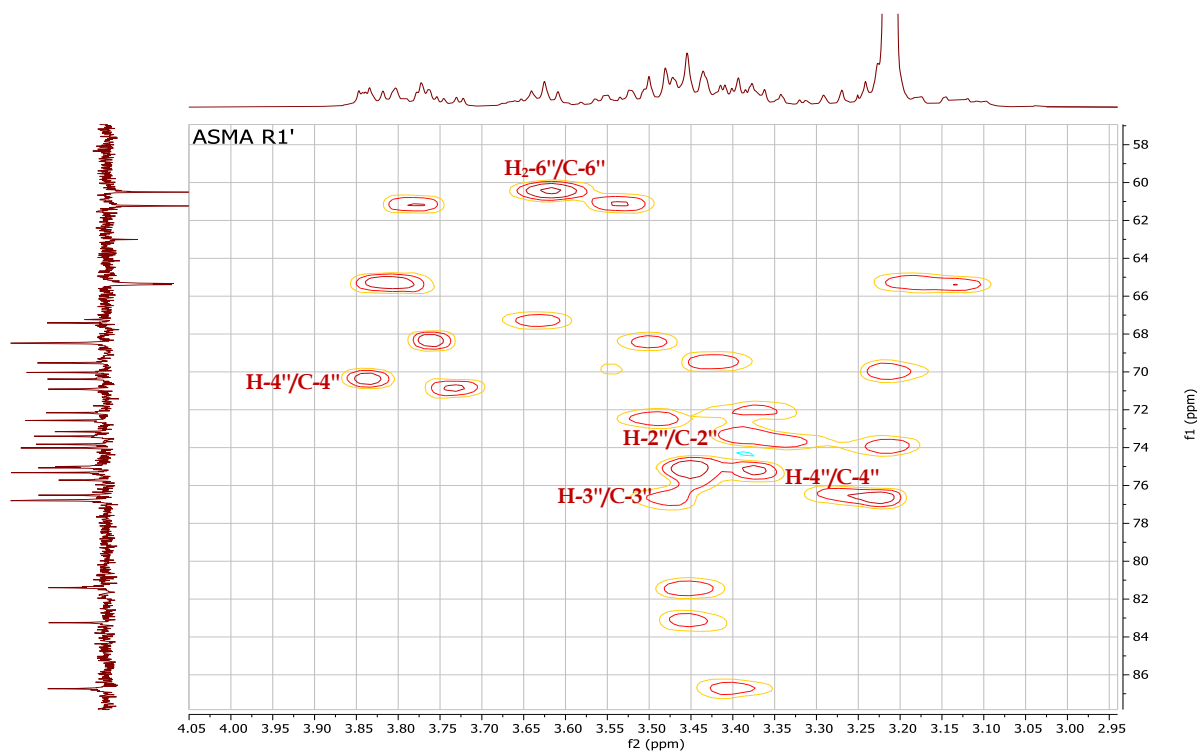
Figure. IV. 147: HSQC spectrum (400 MHz, CD$_3$OD) of galactose of compound **R1**.

The third hexose was identified by the same manner, H-H COSY spectrum (**Figure. IV. 149**) make it possible to determine six spins system of hexose starting from the anomeric proton resonating at δ$_H$ 4.43 (d, J = 7.8 Hz, 1H), show a correlation with an osidic proton resonating at δ$_H$ 3.24 assigned to H-2'''. The H-H COSY spectrum show correlation between H-2''' and H-3''' δ$_H$ 3.38, between H-3''' and H-4''' δ$_H$ 3.51 ppm, the coupling constant of H-4''' (brd, J = 8.8 Hz, 1H) indicated that it is in axial position. This last correlate with H-5''' δ$_H$ 3.40, which show also correlation with two protons of H$_2$-6''' δ$_H$ 3.54 and 3.79 (**Figure. IV. 148**). Based on these results this hexose identified as β-D-glucose.
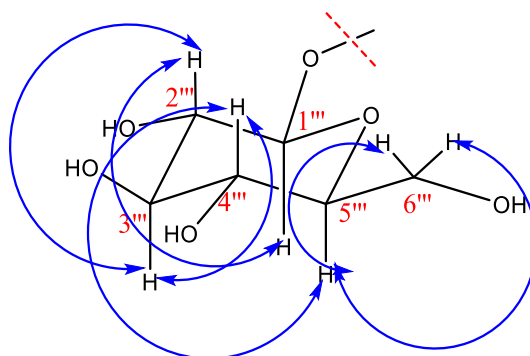
Figure. IV. 148: H-H COSY correlations of β-D-glucose of compound **R1**.
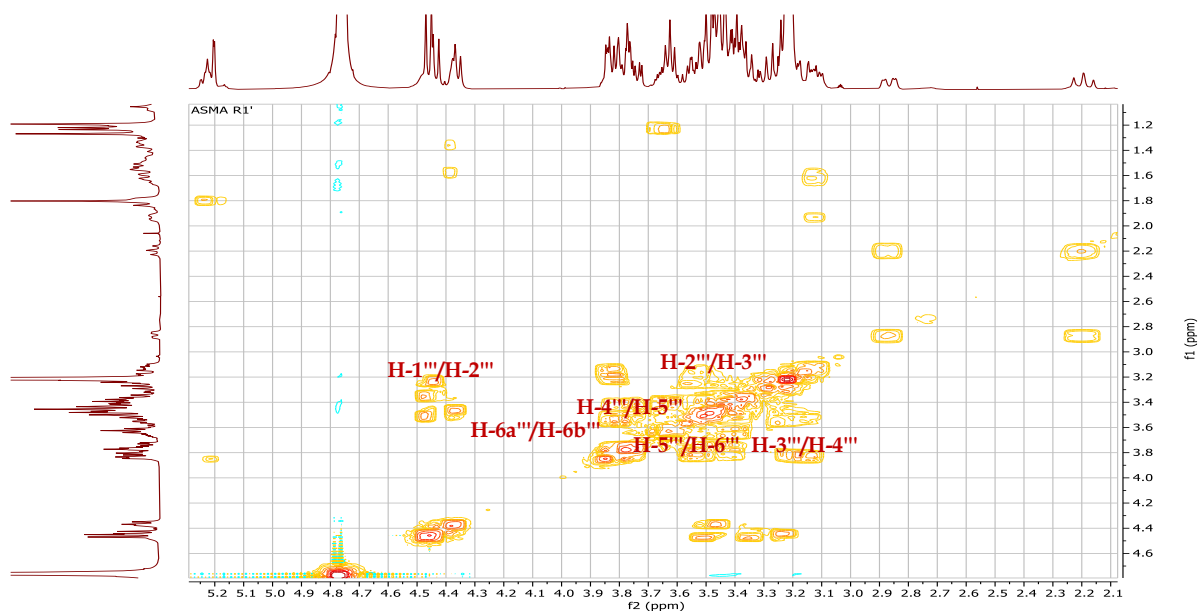
Figure. IV. 149: COSY spectrum (400 MHz, CD₃OD) of β-D-glucose of **R1**.

The corresponding carbons assigned based on the HSQC spectrum (**Figure. IV. 150**) as follow:

- ❖ H-2''' /C-2''' δ_C 76.80.
- ❖ H-3''' /C-3''' δ_C 73.16.
- ❖ H-4''' /C-4''' δ_C 68.40.
- ❖ H-5''' /C-5''' δ_C 75.32.
- ❖ H-6''' /C-6''' δ_C 61.23.
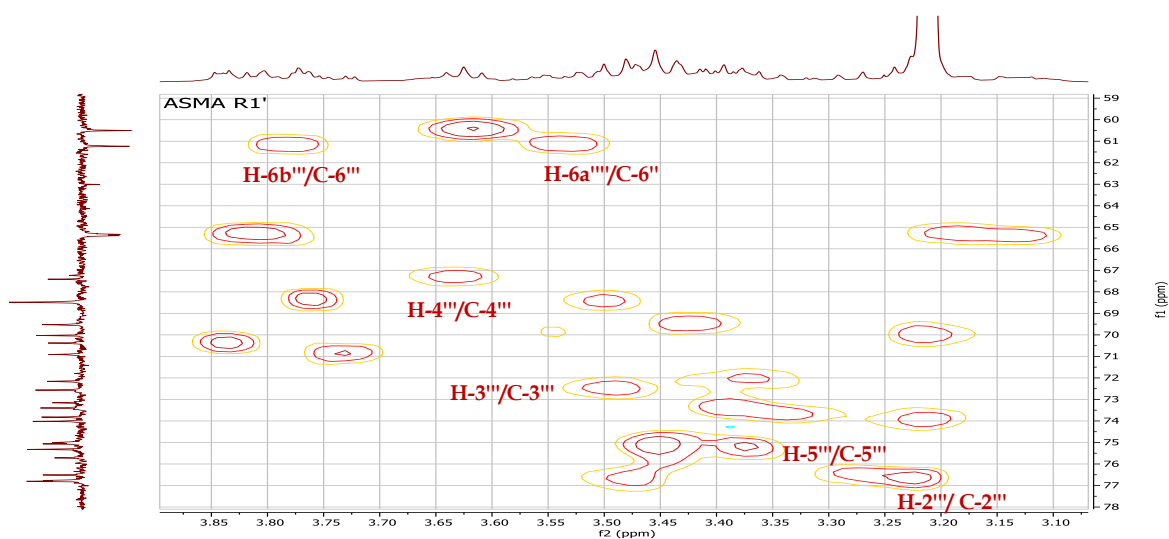
Figure. IV. 150: HSQC spectrum (400 MHz, CD₃OD) of β-D-glucose of **R1**.

The HMBC spectrum show correlations between H-1" of β-D-galactose and C-2' and between H-1''' of β-D-glucose and C-3' (**Figure. IV. 151**).
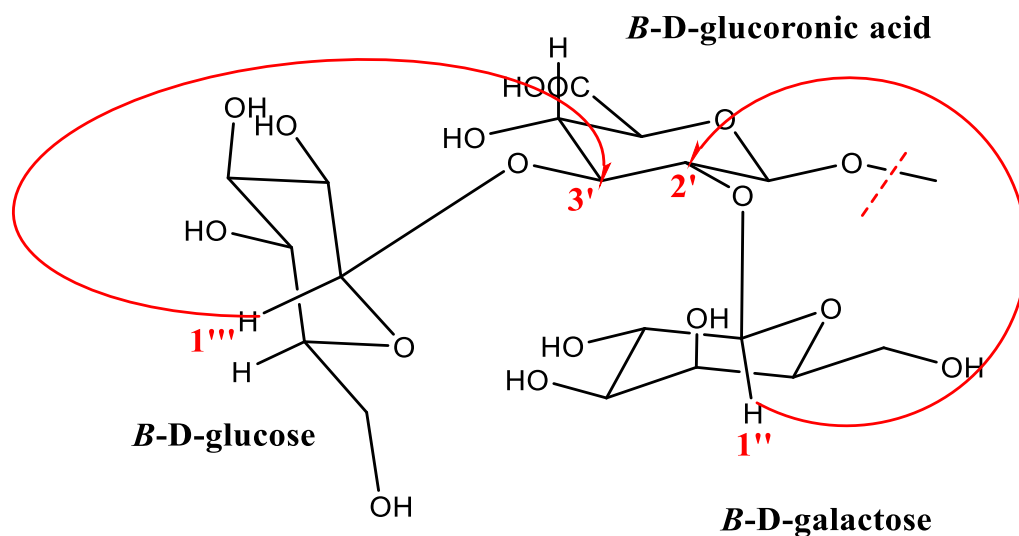
Figure. IV. 151: HMBC correlations between H-1" of β-D-galactose and C-2' and between H-1''' of β-D-glucose and C-3' of the compound **R1**.

By the same way using H-H COSY, TOCSY and HMBC analysis, it is possible to identify the three sugar residues, starting from the anomeric proton resonating at δ_H 5.33 (d, J = 6.3 Hz, 1H). H-H COSY spectrum (**Figure. IV. 153**) displays spins system of six protons corresponding to pentose residue, the H-2'''' resonating at δ_H 3.47 correlates with H-3'''' (δ_H 3.23). The proton H-4'''' resonating at δ_H 3.43 correlates with two protons of H$_2$-5'''' at δ_H 3.82 (dd, 12.0, 5.5Hz, 1H) H-5''''a and δ_H 3.20 (m) H-5''''b (**Figure. IV. 152**). The corresponding carbons assigned using HSQC experiment. According to the analysis of mentioned spectrum this pentose identified that it is a β-D-xylose

❖ H-2'''' /C-2''''δ_C 75.00.

❖ H-3''''/C-3'''' δ_C 76.76.

❖ H-4''''/C-4'''' δ_C 69.53.

❖ H$_2$-5'''' /C-5'''' δ_C 65.39.
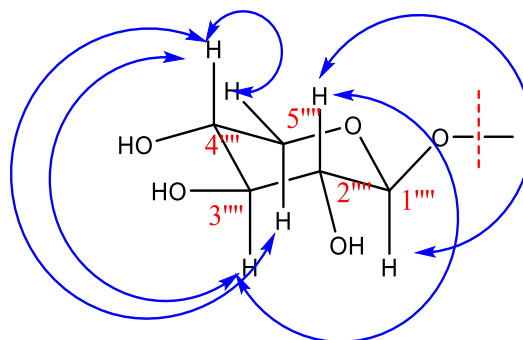
Figure. IV. 152: H-H COSY correlations of β-D-xylose I of the compound **R1**.
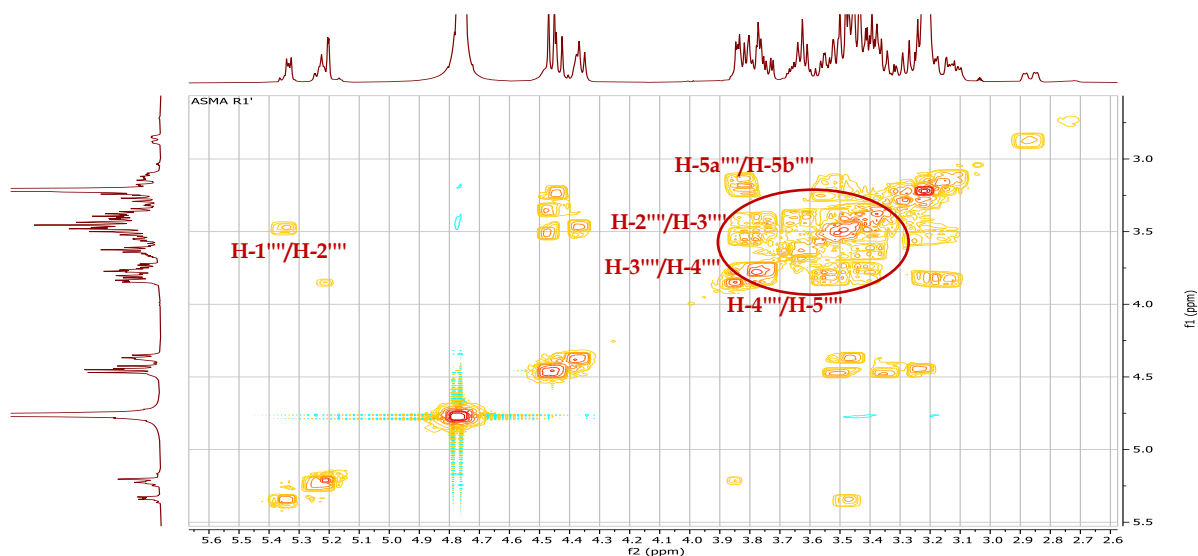
Figure. IV. 153: COSY spectrum (400 MHz, CD$_3$OD) of β-D-xylose I of the compound **R1**.

Based on H-H COSY (**Figure. IV. 155**) and TOCSY (**Figure. IV. 156**) experiments, a spin system of eight protons (8H) was identified of hexose residue starting from the anomeric proton H-1'''' resonating at δ$_H$ 5.20 (d, J = 1.6 Hz, 1H), which correlates with an osidic proton resonating at δ$_H$ 3.84 (dd, J = 3.3, 1.6 Hz, 1H) assigned to H-2''''. The proton resonating at δ$_H$ 3.74 (dd, J = 9.3, 3.3 Hz, 1H) corresponding to H-3'''' correlates with H-4'''' δ$_H$ 3.45. Also, H-5'''' (δ$_H$ 3.65) correlates with H-4'''' and H-6'''' at δ$_H$ 1.23 (d, J = 6.1 Hz, 3H). The coupling constant between H-2'''' and H-3'''' (3.3 Hz) indicates that H-2'''' is on equatorial position. Also, the coupling constant between H-3'''' and H-4'''' (J= 9.3 Hz) indicates the trans di-axial position of these protons (**Figure. IV. 154**). According to these data it could be deduced that this hexose is α-L-rhamnose.
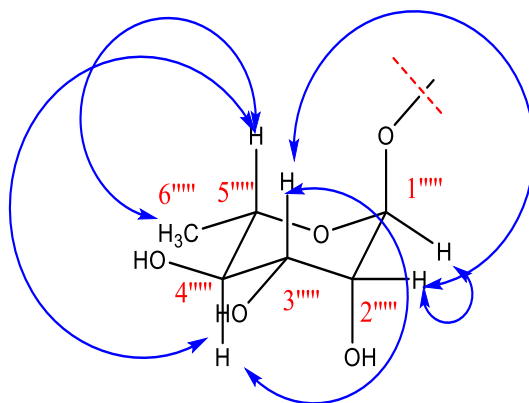
Figure. IV. 154: H-H COSY correlations of α-L-rhamnose of the compound **R1**.
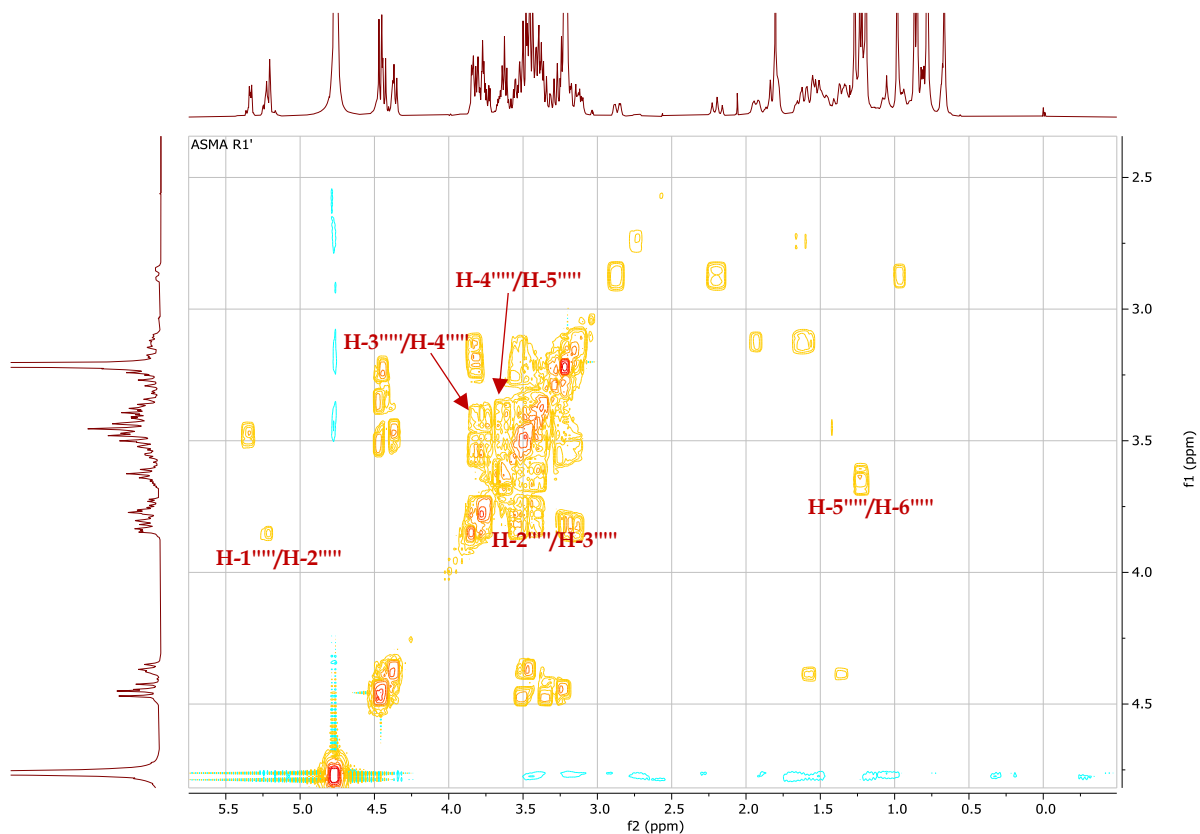
Figure. IV. 155: COSY spectrum (400 MHz, CD$_3$OD) of α-L-rhamnose of the compound **R1**.
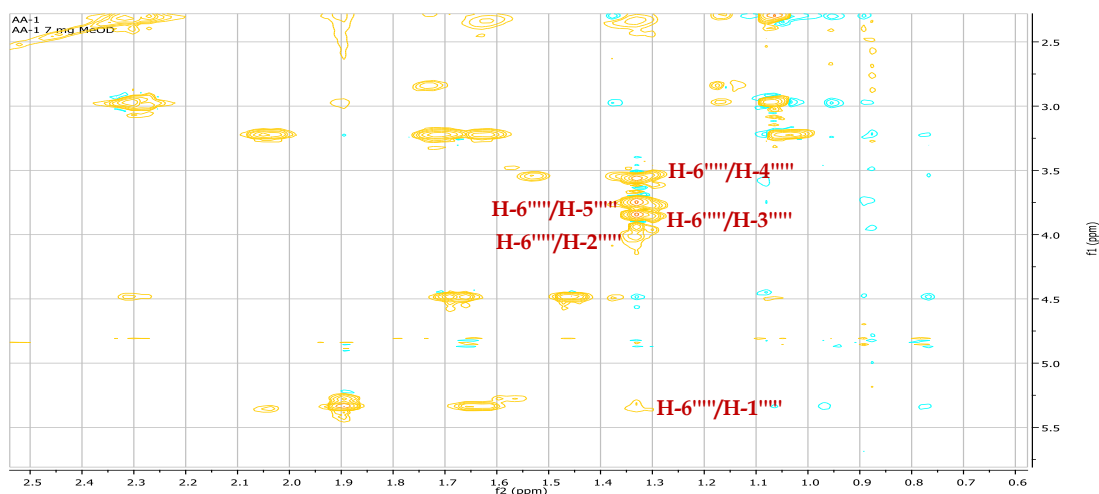
Figure. IV. 156: TOCSY spectrum (600 MHz, CD$_3$OD) of α-L-rhamnose of the compound **R1**.

The HMBC spectrum (**Figure. IV. 157**) reveals a correlation spot between H-6'''' and two carbons resonating at δ$_C$ 67.41 and 83.25, corresponding to C-5'''' and C-4'''' respectively, which confirmed by the HSQC correlations (**Figure. IV. 158**).
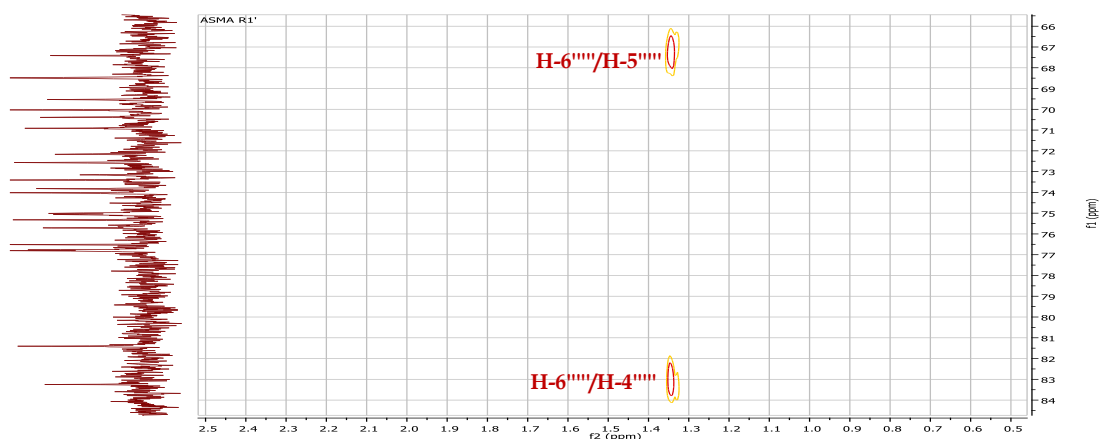
Figure. IV. 157: HMBC spectrum (400 MHz, CD$_3$OD) of correlations of H-6'''' with C-5'''' and C-4'''' of α-L-rhamnose of the compound **R1**.

The others corresponding protons assigned using HSQC spectrum (**Figure. IV. 158**):

- ❖ H-2'''' /C-2'''' δ$_C$ 70.43.
- ❖ H-3''''/C-3'''' δ$_C$ 70.91.
- ❖ H$_3$-6'''' /C-6'''' δ$_C$ 16.91.
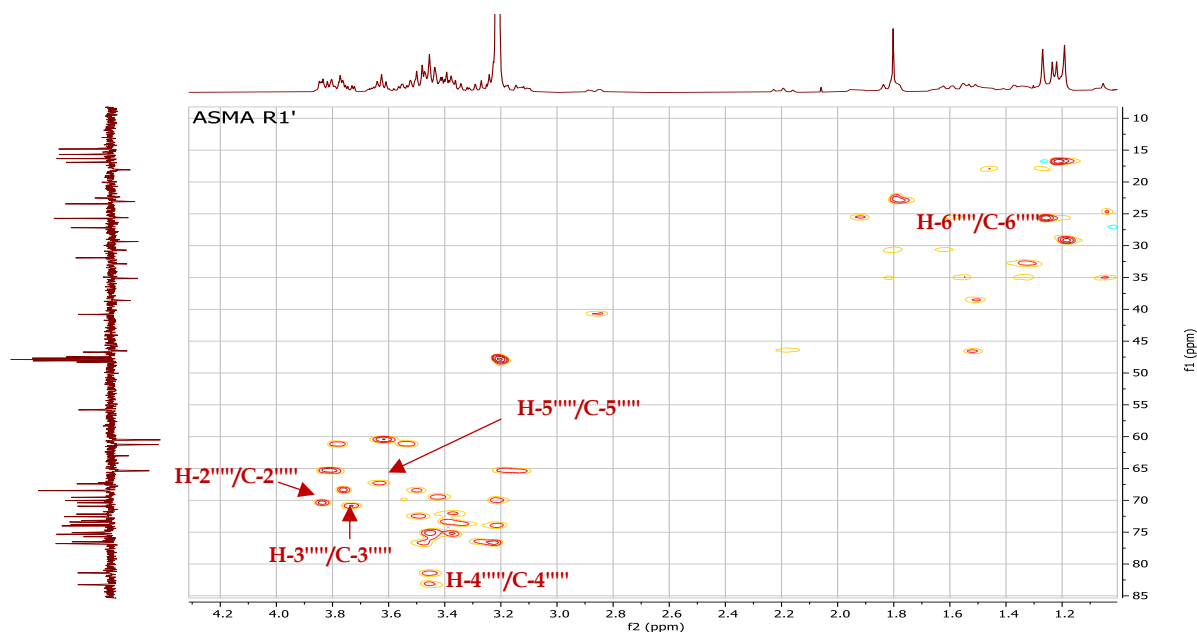
Figure. IV. 158: HSQC spectrum (400 MHz, CD$_3$OD) of α-L-rhamnose of the compound **R1**.

According to H-H COSY (**Figure. IV. 159**) and TOCSY (**Figure. IV. 160**) spectra, that show a spin system of six protons (6H), corresponding to pentose residue,

this spectrum makes it possible to identify these protons starting from the anomeric proton H-1''''' resonating at δ_H 4.46 (d, J = 7.7 Hz, 1H), which correlates with proton resonating at δ_H 3.35 assigned to H-2'''''. The proton resonating at δ_H 3.22 corresponding to H-4''''' correlates with H-3''''' δ_H 3.30 and two protons of H_2-5''''' at δ_H 3.15 (m) H-5'''''b and at δ_H 3.82 H-5'''''a (dd, J = 12.0, 5.5 Hz, 1H) (**Figure. IV. 161**). According to this analysis the pentose residue identified that it is a β-D-xylose.
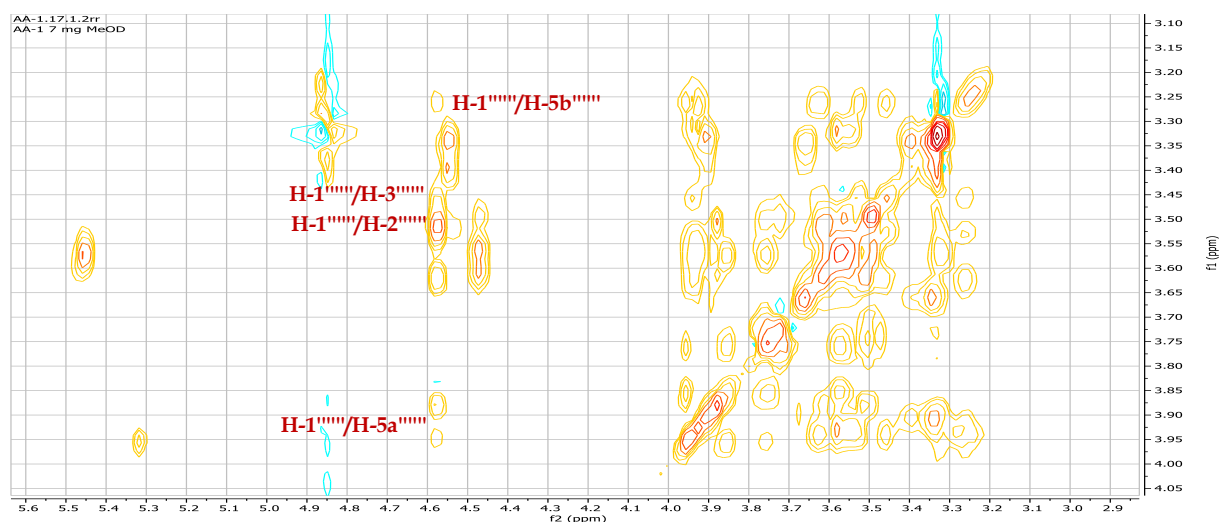
Figure. IV. 159: TOCSY spectrum (600 MHz, CD₃OD) of β-D-xylose II of the compound **R1**.
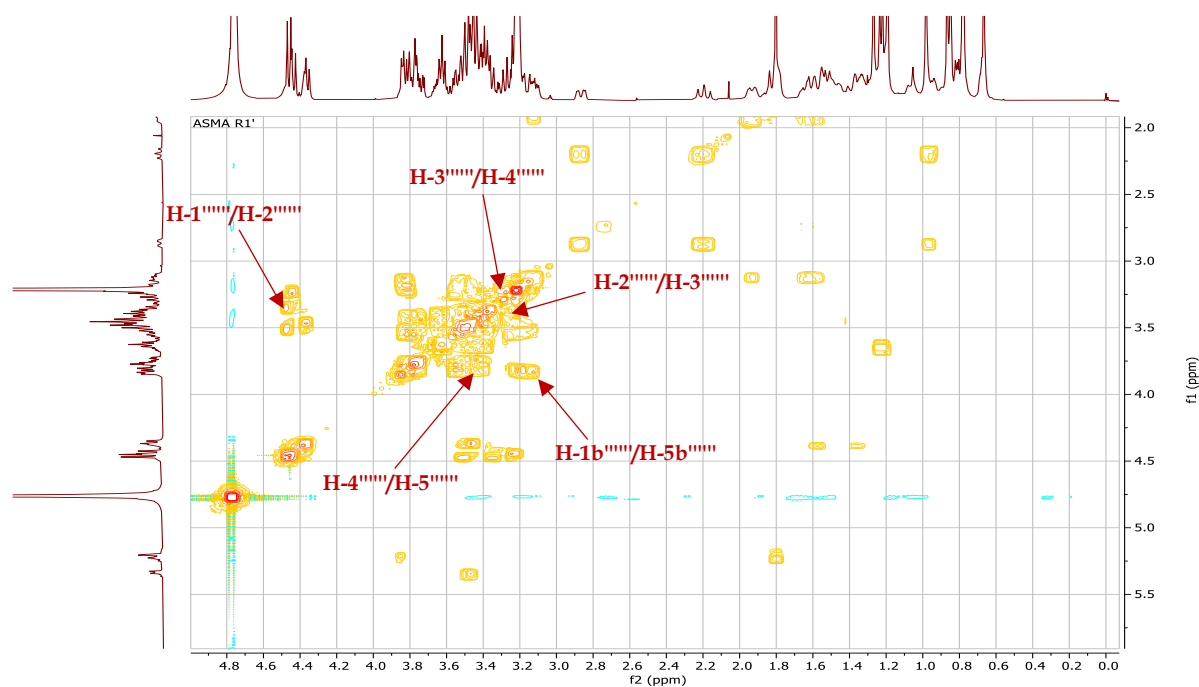
Figure. IV. 160: COSY spectrum (400 MHz, CD₃OD) of β-D-xylose II of the compound **R1**.
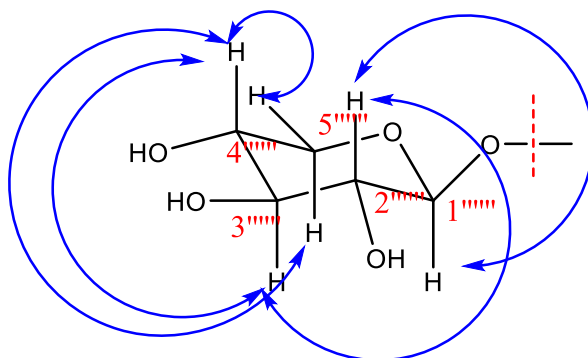
Figure. IV. 161: H-H COSY correlations of β-D-xylose II of the compound **R1**.

The corresponding carbons assigned using HSQC experiment (**Figure. IV. 162**) as follow:

- ❖ H-2"""/C-2""" δ_C 73.82.
- ❖ H-3"""/C-3""" δ_C 76.51.
- ❖ H-4"""/C-4""" δ_C 70.03.
- ❖ H-5"""/C-5""" δ_C 65.33.
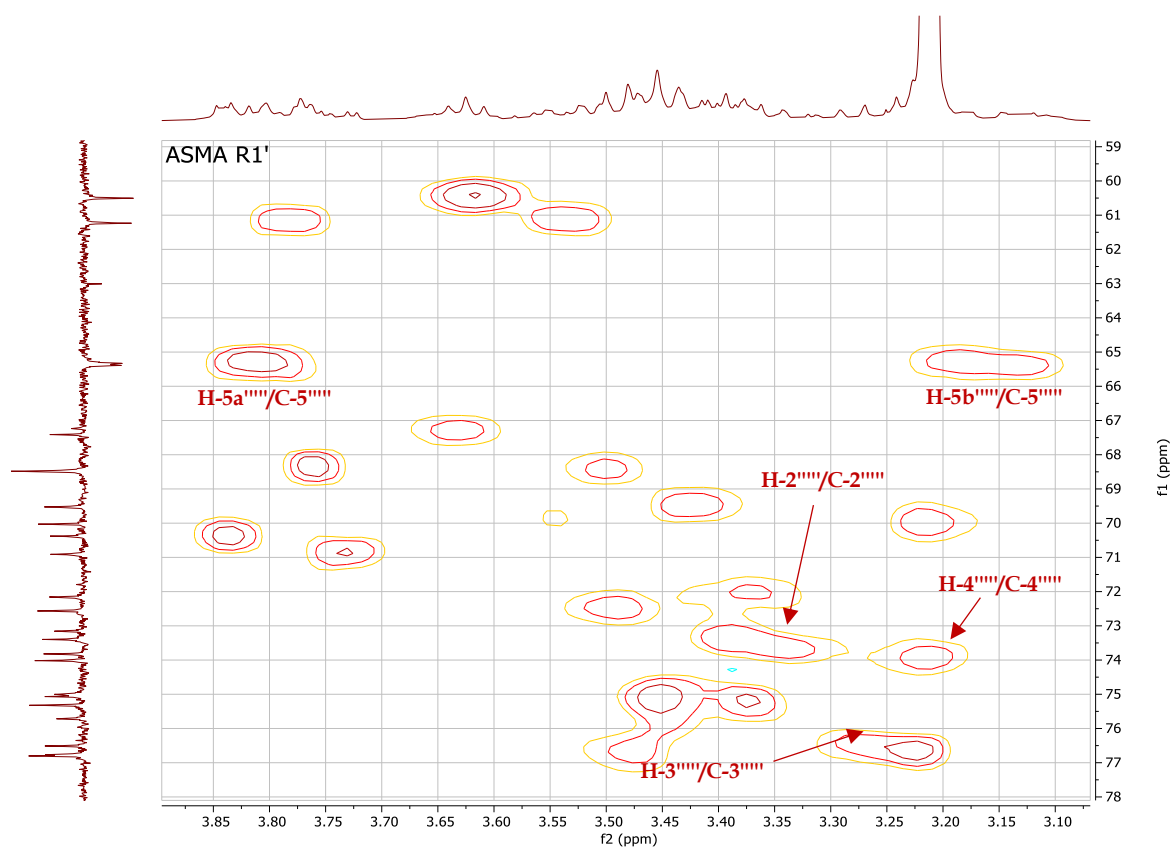
Figure. IV. 162: HSQC spectrum (400 MHz, CD$_3$OD) of β-D-xylose II of the compound **R1**.

The HMBC spectrum (**Figure. IV. 163**) exhibits correlation spots between H-1'''' 5.20 and C-2'''' 75.00. H-1''''' 4.46 and C-4'''' 83.25 (**Figure. IV. 164**).
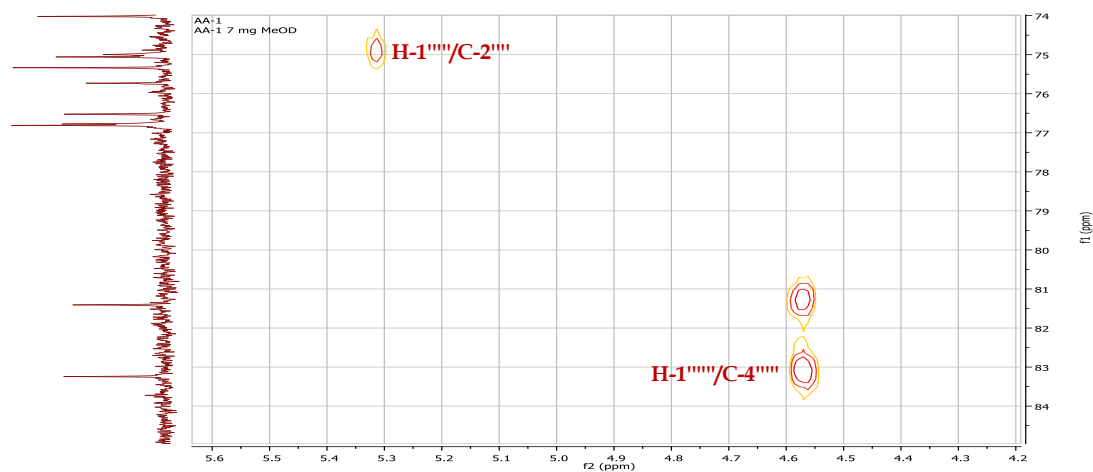
Figure. IV. 163: HMBC correlations (600 MHz, CD₃OD) between osidic moieties at C-28 of the compound **R1**.
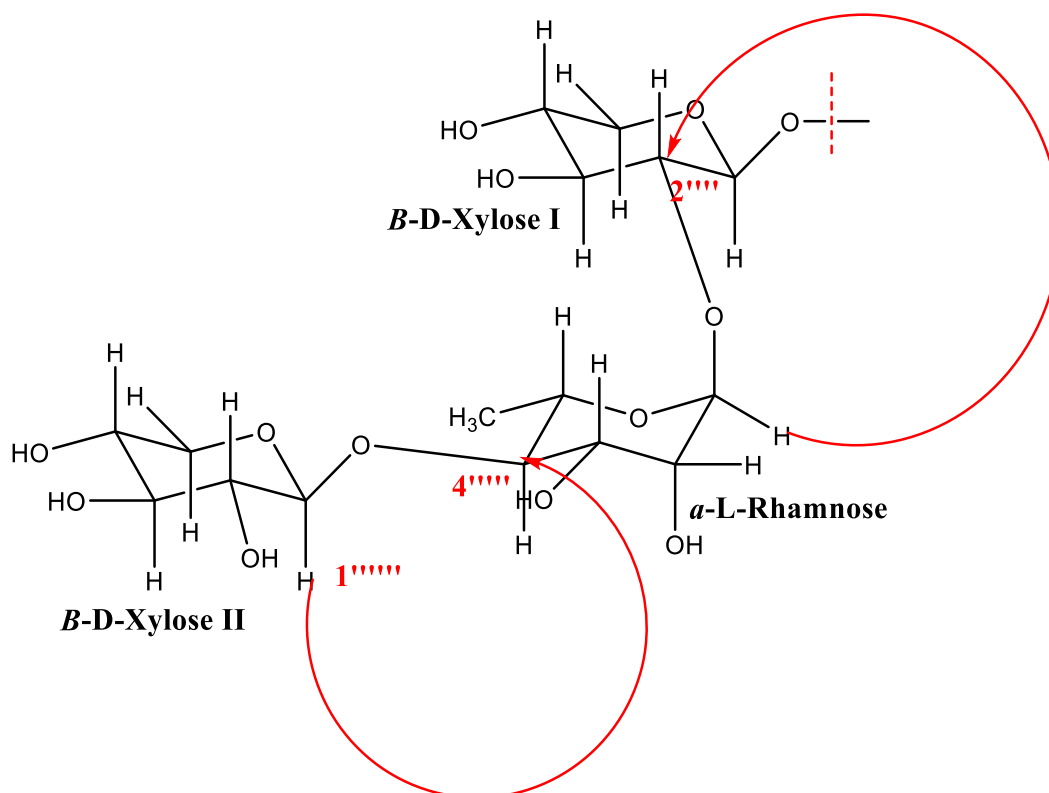
Figure. IV. 164: HMBC correlations between H-1'''' of α-L-rhamnose and C-2'''' of β-D-xylose I and between H-1''''' of β-D-xylose II and C-3'''' of the compound **R1**.

The HMBC spectrum shows a correlations spot between the aglycon part and the osidic part (H-1' 4.36 ppm of glucoronic acid and C-3 89.59 ppm). Also, the chemical shift the anomeric carbon of the xylose I (δ_C 94.04) is a typical of an ester-linked sugar unit [52] (**Figure. IV. 165**) and (**Figure. IV. 166**).
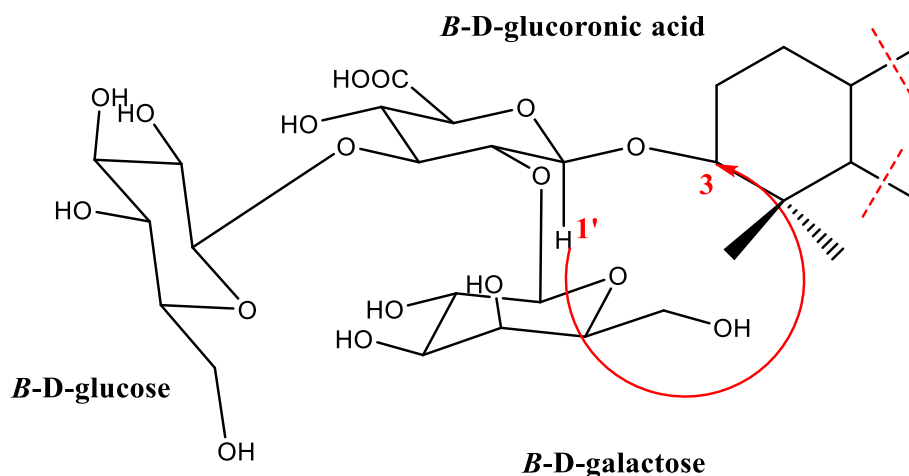
Figure. IV. 165: HMBC correlation between the anomeric proton and the aglycon moiety at C-3 of the compound **R1**.
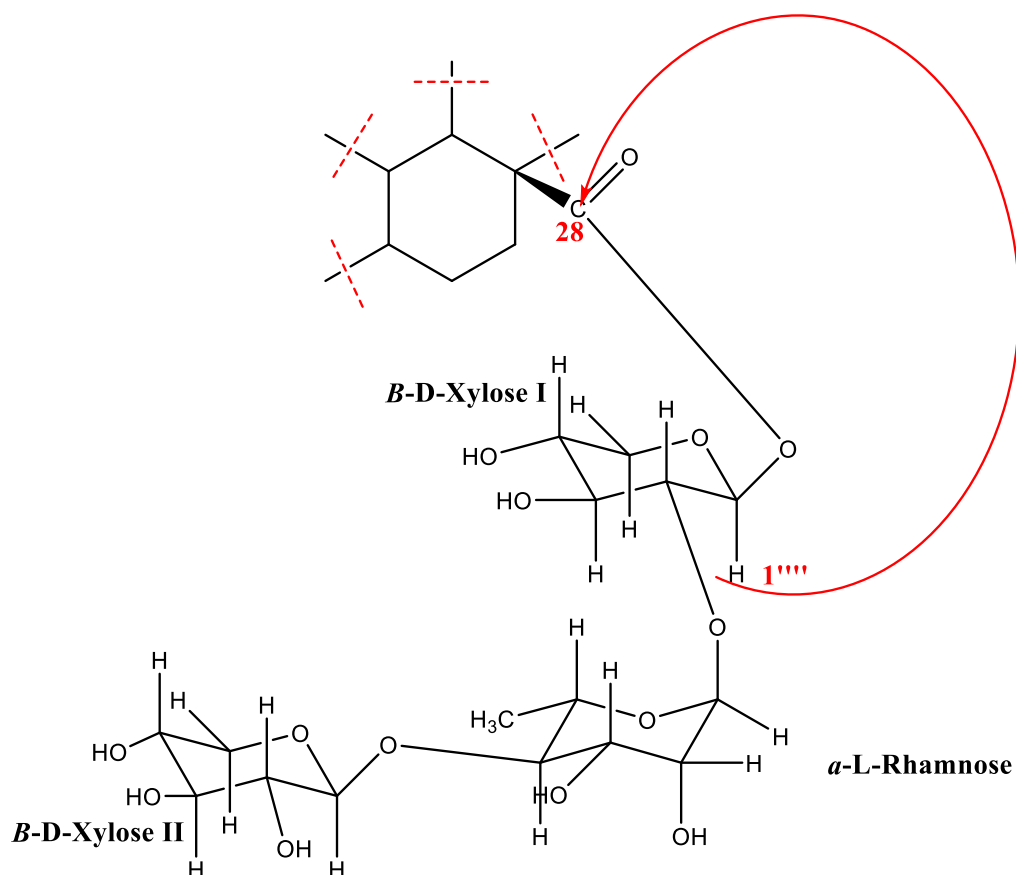
Figure. IV. 166: HMBC correlation between the anomeric proton and the aglycon moiety at C-28 of the compound **R1**.

According to the analysis of all spectra the compound **R1** could be identified as echinocystic acid 3-*O*-β-D-galactopyranosyl-(1"→2')- [β-D-glucopyranosyl- (1'''→3')] -β-D-glucuronopyranosyl-28-O-[β-D-xylopyranosyl-(1'''''→4'''')-α-L-rhamnopyranosyl-(1''''→2'''') -β-D-xylopyranosyl] (**Figure. IV. 167**).
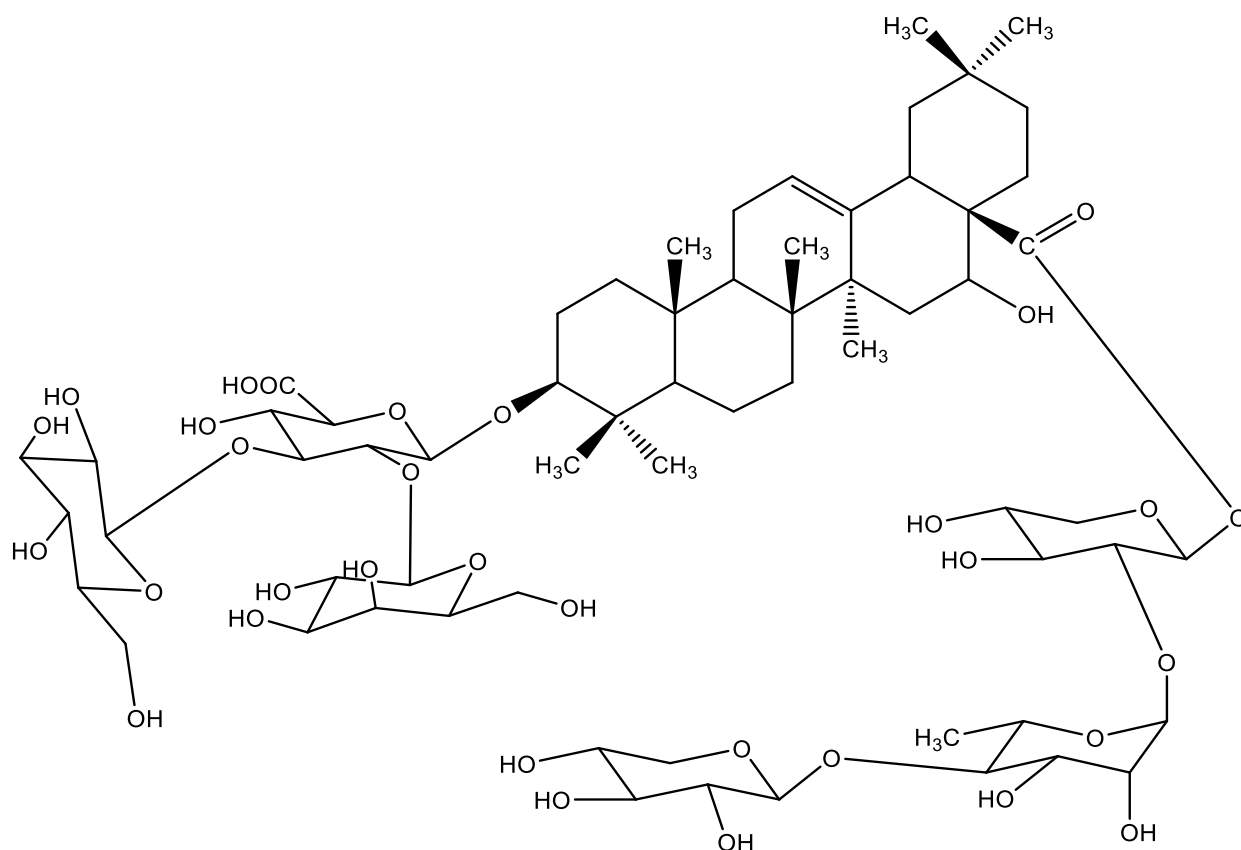
Figure. IV. 167: Structure of compound **R1**; echinocystic acid 3-O-β-D-galactopyranosyl-(1"→2')- [β-D-glucopyranosyl- (1'''→3')] -β-D-glucuronopyranosyl-28-O-[β-D-xylopyranosyl-(1'''''→4'''')-α-L-rhamnopyranosyl-(1''''→2'''') -β-D-xylopyranosyl].

The ^{1}H and ^{13}C NMR data, are summarized in the **Table. IV. 11**, the aglycon parts is in total agreement with that of bidesmosidic echinocystic acid [217, 218]. Also, the osidic part at C-28 is in total agreement with the literature [52]. The compound **R1** is a new compound.

Table. IV. 11: Chemical shifts ^{1}H NMR (400 MHz and 600 MHz) and ^{13}C NMR (100 MHz and 150 MHz) (δ_C in ppm and δ_H in ppm and J in Hz) of compound **R1**.

Position	Carbon	Proton
1	38.61	1.51 (m) H-1a
		0.91 (m) H-1b
2	25.62	1.92 (m) H-2a
		1.58 (m) H-2b
3	89.59	3.10 (dd, J=12.4, 3.8 Hz, 1H)
4	39.05	--
5	55.80	0.67 (m)
6	18.10	1.46 (m) H-6a
		1.26 (m) H-6b
7	32.87	1.34 (m,2H) H-7
8	39.41	--
9	46.71	1.52 (m)
10	36.47	--
11	23.08	1.79 (m)
12	122.7	5.23 (t, 3.5Hz, 1H)
13	143.23	--
14	41.36	--
15	35.14	1.34 (m) H-15a
		1.57 (m) H-15b
16	74.02	4.36 (t, J= 3.4 Hz, 1H)
17	48.85	--
18	40.79	2.87 (dd, 14.3, 4.1 Hz, 1H)
19	46.53	2.19 (dd, 13.4, 3.9 Hz, 1H)
		0.94 (m)
20	29.92	--
21	35.15	1.92 (m) H-21a
		1.14 (m) H-21b
22	30.71	1.62 (m) H-22a
		1.81 (m) H-22b

23	27.19	0.98 (S, 3H)
24	15.67	0.78 (S, 3H)
25	14.83	0.87 (S, 3H)
26	16.33	0.67 (S, 3H)
27	25.71	1.27 (S, 3H)
28	175.65	--
29	31.92	0.78 (S, 3H)
30	23.43	0.85 (S, 3H)
3-O-1'-β-D-glucoronic acid	103.93	4.36 (d, J=7.5 Hz, 1H)
2'	81.40	3.46 (m)
3'	86.73	3.40 (m)
4'	73.82	3.23 (m)
5'	75.32	3.43 (d, J = 9.7 Hz, 1H)
6'	175.65	--
2'-O-1''- β-D-galactose	104.64	4.46 (d, J=7.7 Hz, 1H)
2''	72.56	3.52 (m)
3''	73.40	3.41 (m)
4''	68.40	3.77 (brd, J=3.5 Hz, 1H)
5''	75.00	3.46 (m)
6''	60.50	3.61 (m)
3'-O-1''' β-D-glucose	103.73	4.43 (d, J= 7.8Hz, 1H)
2'''	76.80	3.24 (m)
3'''	73.16	3.38 (m)
4'''	68.40	3.51 (brd, J = 8.8 Hz, 1H)
5'''	75.32	3.40 (m)
6'''	61.23	3.54 (m) 3.79 (m)
28-O-1''''-Xylose	94.04	5.33 (d, J=6.3 Hz, 1H)
2''''	75.00	3.47 (m)
3''''	76.76	3.23 (m)
4''''	69.53	3.43 (m)

5''''	65.39	3.20 (m)
		3.82 (dd, 12.0, 5.5 Hz, 1H)
2''''-O-1'''''-Rhamnose	99.83	5.20 (d, J=1.6 Hz, 1H)
2'''''	70.43	3.84 (dd, J = 3.3, 1.8 Hz, 1H)
3'''''	70.91	3.74 (dd, J=9.3, 3.3 Hz, 1H)
4'''''	83.25	3.45 (m)
5'''''	67.41	3.65 (m)
6'''''	16.91	1.23 (d, J=6.1 Hz, 1H)
4'''''O-1''''''-Xylose	105.33	4.46 (d, J=7.7 Hz, 1H)
2''''''	73.82	3.35 (bd, J = 7.8 Hz, 1H)
3''''''	76.51	3.30 (m)
4''''''	70.03	3.22 (m)
5''''''	65.33	3.15 (m)
		3.82 (dd, 12.0, 5.5 Hz, 1H)

IV.4. 10. Compound R2

Compound **R2** is isolated in the form of a white powder soluble in methanol. It is characterized on TLC test by invisible spot under UV (254 and 366 nm) lamp which turns pink by revelation using acid solution and heating.

The mass spectrum of compound R2, recorded in ESI-MS soft ionization shows a pseudo-molecular ions, in positive mode [M+K]$^+$ at m/z 1238.6 (**Figure. IV. 168**) and in negative mode at m/z 1219.5 [M-H]$^-$ (**Figure. IV. 169**), i.e., a molecular mass of 1220.5 corresponding to a molecular formula $C_{58}H_{92}O_{27}$.
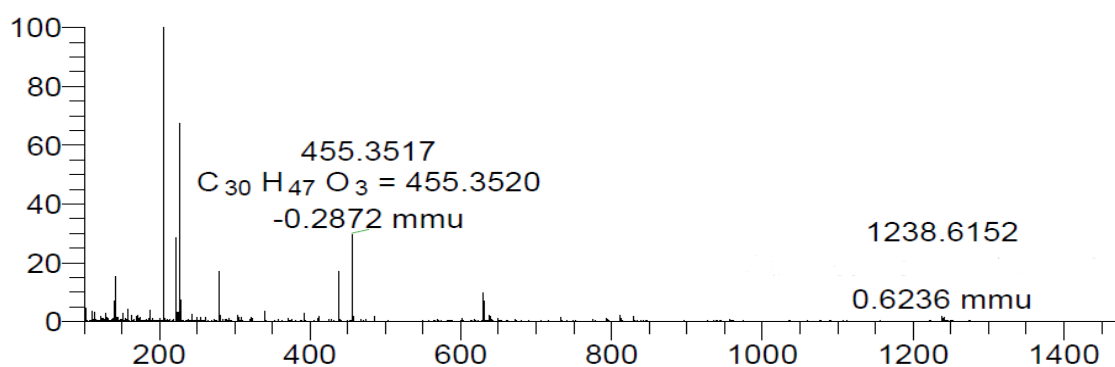
Figure. IV. 168: ESI-MS spectrum of compound **R2**, recorded in positive mode.
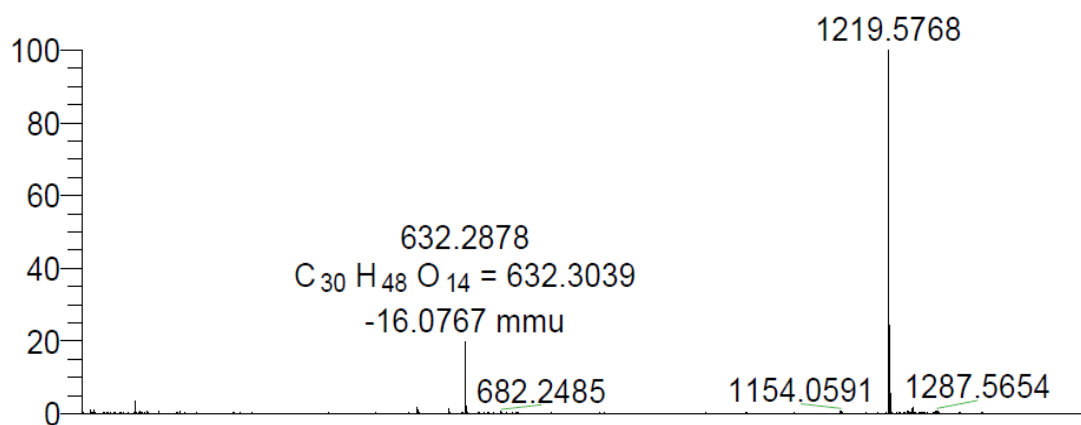
Figure. IV. 169: ESI-MS spectrum of compound **R2**, recorded in negative mode.

The ^{1}H NMR spectrum (**Figure. IV. 171**) recorded in CD$_3$OD, shows seven methyl groups (**Figure. IV. 170**), a characteristic of triterpene skeleton.

The aglycon part:

The seven methyl groups resonating between 0.67 and 1.27 ppm, in the singlet form with integrating oh three protons for each, (S, 3H).

The ^{1}H NMR spectrum displays other signals resonating between 0.9 and 2.18 ppm, corresponding to protons CH and CH$_2$ groups of a triterpene skeleton, other characteristic signals are present in this spectrum:

❖ One olefinic proton at 5.21 (t, J = 3.5 Hz, 1H), assigned to H-12 of the triterpene pentacyclic.

❖ Two oxygenated methine protons resonating at δ_H 3.11 (brd, J = 10.9 Hz, 1H) and 4.37 (t, J = 3.4 Hz) ppm assigned to H-3 and H-16, respectively.

❖ A signal in the form of a double doublet at δ_H 2.87 (dd, J = 14.3, 3.9 Hz, 1H) corresponding to H-18, its multiplicity indicates the presence of two adjacent protons and the coupling constant assigned the β orientation H-18.
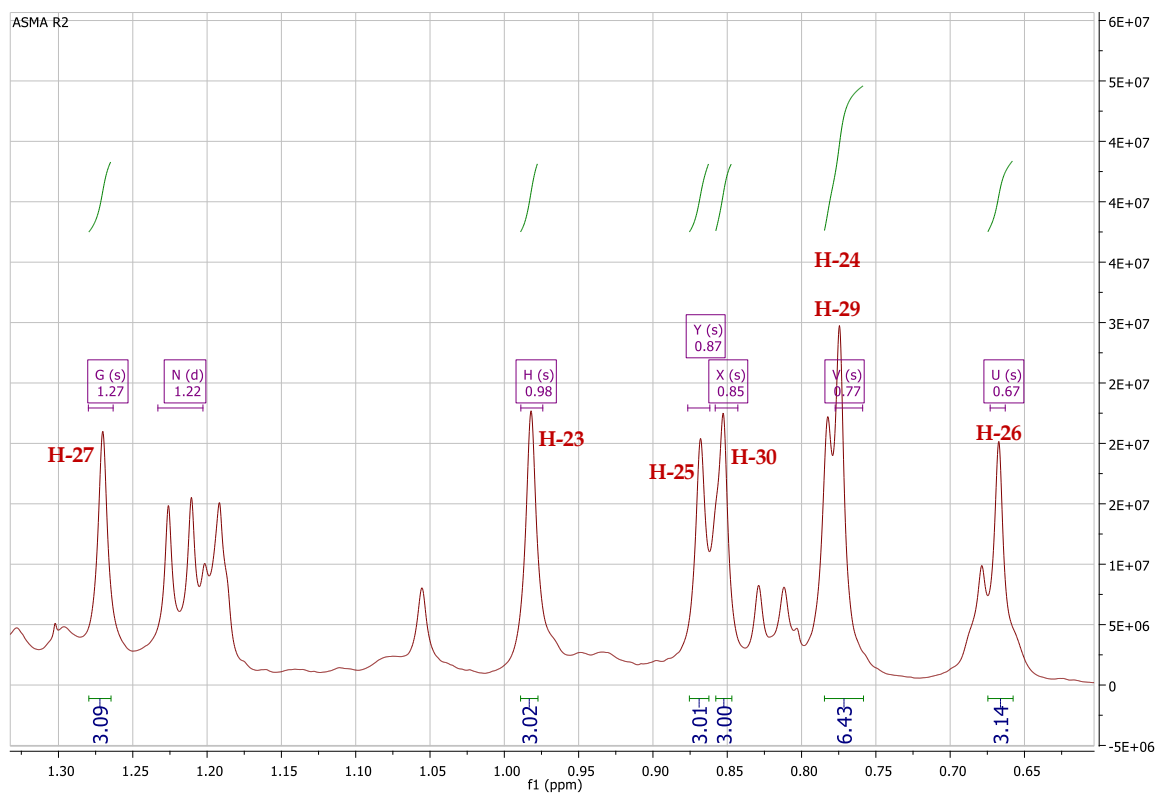
Figure. IV. 170: ^{1}H NMR spectrum (400 MHz, CD$_3$OD) of methyl groups of the compound **R2**.
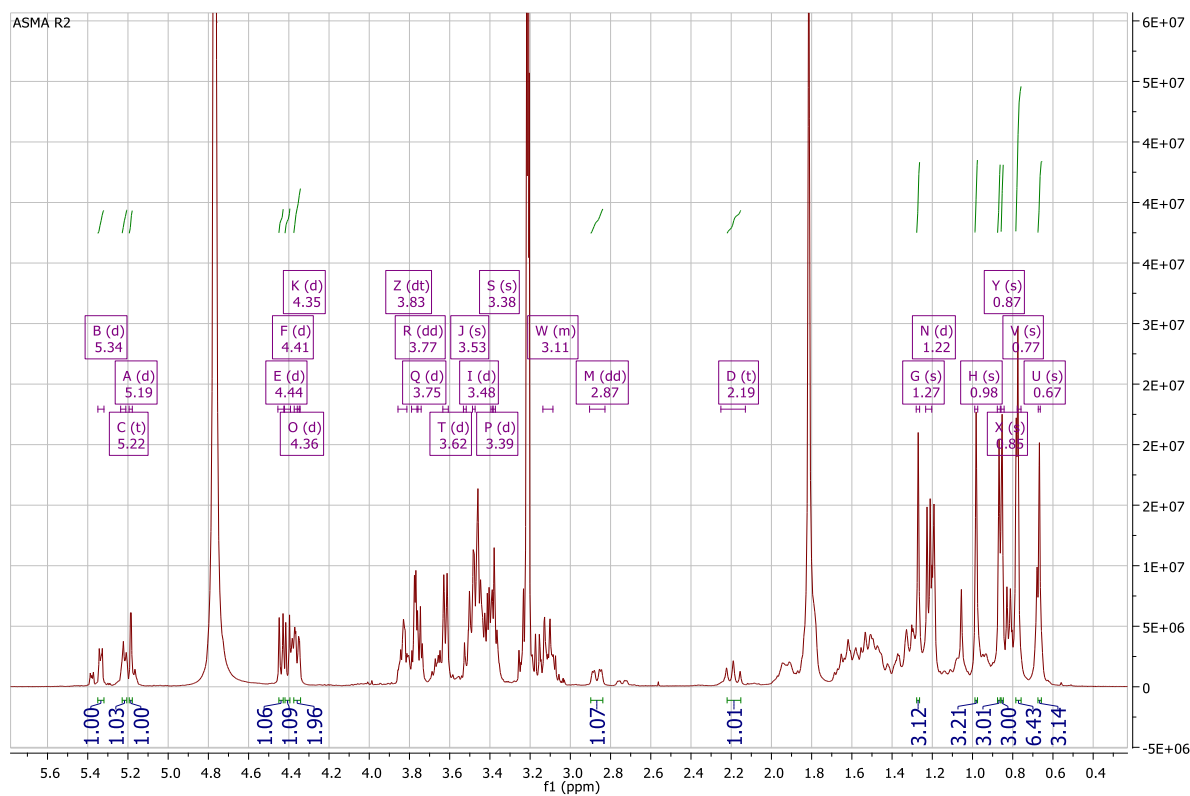
Figure. IV. 171: ^{1}H NMR spectrum (400 MHz, CD$_3$OD) of compound **R2**.

The ^{13}C NMR (**Figure. IV. 172**) and DEPT135 (**Figure. IV. 173**) spectra showed 30 signals were assigned to the aglycone moiety (triterpene pentacyclic), these signals were distributed as follows:

- ❖ Seven tertiary methyl (CH$_3$) groups resonating between δ_C 14 and 32.
- ❖ A carbon signals resonating between δ_C 18 and 55.80, attributable to CH, CH$_2$ and quaternary carbons (C).
- ❖ Two olefinic carbons at δ_C 122.22 and 143.29, were characteristic to an **olean-12-ene** skeleton.
- ❖ Two oxygenated carbons at δ_C 73.25 ppm, attributable to a free hydroxy group C-16 and at δ_C 89.60 ppm, corresponding to C-3. The deshielding effect observed in this position compared to the same carbon with hydroxyl group indicated that C-3 is liked with sugar unit.
- ❖ Carbonyl group observed at δ_C 175.63.
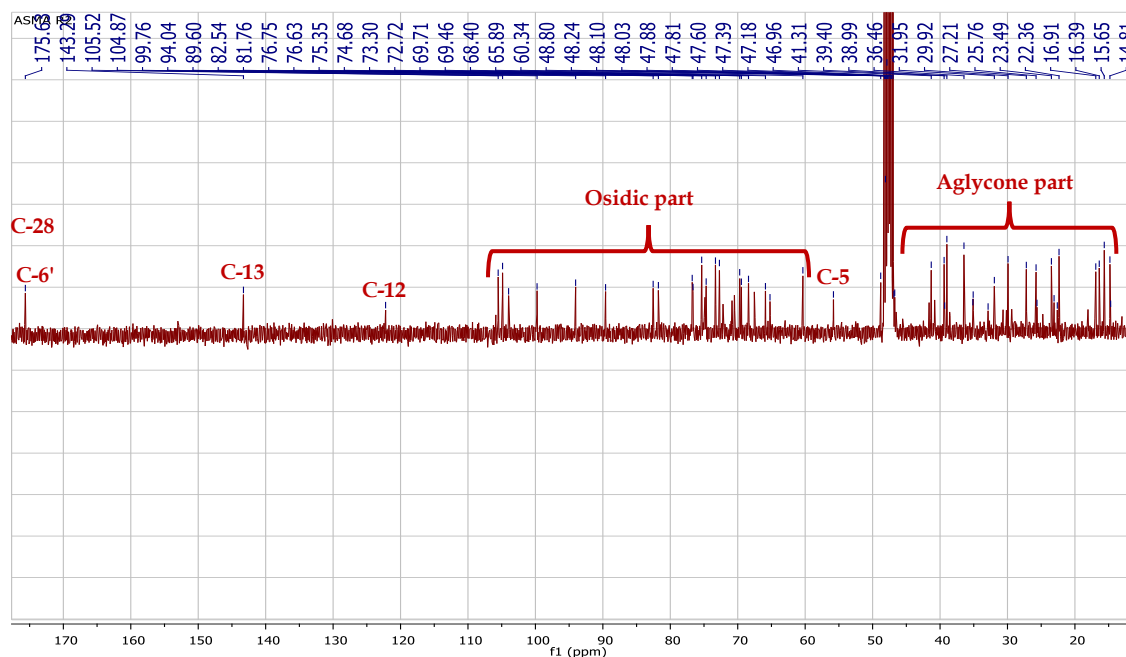
Figure. IV. 172: ^{13}C NMR spectrum (100 MHz, CD$_3$OD) of the compound **R2.**
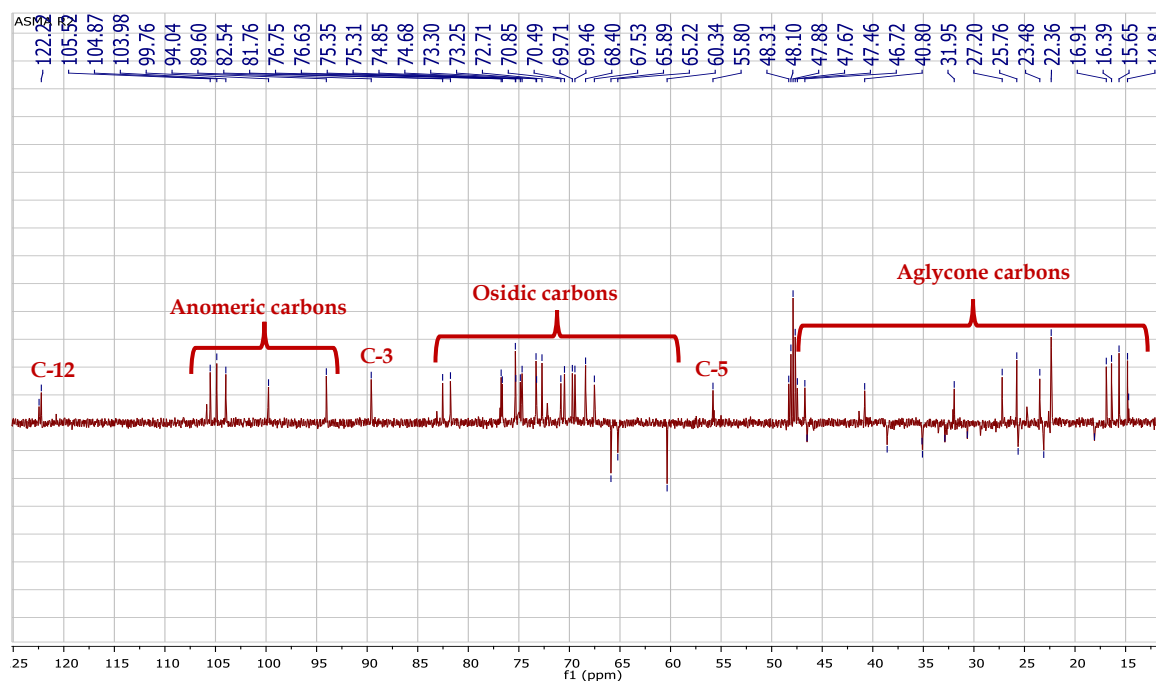
Figure. IV. 173: DEPT 135 spectrum (100 MHz, CD$_3$OD) of compound **R2**.

The results of ^{1}H and ^{13}C NMR spectrum summarized in the **Table. IV. 12** and based on the 2D analysis (HSQC, HMBC and COSY), it could be deduced that the aglycon part of **R2** is in total agreement with the **16-α-hydroxy oleanolic acid** (**echinocystic acid**), by comparison the results of these of **R1** it is clearly that the difference between **R1** and **R2** was in the osidic part.

The osidic part

The ^{1}H NMR (**Figure. IV. 176**) spectrum shows five anomeric proton signals at δ$_H$ 4.36 (d, J = 7.5 Hz, 1H), 4.41 (d, J = 7.6 Hz, 1H), 4.44 (d, J = 7.6 Hz, 1H), 5.19 (d, J = 1.5 Hz, 1H) and 5.33 (d, J = 6.2 Hz, 1H). All the anomeric protons confirm the β configuration, except for anomeric proton at δ$_H$ 5.19 (d, J = 1.5 Hz, 1H) exhibits the α configuration. Also, the ^{1}H NMR spectrum also reveals osidic protons resonating between 3.10 and 3.85 ppm.
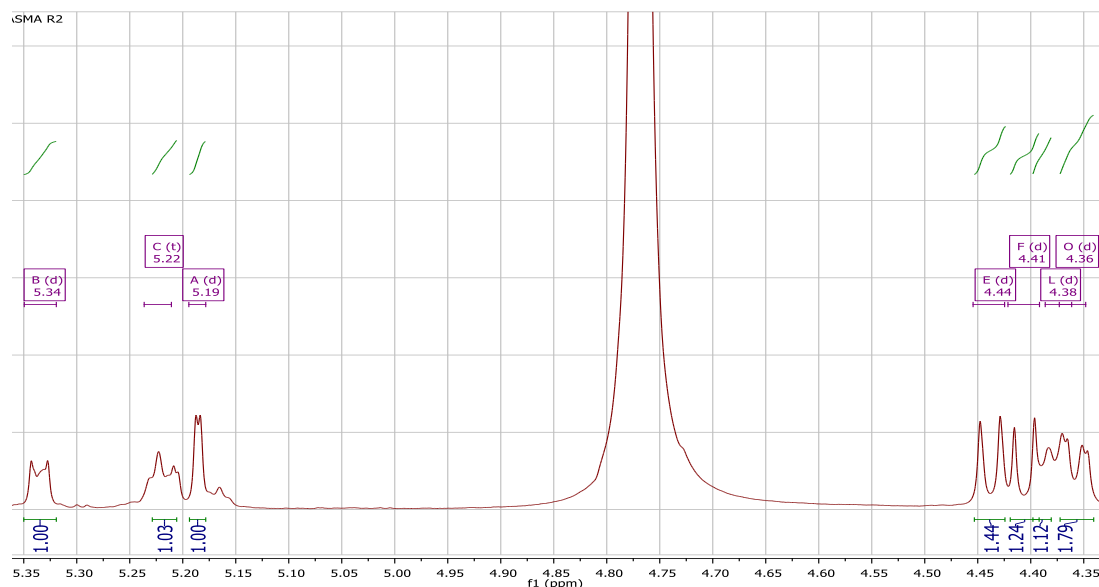
Figure. IV. 174: ^{1}H NMR spectrum (400 MHz, CD$_3$OD) of **R2** anomeric proton region.

The ^{13}C NMR spectrum (**Figure. IV. 175**) shows the presence of five anomeric carbons resonating at 94.04, 99.76, 103.98, 104.87 and 105.33 ppm. This confirmed the suggesting of the occurrence of five sugar units in the compound **R2**.
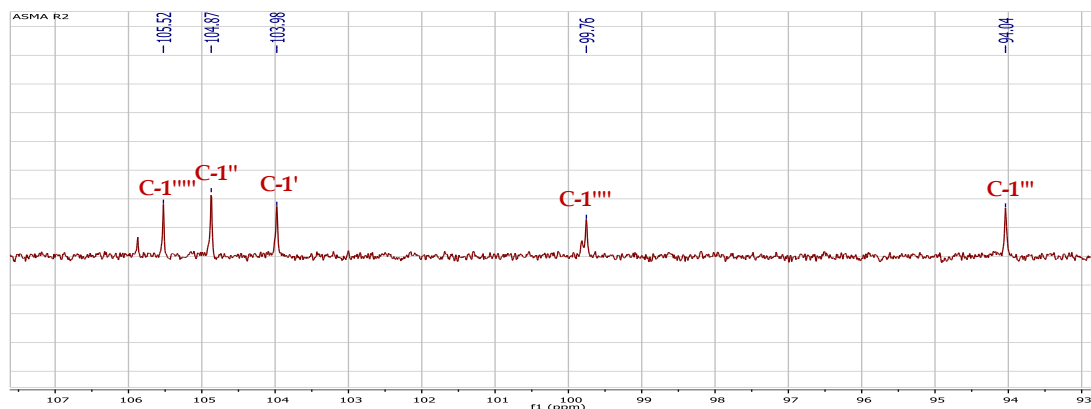
Figure. IV. 175: 13C NMR spectrum (100 MHz, CD$_3$OD) of anomeric proton region of compound **R2**.

The corresponding carbons of anomeric protons, assigned by the HSQC spectrum (**Figure. IV. 176**) as follows:

- ❖ 4.36 correlate with 103.98 ppm.
- ❖ 4.41 correlate with 105.52 ppm.
- ❖ 4.44 correlate with 104.87 ppm.
- ❖ 5.19 correlate with 99.76 ppm.
- ❖ 5.33 correlate with 94.04 ppm.
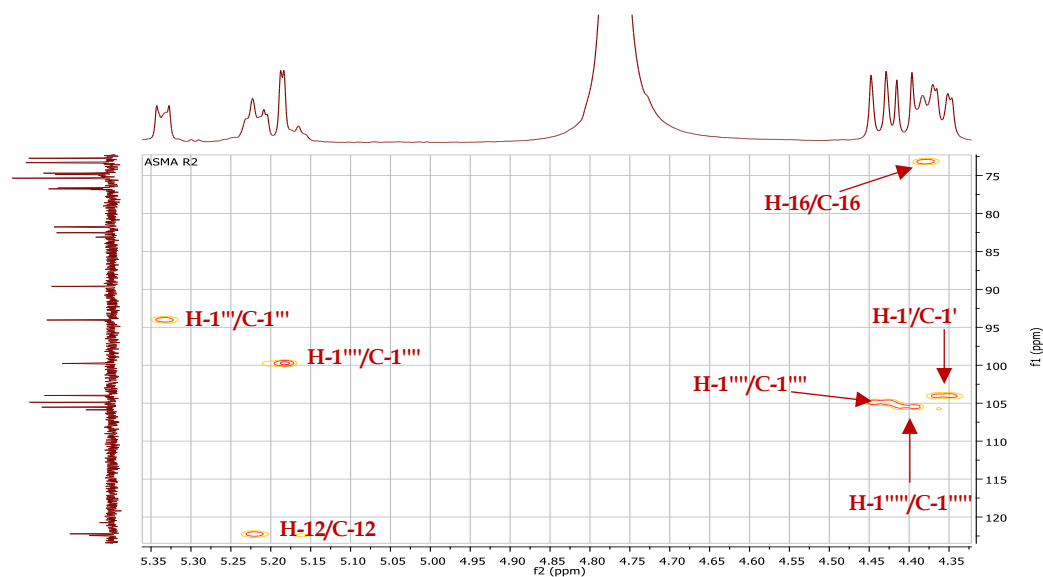
Figure. IV. 176: HSQC spectrum (400 MHz, CD$_3$OD) of anomeric part of **R2**.

The 13C NMR spectrum (**Figure. IV. 177**) also displays osidic carbon signals resonating between 60 and 82.54 ppm distributed on the five sugar residues.
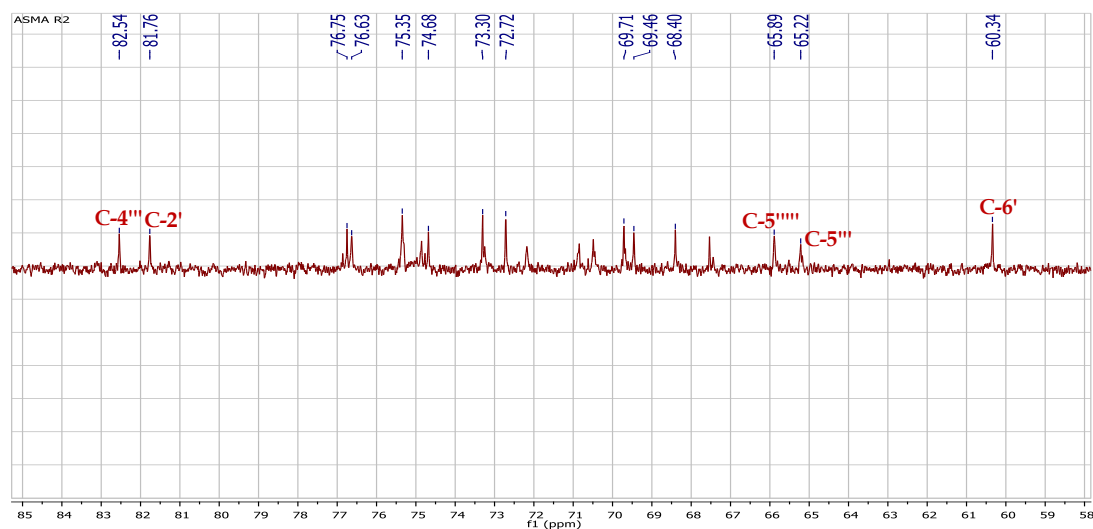
Figure. IV. 177: ^{13}C NMR spectrum (100 MHz, CD$_3$OD) of osidic region of **R2**.

Starting from first anomeric proton H-1' resonating at δ_H 4.36 (d, J = 7.5 Hz, 1H), the comparison of the results with literature data and with saponin **R1**, and based on COSY (**Figure. IV. 178**) and TOCSY (**Figure. IV. 179**) spectra, it is possible to identify a spin system of five protons corresponding to glucoronic acid, H-1' shows correlations with H-2' resonating at δ_H 3.45. H-4' resonating at δ_H 3.53 exhibits correlations with H-3' and H-5' resonating at δ_H 3.48 and δ_H 3.37, respectively.
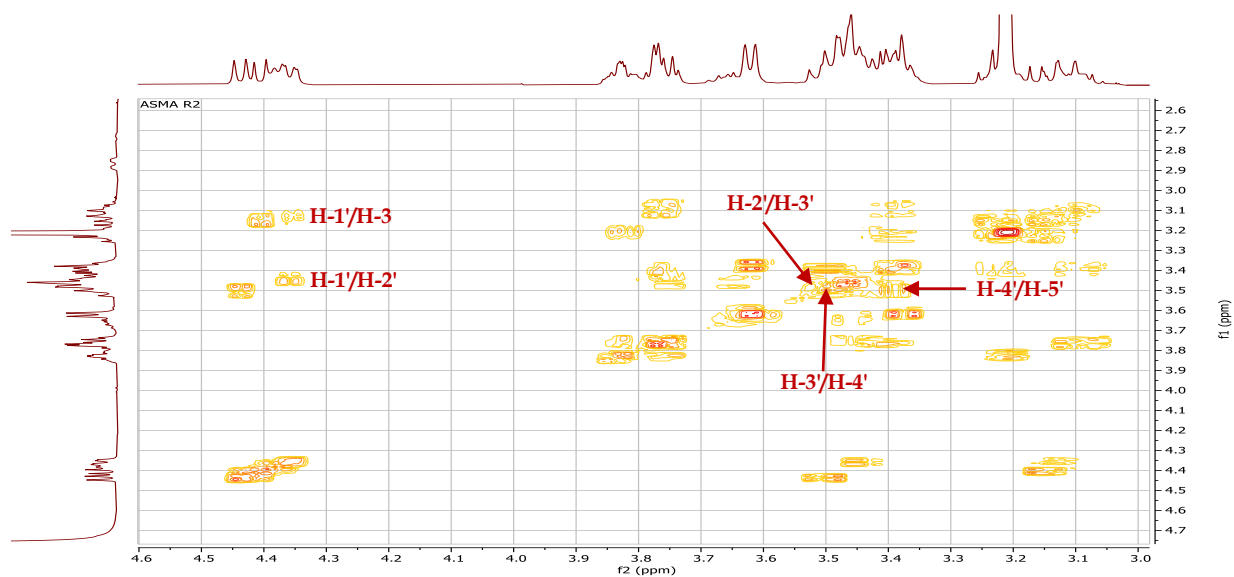
Figure. IV. 178: COSY spectrum (400 MHz, CD₃OD) of glucoronic acid of the **R2**.
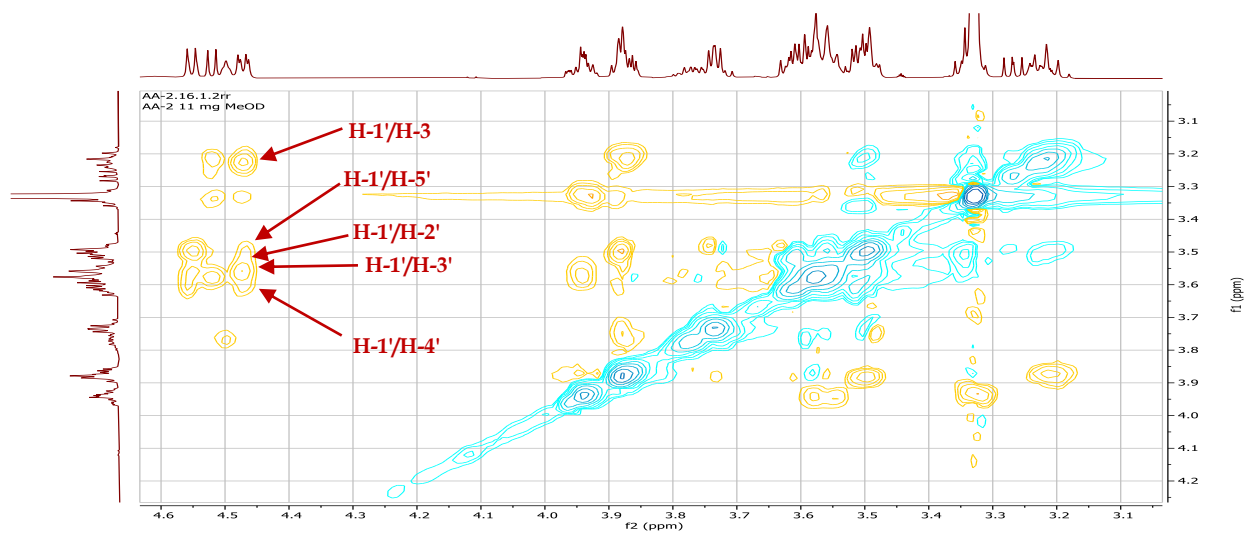
Figure. IV. 179: TOCSY spectrum (600 MHz, CD₃OD) of glucoronic acid of **R2**.

The corresponding carbons assigned using HSQC experiment (**Figure. IV. 180**), as follow:

- ❖ H-2' /C-2' δ_C 81.76.
- ❖ H-3' /C-3' δ_C 76.63.
- ❖ H-4' /C-4' δ_C 72.71.
- ❖ H-5' /C-5' δ_C 75.35.
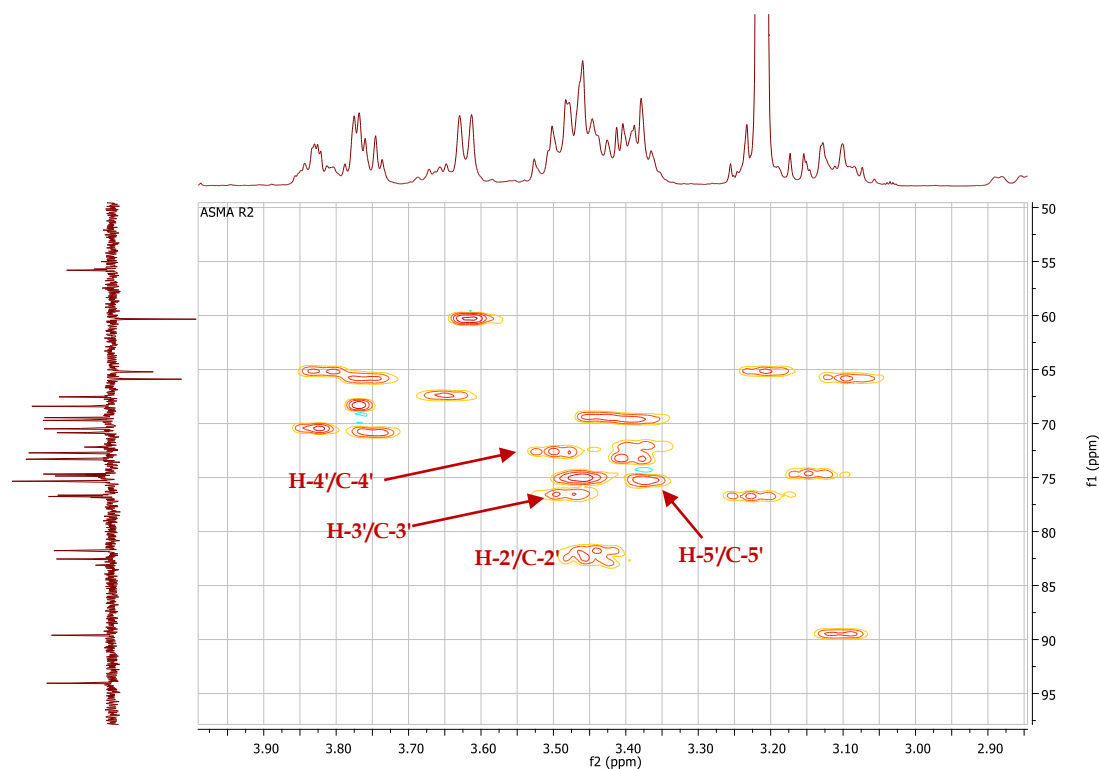
Figure. IV. 180: HSQC spectrum (400 MHz, CD₃OD) of β-D-glucoronic acid of the compound **R2**.

The second spin system corresponding to a hexose residue, six spins system identified based on COSY (**Figure. IV. 181**) and TOCSY (**Figure. IV. 182**) spectra starting from the anomeric proton resonating at δ_H 4.44 (d, J = 7.6 Hz, 1H), which reveals correlations with an osidic proton resonating at δ_H 3.48 assigned to H-2''. The H-H COSY spectrum shows correlations: (H-2'' with H-3'' δ_H 3.39), (H-3'' with H-4'' δ_H 3.77), (H-4'' with H-5'' δ_H 3.46), H-5'' with H₂-6'' δ_H 3.62 (m, 2H).

The H-4'' detected at δ_H 3.77 (brd, J = 2.7 Hz, 1H), the small value of the coupling constant of H-4'' indicated that it is in equatorial position. The coupling constant of H-1'' (7.6 Hz) indicated that it is in β configuration. According to this data the second hexose residue identified as β-D-galactose. The corresponding protons were assigned using HSQC spectrum (**Figure. IV. 183**), which are summarized in the **Table. IV. 12.**
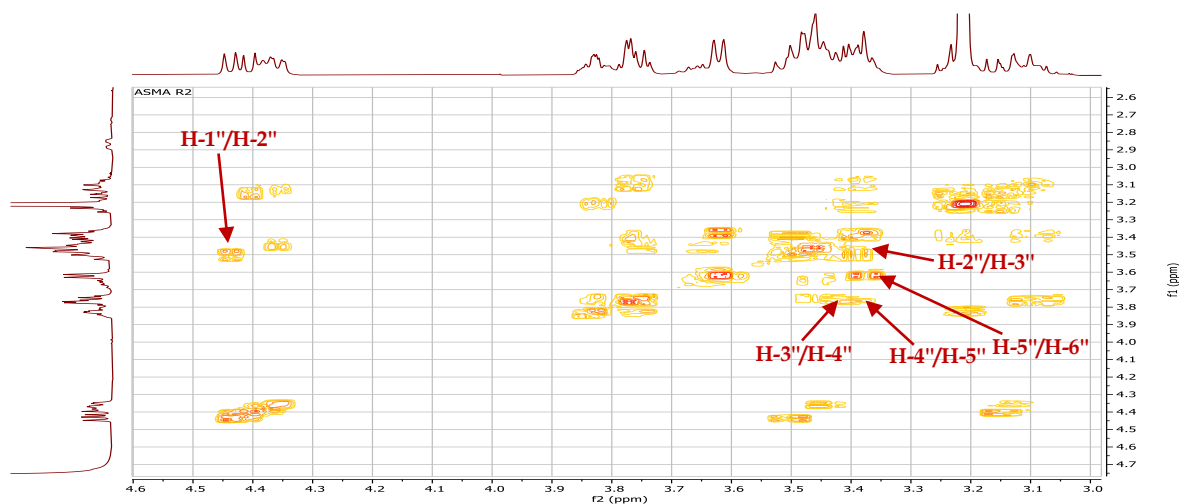
Figure. IV. 181: COSY spectrum (400 MHz, CD₃OD) of second sugar residue, β-D-galactose of the compound **R2**.
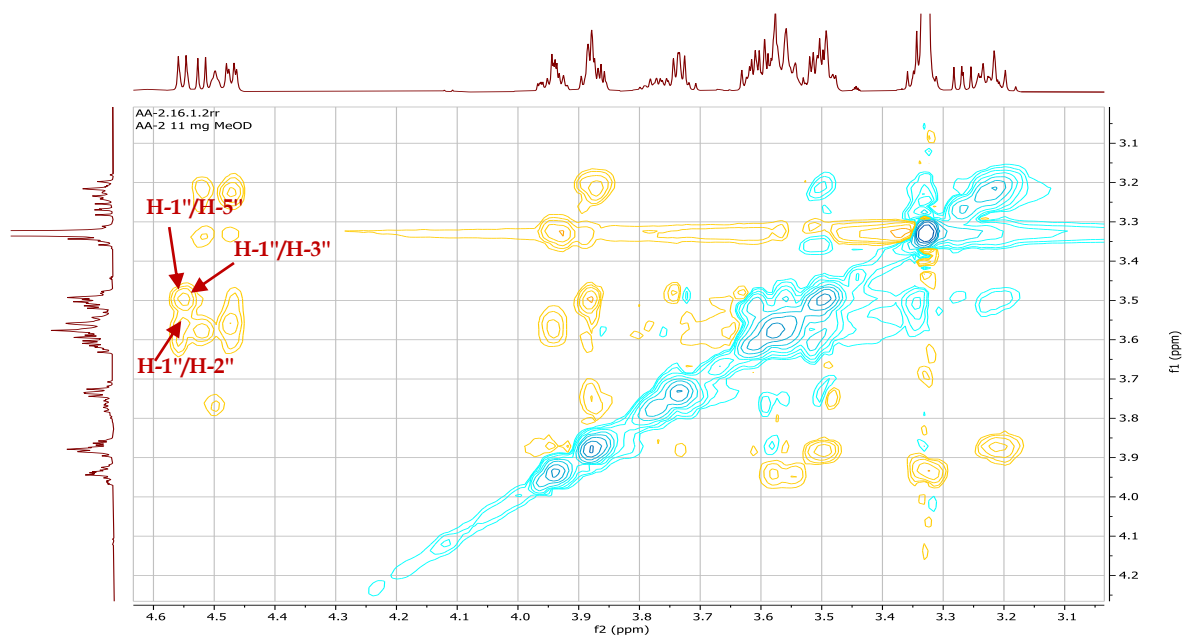
Figure. IV. 182: TOCSY spectrum (600 MHz, CD₃OD) of second sugar residue, β-D-galactose of the compound **R2**.
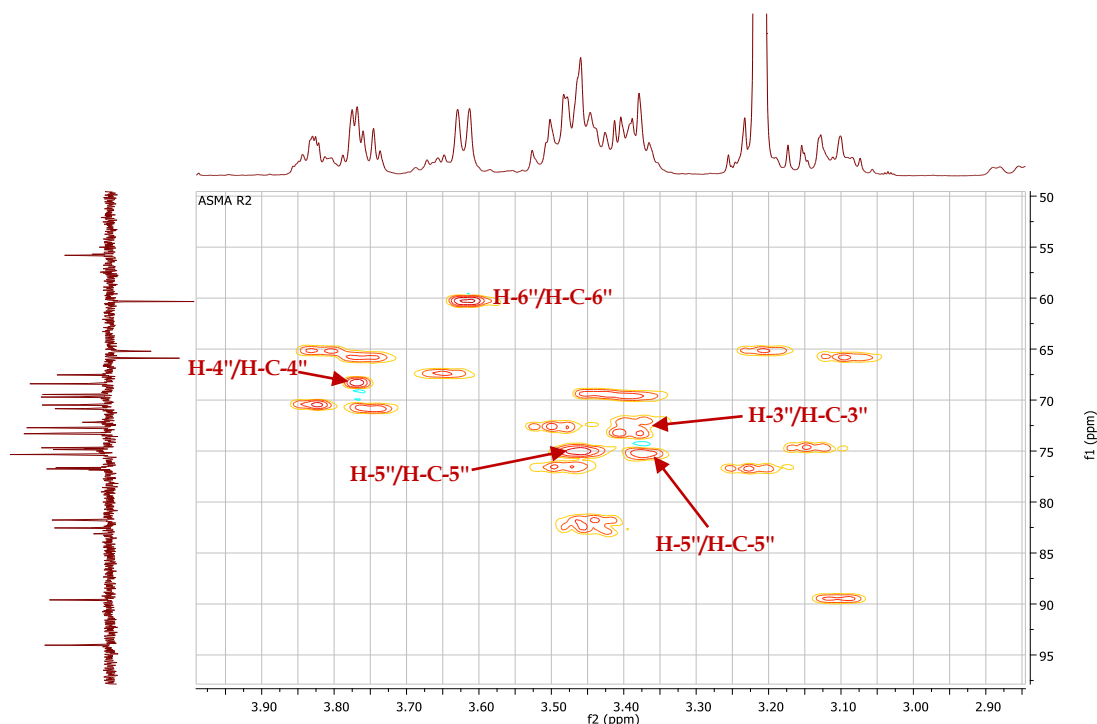
Figure. IV. 183: HSQC spectrum (400 MHz, CD$_3$OD) of β-D-galactose of the compound **R2**.

The linkage of the terminal β-D-galactose at C-2' of the β-D-glucoronic acid was indicated by the correlations between H-1" of the β-D-galactose and C-2' of in the HMBC spectrum (**Figure. IV. 185**). This may be confirmed by the deshielding effect observed on C-2' to 81.76 ppm, comparing with ^{13}C NMR chemical shift with those of β-D-glucoronic acid, showed glycosylation shift of C-2' by 7.8 ppm indicate that the C-2' is site of glycosylation. Also, the HMBC spectrum (**Figure. IV. 185**) reveals cross-peak between H-1' (4.36 ppm) of glucoronic acid and C-3 (89.60 ppm) of aglycon moiety (**Figure. IV. 184**).
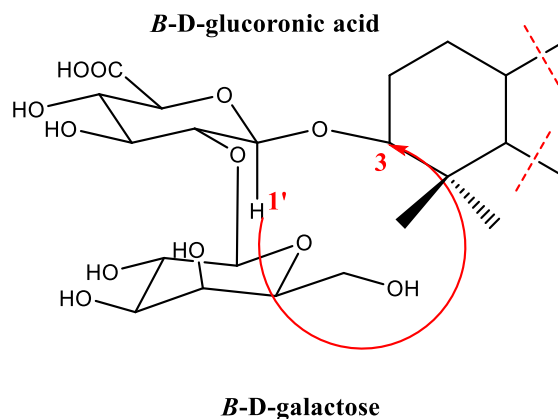
Figure. IV. 184: HMBC correlations between H-1" of galactose and C-2' of **R2**.
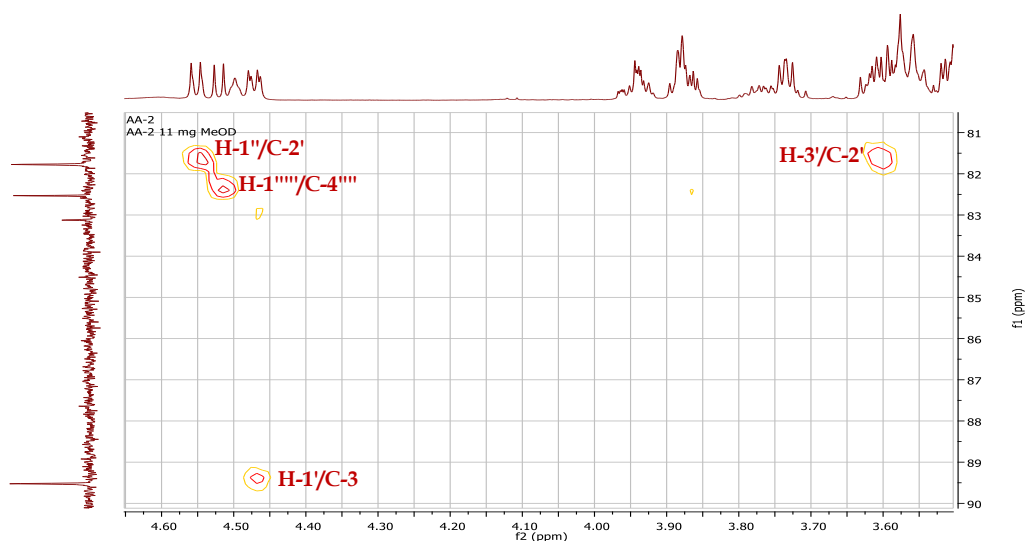
Figure. IV. 185: HMBC spectrum (600 MHz, CD$_3$OD) C-2' and H-1''and between H-1' and C-3 of the compound **R2**.

By the same manner, three sugar units were identified according to their protons and carbons chemical shifts. Starting from the anomeric proton H-1''' resonating at δ$_H$ 5.33 (d, J = 6.2 Hz, 1H), COSY (**Figure. IV. 186**) and TOCSY (**Figure. IV. 187**) experiments displays spins system of six protons corresponding to pentose residue, the H-2''' resonating at δ$_H$ 3.46 correlates with H-3''' (δ$_H$ 3.47). The proton H-4''' resonating at δ$_H$ 3.39 correlates with two protons of H$_2$-5''' at δ$_H$ 3.81 (m) H-5'''a and δ$_H$ 3.20 (m) 5'''b. The corresponding carbons assigned using HSQC experiment (**Figure. IV. 188**) as summarized in the **Table. IV. 12**. According to the analysis of mentioned spectrum this pentose identified that it is a β-D-xylose.

According to COSY (**Figure. IV. 186**) and TOCSY (**Figure. IV. 187**) experiments, a spin system of eight protons were identified of hexose residue starting from the anomeric proton H-1'''' resonating at δ$_H$ 5.18 (d, J = 1.5 Hz, 1H), which correlates with an osidic proton resonating at δ$_H$ 3.83 (dd, J = 3.2, 1.5 Hz, 1H) assigned to H-2''''. The proton resonating at δ$_H$ 3.74 (dd, J = 9.2, 3.2 Hz, 1H) corresponding to H-3'''' correlates with H-4'''' δ$_H$ 3.46. Also, H-5'''' (δ$_H$ 3.65) correlates with H-4'''' and H$_3$-6'''' at δ$_H$ 1.23 (d, J = 6.2 Hz, 3H). The coupling constant between H-2'''' and H-3'''' (3.3 Hz) indicate that H-2'''' is on equatorial position. Also, the coupling constant between H-3'''' and H-4'''' (9.3 Hz) indicate the trans di-axial position of these protons. According to these data it could be deduced that this hexose is α-L-rhamnose. The ^{13}C

chemical shifts of α-L-rhamnose were assigned using HSQC spectrum as shown in (**Figure. IV. 188**), and as summarized in the **Table. IV. 12.**
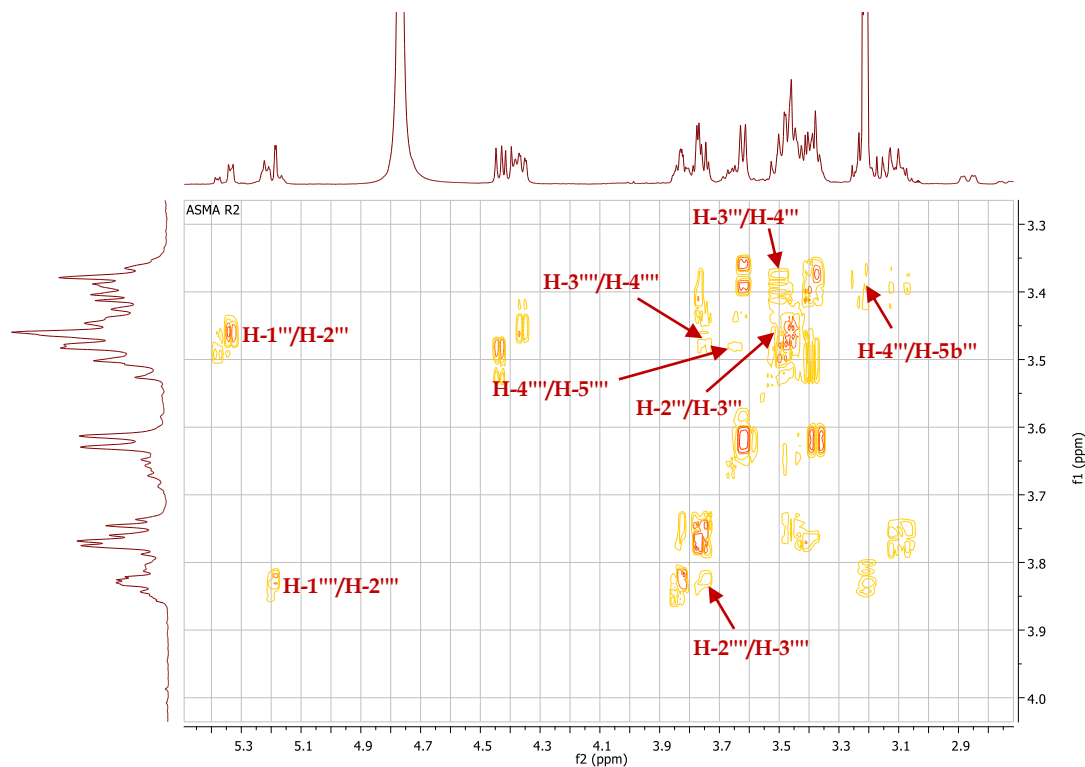
Figure. IV. 186: COSY spectrum (400 MHz, CD₃OD) of β-D-xylose I and α-L-rhamnose of compound **R2**.
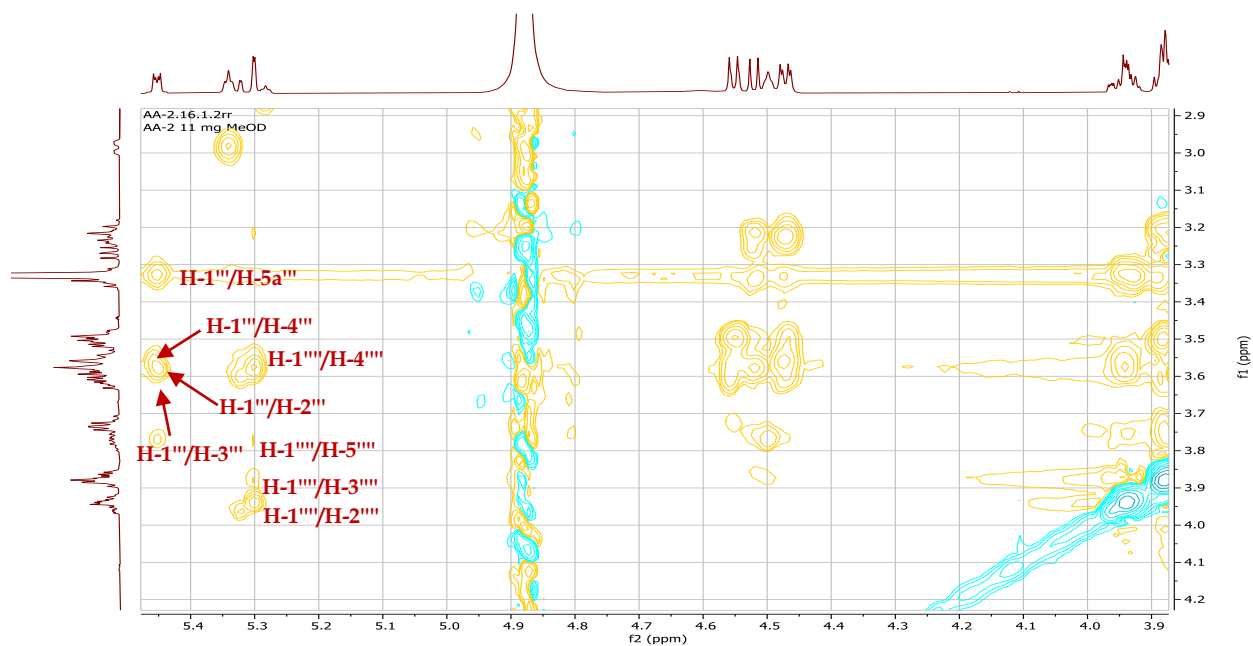
Figure. IV. 187: TOCSY spectrum (600 MHz, CD₃OD) of β-D-xylose I and α-L-rhamnose of compound **R2.**
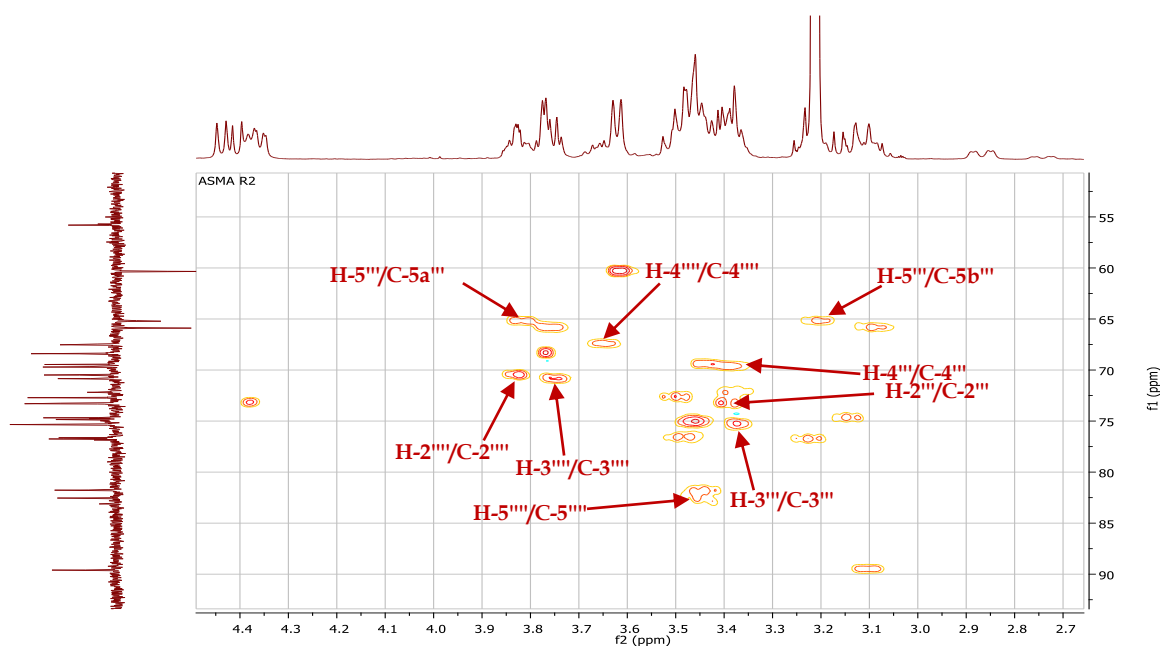
Figure. IV. 188: HSQC spectrum (400 MHz, CD$_3$OD) of β-D-xylose I and α-L-rhamnose of the compound **R2**.

Starting from the anomeric proton H-1'''' resonating at 4.41 (d, J = 7.6 Hz, 1H), COSY (**Figure. IV. 189**) and TOCSY (**Figure. IV. 190**) spectra shows a spin system of six protons corresponding to pentose residue, the H-2'''' resonating at δ$_H$ 3.15 (dd, J = 9.2, 7.6 Hz), correlates with H-3'''' δ$_H$ 3.23 (m). The proton H-4'''' resonating at δ$_H$ 3.40 correlates with two protons of H$_2$-5'''' at δ$_H$ 3.76 (dd, J = 11.1, 4.1 Hz, 1H) H-5''''a and at δ$_H$ 3.08 (m) H-5''''b. The corresponding carbons assigned using HSQC experiments (**Figure. IV. 191**) as summarized in the **Table. IV. 12**. According to the analysis of mentioned spectrum this pentose identified that it is a β-D-xylose.
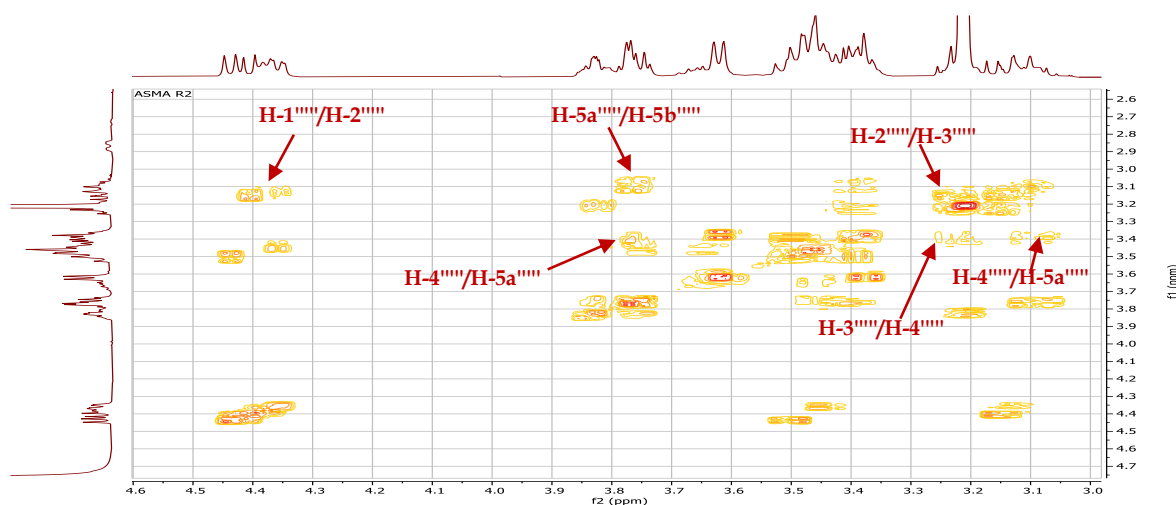
Figure. IV. 189: COSY spectrum (400 MHz, CD$_3$OD) of β-D-xylose II of **R2**.
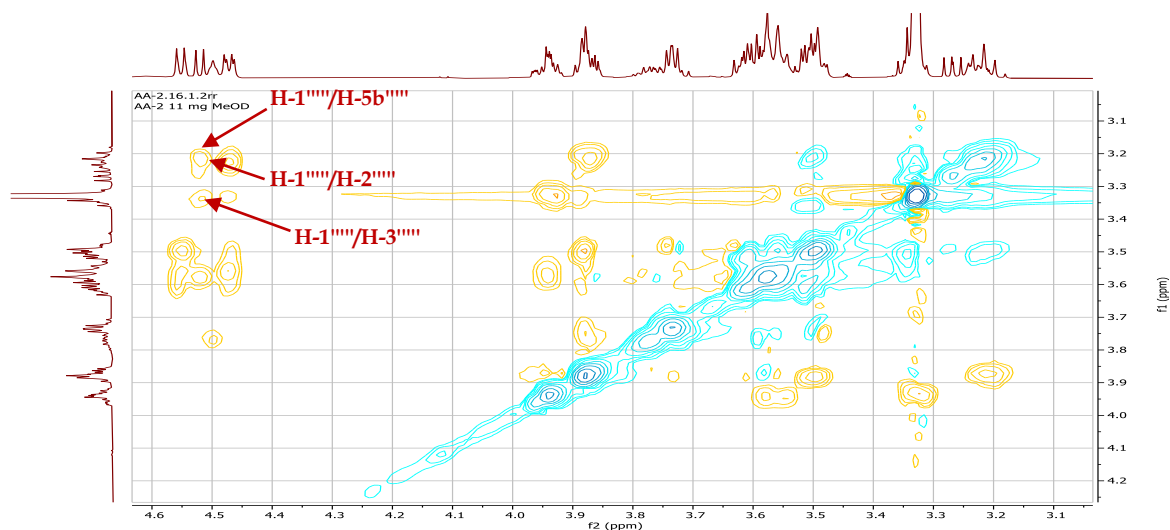
Figure. IV. 190: TOCSY spectrum (600 MHz, CD₃OD) of β-D-xylose II of **R2**.
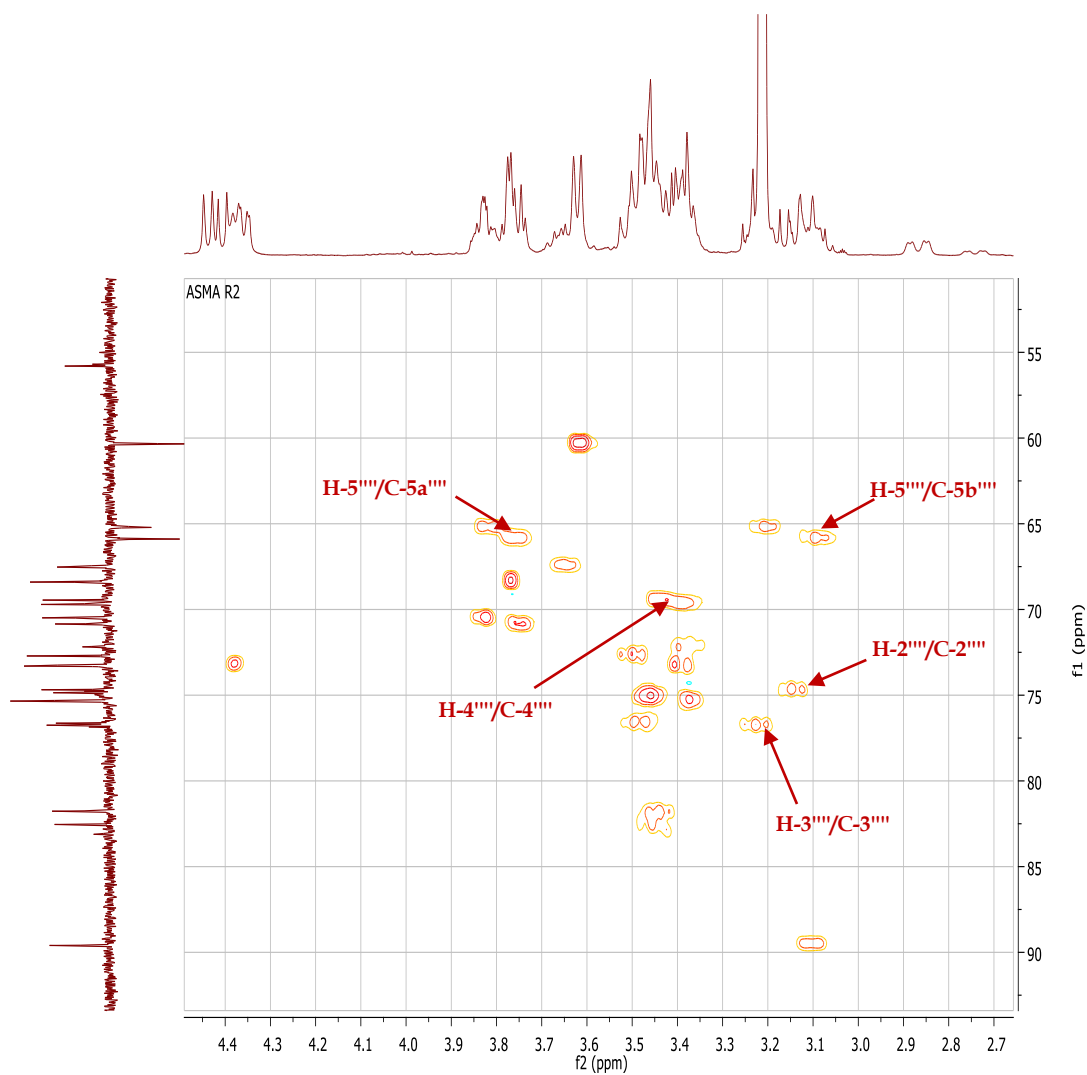
Figure. IV. 191: HSQC spectrum (400 MHz, CD₃OD) of β-D-xylose II of the compound **R2**.

The sequence and the linkage of the trisaccharide chain were deduced from the HMBC experiment (**Figure. IV. 192**), which showed long-range correlations between H-1''''' of xylose II and C-4'''' of rhamnose (δ_C 82.54), H-1'''' of rhamnose and C-2''' of xylose I and of the C-28 of the aglycon (δ_C 179.09).

Comparison of ^{13}C NMR data of **R2** with those of **R1** indicated that **R1** and **R2** possessed the same trisaccharide moiety at C-28, [β-D-xylopyranosyl-(1'''''→4'''')-α-L-rhamnopyranosyl-(1''''→2''') -β-D- xylopyranosyl].
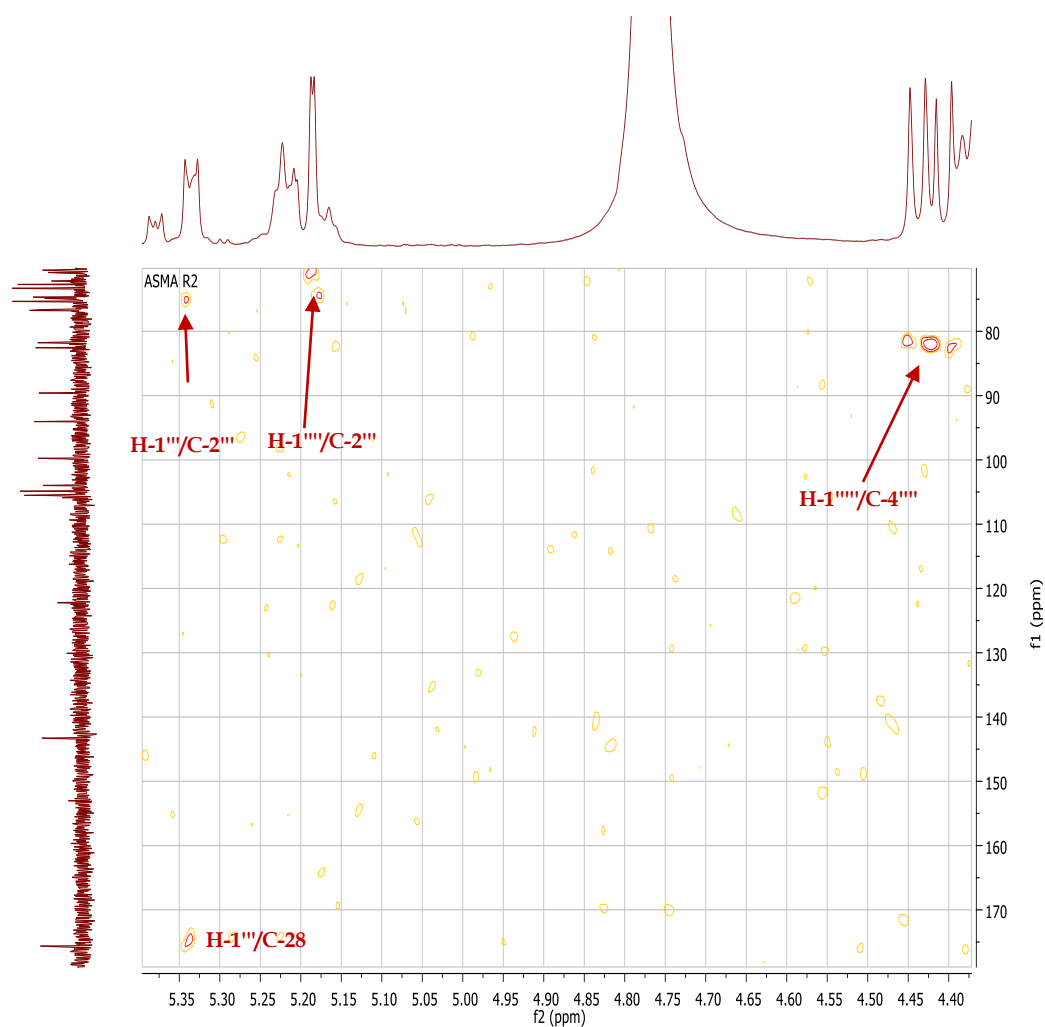
Figure. IV. 192: HMBC spectrum (400 MHz, CD₃OD) of correlations between H-1''''' and C-4'''' of rhamnose, H-1'''' and C-2''' of xylose I and between H-1''' and C-28 of compound **R2**.

According to the analysis of all spectrum the compound **R2** could be identified as echinocystic acid 3-*O*-β-D-galactopyranosyl-(1"→2')- [β-D-β-D-glucuronopyranosyl-28-O-[β-D-xylopyranosyl-(1"""→4"")-α-L-rhamnopyranosyl-(1""→2"')-β-D-xylopyranosyl] (**Figure. IV. 193**).
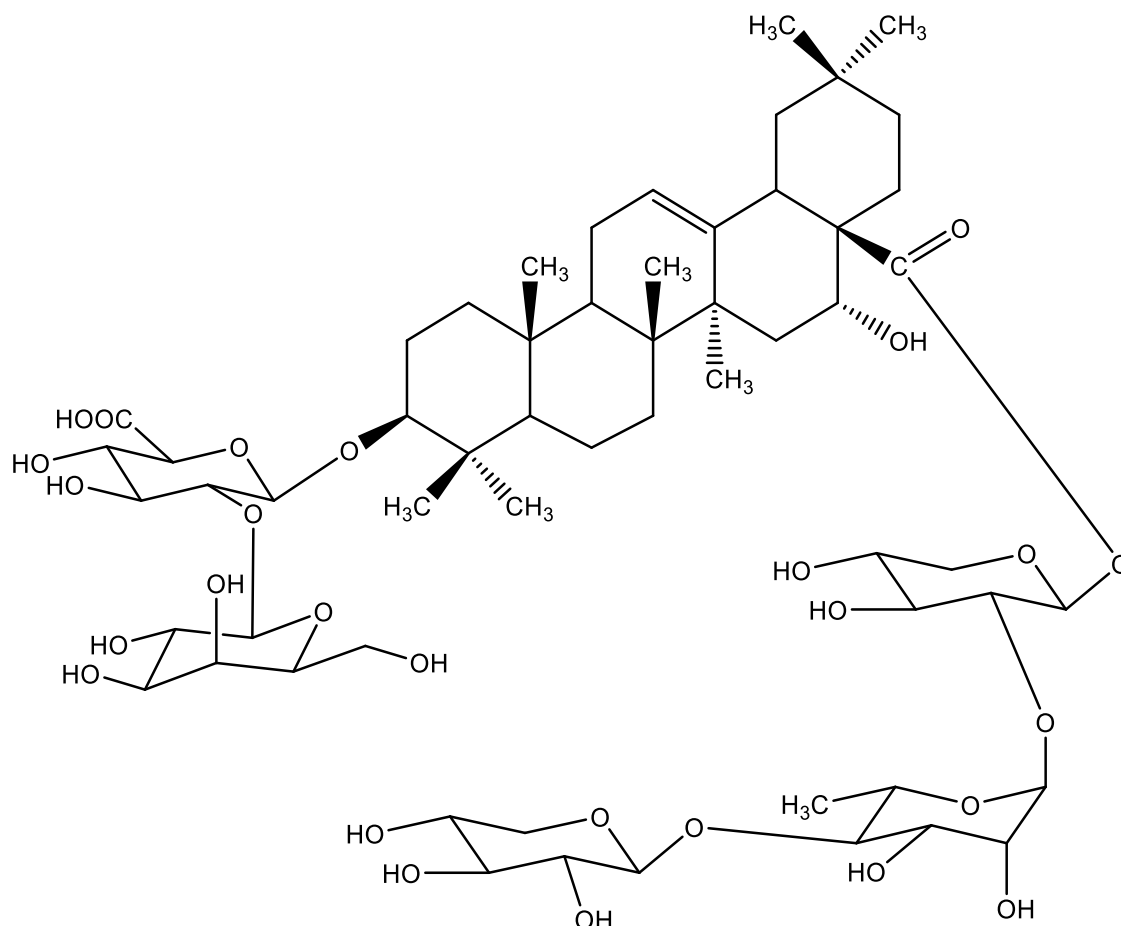
Figure. IV. 193: Structure of compound **R2**; echinocystic acid 3-O-β-D-galactopyranosyl-(1"→2')-β-D-glucuronopyranosyl-28-O-[β-D-xylopyranosyl-(1"""→4"")-α-L-rhamnopyranosyl-(1""→2"') -β-D-xylopyranosyl].

The ^{1}H and ^{13}C NMR data, are summarized in the **Table. IV. 12**, the aglycon parts is in total agreement with that of bidesmosidic echinocystic acid [217, 218]. Also, the osidic part at C-28 and at C-3 are in total agreement with the literature [52]. The compound **R2** is a new compound.

Table. IV. 12: Chemical shifts ^1H NMR (400 and 600 MHz) and ^{13}C NMR (100 and 150 MHz) (da in ppm, J in Hz) of compound **R2** (δ_C in ppm and δ_H in ppm and J in Hz).

Position	Carbon	Proton
1	38.58	1.50 (m) H-1a
		0.9 (m) H-1b
2	25.63	1.92 (m) H-2a
		1.59 (m) H-2b
3	89.30	3.10 (dd, J= 12.4, 3.8Hz, 1H)
4	39.32	--
5	55.80	0.77 (m)
6	18.08	1.47 (m) H-6a
		1.28 (m) H-6b
7	32.87	1.44 (m, 2H)
8	39.40	--
9	46.72	1.52 (m)
10	36.46	--
11	23.09	1.78 (m, 2H)
12	122.22	5.22 (t, J= 3.5 Hz, 1H)
13	143.29	--
14	41.31	--
15	35.09	1.34 (m) H-15b
		1.58 (m) H-15a
16	73.25	4.37 (m)
17	48.80	--
18	40.81	2.86 (dd, J= 14.3, 3.9Hz, 1H)
19	46.51	2.18 (t, 13.6Hz, 1H) H-19a
		0.95 (m) H-19b
20	29.92	--
21	35.13	1.83 (m) H-21a
		1.05 (m) H-21b
22	30.65	1.64 (m) H-22b
		1.80 (m) H-22a

23	27.20	0.97 (S, 3H)
24	15.65	0.77 (S, 3H)
25	14.81	0.86 (S, 3H)
26	16.39	0.66 (S, 3H)
27	25.67	1.27 (S, 3H)
28	175.63	--
29	31.95	0.78 (S, 3H)
30	23.48	0.84 (S, 3H)
3-O-1'-β-D-glucoronic acid	103.98	4.36 (d, J= 7.6Hz, 1H)
2'	81.76	3.45 (m)
3'	76.63	3.48 (m)
4'	72.71	3.53 (m)
5'	75.35	3.37 (m)
6'	175.63	--
2'-O-1''- β-D-galactose	104.87	4.44 (d, J=7.6Hz, 1H)
2''	75.35	3.48 (m)
3''	73.25	3.39 (m)
4''	68.40	3.77 (brd, J = 2.7 Hz, 1H)
5''	72.18	3.38 (brs, 1H)
6''	60.34	3.62 (m, 2H)
28-O-1'''-Xylose	94.04	5.33 (d, J = 6.2 Hz, 1H)
2'''	74.85	3.46 (m)
3'''	75.31	3.47 (m)
4'''	69.46	3.39 (m)
5'''	65.22	3.20 (m)
		3.81 (m)
2'''-O-1''''-Rhamnose	99.76	5.18 (d, J=1.5 Hz, 1H)
2''''	70.49	3.83 (dd, J = 3.2, 1.5 Hz, 1H)
3''''	70.85	3.74 (dd, J = 9.2, 3.2 Hz, 1H)
4''''	82.54	3.46 (m)
5''''	67.53	3.65 (m)
6''''	16.91	1.23 (d, J = 6.2 Hz, 3H)

4''''O-1'''''-Xylose	105.52	4.41 (d, J= 7.7 Hz, 1H)
2'''''	74.68	3.15 (dd, J = 9.2, 7.6 Hz)
3'''''	76.75	3.23 (m)
4'''''	69.71	3.40 (m)
5'''''	65.89	3.08 (m) H-5'''''b
		3.76 (dd, J = 11.1, 4.1 Hz, 1H) H-5'''''a

IV.4. 11. Compound R3

The mass spectrum of compound R3 (**Figure. IV. 194**) obtained in negative mode by ESI-MS soft ionization, shows a pseudo-molecular ion peak at m/z 1087.5 [M-H]⁻, i.e., a molecular mass of 1088.5 corresponding to a molecular formula $C_{53}H_{84}O_{23}$.
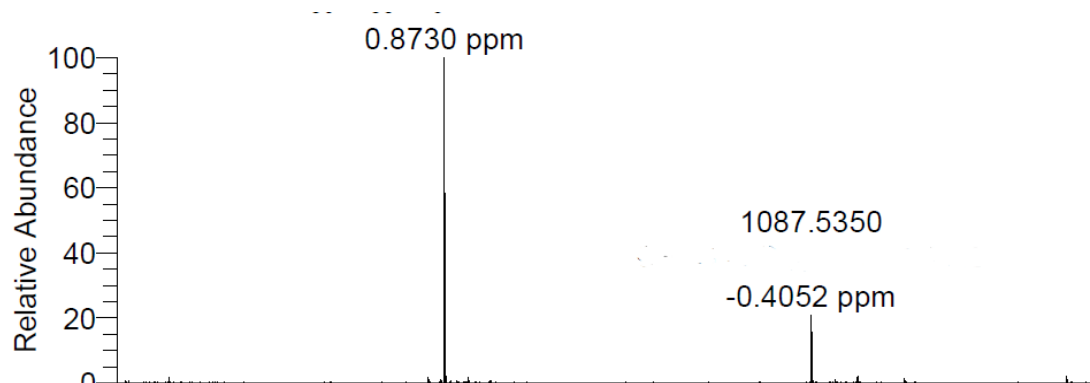
Figure. IV. 194: ESI-MS of compound **R3,** recorded in negative mode.

Compound **R3** is isolated also in the form of a white powder soluble in methanol. It is characterized on TLC test by invisible spot under UV lamp (254 and 366 nm) which turns pink by revelation using acid solution and heating. The ^{1}H NMR spectrum (**Figure. IV. 194**) recorded in CD$_3$OD, reveals seven methyl groups, a characteristic of triterpene skeleton.

The ^{1}H NMR spectrum (**Figure. IV. 195**) of compound **R3** exhibits that this compound is present as two isomers with a (1:1) ratio, we could deduce that by the duplicate peaks in the ^{1}H NMR spectrum. The results of ^{1}H and J-modulated ^{13}C NMR spectra summarized in the **Table. IV. 13** , determined according to the analysis of HSQC, HMBC and COSY spectra, it may deduce that the aglycon parts of one of

isomers of the compound **R3** is an echinocystic acid, the results are in total agreement with the data of compounds **R1** and **R2**.

The aglycon part

The ^{1}H NMR spectrum shows proton signals resonating between 0.9 and 2.18 ppm, corresponding to protons CH and CH$_2$ groups of a triterpene skeleton, other characteristic proton signals are present in this spectrum:

❖ Seven methyl groups resonating between 0.67 and 1.27 ppm, in the singlet form with integrating of three protons for each, (S, 3H).

❖ One olefinic proton at δ_H 5.21 (t, J = 3.5 Hz, 1H), assigned to H-12 of the triterpene pentacyclic.

❖ Two oxygenated methine protons resonating at δ_H 3.11 (dd, J= 12.4, 3.8 Hz, 1H) and δ_H 4.37 (t, J = 3.4 Hz) assigned to H-3 and H-16, respectively.

❖ A signal in the form of a double doublet at δ_H 2.87 (dd, J = 14.3, 3.9 Hz, 1H) corresponding to H-18, its multiplicity indicates the presence of two adjacent protons and the coupling constant assigned the β orientation H-18.
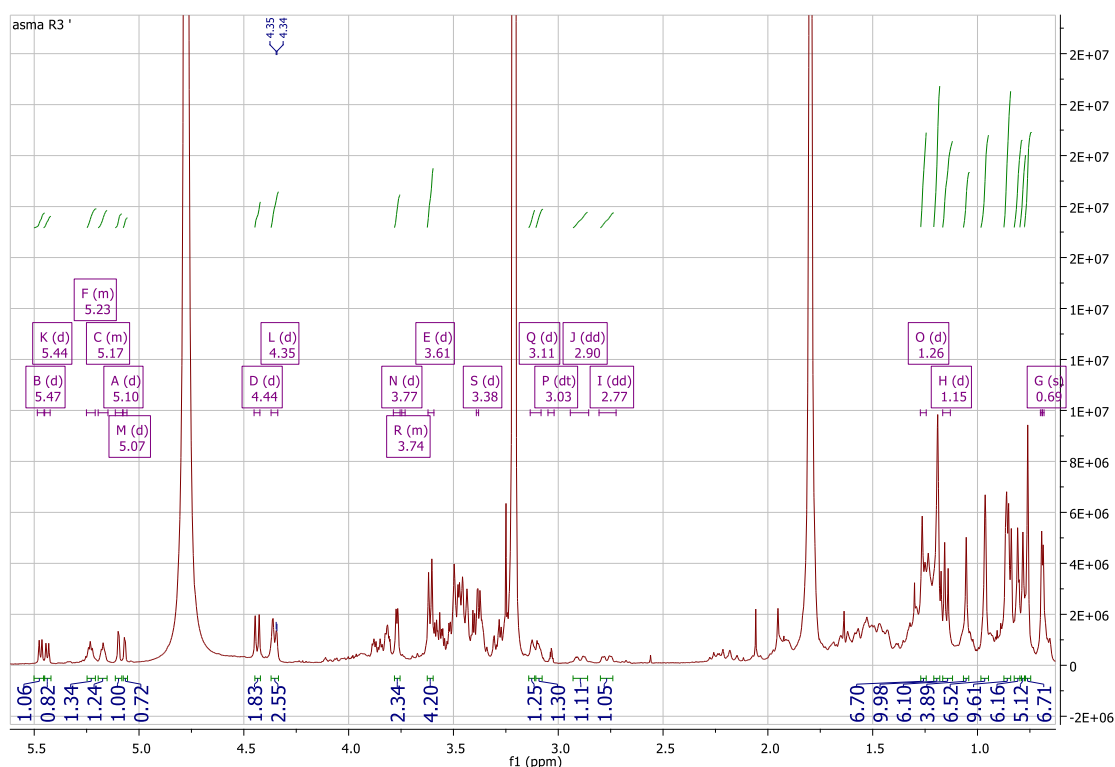
Figure. IV. 195: ^{1}H NMR spectrum (400 MHz, CD$_3$OD) of the compound **R3**.

The J-modulated ^{13}C NMR spectrum (**Figure. IV. 196**) showed signals were assigned to the aglycon moiety (triterpene pentacyclic), these signals were distributed as follows:

- ❖ Seven tertiary methyl (CH$_3$) groups resonating between δ_C 14 and 32.
- ❖ A carbon signals resonating between δ_C 18 and 55.80, attributable to CH, CH$_2$ and quaternary carbons (C).
- ❖ Two olefinic carbons at δ_C 122.22 and 143.29, were characteristic to an olean-12-ene skeleton.
- ❖ Two oxygenated carbons at δ_C 73.25, attributable to a free hydroxy group C-16 and at δ_C 89.60, corresponding to C-3. The deshielding effect observed in this position compared to the same carbon with hydroxyl group indicated that C-3 is liked with sugar unit.
- ❖ Carbonyl group observed at δ_C 175.63.
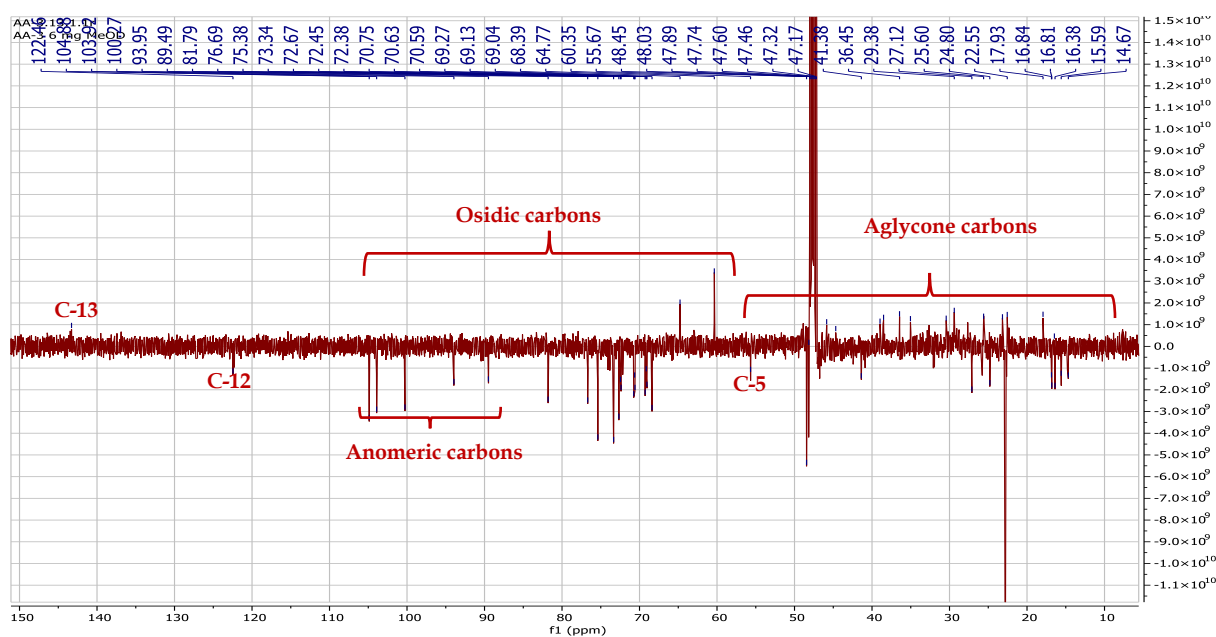
Figure. IV. 196: J-modulated ^{13}C NMR spectrum (600 MHz, CD$_3$OD) of compound **R3**.

Osidic part:

The J-modulated ^{13}C NMR spectrum displays the presence of four anomeric carbons resonating at δ_C 94.00 (C-1'''), 100.27 (C-1''''), 103.92 (C-1') and 104.87 (C-1'') ppm, their corresponding protons assigned by HSQC spectrum (**Figure. IV. 197**) δ_H 5.47, 5.10, 4.35 and 4.44, respectively.
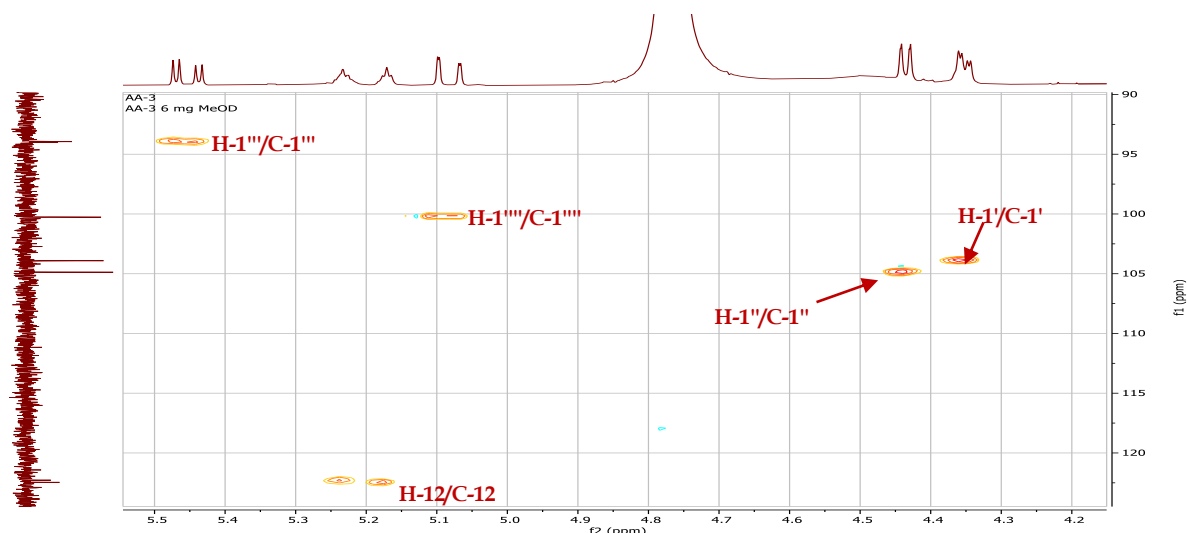
Figure. IV. 197: HSQC spectrum (600 MHz, CD$_3$OD) of anomeric parts of **R3**.

The analysis of COSY (**Figure. IV. 198**) and TOCSY (**Figure. IV. 199**) spectra, make it possible to identify the first spins system of five protons from the anomeric proton H-1' (δ_H 4.35) correlates with the osidic proton H-2' at δ_H 3.45 (m). The H-3' resonating at δ_H 3.48 (m) correlates with H-4' δ_H 3.51 (m). This last correlates with H-5' at δ_H 3.39 (m). The HMBC spectrum (**Figure. IV. 202**) reveals correlations between the osidic protons H-4' and H-5' and carbonyl carbon resonating at 175.63, which confirms that this hexose identified as β-D-glucoronic acid by comparing the chemical shifts with those of the compound **R2**. The chemical shifts of the corresponding carbons of the identified protons of β-D-glucuronic acid are attributed by the analysis of the HSQC spectrum (**Figure. IV. 200**).

The analysis of COSY (**Figure. IV. 198**) and TOCSY (**Figure. IV. 199**) spectra make it possible to identify the second spins system corresponding to hexose, starting from the anomeric proton H-1" resonating at δ_H 4.44 (d, J=7.6 Hz, 1H). The proton H-2" δ_H 3.51 (brd, J = 7.1 Hz, 1H) shows correlations with H-3" resonating at δ_H 3.40 (brd, J = 3.4 Hz, 1H). This last exhibits correlations with H-4" δ_H 3.77 (brd, J = 3.1 Hz, 1H). The H-5" δ_H 3.38 (m) correlate with proton resonating at δ_H 3.61 (m, 2H) corresponding to the protons of H-6". The low value of the coupling constant of the proton H-4" (d, J = 3.1 Hz, 1H) indicates that it is in the equatorial position. According to these results, this hexose is identified as β-D-galactose. The corresponding carbons of the identified protons assigned in the help of HSQC spectrum (**Figure. IV. 200**).
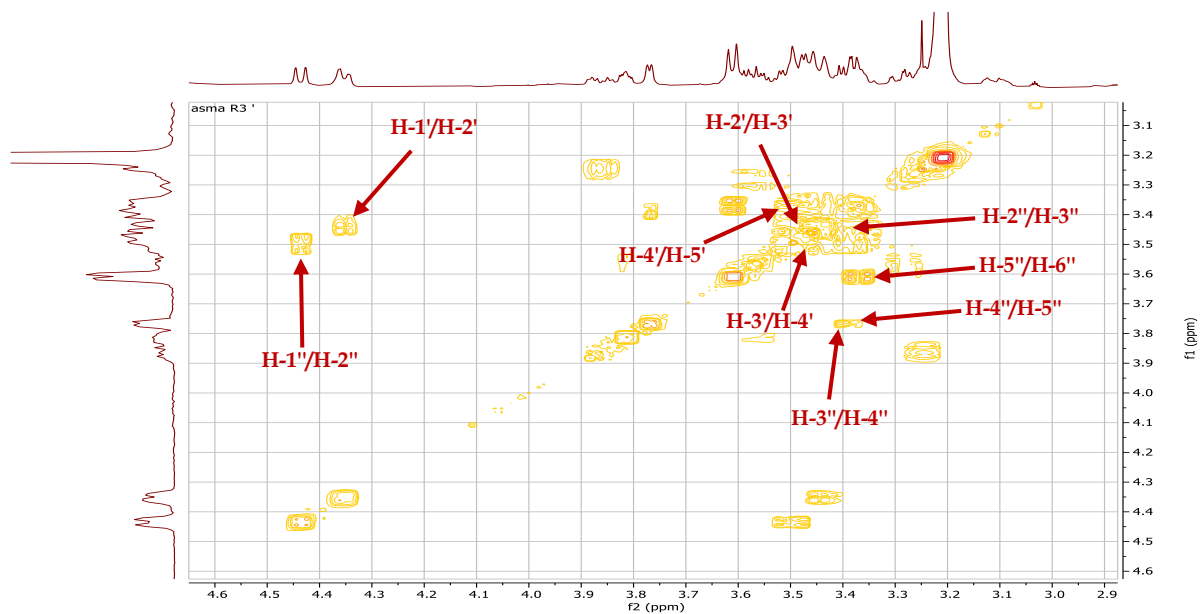
Figure. IV. 198: COSY spectrum (400 MHz, CD₃OD) of the β-D-glucoronic acid and β-D-galactose of **R3.**
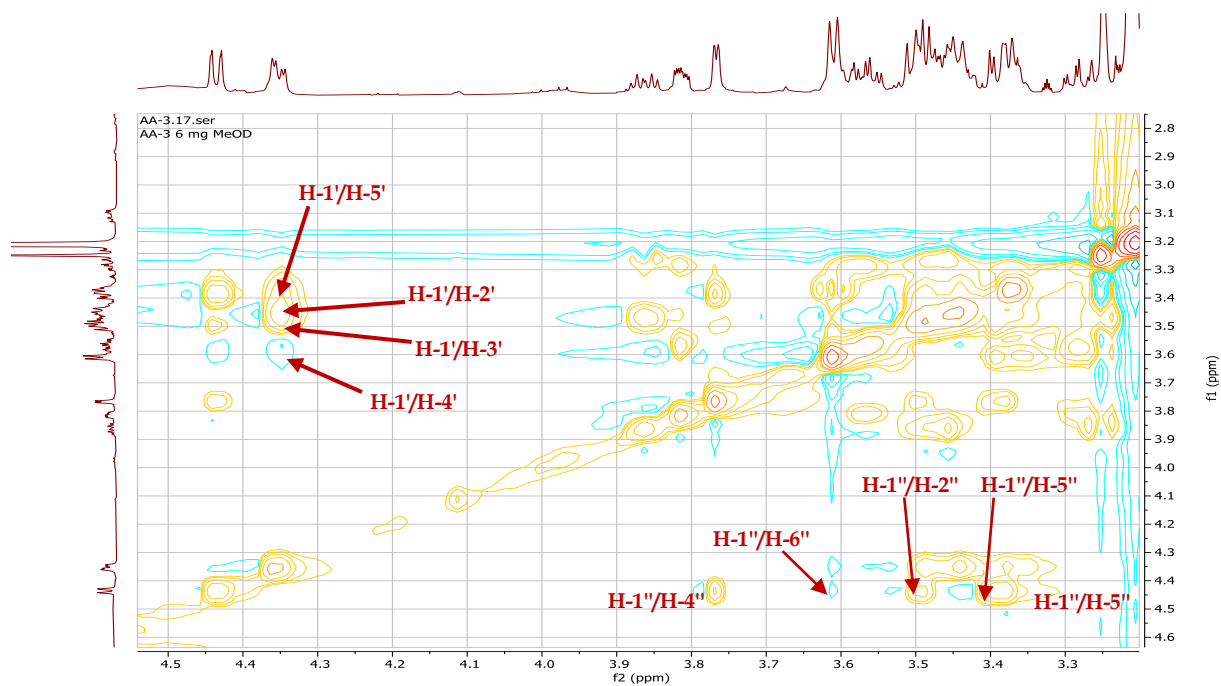
Figure. IV. 199: TOCSY spectrum (600 MHz, CD₃OD) of the β-D-glucoronic acid and β-D-galactose of **R3.**
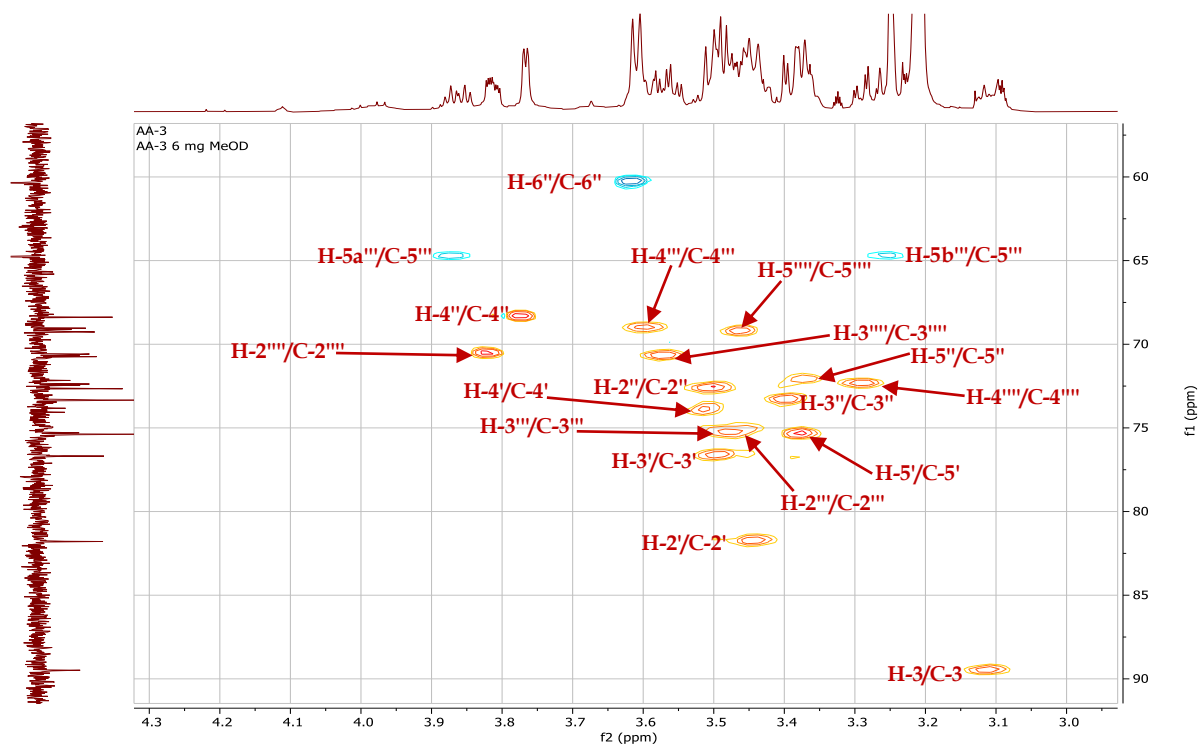
Figure. IV. 200: HSQC spectrum (600 MHz, CD$_3$OD) of osidic parts compound **R3**.

The linkage of the terminal β-D-galactose at C-2' of the glucoronic acid was indicated by the correlation between H-1" of the galactose and C-2' of in the HMBC spectrum. This may be confirmed by the deshielding effect observed on C-2' to 81.79 ppm, comparing with ^{13}C chemical shift with those of glucoronic acid, showed glycosylation shift of C-2' by 7.8 ppm indicate that the C-2' is site of glycosylation (**Figure. IV. 201**). Also, the HMBC spectrum (**Figure. IV. 202**) show cross-peak between H-1' (4.35 ppm) of glucoronic acid and C-3 (89.55 ppm) of aglycon moiety.
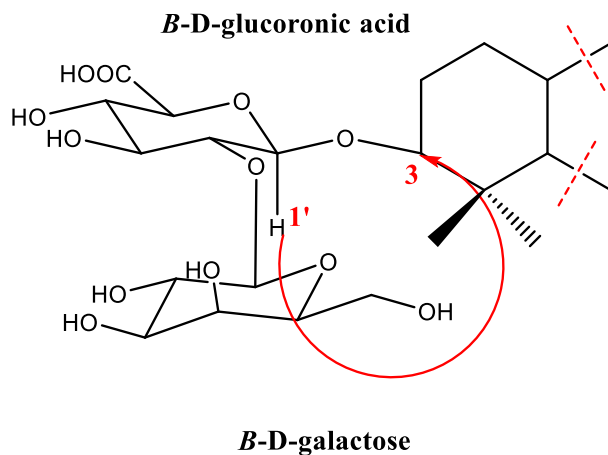
Figure. IV. 201: HMBC correlations between H-1" of galactose and C-2' of compound **R3**.
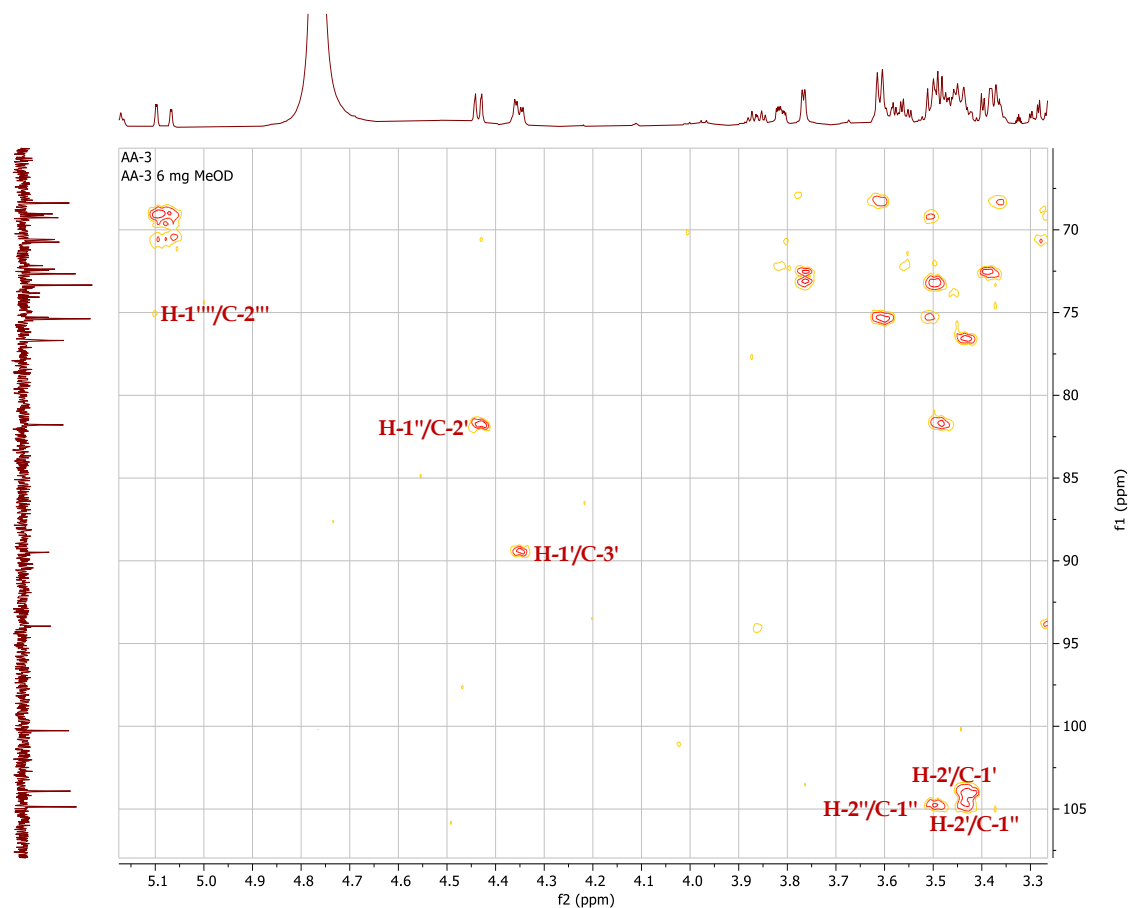
Figure. IV. 202: HMBC spectrum (600 MHz, CD$_3$OD) of glycosidic part at C-3 of **R3**.

From the third anomeric proton H-1''' resonating at δ_H 5.47 (d, J = 5.4 Hz, 1H), the COSY (**Figure. IV. 203**) and TOCSY (**Figure. IV. 204**) spectra displays a spin system of six protons corresponding to a pentose. The proton H-2''' δ_H 3.49 (m) correlates with H-3''' which resonating at δ_H 3.50 (m). The proton H-4''' resonating at correlates with two proton δ_H 3.87 (dd, J = 11.7, 4.7 Hz, 1H) and 3.25 (m), corresponding to H-5'''a and H-5'''b, respectively. The HSQC spectrum (**Figure. IV. 199**) make it possible to the corresponding protons of this pentose. According to these results this pentose identified that it is β-D-xylose.

Also, COSY (**Figure. IV. 203**) and TOCSY (**Figure. IV. 204**) spectra reveals a spin system of eight protons corresponding to a hexose, starting from the anomeric proton H-1'''' that resonating at δ_H 5.10 (d, J=1.5 Hz, 1H). The proton H-2'''' δ_H 3.82 (dd, J = 3.4, 1.7 Hz, 1H) correlates with H-3'''' at δ_H 3.57 (dd, J = 9.2, 3.4 Hz, 1H). The osidic proton H-4'''' δ_H 3.29 (m) correlates with H-5'''' δ_H 3.59 (m), this last shows also correlations with protons corresponding to methyl group H$_3$-6'''' resonating of at δ_H 1.15 (d, J = 6.2 Hz, 3H). The large coupling constant J = 9.2 Hz indicates that the H-3'''' and

H-4"" protons are in the trans-diaxial positions. The corresponding carbons of the identified protons assigned using HSQC spectrum (**Figure. IV. 200**). According to this analysis the hexose identified as α-L-rhamnose.
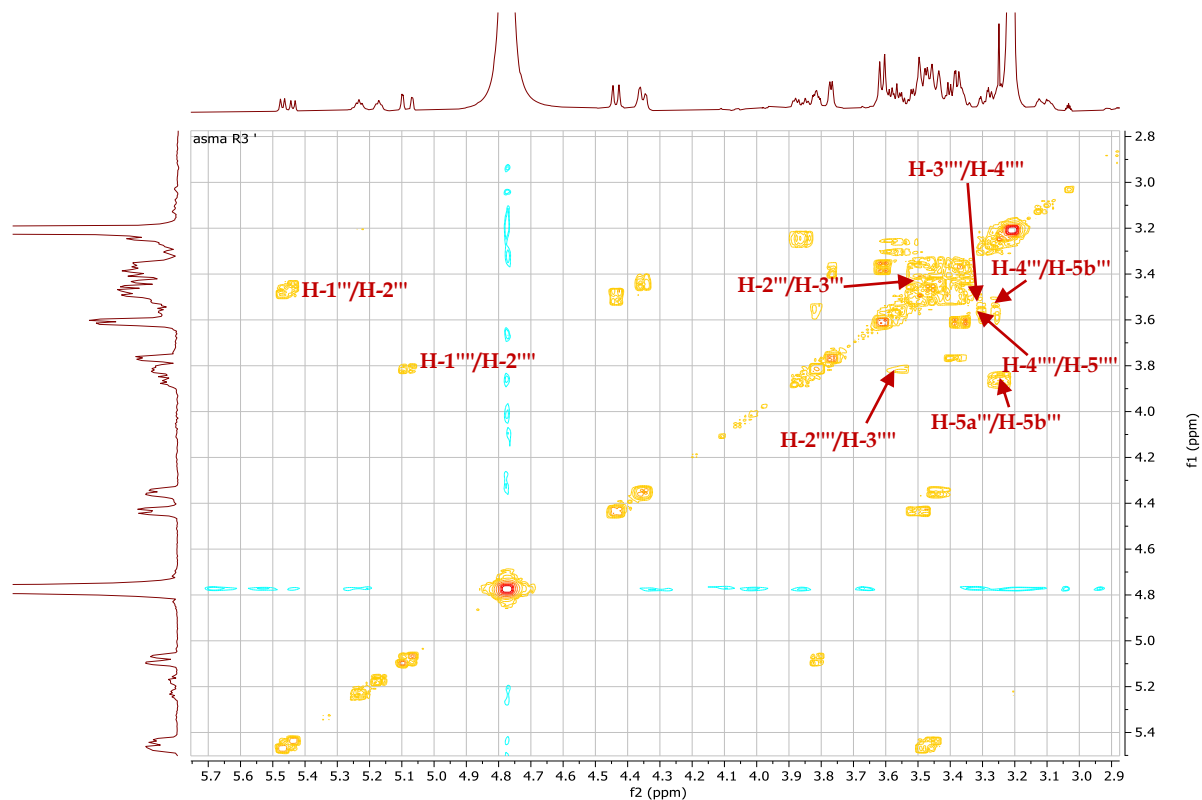
Figure. IV. 203: COSY spectrum (400 MHz, CD$_3$OD) of β-D-xylose and α-L-rhamnose of the compound **R3**.
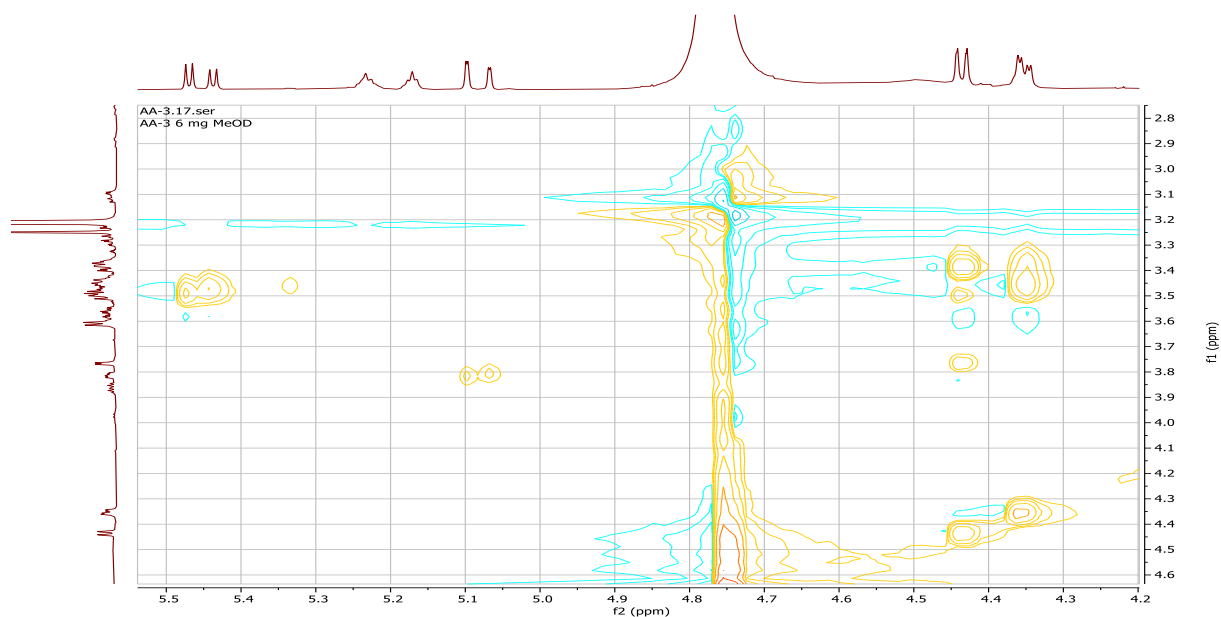
Figure. IV. 204: TOCSY spectrum (600 MHz, CD$_3$OD) of β-D-xylose and α-L-rhamnose of **R3**.

By comparing the results of **R3** and of **R1** and **R2** at C-28, the absence of the anomeric proton and the characteristic peaks of the second β-D-xylose, and the shielded effect observed in C-4'''' of α-L-rhamnose, confirms that the difference between them in the position C-28 was the absence of the second xylose (**Figure. IV. 205**).
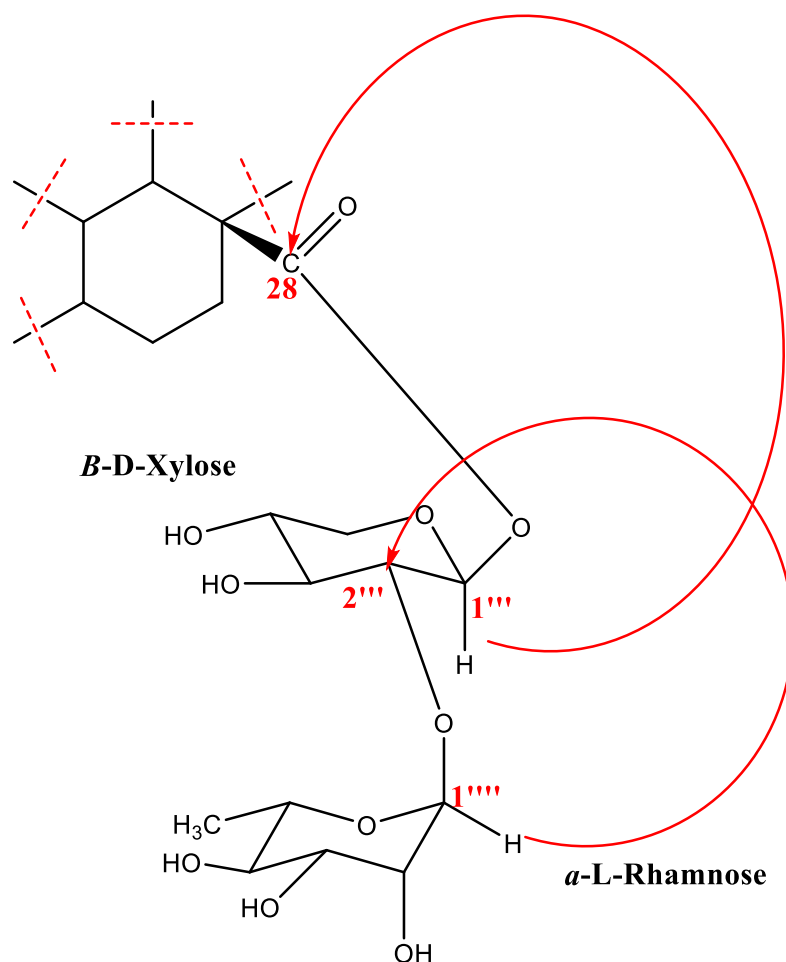
Figure. IV. 205: HMBC correlation between of β-D-xylose and α-L-rhamnose of et C-28 of **R3**.

According to the analysis of all spectrum the compound **R3** could be identified as echinocystic acid 3-*O*-β-D-galactopyranosyl-(1"→2')- [β-D-β-D-glucuronopyranosyl-28-O-[α-L-rhamnopyranosyl-(1''''→2''')-β-D-xylopyranosyl] (**Figure. IV. 206**).

We have tried to verify all the spectra of the compound **R3**, firstly we have excluded the possibility of an α and β amyrin isomers by the absence of characteristic peaks of β amyrin. After that we have checked the stereochemistry of chiral carbons of the positions 3 (α/β), 16 (α/β) and H-18. We have not found the precise position that explained the difference between the peaks of two isomers. It is impossible to separate these two isomers by classical methods except by using accurate HPLC techniques.
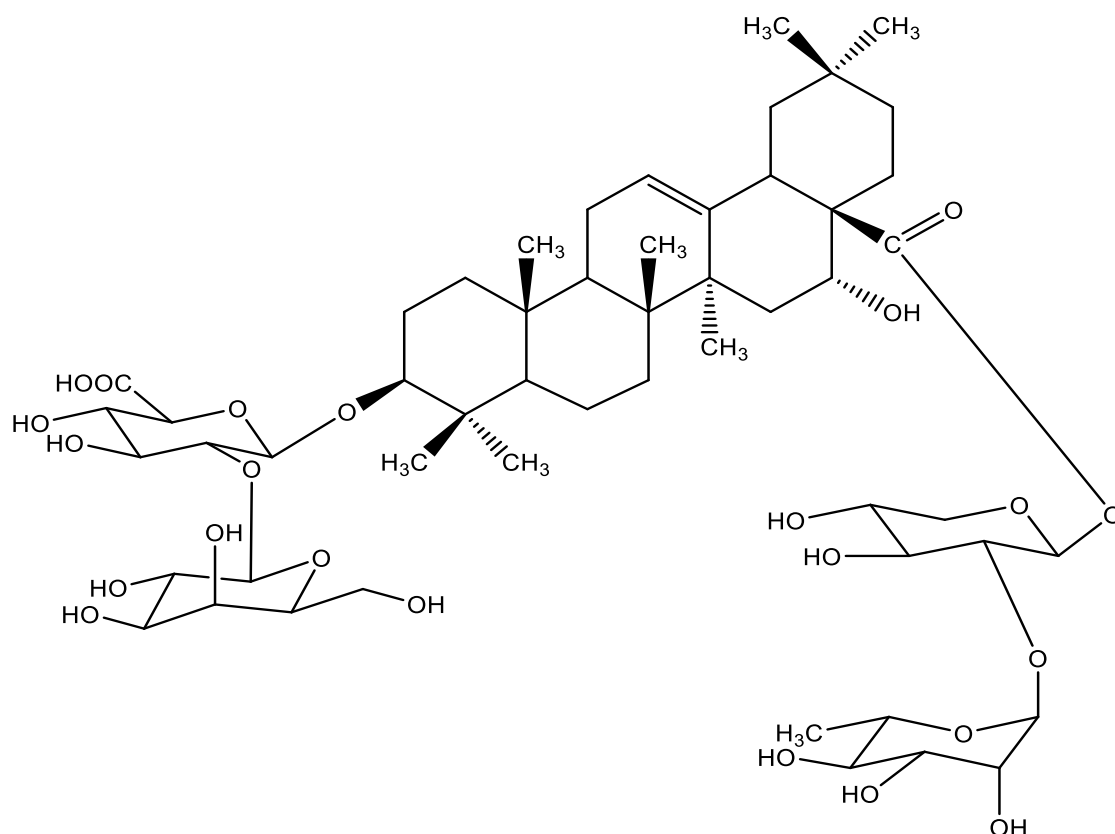
Figure. IV. 206: Structure of compound **R3**; echinocystic acid 3-O-β-D-galactopyranosyl-(1"→2')-β-D-glucuronopyranosyl-28-O-[α-L-rhamnopyranosyl-(1''''→2''') -β-D-xylopyranosyl].

The ^{1}H and ^{13}C NMR data, are summarized in the **Table. IV. 13**, which are in total agreement with the literature of bidesmosidic echinocystic acid [217, 218]. This compound is a new compound.

Table. IV. 13: Chemical shifts ^{1}H NMR (400 and 600 MHz) and ^{13}C NMR (100 and 150 MHz) of compound **R3** (δ_C in ppm and δ_H in ppm and J in Hz).

Position	Carbon	Proton
1	38.54	1.50 (m) H-1a
		0.9 (m) H-1b
2	25.63	1.93 (m) H-2a
		1.61 (m) H-2b
3	89.55	3.11 (dd, J= 12.4, 3.8Hz, 1H)
4	39.27	--
5	55.80	0.66 (m)

6	17.81	1.47 (m) H-6a
		1.29 (m) H-6b
7	32.86	1.42 (m) H-7a
		1.30 (m) H-7b
8	39.40	--
9	46.80	1.52 (m)
10	36.46	--
11	22.97	1.77 (m, 2H)
12	122.22	5.16 (t, J= 3.6 Hz, 1H)
13	143.66	--
14	41.31	--
15	34.37	1.52 (m) H-16a
		1.29 (m) H-16b
16	73.25	4.37 (t, J = 3.4 Hz)
17	48.80	--
18	40.73	2.91 (dd, J = 14.3, 4.0 Hz, 1H)
19	46.30	2.17 (m) H-19a
		0.96 (m) H-19a
20	29.92	--
21	35.00	1.85 (m) H-21a
		1.05 (m) H-21b
22	30.19	1.81 (m) H-22a
		1.65 (m) H-22b
23	27.15	0.96 (S, 3H)
24	15.64	0.75 (S, 3H)
25	14.82	0.85 (S, 3H)
26	16.37	0.68 (S, 3H)
27	25.71	1.26 (S, 3H)
28	175.63	--
29	32.01	0.79 (S, 3H)
30	23.54	0.85 (S, 3H)
3-O-1'-β-D-glucoronic acid	103.92	4.35 (d, J=7.5 Hz, 1H)
2'	81.79	3.45 (m)

3'	76.69	3.48 (m)
4'	73.66	3.51 (m)
5'	75.38	3.39 (m)
6'	175.63	--
2'-O-1''- β-D-galactose	104.87	4.44 (d, J=7.6 Hz, 1H)
2''	72.66	3.51 (brd, J = 7.1 Hz, 1H)
3''	73.34	3.40 (brd, J = 3.4 Hz, 1H)
4''	68.38	3.77 (brd, J = 3.1 Hz, 1H)
5''	72.16	3.38 (m)
6''	60.34	3.61 (m, 2H)
28-O-1'''-Xylose	94.00	5.47 (d, J = 5.4 Hz, 1H)
2'''	75.38	3.49 (m)
3'''	75.41	3.50 (m)
4'''	69.27	3.46 (m)
5'''	64.77	3.25 (m) H-5'''b 3.87 (dd, J = 11.7, 4.7 Hz, 1H) H-5'''a
2'''-O-1''''-Rhamnose	100.27	5.10 (d, J=1.5 Hz, 1H)
2''''	70.58	3.82 (dd, J = 3.4, 1.7 Hz, 1H)
3''''	70.74	3.57 (dd, J = 9.2, 3.4 Hz, 1H)
4''''	72.38	3.29 (m)
5''''	69.04	3.49 (m)
6''''	16.80	1.15 (d, J = 6.2 Hz, 3H)

IV.4. 12. Compound V4

Compound **V4** is isolated in the form of a white powder soluble in methanol. This compound is characterized on TLC test by dark spot under UV lamp (254 and 366 nm), which turns purple by revelation using acid solution and heating.

The ^{1}H NMR spectrum (**Figure. IV. 208**) shows the presence of aromatic protons resonating at δ_H 7.41 (d, J = 7.3Hz, 2H), 7.30 (t, J = 7.3 Hz, 2H) and 7.23 (d, J = 7.3 Hz, 1H), a typical of a monosubstituted benzene ring assignable to H-2,6, H-3,5 and H-4 respectively. This spectrum also reveals the presence of osidic protons resonating between δ_H 3.23 and 3.89, with an anomeric proton at δ 4.38 (d, J = 7.8 Hz, 1H).

The aglycon part

^{1}H NMR spectrum (**Figure. IV. 207**) displays the presence of two protons resonating at δ_H 6.69 (d, J = 16.0 Hz, 1H) and at δ_H 6.37 (ddd, J = 16.0, 6.6, 5.9 Hz, 1H), which suggested the presence of a trans-olefinic double bond, which confirmed by their large coupling constant value J = 16.0 Hz. The ^{1}H NMR spectrum also shows the presence two signals resonating at δ_H 4.52 (dd, J = 5.9, 1.5 Hz, 1H) and δ_H 4.31 (dd, J = 6.6, 1.5 Hz, 1H).
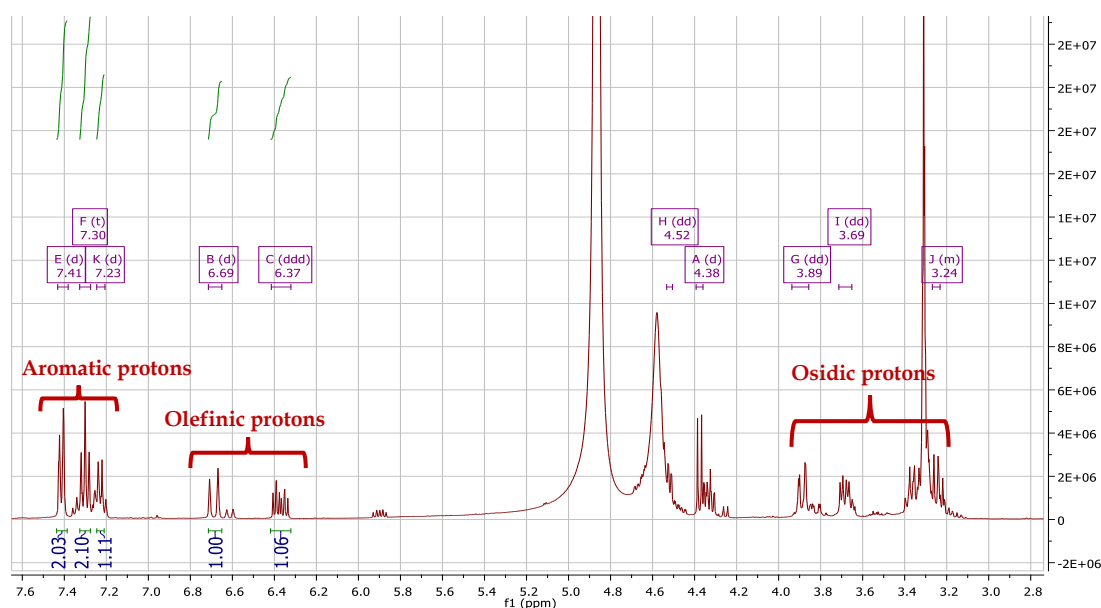
Figure. IV. 207: ^{1}H NMR spectrum (400 MHz, CD$_3$OD) of the compound **V4**.

Figure. IV. 208: ^{1}H NMR spectrum (400 MHz, CD$_3$OD) of aromatic and olefinic part of **V4.**

^{13}C NMR (**Figure. IV. 209**) and DEPT135 (**Figure. IV. 210**) spectra reveals the presence of aromatic carbons resonating between δ_C 126 and 136. The ^{13}C NMR spectrum exhibits two signals at δ_C 132.46 and 125.27, confirmed the presence of a trans-olefinic double bond.

^{13}C NMR and DEPT135 confirms our suggestion of the presence of an oxygenated methylene group (CH$_2$) resonating at δ_C 69.41.
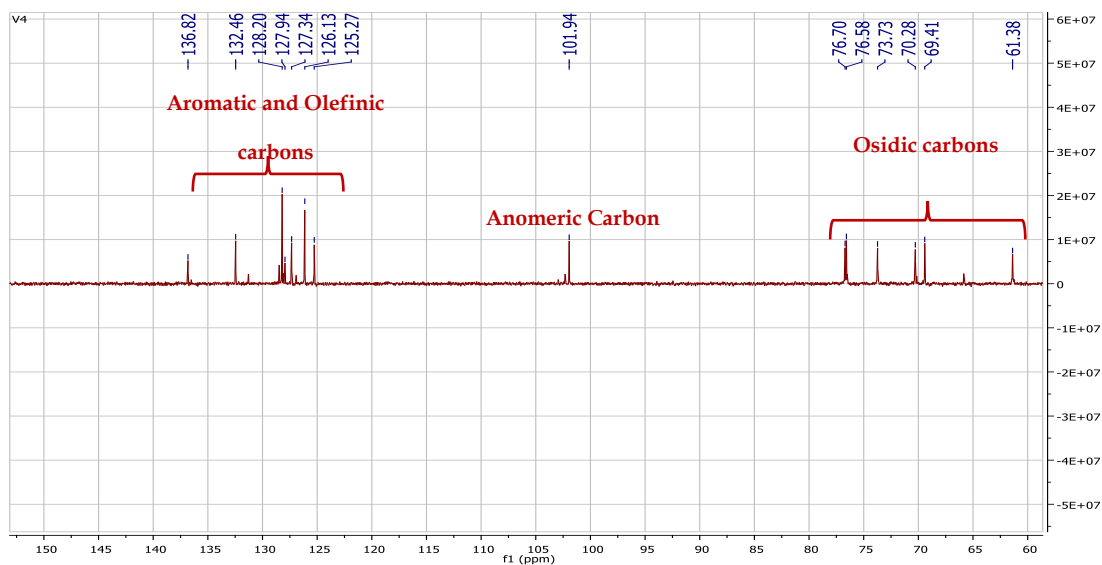
Figure. IV. 209: ^{13}C NMR spectrum (100 MHz, CD$_3$OD) of compound **V4**.
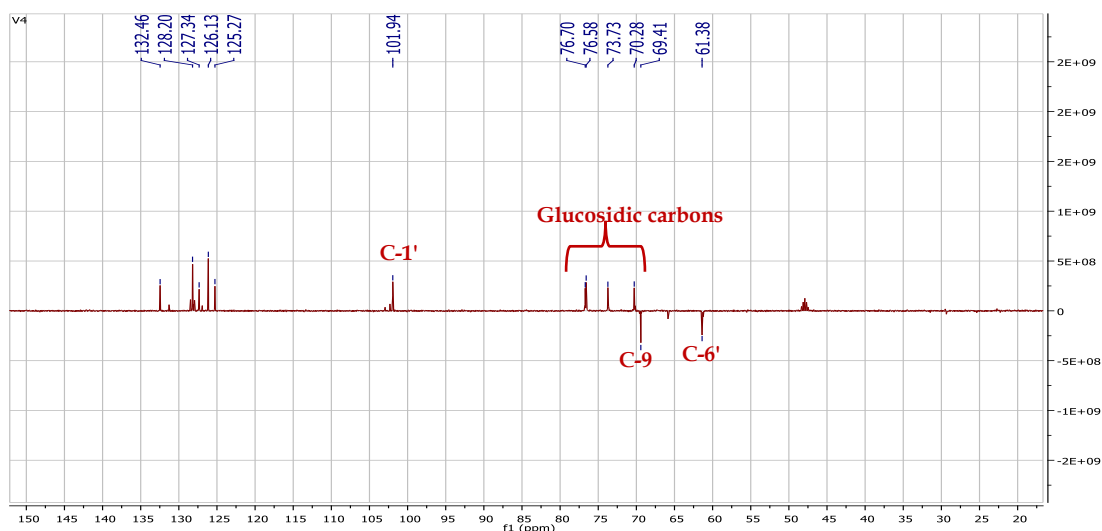
Figure. IV. 210: DEPT135 spectrum (100 MHz, CD$_3$OD) of the compound **V4**.

The HSQC spectrum (**Figure. IV. 211**) make it possible to correlate all the identified protons with their carbons as follow:

- ➢ C-2,6: δ_C 126.13.
- ➢ C-3,5: δ_C 128.20.
- ➢ C-4: δ_C 127.34.
- ➢ C-7: δ_C 132.46.
- ➢ C-8: δ_C 125.27.
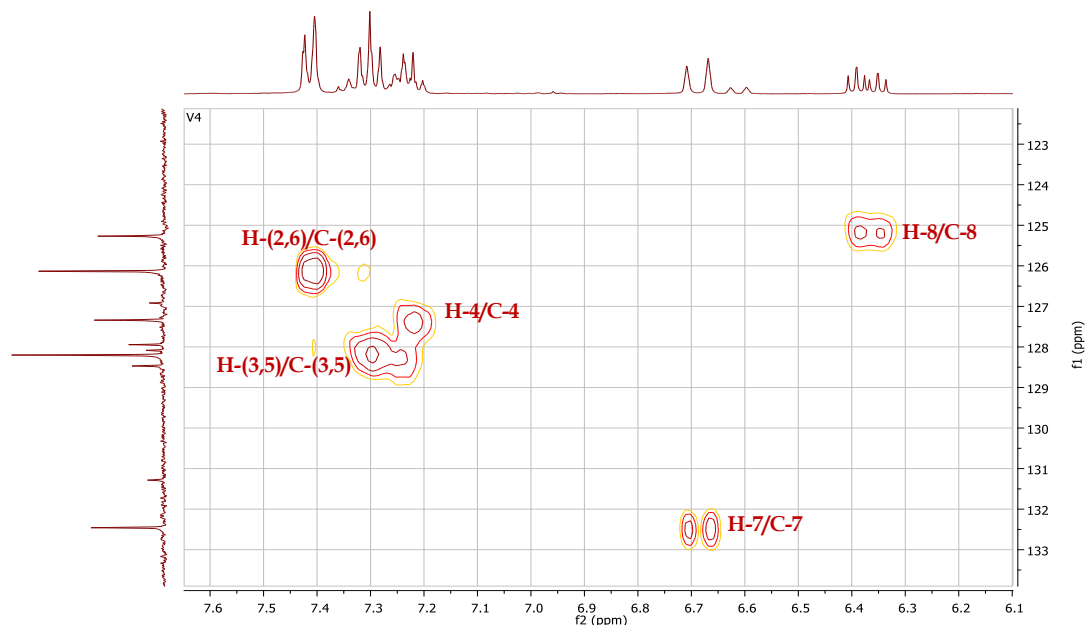
Figure. IV. 211: HSQC spectrum (400 MHz, CD$_3$OD) of aromatic and olefinic parts of **V4**.

The COSY spectrum (**Figure. IV. 212**) shows correlation spots between the olefinic proton H-8 and two protons resonating at δ_H 4.52 and 4.31 ppm. Assigned to an oxygenated methylene group H-9a and H-9b, the HSQC spectrum make it possible to identify its corresponding carbon C-9 δ_C 69.41. Also, correlation spots between H-8 and H-7 resonating at δ_H 6.69 (d, J = 16.0 Hz, 1H).
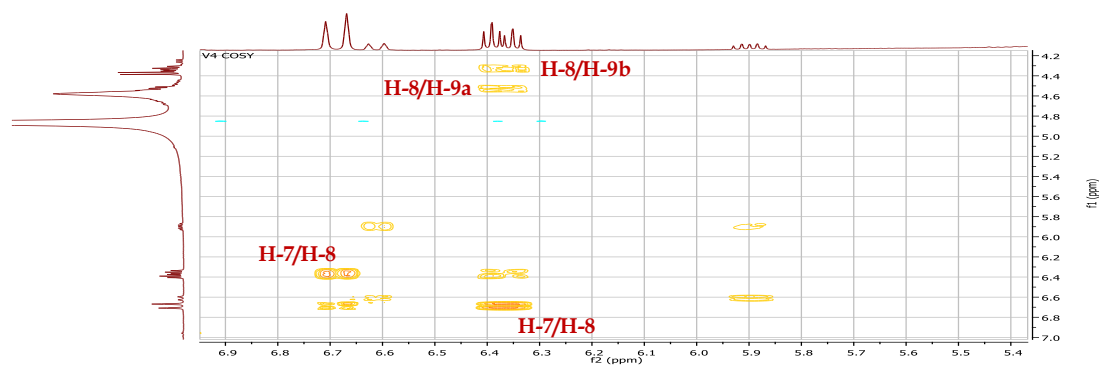
Figure. IV. 212: COSY spectrum (400 MHz, CD$_3$OD) of the compound **V4**.

According to HMBC spectrum (**Figure. IV. 213**), the olefinic protons displays correlations with the identified carbon C-9 δ_C 69.41 and with an aromatic carbon resonating at δ_C 136.82 corresponding to C-1. This spectrum also confirms the correlations between the aromatic protons and its adjacent carbons (**Figure. IV. 214**).
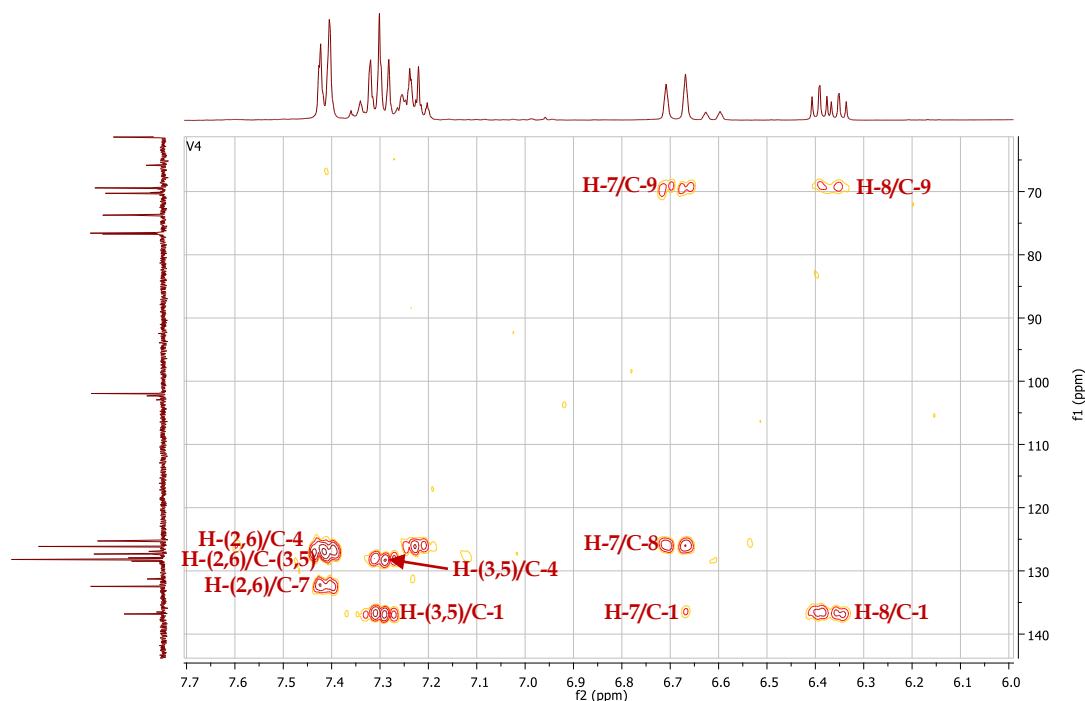
Figure. IV. 213: HMBC spectrum (400 MHz, CD₃OD) of olefinic and aromatic protons of the compound **V4**.
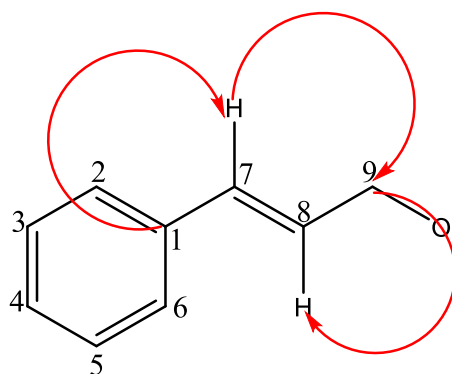
Figure. IV. 214: HMBC correlations of aglycon part of compound **V4**.

The above-mentioned data revealed that the aglycon parts of compound **V4** is cinnamyl alcohol (**Figure. IV. 215**) [219, 220].
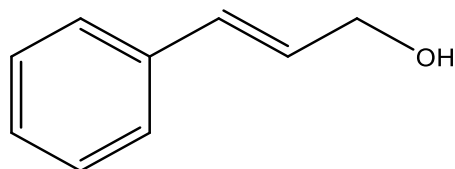
Figure. IV. 215: Structure of cinnamyl alcohol.

The osidic part

The analysis of COSY spectrum (**Figure. IV. 216**), make it possible to identify the osidic protons of a hexose starting from the anomeric proton H-1' δ_H 4.38 (d, J = 7.8 Hz, 1H), which correlates with the osidic proton H-2' resonating at δ_H 3.23 (m). The H-3' δ_H 3.36 (brd, J = 9.1 Hz, 1H) correlates with H-4' δ_H 3.28 (m), showing a trans-diaxial position of the H-2', H-3' and H-4' protons. The H-5' δ_H 3.28(m) exhibits in this spectrum correlations with two osidic protons resonating at δ_H 3.68 (dd, J = 11.8, 5.4 Hz, 1H) and 3.89 (dd, J = 11.9, 1.7 Hz, 1H) assigned to H'-6b and H'-6a. According to these data this hexose identified as β-D-glucose. The corresponding carbons of the identified protons assigned using HSQC spectrum (**Figure. IV. 217**) as follow:

> ➢ C-1': δ_C 101.94.
> ➢ C-2': δ_C 73.73.
> ➢ C-3': δ_C 76.70.
> ➢ C-4': δ_C 70.28.
> ➢ C-5': δ_C 76.58.
> ➢ C-6': δ_C 61.38.
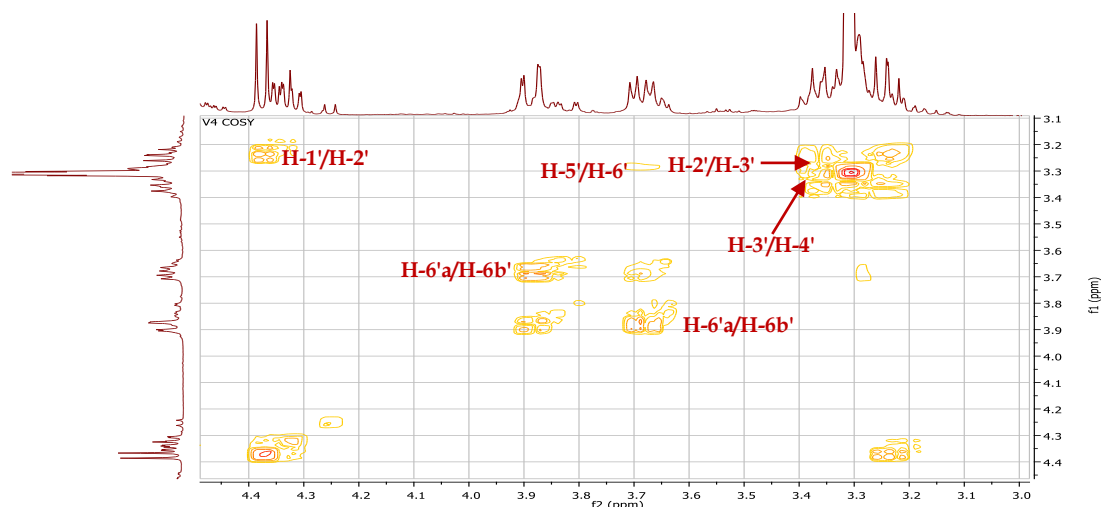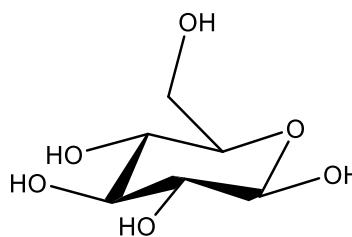
Figure. IV. 216: COSY spectrum (400 MHz, CD₃OD) of osidic part of **V4**.
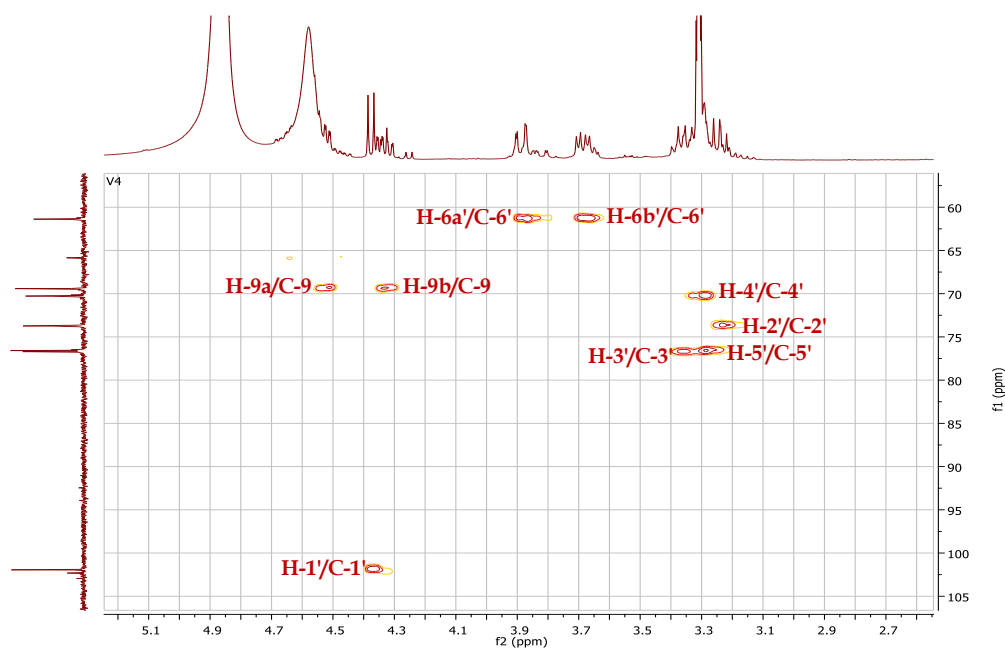
Figure. IV. 217: HSQC spectrum (400 MHz, CD$_3$OD) of osidic protons and the oxygenated methylene group of the compound **V4**.

The analysis of HMBC spectrum (**Figure. IV. 218**) exhibits cross peaks between the protons of the oxygenated methylene group (H-9a and H-9b) and the anomeric carbon C-1' δ_C 101.94. This correlation also confirmed by the cross peaks between the anomeric proton and H-1' δ_H 4.38 and C-9 δ_C 69.41.
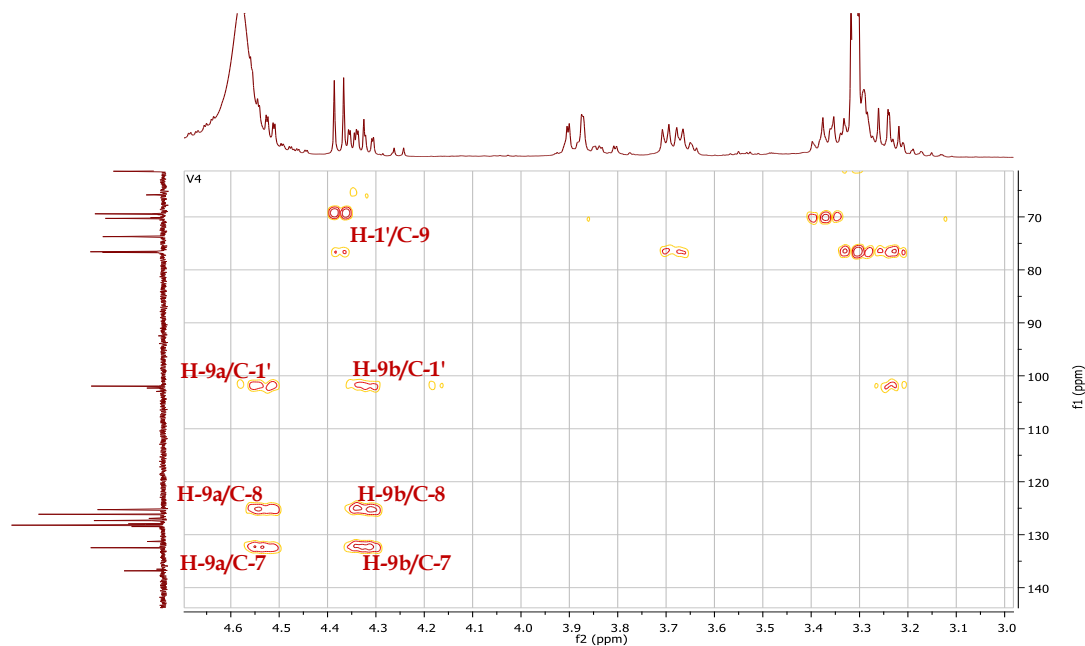
Figure. IV. 218: HMBC spectrum (400 MHz, CD$_3$OD) of compound **V4**.

The ^{1}H and ^{13}C NMR data, are summarized in the **Table. IV. 14**, all the data are in total agreement with; 9-O-β-glucopyranosyl trans-cinnamyl alcohol (Rosin) (**Figure. IV. 219**), which previously isolated from *Sanchezia nobilis* (Acanthaceae) [219], *Piper chaba* (Piperaceae) [220] and *Rhodiola rosea* (Crassulaceae) [221]. The compound **V4** is isolated for the first time from *Atractylis* genus.
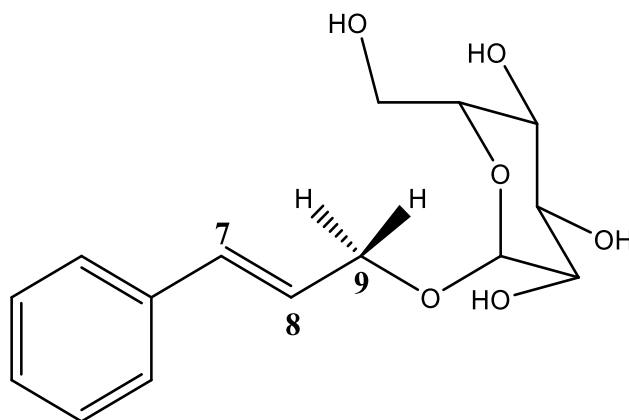
Figure. IV. 219: Structure of the compound **V4;** 9-O-β-glucopyranosyl trans-cinnamyl alcohol (Rosin).

Table. IV. 14: Chemical shifts ^{1}H NMR (400 MHz) and ^{13}C NMR (100 MHz) (da in ppm, J in Hz) of compound **V4**.

Position	Carbon (δ_C in ppm)	Proton (δ_H in ppm and J in Hz)
1	136.82	--
2,6	126.13	7.41 (d, J = 7.3 Hz, 2H)
3,5	128.20	7.30 (t, J = 7.3 Hz, 2H)
4	127.34	7.23 (d, J = 7.3 Hz, 1H)
7	132.46	6.69 (d, J = 16.0 Hz, 1H)
8	125.27	6.37 (ddd, J = 16.0, 6.6, 5.9 Hz, 1H)
9	69.41	4.52 (dd, J = 5.9, 1.5 Hz, 1H)
		4.31 (dd, J = 6.6, 1.5 Hz, 1H)

1'	101.94	4.38 (d, J = 7.8 Hz, 1H)
2'	73.73	3.23 (m)
3'	76.70	3.36 (brd, J = 9.1 Hz, 1H)
4'	70.28	3.28 (m)
5'	76.58	3.28(m)
6'	61.38	3.68 (dd, J = 11.8, 5.4 Hz, 1H) 3.89 (dd, J = 11.9, 1.7 Hz, 1H)

IV.4. 13. Compound V5

Compound **V5** is isolated in the form of a white amorph soluble in methanol. It is characterized on TLC test by visible spot under UV (254 and 366 nm) lamp which turns purple by revelation using acid solution and heating.

The analysis of ^{1}H NMR spectrum (**Figure. IV. 220**) recorded in CD$_3$OD, showed the presence of aromatic proton signals resonating at δ_H 6.83 (d, J = 2.1 Hz, 2H), δ_H 6.84 (m, 2H) and δ_H 6.94 (m, 2H) indicating the presence of two trisubstituted aromatic ring.

It further this spectrum also showed two protons resonating at δ_H 4.47 (d, J = 6.3 Hz, 2H) and proton signals resonating between δ_H 3.28 and 3.66. In addition, four peaks in the singlet form integrating of three protons 3H for each, resonating between δ_H 3.73 and 3.75, characteristic of four methoxy groups.
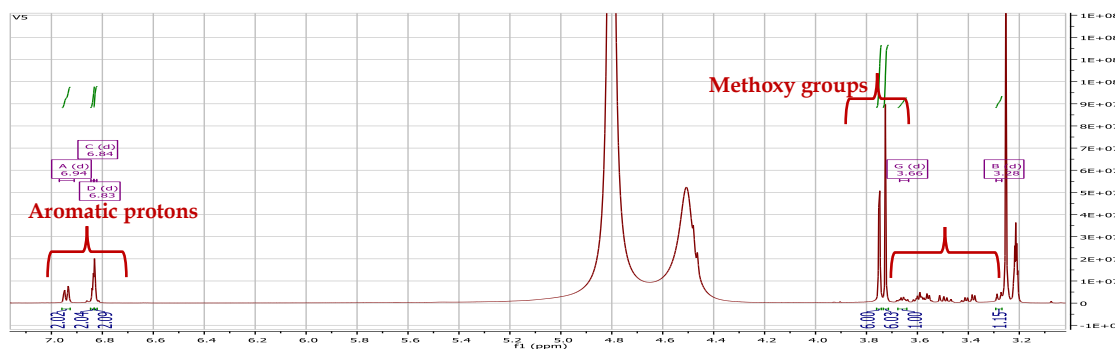
Figure. IV. 220: ^{1}H NMR Spectrum (400 MHz, CD$_3$OD) of compound **V5**.

The analysis of COSY spectrum (**Figure. IV. 222**) shows the presence of correlation between two aromatic protons resonating at δ_H 6.84 (m, 2H) and 6.94 (m, 2H), which indicates that they are two adjacent protons (**Figure. IV. 221**).
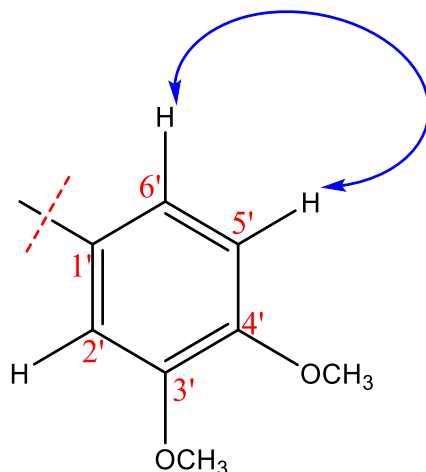
Figure. IV. 221: COSY correlation between the aromatic protons of compound **V5**.
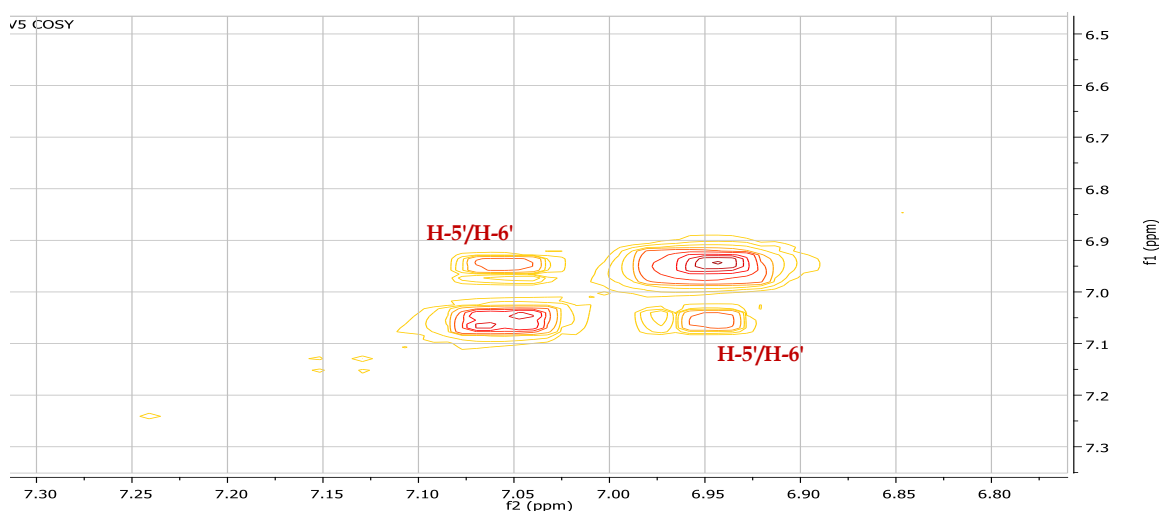
Figure. IV. 222: COSY spectrum (400 MHz, CD$_3$OD) shows the correlation between the aromatic protons of compound **V5**.

The analysis of ^{13}C NMR (**Figure. IV. 223**) and DEPT 135 (**Figure. IV. 224**) spectra reveals:

- ❖ 12 aromatic carbon signals resonating between δ_C 110 and 149.
- ❖ 2 carbon signals intense at δ_C 55.06 and 55.17 corresponding to four methoxy groups.
- ❖ 6 oxygenated carbons four CHOH and two CH$_2$OH groups.
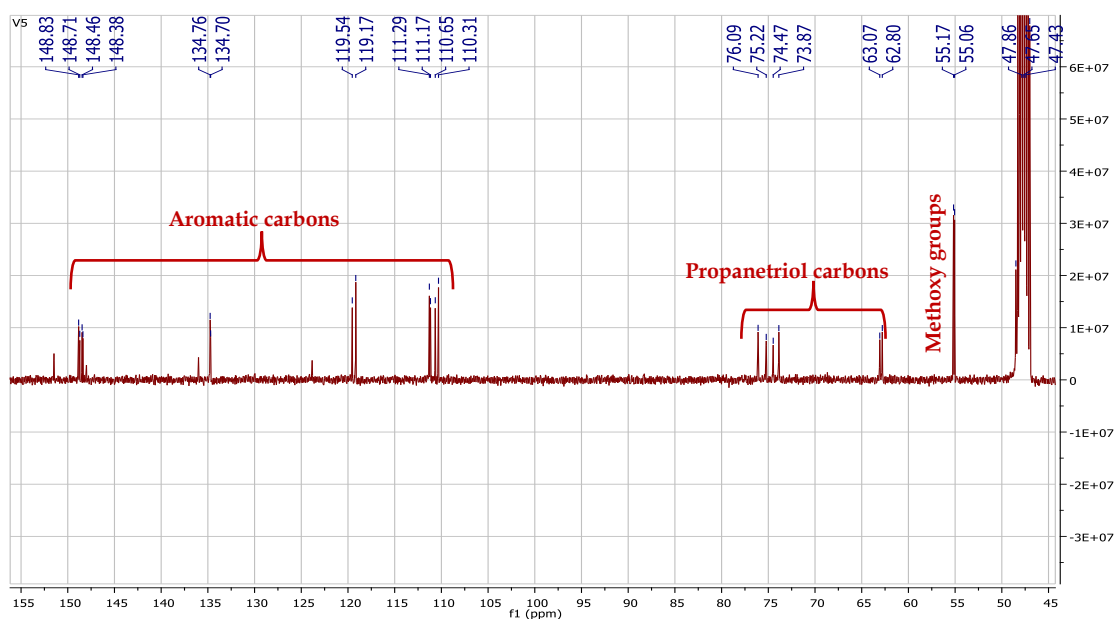
Figure. IV. 223: ^{13}C NMR spectrum (100 MHz, CD$_3$OD) of compound **V5**.
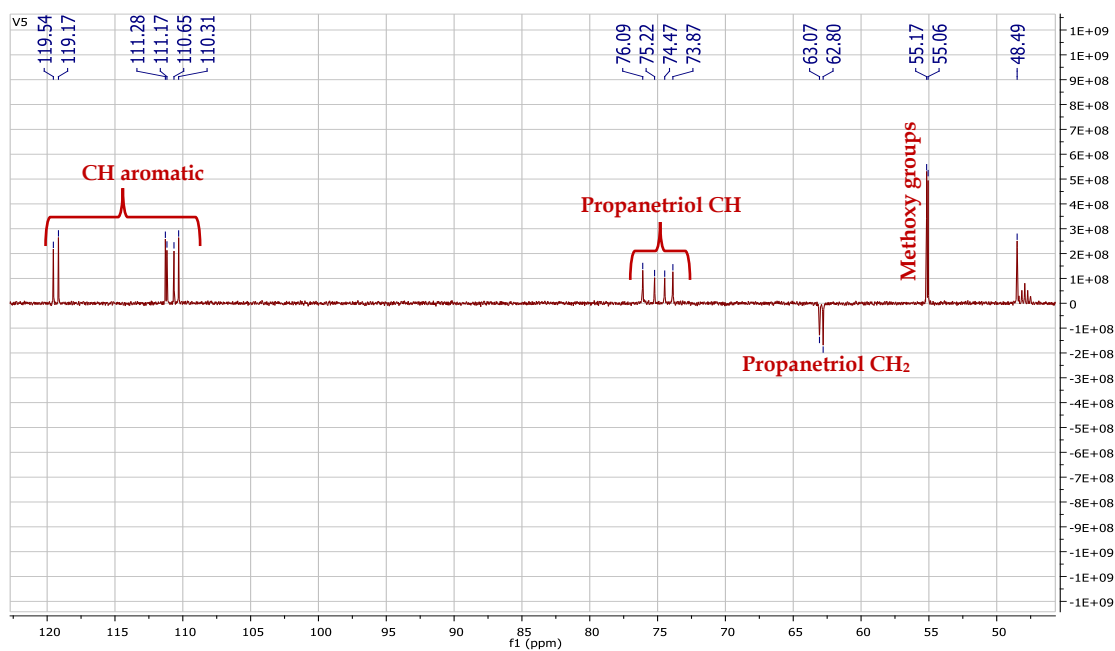
Figure. IV. 224: DEPT 135 spectrum (100 MHz, CD$_3$OD) of compound **V5**.

According the integration of the protons on the ^{1}H NMR spectrum and the number of carbon signals at ^{13}C NMR spectrum, it can be concluded that the compound **V5** exists as a mixture of two isomers (**erythro** and **threo**).

The protons resonating at δ$_H$ 4.47 and proton signals resonating between δ$_H$ 3.28 and 3.66 showed in HSQC spectrum (**Figure. IV. 225**) correlations with the carbons resonating between δ$_C$ 62 and 76 indicating its attachment to hydroxyl group. The

analysis of HSQC spectrum showed also the correlations between the aromatic protons and their corresponding carbons as shown in the **Figure. IV. 225**.
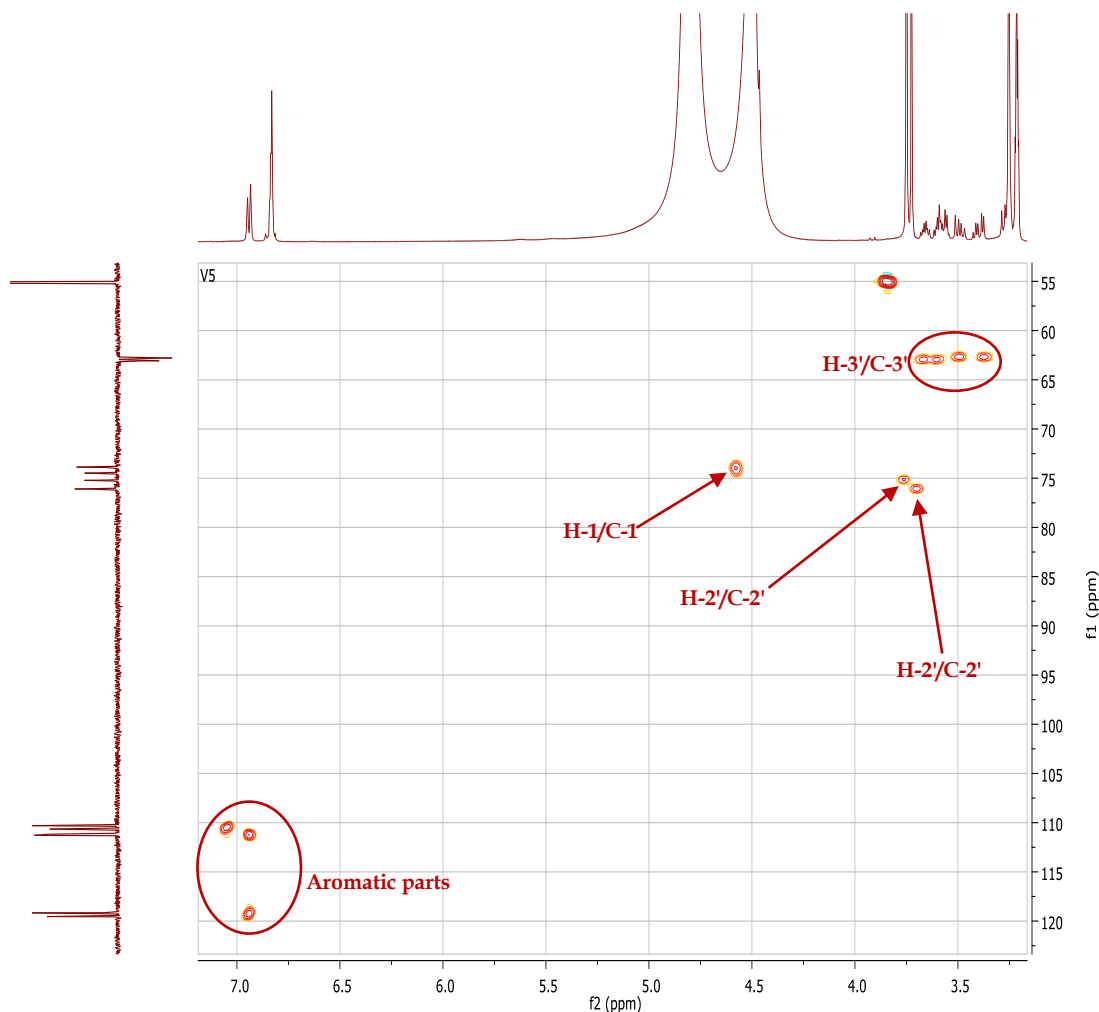
Figure. IV. 225: HSQC spectrum (400 MHz, CD$_3$OD) of compound **V5**.

Based on above data, the compound **V5** was identified as a phenylpropanoid having two methoxy groups at C-3 and C-4. The compound **V5** present as two isomers of 1-(3,4-dimethoxy-phenyl)-1,2,3-propanetriol (veratrylglycerol) [222]. The structure of the compound **V5** was further confirmed by the HMBC (**Figure. IV. 226**) and COSY (**Figure. IV. 227**) spectra.
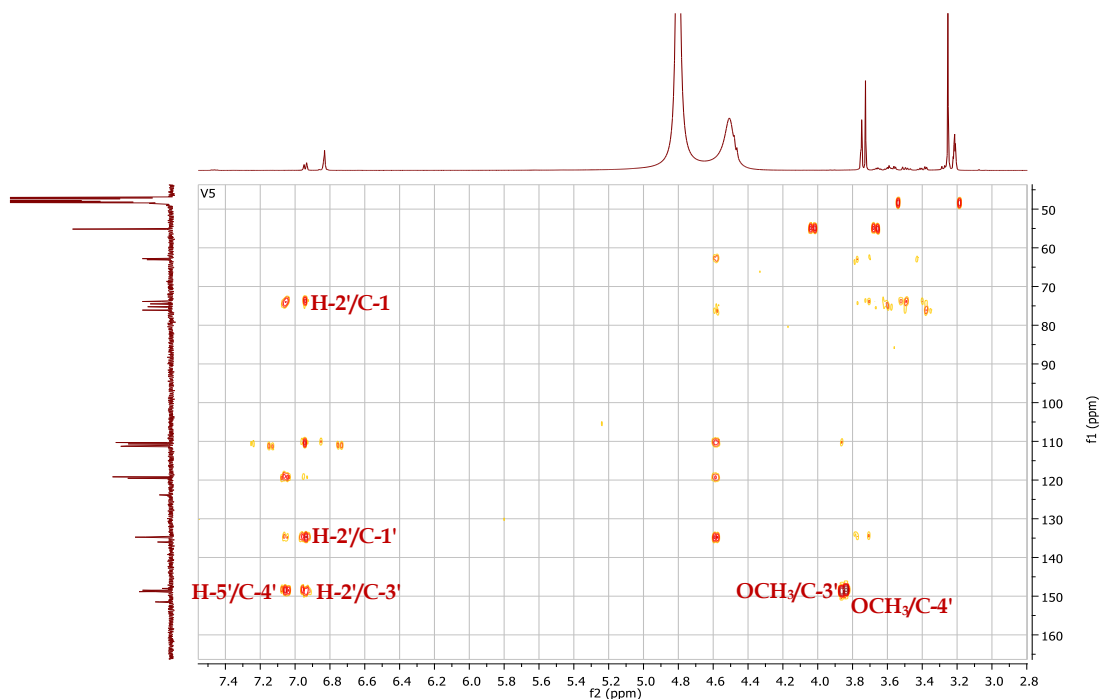
Figure. IV. 226: HMBC spectrum (400 MHz, CD$_3$OD) of compound **V5**.
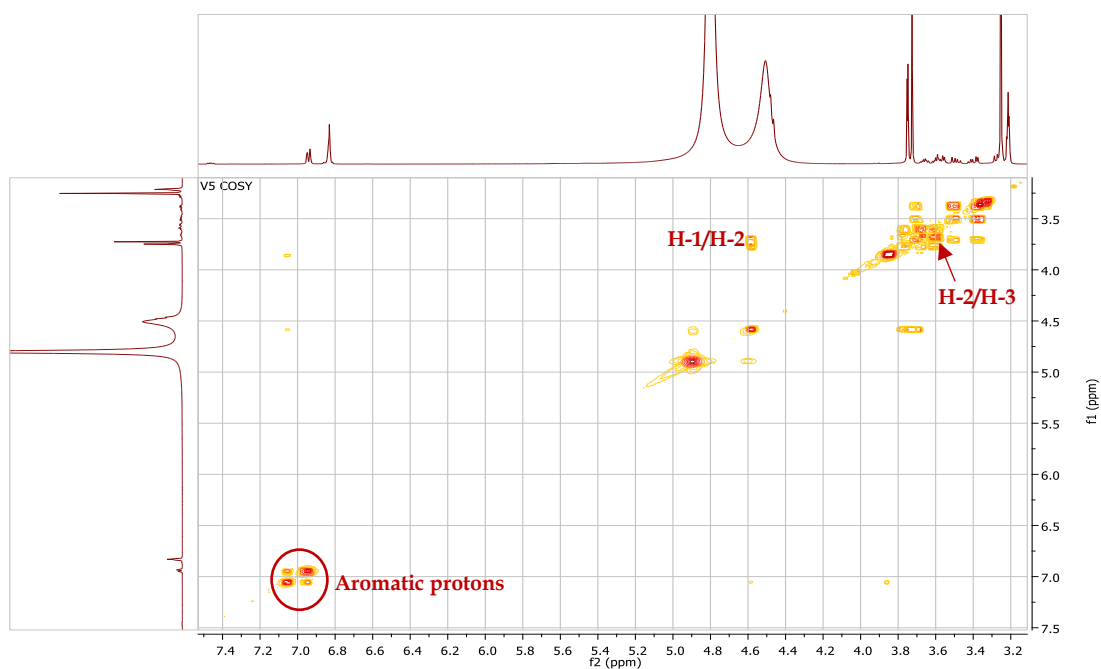
Figure. IV. 227: COSY spectrum (400 MHz, CD$_3$OD) of compound **V5**.

The ^{1}H and ^{13}C NMR data, are summarized in the **Table. IV. 15**, all the data are in total agreement with; 1-(3,4-dimethoxy-phenyl)-1,2,3-propanetriol (veratrylglycerol) (**Figure. IV. 228**), which is previously isolated from the plants

Pimpinella anisum (Apiacees) [222] and *Chrozophora obliqua* (Euphorbiaceae) [223], this compound **V5** is isolated for the first time from the genus *Atractylis*.
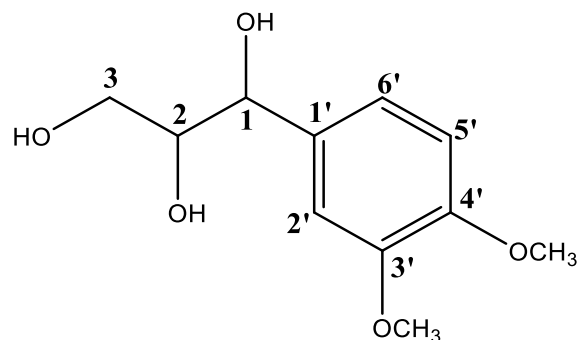
Figure. IV. 228: The chemical structural compound **V5**, 1-(3,4-dimethoxy-phenyl)-1,2,3-propanetriol (veratrylglycerol).

Table. IV. 15: Chemical shifts ^{1}H NMR (400 MHz) and ^{13}C NMR (100 MHz) (da in ppm, J in Hz) on CD_3OD of compound **V5**, isomers of 1-(3,4-dimethoxy-phenyl)-1,2,3-propanetriol (veratrylglycerol) (δ_C in ppm, δ_H in ppm and J in Hz).

	Isomer I		Isomer II	
Position	Carbon	Proton	Carbon	Proton
1	73.87	4.47 (d, J = 6.3 Hz)	74.47	4.47 (d, J = 6.3 Hz)
2	76.09	3.60 (m)	75.22	3.66 (m)
3	62.80	3.28 (m)	63.07	3.49 (dd, J = 11.3, 6.6 Hz, 1H)
		3.39 (dd, J = 11.3, 4.0 Hz, 1H)		3.66 (dd, J = 10.3, 6.4 Hz, 1H)
1'	134.76	--	134.70	--
2'	111.29	6.83 (d, J = 2.1 Hz)	111.17	6.83 (d, J = 2.1 Hz)
3'	148 .83	--	148 .71	--
4'	148.46	--	148.38	--
5'	110.31	6.94 (m)	110.65	6.94 (m)
6'	119.17	6.84 (m)	119.54	6.84 (m)
OCH₃-3'	55.17	3.73 (S, 3H)	55.17	3.73 (S, 3H)
OCH₃-4'	55.06	3.75 (S, 3H)	55.06	3.75 (S, 3H)

IV.4. 14. Compound EP1

The compound **EP1** is isolated in the form of a white powder soluble in the chloroform. This compound is characterized on TLC test by invisible spot under UV lamp (254 and 366 nm), which turns purple by revelation using acid solution and heating.
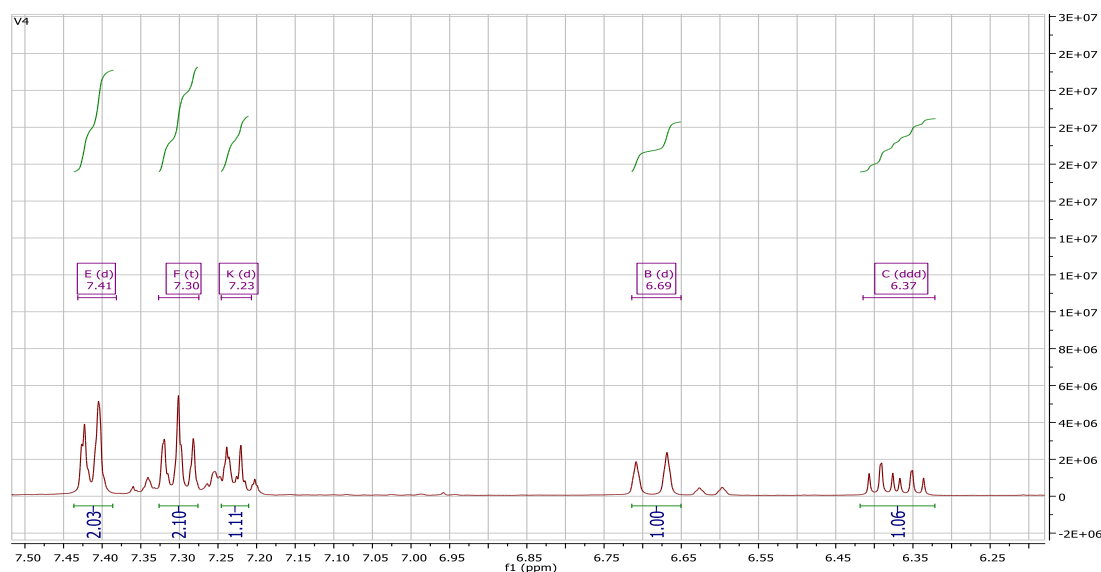
The ^{1}H NMR (**Figure. IV. 229**) and ^{13}C NMR (**Figure. IV. 233**) spectra reveals the presence of high number of signals. Also, the deshielded part of these spectra shows the presence of signals characteristic of different type of compounds, these indicating that **EP1** is isolated in the form of isomeric mixture.

The ^{1}H NMR spectrum (**Figure. IV. 229**) shows a sequence of extremely dense peaks between δ_H 0.70 and 1.7. This indicates the presence of a high number of methyl groups with doublet and singlet multiplicities.
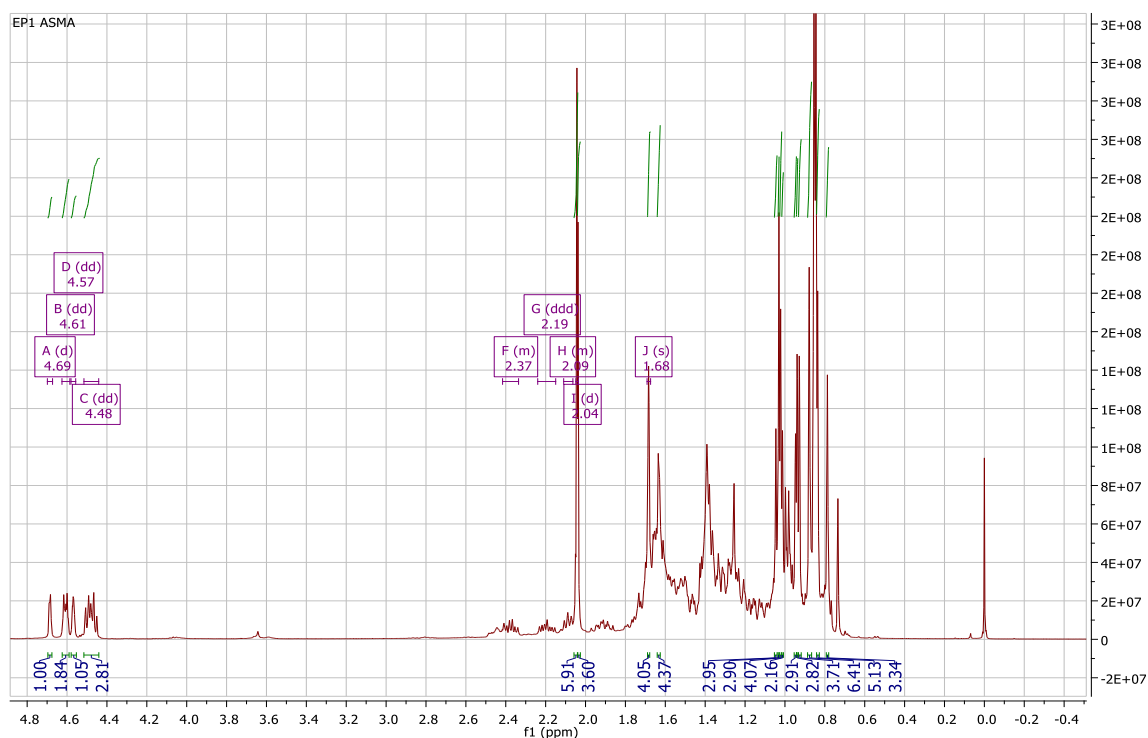
Figure. IV. 229: ^{1}H NMR spectrum (400 MHz, CDCl$_3$) of the compound **EP1**.

In the deshielded parts of the ^{1}H NMR spectrum (**Figure. IV. 230**) displays the presence of five signals corresponding to eight protons resonating at δ_H 4.48 (dd, J = 16.3, 6.0 Hz, 3H), δ_H 4.61 (dd, J = 4.5, 2.2 Hz, 2H), δ_H 4.57 (dd, J = 2.3, 1.3 Hz, 1H), δ_H 4.69 (d, J = 2.2 Hz, 1H) and δ_H 5.26 (d, J = 6.9 Hz, 1H). The analysis of COSY spectrum (**Figure. IV. 231**) shows coupling between the ethylenic protons δ_H 4.57 and

δ_H 4.69. The corresponding carbons of the identified protons were attributed using HSQC spectrum (**Figure. IV. 232**) at δ_C 80.99, 107.13, 109.35 and 118.89, respectively. These carbons split into an oxymethine carbon of position C-3 and three ethylenic carbons.
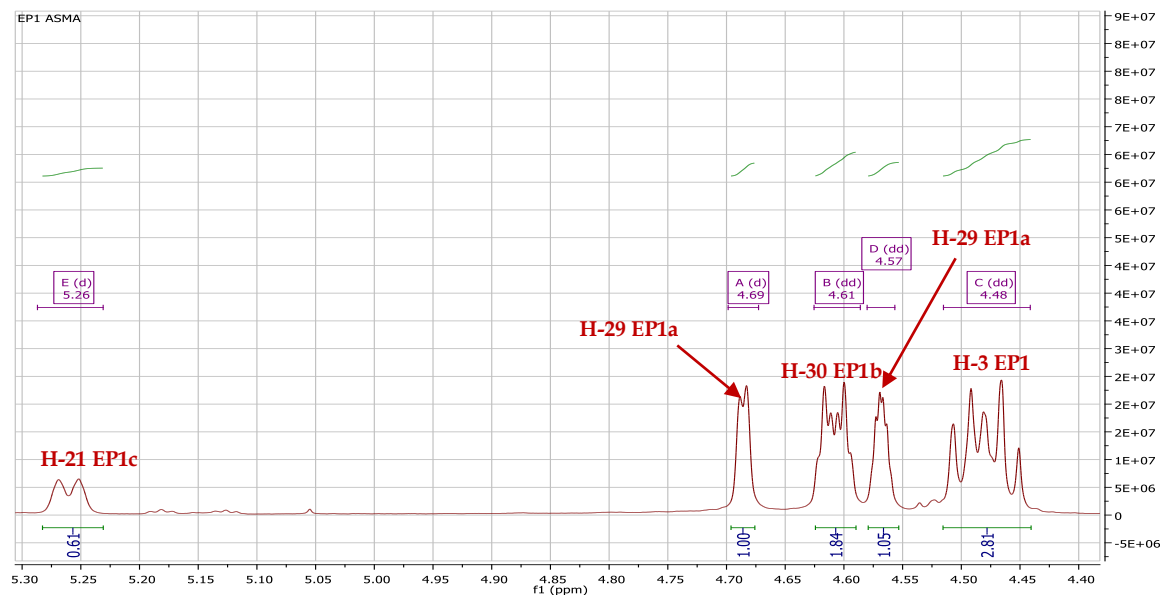
Figure. IV. 230: ^{1}H NMR spectrum (400 MHz, CDCl$_3$) of olefinic region of compound **EP1**.
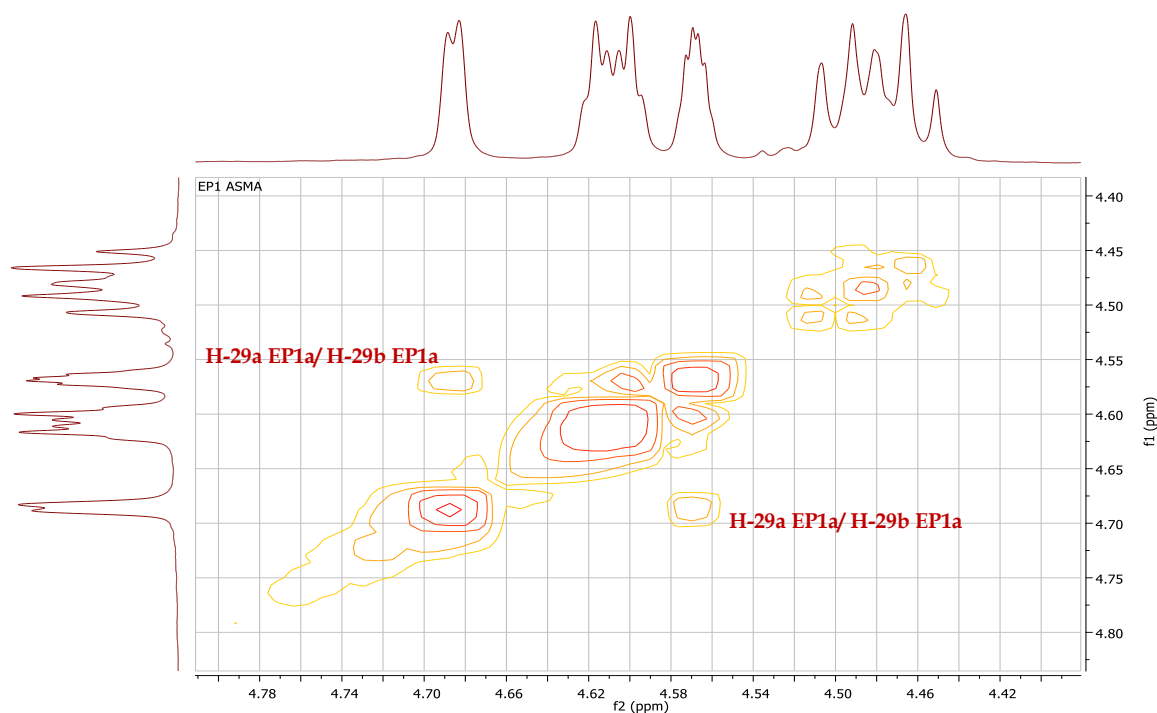
Figure. IV. 231: COSY spectrum (400 MHz, CDCl$_3$) between the olefinic proton of compound **EP1a.**
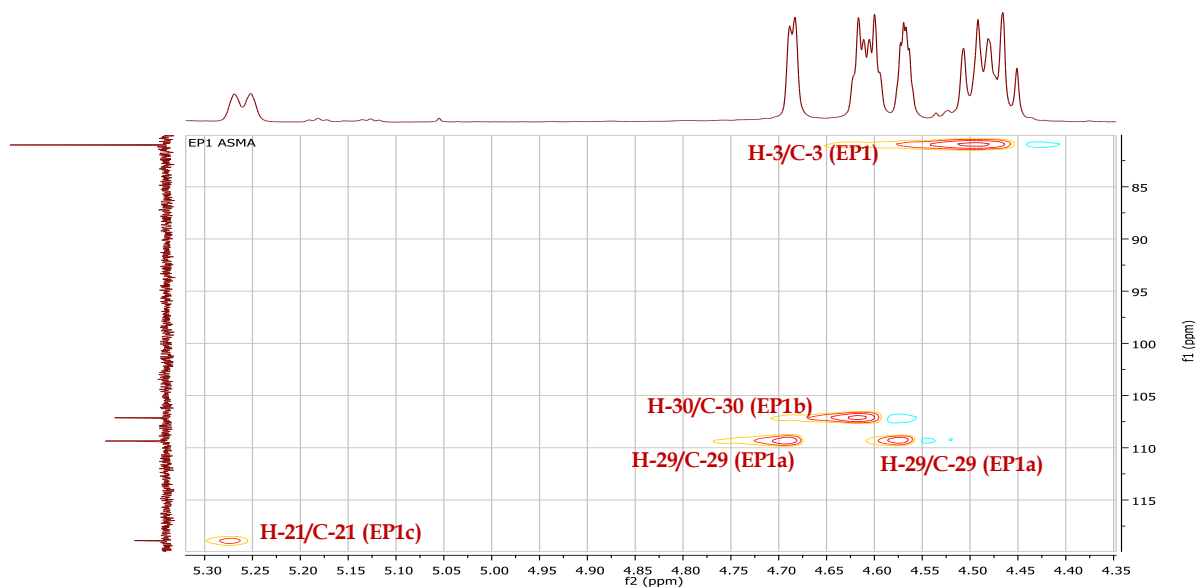
Figure. IV. 232: HSQC spectrum (400 MHz, CDCl$_3$) of olefinic region of **EP1**.

The ^{13}C NMR (**Figure. IV. 233**) and DEPT135 spectra (**Figure. IV. 234**) exhibits more than sixty signals, indicating a mixture of three triterpene. In particular six signals for olefinic carbons were observed, being two secondary (δ_C 107.13 and 109.35), one tertiary (δ_C 118.89) and three quaternary carbons (δ_C 139.87, 150.97 and 154.66). The comparison of these results with literature data suggested the presence of triterpenes type lup-20(29)-ene (δ_C 109.35 and 150.97) **EP1a**, urs-20(30)-ene (δ_C 107.13 and 154.66) **EP1b** and urs-20-ene (δ_C 118.89 and 139.87) **EP1c** [224]. Also, the signal that resonating at δ_C 80.99 is a typical of an acetylated triterpene, in addition to a signal of an ester carbonyl group δ_C 171.01.
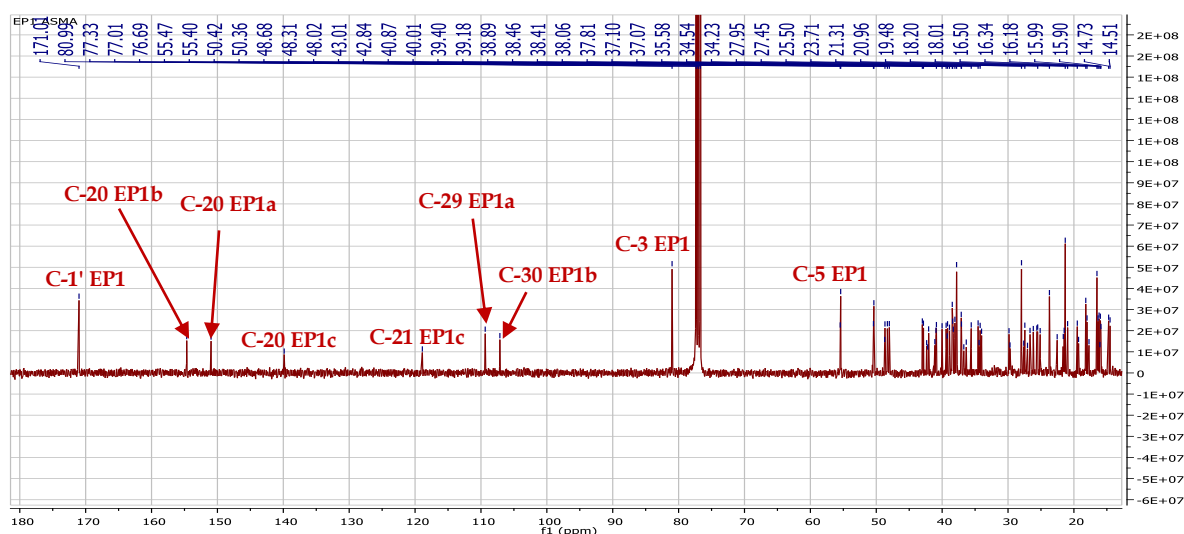
Figure. IV. 233: ^{13}C NMR spectrum (100 MHz, CDCl$_3$) of compound **EP1**.
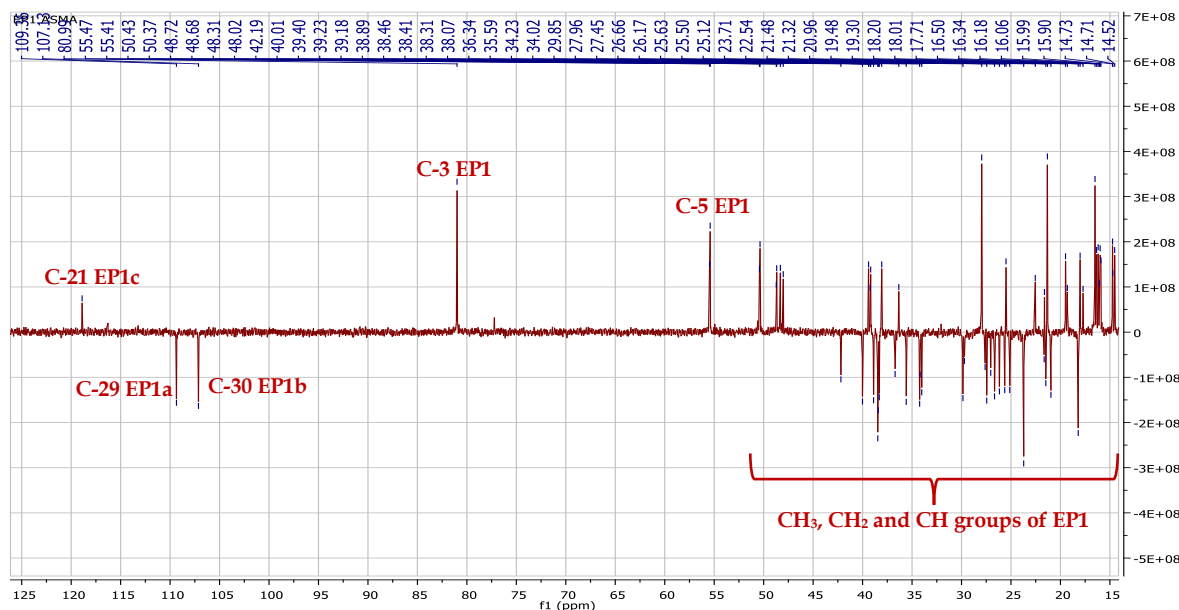
Figure. IV. 234: DEPT135 spectrum (100 MHz, CDCl₃) of compound **EP1**.

The analysis of HSQC spectrum (**Figure. IV. 235**) shows the presence of eight methyl groups at least, correlate with carbons resonating between δ_C 16 and 28. The ^{1}H NMR and HSQC spectra also reveals the presence of signals resonating between δ_H 0.7 and 2.37 corresponding to CH and CH₂ groups. This confirms the pentacyclic triterpene nature of these compounds.
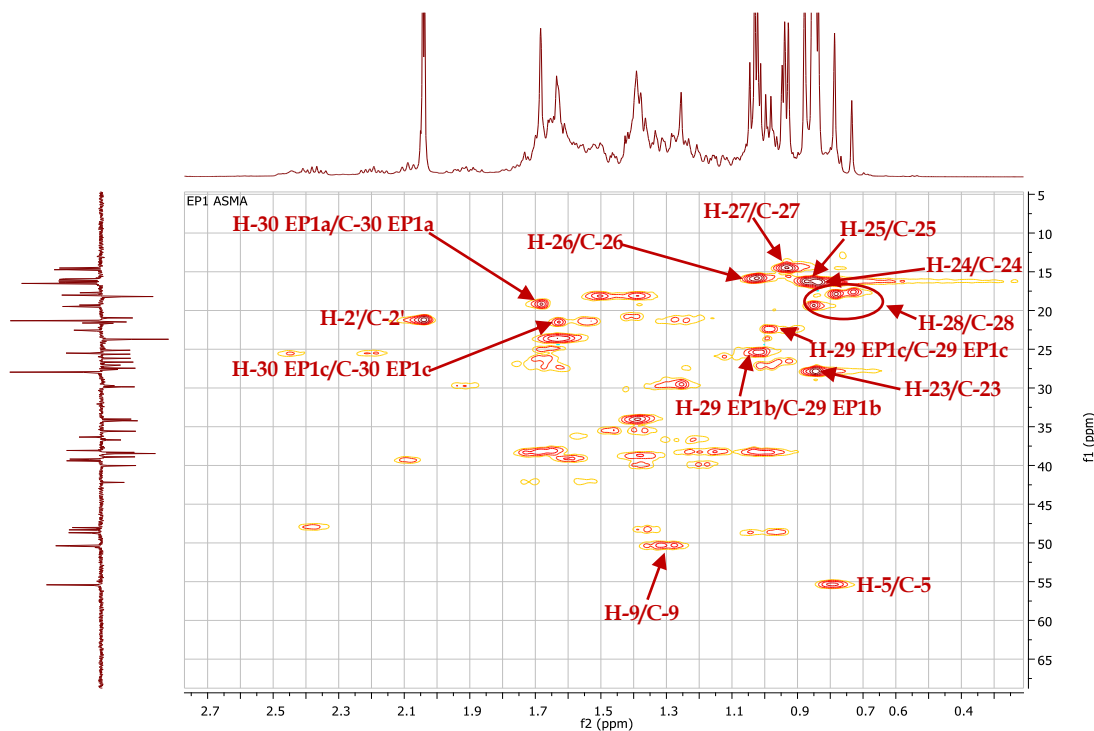
Figure. IV. 235: HSQC spectrum (400 MHz, CDCl₃) of compound **EP1**.

The analysis of ^{1}H NMR and HSQC spectra displays that deference between these molecules is on the cycle **E** of the pentacyclic triterpene. Therefore, the analysis of HMBC (**Figure. IV. 237**) spectrum make it possible to confirms each structure, so in the compound **lup-20(29)-ene**, the correlations between the olefinic carbons (δ_C 109.35 and 150.97) and the methyl group resonating at δ_H 1.68 (H-30) confirming the isopropyl group at C-19. In the compound **urs-20(30)-ene**, the HMBC spectrum shows a correlation between the olefinic carbon δ_C 154.66 and the methyl group resonating at δ_H 1.02 corresponding to H-29. Also, in the compound **urs-20-ene** this spectrum reveals correlations between the olefinic carbon δ_C 139.87 and methyl group resonating at δ_H 0.99 corresponding to H-29 and between the olefinic carbons δ_C 118.89 and 139.87 and methyl group resonating at δ_H 1.64, corresponding to H-30 (**Figure. IV. 236**).
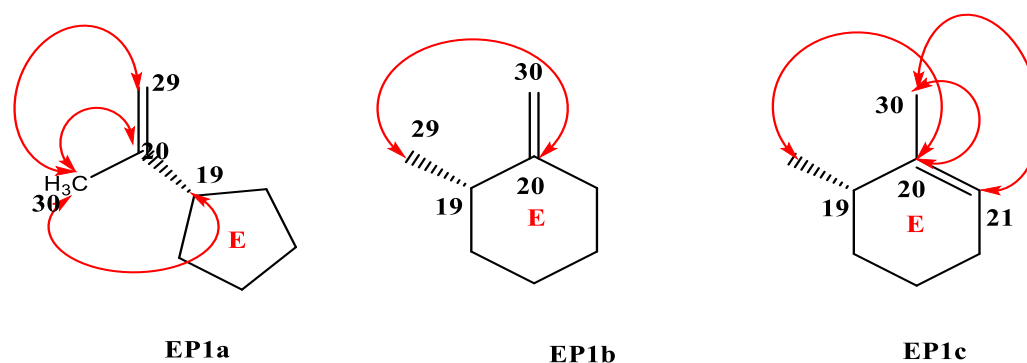
Figure. IV. 236: HMBC correlations of ring E of the compound **EP1**.
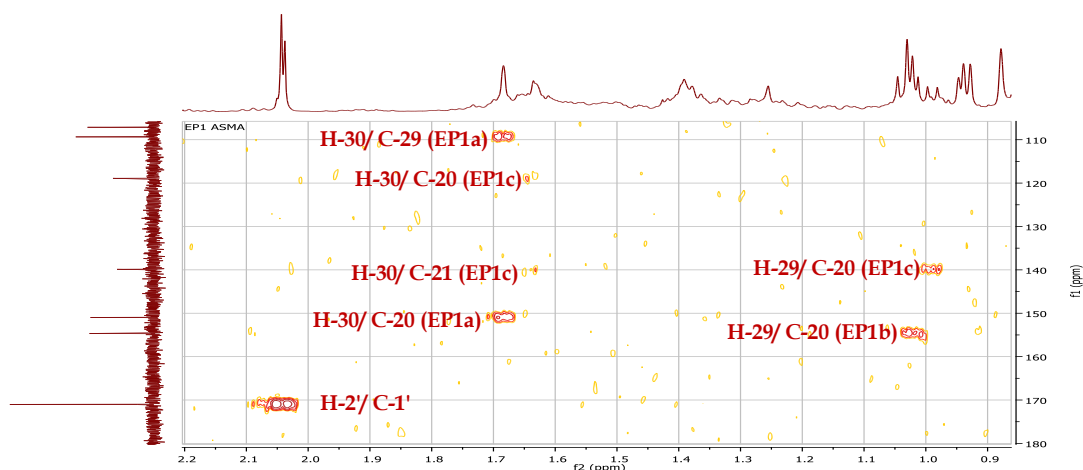
Figure. IV. 237: HMBC spectrum (400 MHz, CDCl₃) of ring **E** the compound **EP1**.

The analysis of HMBC spectrum (**Figure. IV. 238**) also allows to locate the methyl groups (**Figure. IV. 239**), through which the structure of the three isomers can be determined by the comparison with literature data as follow:

➢ Me-23 (δ_H 0.83 (s)) and Me-24 (δ_H 0.85 (s)) exhibits correlations in ^2J with carbon resonating at δ_C 37.81 assigned to C-4 the methyl groups shows also correlations in ^3J with carbon already identified C-3 and with carbon resonating at δ_C 55.4 corresponding to C-5.

➢ Me-25 (δ_H 0.87 (s)) shows correlations in ^2J with carbon resonating at δ_C 37.1 assigned to C-10 and three correlations in ^3J with three carbons resonating at δ_C 38.4, 50.3 and 55.4, these carbons are C-1, C-9 and C-5, respectively.

➢ Me-26 (δ_H 1.02 (s)) displays also correlations in ^3J with three carbons resonating at δ_C 34, 42 and 50.3, these carbons assigned to C-7, C-14, and C-9 already identified, respectively.

➢ Me-27 (δ_H 0.93 (s)) shows correlations in ^2J with the carbon C-14 already identified and correlations in ^3J with C-8, C-13 and C-15.

➢ Me-28 exhibits correlations in ^2J with carbon assigned to C-17 and correlations in ^3J with three carbons assigned to C-16, C-18, and C-22.
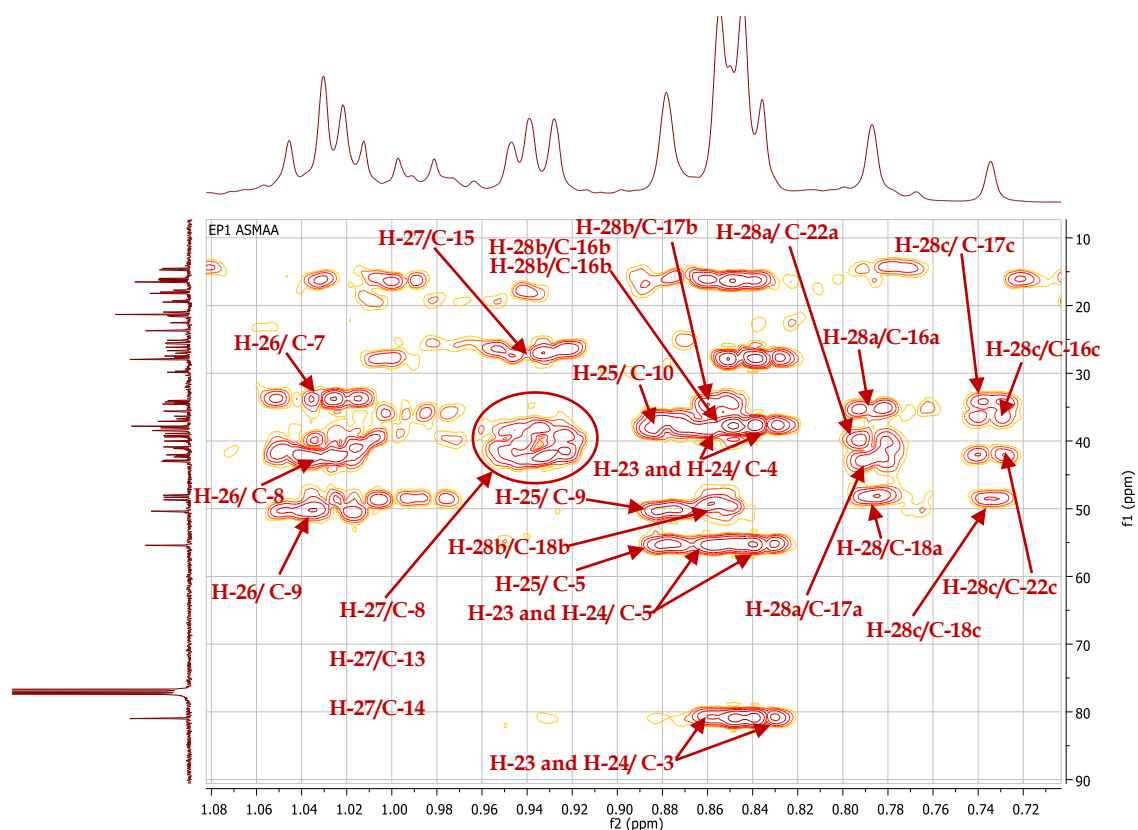
Figure. IV. 238: HMBC spectrum (400 MHz, CDCl₃) of methyl groups of **EP1**.
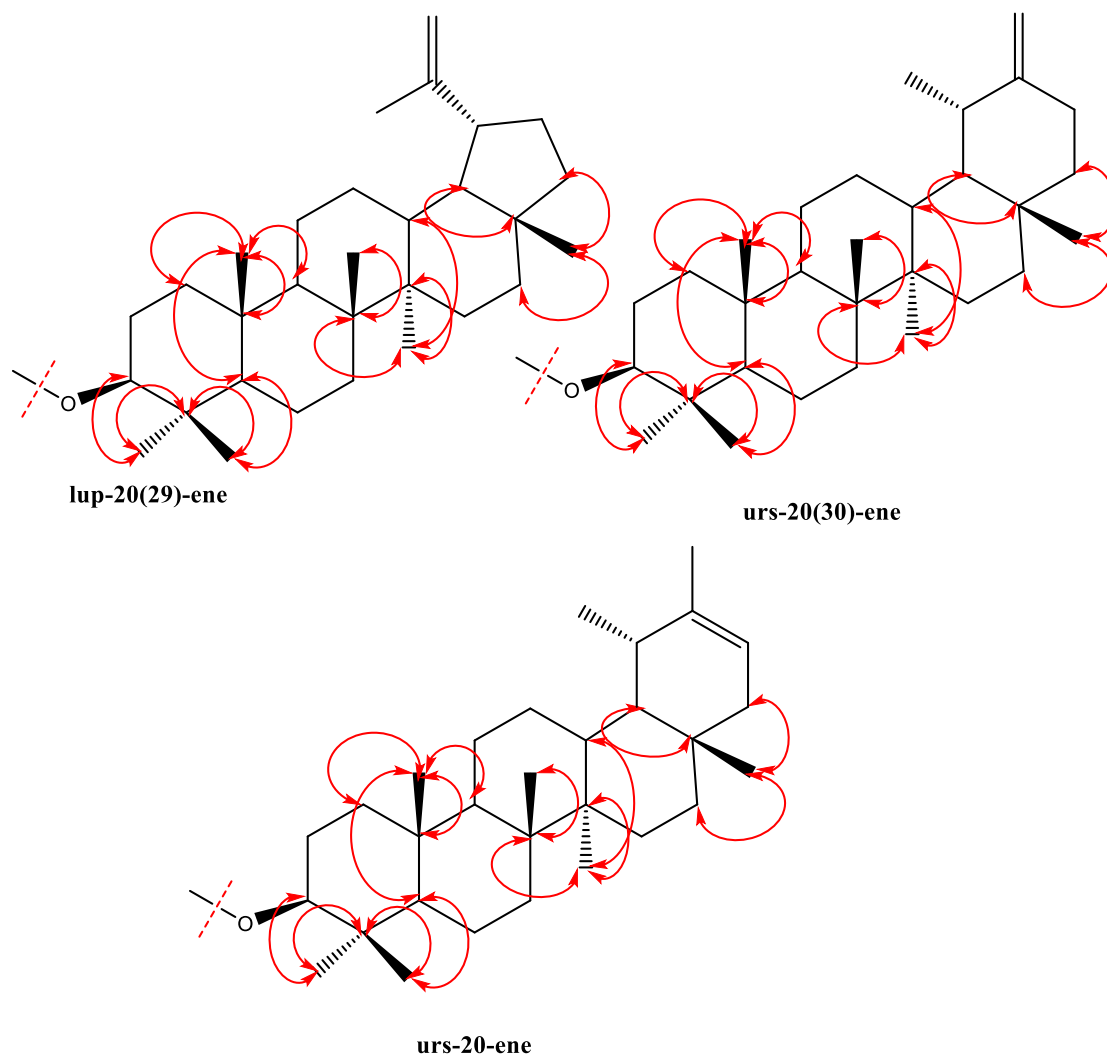
Figure. IV. 239: HMBC correlations of methyl groups of **EP1**.

The chemical shifts of the proton and carbon of the oxymethine group δ_H 4.48/ δ_C 80.99 indicate an acylation at this position. The signal of integration over 9H is observed in ^{1}H NMR at δ_H 2.04 attributable to at least three acetate groups, the carbon of which resonates at δ_C 21.31 ppm. The analysis of HMBC spectrum exhibits a cross peak of between H-3 and the carbonyl group δ_C 171.01, this last also correlate with methyl group resonating at δ_H 2.04 (9H), this confirms the group acetyl at C-3 (**Figure. IV. 240**).
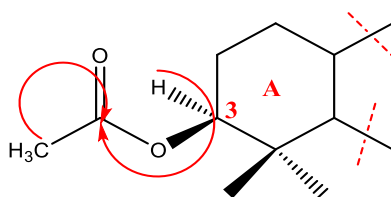
Figure. IV. 240: HMBC correlations at C-3 of compound **EP1**.

According to above mentioned data the components of **EP1** were identified as lupeyl acetate **EP1a**, taraxasteryl acetate **EP1b** and pseudotaraxasteryl acetate (ϕ-taraxasteryl acetate) **EP1c** [195, 224]. The difference in integration between the olefinic protons makes it possible to deduce their proportion at 39.5% lupeyl acetate **EP1a**, 36.3% **taraxasteryl** acetate **EP1b** and 24.1% pseudotaraxasteryl acetate **EP1c**.

The lupeyl acetate **EP1a** is already isolated from the *Atractylis* genus from *A. flava* [52] and *A. serratuloides* [51]. The taraxasteryl acetate **EP1b** is already isolated from the plant *Onopordum acanthium* (Asteraceae) [225] and pseudotaraxasteryl acetate **EP1c** is also already isolated from the plant *Atractylodes lancea* (Asteraceae) [226]. All the data are illustrated in the **Table. IV. 16**, **Table. IV. 17** and **Table. IV. 18** which are in total agreement with; lupeyl acetate **EP1a**, taraxasteryl acetate **EP1b** and pseudotaraxasteryl acetate **EP1c** (**Figure. IV. 241**). The compounds, taraxasteryl acetate **EP1b** and pseudotaraxasteryl acetate **EP1c** identified for the first time from *Atractylis* genus.

Lupeyl acetate

Taraxasteryl acetate

Pseudotaraxasteryl acetate
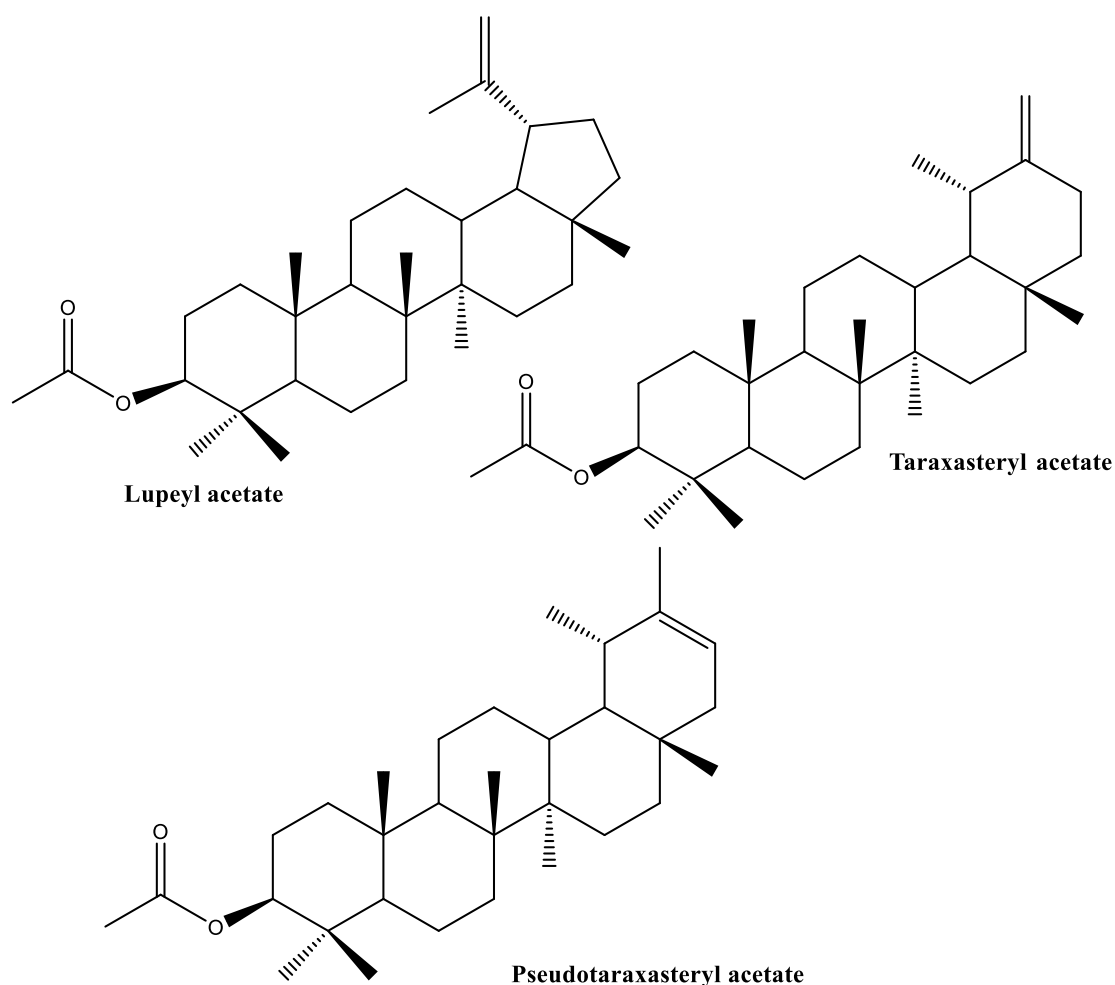
Figure. IV. 241: Chemical structure of **EP1** isomers.

Table. IV. 16: The chemical shifts of ^{1}H NMR (400 MHz) and ^{13}C NMR (100 MHz) on CDCl$_3$ of compound **EP1a**; lupeyl acetate.

Position	Carbon (δ_C in ppm)	Proton (δ_H in ppm and J in Hz)
1	38.4	1.69 (m) H-1a, 1.01 (m) H-1b
2	23.71	1.65 (m) H-2a, 0.99 (m) H-2b
3	80.99	4.48 (dd, J = 16.3, 6.0 Hz)
4	37.81	--
5	55.4	0.79 (m)
6	18.2	1.50 (m) H-6a, 1.39 (m) H-6b
7	34.02	1.39 (m)
8	42.05	--
9	50.3	1.29 (m)
10	37.1	--
11	20.96	1.53 (m) H-11a, 1.25 (m) H-11b
12	25.63	1.67 (m) H-12a, 1.10 (m) H-12b
13	38.06	1.66 (m)
14	42.84	--
15	27	1.64 (m) H-15a, 0.99 (m) H-15b
16	35.59	1.46 (m) H-16a, 1.37 (m) H-16a
17	43.01	--
18	48.31	1.35 (m)

19	48.02	2.37 (m)
20	150.97	--
21	29.85	1.91 (m) H-21a, 1.31 (m) H-21b
22	40.01	1.38 (m) H-22a, 1.18 (m) H-22b
23	27.96	0.83 (s)
24	16.50	0.85 (s)
25	16.34	0.87 (s)
26	15.90	1.02 (s)
27	14.51	0.93 (s)
28	18.01	0.78 (s)
29	109.35	4.57 (dd, J = 2.3, 1.3 Hz, 1H), 4.69 (d, J = 2.2 Hz, 1H)
30	19.49	1.68 (s)
1'	171.01	--
2'	21.31	2.04 (s)

Table. IV. 17: The chemical shifts ^{1}H NMR (400 MHz) and ^{13}C NMR (100 MHz) on CDCl$_3$ of compound **EP1b**; taraxasteryl acetate.

Position	Carbon	proton
1	38.4	1.69 (m) H-1a, 1.01 (m) H-1b
2	23.71	1.65 (m) H-2a, 0.99 (m) H-2b
3	80.99	4.48 (dd, J = 16.3, 6.0 Hz)

4	37.81	--
5	55.4	0.79 (m)
6	18.2	1.50 (m) H-6a, 1.39 (m) H-6b
7	34.19	1.39 (m)
8	40.94	--
9	50.3	1.29 (m)
10	37.1	--
11	21.48	1.63 (m) H-11a, 1.54 (m) H-11b
12	26.17	1.67 (m)
13	39.18	1.58 (m)
14	42.05	--
15	26.66	1.64 (m) H-15a, 0.99 (m) H-15b
16	38.31	1.01 (m) H-16a, 1.18 (m) H-16a
17	34.54	--
18	48.72	0.99 (m)
19	39.40	2.09 (m)
20	154.66	--
21	25.63	2.44 (m) H-21a, 2.20 (m) H-21b
22	38.89	1.58 (m)
23	27.96	0.83 (s)
24	16.50	0.85 (s)

25	16.34	0.87 (s)
26	15.99	1.02 (s)
27	14.73	0.93 (s)
28	19.48	0.85 (s)
29	25.50	1.02 (s)
30	107.13	4.61 (dd, J = 4.5, 2.2 Hz, 2H)
1'	171.01	--
2'	21.31	2.04 (s)

Table. IV. 18: The chemical shifts of ^{1}H NMR (400 MHz) and ^{13}C NMR (100 MHz) on CDCl$_3$ of compound **EP1c**; pseudotaraxasteryl acetate.

Position	Carbon (δ_C in ppm)	Proton (δ_H in ppm and J in Hz)
1	38.4	1.69 (m) H-1a, 1.01 (m) H-1b
2	23.71	1.65 (m) H-2a, 0.99 (m) H-2b
3	80.99	4.48 (dd, J = 16.3, 6.0 Hz)
4	37.81	--
5	55.4	0.79 (m)
6	18.2	1.50 (m) H-6a, 1.39 (m) H-6b
7	34.02	1.39 (m)
8	42.05	--
9	50.4	1.29 (m)

10	37.1	--
11	21.64	1.63 (m) H-11a, 1.54 (m) H-11b
12	27.61	1.62 (m) H-12a, 1.23 (m) H-12b
13	39.23	1.59 (m)
14	42.84	--
15	27	1.64 (m) H-15a, 0.99 (m) H-15b
16	36.71	1.29 (m) H-16a, 1.22 (m) H-16a
17	34.40	--
18	48.72	1.00 (m)
19	36.34	1.57 (m)
20	139.87	--
21	118.89	5.26 (d, J = 6.9 Hz, 1H)
22	42.19	1.71 (m) H-22a, 1.55 (m) H-22b
23	27.96	0.83 (s)
24	16.50	0.85 (s)
25	16.34	0.87 (s)
26	16.06	1.02 (s)
27	14.51	0.93 (s)
28	17.72	0.73 (s)
29	22.54	0.99 (s)
30	21.32	1.63 (s)

1'	171.01	--
2'	21.31	2.04 (s)

IV.4. 15. Compounds EP2

The compounds **EP2** is isolated in the form of a white powder soluble in the chloroform. This compound is characterized on TLC test by invisible spot under UV lamp (254 and 366 nm), which turns purple by revelation using acid solution and heating.

The ^{1}H NMR (**Figure. IV. 242**) and ^{13}C NMR (**Figure. IV. 245**) spectra reveals the presence of high number of signals. Also, the deshielded part of these spectra shows the presence of signals characteristic of different type of compounds, these indicating that **EP2** is isolated in the form of isomeric mixture.

The ^{1}H NMR spectrum (**Figure. IV. 242**) shows a sequence of extremely dense peaks between δ_H 0.70 and 1.7. This indicates the presence of a high number of methyl groups with doublet and singlet multiplicities.
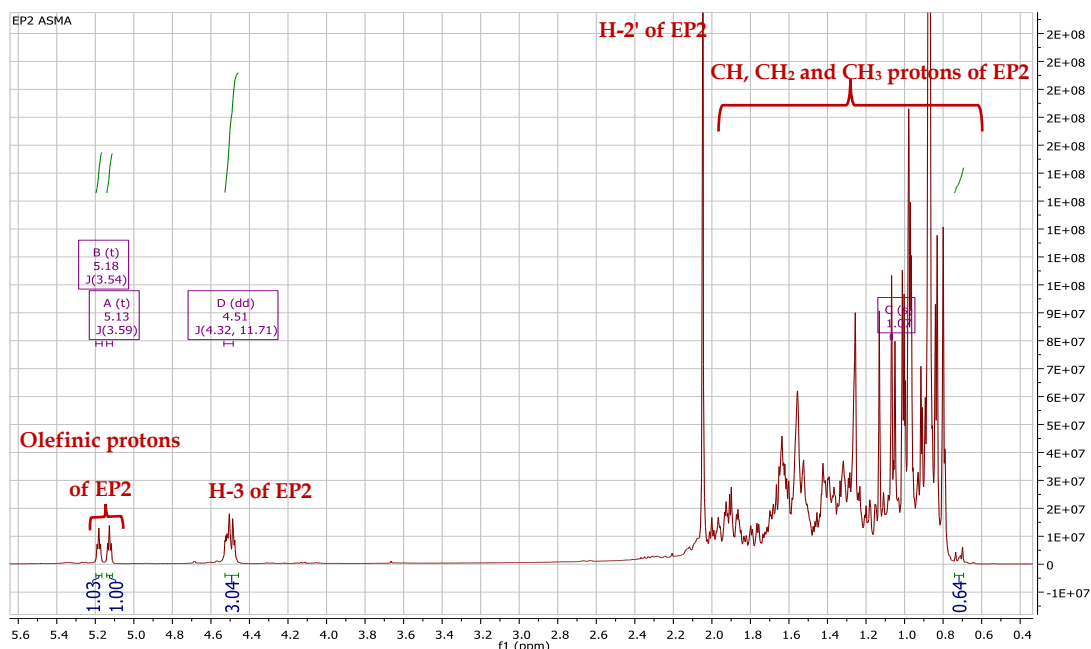
Figure. IV. 242: ^{1}H NMR spectrum (400 MHz, CDCl3) of the compound **EP2**.

The deshielded part of the ^{1}H NMR spectrum (**Figure. IV. 243**) reveals the presence of three signals corresponding to five protons resonating at δ_H 4.51 (dd, J =

11.7, 4.3 Hz, 3H), 5.13 (t, J = 3.6 Hz, 1H) and 5.18 (t, J = 3.5 Hz, 1H). Their corresponding carbons attributed using HSQC spectrum (**Figure. IV. 244**) at δ_C 80.97, 124.34 and 121.66, respectively. These carbons split into an oxymethine carbon assigned to the position C-3 and two ethylenic carbons.
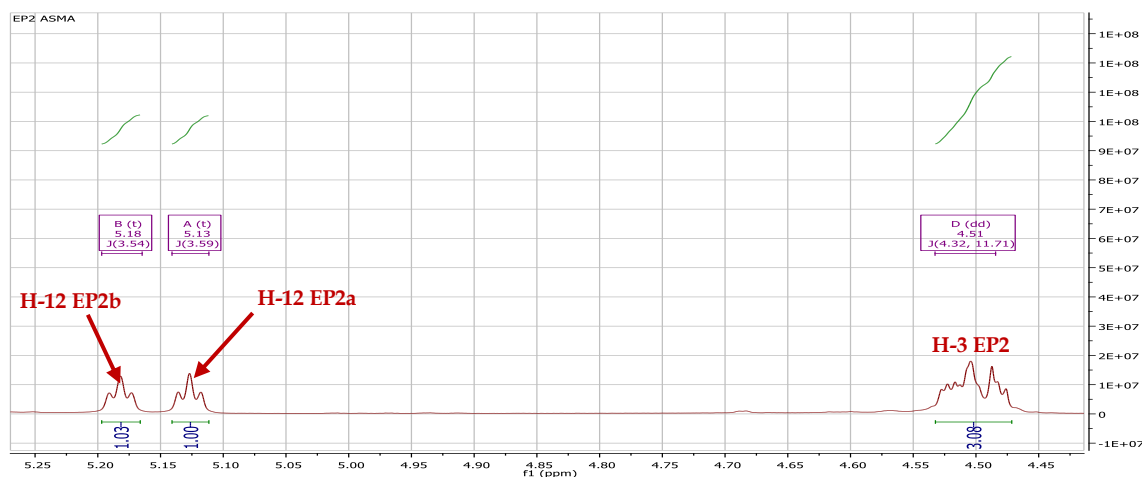
Figure. IV. 243: ^{1}HNMR spectrum (400MHz, CDCl$_3$) of the deshielded parts of **EP2.**
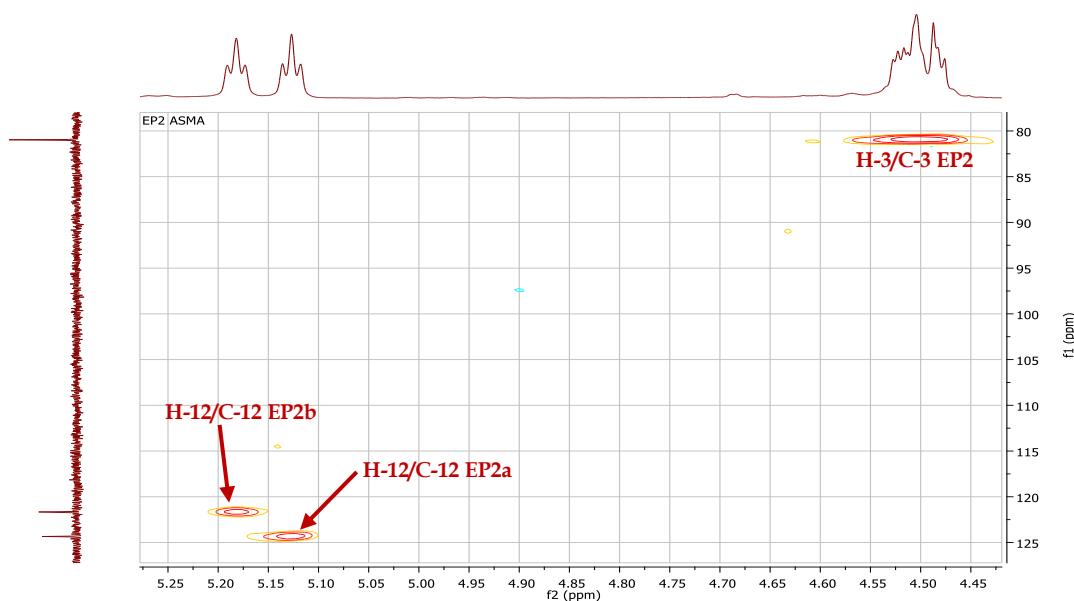
Figure. IV. 244: HSQC spectrum (100 MHz, CDCl$_3$) of the deshielded parts of **EP2**.

The ^{13}C NMR (**Figure. IV. 245**) and DEPT135 (**Figure. IV. 247**) spectra shows more than sixty signals, indicating a mixture of three triterpenes. In particular six signals of olefinic carbons were observed, being two tertiary (δ_C 121.66 and 124.34) and four quaternary carbons (δ_C 134.03, 134.57, 139.65 and 145.23) (**Figure. IV. 246**).
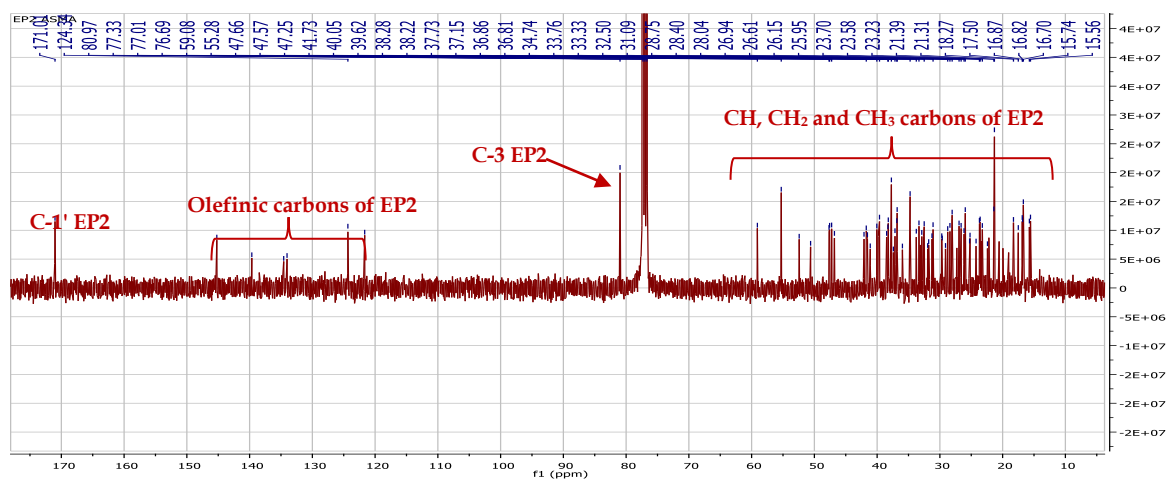
Figure. IV. 245: ^{13}C NMR spectrum (100 MHz, CDCl$_3$) of **EP2**.
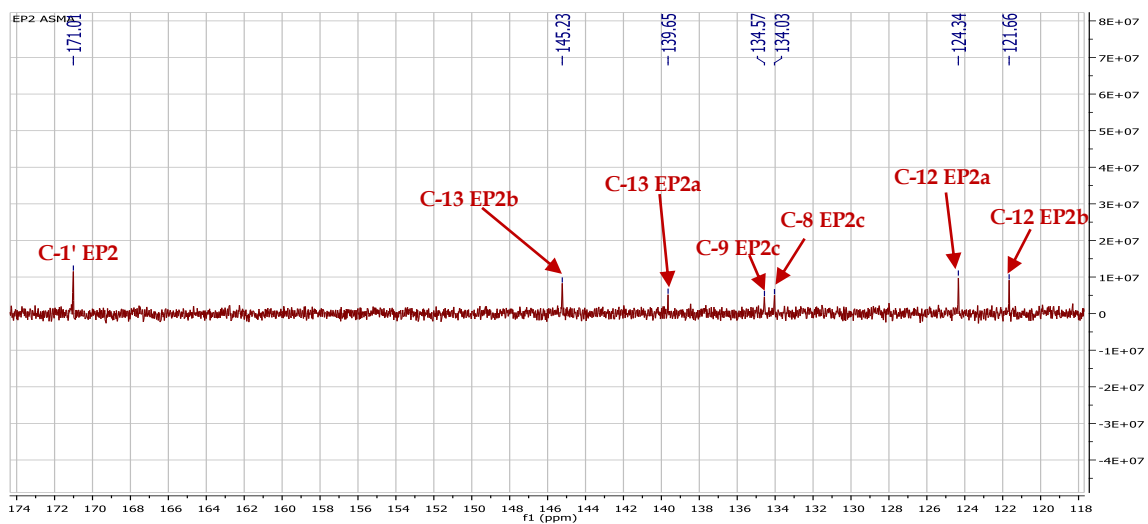
Figure. IV. 246: ^{13}C NMR spectrum (100 MHz, CDCl$_3$) olefinic carbons of **EP2**.
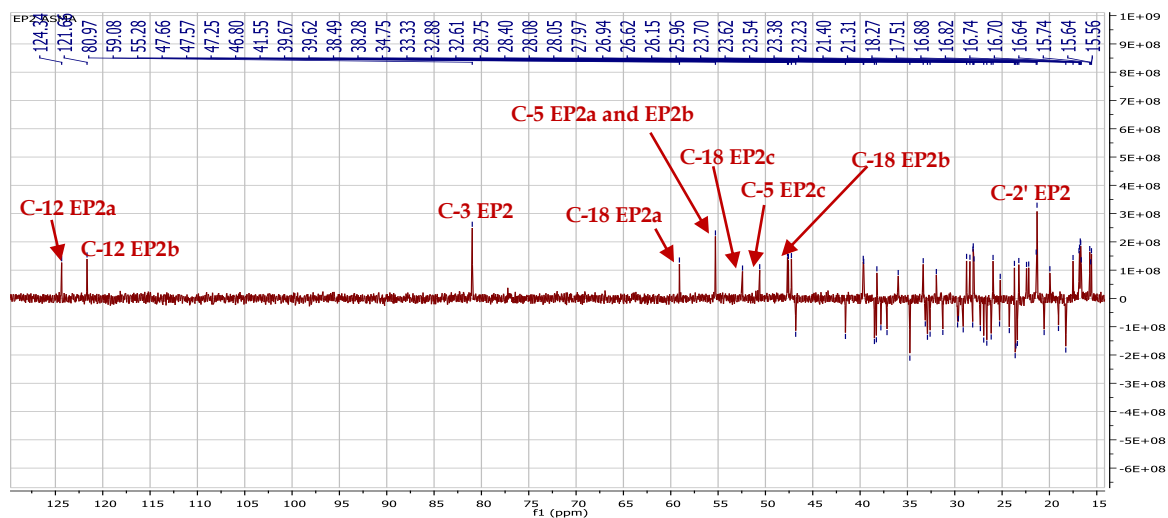
Figure. IV. 247: DEPT 135 spectrum (100 MHz, CDCl$_3$) of the compound **EP2**.

The comparison of these results with literature data suggested that the compound **EP2** compound is in the form of a mixture of three isomers of triterpenes type: **urs-12-ene** (α- amyrin) **EP2a**, **olean-12-ene** (β- amyrin) **EP2b** [224] and **D:C-friedo-ursa-8-ene EP2C** (Isobauerene) [195, 227]. The chemical shifts at δ_C 55.28 (C-5), 59.08 (C-18), 124.34 (C-12) and 139.65 (C-13) are characteristic of the skeleton **urs-12-ene** (α- amyrin) [195], while the values of the chemical shifts at δ_C 47.25 (C-18), 55.28 (C-5), 121.66 (C-12) and 145.23 (C-13) are characteristic of the skeleton **olean-12-ene** (β- amyrin) [195]. Whereas, the values of the chemical shifts at δ_C 50.60, 52.42, 134.03 and 134.57 are compatible with the signals of carbons of skeleton **friedo-ursa-8-ene**: C-5, C-18, C-8 and C-9 respectively [195].

This difference between the chemical shifts of carbons C-12 and C-13 of two structures **EP2a** and **EP2b**, is explained by the environment and the position of the methyl groups relative to the double bond (C12=C13). The C-13 carbon is more deshielded (δ_C 145.23 ppm) in the case of the oleanane skeleton because it receives less the shielding effect of the methyl groups carried by the C-20 carbon (Me-29, Me-30) compared to its homologous in the case of the ursane skeleton which is more shielded (δ_C 139.65 ppm) under the influence of the methyl carried by the C-19 carbon (Me-29) closer to the double bond (**Figure. IV. 248**).
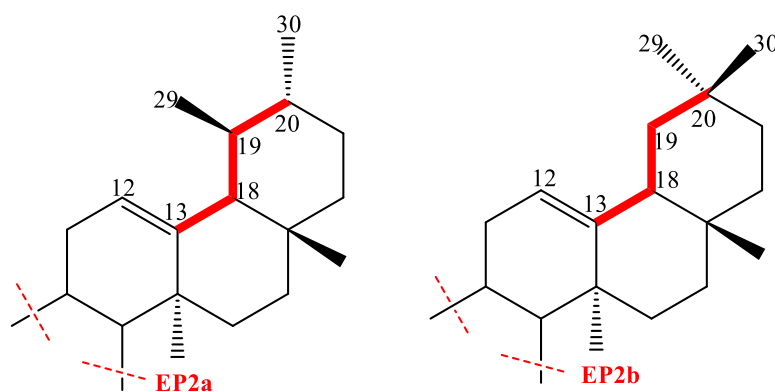
Figure. IV. 248: The effect of the carbons Me-29 and Me-30 on the double bond (C12=C13) of **EP2**.

The analysis of HMBC spectrum (**Figure. IV. 249**) displays correlations between H-12 (δ_H 5.13 **EP2a**) and carbons resonating at δ_C 23.38, 41.73, 47.57 and 59.08 corresponding to C-11, C-14, C-9 and C-18 respectively. Also, correlations

between H-12 (δ_H 5.18 **EP2b**) and carbons resonating at δ_C 42.09, 47.66 and 47.25 corresponding to C-14, C-9 and C-18, respectively (**Figure. IV. 250**).
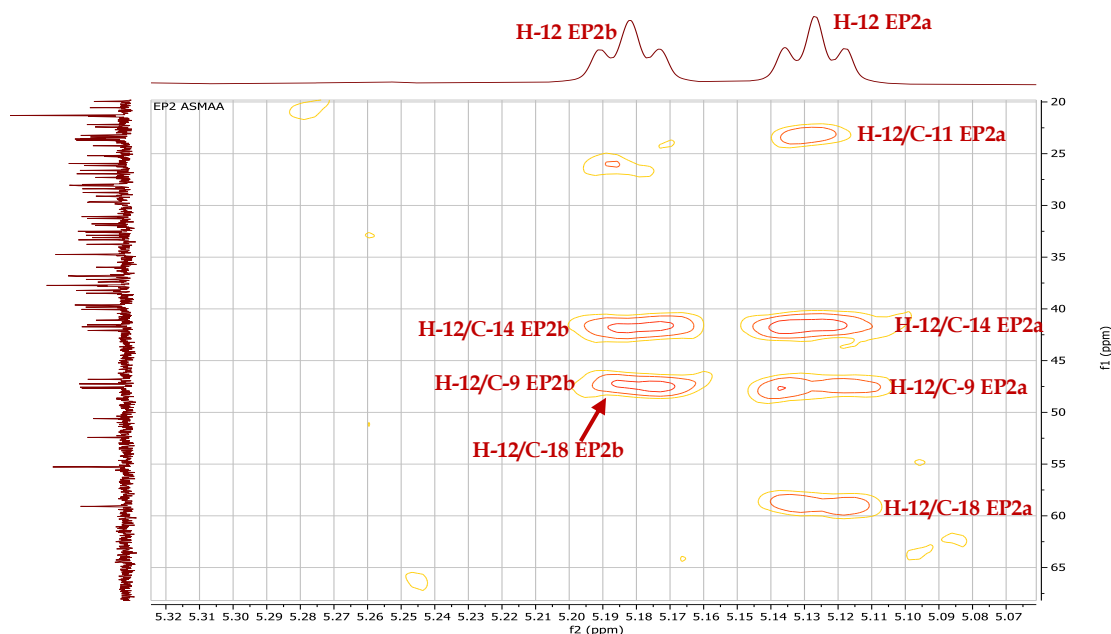
Figure. IV. 249: HMBC spectrum (400 MHz, CDCl₃) of H-12 correlations of **EP2a** and **EP2b**.
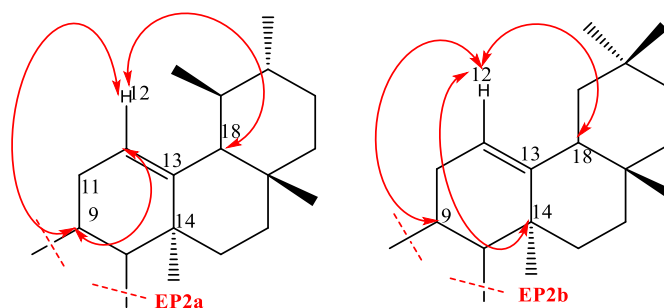
Figure. IV. 250: HMBC correlations of H- 12 of **EP2a** and **EP2b**.

Also, the difference between the chemical shifts of carbons of the double bond (C8=C9) of the structure **EP2c** and the two structures **EP2a** and **EP2b**, is explained by the nature of the olefinic carbons are quaternary carbon, and also the environment and the position of the methyl groups relative to the double bond. The carbon C-9 and C-8 is more shielded (δ_C 134.03, 134.57) in the case of the Isobauerene skeleton because the influence of the methyl closer to the double bond carried by the C-10 and C-14 carbon (Me-25, Me-26) compared to its homologous in the case of **EP2a** and **EP2b** the double bond (C12=C13) the C-13 is more deshielded (δ_C 139.65 and 145.23).

The analysis of HMBC spectrum (**Figure. IV. 251**) exhibits correlations between C-8 (δ_C 134.03) and H_3-25 (δ_H 0.98) and between C-9 (δ_C 134.57) and H_3-26 (δ_H 1.01) (**Figure. IV. 252**).
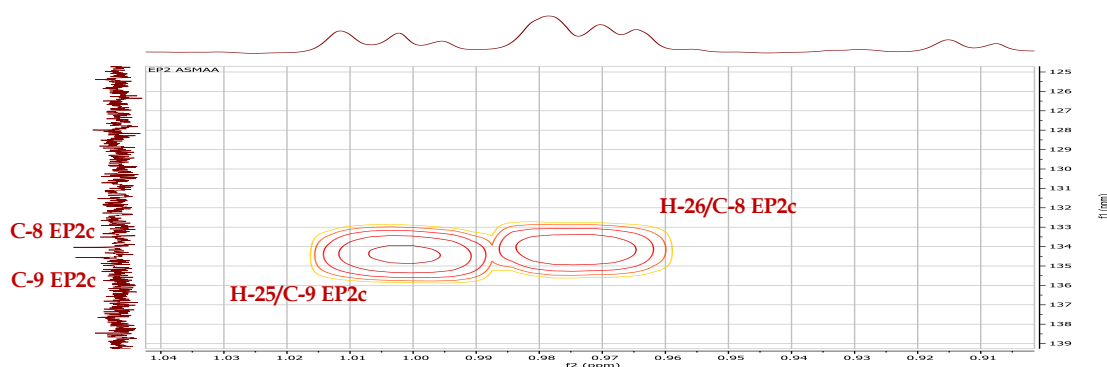
Figure. IV. 251: HMBC spectrum (400 MHz, CDCl$_3$) exhibits the correlations between C-8 and H$_3$-25 and between C-9 and H$_3$-26 of **EP2c**.
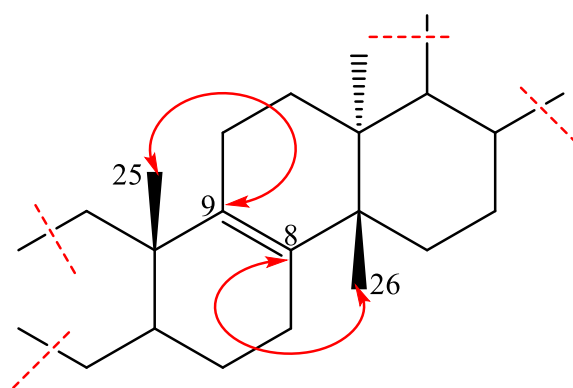
Figure. IV. 252: HMBC correlations between C-8 and H$_3$-25 and between C-9 and H$_3$-26 of **EP3c**.

The HSQC experiment (**Figure. IV. 253**) allows the localization of protons H-18 of **EP2a**, H-18 **EP2b** and H-18 **EP2c** of at δ_H 1.32 (m), 1.95 (dd, J = 12.9, 3.3 Hz) and 1.26 (m) respectively. This difference in chemical shift is due to the different chemical environment around the C-18 carbon.
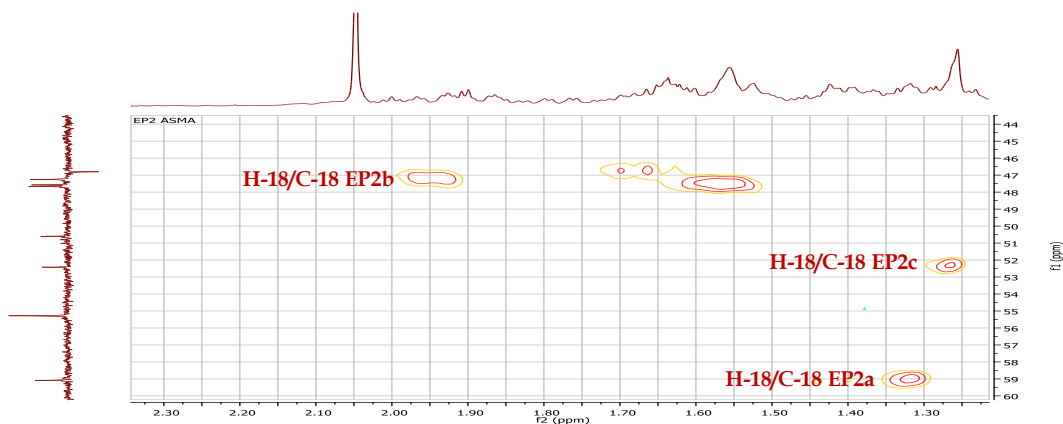
Figure. IV. 253: HSQC spectrum (400 MHz, CDCl$_3$) of C-18/H-18 correlations of **EP2a**, **EP2b** and **EP2c.**

The protons H-18 of **EP2a**, **EP2b** and **EP2c** correlates on COSY spectrum (**Figure. IV. 254**) with the protons H-19 **EP2a** (δ_H 1.32), H$_2$-19 **EP2b** (δ_H 1.68 and 1.02) and H-19 (δ_H 1.10), **EP2c**, their corresponding carbons assigned using HSQC spectrum at δ_C 39.6, 46.8 and 35.97, respectively.
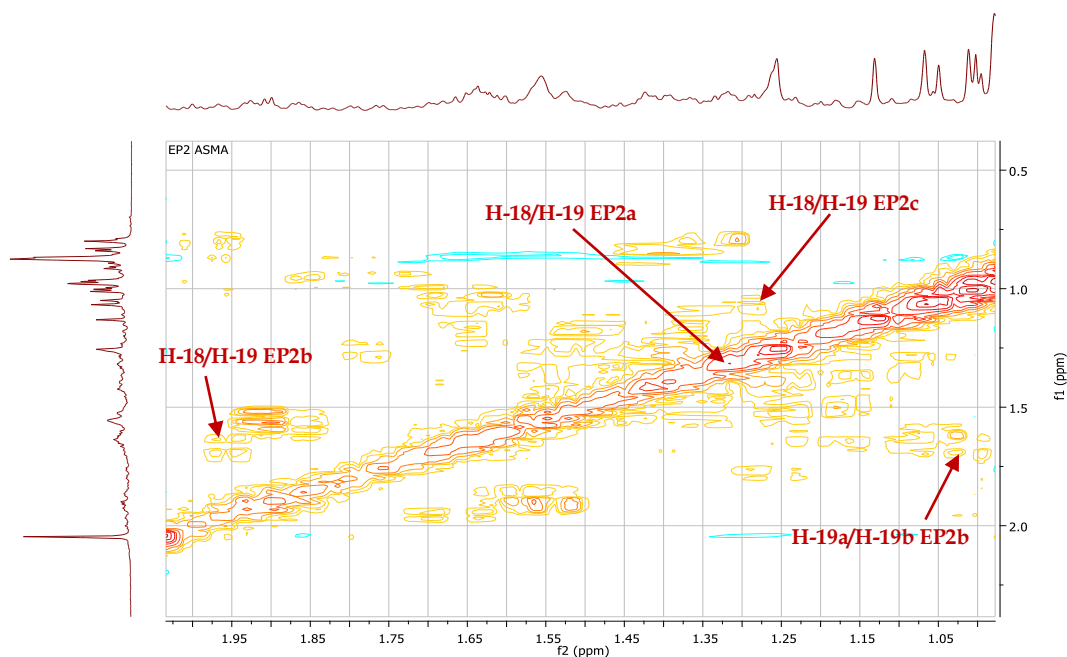
Figure. IV. 254: COSY spectrum (400 MHz, CDCl$_3$) of H-18/H-19 correlations of **EP2a**, **EP2b** and **EP2c.**

According to the identified carbons C-18 and C-19 of **EP2a**, **EP2b** and **EP2c**, it is easy to characterize the three methyl groups Me-28, Me-29 and Me-30: δ_H 0.80,

0.80 and 0.92 of **EP2a**, δ_H 0.83, 0.88 and 0.87 of **EP2b** and δ_H 0.88, 0.99 and 0.90 of **EP2c** respectively, following their correlations in the HMBC spectrum (

Figure. IV. *256*, **Figure. IV. 255**).
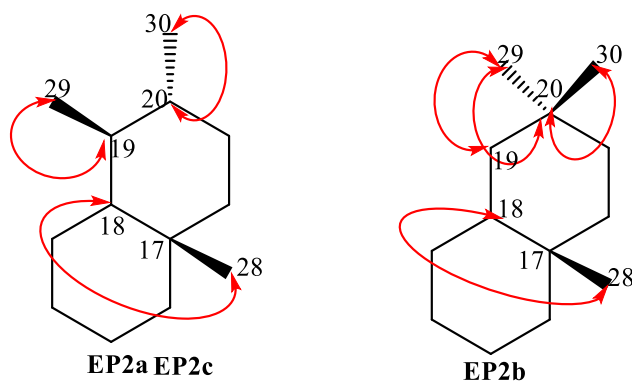
Figure. IV. 255: HMBC correlations of Me-28, 29 and 30 of **EP2a**, **EP2b** and **EP2**
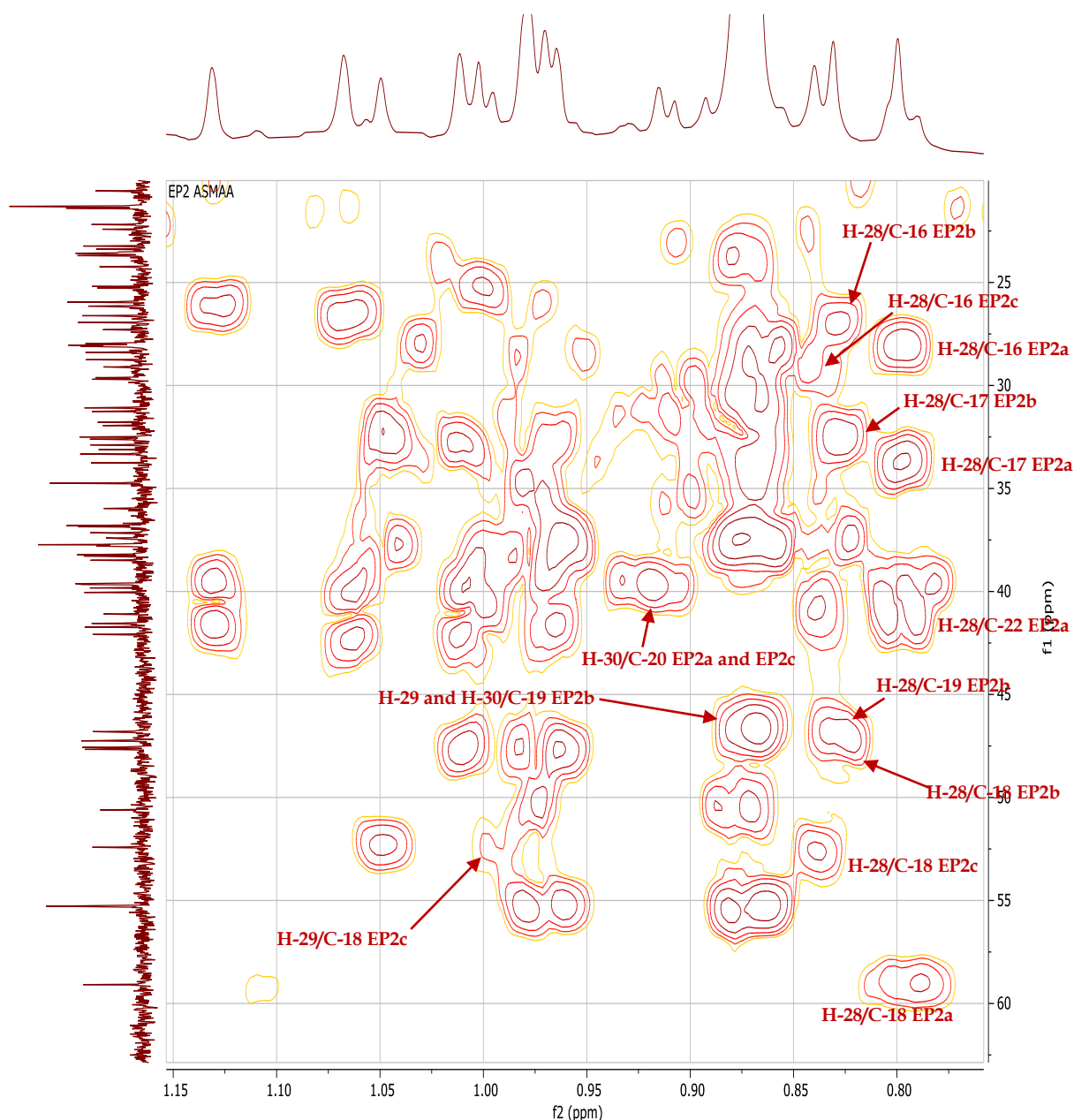
Figure. IV. 256: HMBC spectrum (400 MHz, CDCl₃) of Me-28, Me-29 and Me-30 of **EP2a**, **EP2b** and **EP2c.**

The analysis of HMBC spectrum (**Figure. IV. 257**, **Figure. IV. 258**) also allows the localization of methyl groups Me-25, Me-26 and Me-27: δ_H 0.97, 0.97 and 1.07 ppm of **EP2a** and δ_H 0.97, 1.01 and 1.13 of **EP2b** which reveals correlations with C-9 and C-13 already identified. This spectrum shows also correlations between methyl group Me-27 δ_H 0.87 of **EP2c** and the carbon C-18 already identified. The protons of the methyl group Me-25 of **EP2a** and **EP2b** correlates in HMBC spectrum with the carbons C-5 and C-9 already attributed, also with C-10 and C-1 resonating at δ_C 38.49 and 36.8 of **EP2a** and at δ_C 38.24 and 36.8 of **EP2b** respectively. Their proton assigned

using HSQC spectrum (**Figure. IV. 260**). From the carbons C-3 and C-5, the two methyl groups Me-23 and Me-24 at δ_H 0.87 of **EP2a**, **EP2b** and **EP2c** are easily identified, following their correlations shown on the HMBC spectrum (**Figure. IV. 259**).
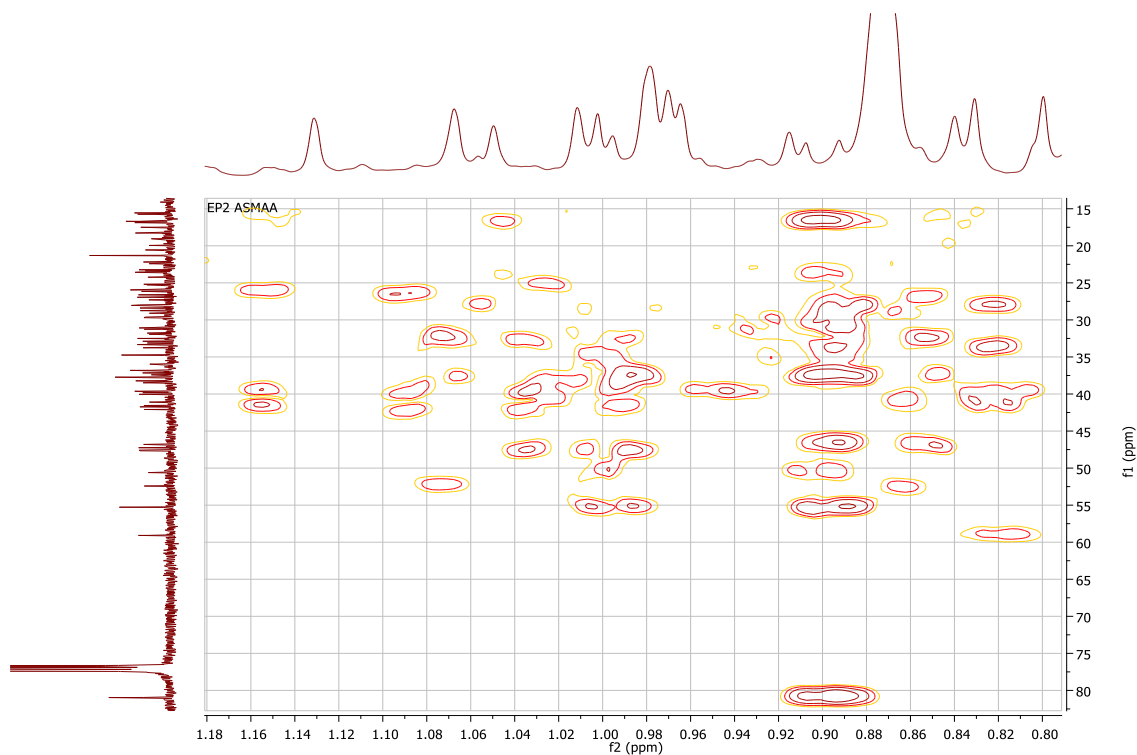
Figure. IV. 257: HMBC spectrum (400 MHz, CDCl₃) shows correlations of Me-25, Me-26 and Me-27 **of EP2a**, **EP2b** and **EP2c**.
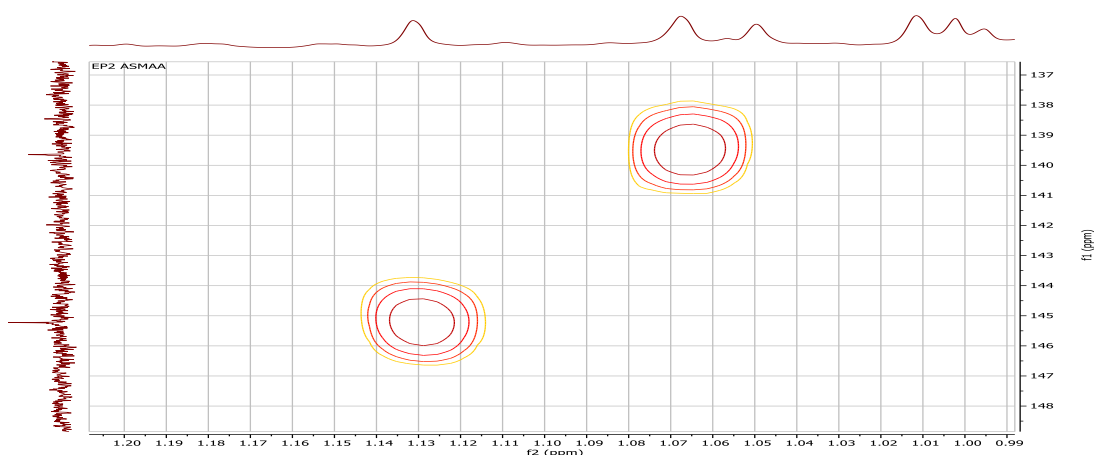
Figure. IV. 258: HMBC spectrum (400 MHz, CDCl₃) reveals correlations of Me-27 of **EP2a** and **EP2b.**
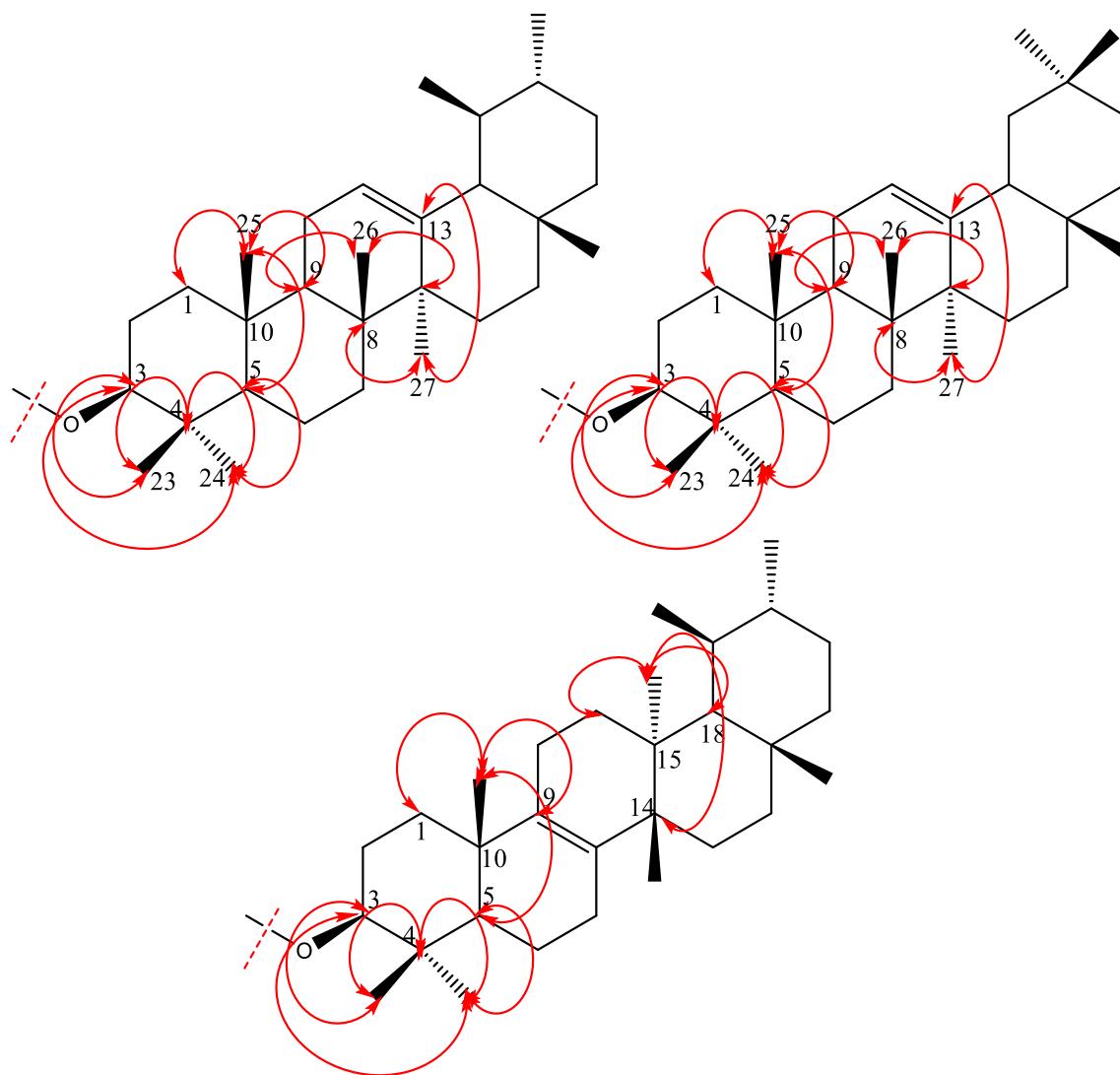
Figure. IV. 259: HMBC correlations of Me-25, Me-26 and Me-27 of **EP2a**, **EP2b** and **EP2c**.

The analysis of HSQC spectrum makes it possible to attribute the carbons of the methyl groups of **EP2a**, **EP2b** and **EP2c** (**Figure. IV. 260**).
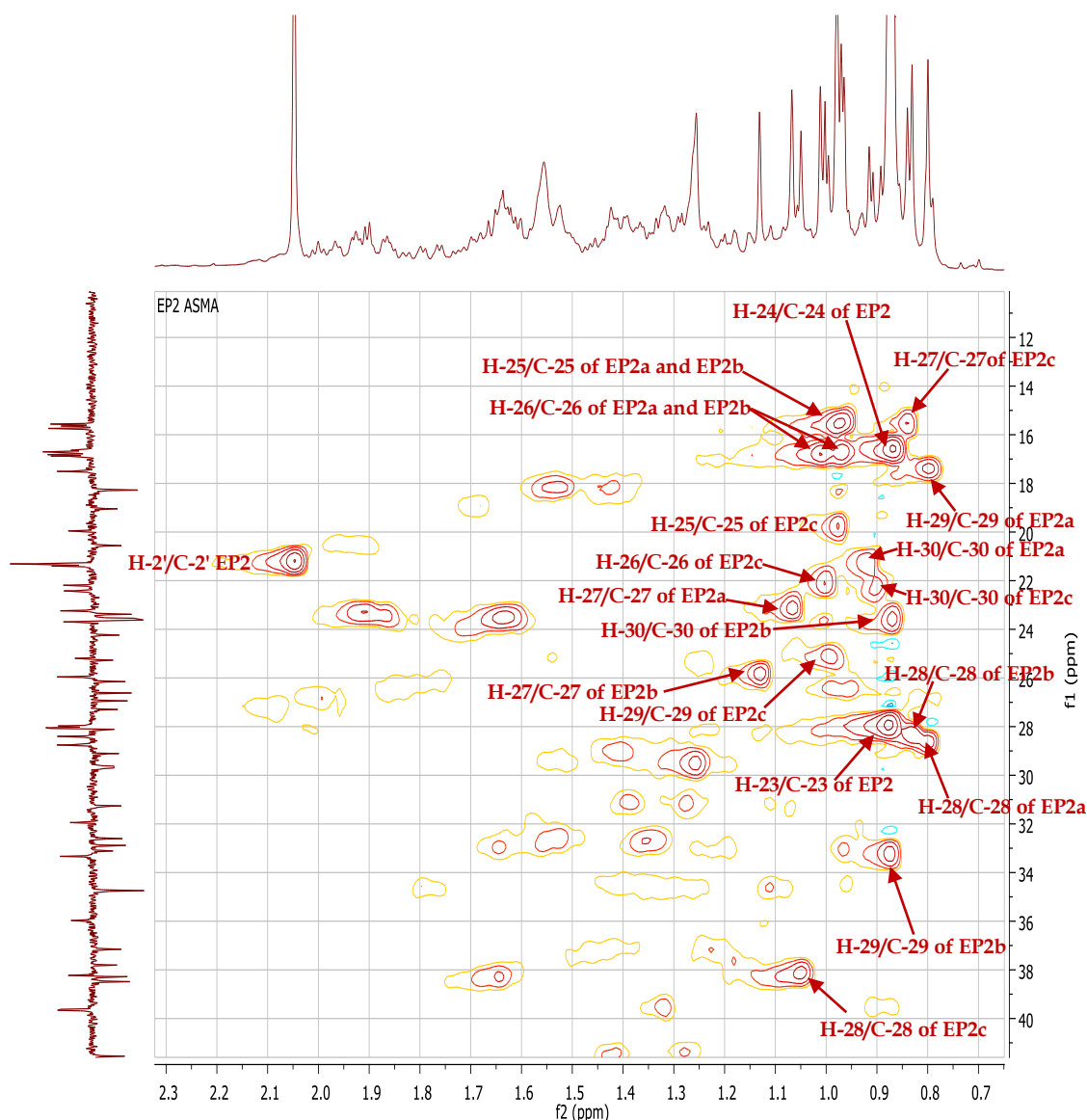
Figure. IV. 260: HSQC spectrum (400 MHz, CDCl$_3$) of methyl groups of **EP2a**, **EP2b** and **EP2c**.

The chemical shifts of the proton and carbon at C-3 δ_H 4.51/ δ_C 80.99, in addition to the signal of an ester carbonyl group δ_C 171.01 are a typical of acetylated triterpene as the compound **EP1**. This was verified by the correlations of H-3 δ_H 4.51 and the ester carbonyl C-1' δ_C 171.01 in the HMBC spectrum (**Figure. IV. 261**). The carbon C-1' displays also correlations with methyl group at δ_H 2.04, this confirms the acetate group at the position C-3. The integration of the signal at δ_H 2.04 more than 9H attributable to at least three acetate groups, the carbon of which resonates at δ_C 21.31. The combined analysis of the different correlations COSY, HSQC and HMBC spectra makes it possible to assign the chemical shifts of all the protons and carbons of **EP2a**, **EP2b** and **EP2c** (**Table. IV. 19** , **Table. IV. 20** and **Table. IV. 21**).
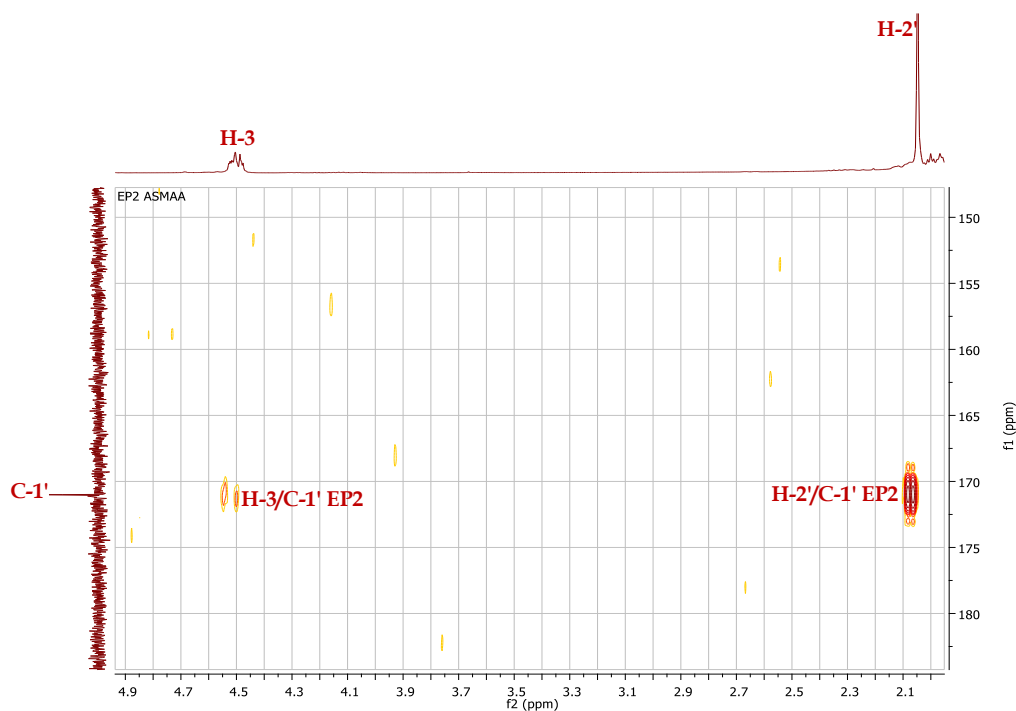
Figure. IV. 261: HMBC spectrum (400 MHz, CDCl$_3$) show the correlation at C-3 of the compound **EP2**.

The difference in integration between the olefinic protons makes it possible to deduce the proportion of the compounds in the mixture **EP2** (**Figure. IV. 262**) at 33.3% α- amyrin acetate **EP2a**, 33.3% β- amyrin acetate **EP2b** and 33.3% isobauerenyl acetate **EP2c**.

The α-amyrin acetate **EP2a** is already isolated from the Asteraceae family from *Microtrichia perotitii* [228] and *Lychnophora pinaster* [229], this compound is also isolated from *Alstonia boonei* (Apocyanaceae) [230] and *Gambeya boiviniana* (Sapotaceae) [231]. The β-amyrin acetate **EP2b** is already isolated from Asteraceae family from the plant *Vernonia auriculifera* [232]. This compound is also isolated from *Chrysophyllum albidium* (Sapotaceae) [233]. The isobauerenyl acetate **EP2c** is isolated for the first time from the plant *Helietta longifoliata* (Rutaceae) [227]. These three compounds are identified for the first time from the *Atractylis* genus. All the data are illustrated in the **Table. IV. 19**, **Table. IV. 20** and **Table. IV. 21**, which are in total agreement with; α-amyrin acetate **EP2a** [228-230], β-amyrin acetate **EP2b** [232, 233] and isobauerenyl acetate **EP2c** [227].
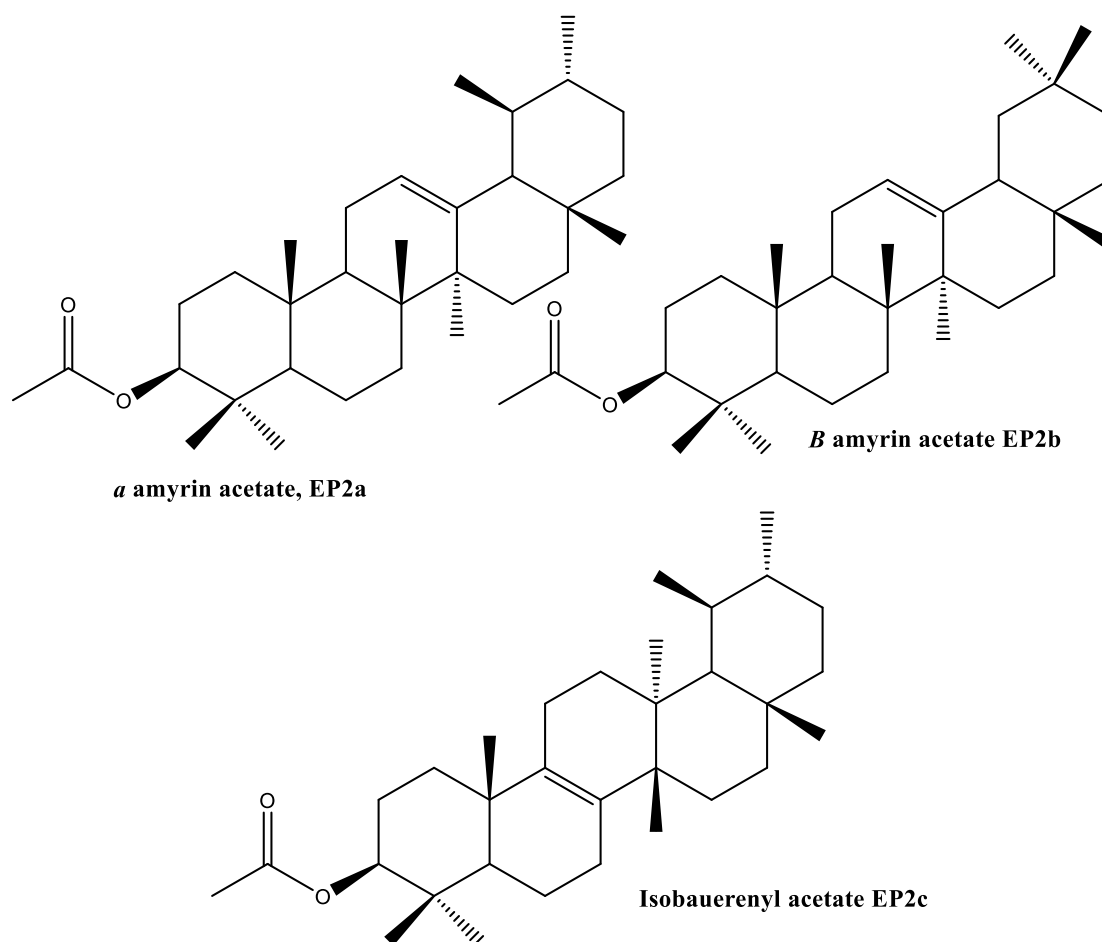
Figure. IV. 262: Structure of the compound **EP2**; **EP2a**: urs-12-ene-3-acetate (α-amyrin acetate), **EP2a**: olean-12-ene-3-acetate (β- amyrin acetate) and **EP2c**: D:C-friedo-ursa-8-ene (Isobauerenyl acetate).

Table. IV. 19: The chemical shifts of ^{1}H NMR (400 MHz) and ^{13}C NMR (100 MHz) on CDCl$_3$ of compound **EP2a**; α- amyrin acetate.

Position	Carbon (δ$_C$ in ppm)	Proton (δ$_H$ in ppm and J in Hz)
1	38.49	1.65 (m) H-1a, 1.06 (m) H-1b
2	23.62	1.64 (m)
3	80.97	4.51 (dd, J = 11.7, 4.3 Hz)
4	37.73	--
5	55.28	0.85

6	18.27	1. 52 (m) H-6a, 1.42 (m) H-6b
7	32.88	1.55 (m) H-7a, 1.35 (m) H-7b
8	40.05	--
9	47.66	1.56 (m)
10	36.8	--
11	23.38	1.91 (m)
12	124.34	5.13 (t, J = 3.6 Hz, 1H)
13	139.65	--
14	42.09	--
15	28.11	2.01 (m) H-15a, 1.23 (m) H-15b
16	26.62	1.84 (m) H-16a
17	33.76	--
18	59.08	1.32 (m)
19	39.6	1.32 (m)
20	39.6	0.89
21	31.26	1.38 (m) H-21a, 1.27 H-21b
22	41.55	1.42 (m) H-22a, 1.27 (m) H-22.
23	28.05	0.87 (s, 3H)
24	16.7	0.87 (s, 3H)
25	15.56	0.97 (S, 3H)
26	16.8	0.97 (S, 3H)

27	23.23	1.07 (S, 3H)
28	28.75	0.80 (S, 3H)
29	17.51	0.80 (S, 3H)
30	21.39	0.92 (S, 3H)
1'	171.01	--
2'	21.31	2.05

Table. IV. 20: The chemical shifts of ^{1}H NMR (400 MHz) and ^{13}C NMR (100 MHz) on CDCl$_3$ of of compound **EP2b**; β- amyrin acetate.

Position	Carbon (δ_C in ppm)	Proton (δ_H in ppm and J in Hz)
1	38.24	1.65 (m) H-1a, 1.06 (m) H-1b
2	23.58	1.64 (m)
3	80.97	4.51 (dd, J = 11.7, 4.3 Hz)
4	37.73	--
5	55.28	0.85
6	18.27	1. 52 (m) H-6a, 1.42 (m) H-6b
7	32.61	1.55 (m) H-7a, 1.35 (m) H-7b
8	39.83	--
9	47.57	1.56 (m)
10	36.8	--
11	23.54	1.91 (m)

12	121.66	5.18 (t, J = 3.5 Hz, 1H)
13	145.23	--
14	41.73	--
15	26.15	1.75 (m) H-15a
16	26.94	1.99 (m) H-16a
17	32.5	--
18	47.25	1.95 (dd, J = 12.9, 3.3 Hz)
19	46.80	1.68 H-19a, 1.02 H-19b
20	31.09	--
21	34.75	1.39 (m) H-21a, 1.29 (m) H-21b
22	37.16	1.42 (m) H-22a, 1.22 (m) H-22b
23	28.08	0.87 (s, 3H)
24	16.7	0.87 (s, 3H)
25	15.74	0.97 (S, 3H)
26	16.88	1.01 (S, 3H)
27	25.96	1.13 (S, 3H)
28	28.40	0.83 (S, 3H)
29	33.33	0.88 (S, 3H)
30	23.70	0.87 (S, 3H)
1'	171.01	--
2'	21.31	2.05

Table. IV. 21: The chemical shifts of ^{1}H NMR (400 MHz) and ^{13}C NMR (100 MHz) on CDCl$_3$ of compound **EP2c**; Isobauerenyl acetate.

Position	Carbon (δ_C in ppm)	Proton (δ_H in ppm and J in Hz)
1	34.75	1.79 (m) H-1a, 1.11 (m) H-1b
2	24.24	1.71 (m)
3	80.97	4.51 (dd, J = 11.7, 4.3 Hz)
4	37.73	--
5	50.60	1.18 (m)
6	19.04	1.68 (m)
7	25.27	1.53 H-7a (m),1.25 H-7b (m)
8	134.03	--
9	134.57	--
10	37.41	--
11	20.56	1.92 (m)
12	33.11	1.24 (m) H-12a, 1.19 H-12b (m)
13	37.76	--
14	41.10	--
15	27.30	2.11 (m)
16	29.62	1.53 (m)
17	31.79	--
18	52.42	1.26 (m)

19	35.97	1.10 (m)
20	34.74	1.28 (m)
21	29.11	1.53 (m)
22	37.81	1.62 (m) H-22a, 1.16 (m) H-22b
23	27.97	0.87 (S, 3H)
24	16.64	0.84 (S, 3H)
25	19.96	0.98 (S, 3H)
26	22.19	1.00 (S, 3H)
27	15.64	0.87 (S, 3H)
28	38.23	1.05 (S, 3H)
29	25.20	0.99 (S, 3H)
30	22.42	0.90 (S, 3H)
1'	171.01	--
2'	21.31	2.05

IV.4. 16. Compounds EP3

The compounds **EP3** is isolated in the form of a white powder soluble in the chloroform. This compound is characterized on TLC test by invisible spot under UV lamp (254 and 366 nm), which turns purple by revelation using acid solution and heating.

The ^{1}H NMR (**Figure. IV. 263**) and ^{13}C NMR (**Figure. IV. 264**) spectra reveals the presence of high number of signals. Also, the deshielded part of these spectra shows the presence of signals characteristic of different type of compounds, these indicating

that **EP3** is isolated in the form of isomeric mixture with characteristics as the compound **EP1** (The same type).

The analysis of ^{1}H NMR spectrum of **EP3** displays the absence of the peak of methyl group at δ_H 2.04 and the appearance of new peak at δ_H 2.29 (td, J = 7.6, 2.1 Hz, 6H) compared to the ^{1}H NMR spectrum of **EP1** (**Figure. IV. 263**).
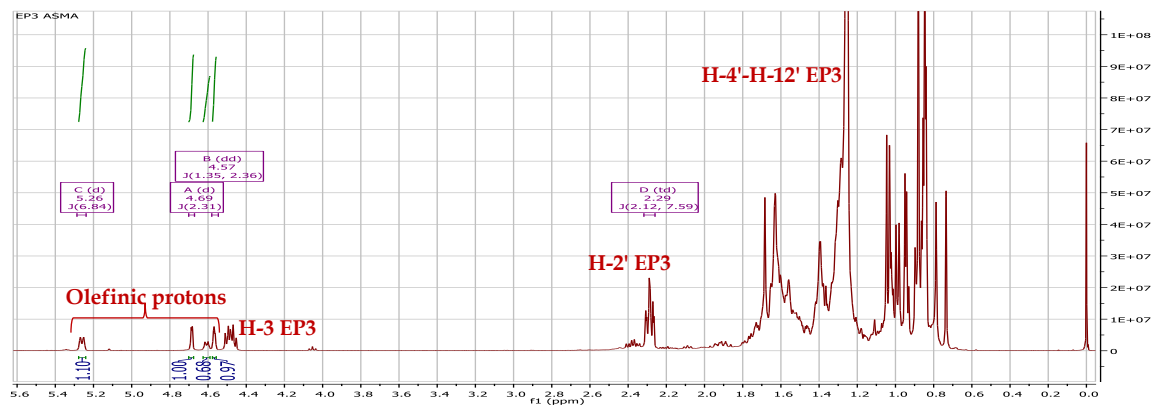
Figure. IV. 263: ^{1}H NMR spectrum (400 MHz, CDCl$_3$) of compound **EP3**.
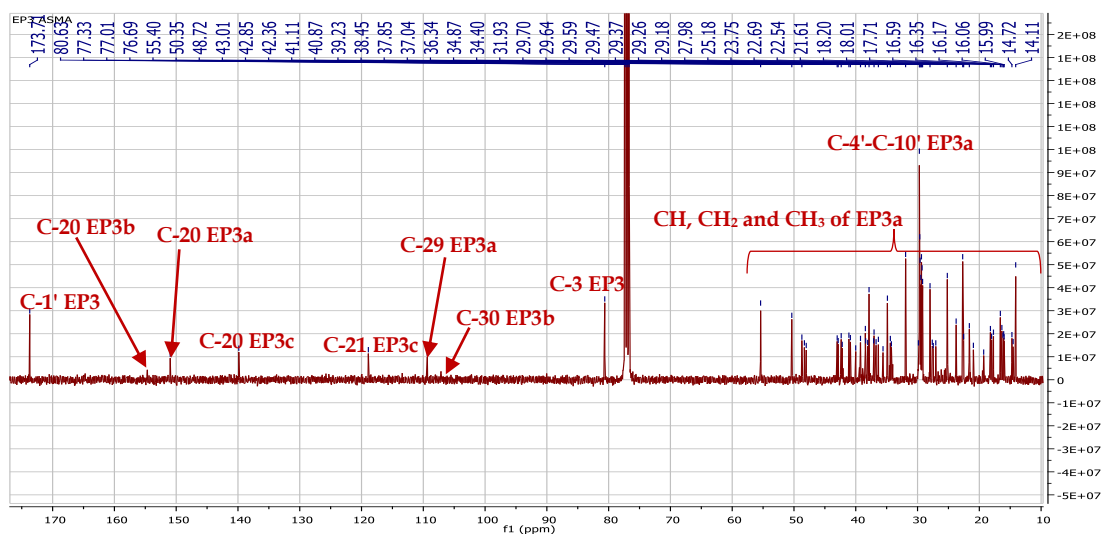
Figure. IV. 264: ^{13}C NMR spectrum (100 MHz, CDCl$_3$) of the compound **EP3**.

Also, the deshielded part of ^{1}H NMR (**Figure. IV. 265**) and ^{13}C NMR spectra (**Figure. IV. 266**) of the compound **EP3** shows the presence of the same characteristic peaks observed in **EP1** spectra. The comparison of these results with **EP1** and the literature data suggested the presence of triterpenes type **lup-20(29)-ene** (δ_C 109.35 and 150.97), **urs-20(30)-ene** (δ_C 107.13 and 154.67) and **urs-20-ene** (δ_C 118.89 and 139.87). The chemical shift of oxygenated carbon also was characteristic of an ester

triterpene (δ_C 80.63), but the carbonyl group was more deshielded (δ_C 173.71 ppm) than in **EP1**.
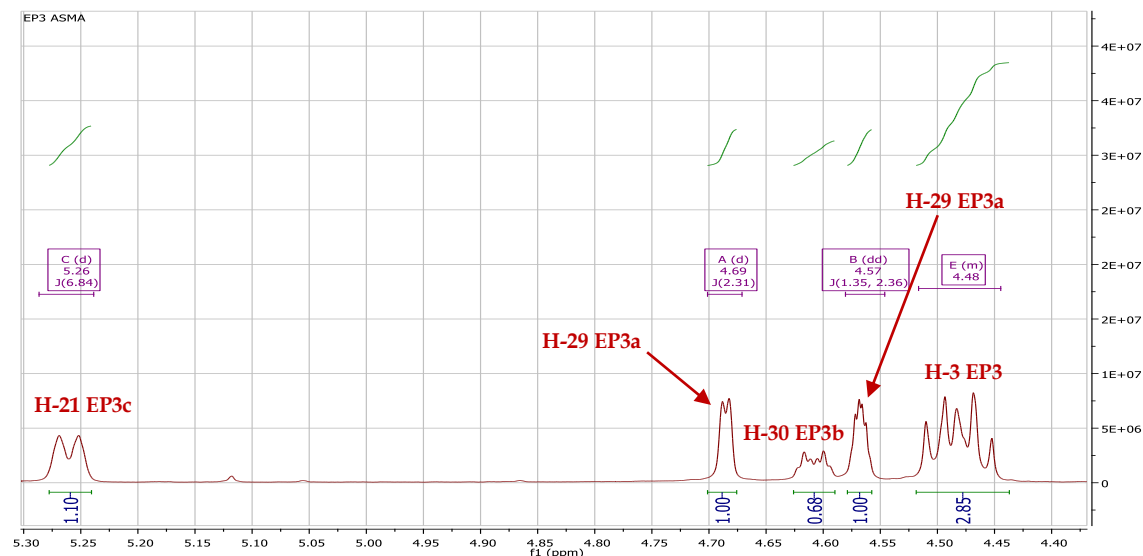
Figure. IV. 265: ^{1}H NMR spectrum (400 MHz, CDCl$_3$) of the deshielded part of **EP3**.
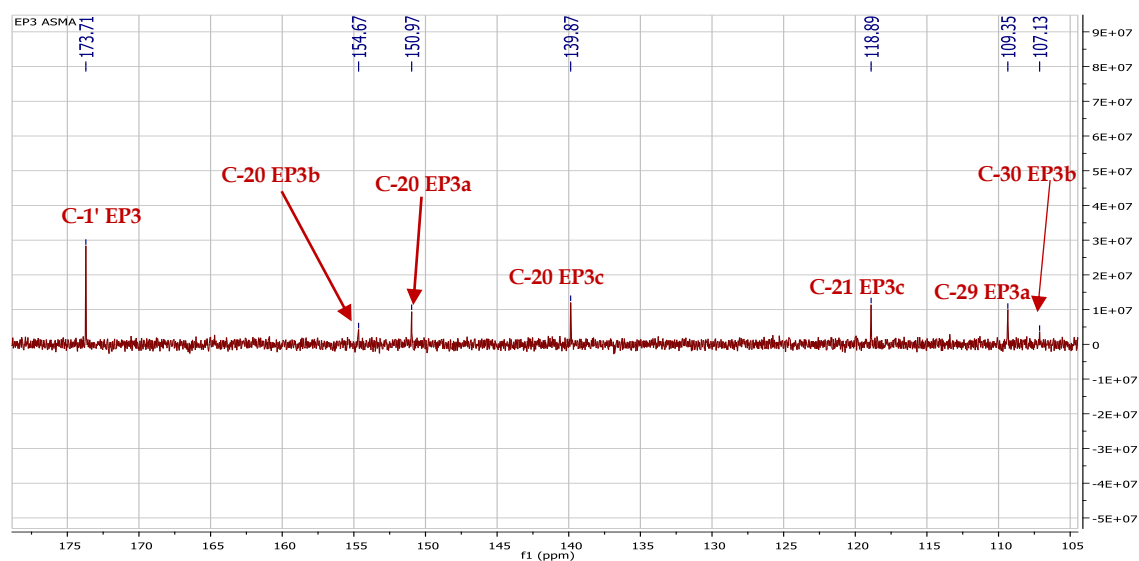
Figure. IV. 266: ^{13}C NMR spectrum (100 MHz, CDCl$_3$) of the deshielded part of **EP3**.

The ^{1}H NMR spectrum (**Figure. IV. 267**) showed protons in form of doublet of a doublet at δ_H 4.46 (dd, J= 7.0, 6.8 Hz) for 3α-H, and in the form of triplet at δ_H 2.29 (J 6.4 Hz) corresponding to the methylene adjacent to ester carbonyl, a multiplet at 1.63 for the β -methylene of the carbonyl, a broad singlet at δ_H 1.25 integrated for 54 protons and a methyl triplet at δ_H 0.88 (J = 6.9 Hz) indicating the presence of a carbon side chain at the C-3 position. This was verified by the deshielding effect observed in the carbonyl group (δ_C 173.71), and confirmed by the correlations of H-3 and the ester

carbonyl C-1 in the HMBC of **EP3**. These results are a typical of long chain carbons at C-3 [224, 234].
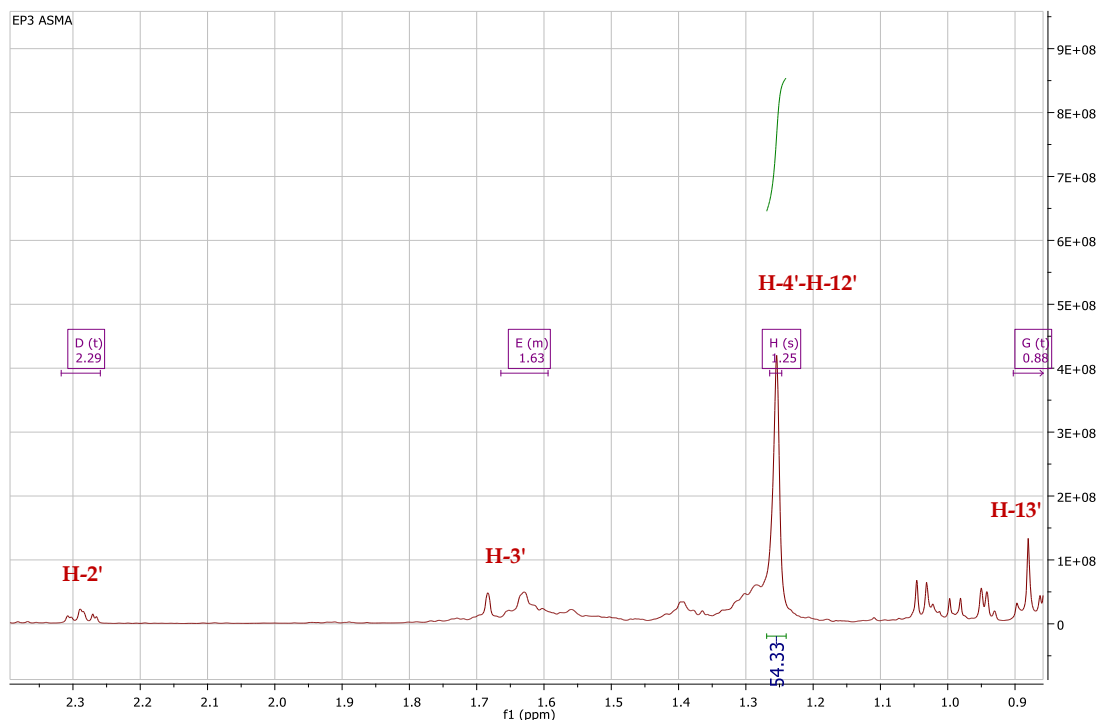
Figure. IV. 267: ^{1}H NMR spectrum (400 MHz, CDCl$_3$) of protons at C-3 of **EP3**.

This long chin of carbon confirmed by the HMBC (**Figure. IV. 269**), COSY (**Figure. IV. 270**) and HSQC (**Figure. IV. 271**, **Figure. IV. 272**) spectra.

The HMBC spectrum displays correlations between H-2' (δ_H 2.29) and carbons resonating at δ_C 25.18 and from 29.2 to 29.85 corresponding to *n* number of CH$_2$ groups (CH$_2$)$_n$. Their corresponding protons assigned using HSQC spectrum as flows:

➢ C-3' δ_C 25.18 its corresponding proton H-3' δ_H 1.63.
➢ The carbons resonating at δ_C 29.2 to 29.85 their corresponding protons resonating at δ_H 1.25.

The protons resonating at δ_H 1.25 a broad singlet integrated for 54 protons. The integration of these protons indicated the presence of 9 CH$_2$ attached to the carbon C-3'.

The correlations between 2' and 3' and between 3' and 4' positions confirmed by the presence of correlations between the identified proton δ_H H-3' 1.63 and C-4' δ_C 29.2 in the HMBC spectrum (**Figure. IV. 269**). Also, confirmed by the presence of

correlation between the identified protons H-2' δ_H 2.29 and H-3' δ_H 1.63 and between H-3' and H-4' δ_H 1.25 in COSY spectrum (**Figure. IV. 270**).

The identified carbon at δ_C 29.85 exhibits correlations in the HMBC spectrum with protons resonating at δ_H 1.25. Its corresponding carbons assigned with the help of HSQC spectrum at δ_C 31.93 and 22.70 corresponding to C-11' and C-12', respectively.

The identified proton at δ_H 1.25 corresponding to H-12' shows a correlation with carbon resonating at δ_C 14.13 in the HMBC spectrum corresponding to C-13' assigned to methyl group, this means the end of the carbon chain. The HSQC spectrum makes it possible to attributed its corresponding proton H-13' at δ_H 0.88. The last correlations (**Figure. IV. 268**) confirmed by:

- ➢ The presence of correlation between C-12' δ_C 22.70 and H-13' δ_H 0.88 in the HMBC spectrum.
- ➢ The presence of correlation between H-12' δ_H 1.25 and H-13' δ_H 0.88 in the COSY spectrum.
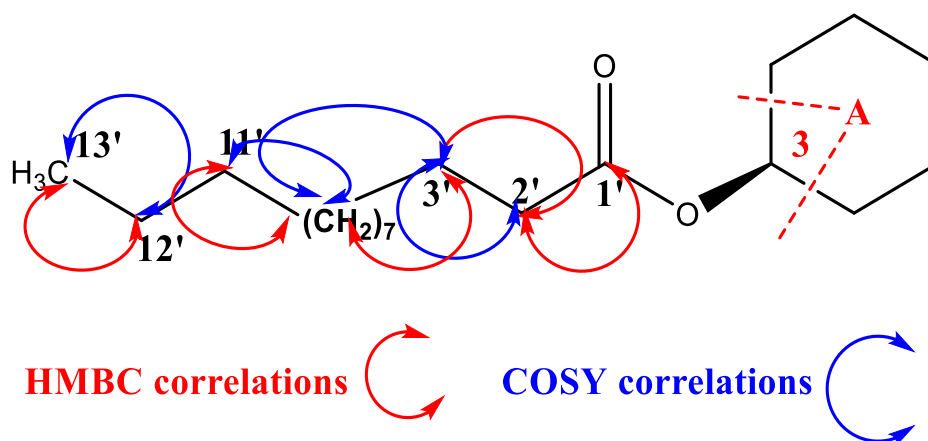
Figure. IV. 268: HMBC and COSY correlations at C-3 of the compound **EP3**.
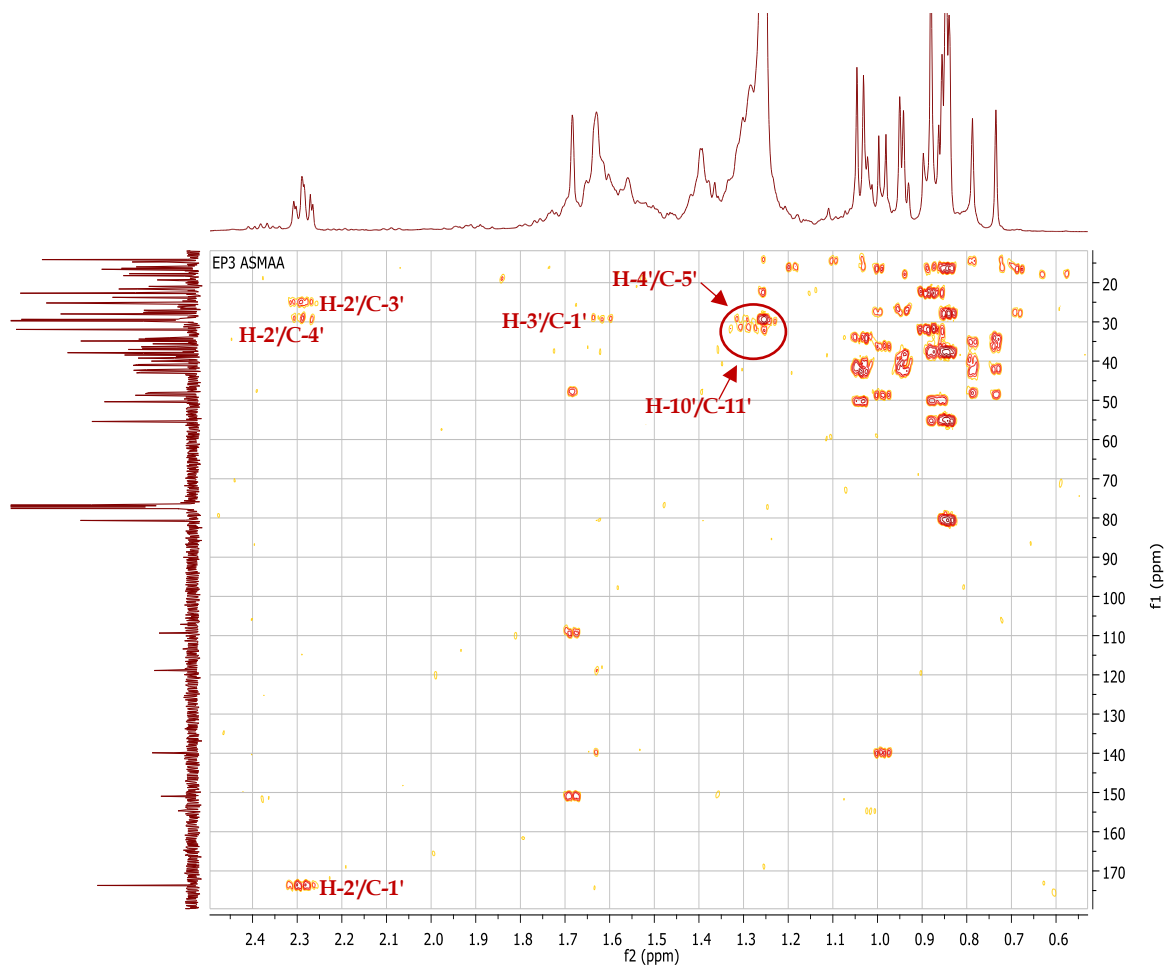
Figure. IV. 269: HMBC spectrum (400 MHz, CDCl$_3$) of the compound **EP3**.
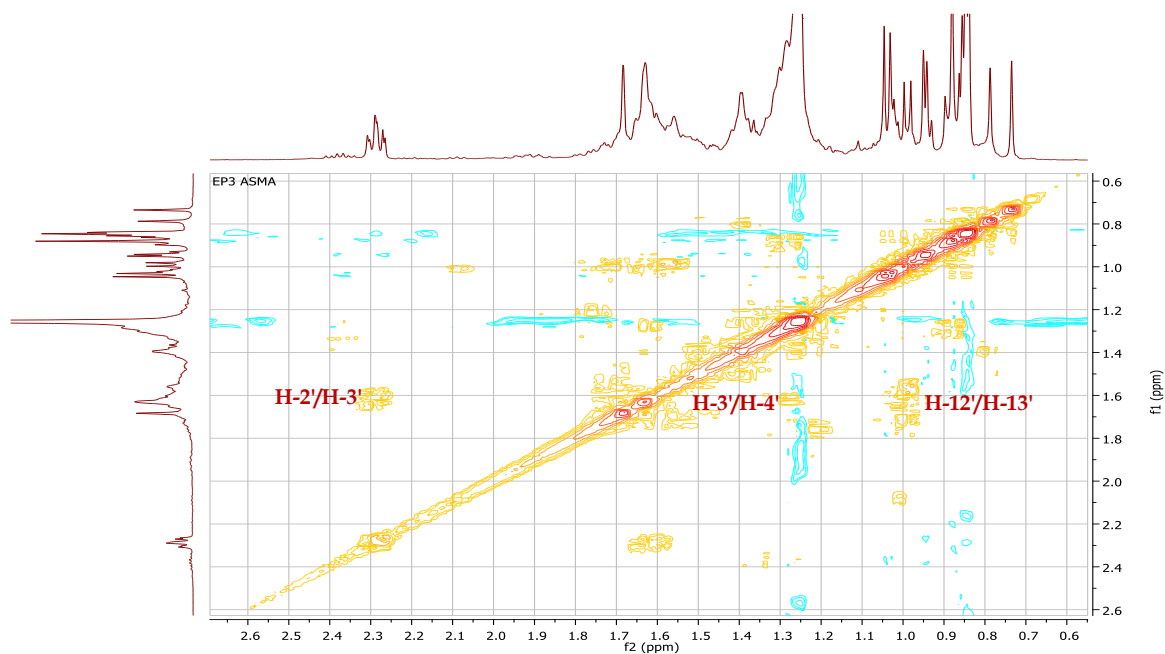
Figure. IV. 270: COSY spectrum (400 MHz, CDCl$_3$) of the compound **EP3**.
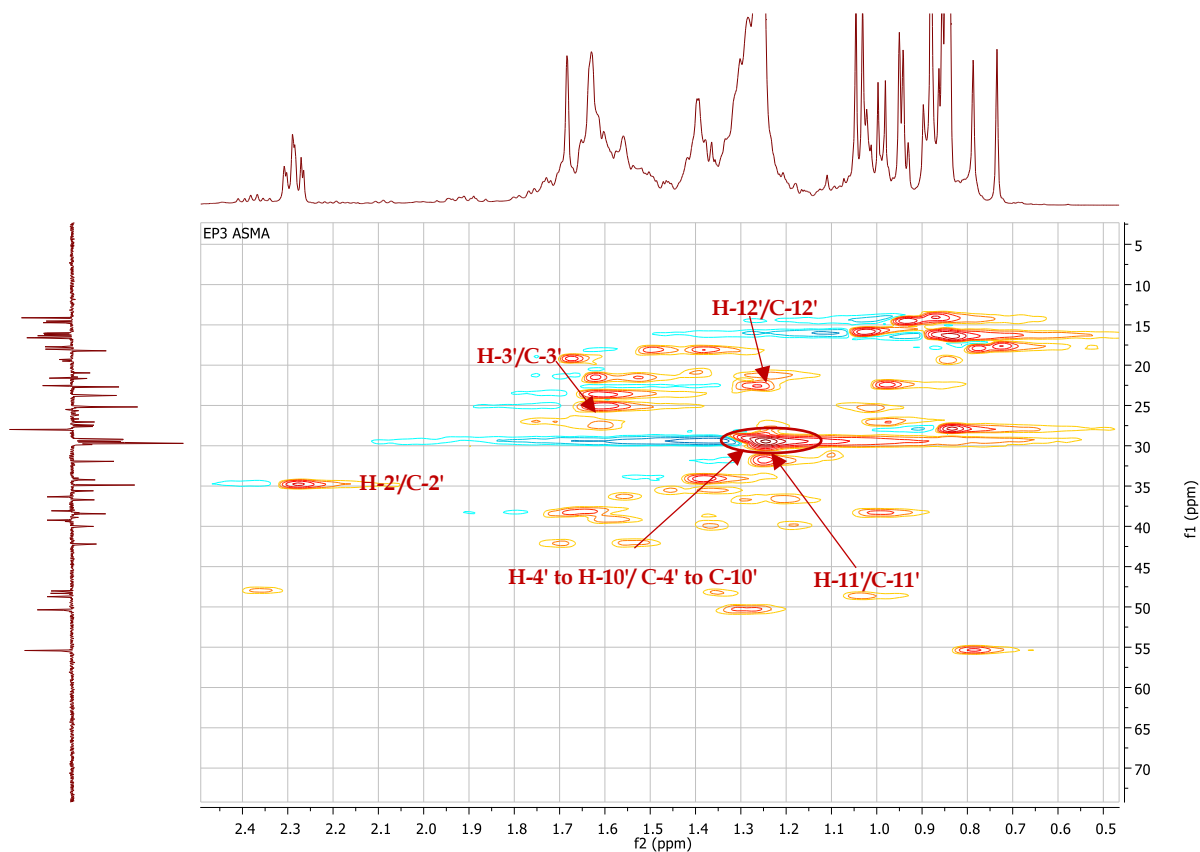
Figure. IV. 271: HSQC spectrum (400 MHz, CDCl$_3$) of the compound **EP3**.
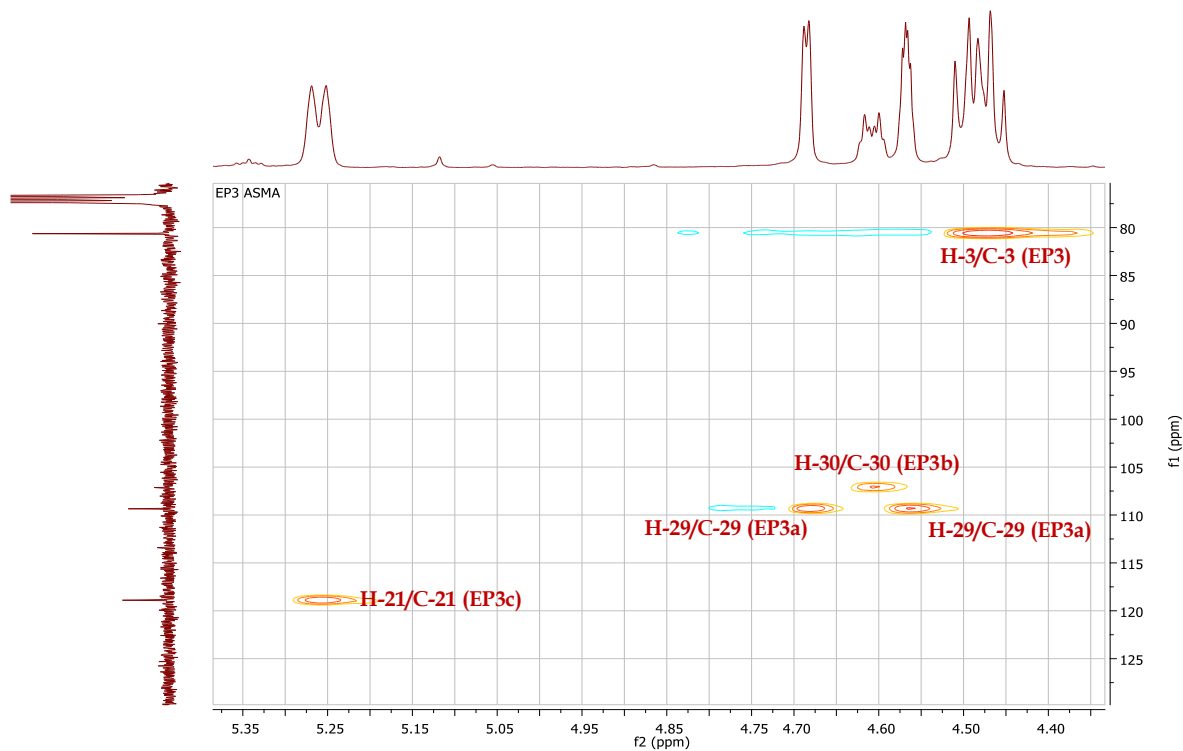
Figure. IV. 272: HSQC spectrum (400 MHz, CDCl$_3$) of olefinic part of the compound **EP3**.

According to above mentioned data the components of **EP3** were identified as lupeyl tridecanoate **EP3a**, taraxasteryl tridecanoate **EP3b** and pseudotaraxasteryl tridecanoate (φ-taraxasteryl tridecanoate) **EP3c** (**Figure. IV. 273**).

The difference in integration between the olefinic protons makes it possible to deduce their proportion at 40.98% lupeyl tridecanoate **EP3a**, 13.93% taraxasteryl tridecanoate **EP3b** and 45.08% pseudotaraxasteryl tridecanoate **EP3c**.
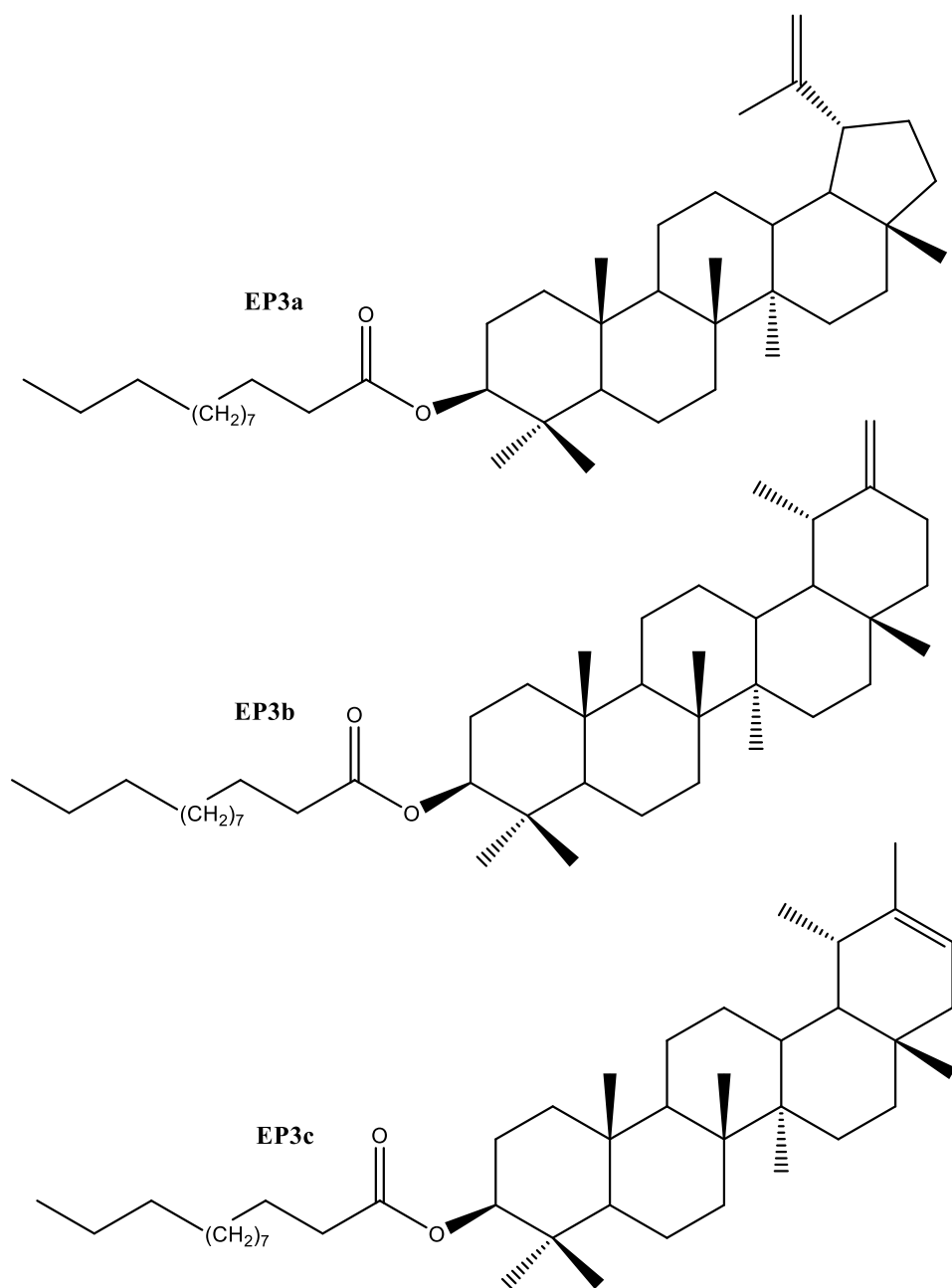
Figure. IV. 273: The chemical structures of compound **EP3**.

The triterpenoid fatty acid asters are already isolated from the plants from Asteraceae family from many plants as: *Gochnatia polymorpha* [224], *Eupatorium glutinosum* [235] and *Calendula officinalis* [236]. All the data are in total agreement with those of **EP1**, the difference is in the substitution at C-3. The **Table. IV. 22** shows the chemical shifts of the protons and carbons of the long chain at C-3 of the compound **EP3**. These compounds are isolated for the first time from *Atractylis* genus.

Table. IV. 22: The chemical shifts of ^{1}H NMR (400 MHz) and ^{13}C NMR (100 MHz) on CDCl$_3$ of the long chain at C-3 of the compound **EP3**.

position	Carbon (δ_C in ppm)	Proton (δ_H in ppm and J in Hz)
1'	173.71	--
2'	34.88	2.29 (t, J = 6.4 Hz, 6H)
3'	25.18	1.63 (m)
4'-10'	29.19-29.85	1.25 (brs)
11'	31.93	1.25 (brs)
12'	22.70	1.25 (brs)
13'	14.13	0.88 (t, J = 6.9 Hz)

IV.4. 17. Compounds EP4

The compounds **EP4** is isolated in the form of a white powder soluble in the chloroform. This compound is characterized on TLC test by invisible spot under UV lamp, which turns purple by revelation using acid solution and heating.

The ^{1}H NMR (**Figure. IV. 275**) and ^{13}C NMR (**Figure. IV. 276**) spectra displays the presence of high number of signals. Also, the deshielded part of these spectra shows the presence of signals characteristic of different type of compounds, these indicating that **EP4** is isolated in the form of isomeric mixture with characteristics as the compound **EP2** (The same type).

The analysis of ^{1}H NMR spectrum of **EP4** (**Figure. IV. 275**) reveals the absence of the peak of methyl group at δ_H 2.04 and the appearance of new peak at δ_H 2.29 (td, J = 7.6, 2.1 Hz, 6H) compared to the ^{1}H NMR spectrum of **EP2** (**Figure. IV. 242**).
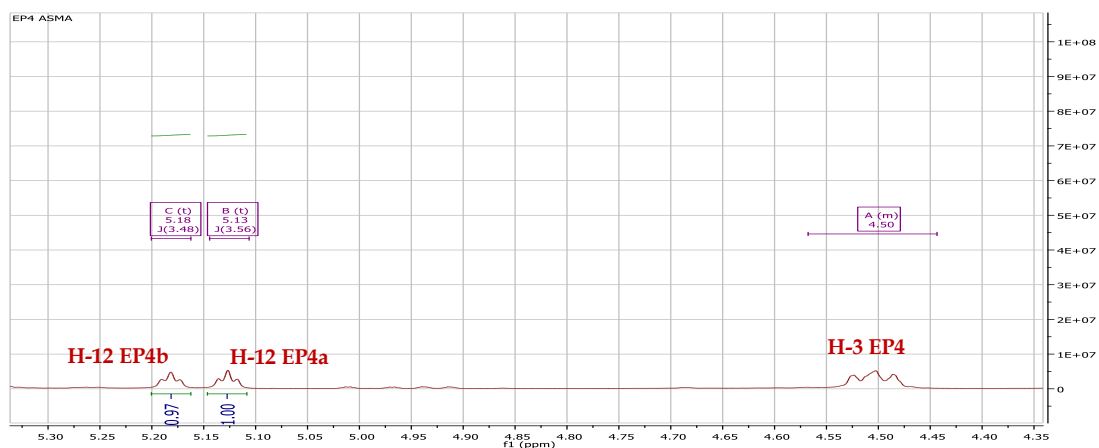
Figure. IV. 274: ^{1}H NMR spectrum (400 MHz, CDCl₃) of the deshielded part of **EP4**.
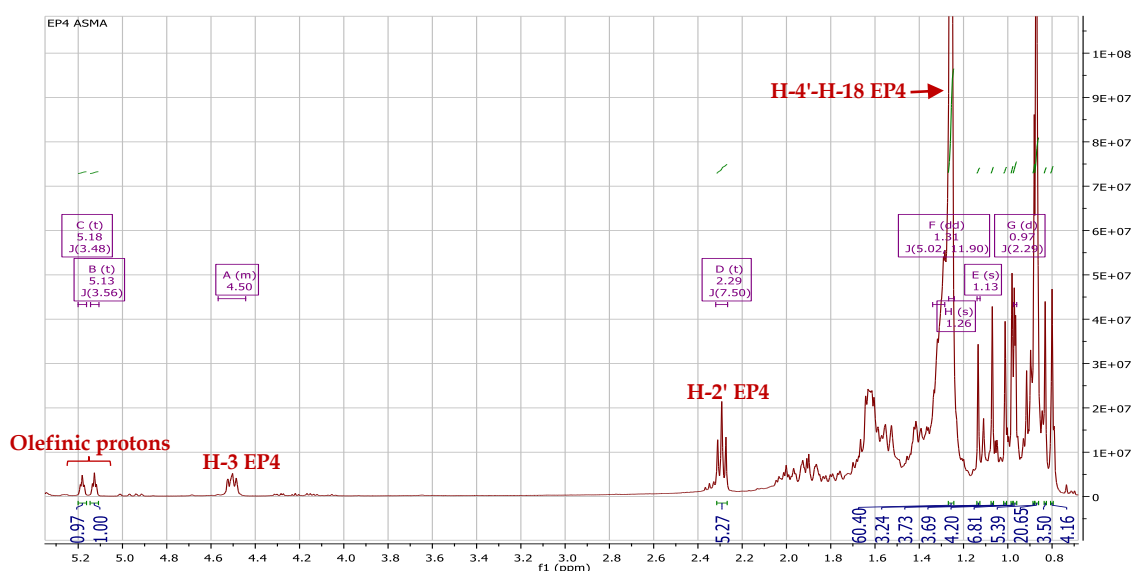
Figure. IV. 275: ^{1}H NMR spectrum (400 MHz, CDCl₃) of the compound **EP4**.

Also, the deshielded part of ^{1}H NMR (**Figure. IV. 274**) and ^{13}C NMR (**Figure. IV. 277**) spectra of the compound **EP4** reveals the presence of the same characteristic peaks observed in **EP2** spectra. The comparison of these results with **EP2** compound is in the form of a mixture of three isomers of triterpenes type: **urs-12-ene** (α- amyrin) (δ_C 124.34 and 139.65) **EP4a**, **olean-12-ene** (β- amyrin) (δ_C 121.66 and 145.23) **EP4b**. The deshielded part of ^{13}C NMR (**Figure. IV. 274**) and HSQC (**Figure. IV. 278**) spectra shows the absence of the characteristic peaks of **EP2c**. The chemical shift of oxygenated carbon also was characteristic of an ester triterpene (δ_C 80.63), but the carbonyl group was more deshielded (δ_C 173.71) than in **EP2**.
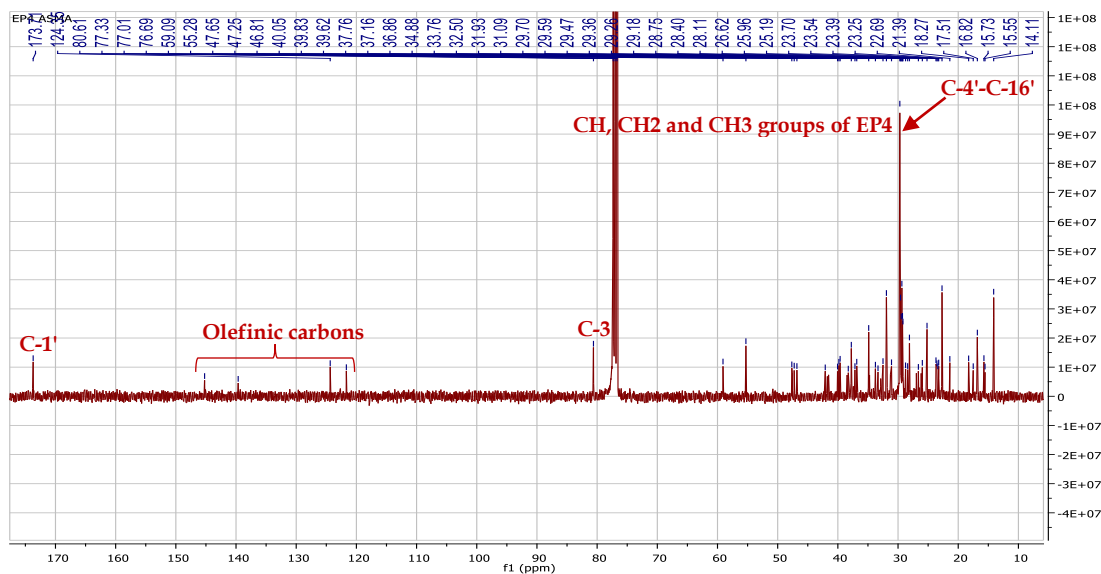
Figure. IV. 276: ^{13}C NMR spectrum (100 MHz, CDCl$_3$) of the compound **EP4**.
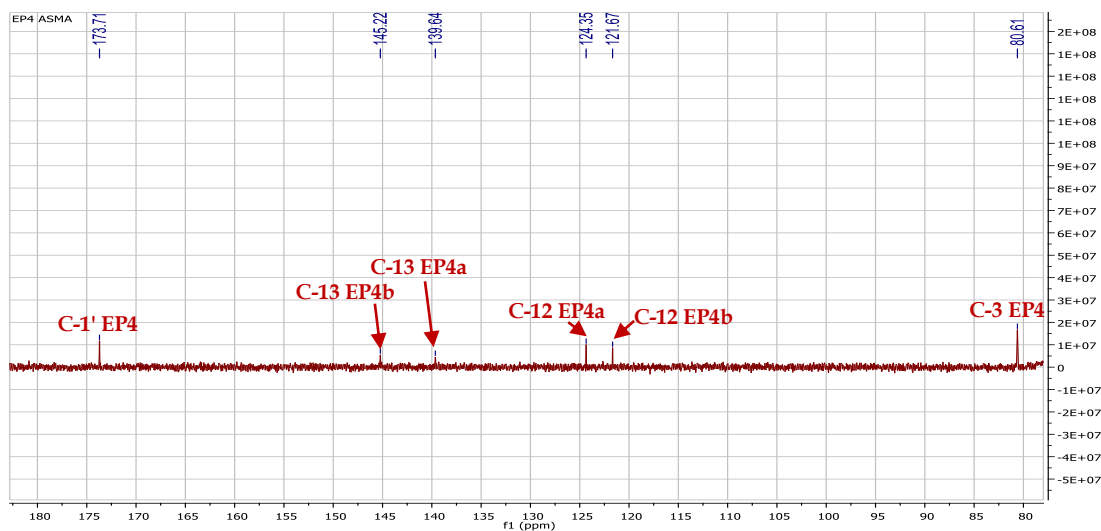
Figure. IV. 277: ^{13}C NMR spectrum (100 MHz, CDCl$_3$) of the deshielded part of **EP4**.
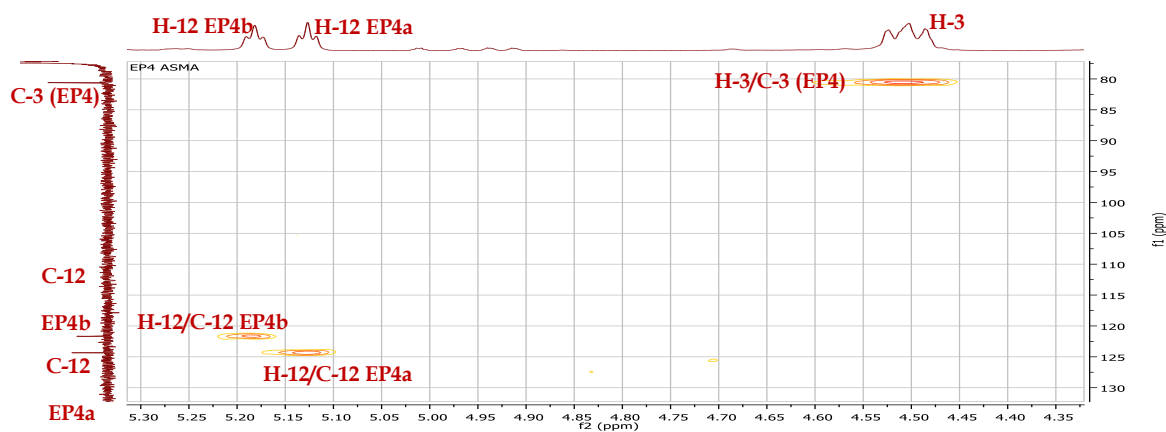
Figure. IV. 278: HSQC spectrum (400 MHz, CDCl$_3$) of the deshielded part of **EP4**.

As we mentioned in the compound **EP3**, the presence of the peaks at δ_H 4.50, 2.29 (J=6.4 Hz) and at δ_H 1.63 on ^{1}H NMR spectrum (**Figure. IV. 273**) corresponding to H-3, methylene adjacent to ester carbonyl and β-methylene of the carbonyl, respectively. Also, a broad singlet at δ_H 1.26 integrated for 60 protons and a methyl triplet at δ_H 0.88 indicating the presence of a carbon side chain at the C-3 position. This was verified by the deshielding effect observed in the carbonyl group (δ_C 173.71), and confirmed by the correlations of H-3 and the ester carbonyl C-1 in the HMBC of **EP4**. These results are a typical of long chain carbons at C-3 [224, 234]. This long chin of carbon confirmed by the HMBC (**Figure. IV. 279**), COSY (**Figure. IV. 280**) and HSQC (**Figure. IV. 281**) spectra. The protons resonating at δ_H 1.26 a broad singlet integrated for 60 protons. The integration of these protons indicated the presence of 15 CH$_2$ group attached to the carbon C-3'.
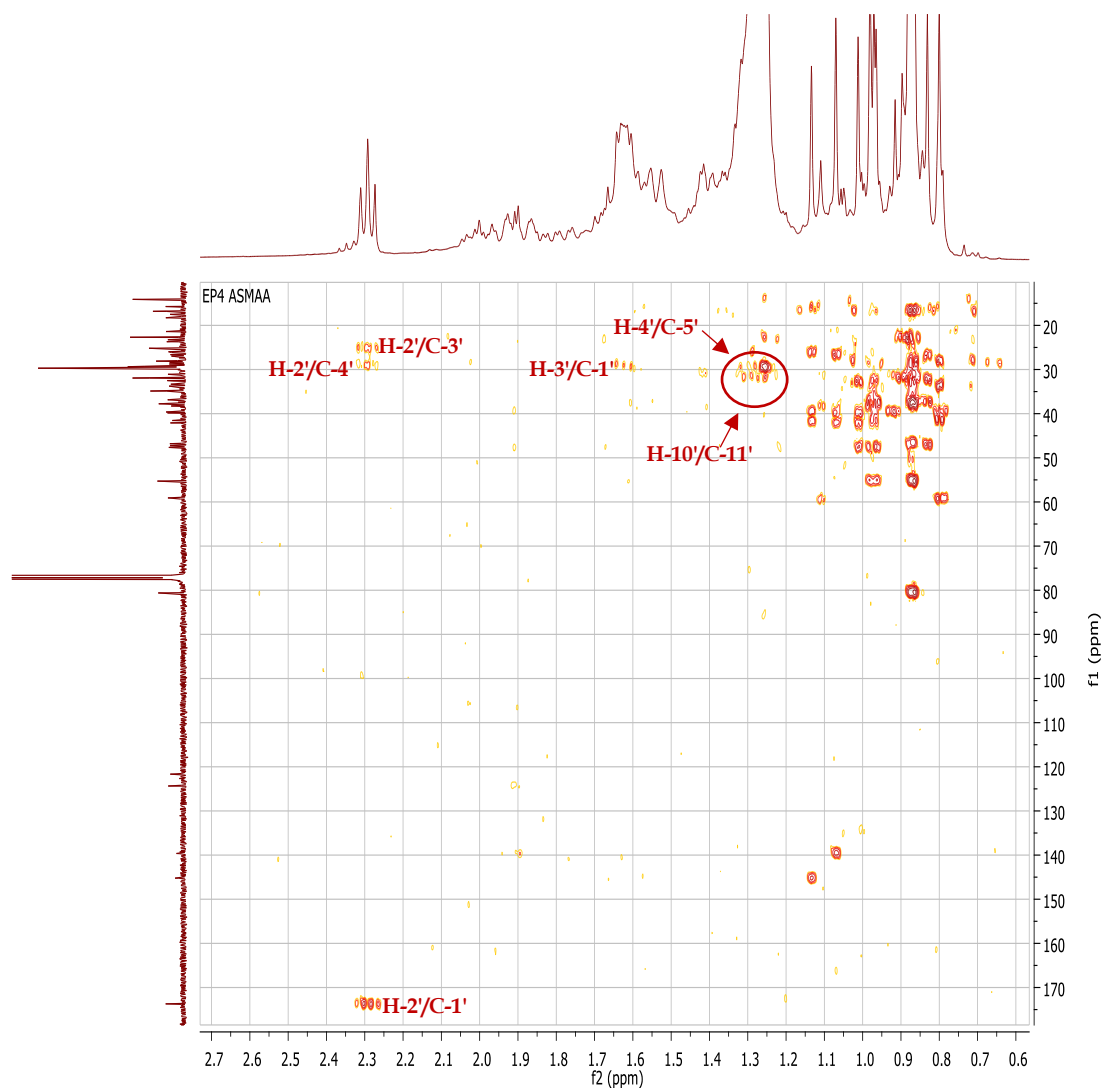
Figure. IV. 279: HMBC spectrum (400 MHz, CDCl$_3$) of the compound **EP4**.
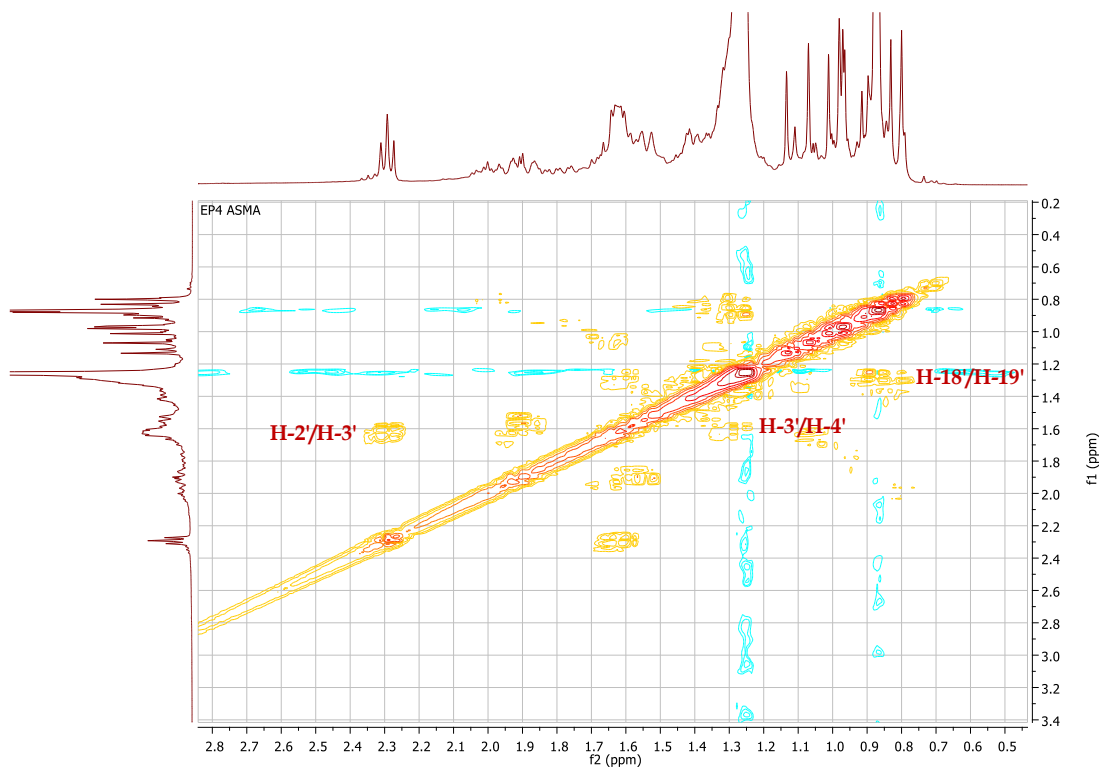
Figure. IV. 280: COSY spectrum (400 MHz, CDCl₃) of the compound **EP4**.
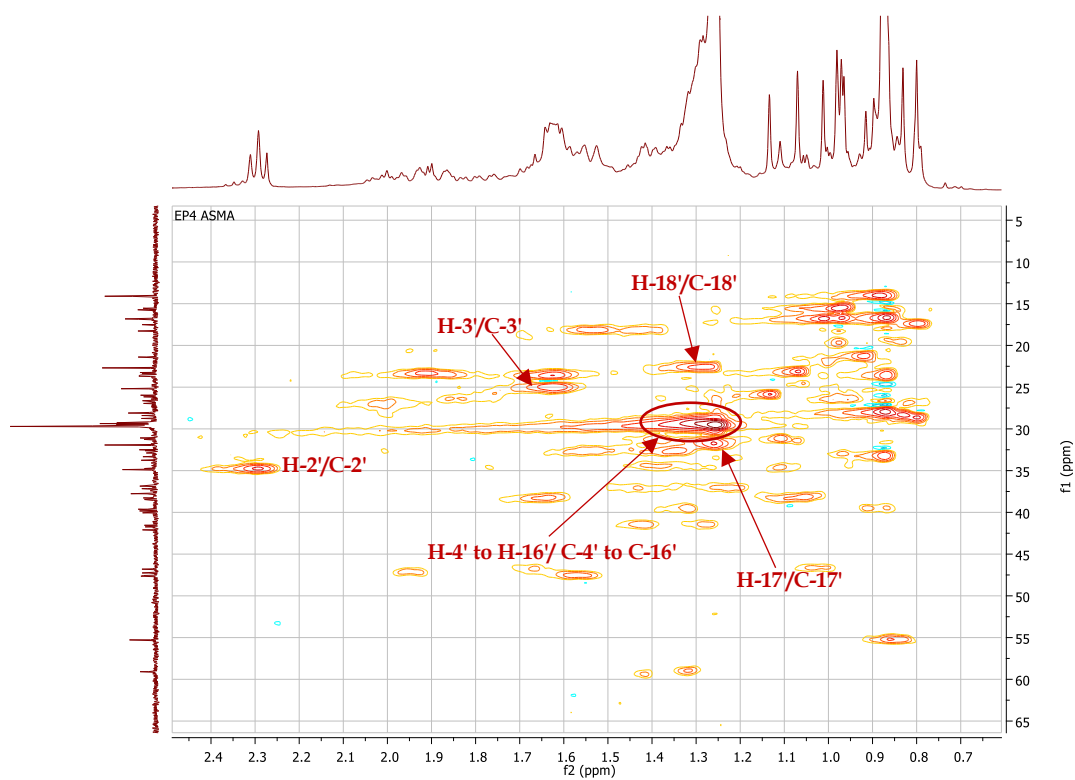
Figure. IV. 281: HSQC spectrum (400 MHz, CDCl₃) of the compound **EP4**.

The analysis of all the spectra of the compound **EP4** shows that all the data are in total agreement with those of **EP2**, the difference is in the substitution at C-3. The **Table. IV. 23** reveals the chemical shifts of the protons and carbons of the long chain at C-3 of the compound **EP4**. These compounds are isolated for the first time from *Atractylis* genus.

Table. IV. 23: The chemical shifts of ^{1}H NMR (400 MHz) and ^{13}C NMR (100 MHz) on CDCl₃ of the long chain at C-3 of the compound **EP4**.

position	Carbon (δ_C in ppm)	Proton (δ_H in ppm and J in Hz)
1'	173.71	--
2'	34.88	2.29 (t, J = 6.4 Hz, 6H)
3'	25.18	1.63 (m)
4'-16'	29.19-29.85	1.26 (brs)
17'	31.93	1.26 (brs)
18'	22.70	1.26 (brs)
19'	14.13	0.88

According to above mentioned data of the compound **EP2** and **EP4** the components of **EP4** were identified as α-amyrin nonadecanoate **EP4a** and β-amyrin nonadecanoate **EP4b** (**Figure. IV. 282**). The difference in integration between the olefinic protons makes it possible to deduce their proportion at 50.76 % α-amyrin nonadecanoate **EP4a** and 49.23% β-amyrin nonadecanoate **EP4b**.

EP4a

EP4b
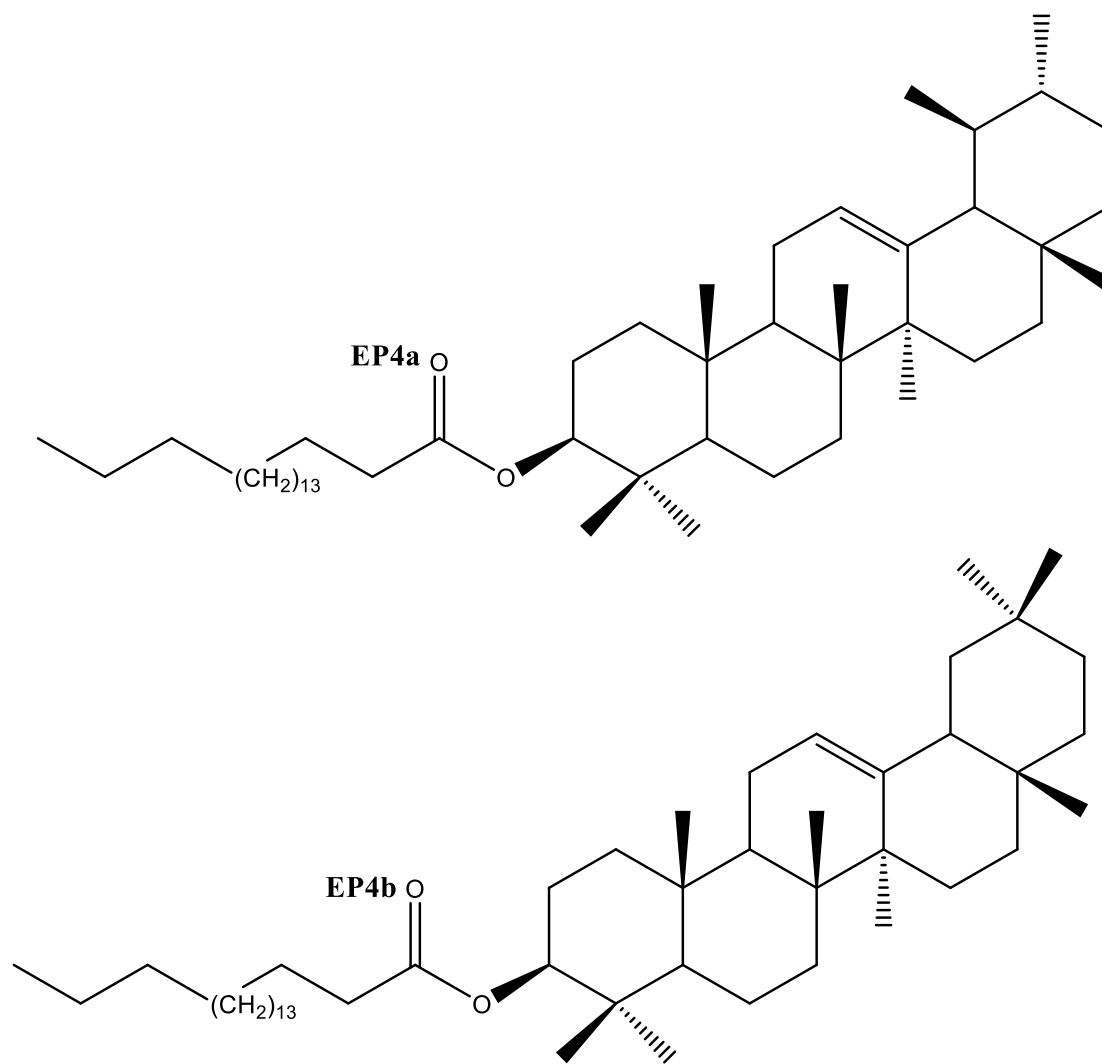
Figure. IV. 282: The chemical structures of compound **EP4**.

Conclusion

———————— *Conclusion* ————————

The present work is interested in the valorization and the promotion of the Saharan plants, by the evaluation of *in vitro* and *in vivo* biological activities and the study of the chemical composition of the plant *Atractylis aristata* batt. belonging to the Asteraceae family, in order to find new molecules with therapeutic effects. In this study new data were obtained on the biological activity and phytochemical composition of *Atractylis aristata* extracts.

The phytochemical screening of the crude extract of the species *Atractylis aristata* reveals the presence of various classes of secondary metabolites namely: flavonoids, steroids, tannins, saponins, terpenoids, reducing compounds, triterpenoids, free quinones and cardenolides known for their interesting biological activities.

The quantitative analysis of the extracts of the plant *A. aristata* by spectroscopic methods have shown moderate levels of polyphenols, flavonoids and condensed tannins. Also, the analysis of the HPLC chromatograms obtained by *Atractylis aristata* shows the richness of the extracts in bioactive compounds.

All extracts exhibit an interesting *in vitro* antioxidant in the different assays: scavenging of DPPH and ABTS radicals, reducing power assay, superoxide anion radical scavenging and Fe^{2+} chelating activity assay. Also, the evaluation of *in vitro* α-amylase inhibitory power show that all extracts of *A. aristata* exhibited high antidiabetic activity. The crude extract shows a very remarkable antioxidant and antidiabetic activities compared to other extracts; this antioxidant power could explain the ability of this extract to inhibit the enzyme α-amylase.

The oral administration of the crude and aqueous extracts did not cause symptoms of intoxication in all animals treated at the concentration 2000 mg/kg for 14 days. Thus, the approximate acute lethal dose of this extract was greater than 2000 mg/kg. In addition, the oral administration of the crude and aqueous extracts at the concentration of 2000 mg/kg inhibits the development of paw edema and exhibit anti-inflammatory activity close to the Ibuprofen that used as positive control. Those extracts also show a sedative activity by the inhibition of the locomotor activity of treated animals compared to the animals treated by the distilled water.

Our results show that the crude extract had the highest biological activity in relation to the antioxidant activity by DPPH and ABTS free radicals and the Fe^{+2} chelating methods, with values IC_{50} 0.04 mg/mL (DPPH), IC_{50} 0.005 mg/mL (ABTS) and I% 95% (Fe^{+2} chelating). The highlighted significant IC_{50} value for the crude extract showed noteworthy activity ten times higher than the standard ascorbic acid against ABTS free radical. It is also important to highlight the antidiabetic activity of the crude extract, which showed an alpha-amylase inhibition rate (I% 57.62 %) very close to the drug acarbose. In the same case, the crude extract also showed a robust capacity of anti-inflammatory and sedative activities *in vivo*, with inhibition values (62.98% and 52.12, respectively). Depending on our findings in the evaluation of *in vitro* and *in vivo* biological activity, the extracts of the plant *A. aristata* could be safely used therapeutically in pharmaceutical formulations aimed at researching new antioxidant, antidiabetic, anti-inflammatory and sedative agents.

The study carried out on the dichloromethane, n-butanol and petroleum ether extracts of the *Atractylis aristata* plant, made it possible to isolate 24 natural compounds, including four phenolic compounds (two flavonoids and two phenolic acids), 16 triterpene compounds (three lupane, thirteen pentacyclic triterpenes) and four polysaccharides. Among these compounds, twenty compounds were identified for the first time in the genus *Atractylis* and 3 new bidesmosidic saponins (for the first time in the Nature). These products belong to carbohydrate classes of primary metabolites and five classes of secondary metabolites:

➢ Four carbohydrate compounds, **N1**; [O-β-d-fructofuranosyl-(2→6)-β-fructofuranosyl-(2→1)-α-d-glucopyranoside] (6- kestose), **N2**; β-d-fructofuranoide, **N5**; [O-β-d-fructopyranosyl-(2→1)-D-fructofuranose] and **N6** [O-β-d-fructofuranosyl-(2→1)-α-d-glucopyranoside] (Sucrose).

➢ Two flavonoids with the same aglycone, **J2**; isorhamnetin 3-O-robinobioside and **J4**; Isorhamnetin 3-O-(2",6"-di-O-α-rhamnopyranosyl-β-galactopyranoside).

➢ Three bidesmosidic saponins **R1** echinocystic acid 3-O-β-D-galactopyranosyl-(1"→2')- [β-D-glucopyranosyl- (1'''→3')] -β-D-glucuronopyranosyl-28-O-[β-D-xylopyranosyl-(1'''''→4'''')-α-L-rhamnopyranosyl-(1''''→2''') -β-D-xylopyranosyl], **R2** echinocystic acid 3-*O*-β-D-galactopyranosyl-(1"→2')- [β-D-β-D-glucuronopyranosyl-28-O-[β-D-xylopyranosyl-(1'''''→4'''')-α-L-

rhamnopyranosyl-(1''''→2''')-β-D-xylopyranosyl] and **R3** echinocystic acid 3-*O*-β-D-galactopyranosyl-(1''→2')- [β-D-β-D-glucuronopyranosyl-28-O-[α-L-rhamnopyranosyl-(1''''→2''')-β-D-xylopyranosyl].

➢ Thirteen pentacyclic triterpenoids: Lupeyl **P1**, Oleanolic acid **P2**, Lupeyl acetate **EP1a**, Taraxasteryl acetate **EP1b**, Pseudotaraxasteryl acetate **EP1c**, α-amyrin acetate **EP2a**, β- amyrin acetate **EP2b** and Isobauerenyl acetate **EP2c**, Lupeyl tridecanoate **EP3a**, Taraxasteryl tridecanoate **EP3b** and Pseudotaraxasteryl tridecanoate (ϕ-taraxasteryl tridecanoate) **EP3c**, α-amyrin nonadecanoate **EP4a** and β-amyrin nonadecanoate **EP4b**.

➢ Two phenolic derivatives: **V4**, 9-O-β-glucopyranosyl trans-cinnamyl alcohol (Rosin)   and   **V5**,   1-(3,4-dimethoxy-phenyl)-1,2,3-propanetriol (veratrylglycerol).

The isolation and purification of these compounds was essentially based on the use of chromatographic techniques, TLC using the support normal silica and column chromatography CC using various supports (normal silica, RP-18 grafted silica, polyamide and Sephadex LH-20).

The structural elucidation of the isolated compounds was carried out by spectroscopic analysis methods, 1D NMR: ^{1}H proton, ^{13}C carbon, J-modulated ^{13}C and DEPT (135 and 90), 2D NMR: H-H COSY, HSQC, HMBC and TOCSY, mass spectrometry ESI-MS and UV spectroscopy, and by comparison with data from the literature.

It was found through this study that our plant contains different types of compounds of primary and secondary metabolites. It is quite clear that the predominant class of secondary metabolites in this study are those of triterpenes, of which these compounds are known for their biological interesting. It is important to note the presence of a series of glycoside derivatives of echinocystic acid in *A. aristata* for the first time in the genus *Atractylis*. Furthermore, it's crucial to recognize that the genus *Atractylis* contains a series of carbohydrates from mono to trisaccharide for the first time.

Despite the development of chromatographic and spectroscopic techniques, the separation and identification of triterpenes and saponins remain very delicate. Indeed, one is faced with a great difficulty during the separation and the distinction between the isomers.

The importance and originality of our work is summarized in the evaluation of biological activities in different ways, as well as the study of phytochemical compounds for the first time of the plant *Atractylis aristata,* as there is no report either in the biological activities or in the phytochemical study, and therefore this is the first study. This work adds as a novelty the separation of carbohydrate for the first time in *Atractylis* genus and bidesmosidic saponins as new compounds in the Nature.

Chemical structure of identified compounds

J4

R1

V4

V5

R2

R3

EP1a

EP1b

EP1c

EP2a

EP2b

EP2c

EP3a

EP3b

EP3c

EP4a

EP4b
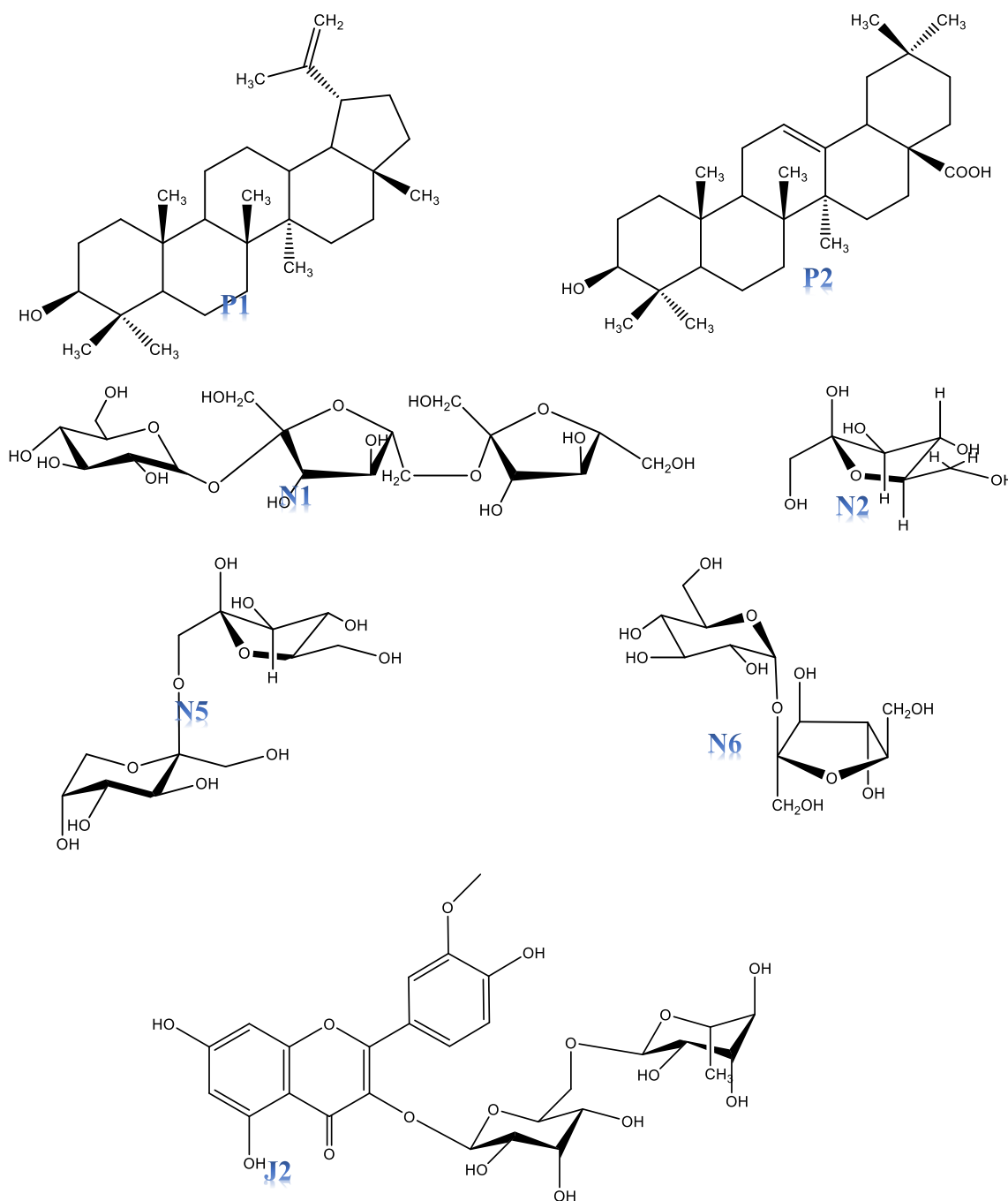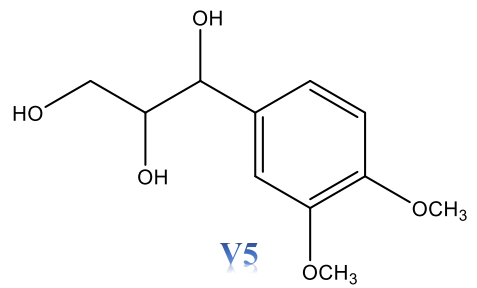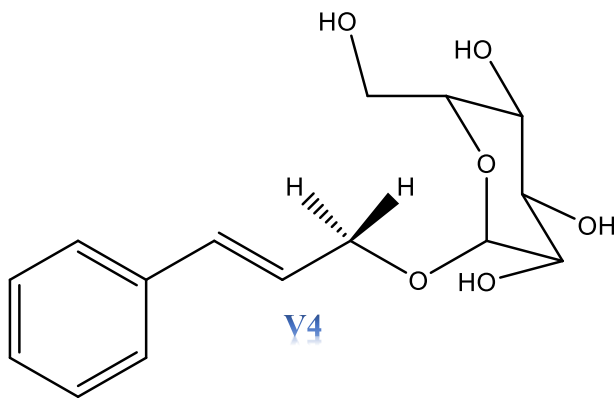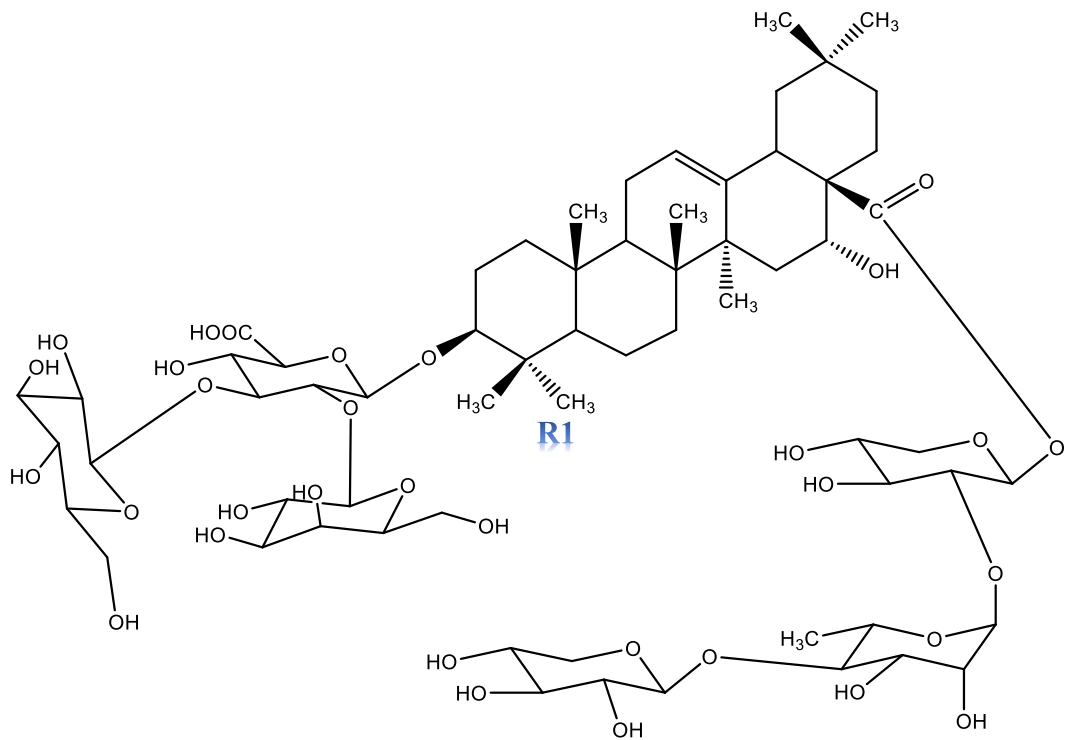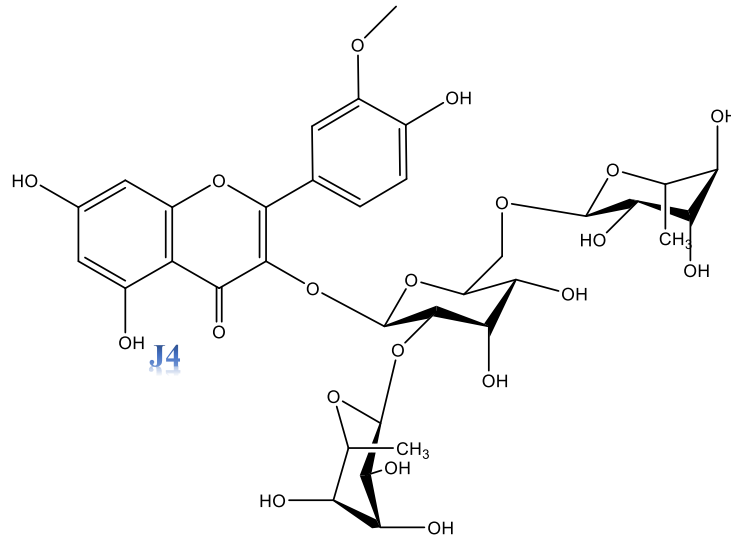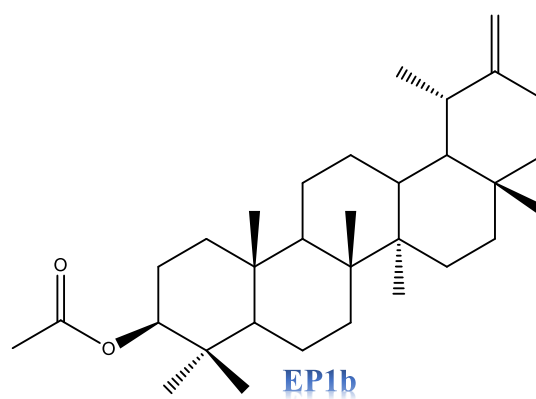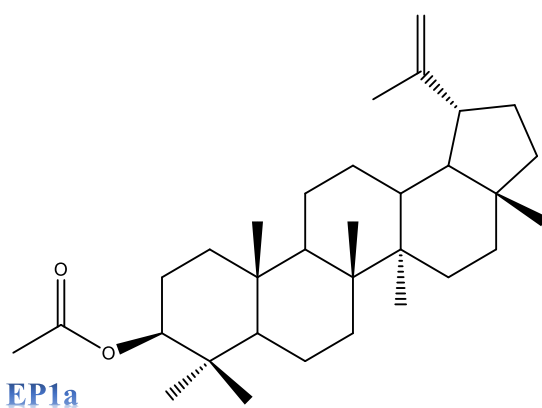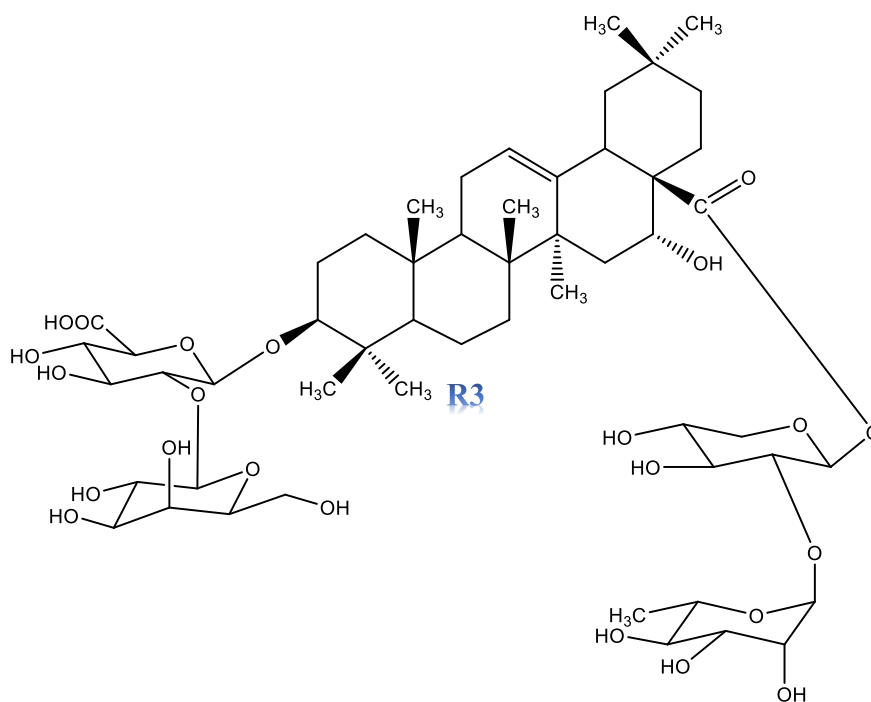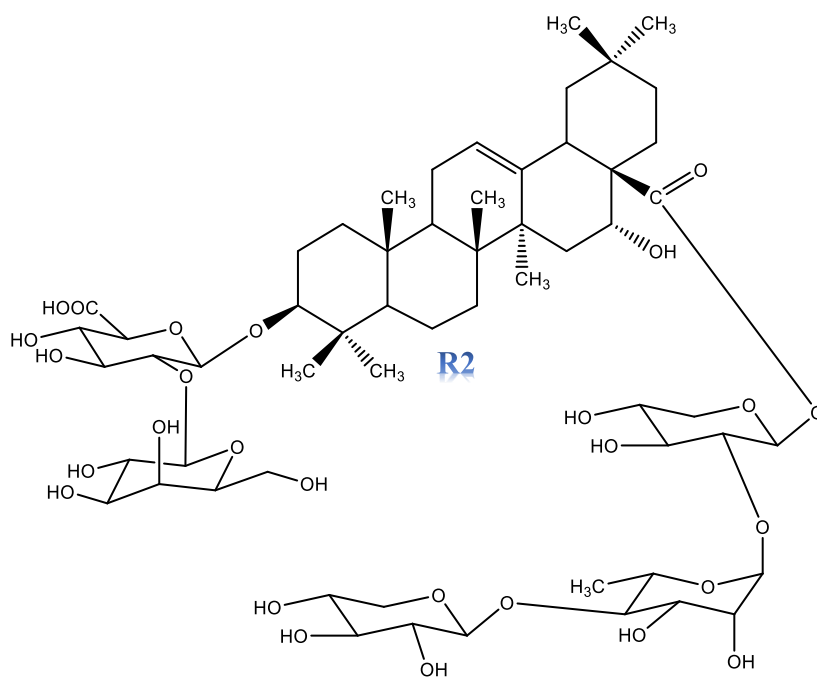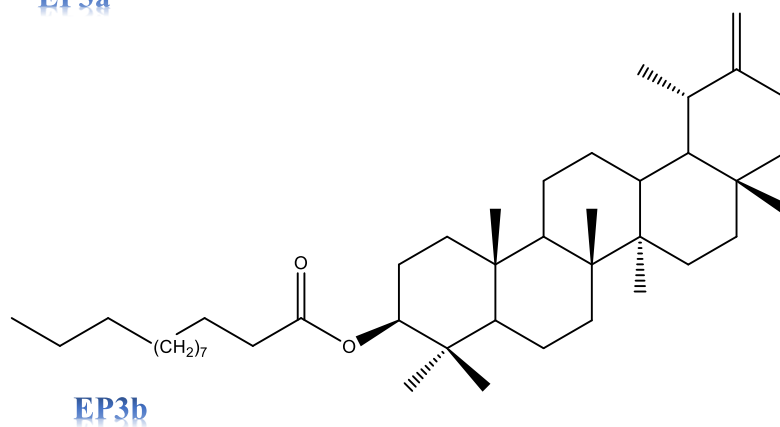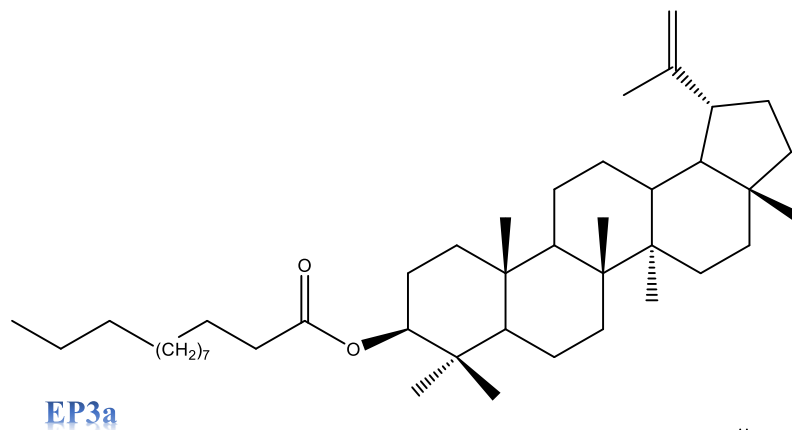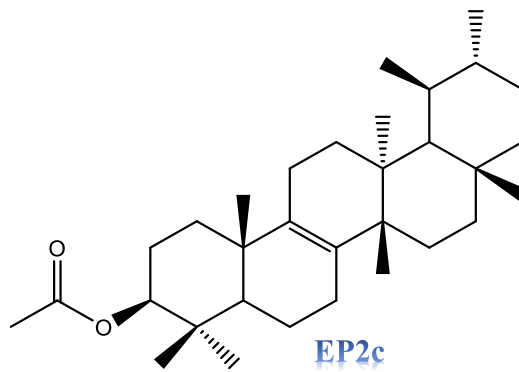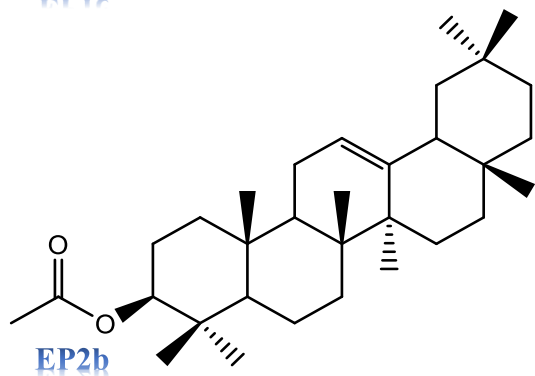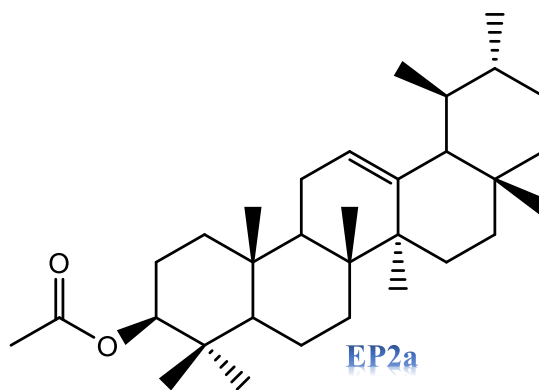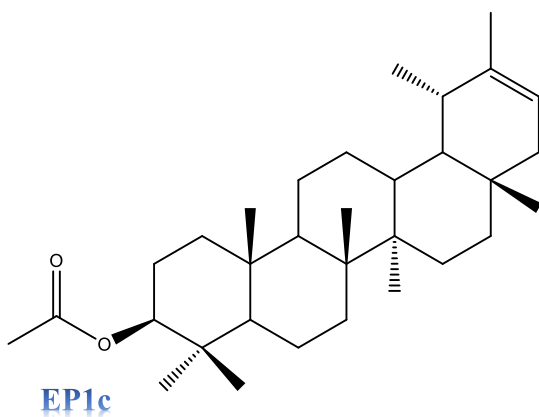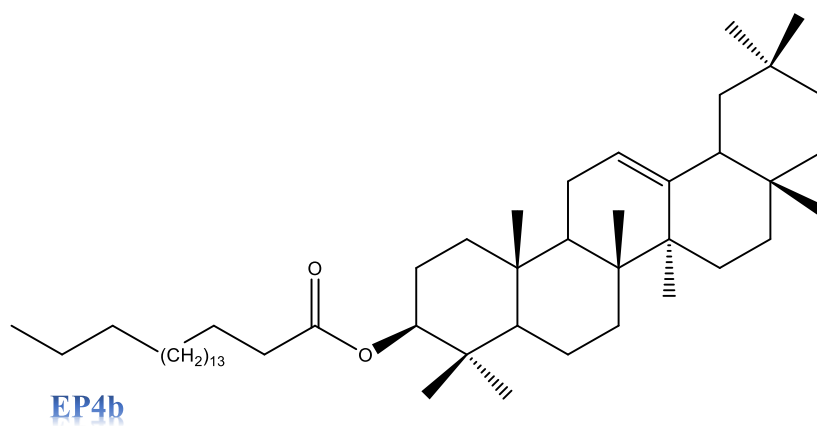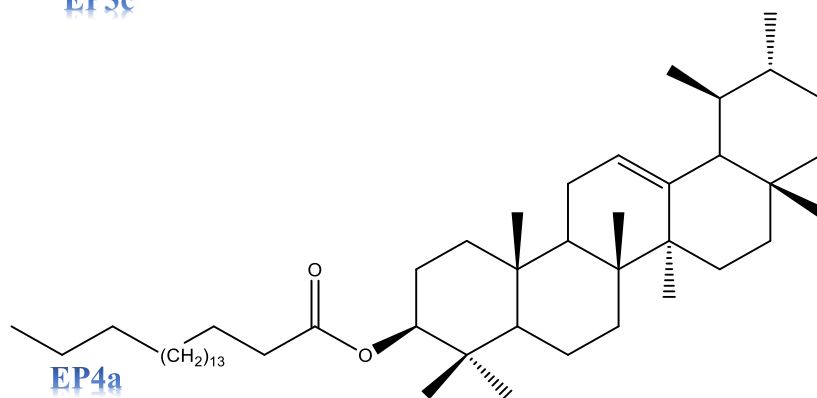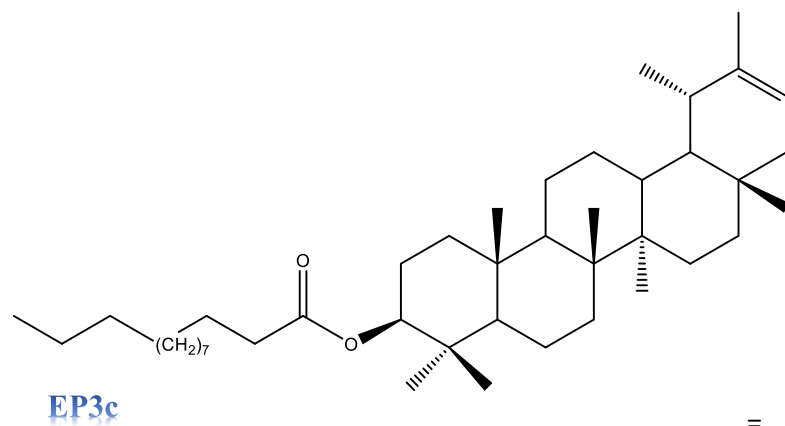
References

References

1. Gurib-Fakim, A., *Medicinal plants: traditions of yesterday and drugs of tomorrow*. Molecular aspects of Medicine, 2006. **27**(1): p. 1-93.
2. Anand, U., et al., *A comprehensive review on medicinal plants as antimicrobial therapeutics: potential avenues of biocompatible drug discovery*. Metabolites, 2019. **9**(11): p. 258.
3. Filleul, E., *Les Astéracées: description botanique, biologique et étude de plantes médicinales et toxiques*, 2019.
4. Chenchouni, H., *Diversité floristique d'un lac du bas-sahara algérien. Flora diversity of a lake at algerian low-sahara*. Acta Botanica Malacitana, 2012. **37**: p. 33-44.
5. Quézel, P., *Analysis of the flora of Mediterranean and Saharan Africa*. Annals of the Missouri Botanical Garden, 1978: p. 479-534.
6. Ozenda, P., *Flora of the Sahara*. Flora of the Sahara., 1977(ed. 2).
7. Ramdane, F., et al., *Ethnobotanical study of some medicinal plants from Hoggar, Algeria*. Journal of medicinal plants research, 2015. **9**(30): p. 820-827.
8. Hammiche, V. and K. Maiza, *Traditional medicine in Central Sahara: pharmacopoeia of Tassili N'ajjer*. Journal of Ethnopharmacology, 2006. **105**(3): p. 358-367.
9. Akram, M.M., et al., *Anti-Inflammatory, Anti-pyretic and Acute Toxicity Effects of n-Butanol Extract of Atractylis flava Desf in Rats*. Pharmacognosy Journal, 2018. **10**(4).
10. Melakhessou, M.A., N. Benkiki, and S.E. Marref, *Determination of antioxidant capacity, flavonoids and total phenolic content of extracts from Atractylis flava Desf*. Research Journal of Pharmacy and Technology, 2018. **11**(12): p. 5221-5228.
11. Bouabid, K., et al., *In vivo anti-diabetic effect of aqueous and methanolic macerated extracts of Atractylis gummifera*. ||| Bangladesh Journal of Pharmacology, 2019. **14**(2): p. 67-73.
12. Bouabid, K., et al., *Phytochemical screening and in vitro evaluation of alpha amylase, alpha glucosidase and beta galactosidase inhibition by aqueous and organic Atractylis gummifera L. extracts*. Plant Science Today, 2018. **5**(3): p. 103-112.
13. Akram, M.M., et al., *Gene Expression Levels of Selected Factors in Monocytic Leukemia Cell Line THP-1 Upon Treatment with n-butanol Extract of Atractylis flava Desf against Cancer*. Journal of Young Pharmacists, 2019. **11**(1): p. 36.
14. Funk, V.A., et al., *Classification of compositae*. Systematics, evolution, and biogeography of Compositae, 2009.
15. PANERO, J.L., et al. *Using a supertree to understand the diversity and distribution of the Compositae*. in *Plant Diversity and Complexity Patterns: Local, Regional, and Global Dimensions: Proceedings of an International Symposium Held at the Royal Danish Academy of Sciences and Letters in Copenhagen, Denmark, 25-28 May, 2003*. 2005. Kgl. Danske Videnskabernes Selskab.
16. Cronquist, A., *Vascular flora of the southeastern United States: Asteraceae*. Vol. 1. 2001: UNC Press Books.
17. Bohm, B.A. and T.F. Stuessy, *Flavonoids of the sunflower family (Asteraceae)* 2001: Springer Science & Business Media.

18.   Baldwin, B.G., B.L. Wessa, and J.L. Panero, *Nuclear rDNA evidence for major lineages of helenioid Heliantheae (Compositae).* Systematic Botany, 2002: p. 161-198.

19.   Panero, J. and V.A. Funk, *Toward a phylogenetic subfamilial classification for the Compositae (Asteraceae).* Proceedings of the Biological society of Washington, 2002.

20.   Panero, J.L. and V.A. Funk, *New infrafamilial taxa in Asteraceae.* Phytologia, 2007.

21.   Panero, J.L. and V.A. Funk, *The value of sampling anomalous taxa in phylogenetic studies: major clades of the Asteraceae revealed.* Molecular Phylogenetics and Evolution, 2008. **47**(2): p. 757-782.

22.   Susanna, A. and N. Garcia-Jacas, *Cardueae (Carduoideae).* Systematics, Evolution and Biogeography of Compositae. Vienna (Austria): IAPT, 2009: p. 293-313.

23.   Alves, M.F., et al., *Chemotaxonomic Study of Sesquiterpene Lactones of Asteraceae: Classical and Modern Methods*, in *Sesquiterpene Lactones*2018, Springer. p. 31-45.

24.   Rolnik, A. and B. Olas, *The plants of the Asteraceae family as agents in the protection of human health.* International Journal of Molecular Sciences, 2021. **22**(6): p. 3009.

25.   Graziose, R., M. Ann Lila, and I. Raskin, *Merging traditional Chinese medicine with modern drug discovery technologies to find novel drugs and functional foods.* Current drug discovery technologies, 2010. **7**(1): p. 2-12.

26.   Kviecinski, M.R., et al., *Study of the antitumor potential of Bidens pilosa (Asteraceae) used in Brazilian folk medicine.* Journal of Ethnopharmacology, 2008. **117**(1): p. 69-75.

27.   Niño, J., et al., *Antibacterial, antifungal and cytotoxic activities of eight Asteraceae and two Rubiaceae plants from Colombian biodiversity.* Brazilian Journal of Microbiology, 2006. **37**: p. 566-570.

28.   Nudo, L.P. and E.S. Catap, *Anti-immunosuppressive effects of Chromolaena odorata (Lf.) King & Robinson (Asteraceae) leaf extract in cyclophosphamide-injected Balb/C mice.* Philippine Journal of Science, 2012. **141**(1): p. 35-43.

29.   Albayrak, S., et al., *Compositions, antioxidant and antimicrobial activities of Helichrysum (Asteraceae) species collected from Turkey.* Food chemistry, 2010. **119**(1): p. 114-122.

30.   Didier, F., et al., *Caffeoyl derivatives: major antioxidant compounds of some wild herbs of the Asteraceae family.* Food and Nutrition Sciences, 2011. **2011**.

31.   Mekinić, I.G., et al., *Antioxidative/acetylcholinesterase inhibitory activity of some Asteraceae plants.* Natural Product Communications, 2013. **8**(4): p. 1934578X1300800416.

32.   Salie, F., P. Eagles, and H. Leng, *Preliminary antimicrobial screening of four South African Asteraceae species.* Journal of Ethnopharmacology, 1996. **52**(1): p. 27-33.

33.   Visintini Jaime, M.F., et al., *In vitro antiviral activity of plant extracts from Asteraceae medicinal plants.* Virology journal, 2013. **10**(1): p. 1-10.

34.   Gazim, Z.C., et al., *Antifungal activity of the essential oil from Calendula officinalis L.(Asteraceae) growing in Brazil.* Brazilian Journal of Microbiology, 2008. **39**: p. 61-63.

35. Santin, J.R., et al., *Antiulcer effects of Achyrocline satureoides (Lam.) DC (Asteraceae)(Marcela), a folk medicine plant, in different experimental models.* Journal of Ethnopharmacology, 2010. **130**(2): p. 334-339.

36. dos Santos, D.A., et al., *Anti-inflammatory and antinociceptive effects of Baccharis dracunculifolia DC (Asteraceae) in different experimental models.* Journal of Ethnopharmacology, 2010. **127**(2): p. 543-550.

37. Al-Hajj, N.Q.M., et al., *In vitro and in vivo evaluation of antidiabetic activity of leaf essential oil of Pulicaria inuloides-Asteraceae.* Journal of Food and Nutrition Research, 2016. **4**(7): p. 461-470.

38. Peng, H.-S., et al., *Molecular Systematics of Genus Atractylodes (Compositae, Cardueae): Evidence from Internal Transcribed Spacer (ITS) and trn L-F Sequences.* International Journal of Molecular Sciences, 2012. **13**(11): p. 14623-14633.

39. Garcia-Jacas, N., et al., *Tribal and subtribal delimitation and phylogeny of the Cardueae (Asteraceae): a combined nuclear and chloroplast DNA analysis.* Molecular Phylogenetics and Evolution, 2002. **22**(1): p. 51-64.

40. Quézel, P. and S. Santa, *Nouvelle flore de l'Algérie et des regions désertoriques meridionales, Tome 2. Centre de la Recherche Scientifique, Paris*, 1963.

41. El Rhaffari, L. and A. Zaid, *Pratique de la phytothérapie dans le sud-est du Maroc (Tafilalet): Un savoir empirique pour une pharmacopée rénovée.* Des sources du savoir aux médicaments du futur, 2002. **1**: p. 293-318.

42. Chen, L.-Y., A. Hu, and C.-J. Chang, *The degradation mechanism of toxic atractyloside in herbal medicines by decoction.* Molecules, 2013. **18**(2): p. 2018-2028.

43. Guo, W.-Q., et al., *Anti-proliferative effects of Atractylis lancea (Thunb.) DC. via down-regulation of the c-myc/hTERT/telomerase pathway in Hep-G2 cells.* Asian Pacific Journal of Cancer Prevention, 2013. **14**(11): p. 6363-6367.

44. Ahid, S., et al. *Atractylis gummifera: de l'intoxication aux méthodes analytiques*. in *Annales de Biologie Clinique*. 2012.

45. Najem, M., et al., *Occurrence de plantes toxiques en phytothérapie traditionnelle dans la région du Moyen Atlas central Maroc.* Journal of Animal & Plant Sciences, 2018. **35**(2): p. 5651-5673.

46. Rahman, S.M.A., et al., *Antibacterial activity of some wild medicinal plants collected from western Mediterranean coast, Egypt: Natural alternatives for infectious disease treatment.* African Journal of Biotechnology, 2011. **10**(52): p. 10733-10743.

47. Melakhessou, M.A., et al., *In vitro, acute and subchronic evaluation of the antidiabetic activity of Atractylis flava Desf n-butanol extract in alloxan-diabetic rats.* Future Journal of Pharmaceutical Sciences, 2021. **7**(1): p. 1-7.

48. Bouaziz, M., et al., *Polyphenols content, antioxidant and antimicrobial activities of extracts of some wild plants collected from the south of Tunisia.* African Journal of Biotechnology, 2009. **8**(24).

49. Boudebaz, K., et al., *The effect of extraction method on antioxidant activity of Atractylis babelii Hochr. leaves and flowers extracts.* Algerian Journal Of Natural Products, 2015. **3**(2): p. 146-152.

50. Badaoui, M.I., et al., *Pyrroloquinolone A, a new alkaloid and other phytochemicals from A tractylis cancellata L. with antioxidant and anticholinesterase activities.* Natural Product Research, 2021. **35**(18): p. 2997-3003.

51. Chabani, S., et al., *Chemical composition of medicinal plant Atractylis serratuloides.* Industrial Crops and Products, 2016. **88**: p. 91-95.

52. Chabani, S., et al., *Three new oleanane-type triterpene saponins from Atractylis flava.* Phytochemistry letters, 2016. **15**: p. 88-93.

53. Sifouane, S., et al., *A new aryltetralin lignan and other phytoconstituents from Atractylis humilis.* Biochemical Systematics and Ecology, 2020. **90**: p. 104018.

54. Melek, F., *Atractylis carduus Christens var-angustifolia flavonoids and anti-inflammatory activity.* Egyptian Journal of Pharmaceutical Sciences, 1992. **33**(2-Jan): p. 11-19.

55. Chabani, S., et al., *Flavonoid glycosides and triterpenoids from Atractylis flava.* Phytochemistry letters, 2013. **6**(1): p. 9-13.

56. Chaboud, A., G. Dellamonica, and J. Raynaud, *Neocorymboside, a di-C-glycosylflavone from Atractylis gummifera.* Phytochemistry, 1988. **27**(7): p. 2360-2361.

57. Riccio, P., B. Scherer, and M. Klingenberg, *Isolation of a new atractyloside type compound.* Febs Letters, 1973. **31**(1): p. 11-14.

58. Calmes, M., et al., *High-performance liquid chromatographic determination of atractyloside and carboxyatractyloside from Atractylis gummifera L.* Journal of Chromatography A, 1994. **663**(1): p. 119-122.

59. Danieli, B., et al., *Structure of the diterpenoid car☐ yatractyloside.* Phytochemistry, 1972. **11**(12): p. 3501-3504.

60. Pachaly, P., A. Lansing, and K.S. Sin, *Constituents of Atractylis koreana.* Planta medica, 1989. **55**(1): p. 59-61.

61. Pachaly, P., et al., *Acetylene aus Atractylis koreana.* Planta medica, 1990. **56**(05): p. 469-471.

62. Hopkins, W.G., *Physiologie végétale*2003: De Boeck Supérieur.

63. Nahar, L. and S.D. Sarker, *Chemistry for pharmacy students: general, organic and natural product chemistry*2019: John Wiley & Sons.

64. Teng, Y., et al., *Sucrose fatty acid esters: synthesis, emulsifying capacities, biological activities and structure-property profiles.* Critical reviews in food science and nutrition, 2021. **61**(19): p. 3297-3317.

65. Wang, Z.-J., et al., *Review on cell models to evaluate the potential antioxidant activity of polysaccharides.* Food & function, 2017. **8**(3): p. 915-926.

66. Wang, Z., et al., *Sulfated Cyclocarya paliurus polysaccharides markedly attenuates inflammation and oxidative damage in lipopolysaccharide-treated macrophage cells and mice.* Scientific reports, 2017. **7**(1): p. 1-12.

67. Fan, L., et al., *Effects of drying methods on the antioxidant activities of polysaccharides extracted from Ganoderma lucidum.* Carbohydrate polymers, 2012. **87**(2): p. 1849-1854.

68. Song, H., et al., *In vitro antioxidant activity of polysaccharides extracted from Bryopsis plumosa.* Carbohydrate polymers, 2010. **80**(4): p. 1057-1061.

69. Joseph, S., et al., *Antitumor and anti-inflammatory activities of polysaccharides isolated from Ganoderma lucidum.* Acta pharmaceutica, 2011. **61**(3): p. 335-342.

70. Yu, Y., et al., *Biological activities and pharmaceutical applications of polysaccharide from natural resources: A review.* Carbohydrate polymers, 2018. **183**: p. 91-101.

71. Wang, P.-C., et al., *Anti-diabetic polysaccharides from natural sources: A review.* Carbohydrate polymers, 2016. **148**: p. 86-97.

72.   TANG, S.-M., *Astragalus polysaccharide improves type 2 diabetes mellitus in rats by protecting islet β cells.* Academic Journal of Second Military Medical University, 2017: p. 482-487.

73.   Zhou, J., et al., *Rehmannia glutinosa (Gaertn.) DC. polysaccharide ameliorates hyperglycemia, hyperlipemia and vascular inflammation in streptozotocin-induced diabetic mice.* Journal of Ethnopharmacology, 2015. **164**: p. 229-238.

74.   Zhang, Y., et al., *Schizophyllan: A review on its structure, properties, bioactivities and recent developments.* Bioactive Carbohydrates and Dietary Fibre, 2013. **1**(1): p. 53-71.

75.   Miyazaki, H., et al., *Effect of antitumor polysaccharide SPR-901 on antitumor activity in combination with 5-FU.* International journal of immunopharmacology, 1994. **16**(2): p. 163-170.

76.   Shi, B.J., et al., *Anticancer activities of a chemically sulfated polysaccharide obtained from Grifola frondosa and its combination with 5-fluorouracil against human gastric carcinoma cells.* Carbohydrate polymers, 2007. **68**(4): p. 687-692.

77.   Zhou, G., et al., *Effect of low molecular λ-carrageenan from Chondrus ocellatus on antitumor H-22 activity of 5-Fu.* Pharmacological Research, 2006. **53**(2): p. 129-134.

78.   Zhou, G., et al., *In vivo growth-inhibition of S180 tumor by mixture of 5-Fu and low molecular λ-carrageenan from Chondrus ocellatus.* Pharmacological Research, 2005. **51**(2): p. 153-157.

79.   Faccin-Galhardi, L.C., et al., *The in vitro antiviral property of Azadirachta indica polysaccharides for poliovirus.* Journal of Ethnopharmacology, 2012. **142**(1): p. 86-90.

80.   Witvrouw, M. and E. De Clercq, *Sulfated polysaccharides extracted from sea algae as potential antiviral drugs.* General Pharmacology: The Vascular System, 1997. **29**(4): p. 497-511.

81.   Muffler, K., et al., *Biotransformation of triterpenes.* Process Biochemistry, 2011. **46**(1): p. 1-15.

82.   Dewick, P.M., *Medicinal natural products: a biosynthetic approach*2002: John Wiley & Sons.

83.   Sheng, H. and H. Sun, *Synthesis, biology and clinical significance of pentacyclic triterpenes: a multi-target approach to prevention and treatment of metabolic and vascular diseases.* Natural product reports, 2011. **28**(3): p. 543-593.

84.   JC Furtado, N.A., et al., *Pentacyclic triterpene bioavailability: An overview of in vitro and in vivo studies.* Molecules, 2017. **22**(3): p. 400.

85.   Moreau, R.A., B.D. Whitaker, and K.B. Hicks, *Phytosterols, phytostanols, and their conjugates in foods: structural diversity, quantitative analysis, and health-promoting uses.* Progress in lipid research, 2002. **41**(6): p. 457-500.

86.   Szakiel, A., et al., *Fruit cuticular waxes as a source of biologically active triterpenoids.* Phytochemistry Reviews, 2012. **11**(2): p. 263-284.

87.   Bruneton, J., *Pharmacognosie-Phytochimie, plantes médicinales, 4e éd., revue et augmentée.* Paris, Tec & Doc-Éditions médicales internationales, 2009: p. 1288.

88.   Thimmappa, R., et al., *Triterpene biosynthesis in plants.* Annual review of plant biology, 2014. **65**: p. 225-257.

89.   Smina, T., et al., *Antioxidant activity and toxicity profile of total triterpenes isolated from Ganoderma lucidum (Fr.) P. Karst occurring in South India.* Environmental toxicology and pharmacology, 2011. **32**(3): p. 438-446.

90.   Rios, J., et al., *Natural triterpenoids as anti-inflammatory agents.* Studies in natural products chemistry, 2000. **22**: p. 93-143.

91.   Nazaruk, J. and M. Borzym-Kluczyk, *The role of triterpenes in the management of diabetes mellitus and its complications.* Phytochemistry Reviews, 2015. **14**(4): p. 675-690.

92.   Zuco, V., et al., *Selective cytotoxicity of betulinic acid on tumor cell lines, but not on normal cells.* Cancer letters, 2002. **175**(1): p. 17-25.

93.   Pisha, E., et al., *Discovery of betulinic acid as a selective inhibitor of human melanoma that functions by induction of apoptosis.* Nature medicine, 1995. **1**(10): p. 1046-1051.

94.   Laszczyk, M.N., *Pentacyclic triterpenes of the lupane, oleanane and ursane group as tools in cancer therapy.* Planta medica, 2009. **75**(15): p. 1549-1560.

95.   Darshani, P., et al., *Anti-viral triterpenes: a review.* Phytochemistry Reviews, 2022: p. 1-82.

96.   Siddique, H.R. and M. Saleem, *Beneficial health effects of lupeol triterpene: a review of preclinical studies.* Life sciences, 2011. **88**(7-8): p. 285-293.

97.   Vincken, J.-P., et al., *Saponins, classification and occurrence in the plant kingdom.* Phytochemistry, 2007. **68**(3): p. 275-297.

98.   Oleszek, W., *Chromatographic determination of plant saponins.* Journal of Chromatography A, 2002. **967**(1): p. 147-162.

99.   Bruneton, J., *Pharmacognosy, phytochemistry, medicinal plants*1995: Lavoisier publishing.

100.   El Aziz, M., A. Ashour, and A. Melad, *A review on saponins from medicinal plants: chemistry, isolation, and determination.* J. Nanomed. Res, 2019. **8**(1): p. 282-288.

101.   Augustin, J.M., et al., *Molecular activities, biosynthesis and evolution of triterpenoid saponins.* Phytochemistry, 2011. **72**(6): p. 435-457.

102.   Sparg, S., M. Light, and J. Van Staden, *Biological activities and distribution of plant saponins.* Journal of Ethnopharmacology, 2004. **94**(2-3): p. 219-243.

103.   Brindhadevi, K., et al., *Extraction, antioxidant, and anticancer activity of saponins extracted from Curcuma angustifolia.* Applied Nanoscience, 2022: p. 1-9.

104.   Pham, H.N.T., et al., *Phytochemical profiles and antioxidant capacity of the crude extracts, aqueous-and saponin-enriched butanol fractions of Helicteres hirsuta Lour. leaves and stems.* Chemical Papers, 2017. **71**(11): p. 2233-2242.

105.   Sirtori, C.R., *Aescin: pharmacology, pharmacokinetics and therapeutic profile.* Pharmacological Research, 2001. **44**(3): p. 183-193.

106.   da Silva, B.P., et al., *A new bioactive steroidal saponin from Agave attenuata.* Zeitschrift für Naturforschung C, 2002. **57**(5-6): p. 423-428.

107.   Dou, F., et al., *α-Glucosidase and-amylase inhibitory activities of saponins from traditional Chinese medicines in the treatment of diabetes mellitus.* Die Pharmazie-An International Journal of Pharmaceutical Sciences, 2013. **68**(4): p. 300-304.

108.   Suresh, P.S., et al., *Steroidal saponins from Trillium govanianum as α-amylase, α-glucosidase, and dipeptidyl peptidase IV inhibitory agents.* Journal of Pharmacy and Pharmacology, 2021. **73**(4): p. 487-495.

109. Ma, S., J. Kou, and B. Yu, *Safety evaluation of steroidal saponin DT-13 isolated from the tuber of Liriope muscari (Decne.) Baily.* Food and chemical toxicology, 2011. **49**(9): p. 2243-2251.

110. Ya-Zheng, Z., et al., *Advances in the antitumor activities and mechanisms of action of steroidal saponins.* Chinese journal of natural medicines, 2018. **16**(10): p. 732-748.

111. Eskander, J., et al., *Steroidal saponins from the leaves of Yucca de-smetiana and their in vitro antitumor activity: structure activity relationships through a molecular modeling approach.* Medicinal Chemistry Research, 2013. **22**(10): p. 4877-4885.

112. Wu, Q., Y. Wang, and M. Guo, *Triterpenoid saponins from the seeds of Celosia argentea and their anti-inflammatory and antitumor activities.* Chemical and Pharmaceutical Bulletin, 2011. **59**(5): p. 666-671.

113. Simões, C., M. Amoros, and L. Girre, *Mechanism of antiviral activity of triterpenoid saponins.* Phytotherapy Research: An International Journal Devoted to Pharmacological and Toxicological Evaluation of Natural Product Derivatives, 1999. **13**(4): p. 323-328.

114. Crozier, A., M.N. Clifford, and H. Ashihara, *Plant secondary metabolites: occurrence, structure and role in the human diet* 2008: John Wiley & Sons.

115. Remesy, C., et al., *Intérêt nutritionnel des flavonoïdes.* Médecine et nutrition, 1996. **32**(1): p. 17-27.

116. Kumar, S. and A.K. Pandey, *Chemistry and biological activities of flavonoids: an overview.* The scientific world journal, 2013. **2013**.

117. Pengfei, L., et al., *Antioxidant properties of isolated isorhamnetin from the sea buckthorn marc.* Plant foods for human nutrition, 2009. **64**(2): p. 141-145.

118. Park, K.-S., Y. Chong, and M.K. Kim, *Myricetin: biological activity related to human health.* Applied Biological Chemistry, 2016. **59**(2): p. 259-269.

119. Vinayagam, R. and B. Xu, *Antidiabetic properties of dietary flavonoids: a cellular mechanism review.* Nutrition & metabolism, 2015. **12**(1): p. 1-20.

120. Yokozawa, T., et al., *Antioxidant effects of isorhamnetin 3, 7-di-O-β-D-glucopyranoside isolated from mustard leaf (Brassica juncea) in rats with streptozotocin-induced diabetes.* Journal of agricultural and food chemistry, 2002. **50**(19): p. 5490-5495.

121. Pari, L. and S. Srinivasan, *Antihyperglycemic effect of diosmin on hepatic key enzymes of carbohydrate metabolism in streptozotocin-nicotinamide-induced diabetic rats.* Biomedicine & Pharmacotherapy, 2010. **64**(7): p. 477-481.

122. Phillips, P., et al., *Myricetin induces pancreatic cancer cell death via the induction of apoptosis and inhibition of the phosphatidylinositol 3-kinase (PI3K) signaling pathway.* Cancer letters, 2011. **308**(2): p. 181-188.

123. Evans, W.C., *Trease and Evans' pharmacognosy* 2009: Elsevier Health Sciences.

124. Yadav, R. and M. Agarwala, *Phytochemical analysis of some medicinal plants.* Journal of phytology, 2011. **3**(12).

125. Oloyede, O., *Chemical profile of unripe pulp of Carica papaya.* Pakistan journal of nutrition, 2005. **4**(6): p. 379-381.

126. Herborne, J., *Phytochemical methods.* A guide to modern techniques of plant analysis, 1973. **2**: p. 5-11.

127. Singleton, V.L. and J.A. Rossi, *Colorimetry of total phenolics with phosphomolybdic-phosphotungstic acid reagents.* American journal of Enology and Viticulture, 1965. **16**(3): p. 144-158.

128.   Lamuela-Raventós, R.M., *Folin–Ciocalteu method for the measurement of total phenolic content and antioxidant capacity.* Measurement of antioxidant activity & capacity: recent trends and applications, 2018: p. 107-115.

129.   Belguidoum, M., H. Dendougui, and Z. Kendour, *In vitro antioxidant properties and phenolic contents of Zygophyllum album L. from Algeria.* J Chem Pharm Res, 2015. **7**(1): p. 510-14.

130.   Chang, C.-C., et al., *Estimation of total flavonoid content in propolis by two complementary colorimetric methods.* Journal of food and drug analysis, 2002. **10**(3).

131.   Mahdi, B., *Étude de métabolites secondaires et quelques activités de plantes algériennes de la famille Zygophyllaceae*, UNIVERSITE KASDI MERBAH OUARGLA.

132.   Kabouche, Z. and C. Bensouici, *Etude phytochimique et évaluation des activités biologiques de deux plantes du genre Sedum.* 2017.

133.   Prieto, P., M. Pineda, and M. Aguilar, *Spectrophotometric quantitation of antioxidant capacity through the formation of a phosphomolybdenum complex: specific application to the determination of vitamin E.* Analytical biochemistry, 1999. **269**(2): p. 337-341.

134.   Falleh, H., et al., *Effect of salt treatment on phenolic compounds and antioxidant activity of two Mesembryanthemum edule provenances.* Plant Physiology and Biochemistry, 2012. **52**: p. 1-8.

135.   Brand-Williams, W., M.-E. Cuvelier, and C. Berset, *Use of a free radical method to evaluate antioxidant activity.* LWT-Food science and Technology, 1995. **28**(1): p. 25-30.

136.   Hsu, B., I.M. Coupar, and K. Ng, *Antioxidant activity of hot water extract from the fruit of the Doum palm, Hyphaene thebaica.* Food chemistry, 2006. **98**(2): p. 317-328.

137.   Re, R., et al., *Antioxidant activity applying an improved ABTS radical cation decolorization assay.* Free radical biology and medicine, 1999. **26**(9-10): p. 1231-1237.

138.   Ramasarma, T. and A.V. Rao, *Catalytic activity of superoxide dismutase: A method based on its concentration-dependent constant decrease in rate of autoxidation of pyrogallol.* Current science, 2007. **92**(11): p. 1481-1482.

139.   Marklund, S. and G. Marklund, *Involvement of the superoxide anion radical in the autoxidation of pyrogallol and a convenient assay for superoxide dismutase.* European journal of biochemistry, 1974. **47**(3): p. 469-474.

140.   Li, H.M., et al., *Preparation of corn (Zea mays) peptides and their protective effect against alcohol-induced acute hepatic injury in NH mice.* Biotechnology and applied biochemistry, 2007. **47**(3): p. 169-174.

141.   Zhao, G.-R., et al., *Antioxidant activities of Salvia miltiorrhiza and Panax notoginseng.* Food chemistry, 2006. **99**(4): p. 767-774.

142.   Prior, R.L., X. Wu, and K. Schaich, *Standardized methods for the determination of antioxidant capacity and phenolics in foods and dietary supplements.* Journal of agricultural and food chemistry, 2005. **53**(10): p. 4290-4302.

143.   Malviya, N., S. Jain, and S. Malviya, *Antidiabetic potential of medicinal plants.* Acta pol pharm, 2010. **67**(2): p. 113-118.

144.   Rasouli, H., et al., *Differential α-amylase/α-glucosidase inhibitory activities of plant-derived phenolic compounds: a virtual screening perspective for the treatment of obesity and diabetes.* Food & function, 2017. **8**(5): p. 1942-1954.

145. Katsarou, A., et al., *Type 1 diabetes mellitus.* Nature reviews Disease primers, 2017. **3**(1): p. 1-17.

146. Daneman, D., *Type 1 diabetes.* The Lancet, 2006. **367**(9513): p. 847-858.

147. DeFronzo, R.A., et al., *Type 2 diabetes mellitus.* Nature reviews Disease primers, 2015. **1**(1): p. 1-22.

148. Miller, G.L., *Use of dinitrosalicylic acid reagent for determination of reducing sugar.* Analytical chemistry, 1959. **31**(3): p. 426-428.

149. Abir, B., *Investigation des effets d'extraits naturels de plantes spontanées locales sur une hydrolase*, 2021.

150. Do, Q.D., et al., *Effect of extraction solvent on total phenol content, total flavonoid content, and antioxidant activity of Limnophila aromatica.* Journal of food and drug analysis, 2014. **22**(3): p. 296-302.

151. Złotek, U., et al., *The effect of different solvents and number of extraction steps on the polyphenol content and antioxidant capacity of basil leaves (Ocimum basilicum L.) extracts.* Saudi journal of biological sciences, 2016. **23**(5): p. 628-633.

152. Khadhri, A., R. El Mokni, and S. Smiti, *Composés phénoliques et activités antioxydantes de deux extraits de chardon à glu: Atractylis gummifera.* Revue Soc. Sci. Nat de Tunisie, 2013. **39**: p. 44-52.

153. Fukushima, Y., et al., *Coffee and green tea as a large source of antioxidant polyphenols in the Japanese population.* Journal of agricultural and food chemistry, 2009. **57**(4): p. 1253-1259.

154. Hertog, M.G., et al., *Intake of potentially anticarcinogenic flavonoids and their determinants in adults in The Netherlands.* 1993.

155. Dehimat, A., et al., *Cytotoxicity and antioxidant activities of leaf extracts of Varthemia sericea (Batt. et Trab.) Diels.* European Journal of Integrative Medicine, 2021. **44**: p. 101338.

156. Ramdane, F., et al., *Phytochemical composition and biological activities of Asteriscus graveolens (Forssk) extracts.* Process Biochemistry, 2017. **56**: p. 186-192.

157. Said, S.A., et al., *Inter-population variability of leaf morpho-anatomical and terpenoid patterns of Pistacia atlantica Desf. ssp. atlantica growing along an aridity gradient in Algeria.* Flora-Morphology, Distribution, Functional Ecology of Plants, 2011. **206**(4): p. 397-405.

158. Ling, L.F. and S. Subramaniam, *Biochemical analyses of Phalaenopsis violacea orchids.* Asian Journal of Biochemistry, 2007. **2**(4): p. 237-246.

159. Tzima, K., N.P. Brunton, and D.K. Rai, *Qualitative and quantitative analysis of polyphenols in Lamiaceae plants—A review.* Plants, 2018. **7**(2): p. 25.

160. Mssillou, I., et al., *Ointment-Based Combination of Dittrichia viscosa L. and Marrubium vulgare L. Accelerate Burn Wound Healing.* Pharmaceuticals, 2022. **15**(3): p. 289.

161. Duangpapeng, P., et al., *Variability in anthocyanins, phenolic compounds and antioxidant capacity in the tassels of collected waxy corn germplasm.* Agronomy, 2019. **9**(3): p. 158.

162. Bouabid, K., et al., *Phytochemical investigation, in vitro and in vivo antioxidant properties of aqueous and organic extracts of toxic plant: Atractylis gummifera L.* Journal of Ethnopharmacology, 2020. **253**: p. 112640.

163. Jacobo-Velázquez, D. and L. Cisneros-Zevallos, *Correlations of antioxidant activity against phenolic content revisited: a new approach in data analysis for food and medicinal plants.* Journal of Food Science, 2009. **74**(9): p. R107-R113.

164. Bors, W. and C. Michel, *Chemistry of the antioxidant effect of polyphenols.* Annals of the New York Academy of Sciences, 2002. **957**(1): p. 57-69.

165. Pietta, P.-G., *Flavonoids as antioxidants.* Journal of Natural Products, 2000. **63**(7): p. 1035-1042.

166. Wojdyło, A., J. Oszmiański, and R. Czemerys, *Antioxidant activity and phenolic compounds in 32 selected herbs.* Food chemistry, 2007. **105**(3): p. 940-949.

167. Hagerman, A.E., et al., *High molecular weight plant polyphenolics (tannins) as biological antioxidants.* Journal of agricultural and food chemistry, 1998. **46**(5): p. 1887-1892.

168. Xu, C., et al., *Superoxide generated by pyrogallol reduces highly water-soluble tetrazolium salt to produce a soluble formazan: A simple assay for measuring superoxide anion radical scavenging activities of biological and abiological samples.* Analytica chimica acta, 2013. **793**: p. 53-60.

169. Gulcin, İ. and S.H. Alwasel, *Metal ions, metal chelators and metal chelating assay as antioxidant method.* Processes, 2022. **10**(1): p. 132.

170. Sarı, Y., et al., *Novel N-propylphthalimide-and 4-vinylbenzyl-substituted benzimidazole salts: Synthesis, characterization, and determination of their metal chelating effects and inhibition profiles against acetylcholinesterase and carbonic anhydrase enzymes.* Journal of Biochemical and Molecular Toxicology, 2018. **32**(1): p. e22009.

171. Sandeepa, K., et al., *In vitro antioxidant activity of Anaphalis lawii (Hook. f) Gamble and Helichrysum buddleioides DC-a comparative study.* J Biosci Agric Res, 2017. **12**(2): p. 1064-1073.

172. Spínola, V. and P.C. Castilho, *Evaluation of Asteraceae herbal extracts in the management of diabetes and obesity. Contribution of caffeoylquinic acids on the inhibition of digestive enzymes activity and formation of advanced glycation end-products (in vitro).* Phytochemistry, 2017. **143**: p. 29-35.

173. Arulselvan, P., et al., *Antidiabetic therapeutics from natural source: A systematic review.* Biomedicine & Preventive Nutrition, 2014. **4**(4): p. 607-617.

174. El-Abhar, H.S. and M.F. Schaalan, *Phytotherapy in diabetes: Review on potential mechanistic perspectives.* World journal of diabetes, 2014. **5**(2): p. 176.

175. Ranilla, L.G., et al., *Phenolic compounds, antioxidant activity and in vitro inhibitory potential against key enzymes relevant for hyperglycemia and hypertension of commonly used medicinal plants, herbs and spices in Latin America.* Bioresource technology, 2010. **101**(12): p. 4676-4689.

176. Nouioua, W., *Ecologie, chorologie et phytochimie et activité biologique d'une Paeoniaceae endémique algérienne (L.) Mill*, 2017, Université Ferhat Abbas.

177. No, O.T., *423: Acute Oral Toxicity—OECD Guideline for the Testing of Chemicals Section 4*, 2002, OECD Publishing: Paris, France.

178. Ferdjioui, S., *Activités biologiques de deux plantes médicinales MentharotundifoliaL. et Lamium amplexicauleL*, 2020.

179. Raghavendra, G.M., K. Varaprasad, and T. Jayaramudu, *Biomaterials: design, development and biomedical applications*, in *Nanotechnology applications for tissue engineering*2015, Elsevier. p. 21-44.

180. Noack, M. and M.-N. Kolopp-Sarda, *Cytokines et inflammation: physiologie, physiopathologie et utilisation thérapeutique.* Revue Francophone des Laboratoires, 2018. **2018**(499): p. 28-37.

181. MOUFFOUK, C., *Evaluation des activités biologiques et étude de la composition chimique de la plante Scabiosa stellata L*, 2019, Université de Batna 2.

182. Marginier, F., *Evaluation des effets sédatifs de quatre protocoles combinant l'alfaxalone, la dexmédétonidine et la méthatone chez le chat: Evaluation of the sedative effects of four protocols combining the alfaxalone, the dexmedetomidine and methadone in the cat*, 2017, École Nationale Vétérinaire Alfort.

183. TEHAMI, W., *Caractérisation phytochimique et évaluation du potentiel antioxydant, antimicrobien et anti-inflammatoire de Salvia argentea*, 2017.

184. Kim, H.P., et al., *Anti-inflammatory plant flavonoids and cellular action mechanisms.* Journal of pharmacological sciences, 2004: p. 0411110005-0411110005.

185. Gupta, G., et al., *Sedative, antiepileptic and antipsychotic effects of Viscum album L.(Loranthaceae) in mice and rats.* Journal of Ethnopharmacology, 2012. **141**(3): p. 810-816.

186. Kim, S., et al., *Marine Polyphenol Phlorotannins as a Natural Sleep Aid for Treatment of Insomnia: A Review of Sedative–Hypnotic Effects and Mechanism of Action.* Marine Drugs, 2022. **20**(12): p. 774.

187. Hennebelle, T., S. Sahpaz, and F. Bailleul, *Plantes sédatives: évaluation pharmacologique et clinique.* Médecine du sommeil, 2007. **4**(13): p. 4-14.

188. Fernández, S., et al., *Sedative and sleep-enhancing properties of linarin, a flavonoid-isolated from Valeriana officinalis.* Pharmacology Biochemistry and Behavior, 2004. **77**(2): p. 399-404.

189. Rauf, A., et al., *In vivo and in silico sedative-hypnotic like activity of 7-methyljuglone isolated from Diospyros lotus L.* Biomedicine & Pharmacotherapy, 2017. **87**: p. 678-682.

190. Shanmugasundaram, J., et al., *Sedative–hypnotic like effect of 5–methoxyflavone in mice and investigation on possible mechanisms by in vivo and in silico methods.* Biomedicine & Pharmacotherapy, 2018. **108**: p. 85-94.

191. Gazola, A.C., et al., *The sedative activity of flavonoids from Passiflora quadrangularis is mediated through the GABAergic pathway.* Biomedicine & Pharmacotherapy, 2018. **100**: p. 388-393.

192. Joullié, M.M. and D.J. Richard, *Cyclopeptide alkaloids: chemistry and biology.* Chemical communications, 2004(18): p. 2011-2015.

193. Jiang, J.-G., et al., *Comparison of the sedative and hypnotic effects of flavonoids, saponins, and polysaccharides extracted from Semen Ziziphus jujube.* Natural Product Research, 2007. **21**(4): p. 310-320.

194. Shwe, H.H., et al., *Isolation and structural characterization of lupeol from the stem bark of Diospyros ehretioides Wall.* IEEE-SEM, 2019. **7**(8): p. 140-144.

195. Mahato, S.B. and A.P. Kundu, *13C NMR spectra of pentacyclic triterpenoids—a compilation and some salient features.* Phytochemistry, 1994. **37**(6): p. 1517-1575.

196. Furuya, T., Y. Orihara, and C. Hayashi, *Triterpenoids from Eucalyptus perriniana cultured cells.* Phytochemistry, 1987. **26**(3): p. 715-719.

197. Arriaga, F.J., A. Rumbero, and P. Vazquez, *Two triterpene glycosides from Isertia haenkeana.* Phytochemistry, 1990. **29**(1): p. 209-213.

198. Seebacher, W., et al., *Complete assignments of 1H and 13C NMR resonances of oleanolic acid, 18α-oleanolic acid, ursolic acid and their 11-oxo derivatives.* Magnetic Resonance in Chemistry, 2003. **41**(8): p. 636-638.

199. Yan, C., et al., *A fructooligosaccharide from Achyranthes bidentata inhibits osteoporosis by stimulating bone formation.* Carbohydrate polymers, 2019. **210**: p. 110-118.

200. Okada, H., et al., *Novel fructopyranose oligosaccharides isolated from fermented beverage of plant extract.* Carbohydrate research, 2010. **345**(3): p. 414-418.

201. Chandrashekar, P.M., K.V.H. Prashanth, and Y.P. Venkatesh, *Isolation, structural elucidation and immunomodulatory activity of fructans from aged garlic extract.* Phytochemistry, 2011. **72**(2-3): p. 255-264.

202. Wang, C., et al., *Structural characterization of a novel oligosaccharide from Achyranthes bidentata and its anti-osteoporosis activities.* Industrial Crops and Products, 2017. **108**: p. 458-469.

203. Chen, X., Y. Xu, and G. Tian, *Physical-chemical properties and structure elucidation of abPS isolated from the root of Achyranthes bidentata.* Yao xue xue bao= Acta Pharmaceutica Sinica, 2005. **40**(1): p. 32-35.

204. Yang, Z., J. Hu, and M. Zhao, *Isolation and quantitative determination of inulin-type oligosaccharides in roots of Morinda officinalis.* Carbohydrate polymers, 2011. **83**(4): p. 1997-2004.

205. Zhang, R., et al., *Achyranthes bidentata root extract prevent OVX-induced osteoporosis in rats.* Journal of Ethnopharmacology, 2012. **139**(1): p. 12-18.

206. Zhang, R., et al., *Du-Zhong (Eucommia ulmoides Oliv.) cortex extract prevent OVX-induced osteoporosis in rats.* Bone, 2009. **45**(3): p. 553-559.

207. Liu, J., A.L. Waterhouse, and N.J. Chatterton, *Proton and carbon chemical-shift assignments for 6-kestose and neokestose from two-dimensional nmr measurements.* Carbohydrate research, 1991. **217**: p. 43-49.

208. Calub, T.M., A.L. Waterhouse, and N.J. Chatterton, *Proton and carbon chemical-shift assignments for 1-kestose, from two-dimensional nmr-spectral measurements.* Carbohydrate research, 1990. **199**(1): p. 11-17.

209. Jones, A., P. Hanisch, and A. McPhail, *Sucrose: an assignment of the 13C NMR parameters by selective decoupling.* Australian Journal of Chemistry, 1979. **32**(12): p. 2763-2766.

210. Markham, K.R., *Techniques of flavonoid identification*1982: Academic press.

211. Buschi, C.A. and A.B. Pomilio, *Isorhamnetin 3-O-robinobioside from Gomphrena martiana.* Journal of Natural Products, 1982. **45**(5): p. 557-559.

212. Markham, K., et al., *Carbon-13 NMR studies of flavonoids—III: Naturally occurring flavonoid glycosides and their acylated derivatives.* Tetrahedron, 1978. **34**(9): p. 1389-1397.

213. Sen, S., N.P. Sahu, and S.B. Mahato, *Flavonol glycosides from Calotropis gigantea.* Phytochemistry, 1992. **31**(8): p. 2919-2921.

214. Halim, A.F., H.-E.A. Saad, and N.E. Hashish, *Flavonol glycosides from Nitraria retusa.* Phytochemistry, 1995. **40**(1): p. 349-351.

215. Yasukawa, K., H. Sekine, and M. Takido, *Two flavonol glycosides from Lysimachia fortunei.* Phytochemistry, 1989. **28**(8): p. 2215-2216.

216. Li, F., et al., *Pancreatic lipase-inhibiting triterpenoid saponins from fruits of Acanthopanax senticosus.* Chemical and Pharmaceutical Bulletin, 2007. **55**(7): p. 1087-1089.

217. Navarro, P., et al., *In vivo anti-inflammatory activity of saponins from Bupleurum rotundifolium.* Life sciences, 2001. **68**(10): p. 1199-1206.

218. Rubio-Moraga, Á., et al., *Triterpenoid saponins from corms of Crocus sativus: localization, extraction and characterization.* Industrial Crops and Products, 2011. **34**(3): p. 1401-1409.

219. Abd Ellah, A.E., et al., *Cinnamyl alcohol, benzyl alcohol, and flavonoid glycosides from Sanchezia nobilis.* Chemistry of natural compounds, 2014. **50**: p. 823-826.

220. Morikawa, T., et al., *A new amide, piperchabamide F, and two new phenylpropanoid glycosides, piperchabaosides A and B, from the fruit of Piper chaba.* Chemical and Pharmaceutical Bulletin, 2009. **57**(11): p. 1292-1295.

221. Bi, H., et al., *Producing Gram-scale unnatural rosavin analogues from glucose by engineered Escherichia coli.* ACS Synthetic Biology, 2019. **8**(8): p. 1931-1940.

222. Bohlin, C., K. Lundquist, and L.J. Jönsson, *Diastereomer selectivity in the degradation of a lignin model compound of the arylglycerol β-aryl ether type by white-rot fungi.* Enzyme and microbial technology, 2008. **43**(2): p. 199-204.

223. Mohamed, K.M., *Phenylpropanoid glucosides from Chrozophora obliqua.* Phytochemistry, 2001. **58**(4): p. 615-618.

224. Silva, L.B., et al., *Triterpenes from the flowers of Gochnatia polymorpha subsp. floccosa.* Revista Brasileira de Farmacognosia, 2011. **21**: p. 556-559.

225. Khalilov, L., et al., *PMR and 13 C NMR spectra of biologically active compounds. XII. Taraxasterol and its acetate from the aerial part of Onopordum acanthium.* Chemistry of natural compounds, 2003. **39**: p. 285-288.

226. Duan, J.-a., et al., *A new cytotoxic prenylated dihydrobenzofuran derivative and other chemical constituents from the rhizomes of Atractylodes lancea DC.* Archives of pharmacal research, 2008. **31**: p. 965-969.

227. Theumann, D. and J. Comin, *Isolation of isobauerenol from Helietta longifoliata.* Phytochemistry, 1969. **8**(4): p. 781-783.

228. Abdullahi, M., et al., *Isolation and Characterisation of an Alpha-amyrin Acetate Isolated from the Leaves of Microtrichia perotitii DC (Asteraceae).* drugs. **1**(2): p. 3-4.

229. Abreu, V.G., et al., *Evaluation of the bactericidal and trypanocidal activities of triterpenes isolated from the leaves, stems, and flowers of Lychnophora pinaster.* Revista Brasileira de Farmacognosia, 2011. **21**: p. 615-621.

230. Okoye, N.N., et al., *beta-Amyrin and alpha-amyrin acetate isolated from the stem bark of Alstonia boonei display profound anti-inflammatory activity.* Pharmaceutical biology, 2014. **52**(11): p. 1478-1486.

231. Wadouachi, A., et al., *Triterpenes and steroids from the stem bark of Gambeya boiviniana Pierre.* Journal of Pharmacognosy and Phytochemistry, 2014. **3**(1): p. 68-72.

232. Kiplimo, J.J., N.A. Koorbanally, and H. Chenia, *Triterpenoids from Vernonia auriculifera Hiern exhibit antimicrobial activity.* African Journal of Pharmacy and Pharmacology, 2011. **5**(8): p. 1150-1156.

233. Ushie, O., H. Adamu, and I. Chindo, *β–amyrin-3-acetate Detected in Methanolic Leaf Extract of Chrysophyllum albidium.* Journal of Chemical Society of Nigeria, 2018. **43**(2).

234. Shen, Y.C., et al., *New triterpenoid fatty acid esters from the small twigs of Viburnum odoratissimum.* Journal of the Chinese Chemical Society, 2003. **50**(2): p. 297-302.

235. El-Seedi, H., et al., *Antimicrobial diterpenoids from Eupatorium glutinosum (Asteraceae).* Journal of Ethnopharmacology, 2002. **81**(2): p. 293-296.

236.   Hamburger, M., et al., *Preparative purification of the major anti-inflammatory triterpenoid esters from Marigold (Calendula officinalis).* Fitoterapia, 2003. **74**(4): p. 328-338.